

Visible Light Mediated Photoredox Catalytic Dehydrogenation and C-H Arylation reactions

Thesis Submitted to AcSIR
For the Award of the Degree of
DOCTOR OF PHILOSOPHY
in
CHEMICAL SCIENCES



by

Manoj Kumar Sahoo

AcSIR No. 10CC13A26007

Under the guidance of

Dr. E. Balaraman

Organic Chemistry Division

CSIR-National Chemical Laboratory (CSIR-NCL)

Pune - 411008, INDIA.

JULY - 2018

Dedicated to All My Beloved

TEACHERS



सीएसआईआर - राष्ट्रीय रासायनिक प्रयोगशाला

(वैज्ञानिक तथा औद्योगिक अनुसंधान परिषद)

डॉ. होमी भाभा मार्ग, पुणे - 411 008, भारत



CSIR - NATIONAL CHEMICAL LABORATORY

(Council of Scientific & Industrial Research)

Dr. Homi Bhabha Road, Pune - 411 008, India

CERTIFICATE

This is to certify that the work incorporated in this Ph.D. thesis entitled “**Visible Light Mediated Photoredox Catalytic Dehydrogenation and C-H Arylation reactions**” submitted by **Mr. Manoj Kumar Sahoo** (AcSIR Registration Number 10CC13A26007) to the Academy of Science and Innovation Research (AcSIR) in the fulfillment of the requirements for the award of the Degree of the Doctor of Philosophy, embodies original research work under my supervision at Organic Chemistry Division, CSIR-National Chemical Laboratory (CSIR-NCL), Pune, India. I further certify that this work has not been submitted to any other University or Institution in part or full for the award of any degree or diploma. Research material obtained from other sources has been duly acknowledged in the thesis. Any text, illustration, table, etc., used in the thesis from other source have been duly cited and acknowledged.

Manoj Kumar Sahoo
Manoj Kumar Sahoo

(Research Student)

(Reg. No. 10CC13A26007)

E. Balaraman
Dr. E. Balaraman

(Research Supervisor)

Date: 30th July, 2018

Place: CSIR-NCL, Pune.

**Communication
Channels**

NCL Level DID : 2590
NCL Board No. : +91-20-25902000
EPABX : +91-20-25893300

FAX

Director's Office : +91-20-25902601
COA's Office : +91-20-25902660
SPO's Office : +91-20-25902664

WEBSITE

www.ncl-india.org

DECLARATION

I hereby declare that the original research work embodied in this thesis entitled “**Visible Light Mediated Photoredox Catalytic Dehydrogenation and C-H Arylation reactions**” submitted to the Academy of Scientific and Innovative Research (AcSIR), New Delhi, for the award of degree of **Doctor of Philosophy in Chemical Sciences** is the outcome of experimental investigations carried out by me under the supervision of **Dr. E. Balaraman**, Senior Scientist, CSIR-National Chemical Laboratory (CSIR-NCL), Pune. I affirm that the work incorporated is in original and has not been submitted to any other academy, university or institution in part or full for the award of any degree or diploma.

Date: 30th July 2018

Manoj Kumar Sahoo

Manoj Kumar Sahoo

Senior Research Fellow

Organic Chemistry Division

CSIR-NCL, Pune-411008.

Acknowledgment

Ph.D. is like a long journey; an experience that takes you through the untraversed path, the green lush meadows and the island of Cyclopes to conquer the final goal fixed in mind. Once you achieve the target and turn back, you realize that all your efforts and the pain were worth going through. The small successes & the serendipitous discoveries, the frustrating failures & unexpected crystallizations, the imparted chemical wisdom & the laboratory camaraderie; they are all important parts of this beautiful voyage. But one can't succeed in this journey without the guidance and support of the research supervisor, friends, and well-wishers. I am taking this opportunity to express my deepest gratitude to everyone who has helped and supported me throughout the course of my research journey.

Firstly, I would like to express my deep sense of gratitude with special thanks to my research supervisor **Dr. E. Balaraman** for his unwavering support, valuable guidance, and scholarly inputs, without which I wouldn't have embarked into the uncharted world of Organometallics and Sustainable Catalysis. His energy, enthusiasm and endless love towards chemistry have been highly inspiring, to me. He provided the consummate knowhow of research and student mentorship through his unique combination of scientific brilliance and personal kindness. I have enjoyed the opportunity to watch and learn from his knowledge and experience. His encouragement, and faith in me throughout my journey have been extremely helpful. He is the one who has moulded me into a good researcher. I am thankful to the Almighty God for giving me the opportunity to pursue my research career under the supervision of such a wonderful and humble person as my mentor. He has given me full freedom to carry out my research work and I could not even imagine having a better mentor than him.

I wish to express my sincere thanks to the Doctoral Advisory Committee members, Dr. Jayaraj Nithyanandhan, Dr. Samir H. Chikkali, Dr. Pradip Maity and former Doctoral Advisory Committee Member Dr. Nitin T. Patil whose contribution in stimulating suggestions and encouragement helped me to coordinate my work.

I am grateful to Prof. A. K. Nangia, Director, CSIR-NCL, Dr. V. K. Pillai and Prof. S. Pal (Former Director, CSIR-NCL), Dr. S. P. Chavan (Head, Organic Chemistry Division), Dr. D. Srinivas (Former Head, Catalysis Division), Dr. C. S. Gopinath (Head, Catalysis

Division) for giving me this opportunity and providing all necessary infrastructure and facilities to carry out my research work. I am also highly thankful to Council of Scientific & Industrial Research (CSIR), New Delhi for the financial assistance.

I am highly grateful to Dr. Satyanarayana Chilukuri, Dr. Chepuri V. Ramana, Dr. Kumar Vanka, Dr. Benudhar Punji, Dr. Rahul Banergee, Dr. Rajesh Gonnade, Dr. M. Sashidhar, Dr. Amitava Das and Dr. Sayam Sen Gupta for their kind help at different part of my research journey which is highly acknowledged.

I would also like to acknowledge Dr. Sunita Barve, Mr. Gati Krushna Nayak and other staff members of the library for all kind of support and for giving access to the library.

I would also like to acknowledge all the support from office staffs of Catalysis and Inorganic Chemistry Division as well as Mrs. Catherine, Deepika, Thangaraj and Fernandes from OCD for their paperwork & other documentation related assistance.

I would like to extend my sincere thanks to Dr. P. R. Rajamohanan and Dr. Udaya Kiran Marelli for their timely help in NMR analysis, Mr. Dinesh Shinde, Mayur More, Pramod, Sanoop, Kavya for NMR recording, Dr. Shantakumari for Mass/HRMS facility, Dr. Borikar for GCMS support. I express my heartiest gratitude towards Ekta Sangtani, Samir, Shridhar and VSSN Swamy for their necessary help in X-Ray crystallographic analysis. I also thank the IP group, CSIR-NCL for their support in the patent filing.

I gratefully acknowledge the kind help and support extended by my seniors especially Dr. Jitendra Kumar Raut, Dr. Chakadola Panda, Dr. Mandakini Tripathi, Dr. Sibanarayana Tripathi, Dr. Gokarneswar Sahoo, Dr. Puspanjali Sahu, Dr. B. P. Biswal, Dr. Kanhu Charan Rout, Dr. Kshirodra Kumar Patra, Dr. Raju Nanda. Also, kind of support from Ms. Prajna, Mr. Sibadatta, Ms. Gitanjali is highly acknowledged.

A special thanks go to Dr. L. N. Nanda, Dr. Balaram Mohapatra, Dr. Devi P. Ojha, Dr. Prasant Nayak, Dr. Subhasis Pati, Dr. Aditya Garai, Mr. Srikanta Patra, Mr. Bikash Sharma, Mr. Pravakar Sethi, for their helping hand and inspiring me during the tenure of my Ph.D.

I especially thank Mr. Sumanta Pradhan, Mr. Debanjan Mondal, Dr. Brijesh Sharma, Dr. Srinivas Kolluru, Dr. Shrikant M. Khake and Dr. Vijay Chaudhari for their exuberant cooperation and support to drive my research in the forward direction.

Special thanks to my labmates Garima, Siba, Vinod, Rana, Akash, Vinita, Subaramanian, Saravanakumar, Sivakumar, Samrin and former labmates Dr. Alok Tripathi, Sopan, Thomas Abraham for their kind support during my research work, which I greatly acknowledge.

A special thanks to all my friends from CSIR-NCL, Sandip Singh, Swamy, Dheerendra, Sandeep Yadav, Virat, Rajan, Manoj, Himansu, Mahitosh, Saibal, Manjur, Amol, Bagle, Aslam, Avinash, Pranab, Sagar, Santi Gopal, Dinesh, Dinesh J. Paymode, Venkannababu, Prabhakar, Mahesh, Dnyanesh, Sharad, Gorakhnath, Dhananjay, Nilesh, Abhijit Bera, Pravin N. Shinde, Arun Nikam, Jayesh, Milan, Ambarish, Punitharasu, Dr-Anil Shelke, Dr. Deva Raj, Dr. Bikash Garai Prabu Kandasamy, Abdul, Tafeek, Indrajeet, Patil, Poulomi Sengupta, Sanjukta, Reshma, Sonali, Suman, Yogita, Govind, Sumanta, Manoj, Sandeep, Anand, Anup, Sweccha, Ragini, Pravin Dwivedi from NCL and Manoj Gupta from IISER Pune for their kind help and support.

My family is always a source of inspiration and a great moral support for me in pursuing my education. I owe a lot to my beloved parents who encouraged and helped me at every stage of my personal and academic life and longed to see this achievement come true. My sincere thanks to my beloved family members my father 'Kailash Chandra Sahoo', mother 'Renuka Sahoo', Grandmother 'Suka Sahoo', other family members Anita, Kanhu, Banamali, Bini, for their endless love, support, and sacrifice. I am very much indebted to my whole family who supported me in every possible way to see the completion of this research work. I especially thank my cousin Rajib Lochan', Atanu Ranjan, Rasmi Ranjan for their kind support and valuable suggestions.

I wish to thank the great scientific community whose achievements are a constant source of inspiration for me. Above all, I extend my gratitude's to the Almighty God for giving me the wisdom, health, and strength to undertake this research work and enabling me to its completion.

Manoj Kumar Sahoo

Table of Contents

Abbreviations

General remarks

Synopsis

Chapter 1: Visible-Light Mediated Photoredox Catalytic Reactions

1.1. Historical Background of Photocatalysis

1.1.1. Radicals in Photocatalysis

1.2. Modern Visible-Light Photoredox Catalysis and Early Work

1.3. Mechanisms Underlying Photoredox Catalysis

1.3.1. Photophysical Properties of a Photocatalyst

1.3.2. Photophysical Properties of $[\text{Ru}(\text{bpy})_3]^{2+}$

1.3.3. Photophysical Properties of Eosin Y and Rose Bengal

1.4. Basic Mechanism of Photoredox Catalysis

1.5. Types of Photoredox Catalysts

1.6. Basic Requirement for Success of a Photoredox Catalytic Reaction

1.7. Recent Trends in Photoredox Catalysis

1.7.1. Dual Catalysis (Merging Photoredox Catalysis with TM or Organocatalysis)

1.7.2. Taxonomy for Dual Catalysis

1.7.3. Importance and Advantages of Dual Catalytic Approach

1.7.4. Challenges for Merging Photoredox Catalysis with Catalytic Cycles from Other Domain

1.8. Scope and Objectives of the Thesis Work

1.9. Organization of thesis

1.10. References

Chapter 2: Organophotoredox Catalyzed Oxidative Dehydrogenation of *N*-Heterocycles

2.1. Introduction

2.2. Statement of the Problem

2.3. Reaction Optimization

2.3.1. Optimization Reaction Conditions

2.3.2. Effect of Catalyst Loading

2.4. Substrate Scope

2.4.1. Scope of Quinoline Derivatives

2.4.2. Scope of Indole Derivatives

2.4.3. Substrate Scope for Other *N*-heteroaromatics

2.4.4. Scope for Pharmaceutically Active Intermediates

2.5. Mechanistic Investigation

2.5.1. Cyclic Voltammetry Analysis

2.5.2. Radical Quenching and Trapping Experiments

2.5.3. Experimental Detection of H₂O₂

2.5.4. Control Experiments

2.5.5. Plausible Mechanism

2.6. Conclusion

2.7. Experimental Section

2.8. Reference

Chapter 3: Dual Catalyzed Acceptorless Dehydrogenation of *N*-Heterocycles to Heteroaromatics by Merging Photoredox Catalysis with Proton Reduction Catalysis

3.1. Introduction

3.2. Statement of the Problem

3.3. Reaction Optimization

3.3.1. Cobalt Complexes Used for the Present Catalytic Study

3.3.2. Synthesis of Cobalt complexes

3.3.3. UV-Visible Spectra of Cobalt Complexes

3.3.4. Cyclic Voltammogram of Cobalt Complex IV

3.3.5. Optimization Table

3.4. Substrate scope

3.4.1. Scope of Quinoline Derivatives

3.4.2. Scope of Indoles and other Heterocycles

3.5. Mechanistic Investigation

3.5.1. Cyclic Voltammetry of Partially Saturated *N*-heterocycles

3.5.2. Analysis for Hydrogen Gas

3.5.2a. Qualitative Analysis of Hydrogen Gas

3.5.2b. Quantitative Measurement of Evolved Hydrogen Gas

3.5.3. Control Experiments

3.5.4. Plausible Mechanism

3.6. Conclusion

3.7. Experimental Section

3.8. References

Chapter 4: Visible-light Photocatalyzed Acceptorless Dehydrogenation of Diaryl Hydrazines

4.1. Introduction

4.2. Statement of the Problem

4.3. Reaction Optimization

4.3.1. Optimization Table

4.3.2. Substrate Scope

4.4. Monitoring of Reaction Progress using UV-Visible Spectroscopy

4.5. Azobenzene and Hydrazobenzene as LOHCs

4.5.1. Substrate Scope

4.6. Derivatization of Azobenzene

4.7. Cis-trans Isomerization upon UV-light Irradiation

4.8. Mechanistic Investigation

4.8.1. Cyclic Voltammetry Experiment

4.8.2. Hydrogen Gas Detection in GC

4.8.3. Control Experiments

4.8.4. Plausible Mechanism

4.9. Conclusion

4.10. Experimental Section

4.11. References

Chapter 5: C-H Arylation of Anilides by Merging Photoredox Catalysis with Palladium Catalysis

Chapter 5A: Dual Catalyzed C-H Arylation of Anilides under External Oxidant-Free Conditions by Merging Organophotoredox Catalysis with Palladium Catalysis

5A.1. Introduction

5A.2. Statement of the Problem

5A.3. Reaction Optimization

5A.4. Substrate Scope

5A.4.1. Scope of Aryldiazonium Salts

5A.4.2. Scope of Anilides

5A.5. Derivatization of ortho-Arylanilines

5A.6. Kinetics of the Reaction

5A.6.1. Representative Procedure: Time-dependent Formation of 3a

5A.6.2. Rate Order Determination

5A.7. Mechanistic Investigation

5A.7.1. Control Experiment

5A.7.2. Light-Dark Experiment

5A.7.3. Light-Dark Experiment (ON/OFF Experiment)

5A.7.4. Identification of Intermediate Pd-complex

5A.7.5. Effect of Other Directing Group

5A.7.6. Plausible Mechanism

5.8. Conclusion

5.9. Experimental Section

5.10. References

**Chapter 5B: Direct Arylation of Anilides under External Oxidant-Free Conditions
using CO₂-Derived Dimethyl Carbonate (DMC) as a 'Green' Solvent under [Ru]-
Catalysis**

5B.1. Introduction

5B.2. Statement of the Problem

5B.3. Reaction Optimization

5B.4. Substrate Scope

5B.5. Mechanistic Investigation

5B.5.1. Control Experiments

5B.5.2. Plausible Mechanism

5B.6. Conclusion

5B.7. Experimental Procedures

5B.8. Reference

Appendix A: NMR and HRMS Data

Appendix B: Copy of ¹H and ¹³C NMR Spectra (Only selected compounds)

Appendix C: Copy of Cyclic Voltammogram (Only selected compounds)

Abbreviations

Units

°C	Degree centigrade
mg	Milligram
h	Hour
Hz	Hertz
μs	Microsecond
mL	Millilitre
min.	Minute
MHz	Megahertz
mmol	Millimole
nm	Nanometre
ppm	Parts per million
%	Percentage
V	Volt
W	Watt

Chemical Notations

Ac	Acetyl
AcOH	Acetic Acid
Ar	Aryl
MeCN	Acetonitrile

BHT	3,5-Di- <i>tert</i> -4-butylhydroxytoluene
bpy	2,2'-Bipyridyl
NBS	<i>N</i> -Bromosuccinimide
CDCl ₃	Deuterated Chloroform
DBAD	Di- <i>tert</i> -butyl azodicarboxylate
DDQ	2,3-Dichloro-5,6-dicyano-1,4-benzoquinone
DMA	<i>N, N'</i> -Dimethylacetamide
DMAP	<i>N, N</i> -Dimethylaminopyridine
DMC	Dimethyl carbonate
DMF	<i>N, N'</i> -Dimethylformamide
dmg	Dimethylglyoxime
DMSO	Dimethyl sulfoxide
DCE	1,2-Dichloroethane
DABCO	1,4-diazabicyclo[2.2.2]- octane
DBU	1,8-Diazabicyclo[5.4.0]undec-7-ene
EtOH	Ethanol
Et	Ethyl
EtOAc	Ethyl Acetate
MeOH	Methanol
Me	Methyl
NMP	1-Methyl-2-pyrrolidinone
2-MeTHF	2-Methyltetrahydrofuran
ppy	2-Phenylpyridine

py	Pyridine
TFA	Trifluoroacetic acid
THF	Tetrahydrofuran
THQ	1,2,3,4-tetrahydroquinolines
TEMPO	2,2,6,6-Tetramethyl-1-piperidinyloxy


Other Notations

δ	Chemical shift
<i>J</i>	Coupling constant in NMR
equiv.	Equivalents
GC	Gas Chromatography
HOMO	Highest occupied molecular orbital
HRMS	High Resolution Mass Spectrometry
LED	Light emitting diode
LUMO	Lowest unoccupied molecular orbital
NMR	Nuclear Magnetic Resonance
PTFE	Polytetrafluoroethylene
rt	Room temperature
UV	Ultraviolet

General remarks

- All catalysts (except proton reduction catalysts prepared according to literature report) were purchased from commercial sources and used as received.
 - Light sources used are of commercial household fluorescent bulbs or LED strips (Blue, Green,) obtained from local market.
 - All reactions were carried out under inert atmosphere following standard procedures using Schlenk techniques.
 - Deuterated solvents for NMR spectroscopic analyses were used as received. All ^1H NMR and ^{13}C NMR analysis were obtained using a Bruker or JEOL 200 MHz, 400 MHz or 500 MHz spectrometers. Coupling constants were measured in Hertz. All chemical shifts are quoted in ppm, relative to TMS, using the residual solvent peak as a reference standard. The following abbreviations are used to explain the multiplicities: s = singlet, d = doublet, t = triplet, q = quartet, m = multiplet, br = broad.
 - HRMS spectra were recorded at UHPLC-MS (Q-exactive-Orbitrap Mass Spectrometer) using electron spray ionization [(ESI⁺, +/- 5kV), solvent medium: water, acetonitrile, methanol and ammonium acetate] technique and mass values are expressed as *m/z*. GC-HRMS (EI) was recorded in Agilent 7200 Accurate-mass-Q-TOF.
 - All reactions are monitored by Thinlayer chromatography (TLC) with 0.25 mm pre-coated silica gel plates (60 F₂₅₄). Visualization was accomplished with either UV light, Iodine adsorbed on silica gel or by immersion in ethanolic solution of phosphomolybdic acid (PMA), p-anisaldehyde or KMnO₄ followed by heating with a heat gun for ~15 sec.
 - All solvents and reagents were purified and dried by according to procedures given in Vogel's Text Book of Practical Organic Chemistry. All reactions were carried out under nitrogen or argon atmosphere with dry, freshly distilled solvents under anhydrous conditions unless otherwise specified. Yields refer to chromatographically and spectroscopically homogeneous materials unless otherwise stated.
 - Column chromatography was performed on silica gel (100-200 or 230-400 mesh size).
 - Chemical nomenclature (IUPAC) and structures were generated using ChemDraw Professional 15.1.
-
-

Preface

 Synopsis of the Thesis to be submitted to the Academy of Scientific and Innovative Research for Award of the Degree of Doctor of Philosophy in Chemistry	
Name of the Candidate	Mr. MANOJ KUMAR SAHOO
Degree Enrolment No. & Date	Ph. D in Chemical Sciences (10CC13A26007); August 2013
Title of the Thesis	Visible Light Mediated Photoredox Catalytic Dehydrogenation and C-H Arylation reactions
Research Supervisor	Dr. E. Balaraman (CSIR-NCL, Pune)

Introduction: In the recent past, visible-light photoredox catalysis experiencing renaissance in organic transformations and development of new synthetic strategies. These catalytic reactions occur under very mild and ambient by employing low energy visible-light from household bulbs. Again photoredox catalytic cycle can be merged with either organocatalysis or transition-metal catalysis. This dual catalysis emerges as a powerful synthetic tool giving unique reactivity and selectivity not observed using either of the catalysts independently. A photoredox catalyst on light irradiation can act as an oxidant or reductant depending on the nature of reactant and reaction environment and hence give unique reactivity.

Statement of the Problem: Nitrogen-containing heterocycles, aryl azobenzenes, and 2-aryl anilines are important families of organic compounds. The *N*-heteroaromatics show profound applications in the synthesis of natural products, bioactive molecules and pharmaceuticals. Similarly azo compound show wide application in drug delivery, material science, conducting polymers, and dye-pigment industry. The ortho-aryl aniline derivatives have shown various application in material sciences, organometallic catalysis and in the synthesis of many pharmaceuticals. Many research groups have reported the synthesis of *N*-heteroaromatics and azobenzenes. But the use of strong oxidants, base, additive and harsh condition are the major drawbacks for these methods. Again for the synthesis of 2,6-bisarylanilines only classical cross-coupling methods were known and not with transition metal catalyzed C-H activation.

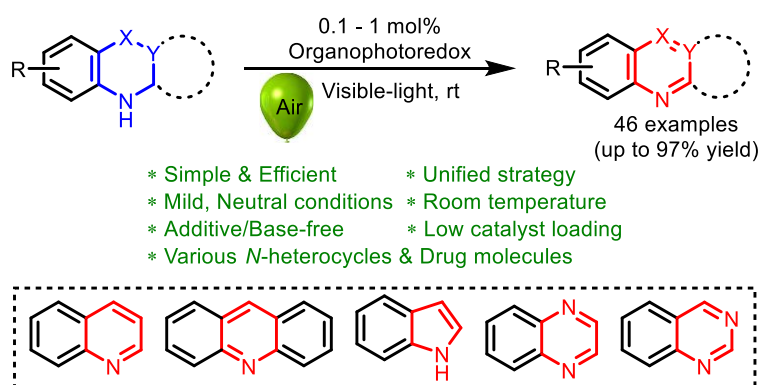
Aims and objectives: The main aim and objective of this thesis is in the development of new methodologies for the synthesis of *N*-heterocycle, azobenzenes and ortho-aryl aniline derivatives under photoredox catalysis sometimes merged with transition metal catalysis. Reactions taking place in dual photoredox and transition metal catalytic condition can be achieved under very mild, ambient and environmentally friendly.

Methodology used: All photoredox catalytic experiments were carried out using standard Schlenk techniques. Commercial household bulbs were used as the light source. All solvents were of AR-grade, obtained from commercial sources and dried following standard protocol prior to use. All photoredox catalysts and metal salts used for the catalytic study were obtained from commercial sources. The proton reduction catalysts used for these study were synthesized according to the literature report and characterized using standard techniques prior to use.

Sample results: The thesis comprises of five chapters. The first chapter gives a brief introduction about the photoredox catalysis, its importance in organic transformation and the recent literature paradigms. From second to fifth, all are working chapters which narrates specific organic transformation under visible-light photoredox catalysis, sometimes merged with a transition metal catalysis as given below.

Chapter II: Organophotoredox Catalyzed Oxidative Dehydrogenation of *N*-Heterocycles

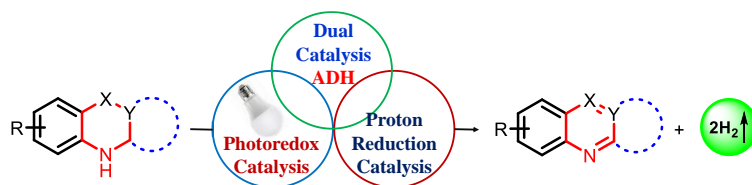
Inspired by the vast application and absence of environmental friendly protocol here, we explored the catalytic oxidative dehydrogenation of diverse *N*-heterocycles using a visible-light organophotoredox catalyst. This reaction proceeds efficiently at room temperature under the base and additive-free conditions, air as oxidant and visible-light from the household bulb. This environmentally benign method shows a broad substrate scope and good functional group compatibility. A thorough mechanistic investigation has been carried out for this oxidative dehydrogenation reaction.



Scheme 1. Organophotoredox catalyzed oxidative dehydrogenation of *N*-heterocycles.

Chapter III: Dual Catalyzed Acceptorless Dehydrogenation of *N*-Heterocycles to Heteroaromatics by Merging Photoredox Catalysis with Proton Reduction Catalysis

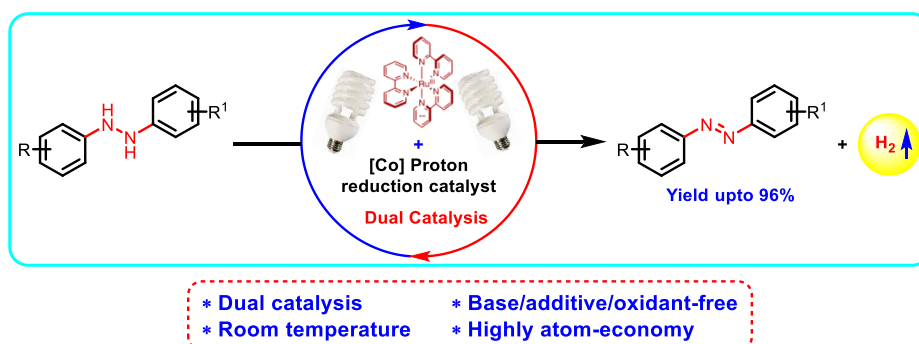
Acceptorless dehydrogenation (ADH) is one of the most important key reactions in catalysis, and proceeds without need of any external oxidants produces less or no waste. These reactions are highly atom economic and environmental benign compared to the oxidative dehydrogenation methods. Here we have explored an ADH reaction strategy for access of *N*-heteroaromatics from their partially saturated counterparts. This ADH reaction was achieved by merging of $[\text{Ru}(\text{bpy})_3]^{2+}$ and Co-oxime based proton reduction catalyst in water using blue light from the LED source. This reaction is additive/base/oxidant-free, proceeds under mild conditions and shows good functional group compatibility as well as broad substrate scope.



Scheme 2. Visible-light photoredox catalyzed acceptorless dehydrogenation of *N*-heterocycles.

Chapter IV: Room Temperature Visible-light Photocatalyzed Acceptorless Dehydrogenation of Diaryl hydrazines

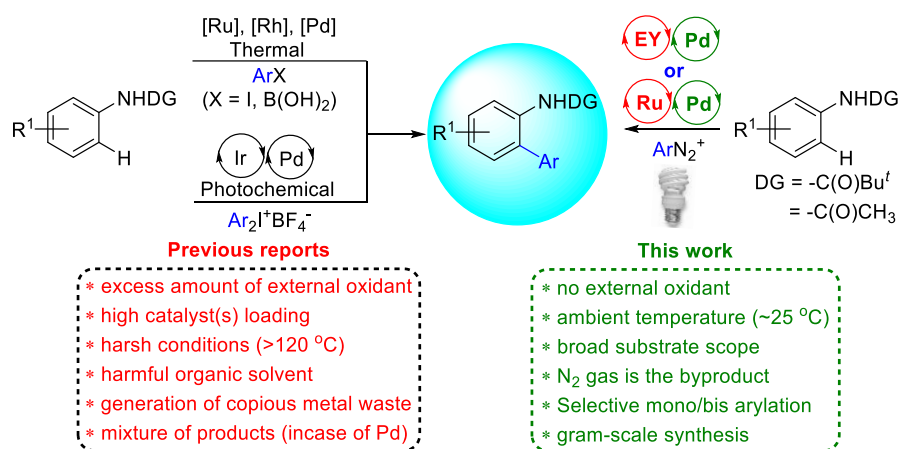
Aromatic azo compounds show profound application as food additives, in dye-pigment industry, as bioactive ligands and therapeutic agents, polymers, photo-responsive soft materials, switches and chemosensors, crystals, and as radical initiators. Herein we report an ADH of hydrazobenzene derivatives using dual catalysis by merging $[\text{Ru}(\text{bpy})_3]^{2+}$ and $\text{Co}(\text{dmgH})_2\text{PyCl}$ catalysis. This additive/oxidant-free reaction takes place at room temperature under very mild eco-benign conditions and is sustainable.



Scheme 3. Visible-light photoredox catalyzed acceptorless dehydrogenation of hydrazobenzene.

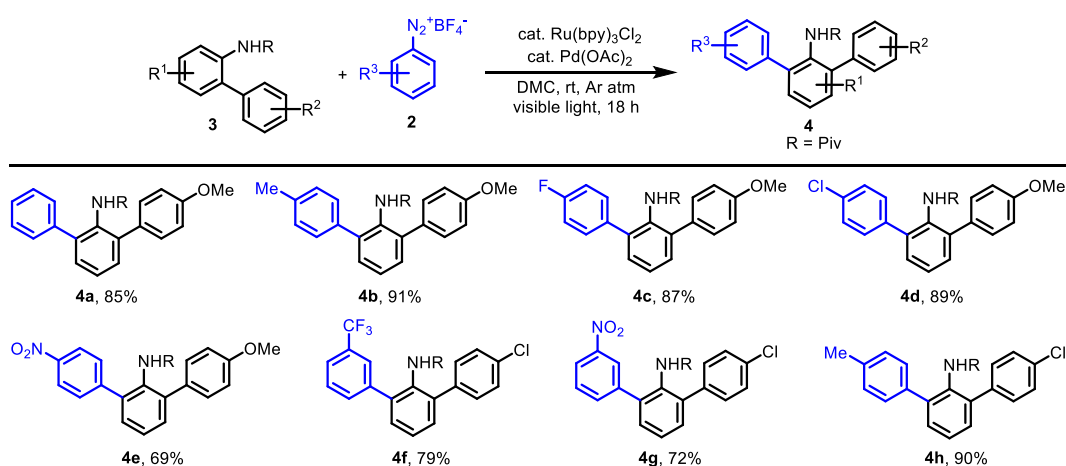
Chapter V: Dual Catalyzed C-H Arylation of Anilides under External Oxidant-Free Conditions by Merging Photoredox Catalysis with Palladium Catalysis

The *ortho*-arylaniline scaffold show numerous applications in pharmaceuticals, material sciences, organometallic catalysis and in synthesizing diverse *N*-heterocyclics. Herein, for the first time, we report a visible-light mediated metal/metal-free photoredox catalyzed tandem with palladium catalytic direct C-H bond arylation of anilides using aryldiazonium salts as arylating agent under mild, ambient and external oxidant/additive/base-free conditions. Under a controlled and modified reaction conditions, this reaction selectively produces mono or 2,6-bisarylated product varying from moderate to excellent yields.



Scheme 4. Dual visible-light photoredox and palladium-catalyzed C-H arylation of anilides.

Table 1. Selected examples of 2,6-bisarylated product



Details of Publications:

1. **M. K. Sahoo**, G. Jaiswal, J. Rana and E. Balaraman, Organo-Photoredox Catalyzed Oxidative Dehydrogenation of N-Heterocycles, *Chem. Eur. J.*, 2017, **23**, 14167-14172.
2. **M. K. Sahoo**, J. Rana, M. Subaramanian and E. Balaraman, Room-Temperature Direct Arylation of Anilides under External Oxidant-Free Conditions Using CO₂-Derived Dimethyl Carbonate (DMC) as a 'Green' Solvent, *ChemistrySelect*, 2017, **2**, 7565-7569.
3. **M. K. Sahoo**, S. P. Midya, V. G. Landge and E. Balaraman, A unified strategy for silver-, base-, and oxidant-free direct arylation of C–H bonds, *Green Chem.*, 2017, **19**, 2111-2117.
4. Room Temperature Visible-light Photocatalyzed Acceptorless Dehydrogenation of Diaryl hydrazines. (Manuscript Accepted in ACS Catalysis)
5. Dual Catalyzed Acceptorless Dehydrogenation of N-Heterocycles to Heteroaromatics by Merging Photoredox Catalysis with Proton Reduction Catalysis. (Manuscript under revision)

Details of Patents:

1. Phenanthroline based pincer complexes useful as catalysts for the preparation of methanol from carbon dioxide, E. Balaraman, V. G. Landge, S. P. Midya, **M. K. Sahoo** and G. Jaiswal.

International Application No.: PCT/IN2016/050050

- 358/DEL/2015 (IN) and 417/DEL/2015 (IN)
- WO2016128997 (A1)
- US2018021766 (A1)
- EP3256250 (A1)

2. Catalytic hydrogenation process for the synthesis of terminal diols from dialkyl aliphatic esters, E. Balaraman and **M. K. Sahoo**

Application number 131/DEL/2015 dt. 15/01/2015.

3. *Ortho*-substituted unsymmetrical diarylaniline compounds and a process for preparation thereof, E. Balaraman, **Manoj K. Sahoo**, G. Jaiswal and S. P. Borikar.

Indian Pat. Appl. (2017), IN 2015DE02331 A 20170203.

Reference:

1. S. Chen, Q. Wan, A. K. Badu-Tawiah, *Angew. Chem. Int. Ed.* **2016**, *55*, 934.
2. K.-H. He, F.-F. Tan, C.-Z. Zhou, G.-J. Zhou, X.-L. Yang, Y. Li, *Angew. Chem. Int. Ed.* **2017**, *56*, 3080
3. L. Wang, A. Ishida, Y. Hashidoko and M. Hashimoto, *Angew. Chem., Int. Ed.*, 2017, **56**, 870
4. D. Kalyani, K. B. McMurtrey, S. R. Neufeldt, M. S. Sanford, *J. Am. Chem. Soc.* **2011**, *133*, 18566.

Chapter 1

Visible-Light Mediated Photoredox Catalytic Reactions

1.1 Historical Background of Photocatalysis

The term “photocatalysis” is derived from the combination of two words originated from the Greek language. The prefix “photo” is derived from Greek word “phos” means light and “catalysis” derived from Greek word “katalyo” means to break down or decompose. In modern chemistry, the term photocatalysis stands for the acceleration of a chemical reaction by light. Each year our earth is receiving the interminable amount of solar energy in the form of light and heat. This is safe, inexpensive, and abundantly available at all places on earth’s surface. Again, directly or indirectly the sun is the ultimate source of all kind of energy available to earth except geothermal energy and hydrothermal energy. The solar spectrum of the sunlight constitutes 44% of visible-light of the overall irradiation and is a ubiquitous form of energy (Figure 1.1).¹⁻² The main objective in complementary science is to efficiently convert the abundantly available solar energy into useful chemical energy.³ It is greatly believed that if it is possible to harness a fraction solar energy, that is reaching on to the earth’s surface, it can be possible to sustainably fulfill all the energy demand of humanity to live without relying on fossil fuels.⁴ In 1912 Giacomo Ciamician has realized the importance of the use of sunlight, the renewable source of energy in chemical synthesis and reported the first photochemical process in organic synthesis.⁵ His concept of utilizing sunlight for chemical transformation was one of the milestones in chemical science. He also predicted that the future energy demand of humanity is going to be fulfilled by harnessing solar energy. In last 100 years, extensive research has been carried out to fulfill the expeditiously growing energy demand by photocatalytic water splitting, carbon dioxide reduction and in the development of new solar cell photovoltaic materials.⁶⁻⁹ Despite significant progress in these above energy-related fields, until last decade the potential in the utilization of visible-light for photocatalysis remained rarely explored in synthetic organic transformations. As most of the organic molecules do not absorb in the visible-light region, rather they absorb the high-energy ultraviolet (UV) light, thus most of the early discovered organic transformations were based on the utilization of high-energy UV light irradiation. However, the solar emission spectrum has only 3% of UV light in it and most of the UV light has been absorbed by the atmosphere (Figure 1.1).¹⁻
² Again, many organic substrates may not be stable enough under the high-energy UV light irradiation, thus can undergo an uncontrolled radical chain process leading to several side reactions and sometimes decomposition. Also handling of high-energy UV light on

industrial scale chemical production is unsafe and require special reaction setup. In this context, utilization of vast visible-light window of the solar spectrum in organic synthesis is highly desirable and demanding. Since most of the organic molecules do not absorb in the visible-light region, thus for chemical transformation to take place, the use of a photocatalyst is necessary. The photocatalyst will absorb visible-light and can induce redox reactions *via* photo-induced electron transfer which is highly attractive as an efficient solar energy harnessing process.

The Spectrum of Solar Radiation (Earth)

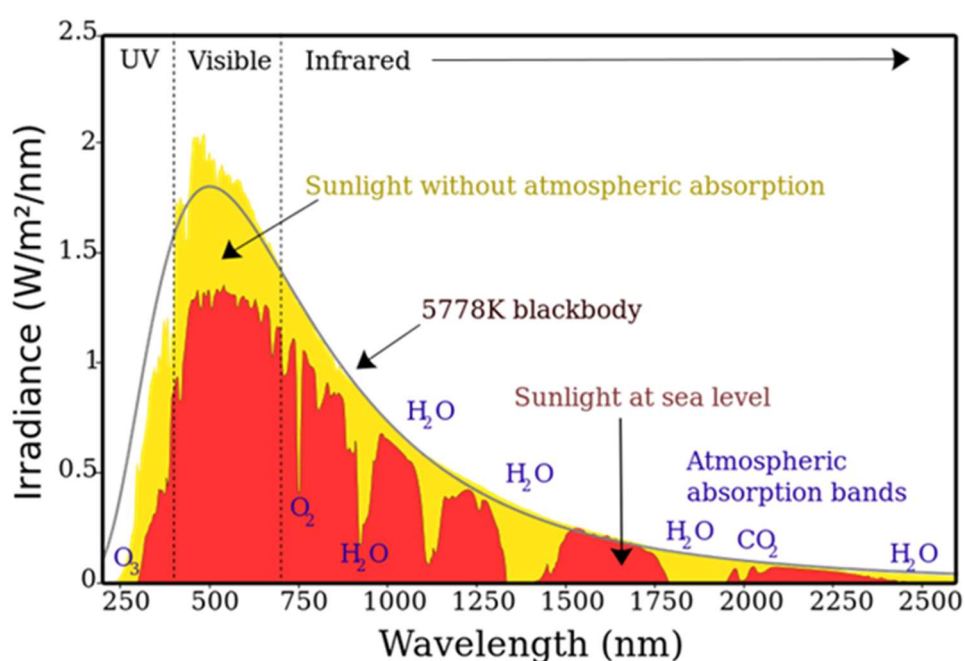


Figure 1.1. Solar emission spectrum received on earth.²

1.1.1 Radicals in Photocatalysis

A photocatalyst upon visible-light irradiation can undergo single electron transfer (SET) with a substrate to generate an odd electron open-shell species in a controlled manner known as radicals. The main advantages of radical intermediates in a chemical reaction is that the radicals are highly reactive and long-lived species. Radical reactions generally take place in salt-free conditions, thus the influence of aggregation and solvation is completely rolled out. Furthermore, the compatibility of the radicals with many functional groups as well as its ability to undergo easy transformations under mild reaction

conditions, have made the free radical reactions a complementary tool to ionic reactions. Traditionally, the reactive radical species were generated by the use of toxic tin reagents, explosive peroxides or azo compounds.¹⁰⁻¹³ However, traditional radical reactions have suffered from a number of limitations which have hampered their routine use in chemical synthesis. First of all, the scale-up of a radical reaction is challenging because these reactions are generally run in dilute media. Although, tributyltin hydride is easily available, extremely versatile and the most effective radical initiator; however, all tin hydrides as well as their byproducts are highly toxic in nature and tend to stick to the products during purification, which consequently eliminates any possibility for industrial use of tin hydrides as radical initiators.¹⁰ Since most of the organic molecules do not absorb in the visible-light region, thus sometimes the high-energy ultraviolet (UV) light is irradiated to generate the reactive radical species. Indeed, free radicals generated using these reagents or upon irradiation of UV light is always problematic. Because it creates several environmental and safety issues as well as the formation of stoichiometric toxic waste. Again, radical reactions initiated *via* traditional method always leads to an uncontrolled radical chain process and hence, give rise to other side reactions as well as copious byproducts. However, under visible-light mediated photoredox catalysis, the light is absorbed only by the photocatalyst and not by the substrate. The photocatalyst upon visible-light irradiation can generate reactive radical species *via* SET in a controlled and continuous manner. Thus, it can overcome the limitations that arise due to radicals generated by the traditional strategies. In the state-of-the-art of catalysis, the photocatalytic reaction with the involvement of SET, a redox process is known as photoredox catalysis. The radical reactions accompanying visible-light photoredox catalysis neither need any toxic radical initiators nor any oxidants/reductants.

1.2. Modern Visible-Light Photoredox Catalysis and Early Work

In general, visible-light photoredox catalysis is the catalytic chemical transformation that uses low-energy visible-light (from 380 nm to 750 nm) to drive the redox reaction which is otherwise energetically disfavoured. In nature, plants use virtually inexhaustible sunlight as the source of energy to make biomass utilizing carbon dioxide and water as key components and allows carbon recycle provided by CO₂, thereby transforming solar

energy into chemical energy. Inspired by such processes, in last decade the scientific community from all over the world are involved in the development of unique, selective and efficient chemical transformations involving redox processes under visible-light irradiation *via* generation of radical species. Recently, visible-light photoredox catalysis has been known and established as one of the most versatile methods to conduct chemical transformations involving reactive radical species under a smooth, continuous and controlled manner. Nowadays, it is also one of the most productive areas in contemporary science. Like, chlorophyll which harvests sunlight responsible for the redox processes involved in photosynthesis, an envisaged chemical transformation also require the involvement of an appropriate photocatalyst which can absorb visible-light for the redox reaction. For that purpose, the photoactive $[\text{Ru}(\text{bpy})_3]^{2+}$ complex was introduced in a catalytic amount. The complex $[\text{Ru}(\text{bpy})_3]\text{Cl}_2$, was discovered by Burstall in 1936,¹⁴ but until last decade it was well known only among the inorganic scientific community as a photoredox catalyst for diverse applications such as photocatalytic water splitting, carbon dioxide reduction to methane, formates etc.⁶⁻⁹ Until recently, however, these complexes had been only sporadically employed as photocatalysts in the area of organic synthesis. The limited exploration of this area is perhaps surprising, as single-electron, radical processes have long been employed in C-C bond construction and often provide access to reactivity that is complementary to that of closed-shell, two electron pathways. After its discovery, the $[\text{Ru}(\text{bpy})_3]^{2+}$ had been sporadically employed as photocatalysts in the area of organic synthesis by the research groups of Kellog,¹⁵ Pac¹⁶ and Deronzier,¹⁷ until recently in 2008 when David MacMillan (Princeton University) merged $[\text{Ru}(\text{bpy})_3]^{2+}$ photoredox catalysis and organocatalysis to develop an asymmetric α -alkylation of aldehydes.¹⁸ Subsequently, researchers from different groups, the Tehshik P. Yoon group (University of Wisconsin, Madison) reported very interesting photocatalytic [2+2] cycloadditions of enones,¹⁹ while the Corey Stephenson group (Boston University) reported photoredox catalyzed dehalogenative cyclization reactions.²⁰

The combined efforts of these three research groups: the research groups of MacMillan, Yoon, and Stephenson independently laid the foundation stone of modern photoredox catalysis in synthetic organic transformations. Their seminal work has helped to initiate a renewed interest in this field, to use photoredox catalysis as a conceptually novel approach in synthetic organic reaction developments. Recently, the field photoredox catalysis has

undergone a significant renaissance and evolved as one of the most emerging fields in catalysis with the development of series of new C-C, C-H, C-N, and C-X bond activation as well as bond formation modes with the development new protocols and synthetic methodologies.²¹⁻²⁴ Nowadays, photoredox catalysis is also the most rapidly expanding area of chemistry with the involvement of different reactive radicals (Figure 1.2). The scientific community has shown immense interest towards visible-light mediated photoredox catalysis. This much-renewed interest among researcher in photoredox catalysis has come due to the unique mode of substrate activation by the photocatalyst in very mild and environmentally benign conditions. The photo-excited photoredox catalyst activates the substrate *via* SET between the photoredox catalyst and the substrate. Under the reaction conditions, a photoredox catalyst can be able to play the role of an oxidant as well as reductant depending on the electron demand which is otherwise difficult or sometimes impossible by other means of chemical catalysis. The energy of a photon absorbed by the photocatalyst is converted back to redox chemical energy and a very low-concentration of reactive radicals is generated *via* photo-induced electron transfer under a controlled and continuous manner. The mild and unique mode of reactive radicals generation *via* photoredox catalysis has been attracting many researchers to quickly embrace and apply this strategy as a surrogate to classical organic transformations.

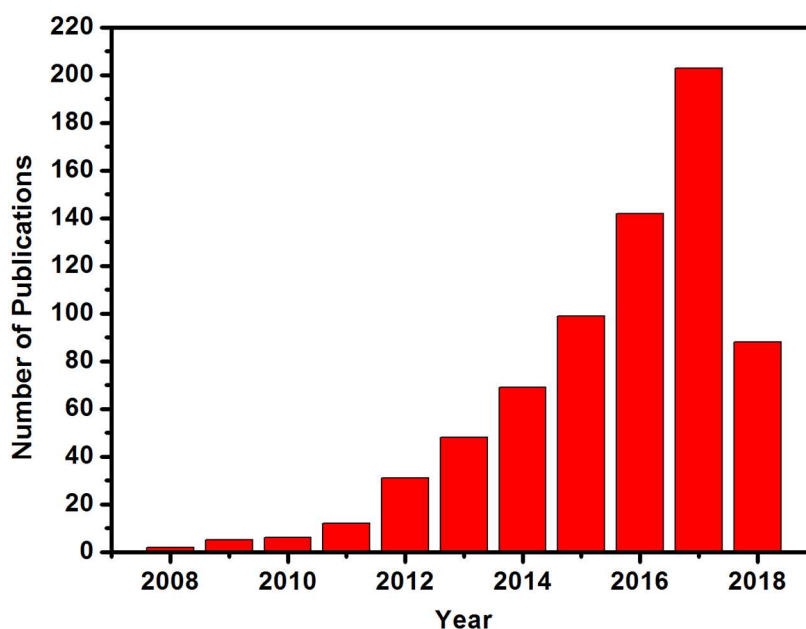


Figure 1.2. Year wise publications on photoredox catalyzed organic transformations (From Web of Science data as on 30th June 2018).

Most of the photoredox catalysts are very poor single-electron oxidants and reductants in their ground state; however, upon visible-light irradiation, these photocatalysts undergo electronic excitation and act as very potent single-electron-transfer reagents. Importantly, the activation of these bench stable, benign catalysts need irradiation from a simple household light bulb to generate redox-active species followed by a chemo-selective trigger to induce unique and valuable catalytic processes. The visible-light mediated photoredox catalysis is capable of achieving unique bond constructions which are may not be possible using established protocols. By employing visible-light photoredox catalysis, it is possible to transiently generate both oxidants and reductants within the same reaction vessel to develop reactions requiring both the electron donation and electron acceptance at different points during the reaction. Thus, photoredox catalysis can be employed to perform overall redox neutral reactions. This approach of generating oxidant or reductant is much superior over the methods requiring stoichiometric chemical oxidants and reductants. Furthermore, during SET process radical ion intermediates are generated whose reactivity pattern is fundamentally different from those of their ground electronic or excited states.²³ Access to these reactive intermediates using other means of activation is often challenging or requires conditions under which their unique reactivity cannot be productively harnessed.

Most of the photoredox catalyzed organic transformations proceed at room temperature under extremely mild and benign conditions without the need of any external reactive radical initiators. Typically a commercial household light bulb is used as the light source in photoredox catalysis, which has significant advantages over the specialized equipment required for processes employing high-energy ultraviolet (UV) light. Additionally, there is a little potential for harmful side reactions that might arise from photoexcitation of the substrate itself. Finally, transition-metal based photoredox catalysts are highly efficient and thus, employed at very low-catalyst loadings, with 1 mole % or even less being typical.

1.3. Mechanisms Underlying Photoredox Catalysis

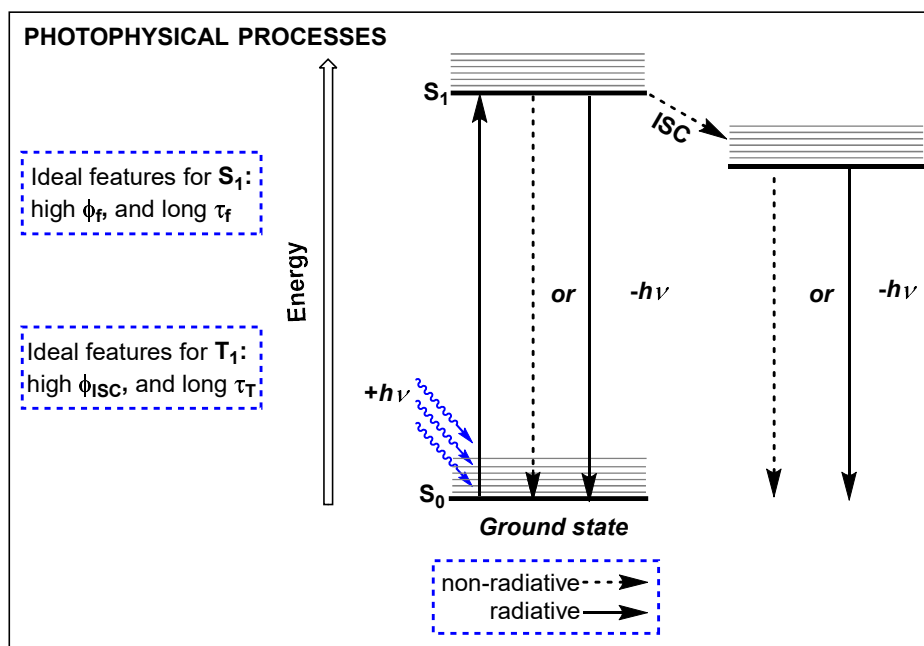
In the process of visible-light mediated photoredox catalysis, the energy of a photon is harnessed by the photocatalyst and is converted to redox chemical energy. Upon visible-light irradiation, the ground state singlet photocatalyst undergoes electronic excitation to

generate highly reactive and short-lived triplet intermediate. This reactive intermediate can act both as a strong oxidant as well as a strong reductant. A reactive radical intermediate is formed by photo-triggered SET between the photoexcited catalyst and the substrate. The SET between the photoredox catalyst and the substrate is beneficial and contributes towards the development of milder reaction conditions as well as energy-efficient transformations. Eventually, the concentration of reactive radical intermediate produced *via* SET at any interval of time will be very less and hence the formation of side product is diminished. The continuous generation of radicals by the photo-triggered SET provides an accelerated reactivity and acts as a driving force for many synthetic organic transformations.

1.3.1. Photophysical Properties of a Photocatalyst

The ground state as well as excited state photophysical and electrochemical properties of a photoredox catalyst are crucial for any organic transformations. Upon visible-light irradiation, the photoredox catalyst undergoes excitation, with the promotion of an electron from its ground state singlet (S_0) to a higher singlet excited state. Within nanosecond, an electron from higher singlet excited state relaxes to the first singlet excited state S_1 . The electron at S_1 state of the photoredox catalyst then may relax to S_0 either by a radiative fluorescence pathway or by a non-radiative process known as internal conversion (IC). The electron at S_1 state can also convert to the first triplet excited state (T_1) by a nonradiative spin-forbidden process known as intersystem crossing (ISC). Similarly, the transition between T_1 to S_0 state is also a spin forbidden process. Hence, T_1 is the longest-lived state and can decay to S_0 by a radiative (known as phosphorescence) or by a non-radiative (IC) pathways. The excited S_1 and T_1 states with lifetime stretching from nanoseconds to the milliseconds are responsible for photoinduced electron transfer between the substrate and the photocatalyst during visible-light mediated chemical reactions.

A good photocatalyst should have properties like high lifetime values for its S_1 and T_1 states. The ideal feature for S_1 state is high quantum yield of fluorescence (ϕ_f) and high fluorescence lifetime (τ_f). Similarly, the ideal feature for T_1 state is high quantum yield of intersystem crossing (ϕ_{ISC}) and high lifetime for triplet states (τ_T).



Scheme 1.1. Photophysical and Electrochemical Processes of Photoredox Catalysts.

1.3.2. Photophysical Properties of $[\text{Ru}(\text{bpy})_3]^{2+}$

The photocatalyst $[\text{Ru}(\text{bpy})_3]^{2+}$ is known for many years for its photochemical properties and its activity in photoredox catalysis. Recently, it has shown surge application in various photoredox catalyzed organic transformations.²¹⁻²⁴ The photophysical properties of $[\text{Ru}(\text{bpy})_3]^{2+}$ based on its UV-Visible spectrum shows three different absorption bands, which corresponds to three different types of electronic transitions: one is ligand centered (LC) electron transfer, the second is metal centered (MC) electron transfer and third the most interesting metal-to-ligand charge-transfer (MLCT), which absorbs in the visible-light region whereas the former transitions occur in the UV region (Figure 1.3). The MLCT transition has a characteristic absorption band at 452 nm and is responsible for the visible-light excitation of the complex $[\text{Ru}(\text{bpy})_3]\text{Cl}_2$, (Scheme 1.1).²⁵ Any tuning to ligand backbone around the Ru-metal center, promote a shift of the MLCT band and hence modification of the photophysical and electrochemical properties of the complex is achievable.

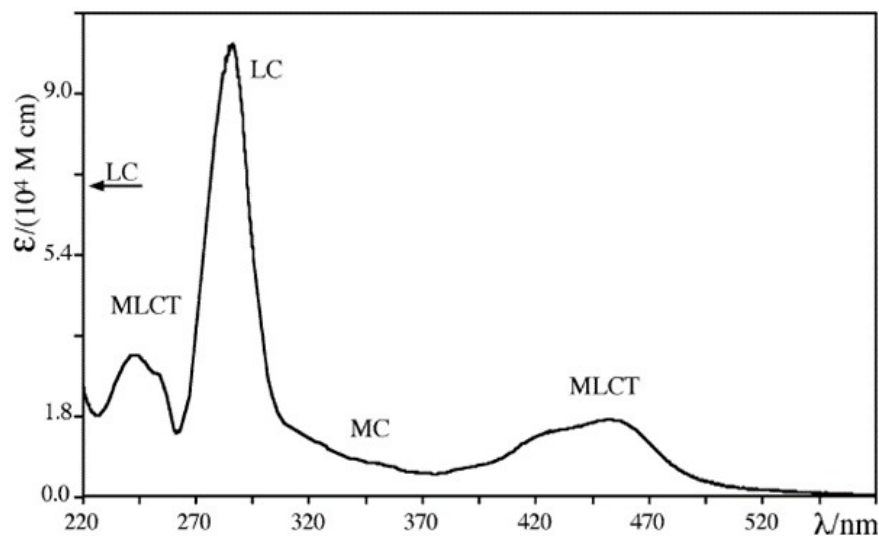
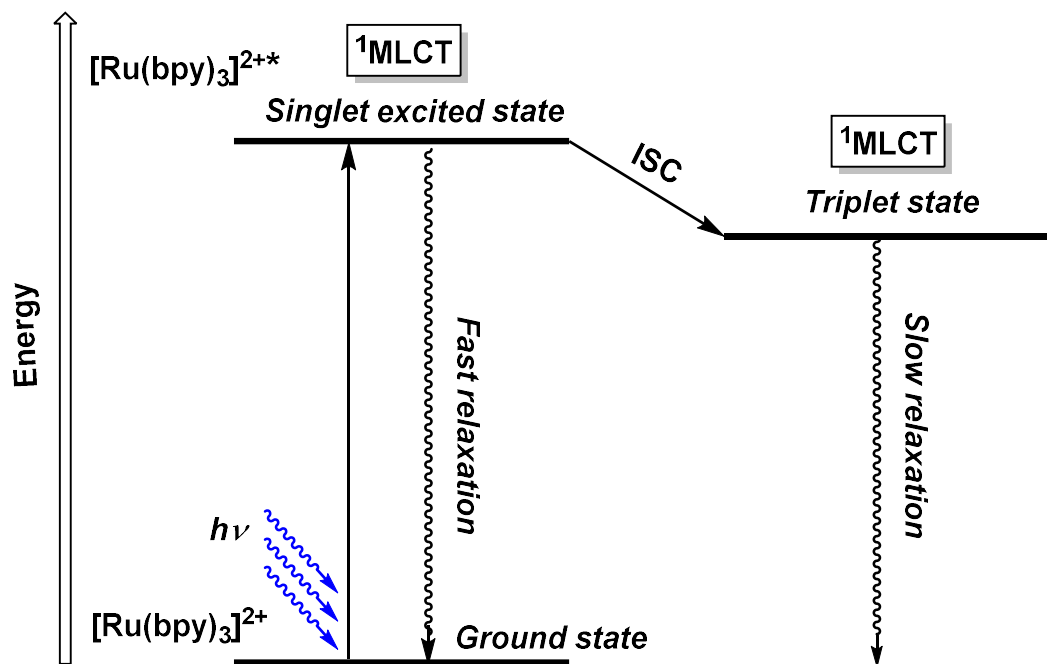


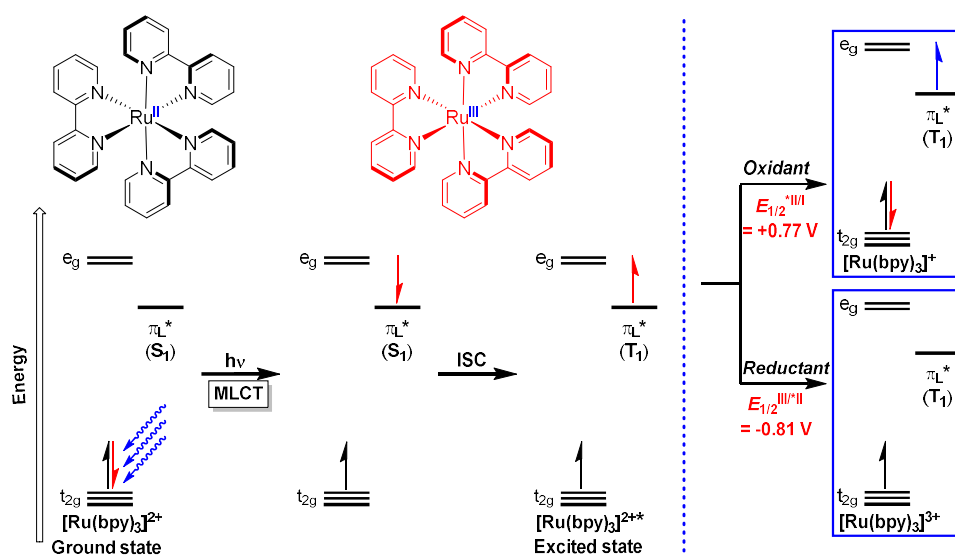
Figure 1.3. The absorption spectrum of $[\text{Ru}(\text{bpy})_3]\text{Cl}_2$ in alcoholic solution.^{25a}

The complex $[\text{Ru}(\text{bpy})_3]^{2+}$ gets activated to $[\text{Ru}(\text{bpy})_3]^{2+*}$ upon irradiation with visible-light ($\lambda_{\text{max}} = 452 \text{ nm}$). After photon absorption the $[\text{Ru}(\text{bpy})_3]^{2+}$ first gets excited to an excited singlet state $^1\text{MLCT}$ which undergoes rapid intersystem crossing (ISC) to a lower in energy excited triplet state $^3\text{MLCT}$ with a relatively long lifetime of 890 ns in acetonitrile and 650 ns in water, long enough to engage in a SET with a substrate through bimolecular reactions.^{24,26} In its triplet excited state $[\text{Ru}(\text{bpy})_3]^{2+}$ acts as an electron donor (energy available = 2.12 eV) (oxidation potential: $[\text{Ru}(\text{bpy})_3]^{3+}/[\text{Ru}(\text{bpy})_3]^{2+*} = -0.86 \text{ V vs SCE in MeCN}$) and as an electron acceptor (reduction potential: $[\text{Ru}(\text{bpy})_3]^{2+*}/[\text{Ru}(\text{bpy})_3]^+ = +0.84 \text{ V vs SCE in MeCN}$). A number of other electronic processes can also deactivate the triplet excited complex. For a controlled and enhanced electron transfer, a cofactor called "quencher" is used along with the photocatalyst. The quencher acts as a rapid electron donor or an acceptor of the electron and is chosen carefully by comparing redox potentials of the photocatalyst and the quencher. Electronic transfer kinetics are important parameters to control and are brought together under the k_q constant that represents the ability of a compound to allow fast electron transfer. To promote an efficient redox process, a rapid electron transfer is necessary to avoid the photocatalyst deactivation in its excited state. A direct consequence of preventing catalyst deactivation is the increase in the catalytic efficiency.²⁵



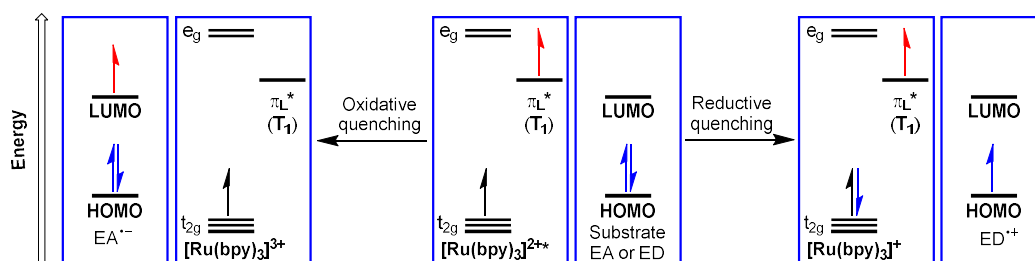
Scheme 1.2. Schematic energy diagram for photoexcitation of $[\text{Ru}(\text{bpy})_3]^{2+}$.

Photoredox catalysts of ruthenium and iridium were extensively used in the photocatalytic organic transformations. Redox properties of tris-chelated Ru(II) complexes of 2,2'-bipyridyl or 1,10-phenanthroline ligands are the most studied complexes because of their excellent photophysical and electrochemical properties. In polypyridyl ruthenium octahedral complexes, Ru^{2+} has a d^6 system. The nitrogen atom of bipyridine ligands coordinates to the metal center through σ donor orbitals localized on the N-atom while the aromatic ring of the ligand possesses both the π donor and π^* acceptor orbitals delocalized over the ring. The HOMO of these Ru(II) complexes is centered on the $d\pi$ orbital of the metal while the LUMO is centered on the π^* orbital of the ligands. Upon visible-light irradiation, an electron from $d\pi$ orbital of Ru(II) is excited to a low-lying π^* orbital of the bipyridyl ligand *via* MLCT (Scheme 1.2). The electron at lowest $^3\text{MLCT}$ has a long half-life, which undergoes SET with other molecules in the solution state even at very low concentration.



Scheme 1.3. Jablonski diagram for visible-light-promoted excitation of $[\text{Ru}(\text{bpy})_3]^{2+}$ ^{21b}

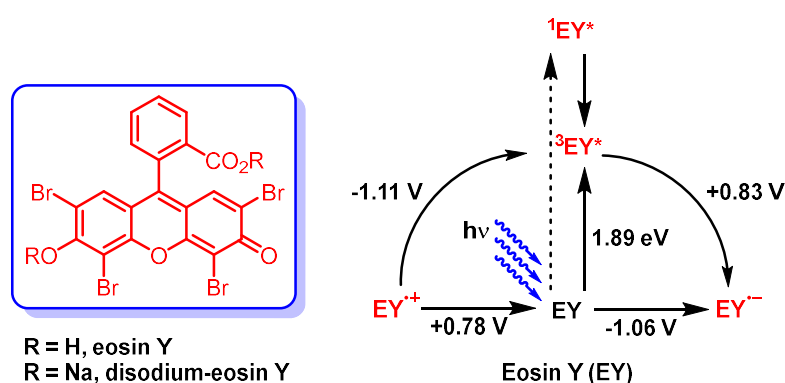
Relative to the ground state Ru(II) species, its excited state species are more reactive which can undergo easy oxidation or reduction, and hence, can serve as either electron donor, or electron acceptor (Scheme 1.3). The photoexcited Ru(II) catalyst takes the advantage of the electron transfer pathway to undergo quenching by donating an electron to an oxidizing agent or by accepting an electron from a reducing agent (Scheme 1.4). These two distinct single electron transfer pathways are term ‘oxidative quenching’ and ‘reductive quenching’. In reductive quenching pathway the quencher reduces the excited state photoredox catalyst to the corresponding low oxidation state species while in oxidative quenching pathway, the quencher oxidizes the excited state photoredox catalyst to the corresponding high oxidation state species.



Scheme 1.4. Jablonski diagram of the oxidative and reductive quenching of $[\text{Ru}(\text{bpy})_3]^{2+*}$. EA = electron acceptor, ED = electron donor.

1.3.3. Photophysical Properties of Eosin Y and Rose Bengal

Like $[\text{Ru}(\text{bpy})_3]^{2+}$, the photochemistry of organic dyes such as eosin Y and rose bengal are also well investigated. The photocatalyst eosin Y absorbs in the green light region with the characteristic absorption peak at 539 nm in the UV-Vis spectrum and has a molar extinction coefficient $\epsilon = 60\,803\text{ M}^{-1}\text{ cm}^{-1}$. Upon visible-light irradiation, eosin Y undergoes singlet excitation followed by rapid intersystem crossing to its lowest energy triplet excited state, having a lifetime of 24 μs .²⁷ At its excited state, eosin Y is more reducing and more oxidizing compared to its ground state. The redox potentials for the excited state of eosin Y can be estimated from its ground state standard redox potentials determined by cyclic voltammetry and the triplet excited state energy. The measured ground state and the estimated excited state oxidation and reduction potentials of eosin Y is given in Scheme 1.5.^{27a, 28}



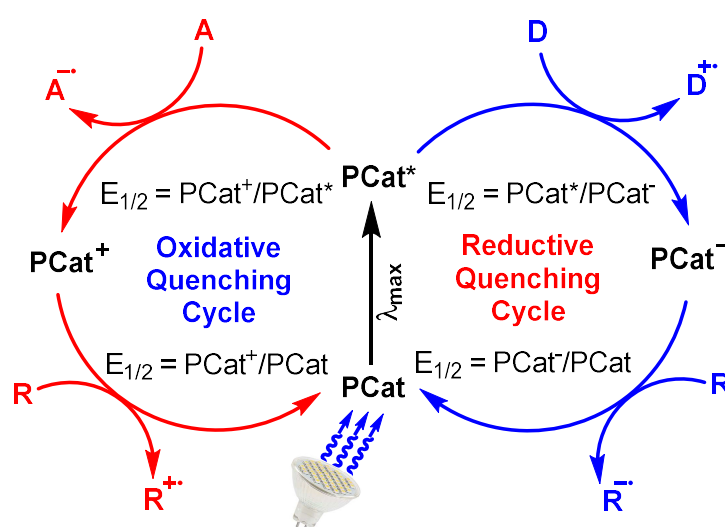
Scheme 1.5. Different forms of eosin Y and redox potentials in MeCN-H₂O (1:1) in the ground and corresponding excited states.

Rose bengal also shows similar photophysical properties like eosin Y. Upon visible-light irradiation rose bengal (RB^{2-}) absorbs the visible-light ($\lambda_{\text{max}} = 550\text{ nm}$) to give a photoexcited singlet state, $\text{RB}^{2-*}(\text{S}_1)$, which undergoes rapid intersystem crossing to its lowest long-lived triplet state $\text{RB}^{2-*}(\text{T}_1)$. This photoexcited $\text{RB}^{2-*}(\text{T}_1)$ acts as a strong oxidant ($E_{1/2}[\text{RB}^{2-*}(\text{T}_1)/\text{RB}^{3-}] = -1.04\text{ V vs SCE}$) and strong reductant.^{21d} Rose bengal is also known as a very good sensitizer for oxygen and generates singlet oxygen.²⁹

1.4. Basic Mechanism of Photoredox Catalysis

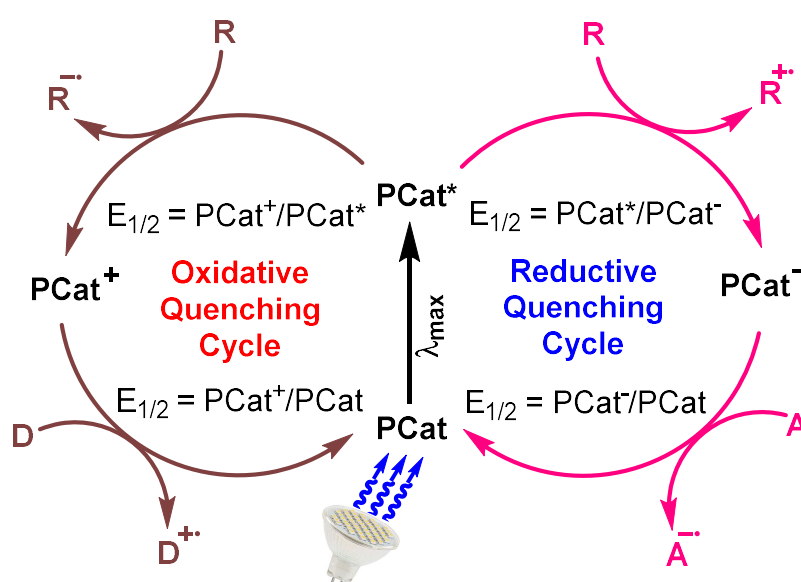
When visible-light of wavelength λ_{\max} is irradiated upon the photocatalyst, the ground state electron jumps to its excited state to give excited **PCat***. At its excited state, the photocatalyst acts as a strong oxidant as well as a strong reductant. Thus two scenarios can happen as explained below.

If a sacrificial electron donor (**D**) with sufficient reduction potential is present in the reaction medium, (Scheme 1.6, right side cycle) the **D** can reduce the excited photocatalyst **PCat*** to generate **PCat⁻**. The process of reduction of the excited photocatalyst is called as reductive quenching and the donor is called as a reductive quencher. Then the reduced photocatalyst transfers an electron to the reactant **R** with concomitant regeneration of ground state photocatalyst **PCat** in the catalytic cycle called as “reductive quenching cycle”. The resulting photocatalytic reduced radical anion **R⁻** undergoes further transformations to give the final product. Similarly, if the reaction has sacrificial electron acceptor (**A**) within it, then the photoexcited catalyst **PCat*** gets oxidized with **A**, to give **PCat⁺**. The substrate **A** acts as oxidative quencher and process of oxidation of excited photocatalyst **PCat*** is known as an oxidative quenching. Further, the **PCat⁺** gets reduced by the reactant **R** (oxidative quenching cycle) with concomitant regeneration of the ground state catalyst **PCat** along with the radical cation **R⁺** which further reacts to give the final product. (Scheme 1.6, left side cycle).

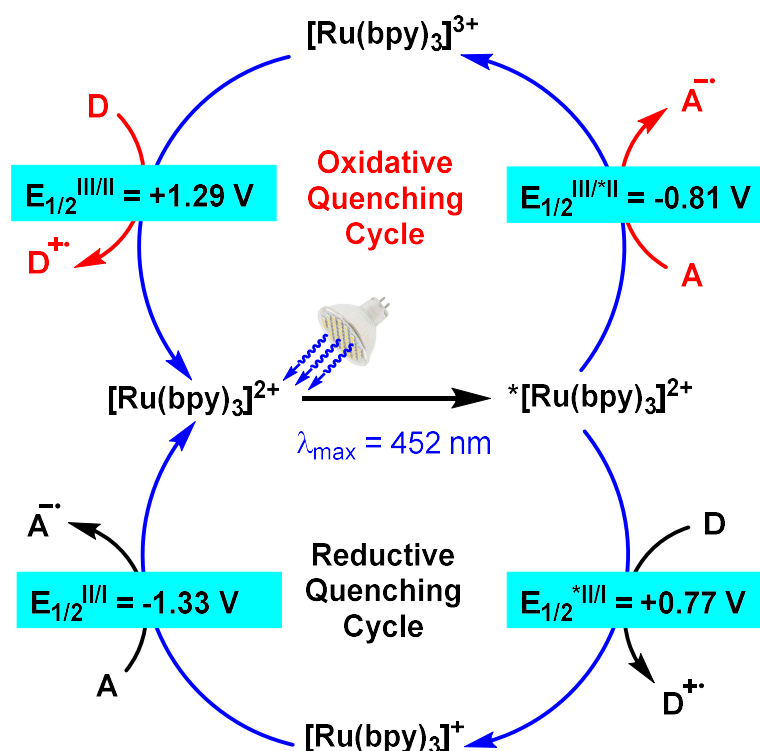


Scheme 1.6. Catalytic cycle in presence of a sacrificial quencher **A** and **D**.

The reactant **R** itself also can act as the quencher. If the **R** acts as reductive quencher by giving an electron to **PCat***, *via* reductive quenching to form **PCat⁻**. The oxidized reactant **R⁺** then participates in radical transformations to give the product. In order to regenerate the catalyst, a sacrificial electron acceptor (**A**) must have to be introduced into the reaction medium (reductive quenching cycle, Scheme 1.7, right side cycle). In an alternative pathway, the activated photocatalyst transfers an electron to the reactant (acts as an oxidative quencher) and generates the oxidized photocatalyst **PCat⁺**. The reduced reactant **R⁻** undergoes radical transformations and the presence of a sacrificial electron donor **D** allows the concomitant regeneration of the photocatalyst **PCat** (oxidative quenching cycle) (Scheme 1.7, left side cycle). The most common oxidative quenchers are polyhalomethanes, dinitro- and dicyanobenzenes, and aryldiazonium salts etc. Similarly, the most common reductive quenchers are tertiary amines.



Scheme 1.7. Catalytic cycle when the reactant itself acts as the quencher.



Scheme 1.8. Oxidative and reductive quenching cycle of $[\text{Ru}(\text{bpy})_3]^{2+}$.

To determine whether a reductive or oxidative quenching cycle is operative in a particular reaction, fluorescence quenching (or Stern-Volmer) studies are commonly employed.³⁰ This technique examines the competition between two deactivation pathways of the photoexcited state: quenching *via* an electron transfer and emission (Figure 1.4).^{21b} In the absence of a quencher, $^*[\text{Ru}(\text{bpy})_3]^{2+}$ undergoes emission, emitting radiation at $\lambda_{\text{max}} = 615 \text{ nm}$ with an inherent intensity.³¹ Increasing concentrations of a quencher, however, additionally deactivate $^*[\text{Ru}(\text{bpy})_3]^{2+}$ *via* electron-transfer pathways and decrease the intensity of the observed emission. This relationship between quencher concentration and emission intensity is given by the Stern-Volmer equation,

$$I_0/I = 1 + k_q\tau_0[\text{Q}],$$

where I_0 and I are the emission intensity in the absence and presence of quencher, respectively, k_q is the quenching rate constant, τ_0 is the excited-state lifetime in the absence of quencher, and $[\text{Q}]$ is the molar concentration of quencher. Plotting the ratio I_0/I against the quencher concentration thus gives a straight line having a y-intercept equal to 1 and a

slope, termed the Stern-Volmer constant (K_{SV}), equal to $k_q\tau_0$. The observation of this relationship between the concentration of a putative quencher and emission intensity constitutes evidence that the molecule engages in single-electron transfer with the photocatalyst. In addition to the electron-transfer pathways described here, the $[\text{Ru}(\text{bpy})_3]^{2+}$ photoexcited state may also engage in energy transfer with organic substrates. It should be noted that energy transfer pathways, like electron-transfer pathways, diminish the emission intensity of the photoexcited species and may be evaluated using the Stern-Volmer analysis.

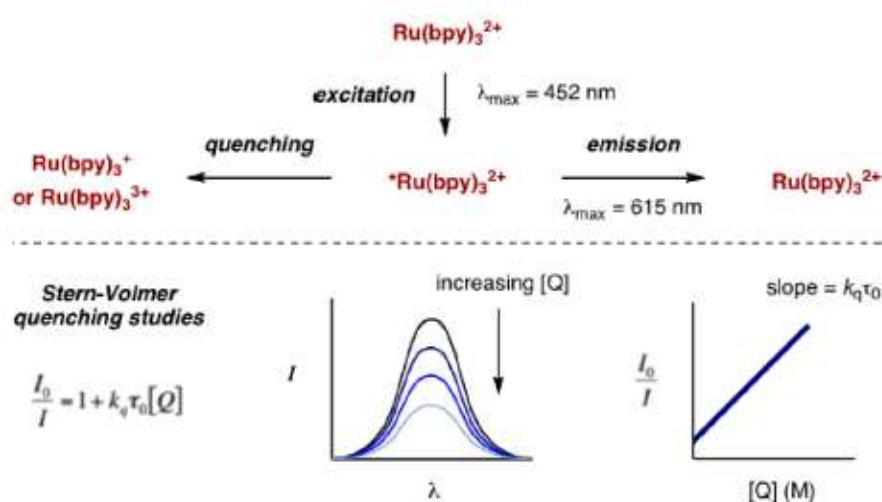


Figure 1.4. Fluorescence quenching Stern-Volmer studies.^{21b}

1.5. Types of Photoredox Catalysts

From time to time there are several types of photoredox catalysts have been reported. All the known photoredox catalysts can be broadly classified into three classes based on the materials they composed off. These are transition-metal complexes, organic dyes, and semiconductors. Similarly, based on the nature of solubility of the material, photoredox catalysts are classified into two categories such homogeneous and heterogeneous photoredox catalysts. Mostly homo- or heteroleptic Ru,²⁵ Ir based polypyridyl complexes³² and few complexes of other transition metals such as copper(I),³³ gold(I)³⁴ and iron(II)³⁵ polypyridine complexes have been used as photoredox catalysts. Below here some commonly used photocatalysts and their redox potential are given. In the early 2000s,

organic photoredox catalysts were dominant but nowadays transition-metal complexes are more commonly used due to high catalytic efficiency.

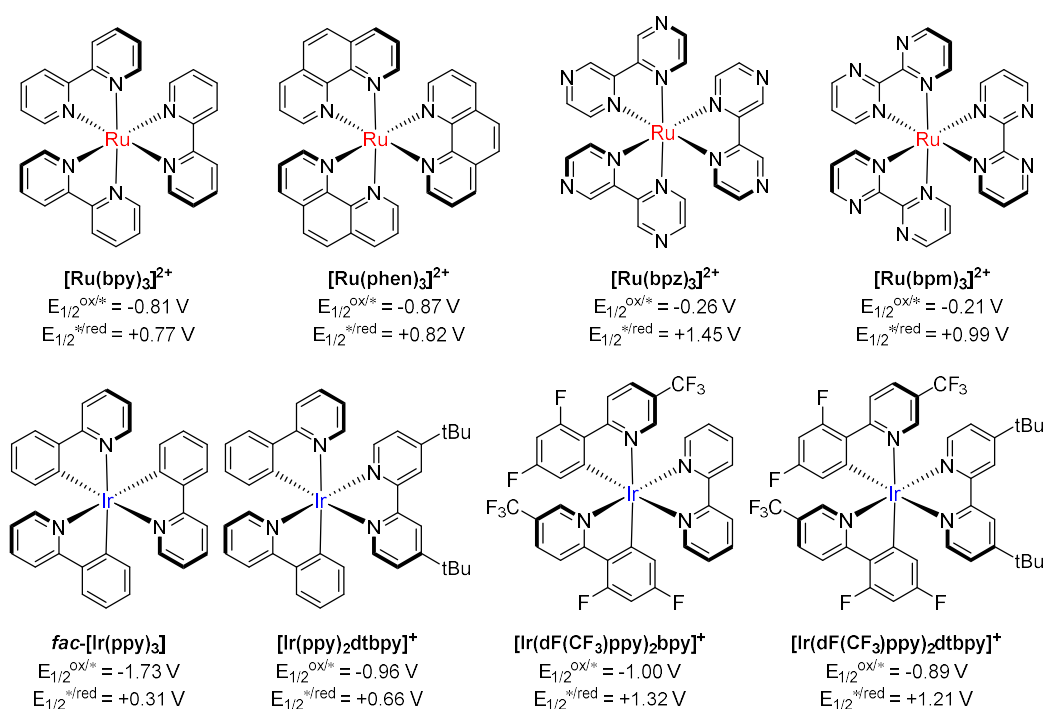


Figure 1.5A. Commonly used transition metal based photoredox catalysts.

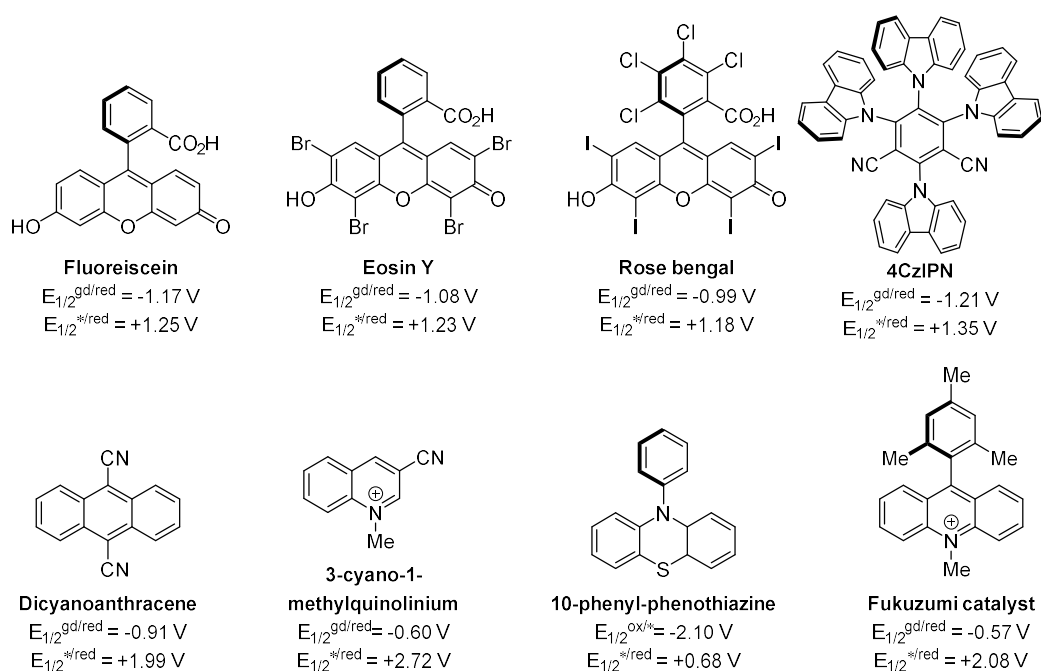


Figure 1.5B. Commonly used organophotoredox catalysts.

1.6. Basic Requirement for Success of a Photoredox Catalytic Reaction

The selection of appropriate photocatalyst plays a very crucial role in the development and success of new photoredox catalytic methods. Appropriate catalysts can be chosen by comparing the redox potentials of the catalyst and the redox potentials needed to oxidize or reduce the desired substrate. After photocatalyst selection, the wavelength of the visible-light source is selected according to the ground state absorption maximum of the selected photocatalyst. If a photocatalyst is new or the absorption data for the photocatalyst is not available, then UV-Visible spectra of the photocatalyst will give information about the wavelength of the visible-light that should be used during the reaction.

The list of commonly used photocatalysts and their redox potentials are presented in Figure 1.5. The most commonly used transition-metal photosensitizers are ruthenium and iridium polypyridyl complexes whereas few other transition-metal complexes were occasionally used as photosensitizer.³⁶ Strong absorbance in visible-light region, long excited state lifetimes and high ISC yields make the Ru and Ir-based photocatalysts the most employed catalysts in synthetic photoredox catalysis. Mostly iridium photocatalysts are used for the production of stronger oxidizing species. This is because iridium is in +III oxidation state with low-spin d^6 configuration and in its higher oxidation state, iridium is capable of accommodating *ortho*-metallated 2-phenylpyridine derived ligands (LX type) to compensate its electron-deficiency.³⁷

The iridium complexes can be heteroleptic without losing their photoactivity. This property of an iridium photocatalyst allows its HOMO and LUMO to separate efficiently in space and thus enables the variation of one potential without affecting the other. This is why by changing the ligand backbone the heteroleptic iridium complexes can be easily tuned to achieve more challenging oxidation and reduction potentials than the homoleptic ruthenium-based polypyridine complexes. As a general rule, strong electron-donating groups on the ligands backbone render the complex to become more strongly reducing, while electron-withdrawing substituent groups cause the complex to become more strongly oxidizing in nature.

Metal-free photocatalysts with a high structural diversity are the rising competitors to commonly used transition metal photocatalysts.^{21d} Although most of these organic photocatalysts possess shorter excited state lifetimes; however, due to their impressive

wide window of redox potential, they have been used in several reactions. There are a few organophotoredox catalysts such as 10-phenyl-phenothiazine are strongly reducing in nature.³⁸ Fluorescein to rose bengal^{24d,27a,39} and the recently developed donor-acceptor scaffolds such as 4CzIPN⁴⁰ offer a well-balanced and large redox window comparable to the commonly used iridium catalysts. The strongly oxidizing 9-mesityl-10-methylacridinium also known as Fukuzumi⁴¹ catalyst is an example of another class of donor-acceptor scaffold which is widely used in photoredox catalysis. The strongest known single-electron-oxidant is probably 3-cyano-1-methylquinolinium⁴² which can be used to perform extremely challenging oxidation reactions.

1.7. Recent Trends in Photoredox Catalysis

1.7.1. Dual Catalysis (Merging Photoredox Catalysis with TM or Organocatalysis)

Under the concept of green chemistry topical interest towards utilization of renewable energy for organic transformations and development of benign and eco-friendly processes has boosted with a renewed interest in visible-light mediated photoredox catalysis. In a sustainable progress, the recent trends of merging photoredox catalysis with another transition-metal catalysis (TM catalysis) or organocatalysis indicates that a cooperative dual catalysis between photoredox catalysis and catalysis from other domains could provide unique reactivity and selectivity. The recently discovered dual catalytic concept by merging two different independent catalyst turns out to be highly promising for performing very exciting sometimes formidable organic transformations. Unlike thermal reactions, visible-light photoredox catalytic reactions occur under extremely mild conditions, and most reactions proceed at room temperature without the need of any external radical initiators, stoichiometric oxidants or reductants. The visible-light irradiation source is typically a low energy commercially available household bulb which does not need any specialized equipment as required for processes employing high-energy ultraviolet (UV) light. The visible-light mediated photoredox catalytic activation of organic substrates is a powerful strategy to generate reactive radical species under very mild conditions. Due to extremely mild reaction conditions, a photoredox catalytic process can be easily combined with other catalytic cycles to develop a dual catalytic system with cooperation between each catalytic cycles. A dual catalytic system by combining

photoredox catalysis with another catalytic cycle such as transition-metal catalysis or organocatalysis can achieve novel and unique reactivity which is otherwise impossible (or) rather difficult to achieve by employing any one of the catalytic systems independently. Recently dual catalysis is a very hot topic in the field of organic chemistry that explores the enormous opportunity provided by combining one area of catalysis with another area to achieve previously unattainable reactions or better the existing reactions. Dual photoredox catalysis generally refers to the merging of a photoredox catalytic cycle with another redox active catalytic cycle but without the involvement of visible-light. Under the dual photoredox catalytic strategy, upon visible-light irradiation, the photoredox catalyst undergoes SET at a given time and allows multi-electron catalysis with the assistance of a second redox catalyst.

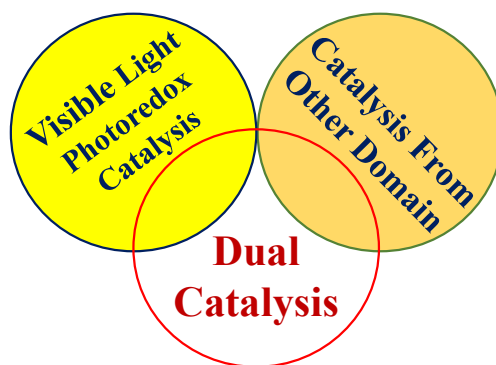


Figure 1.6. Dual catalysis by merging photoredox catalysis and catalysis from other domain.

1.7.2. Taxonomy for Dual Catalysis

The dual catalysis is divided into three types. The first type of catalysis is cooperative photoredox catalysis, wherein both the photoredox catalyst and the other catalyst are directly involved in the same catalytic cycle, working cooperatively with each other to form the product (Figure 1.7a). The second type of catalysis is known as synergistic catalysis wherein both the photoredox catalyst and the other catalyst simultaneously activate two different substrates **A** and **B** in two directly coupled catalytic cycles, leading to the formation of a product (Figure 1.7b). The third one is the sequential catalysis or relay catalysis. In sequential, any one of the two catalysts react with on two different

substrates **A** and **B** to give intermediate **C**. This intermediate again reacts with another independent catalyst to give the final product (**P**) (Figure 1.7c).

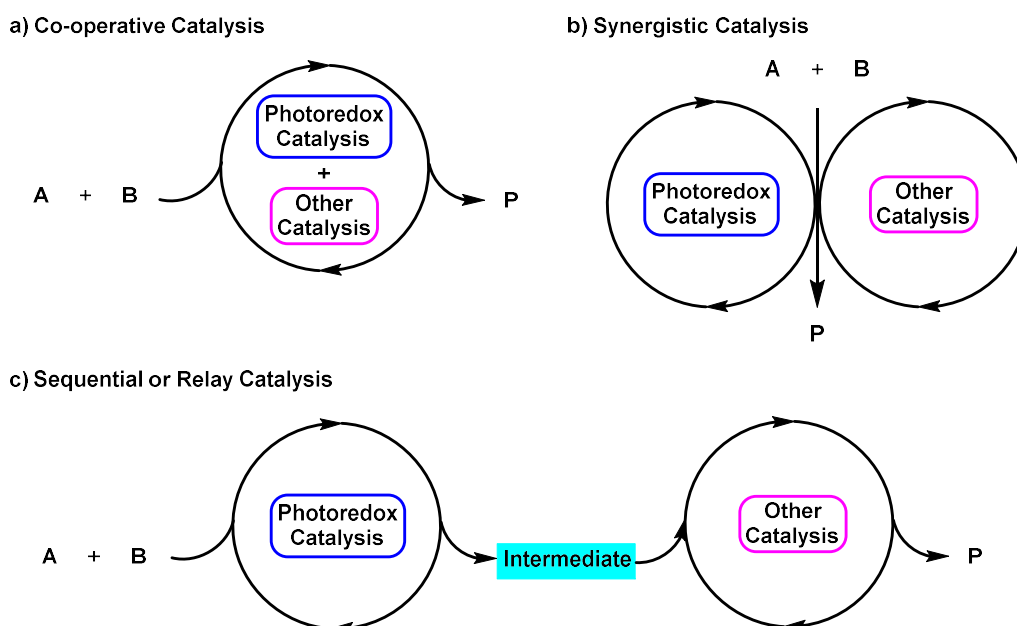


Figure 1.7. (a) The concept of cooperative catalysis. (b) The concept of synergistic catalysis. (c) The concept of sequential or relay catalysis.

1.7.3. Importance and Advantages of Dual Catalytic Approach

While photoredox catalysis and catalysis from other domain individually have their own reactivity and identity in modern organic catalysis. However, the combination of photoredox catalysis and catalysis from other domain such as transition-metal catalysis or organocatalysis is very attractive, as the dual catalysis has many unique advantages such as: (i) Dual catalysis can give rise to new types of reactivity and previously unattainable organic transformations by use of either of the catalytic systems alone. (ii) Dual catalysis can induce or improve the enantioselectivity in the product, where stereochemical control was previously absent or challenging. The combination of photoredox catalysis and catalysis from other domain provides additional possibilities to induce enantioselectivity in a product than the use of a single chiral catalyst. By judicious combinations of a photoredox catalyst and a chiral transition-metal catalyst or a chiral organocatalyst, facile ways for chiral organic transformations can be achieved. Sometimes chiral photoredox catalyst and a chiral catalyst from other domain can be merged where both the chiral

catalysts may control the stereochemistry. A dual catalysis can improve the reaction efficiency and broaden the substrate scope of existing transformations through the cooperative effect of both the catalysts. A dual catalysis by merging photoredox catalysis with catalytic cycles from other domain is attractive in nature and has the following unique advantages:

- (1) A dual catalysis can give rise to the development of new unique reaction as well as reactivities, which was previously impossible to attain by independent use of either of the catalytic systems.
- (2) By combining asymmetric catalysis with photoredox catalysis, it is possible to achieve new challenging enantioselectivity reactions where stereochemical control was previously absent. By selecting appropriate combinations of catalysts for the dual catalysis facile reaction optimization, as well as enantioselective catalysis, may be realized.
- (3) A dual catalysis can significantly improve the catalytic efficiency and can widen the substrate scope of existing transformations through the cooperative effect.

1.7.4. Challenges for Merging Photoredox Catalysis with Catalytic Cycles from Other Domain

Although the combination of photoredox catalysis with a catalytic cycle from another domain can give rise to completely new reactivity and selectivity; however, it is always not straightforward to combine these two catalytic cycles. Despite many advantages, there are several perceived challenges which have to be faced while merging of photoredox catalysis and catalysis from other domain. The most important factor which cannot be overlooked during the development of a dual catalytic cycle is the catalyst compatibility. While combining photoredox catalysis and catalysis from other domain, it should be made sure that the catalysts are compatible with each other, with reactants, additives, intermediates, and solvents throughout the whole reaction sequence. Judicious selection of appropriate catalyst combinations is the key for the development of successful dual catalytic cycle while overcoming the inherent challenges. In addition, strategies like site isolation, phase separation, sequential addition of substrates or catalysts should be applied and adopted during the catalytic transformation. There are many parameters which govern

whether a photoredox catalytic cycle can be merged with other catalytic cycles or not. Few of these points are given below,

- (1). First of all, both the photoredox catalyst and the other catalyst should not react with each other during the reaction.
- (2). Both the photoredox catalyst and the catalyst from other domain should work efficiently under identical reaction conditions.
- (3). Except for photoredox catalyst, the second catalyst should not absorb the visible-light.
- (4.) None of the catalysts should undergo early catalyst deactivation during the reaction.
- (5). The rate of catalytic activity for both photoredox catalyst and the second catalyst should be similar.
- (6). Both photoredox catalyst and the second catalyst should work in co-operation with each other.

1.8. Scope and Objectives of the Thesis Work

This thesis describes the design and development of new visible-light mediated photoredox catalytic methodologies for organic transformations such as dehydrogenation and *ortho*-C-H arylation and related reactions with improved catalytic activity and selectivity. The main objective of the thesis is to develop mild and environmentally benign protocols for organic transformations under visible-light photoredox catalysis sometimes merged with catalytic cycles from other domain such as transition-metal catalysis or organocatalysis.

1.9. Organization of Thesis

The thesis is divided into five chapters. An abstract for each chapter is given below.

Chapter 1: This chapter gives an introduction to visible-light mediated photoredox catalysis, historical background photoredox catalysis, modern photoredox catalysis and the importance of photoredox catalysis. Also, this chapter gives a brief description about

photophysical and photochemical properties of a photocatalyst excitation and mechanism underlying photoredox catalysis such as oxidative quenching and reductive quenching. Towards the end of this chapter merging of photoredox catalysis with catalysis from other domain was described.

Chapter 2: In this chapter, a catalytic oxidative dehydrogenation of *N*-heterocycles by a visible-light organophotoredox catalyst with low catalyst loading (0.1 - 1 mol%) was described. This reaction operates efficiently at room temperature under mild, and in a base- and additive-free conditions with ambient air as the sole oxidant. This reaction has a broad substrate scope and shows excellent functional group compatibility. Also, the utility of this benign approach is demonstrated by the synthesis of various pharmaceutically relevant *N*-heteroarenes such as quinoline, quinoxaline, quinazoline, acridine, and indole.

Chapter 3: Acceptorless dehydrogenation with the extraction of molecular hydrogen under mild conditions from liquid organic hydrogen carriers is highly important and demanding. The third chapter is mainly focused on acceptorless dehydrogenation of partially saturated *N*-heterocycles under a dual visible-light photoredox catalysis merged with proton reduction catalysis. This dual catalytic dehydrogenation reaction operates under mild and benign conditions with the liberation of molecular hydrogen and uses water as the solvent.

Chapter 4: Aromatic azo compounds are privileged structural motifs, as they show myriad pharmaceutical and industrial applications. In this chapter, we have explored a catalytic acceptorless dehydrogenation of diarylhydrazines to access wide variety of aromatic-azo compounds with the removal of H₂ gas as the sole byproduct. This distinctive reactivity has been achieved under dual catalytic conditions by merging [Ru(bpy)₃]²⁺ as the visible-light photoredox catalyst and Co(dmgh)₂(py)Cl as the proton-reduction catalyst. The reaction proceeds smoothly under very mild and benign conditions and operates at room temperature. This dual catalytic approach is highly compatible with various functional groups and has a broad substrate scope. Also, a reversible hydrogen storage and release phenomenon on hydrazobenzene/azobenzene couple has been demonstrated to show the utility of these compounds as hydrogen storage materials.

Chapter 5: The fifth chapter is mainly focused on *ortho*-C-H arylation of anilides under dual visible-light photoredox catalysis and palladium catalysis. This chapter is further divided into two parts based on the nature of photoredox catalysts, reaction conditions as given below:

Chapter 5A: In this sub-chapter, a dual catalytic approach for room temperature C-H arylation of anilides with aryldiazonium salts have been disclosed. This unified strategy has been achieved by the synergistic combination of visible-light metal-free photoredox and palladium catalysis under silver-, base- and/or additive-free conditions. This redox-neutral method shows a broad substrate scope, good functional group tolerance and excellent regioselectivity.

Chapter 5A: In this sub-chapter, an efficient catalytic protocol for direct mono and bis-*ortho*-C-H bond arylation of anilides under base- and external oxidant-free conditions has disclosed. This reaction proceeds smoothly at room temperature using CO₂-derived dimethyl carbonate (DMC) as a 'green' solvent by merging visible-light active [Ru(bpy)₃]²⁺ catalysis and Pd-catalysis. Later, this strategy has been successfully applied for the gram-scale synthesis of fungicide Boscalid.

Overview of the thesis

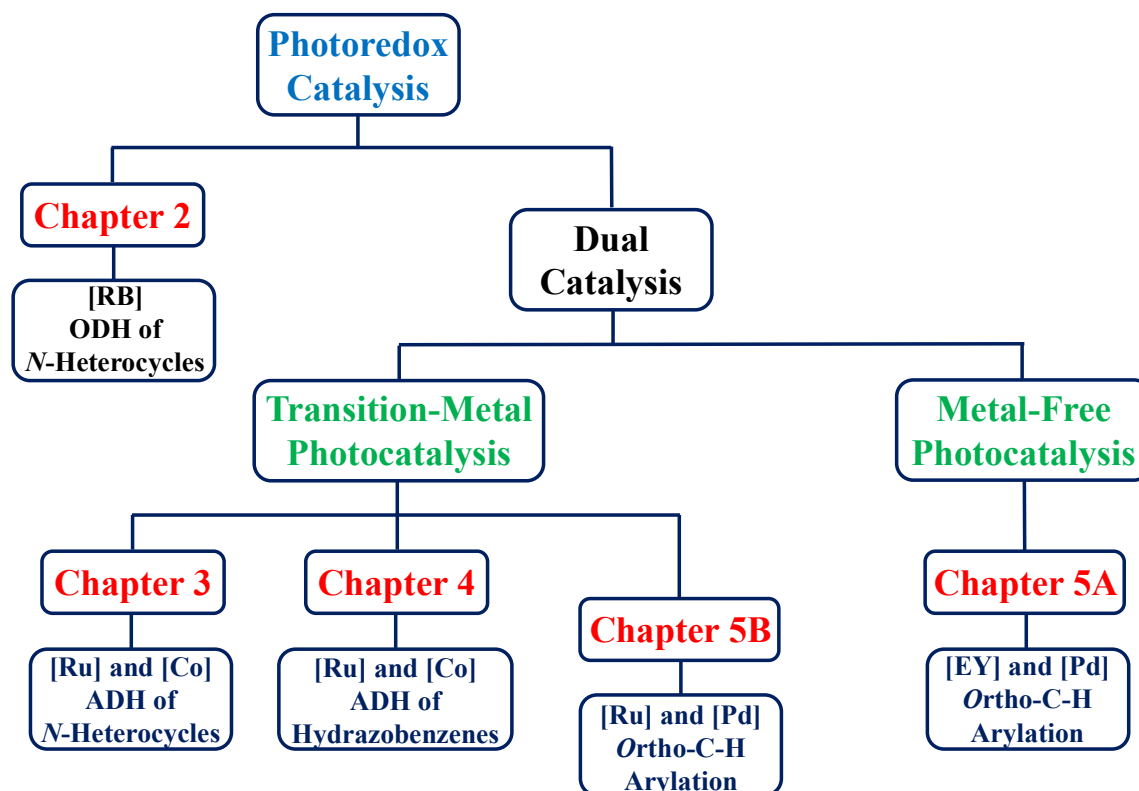


Figure 1.8. Arrangement of working chapters.

1.10. References

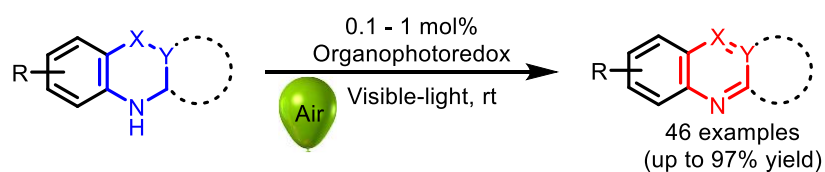
1. Schultz, D. M.; Yoon, T. P. *Science* **2014**, *343*, 985.
2. “Solar_spectrum_en.svg (CC BY-SA 3.0),” can be found under <https://en.wikipedia.org/wiki/Sunlight>, last consulted in January **2018**.
3. Balzani, V.; Credi, A.; Venturi, M. *ChemSusChem* **2008**, *1*, 26-58.
4. Armaroli, N.; Balzani, V. *Angew. Chem., Int. Ed.* **2007**, *46*, 52-66.
5. Ciamician, G. *Science* **1912**, *36*, 385-394.
6. Li, Q.; Guo, B.; Yu, J.; Ran, J.; Zhang, B.; Yan, H.; Gong, J. R. *J. Am. Chem. Soc.* **2011**, *133*, 10878-10884.
7. Ahmad, H.; Kamarudin, S. K.; Minggu, L. J.; Kassim, M. *Renew. Sustain. Energy Rev.* **2015**, *43*, 599-610.
8. Habisreutinger, S. N.; Schmidt-Mende, L.; Stolarczyk, J. K. *Angew. Chem., Int. Ed.* **2013**, *52*, 7372-7408.
9. Albin, A. Photochemistry: Past, Present and Future, *Springer*, Berlin, **2015**.
10. For radical's in organic synthesis, see: (a) Encyclopedia of Radicals in Chemistry, Biology and Materials, Chatgililoglu, C.; Studer, A. Eds. *John Wiley & Sons Ltd. Chichester*, **2012**. (b) Renaud, P.; Sibi, M. P. Radicals in Organic Synthesis, Vol. 1& 2, *Wiley-VCH, Weinheim*, **2001**. (c) Curran, D. P.; Porter, N. A.; Giese, B. Stereochemistry of Radical Reactions, *VCH, Weinheim*, **1996**. (d) Stephenson, C. R. J.; Studer, A.; Curran, D. P. *Beilstein J. Org. Chem.* **2013**, *9*, 2778-2780 and references included.
11. For reviews: (a) Albert, M.; Fensterbank, L.; Lacôte, E.; Malacria, M. *Top. Curr. Chem.* **2006**, *264*, 1. (b) Nicolaou, K. C.; Edmonds, D. J.; Bulger, P. G. *Angew. Chem., Int. Ed.* **2006**, *118*, 7134-7186.
12. For reviews on radical processes, see: (a) Baguley, P. A.; Walton, J. C. *Angew. Chem., Int. Ed.* **1998**, *37*, 3072-3082. (b) Studer, A.; Amrein, S. *Synthesis* **2002**, 835-849. (c) Gilbert, B. C.; Parsons, A. F. *J. Chem. Soc., Perkin Trans 2* **2002**, 367-387.
13. Ollivier, C.; Renaud, P. *Chem. Rev.* **2001**, *101*, 3415-3434.
14. Burstall, F. H. *J. Chem. Soc* **1936**, 173-175.
15. Hedstrand, D. M.; Kruizinga, W. H.; Kellogg, R. M. *Tetrahedron Lett.* **1978**, 1255-1258.
16. Pac, C.; Ihama, M.; Yasuda, M.; Miyauchi, Y.; Sakurai, H. *J. Am. Chem. Soc.* **1981**, *103*, 6495-6497.

-
-
17. Cano-Yelo, H.; Deronzier, A. *Tetrahedron Lett.* **1984**, *25*, 5517-5520.
18. Nicewicz, D.; MacMillan, D. W. C. *Science* **2008**, *322*, 77-80.
19. Ischay, M. A.; Anzovino, M. E.; Du, J.; Yoon, T. P. *J. Am. Chem. Soc.* **2008**, *130*, 12886-12887.
20. Narayanam, J. M. R.; Tucker, J. W.; Stephenson, C. R. J. *J. Am. Chem. Soc.* **2009**, *131*, 8756-8757.
21. For photoredox catalysis in organic synthesis, see: (a) Tucker, J. W.; Stephenson, C. R. J. *J. Org. Chem.* **2012**, *77*, 1617-1622. (b) Prier, C. K.; Rankic, D. A.; MacMillan, D. W. C. *Chem. Rev.* **2013**, *113*, 5322-5363. (c) Shaw, M. H.; Twilton, J.; MacMillan, D. W. C. *J. Org. Chem.* **2016**, *81*, 6898-6926. (d) Romero, N. A.; Nicewicz, D. A. *Chem. Rev.* **2016**, *116*, 10075-10166.
22. Daniel, M.; Fensterbank, L.; Goddard, J.-P.; Ollivier, C. *Org. Chem. Front.* **2014**, *1*, 551-555.
23. Ischay, M. A.; Yoon, T. P. *Eur. J. Org. Chem.* **2012**, 3359-3372.
24. (a) Narayanaman, J. M. R.; Stephenson, C. R. J. *Chem. Soc. Rev.* **2011**, *40*, 102-113. (b) Xuan, J.; Xiao, W.-J. *Angew. Chem., Int. Ed.* **2012**, *51*, 6828-6838. (c) Shi, L.; Xia, W. *Chem. Soc. Rev.* **2012**, *41*, 7687-7697. (d) Hari, D. P.; König, B. *Angew. Chem., Int. Ed.* **2013**, *52*, 4734-4743. (e) Hopkinson, M. N.; Sahoo, B.; Li, J.-L.; Glorius, F. *Chem. Eur. J.* **2014**, *20*, 3874-3886.
25. For reviews on $[\text{Ru}(\text{bpy})_3]^{2+}$ as photoredox catalysts: (a) Campagna, S.; Puntoriero, F.; Nastasi, F.; Bergamini, G.; Balzani, V. *Top. Curr. Chem.* **2007**, *280*, 117-214. (b) Juris, A.; Balzani, V.; Barigelletti, F.; Campagna, S.; Belser, P.; von Zelewsky, A. *Coord. Chem. Rev.* **1988**, *84*, 85. (c) Kalyanasundaram, K. *Coord. Chem. Rev.* **1982**, *46*, 159-244.
26. Montalti, M.; Cedi, A.; Prodi, L.; Gandolfi, M. T. *Handbook of Photochemistry 3rd edition CRC press Taylor & Francis Group*, **2006**, 379.
27. (a) Hari, D. P.; König, B. *Chem. Commun.* **2014**, *50*, 6688-6699. (b) Penzkofer, A.; Beidoun, A.; Daiber, M. *J. Lumin.* **1992**, *51*, 297-314. (c) Penzkofer, A.; Beidoun, A.; Speiser, S. *Chem. Phys.* **1993**, *170*, 139-148.
28. (a) Lazarides, T.; McCormick, T.; Du, P.; Luo, G.; Lindley, B.; Eisenberg, R. *J. Am. Chem. Soc.* **2009**, *131*, 9192-9194. (b) Neumann, M.; Földner, S.; König, B.; Zeitler, K. *Angew. Chem., Int. Ed.* **2011**, *50*, 951-954.
29. (a) Islam, S. D.-M.; Ito, O. *J. Photochem. Photobiol. A: Chemistry* **1999**, *123*, 53-59. (b) Lambert, C. R.; Kochevar, I. E. *J. Am. Chem. Soc.* **1996**, *118*, 3297-3298.
-
-

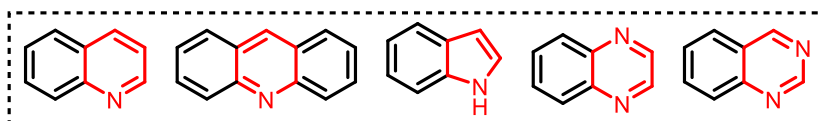
-
-
30. Turro, N. J. *Modern Molecular Photochemistry*; Benjamin/Cummings: Menlo Park, CA, **1978**.
 31. Juris, A.; Balzani, V.; Belser, P.; von Zelewsky, A. *Helv. Chim. Acta* **1981**, *64*, 2175-2182.
 32. Flamigni, L.; Barbieri, A.; Sabatini, C.; Ventura, B.; Barigelletti, F. *Top. Curr. Chem.* **2007**, *281*, 143.
 33. Paria, S.; Reiser, O. *ChemCatChem* **2014**, *6*, 2477-2483.
 34. McTiernan, C. D.; Morin, M.; McCallum, T.; Scaiano, J. C.; Barriault, L. *Catal. Sci. Technol.* **2016**, *6*, 201-207.
 35. Zhang, J.; Campolo, D.; Dumur, F.; Piao, X.; Fouassier, J.-P.; Gigmes, D.; Lalevée, J. *J. Polym. Science, Polym. Chem.* **2016**, *54*, 2247-2253.
 36. Parasram, M.; Gevorgyan, V. *Chem. Soc. Rev.* **2017**, *46*, 6227-6240.
 37. Dixon, I. M.; Collin, J.-P.; Sauvage, J.-P.; Flamigni, L.; Encinas, S.; Barigelletti, F. *Chem. Soc. Rev.* **2000**, *29*, 385-391.
 38. Discekici, E. H.; Treat, N. J.; Poelma, S. O.; Mattson, K. M.; Hudson, Z. M.; Luo, Y.; Hawker, C. J.; de Alaniz, J. R. *Chem. Commun.* **2015**, *51*, 11705-11708.
 39. Nicewicz, D. A.; Nguyen, T. M. *ACS Catal.* **2014**, *4*, 355-360.
 40. Luo, J.; Zhang, J. *ACS Catal.* **2016**, *6*, 873-877.
 41. Fukuzumi, S.; Kotani, H.; Ohkubo, K.; Ogo, S.; Tkachenko, N. V.; Lemmetyinen, H. *J. Am. Chem. Soc.* **2004**, *126*, 1600-1601.
 42. Ohkubo, K.; Kobayashi, T.; Fukuzumi, S. *Angew. Chem., Int. Ed.* **2011**, *50*, 8652-8655.

Chapter 2

Organophotoredox Catalyzed Oxidative Dehydrogenation of *N*-Heterocycles



- * Simple & Efficient
- * Mild, Neutral conditions
- * Additive/Base-free
- * Various *N*-heterocycles & Drug molecules
- * Unified strategy
- * Room temperature
- * Low catalyst loading



Sahoo *et al.*; *Chem. Eur. J.* **2017**, *23*, 14167-14172.

2.1. Introduction

Nitrogen-containing aromatic motifs have been highlighted as important scaffolds as they show profound applications in numerous biologically active natural products, synthetic pharmaceuticals, and in material science (Figure 2.1).¹ Given their importance, the development of efficient strategies for the synthesis of *N*-heteroarenes is a central research area in contemporary science. The site-selective introduction of a new substituent/functional group on *N*-heteroarenes is a grand challenge. It requires multi-step tedious functionalization, and in many cases, it is difficult to install by applying established traditional methods. In recent times, oxidative dehydrogenation of (partially) saturated cyclic compounds have been explored as a complementary route to prepare these substituted *N*-heteroarenes.² However, classical approaches use the super-stoichiometric amount of strong oxidants like DDQ, sulfur, and metal oxides to access *N*-aromatics, and thus produce a large excess of hazardous waste equivalent to the oxidants.³ An alternative to these strong and toxic oxidants is to use air or oxygen, a mild, non-toxic oxidant which produces water as the sole by-product that is superior and highly desirable.

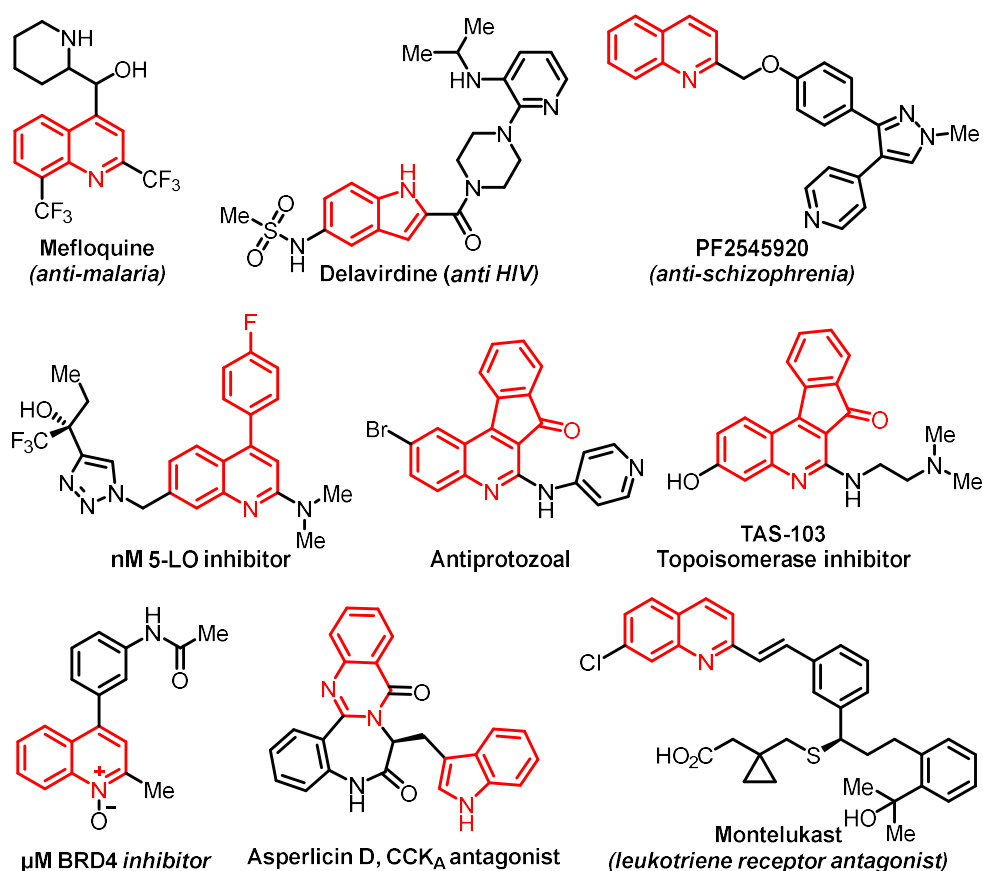
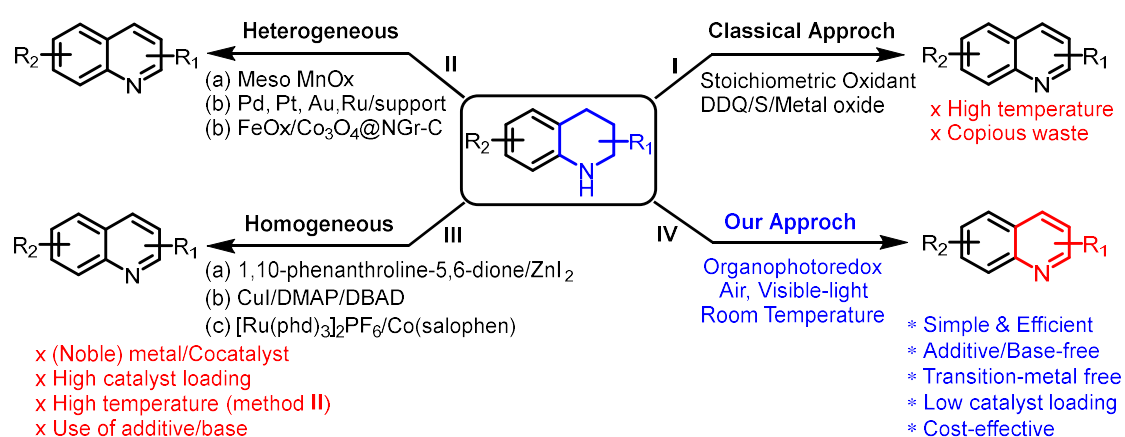


Figure 2.1. The pharmaceutical importance of *N*-heteroaromatics.

Catalytic oxidative dehydrogenation (ODH) is one of the most important strategies in the manufacturing of commodity chemicals.⁴⁻⁷ The ODH reactions based on heterogeneous catalytic systems such as Pt-NW, Pd₃Pb, Ru/TiO₂, Ru/Co₃O₄, Ru/Al₂O₃, and AuNPs/C have been documented.⁸ However, most of these catalytic systems are based on precious metals, require harsh reaction conditions and showed less functional group tolerance. In 2014, Stahl and co-workers reported room temperature aerobic oxidation of diverse 1,2,3,4- tetrahydroquinolines (THQs) by using a homogeneous 1,10-phenanthroline-5,6-dione/ZnI₂^{2c} and the Ru/Co catalyst system.^{2d} Recently, the research group of Beller and Stahl independently reported the oxidative dehydrogenation of THQs and other important *N*-heterocycles using a heterogeneous iron oxide (FeO_x@NGr-C) and cobalt oxide (Co₃O₄-NGr/C) based catalytic system supported on nitrogen-doped carbon respectively.^{2e-2f} A limitation is that the reaction conditions were relatively forcing, e.g. higher temperature (>100 °C), and the use of base and/or additives. Of late, Kim and co-workers have reported the CuI/DBAD based dual catalytic system for the dehydrogenation of THQs under aerobic conditions.^{2j} Despite significant advances have been made using traditional transition-metal catalysis removal of heavy metallic impurities from the final products hinders their practical applicability. Thus, ODH reaction by transition-metal free catalysts are highly desirable and not disclosed prior to our report. In the present chapter, the first report of catalytic oxidative dehydrogenation of diverse *N*-heterocycles by a visible-light⁹ transition-metal free organophotoredox catalyst is reported. The reaction proceeds efficiently under base-free and additive-free conditions with ambient air as the source of O₂ at room temperature (Scheme 2.1).



Scheme 2.1. A general overview of oxidative dehydrogenation of THQs to quinolines.

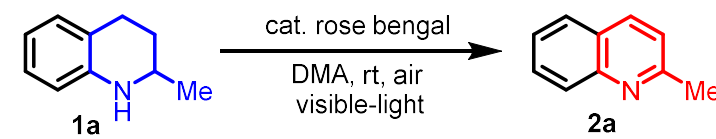
2.2. Statement of the Problem

Various groups have made significant contributions for the synthesis of *N*-heteroaromatics. However, there is no report for the synthesis of these valuable scaffolds under visible-light mediated organophotoredox catalytic oxidative dehydrogenation conditions. The literature precedents have several limitations such as harsh reaction condition, high catalyst loading, use of stoichiometric harmful oxidants or additives *etc.* In this chapter, a photoredox catalytic oxidative dehydrogenation of partially saturated *N*-heterocycles to *N*-heteroaromatics using commercially available rose bengal as photocatalyst and air as the oxidant is described. This reaction operates under very mild, benign, oxidant/additive-free conditions with wide functional group tolerance.

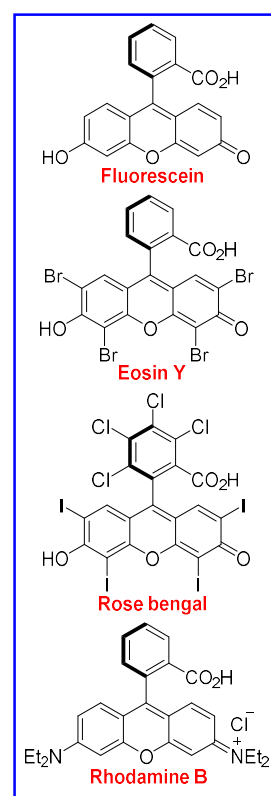
2.3. Reaction Optimization

2.3.1. Optimization Reaction Conditions

We began our catalytic oxidative dehydrogenation of *N*-heterocycles with a screening of various organophotoredox catalysts, solvents and mol% of the catalyst using 2-methyl tetrahydroquinoline (2-MeTHQ) **1a** as a model substrate. After careful investigation, it was observed that irradiation of visible-light upon a catalytic amount of rose bengal (1 mol%) with ambient air as oxidant at room temperature enabled the aromatized 2-methylquinoline **2a** in 91% isolated yield (Table 2.1, entry 1). The necessity of each of the key components (photoredox catalyst, light source, and oxidant) was demonstrated through a series of control experiments. Performing the reaction under dark conditions, in the absence of photoredox catalyst and air did not afford the compound **2a** (Table 2.1, entries 2-4). Various organophotoredox catalysts were examined under identical conditions and among them, rose bengal^{10,11} was found to be an optimal catalyst for this transformation (Table 2.1, entries 1, and 7-9). Gratifyingly, the reaction proceeded readily using 0.1 mol% of the catalyst under identical reaction conditions and gave **2a** in 71% yield (Table 2.1, entry 6). Use of strong oxidants instead of air in the present photocatalytic oxidative dehydrogenation of 2-MeTHQ gave a very poor yield of **2a** (Table 2.1, entries 14-15).

Table 2.1. Optimization of the reaction conditions.^a


Entry	Variation from the initial conditions	Yield of 2a (%)
1	None	99 (91) ^b
2	No light-source	Trace
3	No rose bengal	Trace
4	Under argon atmosphere	Trace
5	No solvent	18
6	0.1 mol % of rose bengal	71 ^b
7	Eosin-Y instead of rose bengal	51
8	Fluorescein instead of rose bengal	23
9	Rhodamine B instead of rose bengal	25
10	MeCN instead of DMA	21
11	DMF instead of DMA	61 ^b
12	MeOH instead of DMA	Trace
13	<i>tert</i> -Butanol instead of DMA	Trace
14 ^c	K ₂ S ₂ O ₈ instead of air	44
15 ^c	Ag ₂ CO ₃ instead of air	19
16	O ₂ balloon	95 ^b



^aReaction conditions: 0.5 mmol of **1a**, 1.0 mol% of photoredox catalyst, and 2 mL of *N,N*-dimethylacetamide (DMA), open-air atm. under visible-light irradiation at room temperature for 24 h, and yields based on GC analysis. ^bIsolated yield. ^c2 equiv. of oxidant.

2.3.2. Effect of Catalyst Loading

The effect of rose bengal was determined by varying the catalyst loading from 0.1 mol% to 2.0 mol% under the standard reaction condition. It was observed that with an increase in catalyst loading the reaction rate increases and gave maximum conversion for 1.0 mol% of the catalyst loading. However, a further increase in photocatalyst loading did not improve the product yield even after 24 h, as shown in Figure 2.2.

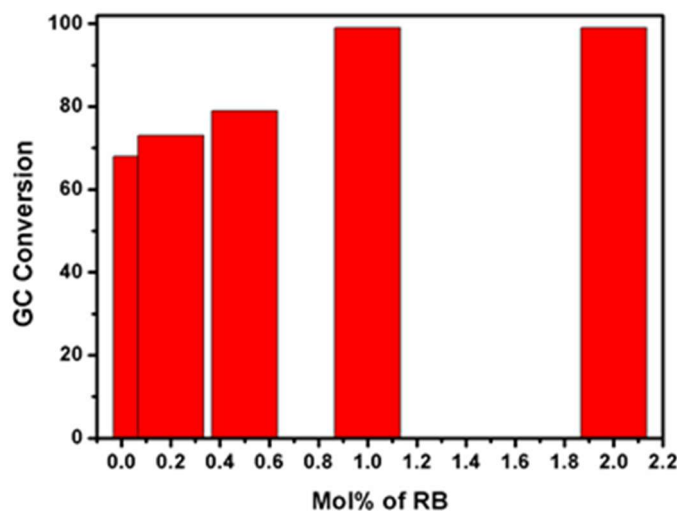
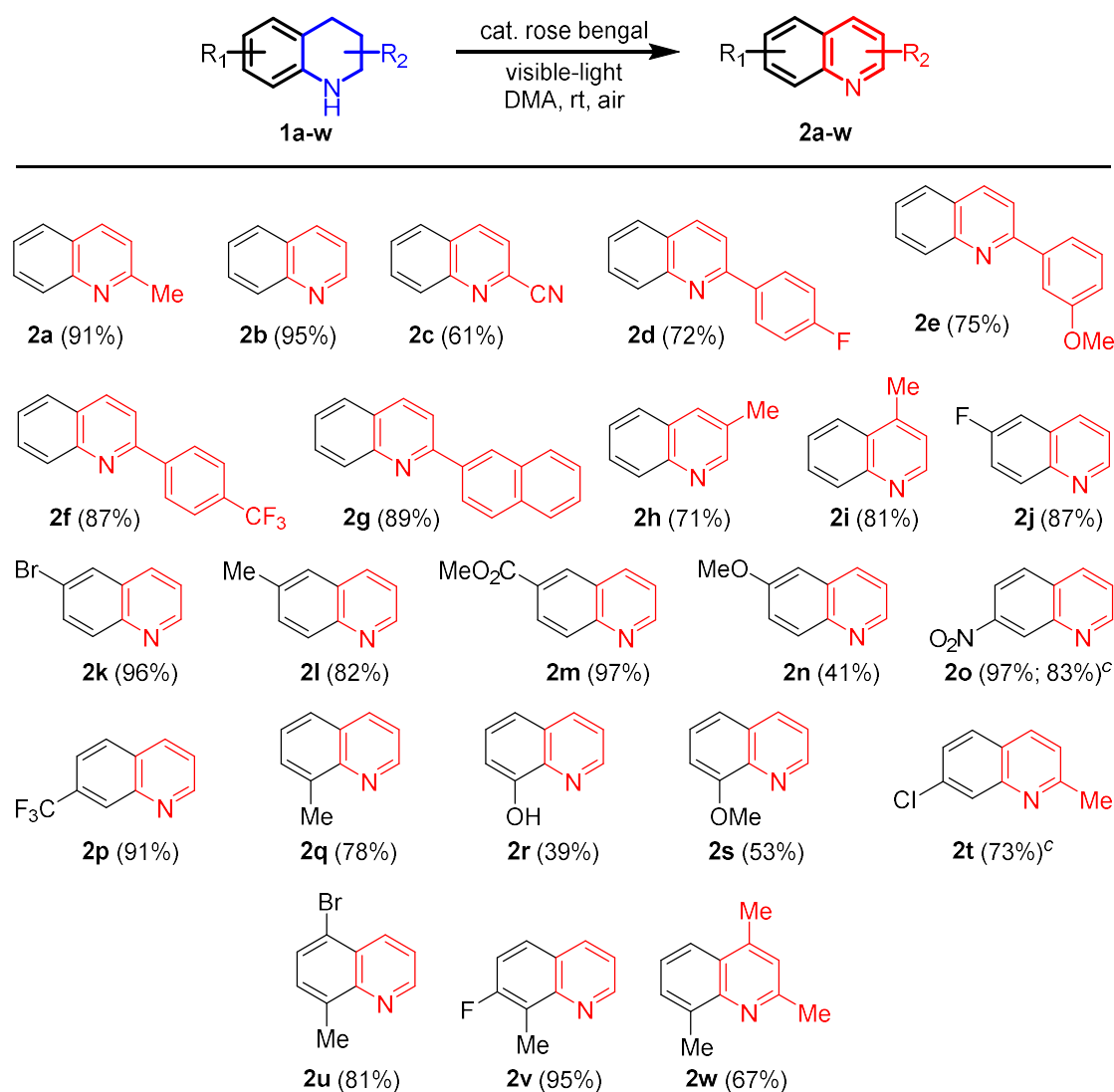


Figure 2.2. Effect of catalyst loading.

2.4. Substrate Scope

2.4.1. Scope of Quinoline Derivatives

With the optimized reaction conditions in hand, the present organophotoredox catalysis was then deployed in the oxidative dehydrogenation (ODH) of diverse (partially) saturated cyclic amines. As shown in Table 2.2, the present ODH strategy is compatible with various substituted THQs containing an electron-rich and electron-deficient group, affording the expected dehydrogenated products in good to excellent yields. The unsubstituted quinoline **2b** was obtained in 95% yield, and substituents at the 2-, 3-, and 4-positions are well tolerated and smoothly underwent dehydrogenation under regular conditions. Interestingly, the photosensitive -CN group is well tolerated and gave the 2-quinoline carbonitrile (**2c**) with 61% isolated yield. The introduction of 2-phenyl, a motif present in pharmaceutically active compounds and 2-(naphtha-2-yl) groups did not influence the reactivities. Thus, 2-aryl substituted THQs, containing -F, -OMe, -CF₃ and 2-naphthyl proceeded efficiently and gave the corresponding dehydrogenated product in excellent yields (**2d** in 72%, **2e** in 75%, **2f** in 87%, and **2g** in 89% yield). The 3-methylquinoline (**2h**) exhibited a moderate yield (71%), while 4-methylquinoline (**2i**) was obtained in 81% isolated yield under optimized conditions. A number of THQs with substitution at 6-, 7-, and 8-positions were also investigated. Indeed, derivatization at these positions is usually accessible *via* selective electrophilic aromatic substitution reactions of THQs. In

Table 2.2. Organophotoredox catalyzed oxidative dehydrogenation of THQs.^{a,b}

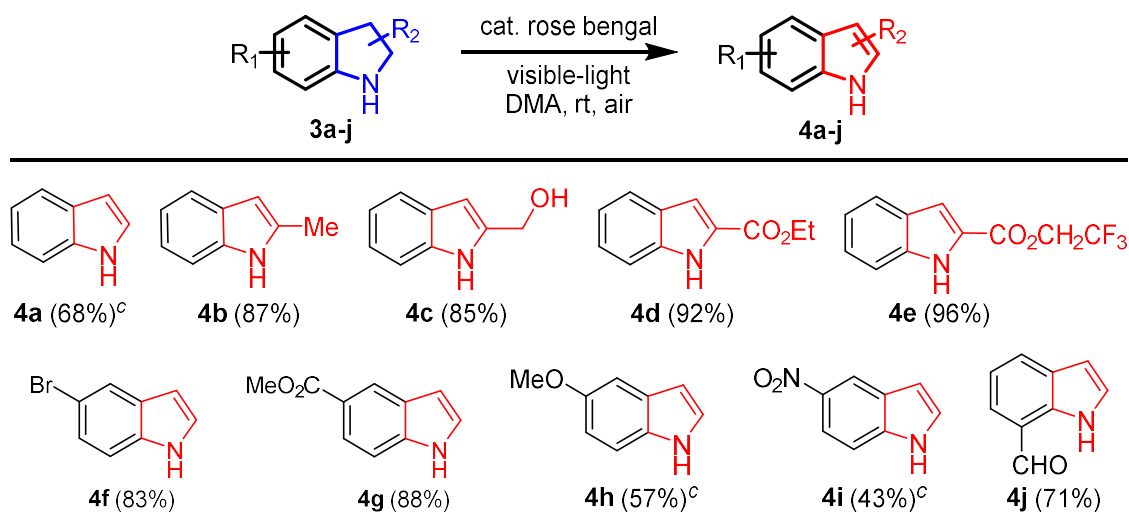
^aReaction conditions: **1** (0.5 mmol), rose bengal (1.0 mol%), DMA (2.0 mL), open-air atm. under visible-light irradiation at room temperature for 24 h. ^bIsolated yields. ^c0.1 mol% of photoredox catalyst for 28 h.

contrast, the reactivity of quinolines in similar reactions is usually unselective, and yielding multiple inseparable products.¹² Under our optimized conditions, 6-substituted quinolines were obtained in high yields (up to 97%). The halo substituents are appealing functional group for late-stage derivatization. Thus, the presence of halogens -F, and -Br at the 6-position led to good yields of dehydrogenated products **2j-2k**. These observations highlight the advantages of the present organophotoredox catalytic system over Pd/C catalysts for oxidative dehydrogenations, as the latter can promote undesired reactivity with aryl halides such as dehalogenation.⁸ Notably, THQ bearing a methoxy substituent

only afforded poor yields (products **2n** in 41%, and **2s** in 53% yield) along with unreacted starting material. Under similar reaction conditions, 7- substituted THQs could also be successfully dehydrogenated. Gratifyingly, products containing more electron-withdrawing groups at 7th-positions such as 7-nitroquinoline (**2o**) and 7-trifluoromethylquinoline (**2p**) were isolated in 97% and 91% yields respectively. However, different groups at 8 position of the aromatic ring (**1q-1s**) do exert a marked influence on the outcome of the reaction and led to the corresponding dehydrogenated products in 39-78% yield. Moreover, THQs bearing multi substituents, such as 2-methyl-7-chloro-THQ (**1t**), 5-bromo-8-methyl-THQ (**1u**), 7-fluoro-4-methyl-THQ (**1v**), and 2,4,8-trimethyl-THQ (**1w**) displayed excellent yields.

2.4.2. Scope of Indole Derivatives

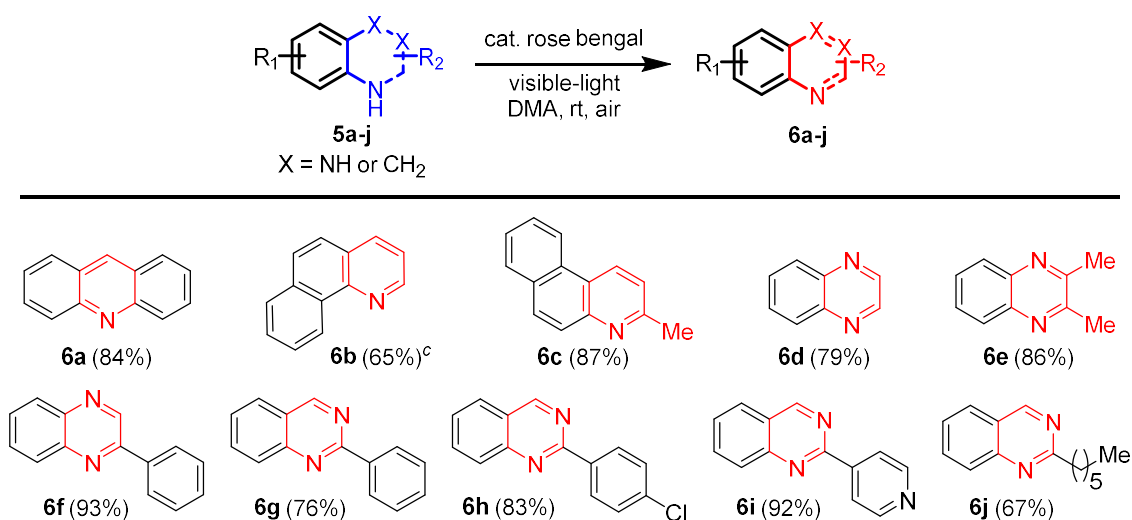
Indoles are another important class of *N*-heteroarenes with interesting bioactivity and are present in pharmaceuticals and natural products. Given that the preparation of indolines is well established,^{1a-b, 13} their metal-free dehydrogenation would provide a direct synthetic route to biologically active indoles. As shown in Table 2.3, the present organophotoredox system displayed excellent activity in the catalytic oxidative dehydrogenation of various indolines to indoles. The readily accessible substrates, indoline **3a**, and 2-methyl indoline **3b** exhibited excellent reactivity under the reaction conditions and afforded the corresponding dehydrogenated products in good yield at room temperature. A variety of 2-substituted indolines were subjected successfully to the present oxidative dehydrogenation and shows that substituent groups had no significant influence on the activity of this catalytic system. Importantly, bromo, ester, methoxy, and nitro-groups were well tolerated under the optimized conditions and yielded the desired products in moderate to good yields. Gratifyingly, an alcoholic group is well tolerated and led to the desired dehydrogenated product **4c** in 85% yield. It is important to note that under classical dehydrogenation conditions using highly reactive DDQ and other reagents, the alcoholic functional group undergoes other side reactions. Importantly, a sensitive aldehyde functional group does not undergo further oxidation, and indole-7-carbaldehyde (**4j**) was isolated in 71% yield.

Table 2.3. Organophotoredox catalyzed oxidative dehydrogenation of indolines.^{a,b}

^aReaction conditions: **3** (0.5 mmol), rose bengal (1.0 mol%), DMA (2.0 mL), open-air atm. under visible-light irradiation at room temperature for 18 h. ^bIsolated yields. ^c0.1 mol% of photoredox catalyst for 24 h.

2.4.3. Substrate Scope for Other *N*-heteroaromatics

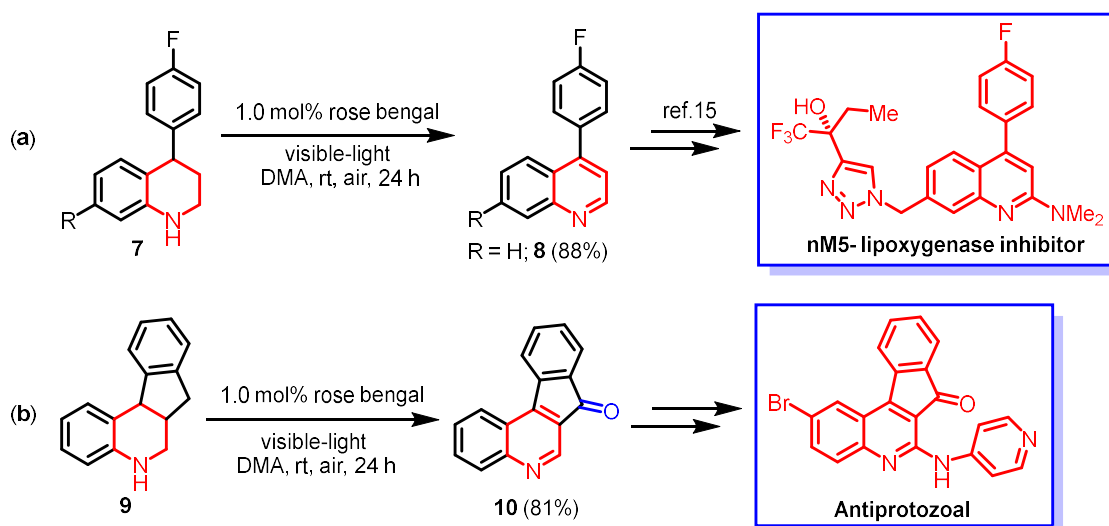
Encouraged by these results, we attempted to apply this transition-metal free oxidative dehydrogenation strategy to other partially saturated *N*-heterocycles. As shown in Table 2.4, acridine (**6a**), benzoquinoline (**6b**), and 3-methylbenzo[f]quinoline (**6c**) generated in 65%-87% yield under our optimized reaction conditions. Quinoxaline derivatives represent a recurring structural motif in antibiotics such as echinomycin.¹⁴ The synthesis of quinoxalines by the present strategy would provide a simple, and robust route to this class of *N*-heteroarenes. Under standard reaction conditions, quinoxaline (**6d**), 2,3-dimethylquinoxaline (**6e**), and 2-phenylquinoxaline (**6f**) were generated in 79%-93% yields. Similarly, 2-substituted 1,2,3,4-tetrahydroquinazoline also gave the corresponding quinazolines (**6g-6h**) in 67%-92% yields.

Table 2.4. Oxidative dehydrogenation of other *N*-heterocycles.^{a,b}

^aReaction conditions: **5** (0.5mmol), rose bengal (1.0 mol%), DMA (2.0 mL), open-air atm. under visible-light irradiation at room temperature for 24 h. ^bIsolated yields. ^c0.1 mol% of photoredox catalyst for 32 h.

2.4.4. Scope for Pharmaceutically Active Intermediates

The unprecedented reactivity of organophotoredox catalyst towards the oxidative dehydrogenation of tetrahydroquinoline derivatives encouraged us to extend its application in the synthesis of pharmaceutically important molecules (Figure 2.1; Scheme 2.2). Thus, dehydrogenation of **7** selectively yielded **8**, a precursor for nM5- lipoxygenase inhibitor.¹⁵ To our delight, the oxidative dehydrogenation of **9** gave **10** in 81% isolated yield, in which along with the principal dehydrogenation of tetrahydroquinoline moiety a benzylic oxidation^{2d} was also observed under our standard reaction conditions. Notably, this reaction provides concise access to the indeno[2,1-c]quinoline substructure present in numerous biologically active compounds, including antiprotozoal agent and phase II topoisomerase inhibitor TAS-103¹⁶ (Figure 2.1).



Scheme 2.2. Synthesis of pharmaceutically relevant molecules.

2.5. Mechanistic Investigation

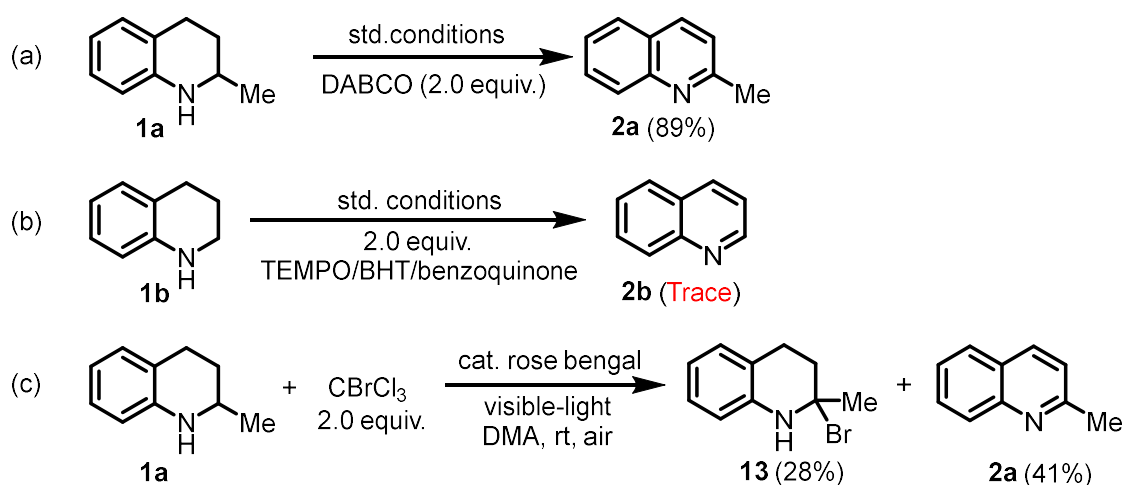
2.5.1. Cyclic Voltammetry Analysis

The redox potential of a compound is very crucial to determine the probable path of the reaction mechanism. We carried out cyclic voltammetry measurement to find out the redox potential of few of partially saturated *N*-heterocycles. The cyclic voltammetry was measured at 10 mV s^{-1} scan rate using Ag/AgCl as reference electrode, a platinum wire as counter electrode and a glassy carbon electrode as working electrode in degassed anhydrous acetonitrile with 0.1 M tetrabutylammonium perchlorate as supporting electrolyte. The oxidation potentials of few compounds were measured which suggests easy oxidation of these compounds by the photocatalyst (For details see Appendix C).

2.5.2. Radical Quenching and Trapping Experiments

To define the possible intermediates and reaction pathway, several control experiments were carried out as shown in Scheme 2.3 and Scheme 2.4. In general, rose bengal (RB) often serves as a photosensitizer to generate the singlet oxygen ($^1\text{O}_2$) from O_2 . In order to find out the generation of $^1\text{O}_2$ and whether it follows oxidative quenching or reductive quenching mechanism in the present reaction, a series of experiments were conducted. Initially, a singlet oxygen quenching experiment was performed under optimized conditions. The reaction was not quenched in the presence of 1,4-diazabicyclo[2.2.2]-

octane (DABCO), which is known as a strong physical quencher of $^1\text{O}_2$.^{11d,17} This result clearly indicated that $^1\text{O}_2$ is not produced in our reaction system and doesn't follow the oxidative quenching mechanism. Next, the ODH reaction of THQs in the presence of 2,2,6,6-tetramethylpiperidine 1-oxyl (TEMPO) free radical, butylated hydroxytoluene (BHT) and benzoquinone was investigated under the optimized reaction conditions. Notably, in presence of a radical scavenger, no quinoline was formed, suggesting that the reaction proceeds with the formation of a radical species, e.g., the superoxide radical anion ($\text{O}_2^{\cdot-}$). It is well-known that BHT suppresses the formation of $\text{O}_2^{\cdot-}$.^{2e,18} Again, when the reaction was carried out in presence of 2.0 equivalents CBrCl_3 , the radical ion intermediate was successfully trapped by CBrCl_3 to give product **13** which was confirmed from GC and GC-MS analysis. Notably, the superoxide anion ($\text{O}_2^{\cdot-}$) generation during visible-light mediated organophotoredox catalysis was confirmed using Nitroblue tetrazolium (NBT) as a selective $\text{O}_2^{\cdot-}$ radical scavenger.¹⁹ Thus, the formation of $\text{O}_2^{\cdot-}$ radical was analyzed by decreasing the absorbance of NBT at 259 nm. As depicted in Figure 2.3, the absorbance of NBT at 259 nm has been significantly decreased with increasing visible-light irradiation time. This observation clearly reveals that the photogenerated $\text{O}_2^{\cdot-}$ radicals react with NBT and thereby decreases the absorbance of NBT. This study strongly supports the effective formation of $\text{O}_2^{\cdot-}$ radicals during the organophotoredox catalyzed oxidative dehydrogenation reaction.



Scheme 2.3. Radical trapping experiments.

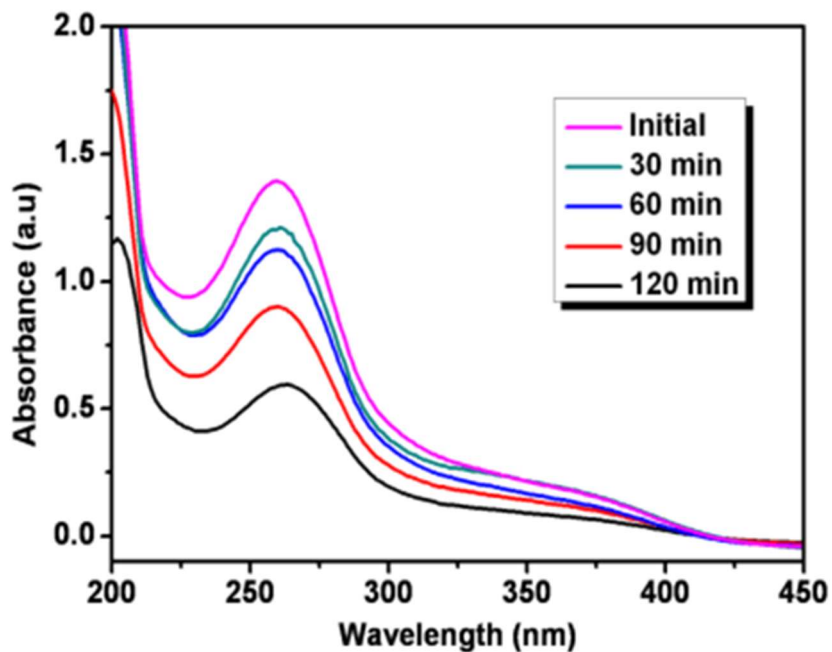


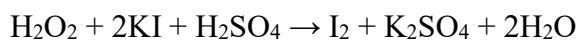
Figure 2.3. Determination of superoxide anion ($O_2^{\cdot-}$) radical.

2.5.3. Experimental Detection of H_2O_2

The formation of H_2O_2 in the reaction mixture was confirmed by a typical iodometric experiment.

Basic Principle of Iodometric Experiment

H_2O_2 oxidizes iodide ion to iodine in the presence of an acid and molybdate catalyst. The liberated iodine can be detected using the starch solution as indicator.



Note: This method is less susceptible to interferences by organic compounds, and is more suitable for measuring mg/L levels of H_2O_2 .

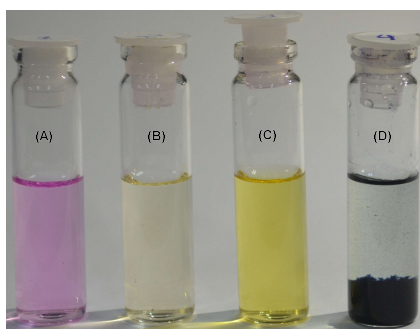
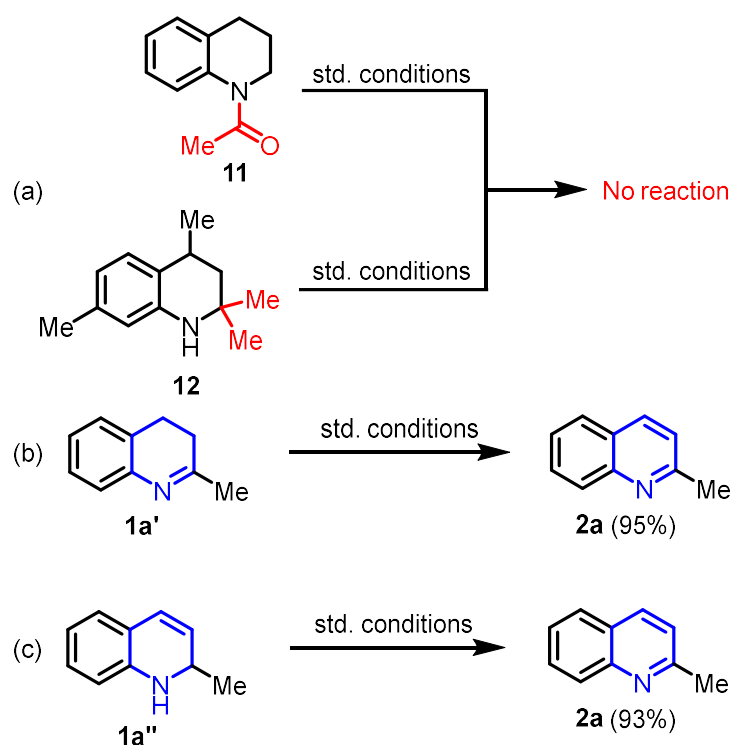


Figure 2.4. Detection of H₂O₂

(A) Reaction mixture; (B) Reaction mixture + dilute H₂SO₄; (C) [Reaction mixture + dilute H₂SO₄] + KI solution; (D) [Reaction mixture + dilute H₂SO₄ + KI solution] + Starch solution.

2.5.4. Control Experiments



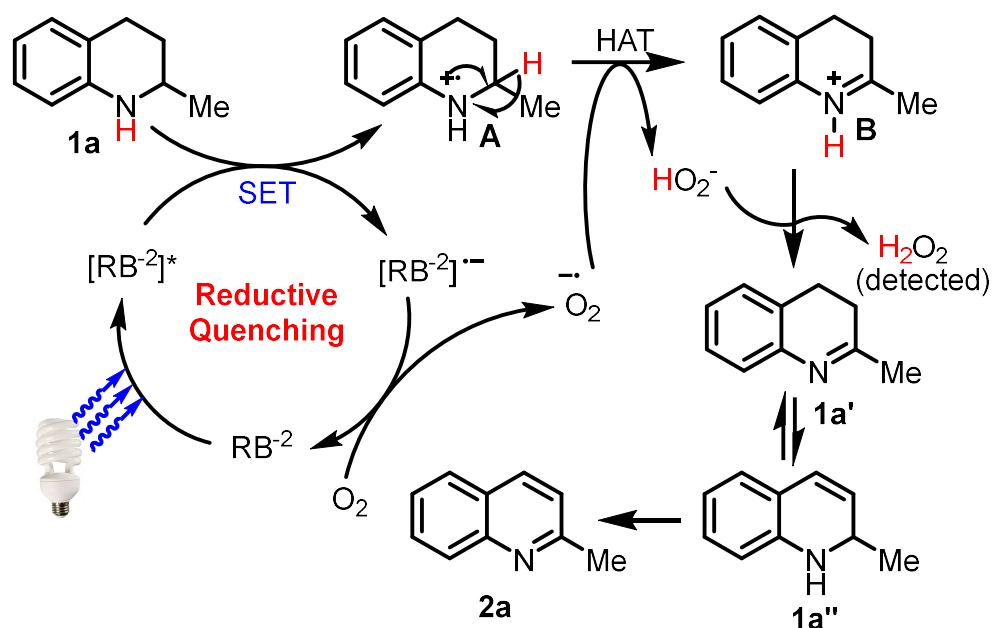
Scheme 2.4. Control experiments.

Notably, no dehydrogenation product was obtained when using 2,2-dimethyl-1,2,3,4-tetrahydroquinoline as substrate. This result signifies that the presence of the N–H motif

in the cycloalkane is critical for the dehydrogenation. Importantly, the dehydrogenation of 1-(3,4-dihydroquinolin-1(2*H*)-yl)ethan-1-one was also not observed, which suggests that the direct formation of a C=C linkage is difficult. Interestingly, ODH of **1a'** and **1a''** were performed and observed that both **1a'** and **1a''** fully dehydrogenated and gave **2a** in excellent yields. Indeed, no isomerization product **1a''** (in case of ODH reaction of **1a'**) was observed under optimized reaction conditions. This result strongly indicates that the isomerization process (**1a'** to **1a''**) is very fast and directly led to product **2a**.

2.5.5. Plausible Mechanism

Based on the above experimental results and known literature,⁹⁻¹¹ we propose a plausible mechanism as shown in Scheme 2.5. Initially, rose bengal (RB²⁻) absorbs the visible-light ($\lambda_{\text{max}} = 550 \text{ nm}$) to give a photoexcited singlet state, RB^{2-*}(S₁), which undergoes rapid intersystem crossing to its lowest long-lived triplet state RB^{2-*}(T₁). This photoexcited RB^{2-*}(T₁) is a strong oxidant ($E_{1/2}[\text{RB}^{2-*}(\text{T}_1)/\text{RB}^{3-}] = -1.04 \text{ V vs SCE}$) and undergoes reductive quenching.^{10d} Thus, the photoexcited rose bengal oxidizes the amine (**1a**; $E^{\text{1a}^+/\text{1a}} = +0.80 \text{ V}$) by single electron transfer (SET) and simultaneously reduces O₂ to O₂^{-•} with the regeneration of RB²⁻.²⁰ Now, the superoxide radical ion (O₂^{-•}) oxidizes the amine radical cation (**A**) to imine (**1a'**) *via* the well-established hydrogen atom transfer (HAT) mechanism with a concomitant generation of H₂O₂.^{2g,7h} Interestingly, the formation of H₂O₂ in the reaction mixture was detected in a typical iodometric experiment (Figure 2.4). The generated H₂O₂ may undergo photocatalytic decomposition under our catalytic condition to lead to water and oxygen (See 2.5.3). Finally, isomerization of **1a'** affords a C=C bonded intermediate (**1a''**) under our conditions and these intermediates are almost energetically equal.²¹ Then, the imine (**1a''**) follows a similar photoredox catalytic cycle through a second dehydrogenation step and led to **2a**. Indeed, indolines may also follow a similar reduction quenching mechanism as discussed in case of THQs (Scheme 2.5). The dehydrogenated imine (3*H*-indole) undergoes isomerization reaction and affords a more stable indole (**4a**) under our photocatalytic conditions. The isomerization of 3*H*-indole to **4a** is mainly due to the formation of the more extended π -conjugated system.



Scheme 2.5. A plausible mechanism for the ODH of tetrahydroquinoline (**1a**).

2.6. Conclusion

In summary, in the first working chapter, an expedient strategy for oxidative dehydrogenation of partially saturated *N*-heterocycles to *N*-hetero-aromatics using a visible-light organophotoredox catalyst is reported. The dehydrogenation reaction occurs in air, at ambient temperature under very mild, base and/or additive-free conditions. The simplicity of the procedure is attractive, which offers wide scope in the synthesis of quinoline, quinoxaline, quinazoline, acridine, and indole derivatives. The mechanistic studies show that the present reaction follows reductive quenching mechanism.

2.7. Experimental Section

2.7.1. General Procedure for Oxidative Dehydrogenation of *N*-heterocycles

In an oven-dried 10 mL reaction tube with a magnetic stirring bar was charged with partially saturated *N*-heterocycles (0.5 mmol), rose bengal (5.1 mg, 1.0 mol %), and 2 mL of anhydrous DMA. The reaction mixture was purged with oxygen for five minutes. Then the reaction tube was placed on a magnetic stirrer with two 32 W household fluorescent

light bulbs kept about 5 cm away from it and irradiated at room temperature with constant stirring. To maintain the temperature a household fan was used. After 24 h, the reaction mixture was diluted with 30 mL of water, and the aqueous layer was extracted with EtOAc (3 x 30 mL). Finally, the combined organic layer was washed with brine (20 mL), dried over Na₂SO₄ and concentrated in *vacuo*. The residue was purified by column chromatography on silica gel with a mixture of EtOAc and petroleum ether to afford the desired *N*-heteroaromatic product.

2.7.2. Determination of Superoxide Anion (O₂^{•-}) Radical

The oxidative dehydrogenation reaction was performed in 25 ppm aqueous NBT solution under standard conditions. The NBT can effectively scavenge the photogenerated O₂^{•-} radicals, and it forms insoluble purple formazan as a precipitate. The O₂^{•-} radicals formation was analyzed by decreasing the absorbance of NBT at 259 nm. As depicted in Figure 2.3, the absorbance of NBT at 259 nm is considerably decreased with increasing irradiation time.

2.7.3. Experimental Procedure for Detection of H₂O₂

The following reagents were prepared for the detection of H₂O₂.

Potassium iodide solution (1% w/v): In a 100 mL Erlenmeyer flask, 1.0 gm of KI was dissolved in 100 mL Milli-Q water, stoppered and stored in a cool place away from light.

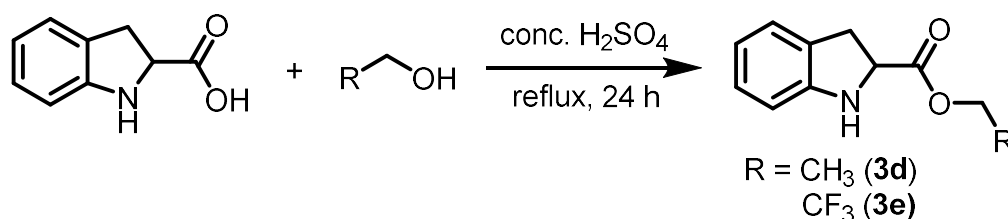
Ammonium molybdate solution: In a 100 mL beaker 4.5 gm of ammonium molybdate was taken. To it 5 mL 6N NH₄OH was added followed by 12.0 gm of NH₄NO₃ and diluted to 50 mL using Milli-Q water.

Sulfuric acid solution: Carefully 3.5M H₂SO₄ solution was prepared by addition of 98% H₂SO₄ to Milli-Q water.

Starch indicator: To 2.5 mL Milli-Q water 250 mg of corn starch was added, shaken well and was poured into a beaker containing 25 mL of boiling Milli-Q water. Boiling continued for further 2 minutes with stirring, cooled down to room temperature, the decanted supernatant was used as an indicator.

Procedure for H₂O₂ detection: To a 100 mL Erlenmeyer flask 0.05 mL of the reaction mixture was taken, diluted with 25 mL of Milli-Q water with stirring to give faint pink coloured solution (Figure 2.4A). To it, 5 mL of 3.5 M H₂SO₄ solution was added which decolourises the solution (Figure 2.4B). To the colourless solution 10 mL of 1% KI solution was added followed by addition of 2 drops of ammonium molybdate solution. The colour of the solution was changed to yellow due to the formation of molecular iodine (Figure 2.4C). Finally to the solution 2 mL of freshly prepared starch solution was added and the colour changes to blue (Figure 2.4D). Excess addition of the starch solution to the mixture results in a dark blue-black solution which precipitates after standing for 30 minutes.

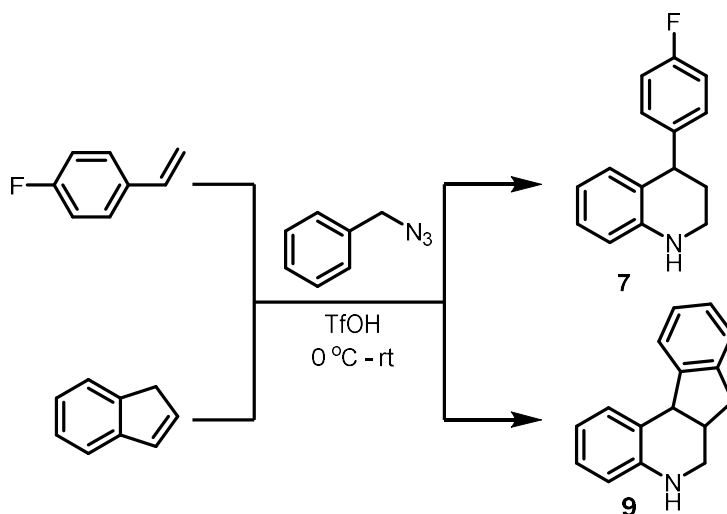
2.7.4. Preparation of Alkyl Indoline-2-carboxylate



Scheme 2.6. Synthesis of alkyl indoline-2-carboxylate.

To indoline-2-carboxylic acid (5 mmol, 1.0 equiv., 0.82 gm), and excess alcohol was added conc. H₂SO₄ (1.0 equiv.) at ambient temperature and heated to reflux for 24 h. The mixture was cooled to room temperature. The excess H₂SO₄ was neutralized by transferring the reaction mixture to a 100 mL beaker containing 20 mL of saturated Na₂CO₃ solution and 20 mL EtOAc. The aqueous layer was extracted with EtOAc (2×20 mL). The combined organic layer was washed with brine solution, dried over Na₂SO₄, and concentrated in *vacuo*. The residue was purified by column chromatography on silica gel with a mixture of EtOAc and petroleum ether to afford the desired indoline-2-carboxylate ester in quantitative yield.

2.7.5. Preparation of Precursor for Pharmaceutically Active Intermediates



Scheme 2.7. Synthesis of precursor for pharmaceutically active intermediates.

(i) To 400 mL of DMSO was added NaN_3 (1.45g, 22 mmol, 1.1 equiv.), and the suspension was allowed to stir for 1 h or until completely dissolved. Then benzyl bromide (20 mmol, 1.0 equiv.) was added, and the mixture was allowed to stir at room temperature for overnight. After completion, 400 mL H_2O was added, the mixture was extracted with 3 x 200 mL diethyl ether, and the organic phase was washed with 2 x 100 mL H_2O followed by 1 x 100 mL brine solution. The organic phase was then dried over Na_2SO_4 and concentrated in *vacuo* to give the corresponding azides, which was used for next reaction without further purification.

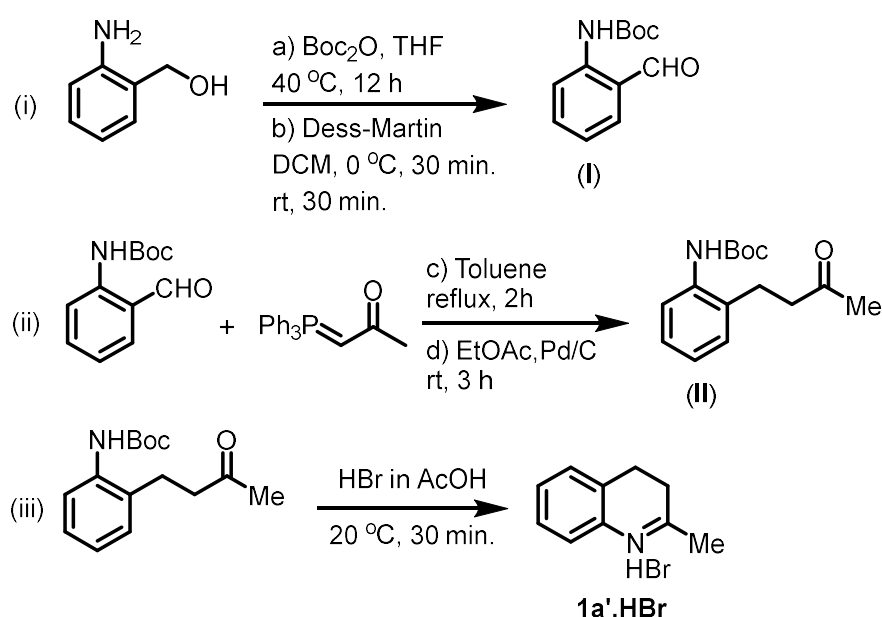
(ii) Similarly, the solution of benzyl azide in dichloromethane was cooled to 0 °C. To it, TfOH (1.1 equiv.) was added, and the solution allowed to stir for 10 min at room temperature. Then 4-fluorostyrene (2.0 equiv.) was added to it at room temperature and was allowed to stir for 1h (TLC shows completion of the reaction). The reaction was quenched by addition of saturated aqueous Na_2CO_3 , and extracted with EtOAc. The organic phase was washed with brine solution, dried over Na_2SO_4 , and finally concentrated in *vacuo*. The crude product was purified by column chromatography on silica gel with a mixture of EtOAc and petroleum ether to afford 7.

(iii) The solution of benzyl azide in dichloromethane was cooled to 0 °C. To it, TfOH (1.1 equiv.) was added, and the solution allowed to stir for 10 min at room temperature. Again the mixture was cooled to 0 °C. Indene (2.0 equiv.) was added at 0 °C, and the reaction

stirred for 1 h at this temperature (TLC shows completion of the reaction). The reaction was quenched by addition of saturated aqueous Na_2CO_3 , and extracted with EtOAc. The organic phase was washed with brine solution, dried over Na_2SO_4 , and finally concentrated in *vacuo*. The crude product was purified by column chromatography on silica gel with a mixture of EtOAc and petroleum ether to afford **9**.

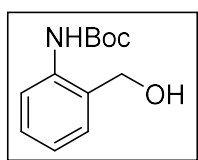
2.7.6. Synthesis of Intermediate Compounds for Mechanistic Investigation

2.7.6a. Synthesis of Intermediate **1a'**



Scheme 2.8. Synthesis of intermediates for mechanistic investigation.

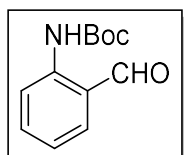
Synthesis of *tert*-butyl (2-(hydroxymethyl)phenyl)carbamate (I)



i) *tert*-butyl (2-(hydroxymethyl)phenyl)carbamate

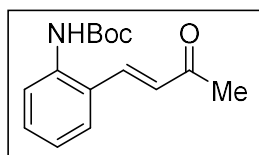
To a solution of $(\text{Boc})_2\text{O}$ (2.27 g, 10.4 mmol) in THF (20 mL) was added 2-aminobenzyl alcohol (1.26 g, 10.0 mmol) in one portion at room temperature. Then the reaction mixture

was stirred at 40 °C for 12 h. The solvent was removed under reduced pressure and the residue was purified by column chromatography using petroleum ether and 30% EtOAc to give the carbamate as a colourless oil (2.16 g, 97% yield).



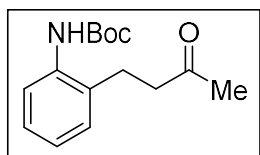
ii) The above *tert*-butyl (2-(hydroxymethyl)phenyl)carbamate (558 mg, 2.5 mmol) in dichloromethane (20 mL) was treated with the Dess-Martin periodinane (2.12 g, 5.0 mmol). The mixture was stirred at 0 °C for 30 min, then at room temperature for 30 min prior to a series of washes with saturated aqueous Na₂S₂O₃, NaHCO₃, and H₂O. The organic layer was extracted with dichloromethane (3 × 25 mL), the combined organic layer was dried over Na₂SO₄, and the solvent was removed under reduced pressure. The residue was purified by column chromatography using petroleum ether and 20% EtOAc to give the desired compound **I** as a pale yellow solid (490mg, 89% yield).

Synthesis of *tert*-butyl (2-(3-oxobutyl)phenyl)carbamate (**II**)



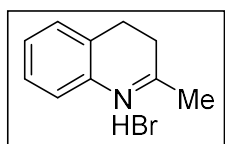
iii) *tert*-butyl (*E*)-(2-(3-oxobut-1-en-1-yl)phenyl)carbamate

To a 50 mL round-bottom flask with a magnetic stirring bar and reflux condenser was charged with compound **I** (2.0 mmol, 440 mg) and 20 mL toluene. Then the mixture was placed on a preheated oil bath at 120 °C. When reflux started Wittig reagent (764 mg, 2.4 mmol) was added at once and the mixture was allowed to reflux for 2 h. The mixture was cooled to room temperature, the solvent was removed under reduced pressure and the residue was purified by column chromatography using petroleum ether and EtOAc as eluent.



iv) *tert*-butyl (2-(3-oxobutyl)phenyl)carbamate (II)

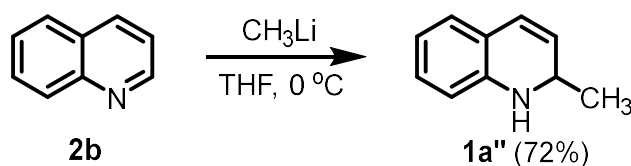
To a 25 mL round-bottom flask with a magnetic stirring bar was charged with) *tert*-butyl (*E*)-(2-(3-oxobut-1-en-1-yl)phenyl)carbamate (1.0 mmol, 261 mg) in 10 mL anhydrous EtOAc. To it, 30 mg of palladium on carbon (5 wt.%, Aldrich-205680) was added and connected to a hydrogen balloon and was allowed to stir at room temperature for 3 h. Then the mixture was passed on a small celite bead (1 cm) and washed with 5 mL of EtOAc. The solvent was removed under reduced pressure to give quantitative of pure product as a colourless oil.



v) 2-methyl-3,4-dihydroquinolinehydrobromide (1a': HBr)

To a 50 mL round-bottom flask with a magnetic stirring bar was charged with compound **II** (0.7 mmol, 180 mg) in 1 mL 33% HBr in acetic acid under an inert atmosphere. The mixture was allowed to stir vigorously at 20 °C for 30 minutes. Then to the reaction mixture, 20 mL cold anhydrous diethyl ether was added, stirred for another one minute and was allowed to settle the white precipitate. The white precipitate was collected by filtration, dried in *vacuo* and (140 mg, 89%) used without further purification in the catalytic experiments.

2.7.6b. Synthesis of Intermediate 1a''



To a solution of 3.0 mL MeLi (3.0 M, in diethoxymethane) at 0° C, **2b** (12 mmol) in 6.0 mL dry THF was added dropwise in an inert atmosphere with stirring. The reaction mixture

was kept at 0° C for 30 minutes and then it was allowed to stir at room temperature. After 6 h, the reaction was quenched with 10 mL water, extracted with diethyl ether (3 × 25 mL). The combined organic layer was dried over Na₂SO₄ and concentrated in *vacuo*. The crude reaction mixture was subjected to NMR analysis which shows 79% 2-Methyl-1,2-dihydroquinoline **1a''**.

(i) For update data of all newly synthesized compounds, see Appendix A.

(ii) For copy of ¹H and ¹³C NMR (only selected compounds) see Appendix B

2.8. Reference

- (a) Hou, X. L.; Yang, Z.; Wong, H. N. C. in *Progress in Heterocyclic Chemistry*, ed. Gribble, G. W.; Gilchrist, T. Pergamon, Oxford, **2005**, *15*, pp. 167. (b) Sützen, S. *Bioactive Heterocycles V*, Springer, **2007**, pp. 145. (c) Michael, J. P. *Nat. Prod. Rep.* **2008**, *25*, 166-187. (d) Vitaku, E.; Smith, D. T.; Njardarson, J. T. *J. Med. Chem.* **2014**, *57*, 10257-10274. (e) Chen, D.; Su, S.-J.; Cao, Y. *J. Mater. Chem. C* **2014**, *2*, 9565-9578. (f) Afzal, O.; Kumar, S.; Haider, M. R.; Ali, M. R.; Kumar, R.; Jaggi, M.; Bawa, S. *Eur. J. Med. Chem.* **2015**, *97*, 871-910.
- (a) Murahashi, S.-I.; Okano, Y.; Sato, H.; Nakae, T.; Komiya, N. *Synlett* **2011**, 1675-1686. (b) Yuan, H.; Yoo, W.-J.; Miyamura, H.; Kobayashi, S. *Adv. Synth. Catal.* **2012**, *354*, 2899-2904. (c) Wendlandt, A. E.; Stahl, S. S. *J. Am. Chem. Soc.* **2014**, *136*, 506-512. (d) Wendlandt, A. E.; Stahl, S. S. *J. Am. Chem. Soc.* **2014**, *136*, 11910-11913. (e) Cui, X.; Li, Y.; Bachmann, S.; Scalone, M.; Surkus, A.-E.; Junge, K.; Topf, C.; Beller, M. *J. Am. Chem. Soc.* **2015**, *137*, 10652-10658. (f) Iosub, A. V.; Stahl, S. S. *Org. Lett.* **2015**, *17*, 4404-4407. (g) Girard, C. A.; Huang, H.; Zhou, F.; Deng, G.-J.; Li, C.-J. *Org. Chem. Front.* **2015**, *2*, 279-287. (h) Giustra, G. X.; Ishibashi, J. S. A.; Liu, S.-Y. *Coord. Chem. Rev.* **2016**, *314*, 134-181. (i) Jung, D.; Kim, M. H.; Kim, J. *Org. Lett.* **2016**, *18*, 6300-6303.
- (a) Fu, P. P.; Harvey, R. G. *Chem. Rev.* **1978**, *78*, 317-361. (b) Buckle, D. R. *Encyclopedia of Reagents for Organic Synthesis*; John Wiley & Sons, Inc.: New York, **2010**.
- For selected reviews on acceptorless dehydrogenation, see: (a) Dobereiner, G. E.; Crabtree, R. H. *Chem. Rev.* **2010**, *110*, 681-703. (b) Gunanathan, G.; Milstein, D. *Science* **2013**, *341*, 249.
- For selected examples on acceptorless dehydrogenation of (partially) saturated cyclic amines, see: (a) Yamaguchi, R.; Ikeda, C.; Takahashi, Y.; Fujita, K.-i. *J. Am. Chem. Soc.* **2009**, *131*, 8410-8412. (b) Muthaiah, S.; Hong, S. H. *Adv. Synth. Catal.* **2012**, *354*, 3045-3053. (c) Wu, J.; Talwar, D.; Johnston, S.; Yan, M.; Xiao, J. *Angew. Chem., Int. Ed.* **2013**, *52*, 6983-6987. (d) Tseng, K. N. T.; Rizzi, A. M.; Szymczak, N. K. *J. Am. Chem. Soc.* **2013**, *135*, 16352-16355. (e) Amende, M.; Gleichweit, C.; Werner, K.; Schernich, S.; Zhao, W.; Lorenz, M. P.; Höfert, O.; Papp, C.; Koch, M.; Wasserscheid, P. *ACS Catal.* **2014**, *4*, 657-665. (f) Fujita, K.-i.; Tanaka, Y.; Kobayashi, M.; Yamaguchi, R. *J. Am. Chem. Soc.* **2014**, *136*, 4829-4832. (g) Chakraborty, S.; Brennessel, W. W.; Jones, W. D. *J. Am. Chem. Soc.* **2014**, *136*, 8564-8567. (h) Yao, W. B.; Zhang, Y. X.; Jia, X. Q.; Huang,

Z. Angew. Chem., Int. Ed. **2014**, *53*, 1390-1394. (i) Manas, M. G.; Sharninghausen, L. S.; Lin, E.; Crabtree, R. H. *J. Organomet. Chem.* **2015**, *792*, 184-189. (j) Xu, R.; Chakraborty, S.; Yuan, H.; Jones, W. D. *ACS Catal.* **2015**, *5*, 6350-6354. (k) Talwar, D.; Gonzalez-de-Castro, A.; Li, H. Y.; Xiao, J. *Angew. Chem., Int. Ed.* **2015**, *54*, 5223-5227 (l) Kojima, M.; Kanai, M. *Angew. Chem., Int. Ed.* **2016**, *55*, 12224-12227. (m) Moromi, S. K.; Siddiki, S. M. A. H.; Kon, K.; Toyao, T.; Shimizu, K.-i. *Catal. Today* **2017**, *281*, 507-511. (n) Forberg, D.; Schwob, T.; Zaheer, M.; Friedrich, M.; Miyajima, N.; Kempe, R. *Nat. Commun.* **2016**, *7*, 13201.

6. For aerobic dehydrogenation of (partially) saturated cyclic compounds, see: (a) Izawa, Y.; Pun, D.; Stahl, S. S. *Science* **2011**, *333*, 209-213. (b) Izawa, Y.; Zheng, C.; Stahl, S. S. *Angew. Chem., Int. Ed.* **2013**, *52*, 3672-3675. (c) Pun, D.; Diao, T.; Stahl, S. S. *J. Am. Chem. Soc.* **2013**, *135*, 8213-8221. (d) Iosub, A. V.; Stahl, S. S. *J. Am. Chem. Soc.* **2015**, *137*, 3454-3457.

7. For selected examples on oxidative dehydrogenation of amines, see: (a) So, M. H.; Liu, Y.; Ho, C. M.; Che, C. M. *Chem. -Asian J.* **2009**, *4*, 1551-1561. (b) Wendlandt, A. E.; Stahl, S. S. *Org. Lett.* **2012**, *14*, 2850-2853. (c) Langeron, M.; Fleury, M.-B. *Angew. Chem., Int. Ed.* **2012**, *51*, 5409-5412. (d) Langeron, M.; Fleury, M.-B. *Science* **2013**, *339*, 43-44. (e) Furukawa, S.; Suga, A.; Komatsu, T. *Chem. Commun.* **2014**, *50*, 3277-3280. (f) Jawale, D. V.; Gravel, E.; Shah, N.; Dauvois, V.; Li, H.; Namboothiri, I. N. N.; Doris, E. *Chem. -Eur. J.* **2015**, *21*, 7039-7042. (g) Suzuki, K.; Tang, F.; Kikukawa, Y.; Yamaguchi, K.; Mizuno, N. *Angew. Chem., Int. Ed.* **2014**, *53*, 5356-5360. (h) Chen, B.; Wang, L.; Gao, S. *ACS Catal.* **2015**, *5*, 5851-5876.

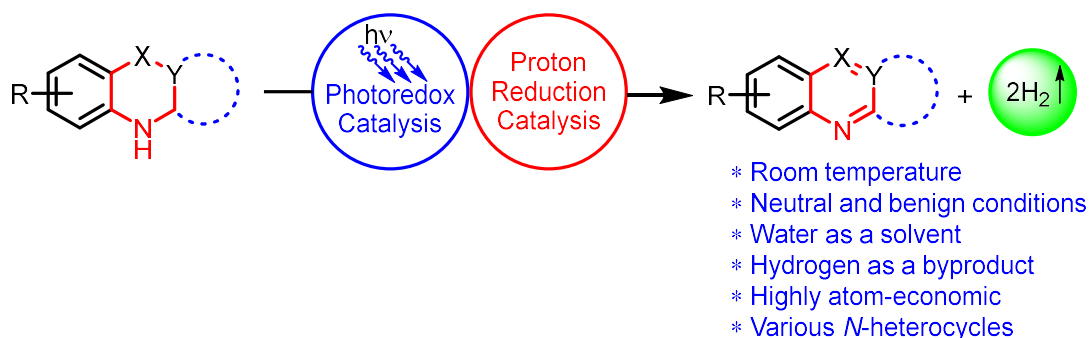
8. (a) Yamaguchi, K.; Mizuno, N. *Angew. Chem., Int. Ed.* **2003**, *42*, 1480-1483. (b) Yamaguchi, K.; Mizuno, N. *Chem. -Eur. J.* **2003**, *9*, 4353-4361. (c) Kamata, K.; Kasai, J.; Yamaguchi, K.; Mizuno, N. *Org. Lett.* **2004**, *6*, 3577-3580. (d) Choi, H.; Doyle, M. P. *Chem. Commun.* **2007**, 745-747. (e) Li, F.; Chen, J.; Zhang, Q.; Wang, Y. *Green Chem.* **2008**, *10*, 553-562. (f) Yamaguchi, K.; Kim, J. W.; He, J. L.; Mizuno, N. *J. Catal.* **2009**, *268*, 343-349. (g) Yuan, H.; Yoo, W. J.; Miyamura, H.; Kobayashi, S. *J. Am. Chem. Soc.* **2012**, *134*, 13970-13973. (h) Ge, D. H.; Hu, L.; Wang, J. Q.; Li, X. M.; Qi, F. Q.; Lu, J. M.; Cao, X. Q.; Gu, H. W. *ChemCatChem* **2013**, *5*, 2183-2186.

9. Recent examples on dehydrogenation of THQs under photoredox catalysis see: (a) Zhou, L.; Hossain, M. L.; Xiao, T. *Chem. Rec.* **2016**, *16*, 319-334. (b) Chen, S.; Wan, Q.; Badu-Tawiah, A. K. *Angew. Chem., Int. Ed.* **2016**, *55*, 9345-9349. (c) He, K.-H.; Tan, F.-

- F.; Zhou, C.-Z.; Zhou, G.-J.; Yang, X.-L.; Li, Y. *Angew. Chem., Int. Ed.* **2017**, *56*, 3080-3084. (d) Yin, Q.; Oestreich, M. *Angew. Chem., Int. Ed.* **2017**, *56*, 7716-7718. (e) Kato, S.; Saga, Y.; Kojima, M.; Fuse, H.; Matsunaga, S.; Fukatsu, A.; Kondo, M.; Masaoka, S.; Kanai, M. *J. Am. Chem. Soc.* **2017**, *139*, 2204-2207.
10. Recent reviews on organophotoredox catalysis, see: (a) Ravelli, D.; Fagnoni, M.; Albini, A. *Chem. Soc. Rev.* **2013**, *42*, 97-113. (b) Nicewicz, D. A.; Nguyen, T. M. *ACS Catal.* **2014**, *4*, 355-360. (c) Hari, D. P.; König, B. *Chem. Commun.* **2014**, *50*, 6688-6699. (d) Romero, N. A.; Nicewicz, D. A.; *Chem. Rev.* **2016**, *116*, 10075-10166.
11. Selected examples of rose bengal catalyzed reactions, (a) Pan, Y.; Kee, C. W.; Chen, L.; Tan, C.-H. *Green Chem.* **2011**, *13*, 2682-2685. (b) Pan, Y.; Wang, S.; Kee, C. W.; Dubuisson, E.; Yang, Y.; Loh, K. P.; Tan, C.-H. *Green Chem.* **2011**, *13*, 3341-3344. (c) Teo, Y. C.; Pan, Y.; Tan, C.-H. *ChemCatChem* **2013**, *5*, 235-240. (d) Sun, J.-G.; Yang, H.; Li, P.; Zhang, B. *Org. Lett.* **2016**, *18*, 5114-5117.
12. (a) Prajapati, S. M.; Patel, K. D.; Vekariya, R. H.; Panchal, S. N.; Patel, H. D. *RSC Adv.* **2014**, *4*, 24463-24476. (b) Iwai, T.; Sawamura, M. *ACS Catal.* **2015**, *5*, 5031-5040 and references therein.
13. Zhang, M.-Z.; Chen, Q.; Yang, G.-F. *Eur. J. Med. Chem.* **2015**, *89*, 421-441.
14. Zolova, O. E.; Mady, A. S. A.; Garneau-Tsodikova, S. *Biopolymers* **2010**, *93*, 777-790.
15. Delorme, D.; Dubé, D.; Ducharme, Y.; Grimm, E. L.; Friesen, R.; Lepine, C. (Merck Frosst, Canada). U.S. Patent 5, 552, 437, Sept 3, **1996**.
16. Upadhyaya, R. S.; Dixit, S. S.; Földesi, A.; Chattopadhyaya, J. *Bioorg. Med. Chem. Lett.* **2013**, *23*, 2750-2758.
17. (a) Ouannes, C.; Wilson, T. *J. Am. Chem. Soc.* **1968**, *90*, 6527-6528. (b) Silverman, S. K.; Foote, C. S. *J. Am. Chem. Soc.* **1991**, *113*, 7672-7675. (c) Klaper, M.; Linker, T. *J. Am. Chem. Soc.* **2015**, *137*, 13744-13747.
18. Su, F. Z.; Mathew, S. C.; Lipner, G.; Fu, X. Z.; Antonietti, M.; Blechert, S.; Wang, X. C. *J. Am. Chem. Soc.* **2010**, *132*, 16299-16301.
19. Czoska, A.; Livraghi, S.; Chiesa, M.; Giamello, E.; Agnoli, S.; Granozzi, G.; Finazzi, E.; Valentin, C. D.; Pacchioni, G. *J. Phys. Chem. C* **2008**, *112*, 8951-8956.
20. (a) Islam, S. D.-M.; Ito, O. *J. Photochem. Photobiol. A: Chemistry* **1999**, *123*, 53-59. (b) Lambert, C. R.; Kochevar, I. E. *J. Am. Chem. Soc.* **1996**, *118*, 3297-3298.
21. Li, H.; Jiang, J.; Lu, G.; Huang, F.; Wang, Z. X. *Organometallics* **2011**, *30*, 3131-3141.

Chapter 3

Dual Catalyzed Acceptorless Dehydrogenation of *N*-Heterocycles to Heteroaromatics by Merging Photoredox Catalysis with Proton Reduction Catalysis



(Manuscript under Revision)

3.1. Introduction

Dehydrogenation reactions are fundamental reactions in synthetic organic chemistry and widely used in processes for manufacturing commodity chemicals, and pharmaceuticals.¹ The catalytic acceptorless dehydrogenation (ADH) reactions are fascinating over catalytic oxidative dehydrogenation reactions, as the ADH reaction avoids any use of stoichiometric oxidants, and thus, making the process greener, and sustainable.² Significantly, the evolved hydrogen gas; an energy carrier is valuable in itself. Indeed, removal of hydrogen atoms from adjacent atomic centres of an organic molecule is a thermodynamically uphill process.³ However, recent experimental and computational studies revealed that the presence of one or more nitrogen atoms in the ring brings down the endothermicity of the reaction and thus, making the ADH reaction facile under ambient conditions.³

In recent times, the non-oxidative dehydrogenation of partially saturated *N*-heterocycles has been considered to be the promising method to produce *N*-heterocyclic arenes and hydrogen gas which remain challenging. Undoubtedly, nitrogen-containing heterocyclic scaffolds show numerous applications in the synthesis of active pharmaceutical ingredients,⁴ including to use as liquid organic hydrogen carriers (LOHCs) for fuel cell applications (Fig. 3.1).⁵ In this context, the ADH of partially saturated *N*-heterocycles is important and highly demanding.⁶

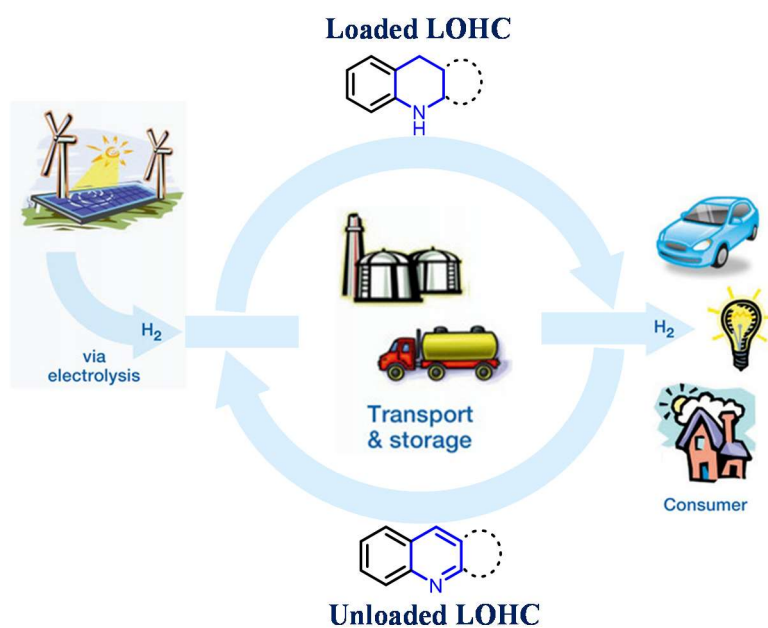
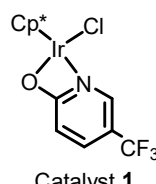
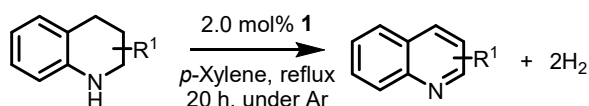


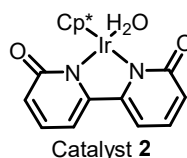
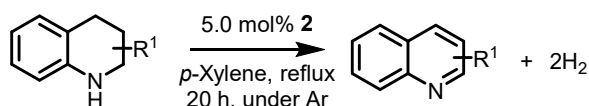
Figure 3.1. The importance of *N*-heterocycles as LOHC.

Significant contributions have been made by the research groups of Fujita and Yamaguchi,^{6a,6c} Xiao,^{6b,6g} Crabtree^{6e} using well-defined molecular catalysts (Scheme 3.1A). Independently, Jones and co-workers have reported the ADH reaction of partially saturated *N*-heterocycle to *N*-heteroaromatics catalyzed by well-defined Fe-, and Co-complexes.^{6d,6f} Kanai^{6h} and co-workers used borane as a catalyst whereas Kempe⁶ⁱ used heterogeneous Pd₂Ru@SiCN catalyst for the dehydrogenation reaction (Scheme 3.1A). However, these catalytic systems operate under thermal conditions (at elevated temperature). The use of non-eco-friendly high boiling solvents such as chlorobenzene or unconventional trifluoroethanol is other limitations. In our previous chapter, we have described oxidative dehydrogenation of *N*-heterocycles to *N*-heteroaromatics under visible-light metal-free photoredox catalytic conditions using air as an oxidant. In the present chapter, we report dehydrogenation of partially saturated *N*-heterocycles to *N*-heterocyclic arenes with the liberation of hydrogen gas using newly synthesized Co-glyoxime based proton reduction catalyst (Scheme 3.1B). The reaction operates at room temperature under mild, neutral conditions using water as a solvent. The present AHD reaction has been achieved by merging of Ru-based photoredox catalysis with Co-based proton reduction catalysis under visible-light irradiation.⁷⁻⁹ The 2-methyl-1,2,3,4-tetrahydroquinoline (2-MeTHQ) (**1a**) was chosen as the model substrate for our dehydrogenation reaction. Initially, we have investigated the effect of various photoredox catalysts, proton reduction catalysts, solvents, light source and mol% of catalyst loading under various reaction conditions. From the initial screening, it was observed that Ru-based photoredox catalyst merged with a newly synthesized Co-oxime based proton reduction catalyst (**IV**) using water as the solvent is the best optimal catalytic system for the present external oxidant-free dehydrogenation reaction.

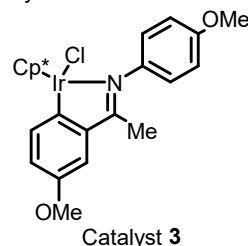
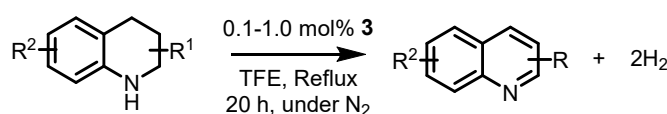
Yamaguchi, Fujita and Co-workers



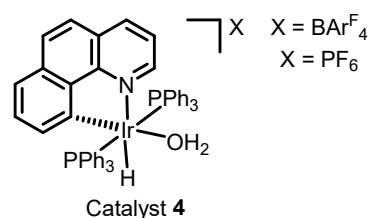
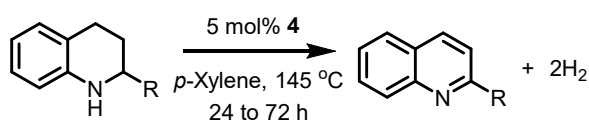
Yamaguchi, Fujita and Co-workers



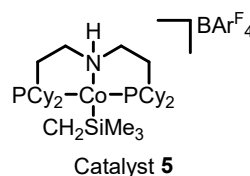
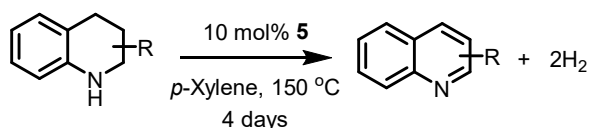
Xiao and Co-workers



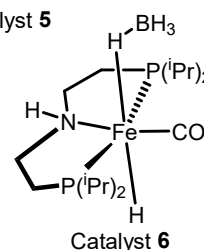
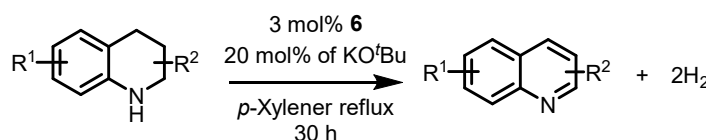
Crabtree and Co-workers



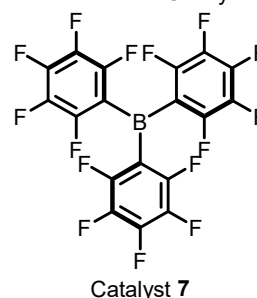
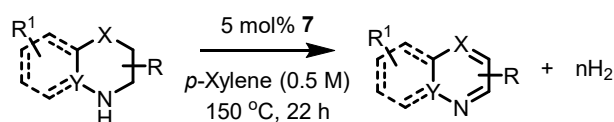
Jones and Co-workers



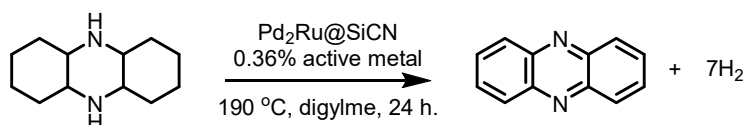
Jones and Co-workers

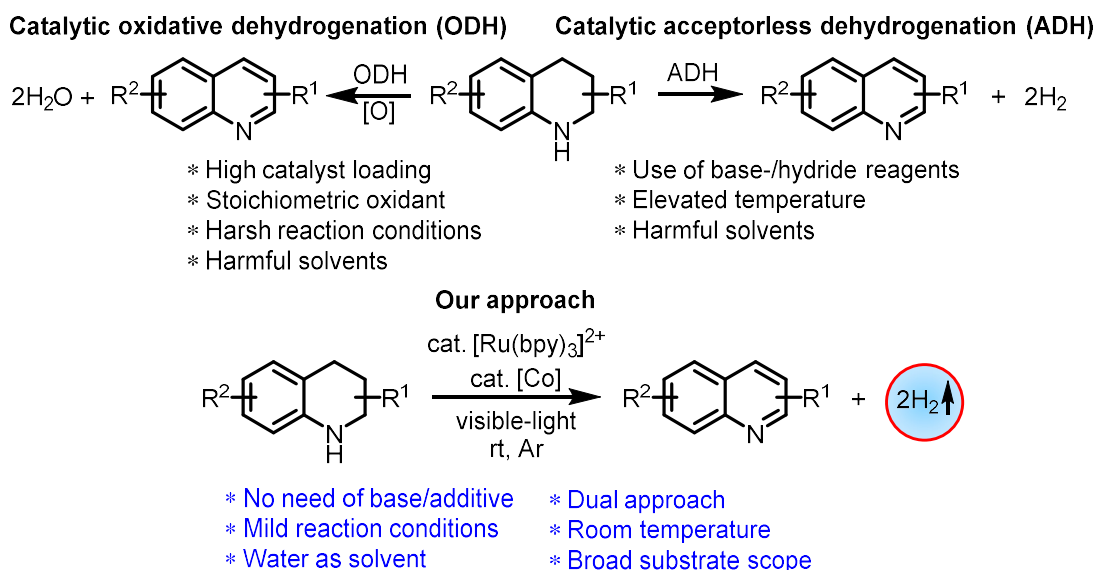


Kanai and Co-workers



Kemppe and Co-workers

Scheme 3.1A. Literature report on acceptorless dehydrogenation of *N*-heterocycles.



Scheme 3.1B. Various strategies to access *N*-heteroaromatics (Literature precedents vs present work).

3.2. Statement of the Problem

Catalytic acceptorless dehydrogenation of *N*-heterocycles has been well studied by many research groups (Scheme 3.1B). However, the need for harsh reaction conditions to overcome thermodynamic parameters, use of precious metal-based catalysts, bases/additives, harmful organic solvents and high catalyst loading are the major concerns. Thus, an efficient catalytic method needs to be developed for acceptorless dehydrogenation, which has overcome all these drawbacks. In this chapter, we report a visible-light mediated dual catalytic approach for dehydrogenation of *N*-heterocycles to *N*-heteroaromatics with H₂ liberation. This reactivity was achieved by merging [Ru(bpy)₃]²⁺ catalysis with newly synthesized [Co]-based proton reduction catalysis in water. The current method operates under very mild, benign conditions. Under this catalytic dehydrogenation, a variety of substrates with different functional groups can be easily dehydrogenated.

3.3. Reaction Optimization

3.3.1. Cobalt Complexes Used for the Present Catalytic Study

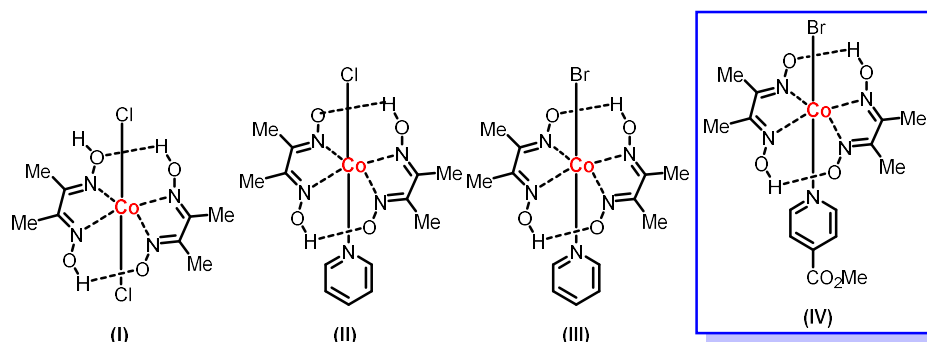
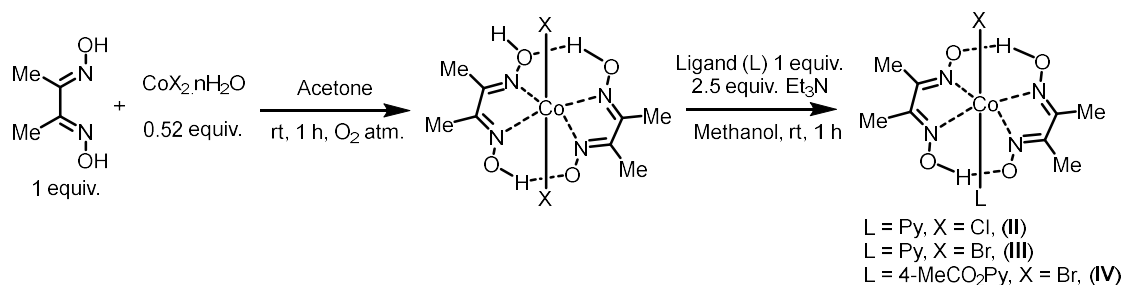


Figure 3.2. Cobalt-based proton reduction catalysts used for the present study.

3.3.2. Synthesis of Cobalt complexes

The above Co-dimethylglyoxime proton reduction catalysts were synthesized according to a two-step procedure as shown in scheme 3.2.



Scheme 3.2. Synthesis of proton reduction catalyst.

3.3.3. UV-Visible Spectra of Cobalt Complexes

The solid-state UV-Visible spectra of various proton reduction catalysts were recorded and are given in Figure 3.3. From the solid-state UV-visible absorption spectra of proton reduction catalysts, it is found that the absorption maximum (λ_{\max}) for these catalysts are below 450 nm. Therefore it is believed that $[\text{Ru}(\text{bpy})_3]^{2+}$ will absorb the visible-light to initiate the redox reaction and not the proton reduction catalysts.

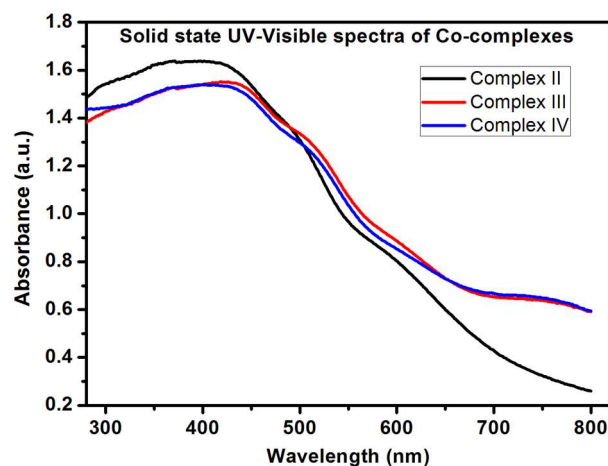


Figure 3.3. Solid-state UV-Visible spectra of Co-complexes (II-IV).

3.3.4. Cyclic Voltammogram of Cobalt Complex IV

Redox potentials of proton reduction catalyst and photocatalyst were judged through cyclic voltammetric (CV) investigations. Typically three electrode systems comprising glassy carbon (GC, 3mm dia.) was used as working electrode and Ag/Ag^+ (0.1M TBAP in acetonitrile) as reference electrode and a platinum wire was used as counter electrode, respectively. CVs were recorded in acetonitrile containing 0.1M TBAP as an electrolytic medium. Solutions were purged with argon for 30 minutes before scans and also jacketed during the measurements. Potentials were calibrated using the ferrocene as an internal standard.

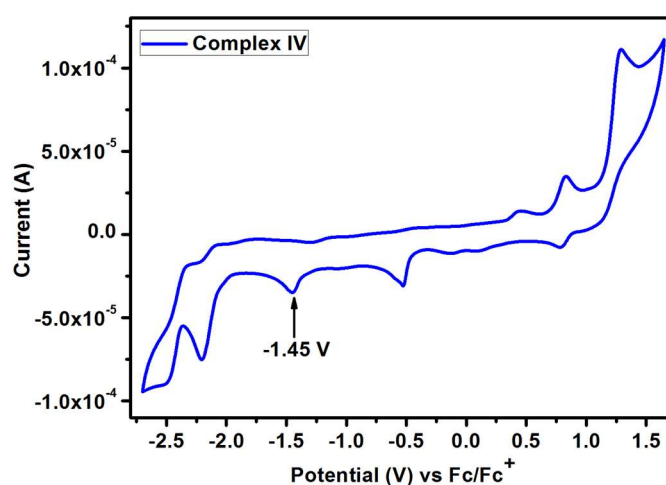


Figure 3.4. CV of IV (0.001 M) in 0.1 M NBu_4PF_6 in degassed CH_3CN with scan rate 100 mV/s.

Interestingly, the newly synthesized Co-oxime complex **IV** is highly stable in water. This result prompted us to perform the ADH reaction using water as a solvent.

3.3.5. Optimization Table

Table 3.1. Optimization of the reaction conditions^a

Entry	Variation from initial conditions	Yield ^b
1	None	99 (96) ^c
2	No light-source	NR
3	No [Ru(bpy) ₃]Cl ₂	NR
4	No Co-IV	NR
5	[Ru(bpy) ₃][PF ₆] ₂ instead of [Ru(bpy) ₃]Cl ₂	99
6	[Ru(1,10-phen) ₃]Cl ₂ instead of [Ru(bpy) ₃]Cl ₂	89 ^c
7	Eosin-Y instead of [Ru(bpy) ₃]Cl ₂	23
8	Fluorescein instead of [Ru(bpy) ₃]Cl ₂	NR
9	I instead of IV	NR
10	II instead of IV	24
11	III instead of IV	58
12	MeCN instead of water	NR
13	DMF instead of water	NR
14	2-MeTHF instead of water	56
15	0.5 mol % of [Ru(bpy) ₃]Cl ₂	66
16	1.0 mol % of IV	48

^aReaction conditions: **1a** (0.25 mmol), photoredox catalyst (1.0 mol%), proton reduction catalyst (2.5 mol%), water (8 mL), Ar atm., visible-light irradiation from the blue LED at 28 °C for 12 h. ^bGC yield using mesitylene as an internal standard. ^cIsolated yields. NR = no reaction.

Upon irradiation of visible-light in presence of catalytic amount of $[\text{Ru}(\text{bpy})_3]\text{Cl}_2$ (1 mol%) and a newly synthesized proton reduction catalyst **IV** (2.5 mol%) in water under argon atmosphere the substrate **1a** gave the corresponding dehydrogenated product **2a** in 96% isolated yield (Table 3.1, entry 1). Gratifyingly, the generation of molecular hydrogen was qualitatively analyzed by gas chromatography. Performing the reaction in absence of the light source, photoredox catalyst or proton reduction catalyst, no formation of product **2a** was observed (Table 3.1, entries 2-4). This result confirms that light source, photoredox catalyst and proton reduction catalyst are essential for the success of the reaction. Among different photoredox catalysts screened, the Ru-based photoredox catalyst was found to be optimal for this reaction. The organophotoredox catalysts either gave very poor yield or no product formation **2a** under optimal conditions (Table 3.1, entries 1 and 5-8). Remarkably, the proton reduction catalyst **IV** synthesized by our group (Figure 3.2) worked efficiently and offered the dehydrogenated product (**2a**) in 96% isolated yield. Recently, Li and co-workers reported a similar ADH reaction of *N*-heterocycles using Co-oxime (**II**) as the proton reduction catalyst in ethanol.⁹ It was noteworthy that under our catalytic conditions using water as a solvent the Co-oxime complex (**II**) gave only 24% yield of the desired dehydrogenated product **2a** (Table 3.1, entry 10). Indeed, the other well-established Co(III)-oxime complexes (**I** and **III**) gave unsatisfactory results under optimized conditions (Table 3.1, entries 1 and 9 and 10). This result clearly showed the superiority of our proton reduction catalyst **IV**. Notably, water was found to be the optimal solvent for this transformation (Table 3.1, entries 1 and 12-14). Under standard reaction conditions, a low catalyst loading (0.5 mol%) of $[\text{Ru}(\text{bpy})_3]\text{Cl}_2$ gave **2a** in 66% yield, while 1 mol% of proton reduction catalyst **IV** gave a moderate yield of the product **2a** (Table 3.1, entries 15-16).



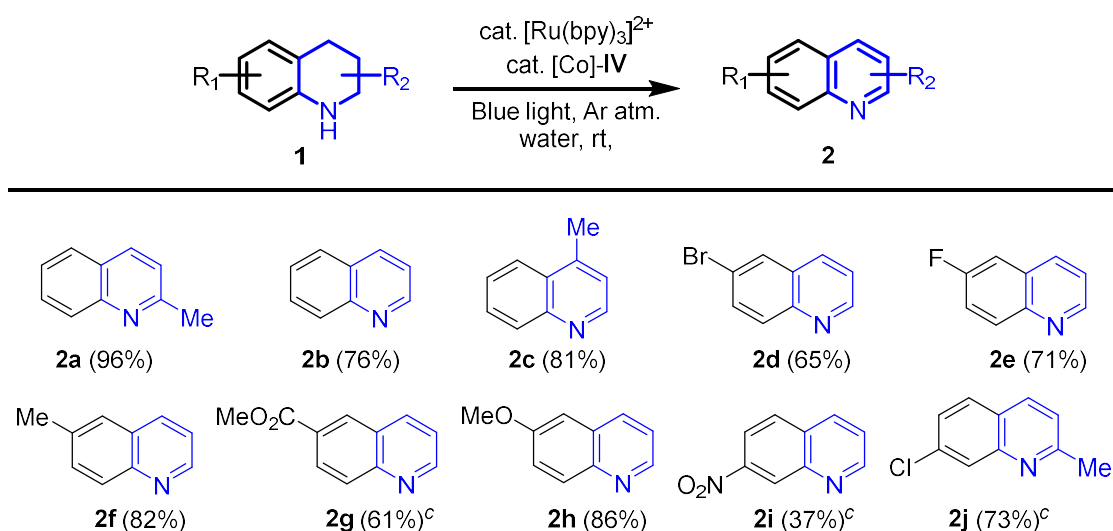
Figure 3.5. (A) Reaction setup for ADH of *N*-heterocycles. (B) Reaction after 12 h.

3.4. Substrate scope

3.4.1. Scope of Quinoline Derivatives

With the optimized reaction condition in hand, we next investigated the scope of the dual catalytic approach for the ADH of 1,2,3,4-tetrahydroquinoline (THQ) derivatives (Table 3.2). We found that various important THQs can be dehydrogenated to the corresponding *N*-heteroarenes in moderate to good yields with the liberation of H₂ gas in water using our catalytic system. The unsubstituted substrate **1b** gave the expected product **2b** in 76% isolated yield. The presence of an electron-donating group at the different position of the THQs enhanced the reactivity of the substrate and offered very good yields of dehydrogenated product compared to that of substrates with electron-deficient groups. Thus, THQs with an electron-donating alkyl or methoxy group reacted efficiently to lead to the corresponding dehydrogenated product in excellent yields (up to 96%) (Table 3.2, entries 1, 3, 6 and 8). Under optimal conditions, the electron-deficient groups such as -Br, -F, -CO₂Me, and -NO₂ underwent the dehydrogenation reaction and offered the expected product in moderate yields (37% to 71%). The disubstituted substrate **1j** smoothly dehydrogenated under our dual catalytic condition and gave the product **2j** in 73% isolated yield after 24 h.

Table 3.2. Room temperature ADH of THQs in water.^a

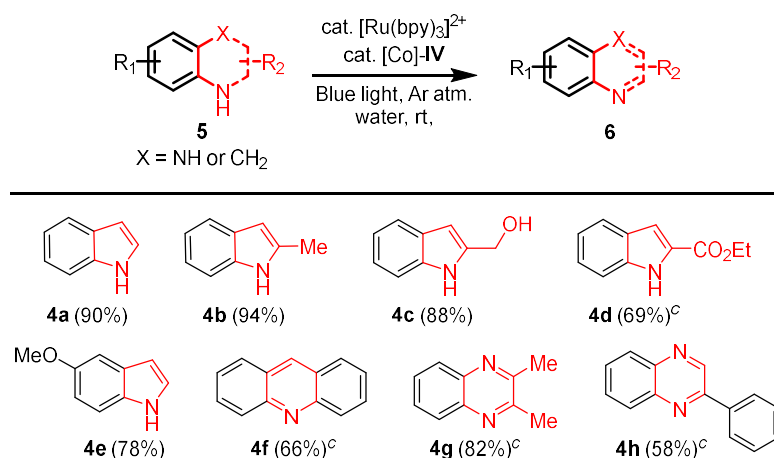


^aReaction conditions: substrate **1** (0.25 mmol), [Ru(bpy)₃]²⁺ (1.0 mol%), [Co]-IV (2.5 mol%), water (8 mL), Ar atm., 36 W blue LED, 28 °C, 12 h. ^bIsolated yields. ^cAfter 24 h.

3.4.2. Scope of Indoles and other Heterocycles

Our methodology was applied successfully for the synthesis of other important *N*-heterocyclic compounds e.g. indoles, acridine and quinoxaline. Many of these *N*-heterocycles are present in pharmaceuticals, natural products, and are found to be biologically active motifs.¹⁰ When unsubstituted indoline **3a** and 2-methyl indoline **3b** subjected to the dehydrogenation reaction under optimized conditions showed excellent reactivity and gave the products **4a**, and **4b** in 90%, and 94% isolated yields, respectively. Interestingly, the substrate **3c** with a hydroxyl group selectively gave the expected product **4c** in 88% isolated yield with retaining the alcoholic functionality. It is noteworthy that the primary alcohol functionality cannot be preserved in transition-metal catalyzed dehydrogenation reaction due to higher reactivity of alcohols to lead to several other products. This is the advantage of our present catalytic system. The substrate **3d** with an electron deficient ester group gave moderate (69%) yield of product **4d** after 24 h. An electron rich indoline **3e** gave the desired product **4e** in 78% isolated yield after 12 h. The 1,10-dihydroacridine **3f** underwent ADH reaction under our dual catalytic conditions and offered the product **4f** in 66% isolated yield after 24 h. The substituted tetrahydroquinoxalines also smoothly proceeded under standard reaction conditions and gave the desired products **4g**, and **4h** in 82% and 58% isolated yields, respectively. Notably, the liberated hydrogen gas was detected by gas chromatography and also quantified.

Table 3.3. Room temperature ADH of indolines and other heterocycles in water.^a



^aReaction conditions: substrate **3** (0.25 mmol), [Ru(bpy)₃]²⁺ (1.0 mol%), [Co]-IV (2.5 mol%), water (8 mL), Ar atm., 36 W blue LED, 28 °C, 12 h. ^bIsolated yields. ^cAfter 24 h.

3.5. Mechanistic Investigation

3.5.1. Cyclic Voltammetry of Partially Saturated *N*-heterocycles

In order to get insight into the oxidation potential of the partially saturated *N*-heterocycles, we recorded the cyclic voltammetry data for few of the compounds. The cyclic voltammetry was measured at 10 mV s^{-1} scan rate using Ag/AgCl as reference electrode, Pt wire as counter electrode and a glassy carbon electrode as working electrode in anhydrous degassed acetonitrile with 0.1 M tetrabutylammonium perchlorate as supporting electrolyte. For the oxidation potential for **1a**, **3f** and **3h** see Appendix C.

3.5.2. Analysis for Hydrogen Gas

3.5.2a. Qualitative Analysis of Hydrogen Gas

The liberated hydrogen gas was detected in GC and quantified after completion of the reaction for the substrate **1a**.

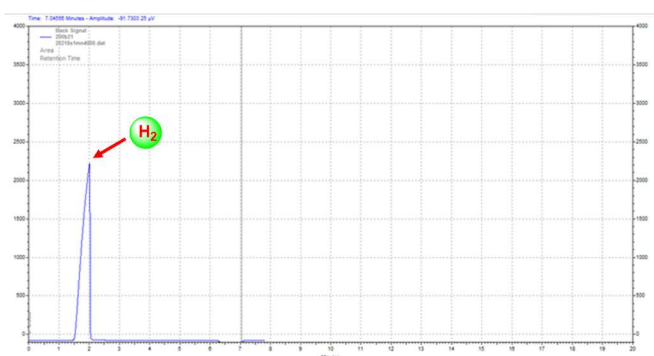
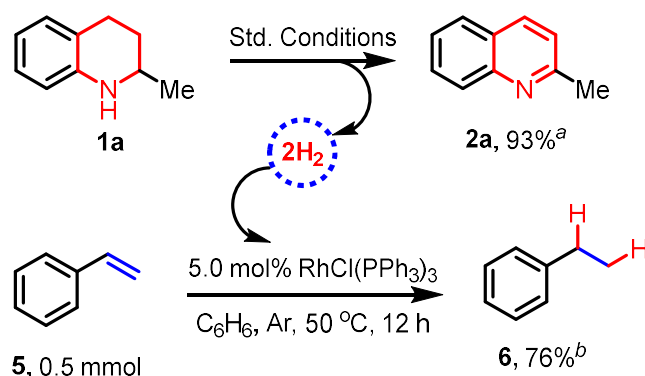


Figure 3.6. Hydrogen gas detection on GC.

3.5.2b. Quantitative Measurement of Evolved Hydrogen Gas

The evolved hydrogen gas was utilized for hydrogenation of styrene. Simultaneously two parallel reactions were carried out. In one reaction vial, visible-light mediated photocatalytic acceptorless dehydrogenation of **1a** was carried out under the optimal reaction condition. Whereas in another reaction vial thermal hydrogenation of styrene **5** was carried out using $\text{RhCl}(\text{PPh}_3)_3$ as the catalyst. Both the reaction vials are connected to

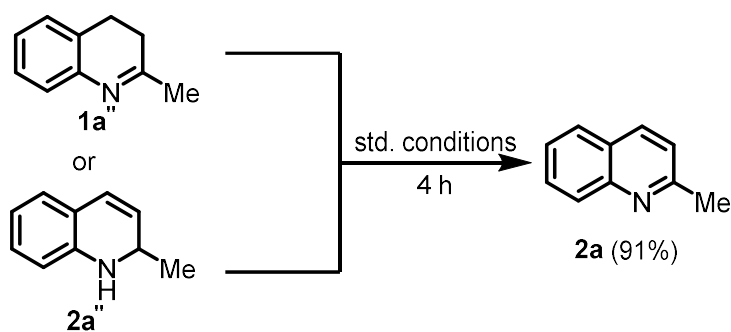
each other by a cannula and were allowed to continue for 12 h. After the stipulated time, the reaction mixtures were analyzed in GC and the results are given below.



Scheme 3.3. Quantification of H₂ gas.

Reaction conditions: Substrate (0.25 mmol), [Ru(bpy)₃]Cl₂ (1.0 mol %), [Co] (2.5 mol %), water 8.0 mL, ambient temperature, 12 h, 36 W blue LED, ^aIsolated yield, ^bGC yield using *n*-decane as internal standard.

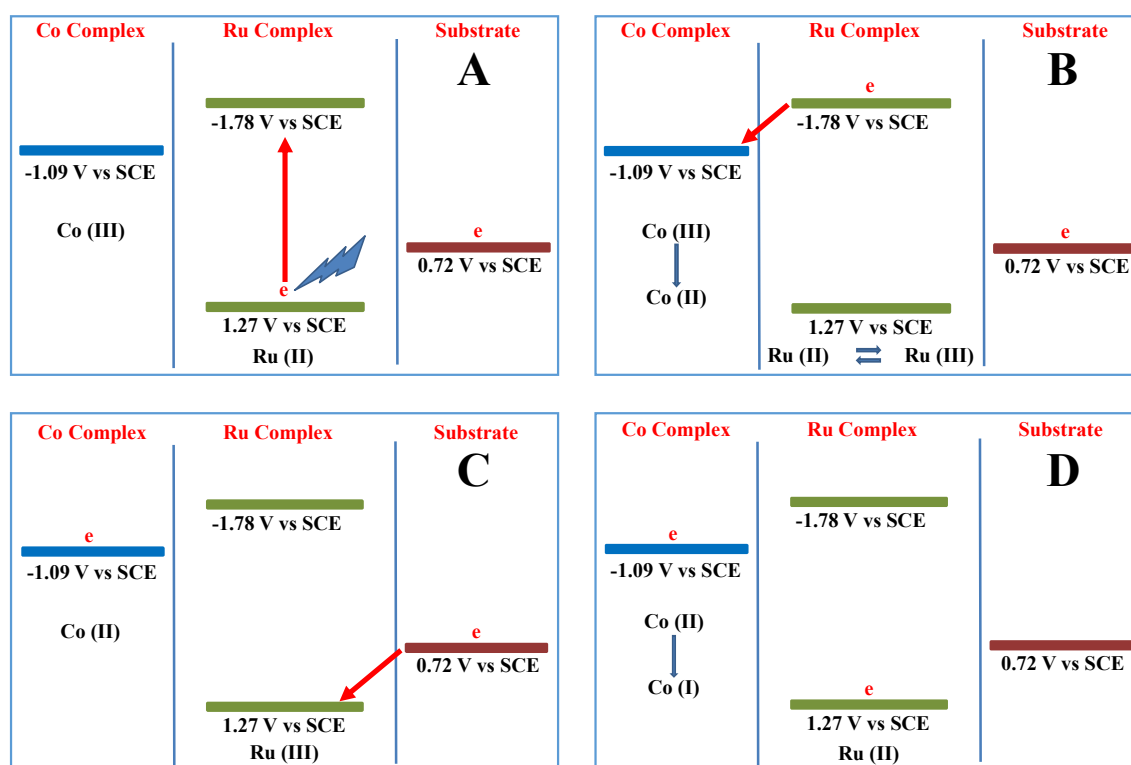
3.5.3. Control Experiments



Scheme 3.4. Control experiment study.

To gain insight into the mechanism, several control experiments were performed under optimized reaction conditions. No product formation was observed when the reaction was carried out in the absence of the light source, photoredox catalyst or proton reduction catalyst. These control experiments confirm the necessity of each key reaction components. The λ_{max} of the proton reduction catalyst was found to be less than 435 nm from their solid state UV-visible spectroscopy, which confirms that visible-light absorbed

by the Ru-based photoredox catalyst is responsible for the success of the reaction. From cyclic voltammetry studies, the oxidation potential of **1a** was found to be 0.81 V. The reduction potentials $E^{\text{III/II}}$ and $E^{\text{II*/I}}$ of tris(2,2'-bipyridine)ruthenium, $[\text{Ru}(\text{bpy})_3]^{2+}$ were determined to be +1.29 V vs SCE and +0.77 V vs SCE, respectively.¹¹⁻¹² From cyclic voltammetry analysis, the reduction potential for $E^{\text{III/II}}$ of our newly synthesized $\text{Co}(\text{dmgH})_2(4\text{MeCO}_2\text{Py})\text{Br}$ complex (**IV**) was found to be -1.05 V vs SCE. The oxidation potential for $E^{\text{III/II*}}$ of $[\text{Ru}(\text{bpy})_3]^{2+}$ were reported as -0.81 V vs SCE.¹² By comparing the electrode potential of the compounds, we believe that the excited state of $^*[\text{Ru}(\text{bpy})_3]^{2+}$ could reduce Co^{III} via single electron transfer (SET) while the 2-MeTHQ **1a** could reduce the $[\text{Ru}(\text{bpy})_3]^{3+}$ with one electron transfer and thus, the catalytic cycle follows the oxidative quenching mechanism (Scheme 3.5 and Scheme 3.6).

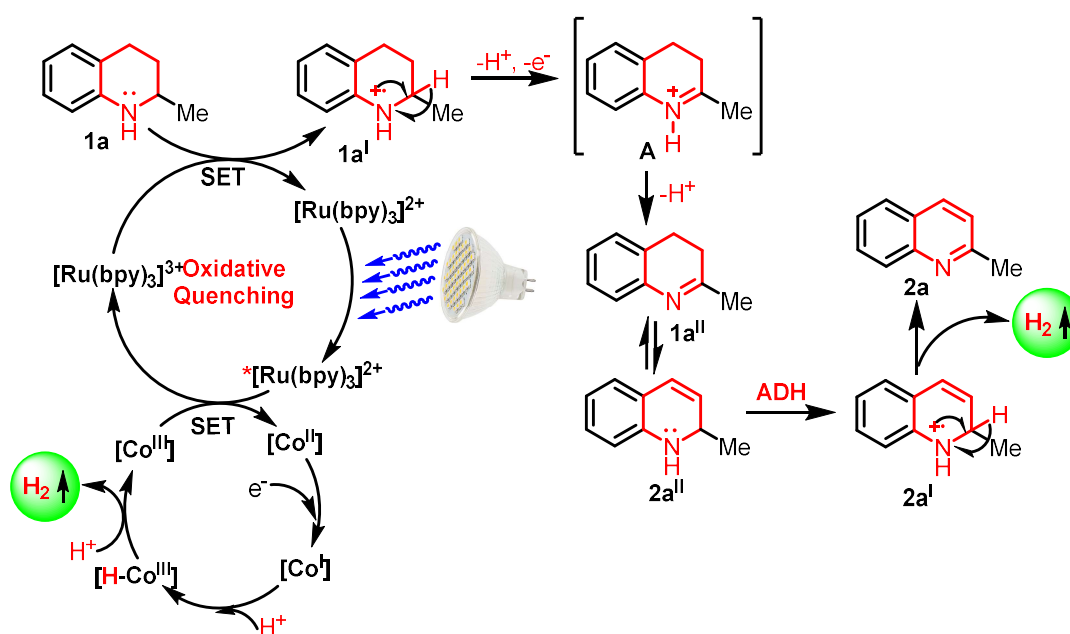


Scheme 3.5. Electron transfer between catalysts and substrate.

(A) Visible-light irradiation on $[\text{Ru}(\text{bpy})_3]^{2+}$. (B) Electron excitation from ^0S to ^1T of $[\text{Ru}(\text{bpy})_3]^{2+}$. (C) One electron reduction of Co^{3+} by $^*[\text{Ru}(\text{bpy})_3]^{2+}$. (D) One electron oxidation of the substrate by $[\text{Ru}(\text{bpy})_3]^{3+}$.

3.5.4. Plausible Mechanism

Based on the literature precedents,^{7-8,12-13} and experimental observation, we propose the following plausible mechanism for the dual ADH reaction of **1a** (Scheme 3.6). Upon visible-light irradiation, the $[\text{Ru}(\text{bpy})_3]^{2+}$ generates highly reactive triplet excited state $^*[\text{Ru}(\text{bpy})_3]^{2+}$ which can reduce Co^{III} to Co^{II} via a SET through oxidative quenching pathway, and to lead to $[\text{Ru}(\text{bpy})_3]^{3+}$. The $[\text{Ru}(\text{bpy})_3]^{3+}$ acts as a potent oxidant, and reduced by **1a** to regenerate $[\text{Ru}(\text{bpy})_3]^{2+}$, and with the formation of an amine radical cation **1a'**. This amine radical cation undergoes further one electron oxidation by Co^{II} to provide highly reducing Co^{I} and intermediate **1a''** with subsequent releases two protons. The formed Co^{I} -species immediately reacts with a proton to give $\text{Co}^{\text{III}}\text{-H}$, which can react further with a second proton, and thus releasing a molecule of H_2 and Co^{III} . However, at this stage, the $\text{Co}^{\text{III}}\text{-H}$ may undergo single electron reduction to $\text{Co}^{\text{II}}\text{-H}$ followed by protonation to release an H_2 molecule and Co^{II} . The homolytic cleavage involving two $\text{Co}^{\text{III}}\text{-H}$ to evolve H_2 could also not be ruled out.¹⁴ The intermediate **1a''** can isomerize to give intermediate **2a''**. Finally, the product **2a** is formed from intermediate **2a''** with repetition of the above catalytic cycles via the formation of amine radical cation **2a'**, to give the complete dehydrogenated product **2a**. To support our hypothesis, we have separately synthesized **1a''** and **2a''** and subjected to dual catalytic conditions and indeed, both the substrates offered the dehydrogenated product **2a** in excellent yield.



Scheme 3.6. A plausible mechanism for acceptorless dehydrogenation of **1a**.

3.6. Conclusion

In summary, an expedient strategy for the catalytic non-oxidative dehydrogenation of partially saturated *N*-heterocycles with H₂ evolution under oxidant-free conditions using water as solvent is reported. This acceptorless dehydrogenation reaction enabled by merging a photoredox catalyst with a newly synthesized proton reduction catalyst and operates at room temperature. The present atom-economic and sustainable catalytic approach is successfully applied for the synthesis of various *N*-heterocyclic arenes such as quinoline, quinoxaline, acridine, and indole derivatives.

3.7. Experimental Section

3.7.1. Synthesis of Proton Reduction Catalysts

The Co-dimethylglyoxime proton reduction catalysts were synthesized according to the procedure given below.

3.7.1a. Synthesis of dihalo(dimethylglyoxime)(dimethylglyoximato)cobalt(III)

To a 50 mL round-bottomed flask, 25 mL of acetone (AR grade), 10 mmol of dimethylglyoxime and 5.2 mmol of CoCl₂·6H₂O (CoBr₂·nH₂O) was taken and stirred for 1h at room temperature with oxygen purging from a balloon. After 1h, the reaction mixture was kept at -10 °C for 6 h and the precipitate was filtered, washed with cold acetone (2 x 10 mL) and air-dried to give green solid (quantitative yield). The spectroscopic analysis is consistent with the reported compound.

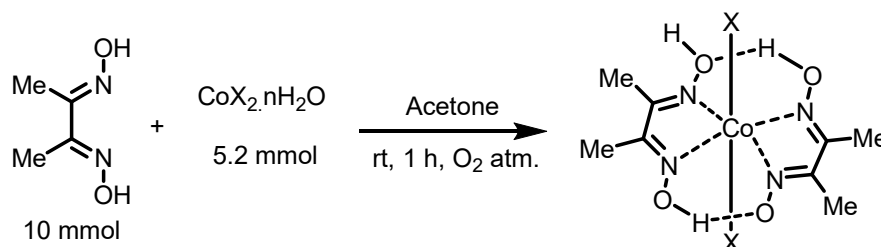


Figure 3.7. Synthesis of Co(dmgh)(dmgh₂)X₂

3.7.1b. Synthesis of halo-L-bis(dimethylglyoximate)cobalt(III)

To a suspension of dihalo(dimethylglyoxime)(dimethylglyoximate)cobalt(III), (2.5 mmol) in 50 mL of MeOH, 2.5 mmol of triethylamine was added at room temperature. The mixture was allowed to stir for 30 min till the colour of mixture turned from green to a clear dark brown solution. Then to the solution, one equivalent of pyridine (4-MeCO₂Py) was added and was allowed to stir for further 1h. After 1h, the reaction mixture was kept at -10 °C for 6h and the precipitate was filtered, washed with cold methanol (2 x 10 mL) followed by 10 mL water and the obtained brown solid was air dried. The complexes were characterized by ¹H, ¹³C-NMR and HRMS.

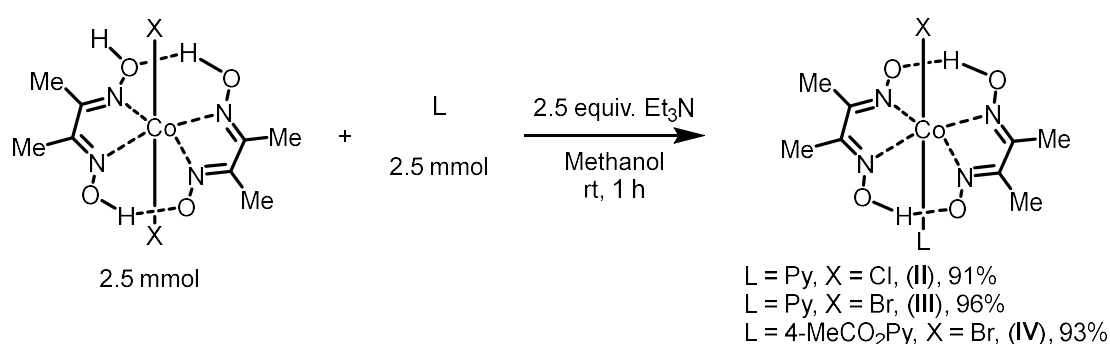


Figure 3.8. Synthesis of Co(dmgh)₂LX.

3.7.2. General Procedure for Catalytic ADH of *N*-heterocycles

In an oven-dried 20 mL headspace vial with a magnetic stirring bar was charged with **1** or **3** (0.25 mmol), Ru(bpy)₃Cl₂·6H₂O (1 mol %), Co(dmgh)₂(4-MeCO₂Py)Cl (**IV**) (2.5 mol %), and 8.0 mL of degassed mili-Q water (degassed by bubbling argon for 30 minutes) under argon atmosphere. The headspace vial was sealed with a Teflon/PTFE cap, and then the reaction vial was placed on a magnetic stirrer with blue LED light bulbs strips (36 W) kept about 3 cm away from it and irradiated at room temperature with constant stirring. A cooling fan was used to maintain the reaction temperature. The residue was purified by column chromatography on silica gel with a mixture of petroleum ether and EtOAc to afford the desired product **2** or **4**.

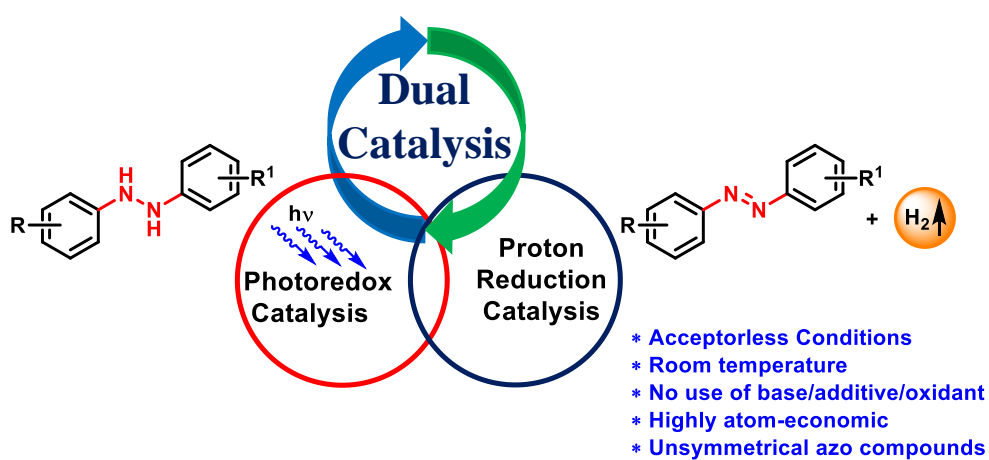
3.8. References

1. (a) Arpe, H. J. *Industrial Organic Chemistry*, Wiley-VCH, Weinheim **2010**. (b) Ahmed, M. S.; Mannel, D. S.; Root, T. W.; Stahl, S. S. *Org. Process Res. Dev.* **2017**, *21*, 1388-1393.
2. (a) Gorgas, N.; Kirchner, K. *Acc. Chem. Res.* **2018**, *51*, 1558-1569. (b) Sordakis, K.; Tang, C.; Vogt, L. K.; Junge, H.; Dyson, P. J.; Beller, M.; Laurenczy, G. *Chem. Rev.* **2018**, *118*, 372-433. (c) Filonenko, G. A.; van Putten, R.; Hensen, E. J. M.; Pidko, E. A. *Chem. Soc. Rev.* **2018**, *47*, 1459-1483. (d) Crabtree, R. H. *Chem. Rev.* **2017**, *117*, 9228-9246. (e) Balaraman, E.; Nandakumar, A.; Jaiswal, G.; Sahoo, M. K. *Catal. Sci. Technol.* **2017**, *7*, 3177-3195. (f) Kumar, A.; Bhatti, T. M.; Goldman, A. S. *Chem. Rev.* **2017**, *117*, 12357-12384. (g) Thoi, V. S.; Sun, Y.; Long J. R.; Chang, C. J. *Chem. Soc. Rev.* **2013**, *42*, 2388-2400. (h) Gunanathan, C.; Milstein, D. *Science* **2013**, *341*, 1229712. (i) Dobereiner, G. E.; Crabtree, R. H. *Chem. Rev.* **2010**, *110*, 681-703. (j) Buckle, D. R. *Encyclopedia of Reagents for Organic Synthesis*; John Wiley & Sons, Inc.: New York, **2010**.
3. (a) Clot, E.; Eisenstein, O.; Crabtree, R. H. *Chem. Commun.* **2007**, 2231-2233. (b) Crabtree, R. H. *Energy Environ. Sci.* **2008**, *1*, 134-138. (c) Cui, Y.; Kwok, S.; Bucholtz, A.; Davis, B.; Whitney, R. A.; Jessop, P. G. *New J. Chem.* **2008**, *32*, 1027-1037. (d) Jessop, P. *Nat. Chem.* **2009**, *1*, 350-351.
4. (a) Süzen, S. *Bioactive Heterocycles V*, Springer **2007**, 145. (b) Vitaku, E.; Smith, D. T.; Njardarson, J. T. *J. Med. Chem.* **2014**, *57*, 10257-10274.
5. (a) Teichmann, D.; Arlt, W.; Wasserscheid, P.; Freymann, R. *Energy Environ. Sci.* **2011**, *4*, 2767-2773. (b) Klebanoff, L. *Hydrogen Storage Technology: Materials and Applications*, 1st ed., Taylor and Francis **2012**, pp. 287-328. (c) Preuster, P.; Papp, C.; Wasserscheid, P. *Acc. Chem. Res.* **2017**, *50*, 74-85. (d) Zhu, Q.-L.; Xu, Q. *Energy Environ. Sci.* **2015**, *8*, 478-512. (e) Eberle, U.; Felderhoff, M.; Schüth, F. *Angew. Chem., Int. Ed.* **2009**, *48*, 6608-6630.
6. (a) Yamaguchi, R.; Ikeda, C.; Takahashi, Y.; Fujita, K.-i. *J. Am. Chem. Soc.* **2009**, *131*, 8410-8412. (b) Wu, J.; Talwar, D.; Johnston, S.; Yan, M.; Xiao, J. *Angew. Chem., Int. Ed.* **2013**, *52*, 6983-6987. (c) Fujita, K.-i.; Tanaka, Y.; Kobayashi, M.; Yamaguchi, R. *J. Am. Chem. Soc.* **2014**, *136*, 4829-4832. (d) Chakraborty, S.; Brennessel, W. W.; Jones, W. D. *J. Am. Chem. Soc.* **2014**, *136*, 8564-8567. (e) Manas, M. G.; Sharninghausen, L. S.; Lin, E.; Crabtree, R. H. *J. Organomet. Chem.* **2015**, *792*, 184-189. (f) Xu, R.; Chakraborty, S.; Yuan, H.; Jones, W. D. *ACS Catal.* **2015**, *5*, 6350-6354. (g) Talwar, D.; Gonzalez-de-

- Castro, A.; Li, H. Y.; Xiao, J. *Angew. Chem., Int. Ed.* **2015**, *54*, 5223-5227. (h) Kojima, M.; Kanai, M. *Angew. Chem., Int. Ed.* **2016**, *55*, 12224-12227. (i) Forberg, D.; Schwob, T.; Zaheer, M.; Friedrich, M.; Miyajima, N.; Kempe, R. *Nat. Commun.* **2016**, *7*, 13201-13206. (j) Moromi, S. K.; Siddiki, S. M. A. H.; Kon, K.; Toyao, T.; Shimizu, K.-i. *Catal. Today* **2017**, *281*, 507-511. (k) Jaiswal, G.; Landge, V.; Jagadeesan, D.; Balaraman, E. *Nature Commun.* **2017**, *8*, 2147.
7. (a) Chen, S.; Wan, Q.; Badu-Tawiah, A. K. *Angew. Chem., Int. Ed.* **2016**, *55*, 9345-9349. (b) Kato, S.; Saga, Y.; Kojima, M.; Fuse, H.; Matsunaga, S.; Fukatsu, A.; Kondo, M.; Masaoka, S.; Kanai, M. *J. Am. Chem. Soc.* **2017**, *139*, 2204-2207. (c) Sahoo, M. K.; Jaiswal, G.; Rana, J.; Balaraman, E. *Chem. -Eur. J.* **2017**, *23*, 14167-14172. (d) Zheng, M.; Shi, J.; Yuan, T.; Wang, X. *Angew. Chem., Int. Ed.* **2018**, *57*, 5487-5491.
8. (a) Zhang, G.; Liu, C.; Yi, H.; Meng, Q.; Bian, C.; Chen, H.; Jian, J.-X.; Wu, L.-Z.; Lei, A. *J. Am. Chem. Soc.* **2015**, *137*, 9273-9276. (b) Wu, C.-J.; Meng, Q.-Y.; Lei, T.; Zhong, J.-J.; Liu, W.-Q.; Zhao, L.-M.; Li, Z.-J.; Chen, B.; Tung, C.-H.; Wu, L.-Z. *ACS Catal.* **2016**, *6*, 4635-4639. (c) Zheng, Y.-W.; Chen, B.; Ye, P.; Feng, K.; Wang, W.; Meng, Q.-Y.; Wu, L.-Z.; Tung, C.-H. *J. Am. Chem. Soc.* **2016**, *138*, 10080-10083. (d) Zheng, Y.-W.; Ye, P.; Chen, B.; Meng, Q.-Y.; Feng, K.; Wang, W.; Wu, L.-Z.; Tung, C.-H. *Org. Lett.* **2017**, *19*, 2206-2209.
9. He, K.-H.; Tan, F.-F.; Zhou, C.-Z.; Zhou, G.-J.; Yang, X.-L.; Li, Y. *Angew. Chem., Int. Ed.* **2017**, *129*, 3080-3084.
10. Zhang, M.-Z.; Chen, Q.; Yang, G.-F. *Eur. J. Med. Chem.* **2015**, *89*, 421-441.
11. Bock, C. R.; Connor, J. A.; Gutierrez, A. R.; Meyer, T. J.; Whitten, D. G.; Sullivan, B. P.; Nagle, J. K. *J. Am. Chem. Soc.* **1979**, *101*, 4815-4824.
12. (a) Prier, C. K.; Rankic, D. A.; MacMillan, D. W. C. *Chem. Rev.* **2013**, *113*, 5322-5363. (b) Xi, Y.; Yi, H.; Lei, A. *Org. Biomol. Chem.* **2013**, *11*, 2387-2403. (c) Schultz, D. M.; Yoon, T. P. *Science* **2014**, *343*, 985.
13. (a) Hopkinson, M. N.; Sahoo, B.; Li, J.-L.; Glorius, F. *Chem. Eur. J.* **2014**, *20*, 3874-3886. (b) Tóth, B. L.; Tischler, O.; Novák, Z. *Tetrahedron Lett.* **2016**, *57*, 4505-4513. (c) Skubi, K. L.; Blum, T. R.; Yoon, T. P. *Chem. Rev.* **2016**, *116*, 10035-10074.
14. Dempsey, J. L.; Brunschwig, B. S.; Winkler, J. R.; Gray, H. B. *Acc. Chem. Res.* **2009**, *42*, 1995-2004.
15. (a) Schrauzer, G. N. *Inorg. Synth.* **1968**, *11*, 61-70. (b) Du, P.; Schneider, J.; Luo, G.; Brennessel, W.W.; Eisenberg, R. *Inorg. Chem.* **2009**, *48*, 4952-4962.

Chapter 4

Visible-light Photocatalyzed Acceptorless Dehydrogenation of Diaryl Hydrazines



Sahoo *et al.*; *ACS Catal.* **2018**, *8*, 7727-7733.

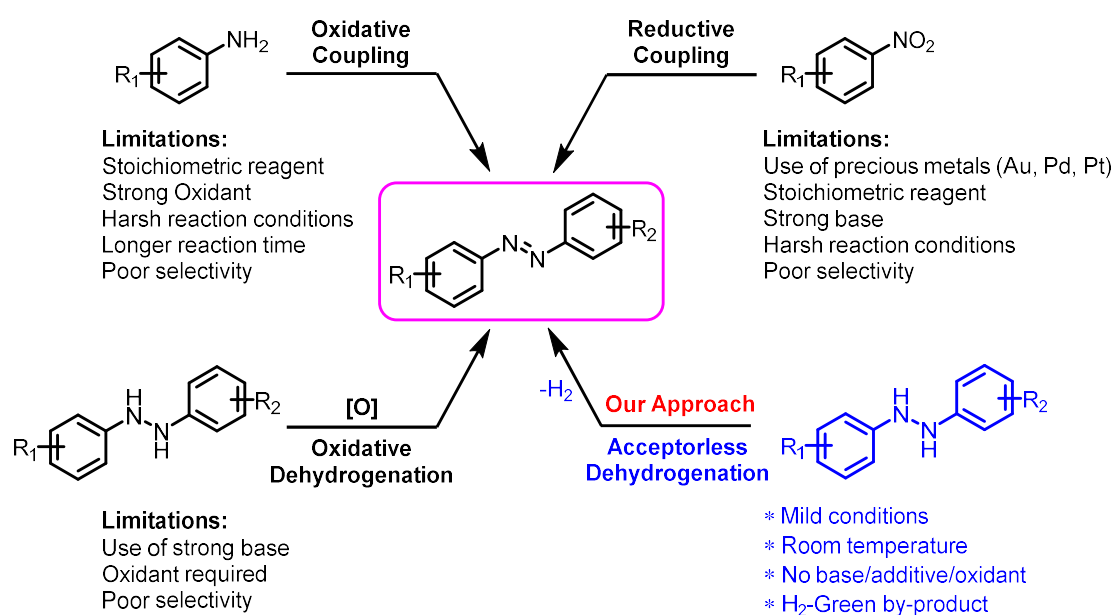
4.1. Introduction

Aromatic compounds with the N=N motifs are privileged structural compounds as they show myriad applications¹⁻⁶ in dyes and pigment industry,¹ therapeutic agents,² photo-responsive switches and chemosensors, polymers, soft materials, radical initiators, bioactive ligands, and food additives.³⁻⁶ In recent times, several methods have been reported for the synthesis of aromatic azo derivatives (Scheme 4.1).⁷⁻¹¹ These methods include oxidative dehydrogenative couplings of anilines,⁷ reductive coupling of aromatic nitro compounds,⁸ the coupling of aromatic compounds with aryl diazonium salts,⁹ and Mills reaction.¹⁰ There are few reports on direct oxidative dehydrogenation (ODH) of hydrazobenzene derivatives to azobenzenes.¹¹⁻¹² These synthetic methods suffer from harsh reaction conditions such as high catalyst loading, need of stoichiometric reagents, strong oxidants or additives and thus, generate an equivalent amount of waste.

Jiao and co-workers reported a Cu-catalyzed oxidative dehydrogenation of anilines^{7d} to azobenzenes using air as the oxidant. Notably, due to the competing self-coupling of anilines, the unsymmetrical azo compounds were obtained in poor yields. Of late, Suib and his group reported the synthesis of symmetrical azobenzene derivatives by oxidative dehydrogenation of anilines using *meso*-Mn₂O₃.^{7e} The reaction operates at elevated temperature with very high catalyst loading. Very recently, Lin and co-workers reported a method to prepare azo compounds by oxidative dehydrogenation of anilines using a stoichiometric amount of NBS and DBU under cryogenic conditions.^{7a} Ma and co-workers described the synthesis of diaryl hydrazines using heterogeneous graphene oxide system with high catalyst loading (10 weight%) under oxidative conditions.^{11c} Gozin and co-workers reported oxidative dehydrogenation of hydrazobenzene using the toxic TiCl₃/HBr system.^{11e} Of late, Hashimoto and co-workers reported oxidative dehydrogenation of hydrazobenzene using strong base (KO^tBu).^{11a} Although this method has a broad substrate scope, the use of liquid NH₃ as solvent medium and strong base limited the practical applicability of the reaction.

In recent times, catalytic dehydrogenation of organic molecules with the liberation of molecular hydrogen is one of the most important key reactions in contemporary science.¹³ The catalytic acceptorless dehydrogenation reactions (ADH) obviate the requirement of external oxidants and produce less toxic waste. The ADH method with the liberation of hydrogen gas is much superior over the classical oxidative dehydrogenation methods in

view of atom-economy, and environmental sustainability.¹⁴ Removal of hydrogen atoms from adjacent atomic centers of an organic molecule is a thermodynamically uphill process; however, recent experimental and computational studies showed that the presence of nitrogen atom makes the removal of hydrogen atom more easier.¹⁵ In our previous chapter, we have shown ADH of partially saturated *N*-heterocyclic compounds under dual catalytic conditions by merging visible-light photo-active $[\text{Ru}(\text{bpy})_3]^{2+}$ catalysis and Co-based proton reduction catalysis. In this chapter, we have extended our previous work and report ADH of hydrazobenzene derivatives under dual catalytic conditions. This unprecedented reaction operates under very mild, benign conditions and room temperature. A consequence of this finding with only molecular hydrogen as the byproduct makes this process more eco-benign and sustainable for the effective synthesis of a wide range of aromatic azo compounds for various applications. Interestingly, we have also developed a catalytic method for efficient hydrogenation of azobenzenes to hydrazobenzenes using H_2 gas to demonstrate the reversible hydrogen storage/release phenomenon on this system (Figure 4.1).



Scheme 4.1. Previous reports on catalytic approaches to the synthesis of azobenzene derivatives.

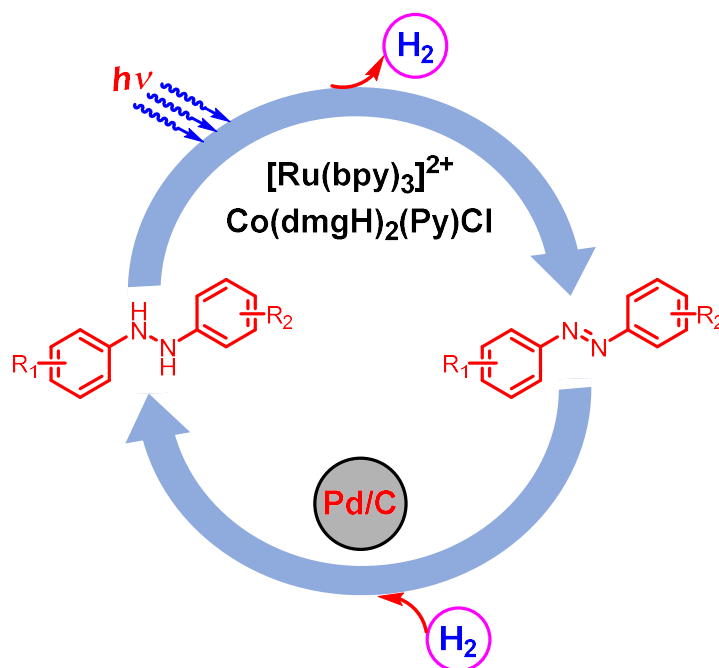


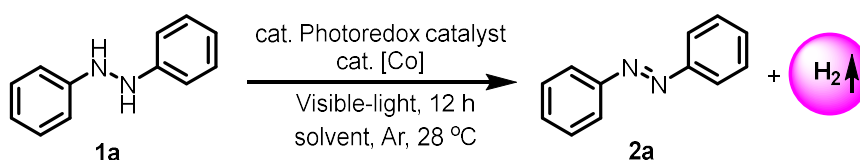
Figure 4.1. Reversible hydrogen storage and release phenomenon on azobenzene/hydrazobenzene couple.

4.2. Statement of the Problem

Aromatic azo compounds are privileged structural motifs as they show myriad pharmaceutical as well as industrial applications. Therefore numerous research has been dedicated to the synthesis of these azo compounds. However, the current literature precedents lack the sustainability due to harsh reaction conditions such as the use of a quantitative amount of oxidant, base, additive or need of high catalyst loading. Hence, development of an efficient catalytic method is essential for the synthesis of varieties of azobenzenes. In this chapter, we report a dual catalytic approach for the acceptorless dehydrogenation of hydrazobenzenes to the corresponding azobenzenes. This dual catalytic activity has been achieved by merging visible-light active $[\text{Ru}(\text{bpy})_3]^{2+}$ as photoredox catalyst with a catalytic amount of $\text{Co}(\text{dmgH})_2(\text{Py})\text{Cl}$ as proton reduction catalyst. The current method operates under very mild, benign conditions and has a wide substrate scope as well as broad functional group tolerance.

4.3. Reaction Optimization

4.3.1. Optimization Table

Table 4.1. Optimization of the reaction conditions.^a

Entry	[Co] source	Photoredox catalyst	Solvent	Yield (%) ^b
1	III	[Ru(bpy) ₃]Cl ₂	EtOH	93 ^c
2	III	[Ru(bpy) ₃][PF ₆] ₂	EtOH	95 ^[c]
3	III	Eosin Y	EtOH	trace
4	III	Rose bengal	EtOH	trace
5	I	[Ru(bpy) ₃]Cl ₂	EtOH	36
6	II	[Ru(bpy) ₃]Cl ₂	EtOH	42
7	III	[Ru(bpy) ₃]Cl ₂	MeOH	89 ^c
8	III	[Ru(bpy) ₃]Cl ₂	MeCN	0
9	---	[Ru(bpy) ₃]Cl ₂	EtOH	0
10	III	---	EtOH	0
11	III	[Ru(bpy) ₃]Cl ₂	EtOH	0 ^d
12	III	[Ru(bpy) ₃]Cl ₂	EtOH	69 ^e

^aGeneral reaction conditions: Substrate **1a** (0.25 mmol), photoredox catalyst (1.0 mol%), proton-reduction (**I-III**) catalyst (2.0 mol%), solvent 2.5 mL, 28 °C, visible-light, 12 h.

^bBased on ¹H NMR yield. ^cIsolated yield. ^dDark conditions. ^e0.5 mol% of photoredox catalyst.

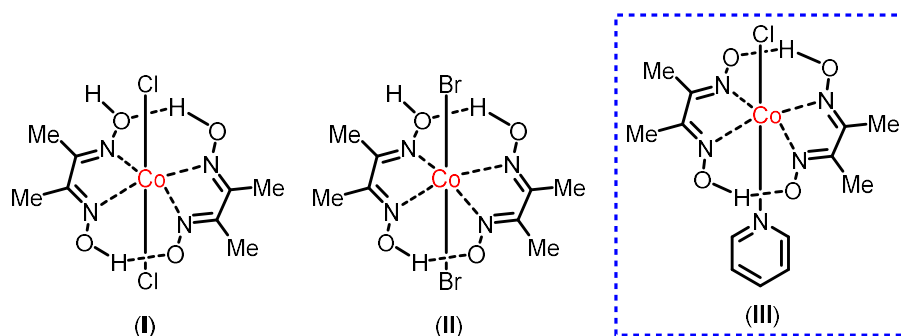


Figure 4.2. Co-glyoxime based proton reduction catalysts used for the present study.

We began optimization of the ADH reaction using diphenyl hydrazine **1a** as a model substrate. We screened a number of photoredox catalysts merged with different proton reduction catalysts (**I-III**) in various solvent systems (Table 4.1). We found that 1 mol% of photoredox catalyst, 2.0 mol % of Co-based proton reduction catalyst, in 0.1 M ethanol gave the desired dehydrogenated azobenzene **2a** in 93% isolated yield (Table 4.1, entry 1). Among the various photoredox catalysts, $[\text{Ru}(\text{bpy})_3]^{2+}$ catalyst was found to be optimal for this reaction (Table 4.1, entries 1-4). Similarly, $\text{Co}(\text{dmgH})_2(\text{py})\text{Cl}$ (**III**) proton reduction catalyst was found to give superior activity and gave the maximum yield of **2a** (Table 4.1, entries 1, 5-6). The liberated hydrogen gas was qualitatively analyzed by gas chromatography (GC-TCD) (Section 4.7.2). Among a number of solvents screened, EtOH was found to be the most suitable solvent for this ADH reaction (Table 4.1, entries 1, 7-8). A series of control experiments were carried out to show the necessity of each of the reaction components such as photoredox catalyst, proton reduction catalyst, and the light source (Table 4.1, entries 9-11). The product **2a** formation was not observed in the absence of either photoredox or proton reduction catalyst (Table 4.1, entries 9-10). Similarly, in the absence of the light source, no formation of **2a** was observed (Table 4.1, entry 11). Notably, reducing the photoredox catalyst loading to 0.5 mol% gave the desired product **2a** in moderate yield (Table 4.1, entry 12). Gratifyingly, this unprecedented catalytic ADH reaction proceeds very smoothly at ambient temperature under neutral conditions in presence of visible-light source with no generation of waste except hydrogen gas.

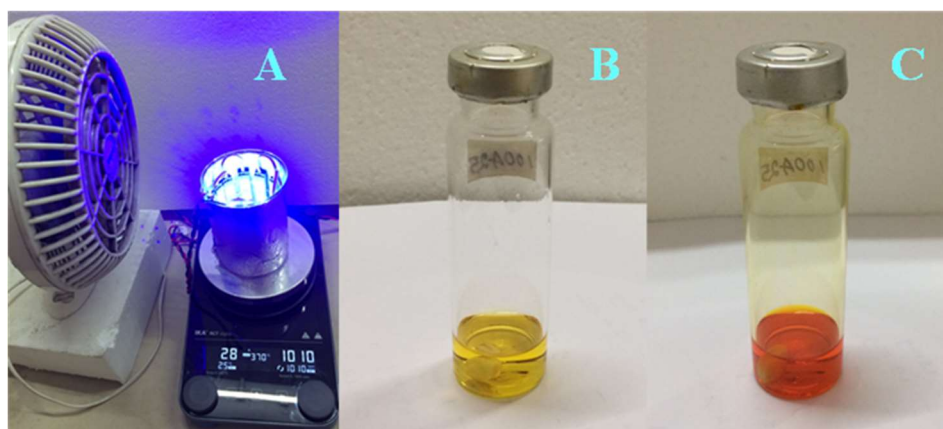


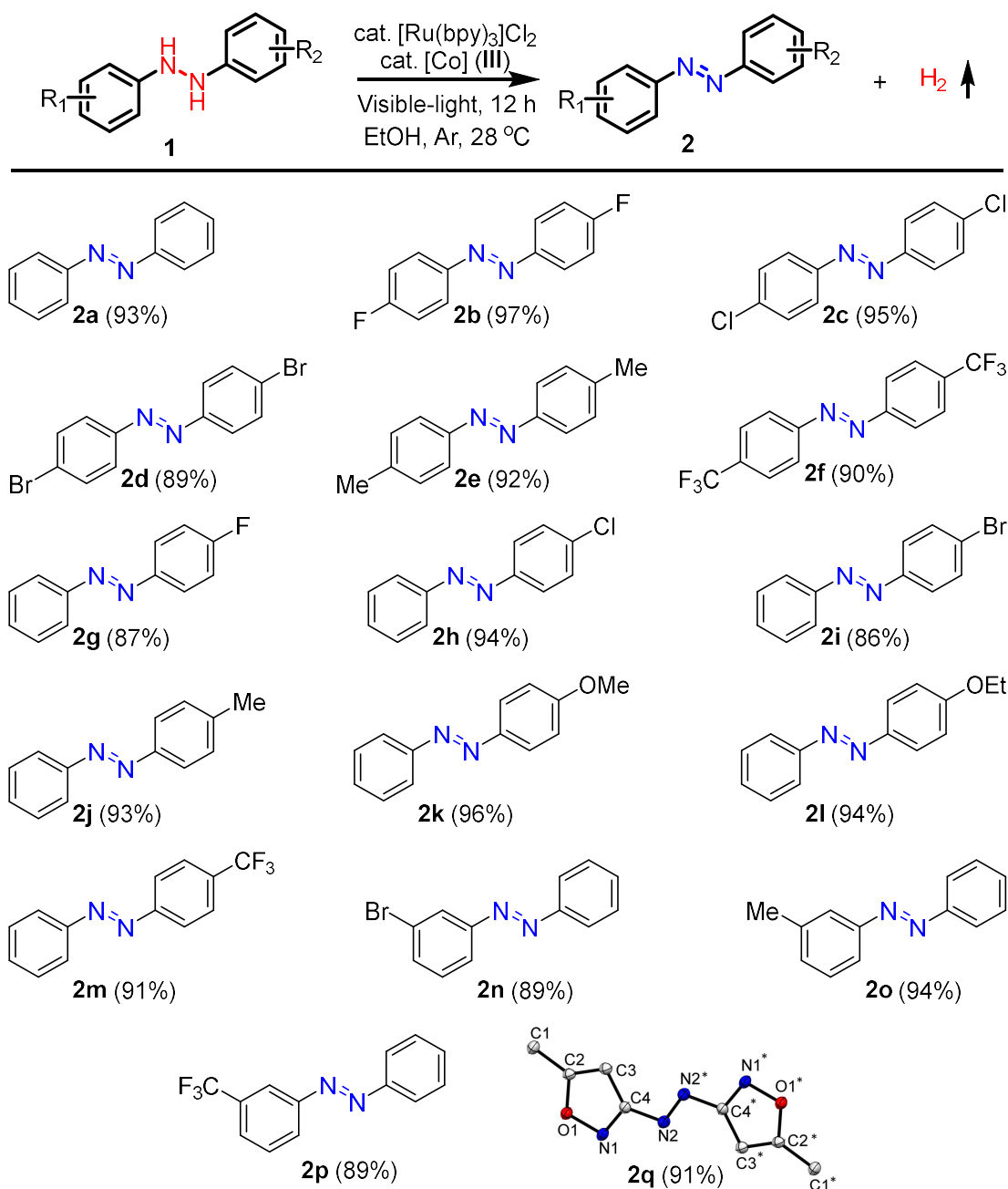
Figure 4.3. (A) Reaction Setup. (B) Reaction mixture before reaction. (C) Reaction mixture after visible-light irradiation for 12 h.

4.3.2. Substrate Scope

With the optimal reaction conditions in hand, several hydrazobenzene derivatives **1** were subjected to the ADH reaction in presence of [Ru(bpy)₃]Cl₂ (1 mol%), proton-reduction cobalt catalyst (**III**) (2 mol%) under visible-light irradiation in ethanol at room temperature. As shown in Table 4.2, the present ADH strategy shows a wide substrate scope and high functional-group tolerance and gives dehydrogenated azobenzene derivatives in good to excellent yields (up to 97%). Electron-donating as well as electron-withdrawing groups at different position in the phenyl ring of the hydrazobenzene derivatives did not affect the reactivity and yielded the corresponding dehydrogenated products (Table 4.2).

Among symmetrical hydrazobenzene derivatives, substrates bearing electron-withdrawing group at the *para* position of the phenyl ring, such as fluoro, chloro, bromo and trifluoromethyl proceeded smoothly to give the corresponding azobenzenes in 89%-97% isolated yields (products **2b-2d**, and **2f**) under the optimized conditions. Also, substrates with electron-donating groups such as *p*-methyl gave **2e** in 92% isolated yield. Like symmetrical hydrazobenzenes, unsymmetrically substituted hydrazobenzenes showed a similar trend in their reactivity. Thus, substrates with electron-withdrawing groups such as 4-F, 4-Cl, 4-Br, 4-CF₃, 3-Br, and 3-CF₃ were well tolerated and afforded the corresponding azobenzenes in good to excellent yields of 86% to 94% (Table 4.2, products **2g-2i**, **2m-2n**, and **2p**). The diaryl hydrazines with electron-donating groups such as 4-Me, 4-MeO, 4-EtO, and 3-Me were well tolerated and offered the corresponding dehydrogenated products in excellent yields (Table 4.2, products **2j-2l**, and **2o**). Similarly, a heterocyclic azo derivative was obtained with 91% isolated yield under the optimized condition (Table 4.2, product **2q**).

Table 4.2. Substrate scope for room temperature dual catalyzed ADH of hydrazobenzene.^{a-b}



^aReaction conditions: **1** (0.25 mmol), [Ru(bpy)₃]Cl₂ (1 mol%), Co-catalyst (**III**) (2 mol%), EtOH (2.5 mL), Ar atm., 36 W blue LED, 28 °C, 12 h. ^bIsolated yields.

Note: In single crystal X-ray structure of **2q**, for clarity hydrogen atoms are omitted.

4.4. Monitoring of Reaction Progress using UV-Visible Spectroscopy

The progress of the present ADH reaction was monitored by UV-Visible absorption spectroscopy (Figure 4.4). From UV-Visible absorption spectroscopic analysis, it is observed that the rate of the reaction decreases as the concentration of product (**2a**) increases. This is because azo products are typically absorbing in a visible range, and as more and more azo product is generated in the reaction mixture, it obscures the activity of the photocatalyst. The reaction kinetics was measured by applying the Beer Lambert's law. By UV-Visible absorption spectroscopic analysis, the concentration of azobenzene was measured at different time intervals of the reaction, and a plot was drawn between azobenzene yield *vs* time. This plot clearly shows that the rate of azobenzene formation decreases with increase in time.

At different time interval, a known volume of reaction mixture was withdrawn into a sample vial and was diluted with ethanol to adjust the concentration to 10^{-4} M. Then, the UV-Visible absorbance of the sample was measured which is given in plot **B**. The graph **C** represents the UV-Visible absorption spectra of azobenzene at different known concentrations. The plot **D** is a straight line and represents the plot between absorbance *vs* different known concentrations of azobenzene, and thus obeys the Beer Lambert's law. The plot **E** represents the plot between yields of azobenzene *vs* time. The yield of azobenzene was calculated from the equation,

$$y = mx + c$$

wherein, *y* is the absorbance of the reaction mixture at a different time interval, 'm' is the slope and 'c' is the intercept. The slope 'm' and intercept 'c' were obtained from plot **D**. From plot **E**, it is observed that the rate of the reaction decreases with time. Again at time 0 hour, the yield from UV-Visible absorbance was 30% which is because of the absorbance of the photoredox catalyst $[\text{Ru}(\text{bpy})_3]\text{Cl}_2$. After 12 h, the yield from UV-Visible absorbance was found to be 89%.

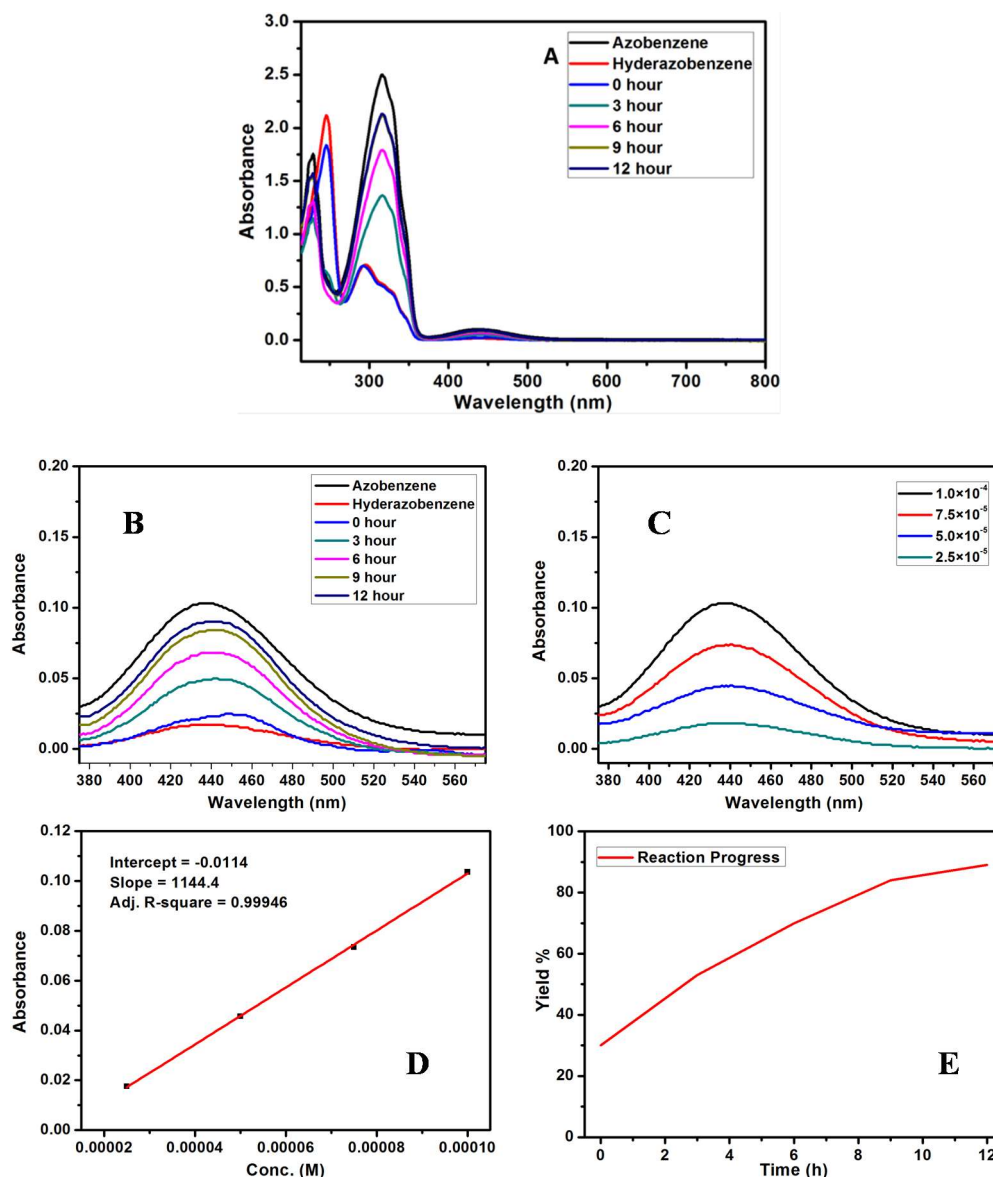


Figure 4.4. Plot A and B represent the UV-Visible absorption spectroscopy of the reaction mixture at different time intervals, while C represents absorbance at different known concentrations of azobenzene. The Plot D is absorbance vs known conc, and plot E represents the reaction progress with time calculated by measuring the UV-Visible spectra at different time interval

4.5. Azobenzene and Hydrazobenzene as LOHCs

In recent times, liquid organic hydrogen carriers (LOHCs) as efficient hydrogen storage have been paid much attention in contemporary science.^{15a-c,16-17} However, the viability of azobenzene as hydrogen storage system is only possible when both the dehydrogenation

of hydrazobenzenes and hydrogenation of azobenzenes become feasible under mild reaction conditions. Gratifyingly, the reversible hydrogen storage/release phenomenon on hydrazobenzene/azobenzene couple is successfully demonstrated. This is the first time we are showing that diazohydrazine can be used as LOHC, although it has poor % of hydrogen storage capacity. In this context, we have developed an efficient method for hydrogenation of azobenzene to hydrazobenzene under very mild conditions using a commercially available heterogeneous catalyst. The hydrogenation reaction was carried out using a catalytic amount of Pd/C (5 weight% of Pd) and a catalytic amount of pyridine as additive under 1 atmospheric pressure of hydrogen at ambient temperature (Table 4.3).

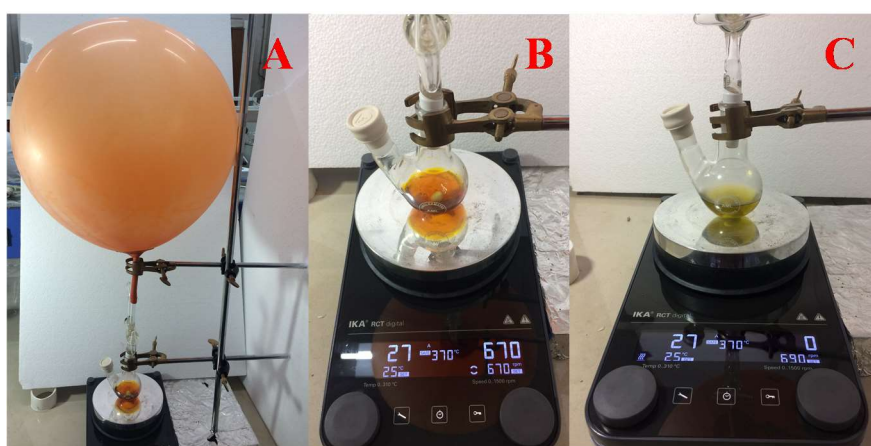
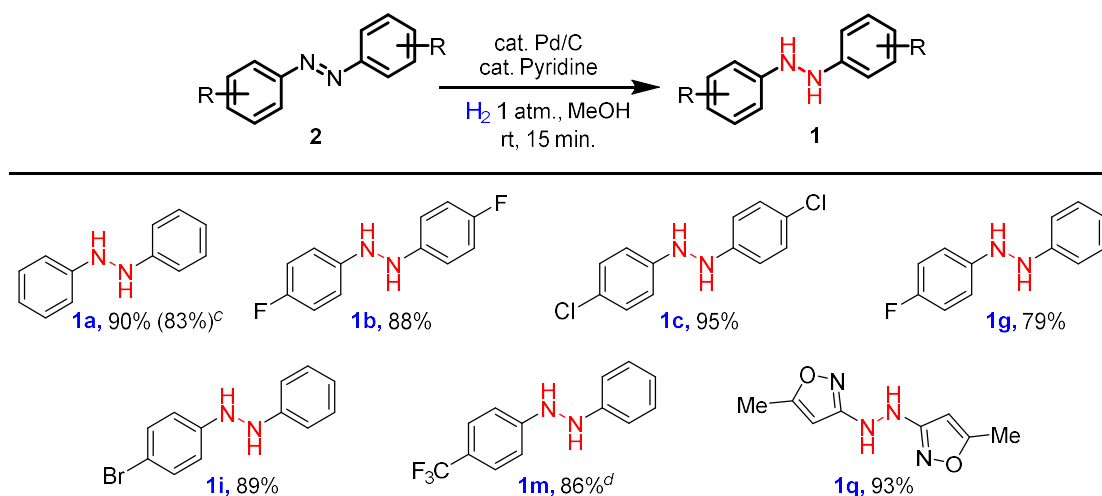


Figure 4.5. (A) Reaction setup for hydrogenation of azobenzene. (B) Reaction mixture before hydrogenation. (C) Reaction mixture after hydrogenation.

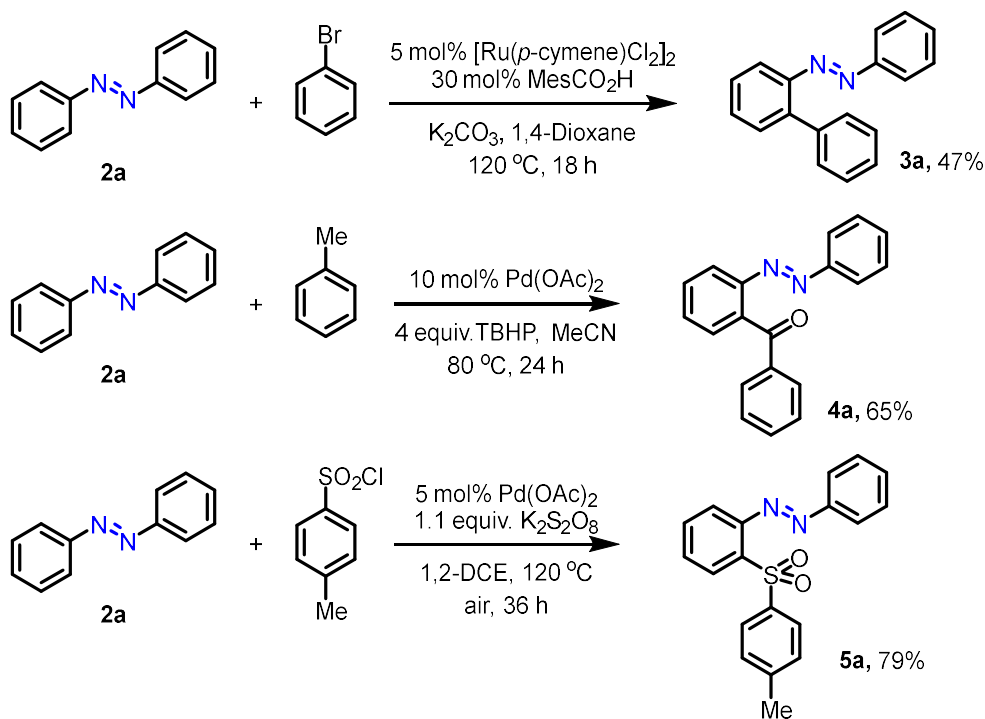
4.5.1. Substrate Scope

This catalytic hydrogenation of azobenzenes to corresponding hydrazobenzenes is a general process. This methodology was applied for hydrogenation of few substrates with different functional groups. Symmetrical azobenzenes with and without substituent group underwent hydrogenation smoothly and gave excellent isolated yields up to 95% (Table 4.3, entries **1a-1c**). Similarly, unsymmetrical substrates with electron withdrawing groups (-Cl, -Br, -CF₃) underwent hydrogenation to give yields up to 89% of corresponding hydrogenated product (Table 4.3, **1g, 1i, 1m**). Notable, heterocyclic azocompound underwent smooth hydrogenation to give **1q** in 93% isolated yield. Also, this hydrogenation strategy was used for the gram-scale synthesis of **1a** and give 83% isolated yield.

Table 4.3. Pd/C catalyzed hydrogenation of azobenzenes (substrate scope).^{a,b}

^aReaction conditions: **2a** (0.25 mmol), Pd/C (1.0 mg), pyridine (10 mol%), methanol (5.0 mL), 1 atm. H_2 , rt, 15 min. ^bIsolated yields. ^cGram-scale synthesis. ^dReaction continued for 30 min.

4.6. Derivatization of Azobenzene

**Scheme 4.2.** Diversification of azobenzene derivatives.

Next, we have shown the diversification of azobenzene (acts as a good directing group¹⁸ in the C-H bond activation chemistry) and illustrated in Scheme 4.2. The Ru-catalyzed *ortho* C-H bond arylation of azobenzene gave **3a** in 47% isolated yield.^{18a} Similarly, Pd-catalyzed *ortho*-C-H bond acylation was achieved using toluene as the acyl equivalent and TBHP as the oxidant gave **4a** in 65% isolated yield.^{18b} The Pd-catalyzed *ortho*-C-H bond sulfonylation of azobenzene (**2a**) proceeded smoothly in the presence of catalytic amount of Pd(OAc)₂ and K₂S₂O₈ as the oxidant yielding **5a** in 79% isolated yields.^{18c}

4.7. Cis-trans Isomerization upon UV-light Irradiation

For two of the azo compounds, the UV-Visible spectra were recorded before and after UV exposure in hexane solvent. The UV-exposure was given for 10 min by Omni Cure 2000 lamp with 100% of its power. Immediately after UV-exposure and after a certain time interval, the UV-Vis spectra were recorded. During this experiment, we observed a slight color change of these azo compounds upon UV exposure (for 10 min), but it was not possible to distinguish the difference in the photograph (snapshot).

Significant changes in the UV-Visible spectra's of the azo compound was observed between before UV light irradiation and after irradiation, which is due cis-trans isomerization around N=N double bond (Figure 4.7).

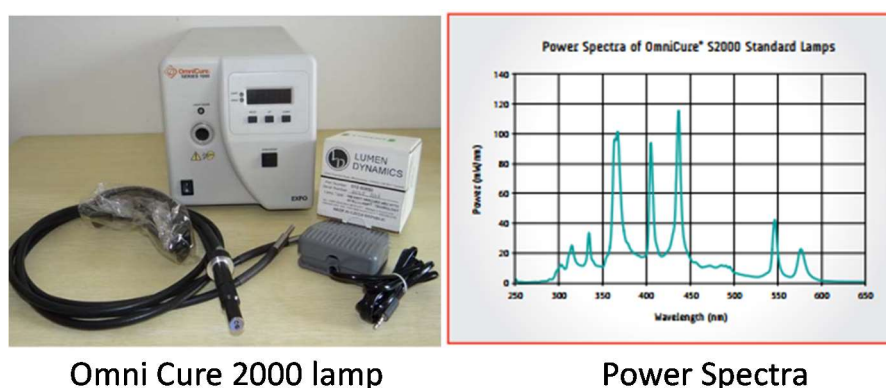


Figure 4.6. Omni Cure 2000 lamp and its power spectra.

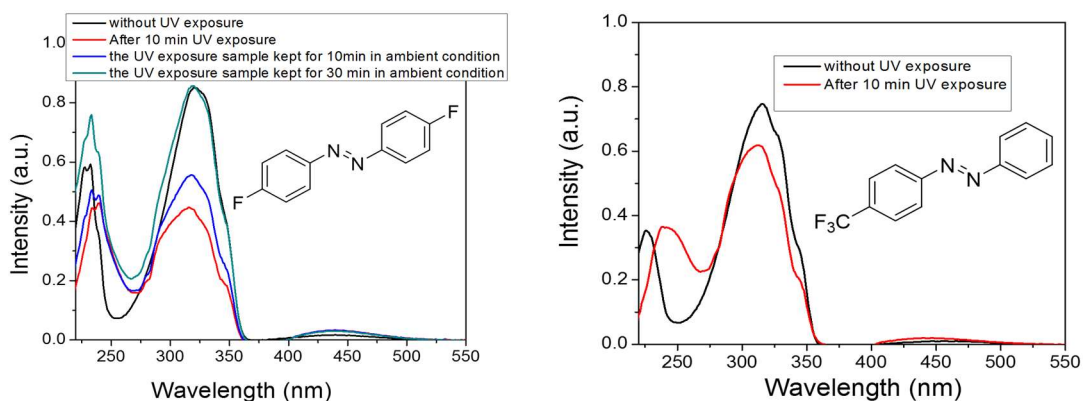


Figure 4.7. Comparison between UV-Visible spectra of azo compounds before UV light irradiation and after UV light irradiation.

4.8. Mechanistic Investigation

4.8.1. Cyclic Voltammetry Experiment

In order to get insight into the oxidation potential of the hydrazobenzene derivatives, cyclic voltammetry was recorded for two of the compounds **1a** and **1c**. The cyclic voltammetry was measured at 10 mV s^{-1} scan rate using Ag/AgCl as reference electrode, Pt wire as counter electrode and a glassy carbon electrode as working electrode in anhydrous acetonitrile with 0.1 M tetrabutylammonium perchlorate as supporting electrolyte. The oxidation potential for compounds **1a** and **1c** was found to be 0.58 V vs SCE and 0.66 V vs SCE respectively.

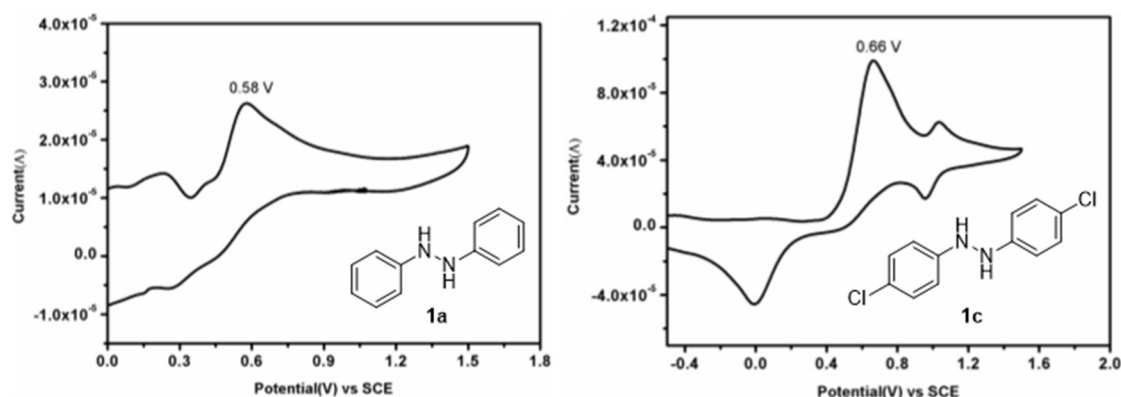


Figure 4.8. Oxidation potential measured for hydrazobenzenes using CV technique.

4.8.2. Hydrogen Gas Detection in GC

The hydrogen gas evolved during the photocatalytic acceptorless dehydrogenation hydrazobenzene was qualitatively detected in GC as shown in Figure 4.9.

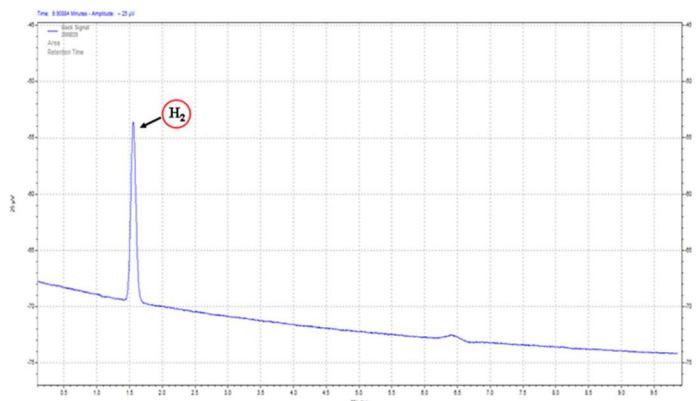
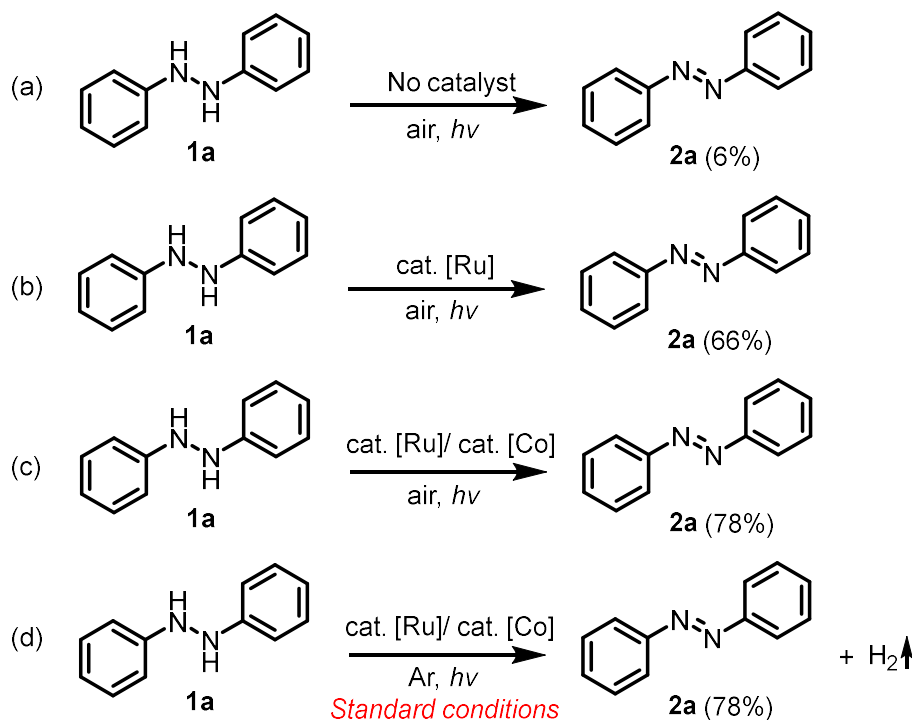


Figure 4.9. Qualitative hydrogen gas detection in GC.

4.8.3. Control Experiments

To better understand the reaction mechanism, a series of control experiments were carried out. In the absence of the catalysts or under the dark conditions, no formation of product was observed. This clearly confirms that all the key reaction components are essential for the success of the present ADH reaction. When the reaction was carried out in the air upon visible-light irradiation (in the absence of both photoredox and proton reduction catalyst), a trace amount of **2a** was detected. Similarly, when the reaction was carried out in the air only in presence of the photoredox catalyst (i.e. in absence of proton reduction Co-catalyst), upon visible-light irradiation, 66% yield of **2a** was formed. Performing the reaction under standard conditions under air, 78% yield of **2a** was obtained. However, in all the cases there is no formation of hydrogen gas was observed on GC. These results showed that the product formation is due to purely by oxidative dehydrogenation and not *via* acceptorless dehydrogenation.¹¹⁻¹² Cyclic voltammetry experiment of **1a** and **1c** shows the oxidation potential of the two compounds are +0.58 V *vs* SCE, and +0.66 V *vs* SCE, respectively (Figure 4.8). The reduction potentials $E^{\text{III/II}}$ and $E^{\text{II}^*/\text{I}}$ of tris(2,2'-bipyridine)ruthenium, $[\text{Ru}(\text{bpy})_3]^{+2}$ were determined to be +1.29 V *vs* SCE, and +0.77 V *vs* SCE, respectively.¹⁹ The reduction potential $E^{\text{III/II}}$ (**III**) of $\text{Co}(\text{dmgH})_2(\text{py})\text{Cl}$ and the oxidation potential $E^{\text{III/II}^*}$ of $[\text{Ru}(\text{bpy})_3]^{+2}$ were reported as -0.67 V *vs* SCE,²⁰ and -0.81 V

vs SCE, respectively.¹⁹ Thus, it is expected that the excited state of $^*[\text{Ru}(\text{bpy})_3]^{2+}$ could transfer an electron to Co^{III} while hydrazobenzene **1a** could transfer an electron to $[\text{Ru}(\text{bpy})_3]^{3+}$ and in this way the catalytic cycle will be completed, and thus may follow the oxidative quenching mechanism.

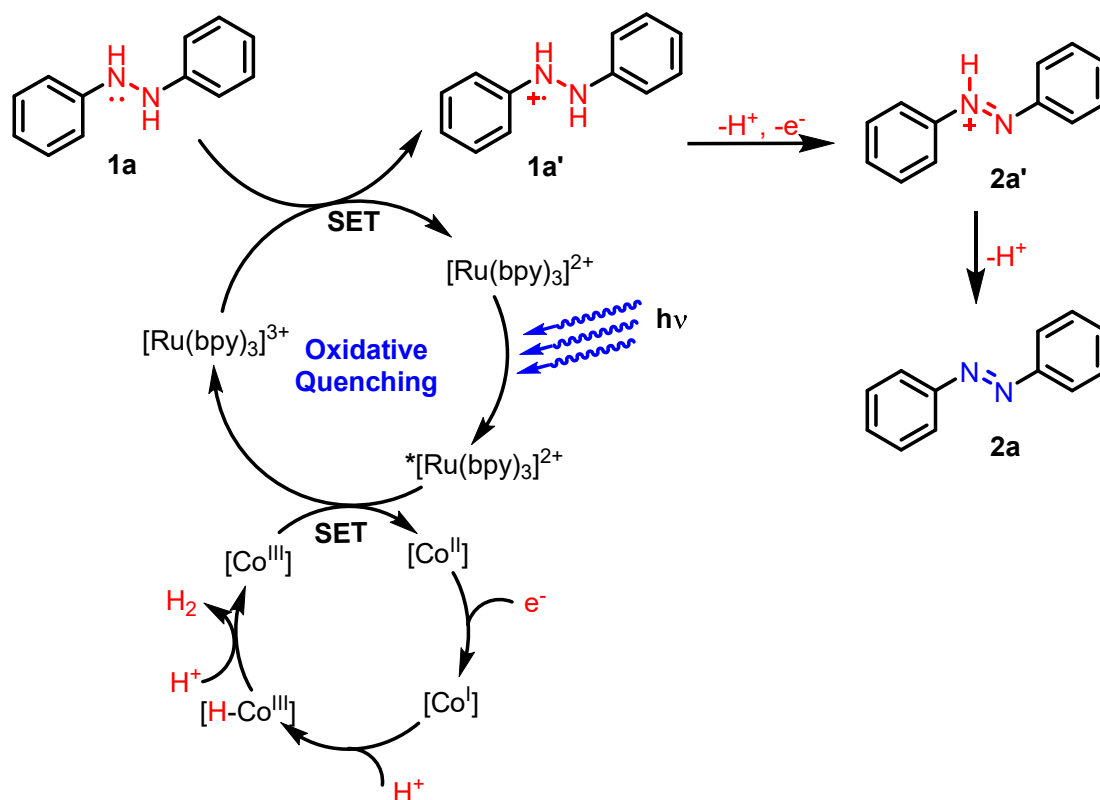


Scheme 4.3. Control experiments in presence of air and Ar atm.

4.8.4. Plausible Mechanism

Based on the above experimental observation, and recent literature precedents¹⁹ on dual catalysis²⁰ and hydrogen evolving reactions by proton reduction cobalt complexes,²¹ we have proposed a plausible mechanism as follows in Scheme 4.4. Under the visible-light irradiation the photocatalyst, $[\text{Ru}(\text{bpy})_3]^{2+}$ generates the excited state $^*[\text{Ru}(\text{bpy})_3]^{2+}$ which can reduce Co^{III} to Co^{II} via the single electron transfer (SET) through oxidative quenching and lead to $[\text{Ru}(\text{bpy})_3]^{3+}$. Then, the formed $[\text{Ru}(\text{bpy})_3]^{3+}$ is reduced by **1a** to regenerate $[\text{Ru}(\text{bpy})_3]^{2+}$ and an amine radical cation **1a'**. This radical cation **1a'** can undergo hydrogen-atom transfer with Co^{II} to produce the intermediate **2a'** and a highly reducing Co^{I} or can directly produce $\text{Co}^{\text{III}}\text{-H}$ intermediate. Subsequently, the highly reducing Co^{I} species immediately reacts with an H^+ ion (released from **1a'**) to give $\text{Co}^{\text{III}}\text{-H}$ intermediate. This $\text{Co}^{\text{III}}\text{-H}$ intermediate may react with the second proton (released from **2a'**) releasing

a molecule of H_2 and Co^{III} or may undergo reduction to $\text{Co}^{\text{II}}\text{-H}$ followed by protonation to release H_2 molecule and Co^{II} . However, the homolytic cleavage that involving the two $\text{Co}^{\text{III}}\text{-H}$ intermediate to evolve hydrogen gas could also not be ruled out.²¹⁻²²



Scheme 4.4. Plausible mechanism for ADH of hydrazobenzene (1a).

4.9. Conclusion

In conclusion, we have developed a dual transition-metal catalyzed acceptorless dehydrogenation of hydrazobenzene derivatives to the corresponding azobenzenes with the liberation of hydrogen gas. This unprecedented ADH strategy was achieved under environmentally benign conditions by merging the visible-light photoredox catalysis with Co-based proton reduction catalysis at room temperature under base-, and oxidant-free conditions. Interestingly, reversible hydrogen storage/release phenomenon on hydrazobenzene/ azobenzene couple is also demonstrated.

4.10. Experimental Section

4.10.1. General Procedure for Acceptorless Dehydrogenation of Hydrazobenzenes

In an oven-dried 20 mL headspace vial with a magnetic stirring bar was charged with **1** (0.25 mmol), [Ru(bpy)₃]Cl₂·6H₂O (1 mol %), Co(dmgh)₂(py)Cl (**III**) (2 mol %), and 2.5 mL of anhydrous ethanol under argon atmosphere. The headspace vial was sealed with a Teflon/PTFE cap, and then the reaction vial was placed on a magnetic stirrer with blue LED light bulbs strip (36 W) kept about 3 cm away from it and irradiated at room temperature with constant stirring. A cooling fan was used to maintain the reaction temperature. After 12 h, the solvent of the reaction mixture was removed under reduced pressure, diluted with 30 mL diethyl ether and 30 mL water and the aqueous layer was extracted with diethyl ether (1 x 30 mL). Finally, the combined organic layer was washed with brine solution (20 mL), dried over Na₂SO₄ and concentrated in *vacuo*. The residue was crystallized or purified by column chromatography on silica gel with a mixture of petroleum ether and EtOAc (1% EtOAc in petroleum ether) to afford desired product **2**.

4.10.2. General Procedure for Hydrogenation of Azobenzenes

To a 25 mL round-bottomed flask 0.25 mmol of azobenzene **1** and 1.0 mg of Pd/C (5 weight % Pd loading) was taken. To it, 5 mL of anhydrous methanol was added followed by 10 mol% of pyridine under an inert atmosphere. The round-bottomed flask was connected to a hydrogen balloon, flushed twice and was allowed to stir at room temperature. The reaction was monitored using TLC, and when the solution becomes colourless (nearly after 15 minutes), the hydrogen balloon was removed. The reaction mixture was quickly filtered through a small pad of celite and the solvent was removed in *vacuo*. Then the solid was washed with small amount of n-hexane (twice) followed by removal of traces of solvent in *vacuo* to get the desired hydrazobenzene in quantitative yield.

4.11. References

1. (a) Merino, E. *Chem. Soc. Rev.* **2011**, *40*, 3835-3853. (b) Hunger, K. *Industrial Dyes: Chemistry, Properties, Applications; Wiley-VCH: Weinheim (Germany)* **2003**. (c) Zollinger, H. *Color Chemistry: Syntheses, Properties and Applications of Organic Dyes and Pigments. VCH: New York* **1987**, 85.
2. (a) Lee, S. H.; Moroz, E.; Castagner, B.; Leroux, J.-C. *J. Am. Chem. Soc.* **2014**, *136*, 12868-12871. (b) Singh, A. K.; Das J.; Majumdar, N. *J. Am. Chem. Soc.* **1996**, *118*, 6185-6191.
3. (a) Bandara, H. M.; Burdette, S. C. *Chem. Soc. Rev.* **2012**, *41*, 1809-1825. (b) Beharry, A. A.; Woolley, G. A. *Chem. Soc. Rev.* **2011**, *40*, 4422-4437. (c) Gorostiza, P.; Isacoff, Y. E. *Science* **2008**, *322*, 395-399. (d) Banghart, M.; Borges, K.; Isacoff, E.; Trauner, D.; Kramer, R. H. *Nat. Neurosci.* **2004**, *7*, 1381-1386. (e) DiCesare, N.; Lakowicz, J. R. *Org. Lett.* **2001**, *3*, 3891-3893.
4. (a) Zhou, Q.; Fursule, I.; Berron, B. J.; Beck, M. J. *J. Phys. Chem. A* **2016**, *120*, 7101-7111. (b) Zhao, Y.; He, J. *Soft Matter* **2009**, *5*, 2686-2693. (c) Kumar, G. S.; Neckers, D. C. *Chem. Rev.* **1989**, *89*, 1915-1925.
5. Barrett, C. J.; Mamiya, J.-I.; Yager, K. G.; Ikeda, T. *Soft Matter* **2007**, *3*, 1249-1261.
6. (a) Bushuyev, O. S.; Tomberg, A.; Friscic, T.; Barrett, C. J. *J. Am. Chem. Soc.* **2013**, *135*, 12556-12559. (b) Ikeda, T. *J. Mater. Chem.* **2003**, *13*, 2037-2057.
7. (a) John, A. A.; Lin, Q. *J. Org. Chem.* **2017**, *82*, 9873-9876. (b) Okumura, S.; Lin, C. H.; Takeda, Y.; Minakata, S. *J. Org. Chem.* **2013**, *78*, 12090-12105. (c) Takeda, Y.; Okumura, S.; Minakata, S. *Angew. Chem., Int. Ed.* **2012**, *51*, 7804-7808. (d) Zhang, C.; Jiao, N. *Angew. Chem., Int. Ed.* **2010**, *49*, 6174-6177. (e) Dutta, B.; Biswas, S.; Sharma, V.; Savage, N. O.; Alpay, S. P.; Suib, S. L. *Angew. Chem., Int. Ed.* **2016**, *55*, 2171-2175. (f) Gorrane, A.; Corma, A.; García, H. *Science* **2008**, *322*, 1661-1664. (g) Lu, W.; Xi, C. *Tetrahedron Lett.* **2008**, *49*, 4011-4015. (h) Farhadi, S.; Zaringhadam, P.; Sahamieh, R. Z. *Acta Chim. Slov.* **2007**, *54*, 647-653. (i) Lim, Y.-K.; Lee, K.-S.; Cho, C.-G. *Org. Lett.* **2003**, *5*, 979-982. (j) Zhu, Z.; Espenson, J. H. *J. Org. Chem.* **1995**, *60*, 1326-1332.
8. (a) Combita, D.; Concepci3n, P.; Corma, A. *J. Catal.* **2014**, *311*, 339-349. (b) Hu, L.; Cao, X.; Chen, L.; Zheng, J.; Lu, J.; Sun, X.; Gu, H. *Chem. Commun.* **2012**, *48*, 3445-3447. (c) Hu, L.; Cao, X.; Shi, L.; Qi, F.; Guo, Z.; Lu, J.; Gu, H. *Org. Lett.* **2011**, *13*, 5640-5643. (d) Zhu, H.; Ke, X.; Yang, X.; Sarina, S.; Liu, H. *Angew. Chem., Int. Ed.* **2010**, *49*,

- 9657-9661. (e) Grirrane, A.; Corma, A.; Garcia, H. *Nat. Protoc.* **2010**, *11*, 429-438. (f) Corma, A.; Concepci3n, P.; Serna, P. *Angew. Chem., Int. Ed.* **2007**, *46*, 7266-7269.
9. (a) Dabbagh, H. A.; Teimouri, A.; Chermahini, A. N. *Dyes Pigm.* **2007**, *73*, 239-244. (b) Barbero, M.; Cadamuro, S.; Dughera, S.; Giaveno, C. *Eur. J. Org. Chem.* **2006**, 4884-4890. (c) Gung, B. W.; Taylor, R. T. *J. Chem. Educ.* **2004**, *81*, 1630-1632. (d) Haghbeen, K.; Tan, E. W. *J. Org. Chem.* **1998**, *63*, 4503-4505. (e) Barbero, M.; Degani, I.; Dughera, S.; Fochi, R.; Perracino, P. *Synthesis* **1998**, 1235-1237.
10. Smith M. B.; March. J. March's Advanced Organic Chemistry Reactions, Mechanisms, and Structure. *John Wiley & Sons, Inc.* **2007**.
11. (a) Wang, L.; Ishida, A.; Hashidoko, Y.; Hashimoto, M. *Angew. Chem., Int. Ed.* **2017**, *56*, 870-873. (b) Donck, S.; Gravel, E.; Li, A.; Prakash, P.; Shah, N.; Leroy, J.; Li, H.; Namboothiri, I. N. N.; Doris, E. *Catal. Sci. Technol.* **2015**, *5*, 4542-4546. (c) Bai, L.-S.; Gao, X.-M.; Zhang, X.; Sun, F.-F.; Ma, N. *Tetrahedron Lett.* **2014**, *55*, 4545-4548. (d) Gao, W.; He, Z.; Qian, Y.; Zhao, J.; Huang, Y. *Chem. Sci.* **2012**, *3*, 883-886. (e) Drug, E.; Gozin, M. *J. Am. Chem. Soc.* **2007**, *129*, 13784-13785. (f) Kim, S. S. B.; Hommer, R. B.; Cannon, R. D. *Bull. Korean Chem. Soc.* **2006**, *27*, 255-265.
12. Azobenzene synthesis by oxidation methods, see: (a) Noureldin, N. A.; Bellegarde, J. W. *Synthesis* **1999**, 939-942. (b) Zuman, P.; Shah, B. *Chem. Rev.* **1994**, *94*, 1621-1641.
13. Recent representative reviews on acceptorless dehydrogenation (ADH) reactions: (a) Gorgas, N.; Kirchner, K. *Acc. Chem. Res.* **2018**, *51*, 1558-1569. (b) Sordakis, K.; Tang, C.; Vogt, L. K.; Junge, H.; Dyson, P. J.; Beller, M.; Laurenczy, G. *Chem. Rev.* **2018**, *118*, 372-433. (c) Filonenko, G. A.; van Putten, R.; Hensen, E. J. M.; Pidko, E. A. *Chem. Soc. Rev.*, **2018**, *47*, 1459-1483. (d) Crabtree, R. H. *Chem. Rev.* **2017**, *117*, 9228-9246. (e) Balaraman, E.; Nandakumar, A.; Jaiswal, G.; Sahoo, M. K. *Catal. Sci. Technol.* **2017**, *7*, 3177-3195. (f) Kumar, A.; Bhatti, T. M.; Goldman, A. S. *Chem. Rev.* **2017**, *117*, 12357-12384. (g) Thoi, V. S.; Sun, Y.; Long J. R.; Chang, C. J. *Chem. Soc. Rev.* **2013**, *42*, 2388-2400. (h) Gunanathan, C.; Milstein, D. *Science*. **2013**, *341*, 1229712. (i) Dobereiner, G. E.; Crabtree, R. H. *Chem. Rev.* **2010**, *110*, 681-703.
14. Buckle, D. R. Encyclopedia of Reagents for Organic Synthesis; *John Wiley & Sons, Inc.*: New York, **2010**.
15. (a) Jessop, P. *Nat. Chem.* **2009**, *1*, 350-351. (b) Cui, Y.; Kwok, S.; Bucholtz, A.; Davis, B.; Whitney, R. A.; Jessop, P. G. *New J. Chem.* **2008**, *32*, 1027-1037. (c) Crabtree, R. H.

Energy Environ. Sci. **2008**, *1*, 134-138. (d) Clot, E.; Eisenstein, O.; Crabtree, R. H. *Chem. Commun.* **2007**, 2231-2233.

16. Recent representative reviews on LOHCs: (a) Preuster, P.; Papp, C; Wasserscheid, P. *Acc. Chem. Res.* **2017**, *50*, 74-85. (b) Zhu, Q.-L.; Xu, Q. *Energy Environ. Sci.* **2015**, *8*, 478-512. (c) Fukuzumi, S.; Suenobu, T. *Dalton Trans.* **2013**, *42*, 18-28. (d) Yadav, M.; Xu, Q. *Energy Environ. Sci.* **2012**, *12*, 9698-9725. (e) Teichmann, D.; Arlt, W.; Wasserscheid, P.; Freymann, R. *Energy Environ. Sci.* **2011**, *4*, 2767-2773. (f) Makowski, P.; Thomas, A.; Kuhn, P.; Goettmann, P. *Energy Environ. Sci.* **2009**, *2*, 480-490. (g) Eberle, U.; Felderhoff, M.; Schüth, F. *Angew. Chem., Int. Ed.* **2009**, *48*, 6608-6630.

17. Selected examples on reversible hydrogenation-dehydrogenation reactions: (a) Forberg, D.; Schwob, T.; Zaheer, M.; Friedrich, M.; Miyajima, N.; Kempe, R. *Nat. Commun.* **2016**, *7*, 13201-13207. (b) Manas, M. G.; Sharninghausen, L. S.; Lin, E.; Crabtree, R. H. *J. Organomet. Chem.* **2015**, *792*, 184-189. (c) Xu, R.; Chakraborty, S.; Yuan, H.; Jones, W. D. *ACS Catal.* **2015**, *5*, 6350-6354. (d) Hu, P.; Fogler, E.; Diskin-Posner, Y.; Iron, M. A.; Milstein, D. *Nat. Commun.* **2015**, *6*, 6859-6866. (e) Fujita, K.-i.; Tanaka, Y.; Kobayashi, M.; Yamaguchi, R. *J. Am. Chem. Soc.* **2014**, *136*, 4829-4832. (f) Chakraborty, S.; Brennessel, W. W.; Jones, W. D. *J. Am. Chem. Soc.* **2014**, *136*, 8564-8567. (g) Yamaguchi, R.; Ikeda, C.; Takahashi, Y.; Fujita, K.-i. *J. Am. Chem. Soc.* **2009**, *131*, 8410-8412.

18. (a) Hubrich, J.; Himmler, T.; Rodefeld, L.; Ackermann, L. *ACS Catal.* **2015**, *5*, 4089-4093. (b) Song, H.; Chen, D.; Pi, C.; Cui, X.; Wu, Y. *J. Org. Chem.* **2014**, *79*, 2955-2962. (c) Zhang, D.; Cui, X.; Zhang, Q.; Wu, Y. *J. Org. Chem.* **2015**, *80*, 1517-1522.

19. (a) Prier, C. K.; Rankic, D. A.; MacMillan, D. W. C. *Chem. Rev.* **2013**, *113*, 5322-5363. (b) Bock, C. R.; Connor, J. A.; Gutierrez, A. R.; Meyer, T. J.; Whitten, D. G.; Sullivan, B. P.; Nagle, J. K. *J. Am. Chem. Soc.* **2008**, *101*, 4815-4824.

20. Selected examples on merging photoredox catalysis and proton-reduction catalysis: (a) Twilton, J.; (Chip) Le, C.; Zhang, P.; H. Shaw, M. H.; Evans, R. W.; MacMillan, D. W. C. *Nat. Rev. Chem.* **2017**, *1*, 52. (b) He, K.-H.; Tan, F.-F.; Zhou, C.-Z.; Zhou, G.-J.; Yang, X.-L.; Li, Y. *Angew. Chem., Int. Ed.* **2017**, *129*, 3080-3084. (c) Zheng, Y.-W.; Chen, B.; Ye, P.; Feng, K.; Wang, W.; Meng, Q.-Y.; Wu, L.-Z.; Tung, C.-H. *J. Am. Chem. Soc.* **2016**, *138*, 10080-10083. (d) Wu, C.-J.; Meng, Q.-Y.; Lei, T.; Zhong, J.-J.; Liu, W.-Q.; Zhao, L.-M.; Li, Z.-J.; Chen, B.; Tung, C.-H.; Wu, L.-Z. *ACS Catal.* **2016**, *6*, 4635-4639. (e)

Zhang, G.; Liu, C.; Yi, H.; Meng, Q.; Bian, C.; Chen, H.; Jian, J.-X.; Wu, L.-Z, Lei, A. *J. Am. Chem. Soc.* **2015**, *137*, 9273-9280.

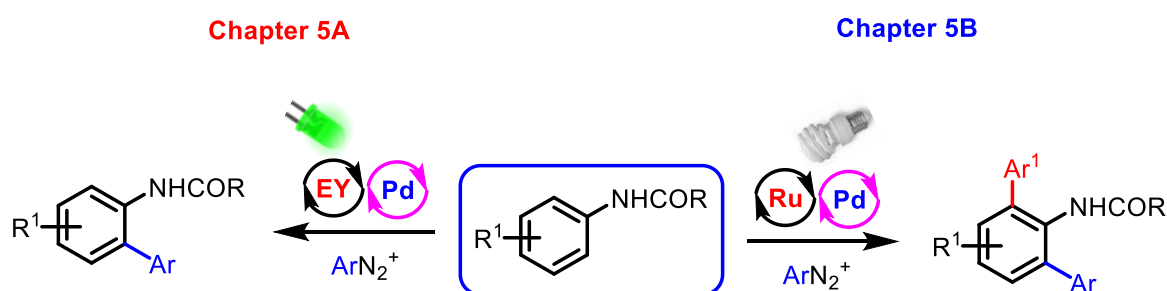
21. (a) Bhattacharjee, A.; Andreiadis, E. S.; Chavarot-Kerlidou, M.; Fontecave, M.; Field, M. J.; Artero, V. *Chem. Eur. J.* **2013**, *19*, 15166-15174. (b) Marinescu, S. C.; Winkler, J. R.; Gray, H. B. *Proc Natl Acad Sci USA* **2012**, *109*, 15127-15131. (c) Dempsey, J. L.; Winkler, J. R.; Gray, H. B. *J. Am. Chem. Soc.* **2010**, *132*, 16774-16776. (d) Dempsey, J. L.; Brunschwig, B. S.; Winkler, J. R.; Gray, H. B. *Acc. Chem. Res.* **2009**, *42*, 1995-2004. (e) Du, P.; Schneider, J.; Luo, G.; Brennessel, W.W.; Eisenberg, R. *Inorg. Chem.* **2009**, *48*, 4952-4962.

22. Lazarides, T.; Du, T.; McCormick, P.; Luo, G.; Lindley, B.; Eisenberg, R. *J. Am. Chem. Soc.* **2009**, *131*, 9192-9194.

Chapter 5

C-H Arylation of Anilides by Merging Photoredox Catalysis with Palladium Catalysis

This chapter is divided into two parts. Part A describes direct arylation of anilides using dual catalysis by merging visible-light organophotoredox catalysis with Pd-catalysis. Part B describes arylation of anilides using Ru-photoredox catalysis merged with Pd-catalysis using CO₂ derived dimethyl carbonate as a 'green solvent'. This work has extended in the synthesis of unsymmetrical *bis-ortho* arylation of anilides.

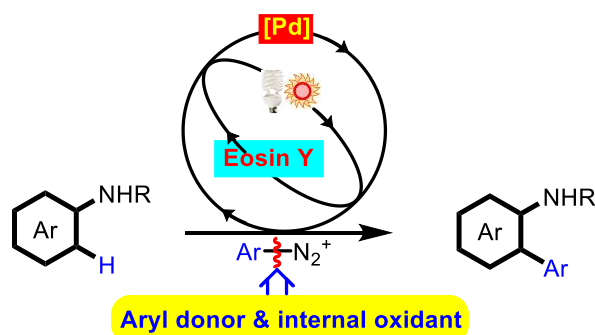


- * Metal-free photocatalyst
- * MeOH as solvent
- * Only mono *ortho*-C-H arylation
- * Green LED as light source

- * Ru-metal based photocatalyst
- * DMC as solvent
- * Bis *ortho*-C-H arylation
- * Fluorescent bulb as light source

Chapter 5A

Dual Catalyzed C-H Arylation of Anilides under External Oxidant-Free Conditions by Merging Organophotoredox Catalysis with Palladium Catalysis



Pd/Eosin Y Dual Catalysis

- * Silver-free
- * Additive-free
- * No external oxidant
- * Visible-light
- * Room temperature
- * Heterocycle formation

Sahoo *et al.*, *Green Chem.* **2017**, *19*, 2111-2117.

5A.1. Introduction

Development of new chemical approaches for the synthesis of industrially relevant compounds and pharmaceutical drugs is of great demand and fuels the efforts of the present scientific community. In this context, the biaryl motif is an important structural component of numerous natural products, pharmaceutical agents, organic materials and many of them of industrial importance.¹ Classical transition-metal catalyzed cross-coupling reactions are the powerful methods for the construction of the biaryl skeleton.²⁻³ In contrast to the well-established cross-coupling reactions, ubiquitous C-H bond direct arylation has recently emerged as more promising and practical approach to access biaryl motifs with great step- and atom-economy.³ Indeed, it circumvents the necessity of prefunctionalization of an organic molecule and has more advantages when the regioselective introduction of (pseudo)halides in an organic molecule involves multistep synthetic strategy and required harsh reaction conditions or sometimes problematic. In particular, owing to the prevalence of 2-arylaniline scaffolds in pharmaceuticals, agrochemicals, and material science much attention has been paid to the transition-metal catalyzed direct C-H arylation of (electron-rich) arenes (Figure 5A.1).⁴ Despite a few notable progress in this field over the last decade, the majority of the approaches still suffer from harsh conditions such as operates at elevated temperature, and the need for excess amounts (super-stoichiometric) of oxidants, bases and/or additives and results in copious waste and functional-group incompatibilities.⁵ Hence, it would be desirable to develop a mild, and environmentally benign C-H arylation under oxidant-, base/ additive-free conditions.

In recent times, aryldiazonium salts emerge as a convenient arylating reagent;⁶⁻⁷ however, their exploitation in transition-metal catalyzed expedient C-H arylation is rare. This is due to its high electrophilic character, reactivity towards many classes of nucleophilic coupling partners, and sensitivity towards ligand-additives and bases employed in the majority of C-H bond activation and cross-coupling reactions.⁸ Recently, Sanford and co-workers reported the Ru/Pd-catalyzed C-H arylation of 2-phenylpyridine, which is a good substrate because of its chelating ability, and cyclic *tert*-amides by using aryldiazonium tetrafluoroborates as aryl group donor.^{9a} However, this reaction still requires a large excess of aryldiazonium salts and notably, the role of silver salt (Ag_2CO_3 , a mild oxidant) used as an additive is not always straightforward. Chang and co-workers reported $\text{Cp}^*\text{Ir(III)}$ -

catalyzed (10 mol% w.r.t to Ir atom) oxidant-free C-H arylation of electron-deficient amides using aryldiazonium salts as an unconventional arylating agent, also working as an internal oxidant;^{9b} nevertheless, often required a catalytic amount of silver salt and a base (Scheme 5A.1a). Gaunt and co-workers developed a direct approach to C-H arylation of anilides at 50–70 °C using diaryliodonium salts as the aryl coupling partner under oxidant-free copper catalysis,¹⁰ but unfortunately, only *meta*-arylation of anilides was accomplished (Scheme 5A.1b). Thus, a general and efficient strategy for direct C-H arylation of anilides under oxidant-, additive- and/or base-free conditions is still elusive.¹¹ In the present chapter, we describe a dual catalytic approach¹² by merging of a visible-light metal-free photoredox catalysis with a palladium catalysis to expedient C-H arylation of anilides using aryldiazonium salts as a convenient aryl group donor, also working as an internal oxidant *via* C-N₂ bond cleavage under silver-, and base-free conditions. A consequence of this finding could be a safer and cleaner process for the effective synthesis of a wide range of important *N*-heterocyclic commodities.

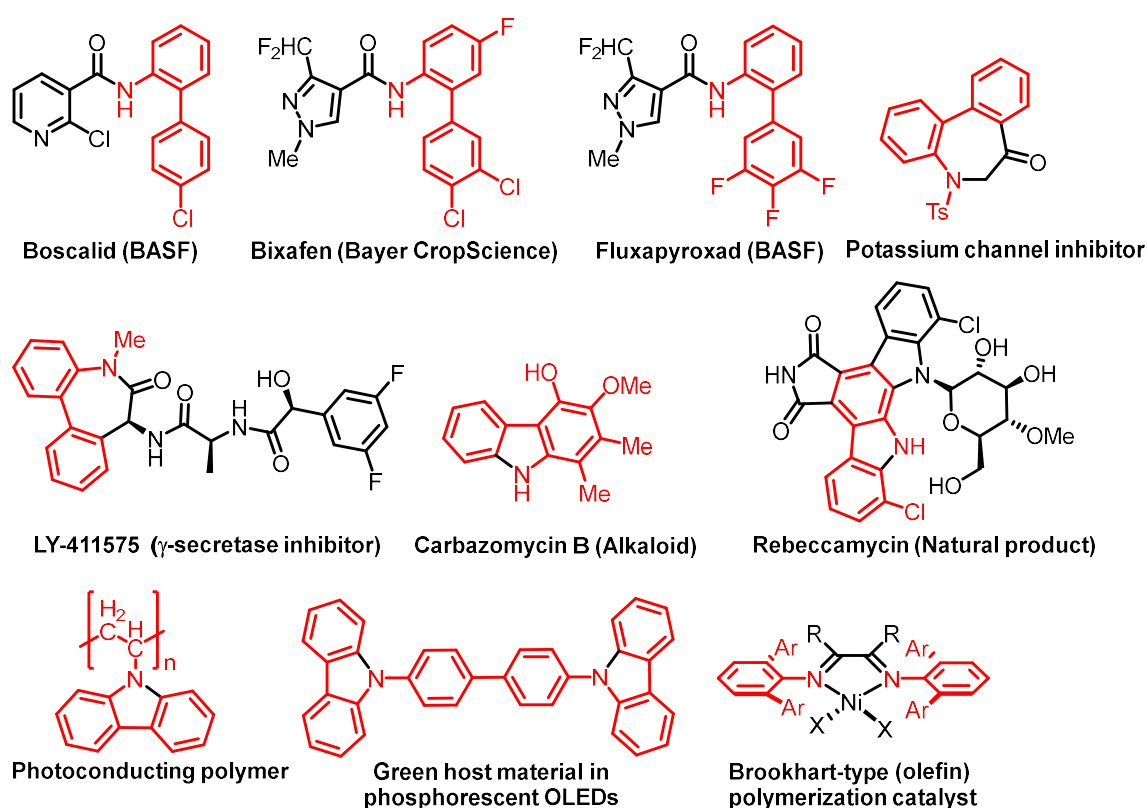
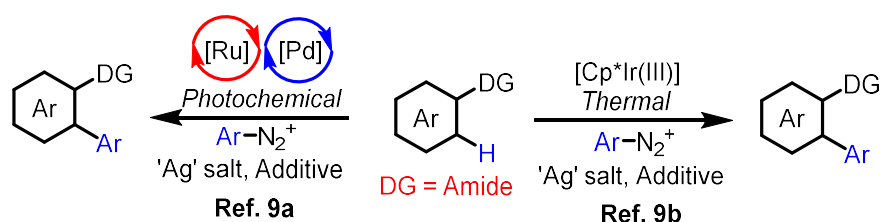
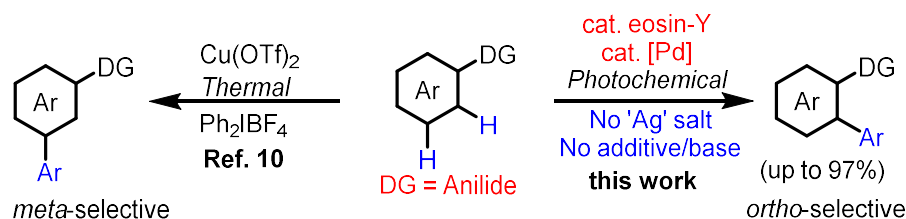


Figure 5A.1. Importance of 2-aryl anilines.

(a) Direct C-H arylation of electron-deficient arenes using aryldiazonium salts



(b) Direct C-H arylation of electron-rich arenes under external-oxidant free conditions



- * Silver-free
- * No external oxidant
- * Low-energy irradiation
- * Broad substrate scope
- * Base/Additive-free
- * Room temperature
- * Kinetic study
- * Gram-scale synthesis

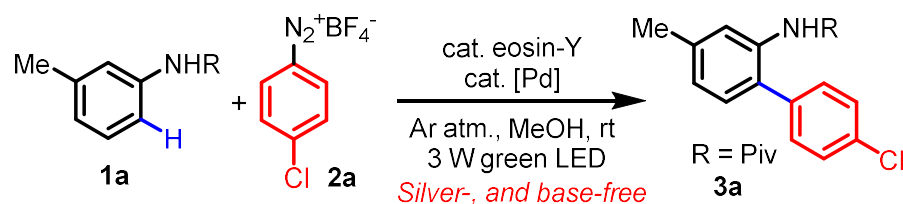
Scheme 5A.1. Direct C-H bond arylation of arenes under oxidant-free conditions.

5A.2. Statement of the Problem

Ortho-aryl anilines and related structural motifs have shown significant and innumerable pharmaceutical as well as industrial applications. However, the present literature precedent has very few reports towards the synthesis of these compounds. Often, these reactions were carried out under harsh reaction conditions such as the need of high temperature, harmful solvents, stoichiometric oxidant, base, or additive. Hence, development of a catalytic C-H bond activation method is essential for the efficient synthesis of varieties of *ortho*-aryl anilines. In this chapter, we describe a dual catalytic approach for the efficient, selective and controlled synthesis of *ortho*-aryl anilines *via* C-H bond activation. This dual catalytic C-H bond activation process has been achieved by merging both a metal-free and transition-metal based visible-light photoredox catalysis with palladium catalysis. These reactions operate under very mild, benign conditions, has a broad substrate scope, excellent functional group tolerance and has been achieved in gram scale synthesis.

5A.3. Reaction Optimization

We began our external oxidant-free site-selective C-H arylation of anilides with an evaluation of a range of solvents, mol% of the photoredox catalyst, and palladium salts in the presence of **1a** as arene partner and 4-chlorobenzenediazonium salt **2a** as aryl group donor (Table 5A.1). We found that the use of light (from 3 W green LED) in the presence of catalytic amounts of eosin-Y, and Pd(OAc)₂ enabled the desired *ortho* C-H arylated anilide **3a** in 93% isolated yield (Table 5A.1, entry 1). The necessity of each of the key reaction components (photoredox catalyst, Pd-catalyst, and light source) was demonstrated through a series of control experiments (Table 5A.1, entries 2-4). Reactions in the dark and at increased temperature (80 °C) gave the desired product **3a** in very poor yield (17%), which excludes homolytic bond cleavage of the starting material to an aryl radical under these conditions (Table 5A.1, entry 2). While trace amounts (only 8%) of the product were formed in the absence of photoredox catalyst; no reaction was observed upon exclusion of light. No formation of **3a** was observed in the absence of Pd(OAc)₂ (Table 5A.1, entry 4), and reducing the catalytic amount of Pd(OAc)₂ gave moderate yields (Table 5A.1, entries 14-15). We also examined other [Pd] sources (Table 5A.1, entries 16-20) and also replacing the palladium catalyst with those derived from gold, nickel or copper salts; however, only excellent yield was obtained when Pd(OAc)₂ was used, and no product was detected with other metal catalysts. A series of solvents were examined and among them, methanol was found to be an optimal solvent for this transformation (Table 5A.1, entries 1, and 8-13). Gratifyingly, these optimal conditions employ a low-energy 3 W green LED light source and proceed readily at room temperature under silver-, base-, and external oxidant-free conditions with no generation of copious metal waste.

Table 5A.1. Optimization of the reaction conditions.^{a,b}

Entry	Variation from the initial conditions ^a	Yield of 3a (%) ^b
1	none	93
2	no light	trace (17) ^c
3 ^d	no eosin-Y	8
4	no [Pd] source	trace
5	Rose bengal instead of eosin-Y	81
6 ^d	Fluorescein instead of eosin-Y	23
7 ^d	Ru(bpy) ₃ Cl ₂ instead of eosin-Y	46
8	CH ₃ CN instead of MeOH	trace
9 ^d	DMF instead of MeOH	20
10	CF ₃ CH ₂ OH instead of MeOH	57
11	DCE instead of MeOH	59
12 ^d	1,4-Dioxane instead of MeOH	26
13	Toluene instead of MeOH	trace
14	5.0 mol% Pd(OAc) ₂	61 (82) ^e
15	2.5 mol% Pd(OAc) ₂	43
16 ^{d,f}	Pd(II)-pivalate as [Pd] source	49
17 ^{d,f}	PdCl ₂ as [Pd] source	30
18 ^f	(PPh ₃) ₂ PdCl ₂ as [Pd] source	trace
19 ^{d,f}	Pd(acac) ₂ as [Pd] source	10
20 ^f	(dppe)PdCl ₂ as [Pd] source	trace

^aReaction conditions: **1a** (0.2 mmol), **2a** (0.3 mmol), eosin-Y (1.0 mol%), Pd(OAc)₂ (10 mol%), MeOH (1 mL), Ar atm., 3 W green LED for 12 h (R = Piv). ^bIsolated yields. ^cAt 80 °C. ^dYield determined by ¹H NMR. ^e24 h. ^f5 mol%.

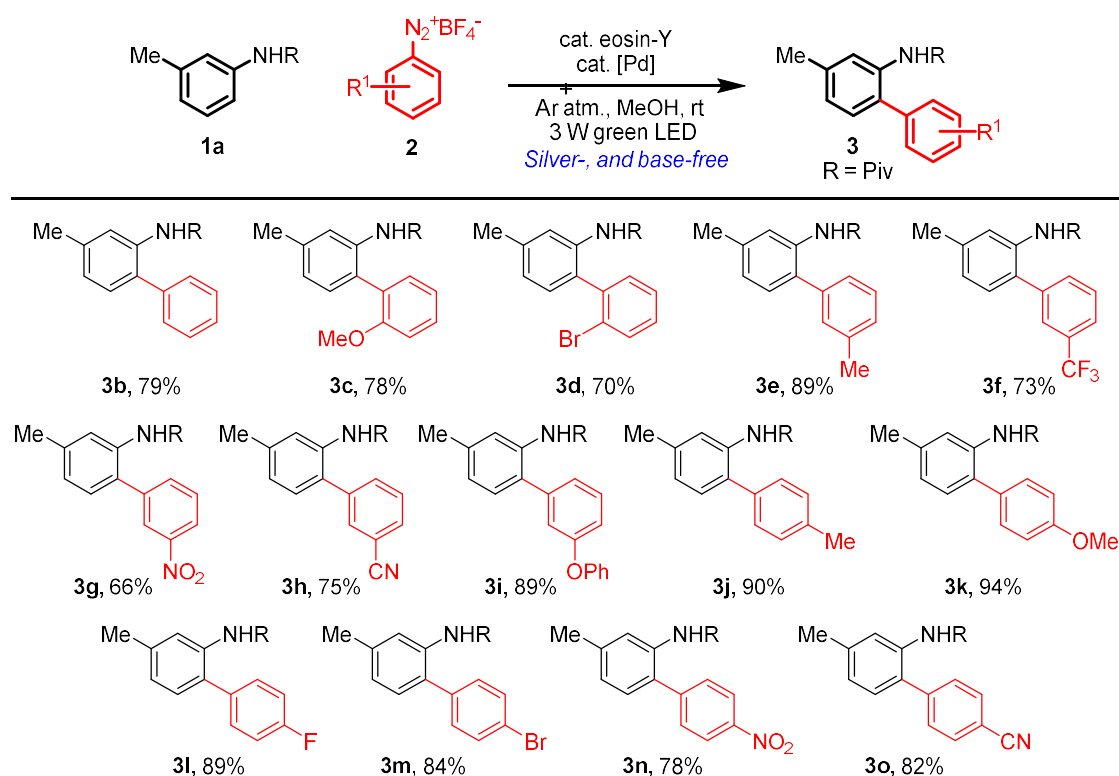
5A.4. Substrate Scope

5A.4.1. Scope of Aryldiazonium Salts

Having identified the optimal condition for the room temperature external oxidant-, base-, silver-free strategy, next sought to define the scope of both anilides **1** and aryldiazonium salts **2**. The scope of aryldiazonium salts **2** was initially explored using *N*-(*m*-

tolyl)pivalamide **1a** as a benchmark substrate at room temperature. As shown in Table 5A.2, the present direct C-H arylation strategy displayed a high functional-group tolerance and proved to be a general method for the preparation of mono-selective *ortho* C-H arylated anilides in good to excellent yields (up to 94%) under very mild conditions. Aryldiazonium salts bearing electron-donating groups at the *meta* and *para* position of the phenyl ring, such as methyl and methoxy, proceeded smoothly and gave the corresponding *ortho*-arylated anilides in 89%-94% isolated yields (products **3e**, and **3j-3k**). Indeed, electron-withdrawing group substituted (-CF₃, -NO₂, -CN, and -F) aryldiazonium salts, such as **3f-3h**, **3l**, and **3n-3o** were also well tolerated and afforded the corresponding C-H arylated products in good yields (66%-89%) (Table 5A.2). These results indicate that the electronic nature of the aryldiazonium salts has little influence on the present C-H arylation reaction. However, a substituent at the *ortho* position of the phenyl ring gave the desired product with a slightly decreasing yield (products **3c** in 78% yield and **3d** in 70% yield) which could be explained by steric reasons.

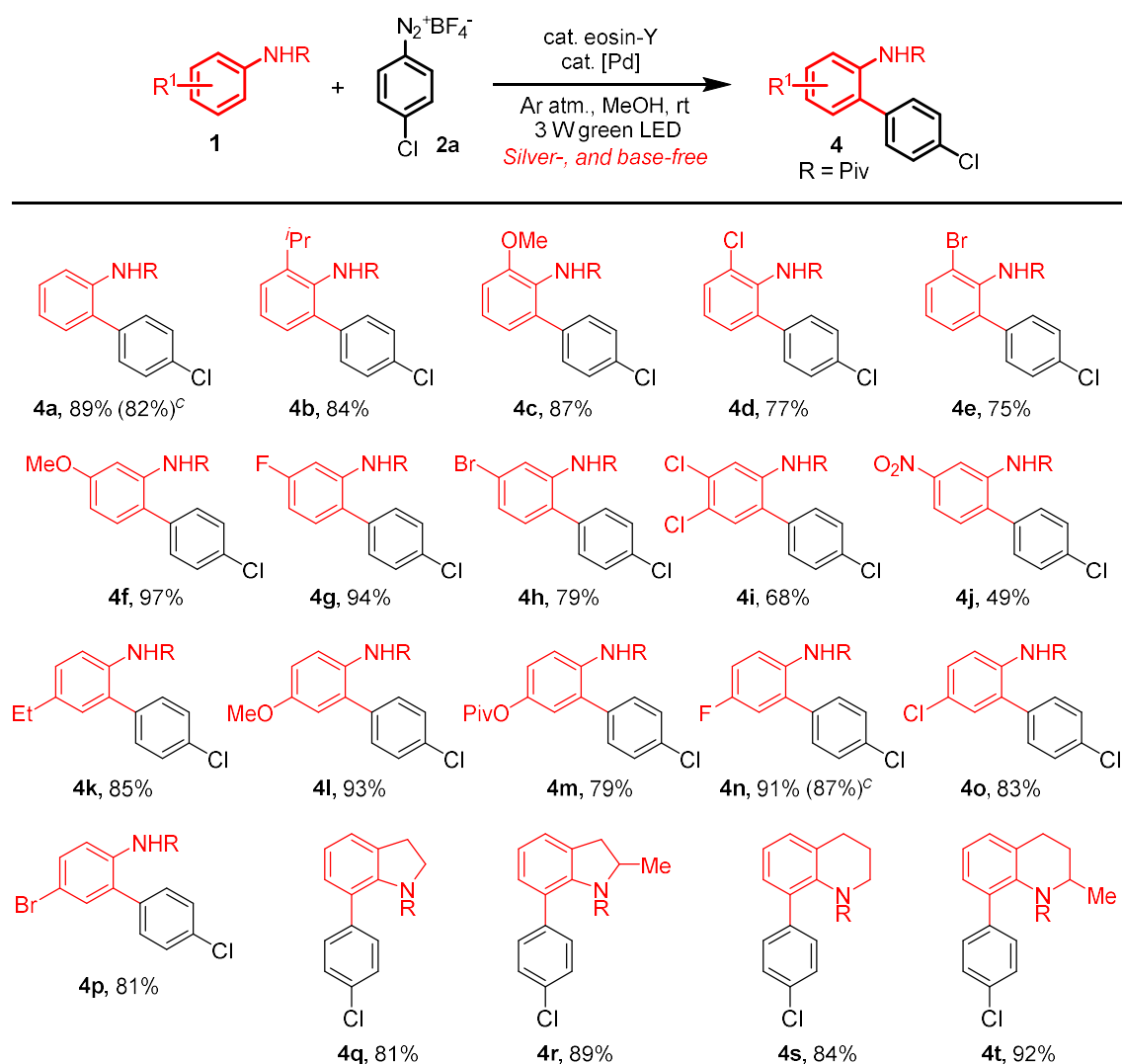
Table 5A.2. Scope of aryldiazonium salts.^{a,b}



^aReaction conditions: **1a** (0.2 mmol), **2** (0.3 mmol), eosin-Y (1 mol%), Pd(OAc)₂ (10 mol%), MeOH (1 mL), Ar atm., 3 W green LED for 12 h (R = Piv). ^bIsolated yields.

5A.4.2. Scope of Anilides

We next focused our attention on the scope of the anilide coupling partner. As exemplified in Table 5A.3, electron-donating, as well as electron-withdrawing groups on the *N*-phenyl ring, gave the desired mono-selective arylated products in excellent yields (up to 97%). Thus, *N*-phenylpivalamide **1** with electron-donating substituents such as *o*-^{*i*}Pr, *o*-OMe, *m*-OMe, *p*-Et, and *p*-OMe afforded the corresponding site-selective *ortho*-arylated products in very good yields (Table 5A.3, products **4b** in 84%, **4c** in 87%, **4f** in 97%, **4k** in 85%, and **4l** in 93% isolated yields). Under optimized conditions, **1** with electron-withdrawing substituents (*p*-F and *m*-NO₂) on the phenyl group successfully reacted with **2a** and yielded the corresponding C-H arylated products in 91% and 49% respectively. Halide substituents are also well tolerated and gave the expected C-H arylated products in good yields (up to 94%). It is noteworthy that a benzene ring substituted with both *O*-pivaloyl and *N*-pivaloyl moieties undergo C-H arylation only on *ortho*-position to *N*-pivaloyl group. Thus, the reaction of **1m** with **2a** under optimized conditions selectively gave **4m** in 79% isolated yield. Next, the scope of our C-H arylation strategy extended to cyclic systems. Thus, under optimized conditions, indoline derivatives (products **4q** in 81% and **4r** in 89% isolated yields) and tetrahydroquinolines (products **4s** in 84% and **4t** in 92% isolated yields) gave the corresponding C-H bond arylated products in excellent yields. We have also successfully shown the scalability and practical viability of this catalytic protocol under standard conditions (products **4a** in 82%, and **4n** in 87% isolated yields). Notably, the present catalytic system can be reusable. Thus, after the first catalytic run between **1a** and **2a** in the presence of catalytic amounts of eosin-Y and [Pd] source under standard conditions, the yield of the *ortho*-arylated product **3a** observed was 95% (GC yield). In the same reaction vessel were placed a fresh **1a** and **2a**, and the reaction was continued further without the addition of catalysts. After 18 h, the yield of **3a** determined for the second cycle was 91%.

Table 5A.3. Scope of anilides.^{a,b}

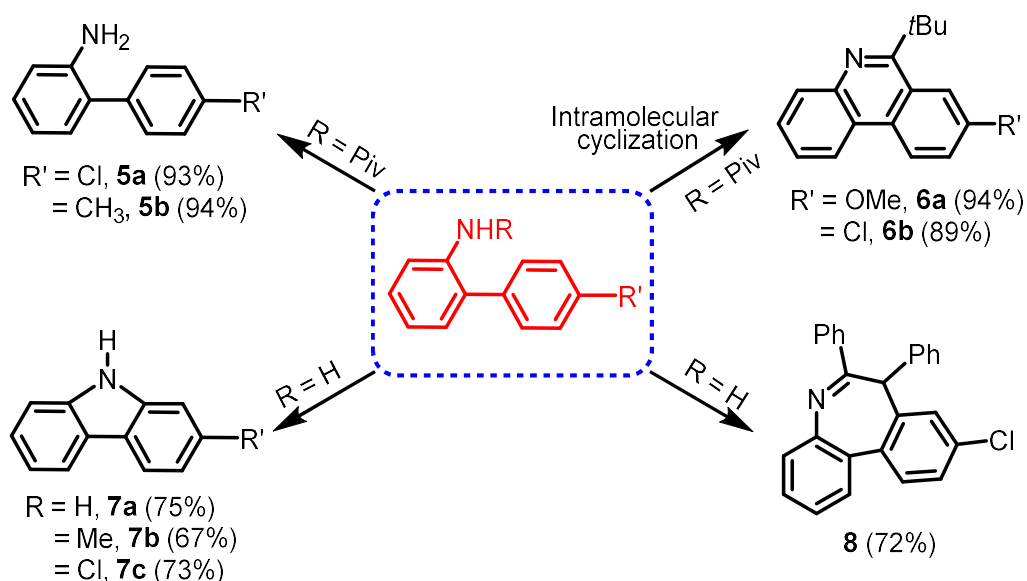
^aReaction conditions: **1** (0.2 mmol), **2a** (0.3 mmol), eosin-Y (1 mol%), Pd(OAc)₂ (10 mol%), MeOH (1 mL), Ar atm., 3 W green LED, 12 h (R = Piv). ^bIsolated yields. ^cGram-scale synthesis.

5A.5. Derivatization of ortho-Arylanilines

5A.5.1. Cyclization of Anilides

A consequence of the present direct C-H arylation strategy could be a safer and cleaner process for the effective synthesis of a wide range of important *N*-heterocyclic commodities such as phenanthridine, carbazole, and dibenzo[*b,d*]azepine. The removal of the directing group (pivaloyl group) was easily accomplished under mild reaction

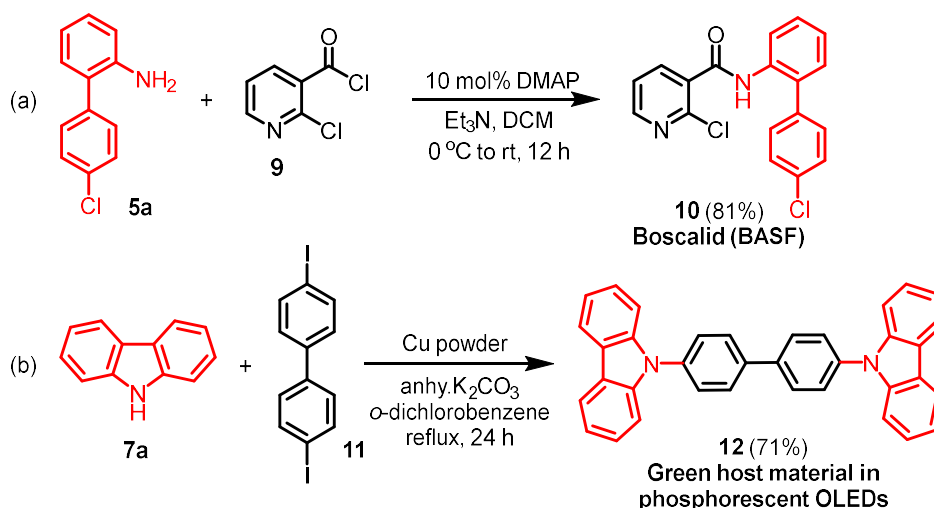
conditions to access *ortho*-aryl anilines in excellent yields (products **5a** in 93%, and **5b** in 94% yields; Scheme 5A.2). The intramolecular cyclization of *ortho*-aryl anilides proceeded smoothly in the presence of POCl₃, yielding phenanthridine derivatives **6a** and **6b** in 94%, and 89% yields, respectively. In addition, *ortho*-aryl anilines were converted into carbazole derivatives **7a-c** in good yields in the presence of catalytic amounts of [Cp*IrCl₂]₂ (2 mol %) and Cu(OAc)₂ (20 mol %) as well as PivOH (1 mmol) under air.^{4d} A palladium(II)-catalyzed [5+2] oxidative annulations of *o*-arylanilines with alkynes to access to an imine-containing dibenzo[*b,d*]azepines (**8**; 72% isolated yield) with great stereoselectivity was demonstrated.^{4f}



Scheme 5A.2. Diversification of *ortho*-arylaniline derivatives.

5A.5.2. Synthesis of Industrially Valuable Products

To our delight, a potential synthetic application of the *ortho* C-H bond arylated anilides was successfully shown in Scheme 5A.3. Treatment of **5a** with **9** in the presence of a catalytic amount of *N,N*-dimethylaminopyridine (DMAP) led to Boscalid (**10**) in 81%, which is used as a potent fungicide.^{4c} A copper powder mediated *N*-arylation of carbazole (**7a**) with 4,4'-diiodobiphenyl (**11**) to access **12**, a green host material in phosphorescent OLEDs was also shown.^{4e}



Scheme 5A.3. Synthetic applications of *ortho* C-H arylated anilines.

5A.6. Kinetics of the Reaction

Time-dependent experiments on external oxidant-free direct C-H arylation of anilides were also conducted to study the reaction kinetics (Figure. 5A.2). Thus, continuous sampling was undertaken with the different time intervals, and the conversion of anilide (**1a**) and the yield of *ortho*-aryl anilide (**3a**) were determined. The formation of **3a** followed a linear line, indicating a constant reaction rate. To find the order of reaction in each component (**1a**, **2a**, and catalyst) of the current dual catalytic approach to direct arylation of anilides with aryldiazonium salts was determined individually by using the initial rate approximation. The progress of the reaction studied with the kinetic analyses and revealed that the arylation reaction is fractional order in anilide, aryldiazonium salt, and the catalyst concentration.

5A.6.1. Representative Procedure: Time-dependent Formation of **3a**

Representative procedure (Sec 5A.6.2a.) was followed, employing *N*-(*m*-tolyl)pivalamide (76.5 mg, 0.4 mmol), 4-chlorobenzenediazonium tetrafluoroborate (136 mg, 0.6 mmol), Pd(OAc)₂ (9.0 mg, 0.04 mmol), mesitylene as internal standard (0.056 mL, 0.4 mmol) and eosin-Y (2.6 mg, 0.004 mmol), in 2.0 mL of dry methanol. At various time interval, from the reaction vessel, an aliquot of sample was withdrawn to the GC vial. The sample was

diluted with methanol and subjected to GC analysis. The final data was obtained by averaging the results of two independent runs for each experiment.

Table 5A.4. GC yield of **3a** and conversion of **1a** at different time intervals.

Experiment no.	Time (h)	Yield of 3a (%)	Conversion of 1a (%)
1	0	0	100
2	1	30	70
3	2	45	55
4	3	60	40
5	4	69	31
6	6	84	26
7	8	95	5
8	12	98	2

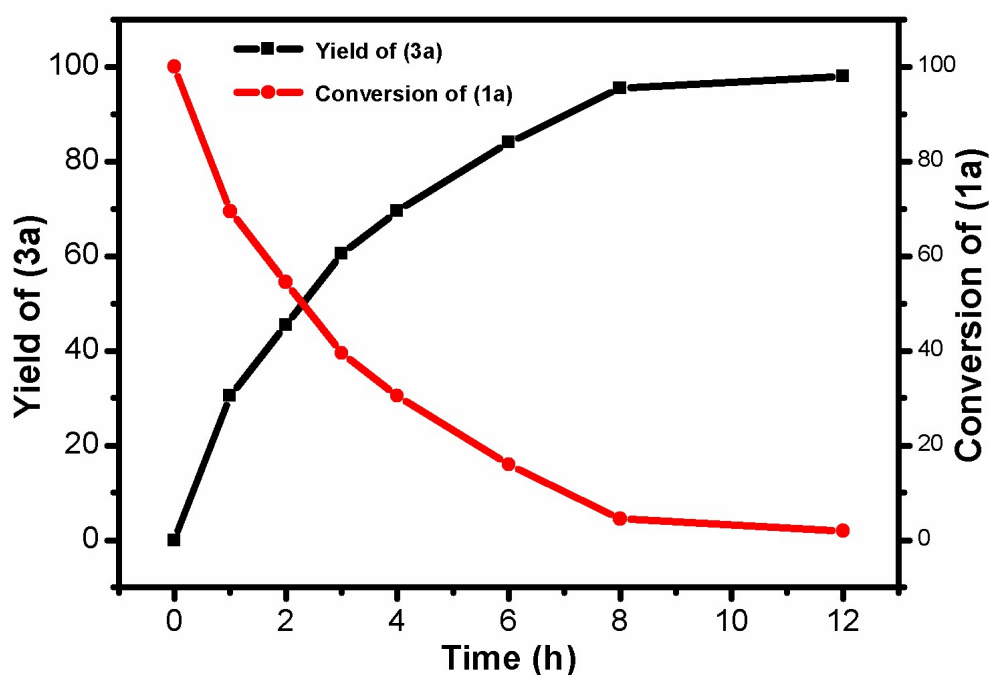


Figure 5A.2. Reaction profile for the formation of **3a** and conversion of **1a**.

5A.6.2. Rate Order Determination

The order for the *ortho* C-H arylation reaction of anilides with various reaction components was determined by the initial rate method. The data of the concentration of the product vs time (h) plot was fitted linearly with Origin Pro 8. The slope of the linear fitting is the reaction rate. The order of the reaction was then determined by plotting the log (rate) vs log (conc.) for a particular component.

5A.6.2a. Representative Procedure: Rate Order Determination for *N*-(*m*-tolyl)pivalamide

To determine the order for *N*-(*m*-tolyl)pivalamide in the *ortho* C-H arylation of anilides, the initial rates at different initial concentrations of *N*-(*m*-tolyl)pivalamide were recorded. The final data was obtained by averaging the results of two independent runs for each experiment.

In an oven-dried 15 mL Schlenk tube with a magnetic stirring bar was charged with 4-chlorobenzenediazonium tetrafluoroborate (136 mg, 0.6 mmol), Pd(OAc)₂ (9.0 mg, 0.04 mmol), eosin-Y (2.6 mg, 0.004 mmol) and specific amount of *N*-(*m*-tolyl)pivalamide (as shown in Table 5A.5). To it 2.0 mL of dry methanol was added, followed by addition of mesitylene as internal standard (0.056 mL, 0.4 mmol) under argon atmosphere. Then the reaction tube was freeze-dried in liquid N₂, degassed by the freeze-pump-thaw procedure (3×), refilled with argon gas. The temperature of Schlenk tube was brought to room temperature, then the Schlenk tube was placed on a magnetic stirrer with two 3 W green LED light bulbs kept about 5 cm away from it and irradiated at room temperature with constant stirring. At regular intervals, from the reaction vessel, an aliquot of sample was withdrawn to the GC vial. The sample was diluted with methanol and subjected to GC analysis. The concentration of the product **3a** obtained in each sample was determined with respect to the internal standard mesitylene.

Table 5A.5 Rate of *ortho* C-H arylation reaction at different initial concentration of *N*-(*m*-tolyl)pivalamide

Experiment no.	Amount of <i>N</i> -(<i>m</i> -tolyl)pivalamide (mg)	Initial conc. of <i>N</i> -(<i>m</i> -tolyl)pivalamide [M]	Initial Rate [Mh ⁻¹] x 10 ⁻²
1	77	0.2	1.6
2	115	0.3	2.1
3	153	0.4	2.4
4	191	0.5	2.8

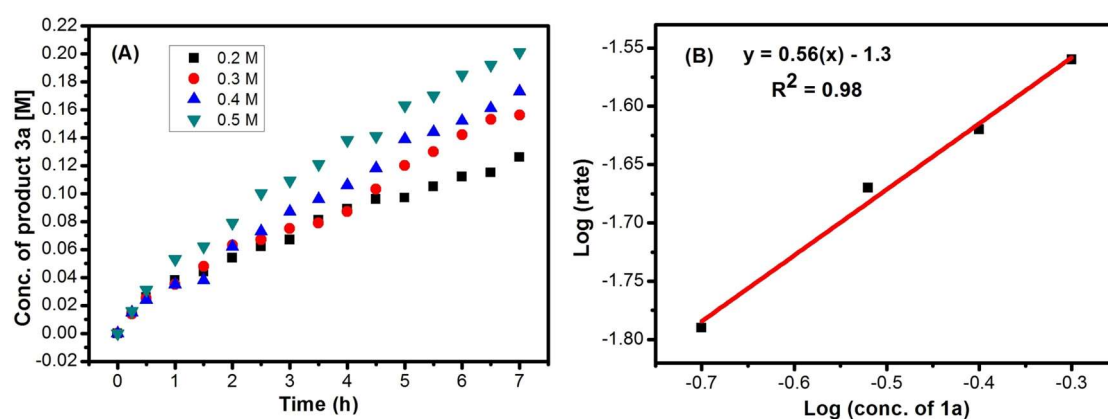


Figure 5A.3. (A) Time-dependent formation of **3a** at different initial concentration of *N*-(*m*-tolyl)pivalamide **1a**. (B) Plot of log(rate) vs log(conc. of **1a**).

5A.6.2b Representative Procedure: Rate Order Determination for 4-chlorobenzenediazonium tetrafluoroborate

To determine the order for 4-chlorobenzenediazonium tetrafluoroborate in the *ortho* C-H arylation of anilides, the initial rates at different initial concentrations of 4-chlorobenzenediazonium tetrafluoroborate were recorded. The final data was obtained by averaging the results of two independent runs for each experiment.

Representative procedure (Sec 5A.6.2a.) was followed, employing *N*-(*m*-tolyl)pivalamide (76.5 mg, 0.4 mmol), Pd(OAc)₂ (9.0 mg, 0.04 mmol), eosin-Y (2.6 mg, 0.004 mmol), mesitylene as internal standard (0.056 mL, 0.4 mmol) and specific amount of 4-

chlorobenzenediazonium tetrafluoroborate (as shown in Table 5A.6) in 2.0 mL of dry methanol.

Table 5A.6. Rate of *ortho* C-H arylation reaction at different initial concentration of 4-chlorobenzenediazonium tetrafluoroborate.

Experim ent no.	4-chlorobenzenediazonium tetrafluoroborate (mg)	Initial conc. of 4-chlorobenzenediazonium tetrafluoroborate [M]	Initial Rate [Mh ⁻¹] x 10 ⁻²
1	91	0.2	1.8
2	136	0.3	2.0
3	181	0.4	2.1
4	226	0.5	2.2

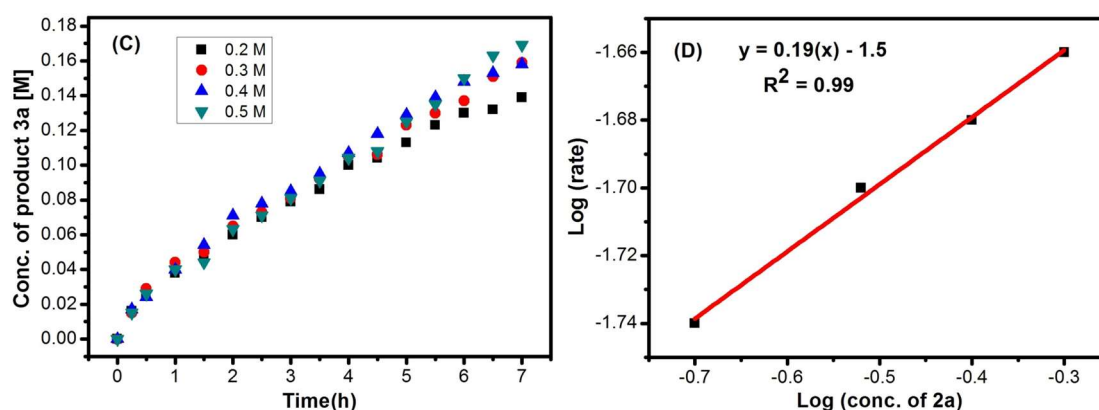


Figure 5A.4. (C) Time-dependent formation of **3a** at different initial concentration of 4-chlorobenzenediazonium tetrafluoroborate. **2a**. (D) Plot of log(rate) vs log(conc. of **2a**).

5A.6.2c Representative Procedure: Rate Order Determination for Eosin-Y

To determine the order for eosin-Y in the *ortho* C-H arylation of anilides, the initial rates at different initial concentrations of eosin-Y were recorded. The final data was obtained by averaging the results of two independent runs for each experiment.

Representative procedure (Sec 5A.6.2a.) was followed, employing *N*-(*m*-tolyl)pivalamide (76.5 mg, 0.4 mmol), 4-chlorobenzenediazonium tetrafluoroborate (136 mg, 0.6 mmol),

Pd(OAc)₂ (9.0 mg, 0.04 mmol), mesitylene as internal standard (0.056 mL, 0.4 mmol) and specific amount of eosin-Y (as shown in Table 5A.7) in 2.0 mL of dry methanol.

Table 5A.7. Rate of *ortho* C-H arylation reaction at different initial concentration of Eosin-Y.

Experiment no.	Eosin-Y (mg)	Initial conc. of Eosin-Y [M]	Initial Rate [Mh ⁻¹] x 10 ⁻²
1	2.6	0.002	2.79
2	13	0.01	3.45
3	25.9	0.02	4.40
4	38.9	0.03	4.82

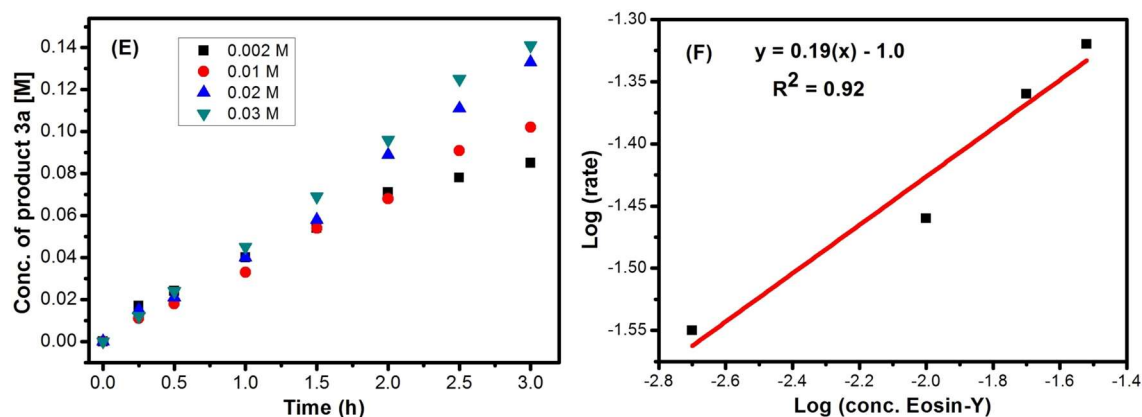


Figure 5A.5. (A) Time-dependent formation of **3a** at different initial concentration of Eosin-Y. (B) Plot of log(rate) vs log(conc. of Eosin-Y).

5A.6.2d Representative Procedure: Yield Determination for Pd(OAc)₂

To determine the effect of mol% of Pd(OAc)₂ in the *ortho* C-H arylation of anilides **3a**, the yields at different initial concentrations of Pd(OAc)₂ were recorded.

Representative procedure (Sec 5A.6.2a.) was followed, employing *N*-(*m*-tolyl)pivalamide (38 mg, 0.2 mmol), 4-chlorobenzenediazonium tetrafluoroborate (38 mg, 0.3 mmol), eosin-Y (1.3 mg, 0.002 mmol) and specific amount of Pd(OAc)₂ (as shown in Table 5A.8) in 1.0 mL of dry methanol.

Table 5A.8. Yield of *ortho* C-H arylation reaction at different initial concentration of Pd(OAc)₂.

Experiment no.	Amount of Pd(OAc) ₂ (mg)	Initial conc. of Pd(OAc) ₂ [M]	Yield (%)
1	0.5	0.002	4 (by GC)
2	1.1	0.005	43 (isolated yield)
3	2.2	0.01	61 (isolated yield)
4	4.5	0.02	93 (isolated yield)

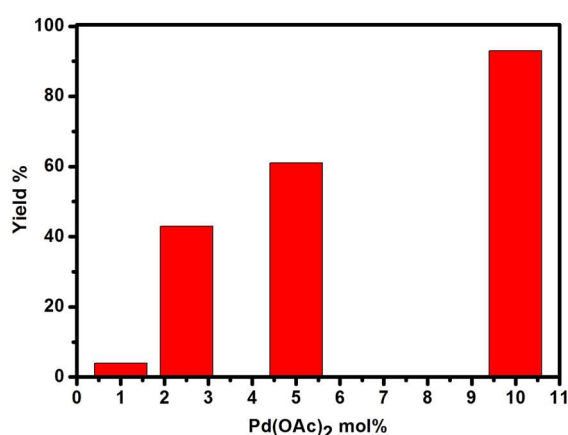


Figure 5A.6. Yield formation of **3a** at different initial concentration of Pd(OAc)₂

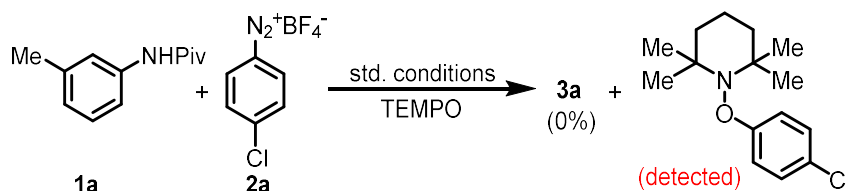
5A.7. Mechanistic Investigation

5A.7.1. Control Experiment

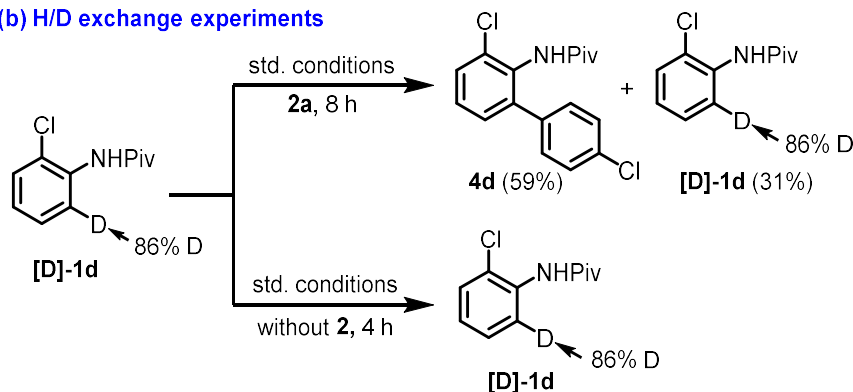
Performing the reaction in the presence of the radical scavenger 2,2,6,6-tetramethylpiperidine-1-oxyl (TEMPO), the reaction was completely inhibited (Scheme 5A.4a). Indeed, the *O*-arylated-TEMPO product was detected on GC-MS, indicating that the radical reaction pathway could be involved in the catalytic cycle. Furthermore, the yield of **3a** was completely dropped when no photocatalyst was present in the reaction and/or under dark conditions (Table 5A.1, entry 3). A “light/dark” experiment indicates that a radical chain process in the present dual catalytic system may be operative.¹³ Notably, the C-H arylation of the isotopically labeled substrate [D]-**1d** was not accompanied by H/D exchange reactions, which is indicative of a kinetically relevant C-

H palladation step (Scheme 5A.4b). In a preliminary experiment, the formation of palladacycle intermediate **14** was identified by the stoichiometric reaction of **1a** with Pd(OAc)₂.¹⁴

(a) Radical trapping experiment

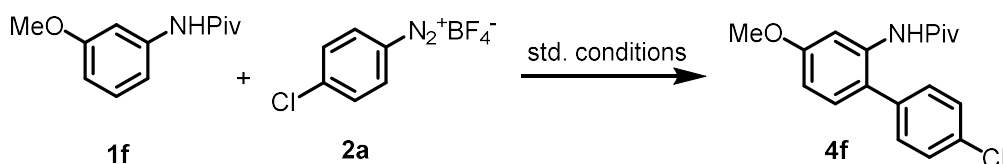


(b) H/D exchange experiments



Scheme 5A.4. Mechanistic studies.

5A.7.2. Light-Dark Experiment



Following representative procedure (Sec 5A.6.2a.), two parallel experiments {**A** (Light) and **B** (Dark)} were carried out employing *N*-(3-methoxyphenyl)pivalamide **1f** (83 mg, 0.4 mmol), 4-chlorobenzenediazonium tetrafluoroborate **2a** (136 mg, 0.6 mmol), Pd(OAc)₂ (9.0 mg, 0.04 mmol), eosin-Y (2.6 mg, 0.004 mmol) and mesitylene (0.056 mL, 0.4 mmol) as internal standard in 2.0 mL of dry methanol. Initially, the reaction (**B**) was irradiated with a light source under the standard condition for the first 60 minutes and then carried out in the dark condition. However, reaction (**A**) was irradiated with continuous irradiation. Continuous sampling was undertaken with the different time intervals, and yield of *ortho*-arylated product (**4f**) was determined by gas chromatography.

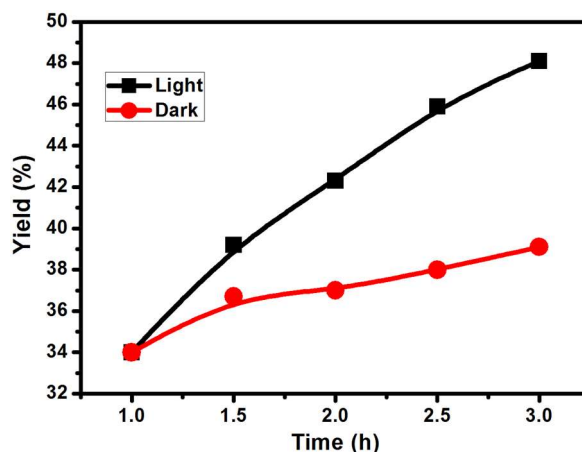


Figure 5A.7. Kinetic profile **4f** at different time intervals for two separate (dark and light) experiments.

5A.7.3. Light-Dark Experiment (ON/OFF Experiment)

Following representative procedure (Sec 5A.6.2a.), the reaction was carried out employing *N*-(3-methoxyphenyl)pivalamide **1f** (83 mg, 0.4 mmol), 4-chlorobenzenediazonium tetrafluoroborate **2a** (136 mg, 0.6 mmol), Pd(OAc)₂ (9.0 mg, 0.04 mmol), eosin-Y (2.6 mg, 0.004 mmol) and mesitylene (0.056 mL, 0.4 mmol) as internal standard in 2.0 mL of dry methanol. The reaction is conducted using alternating intervals of light and dark. In each interval, continuous sampling was undertaken with the different time intervals, and yield of *ortho*-arylated product (**4f**) was determined by gas chromatography.

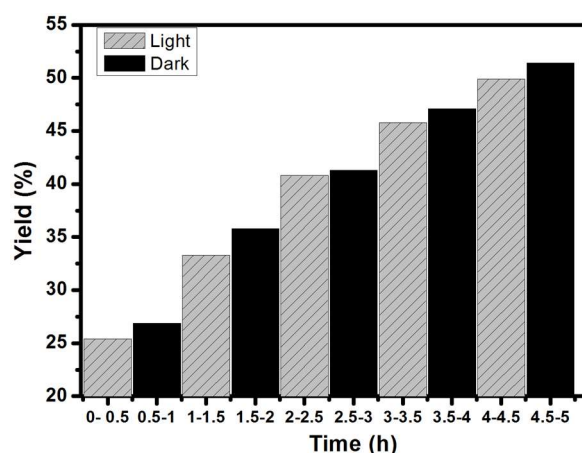


Figure 5A.8. GC yield of **4f** with different time intervals (Light-Dark experiment).

5A.7.4. Identification of Intermediate Pd-complex

To an oven-dried 5 mL screw-capped vial, **1f** (70 mg, 0.33 mmol), Pd(OAc)₂ (75mg, 1 equiv.), *N*-Formylglycine (35mg, 1 equiv.) and hexafluoroisopropanol (2 mL) were added under argon atmosphere. The mixture was stirred for 3 hr at 100 °C followed by cooling to room temperature. The solution was filtered through a celite pad and submitted to HRMS analysis. HRMS (EI): *m/z* Calcd for [M-H] C₁₅H₁₉N₂O₅Pd: 413.0323; Found: 413.0317.

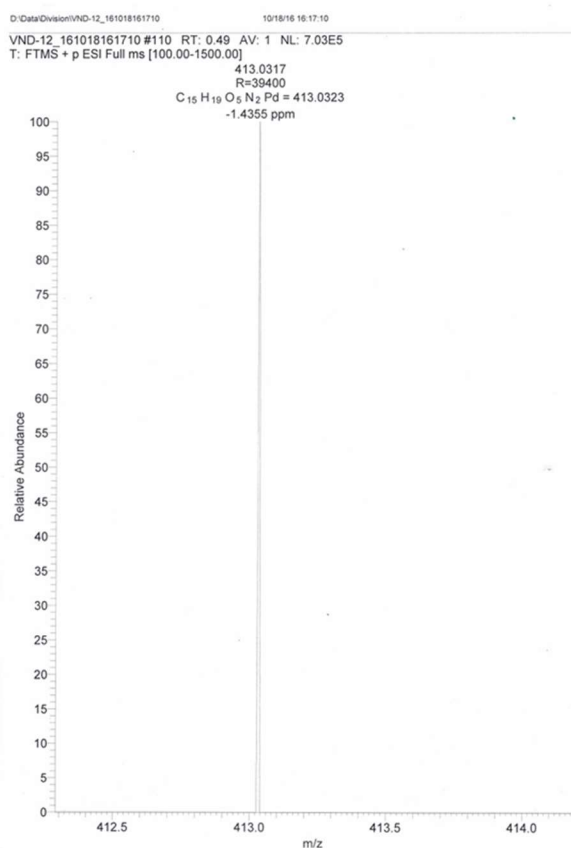


Figure 5A.9a. HRMS of intermediate Pd-complex

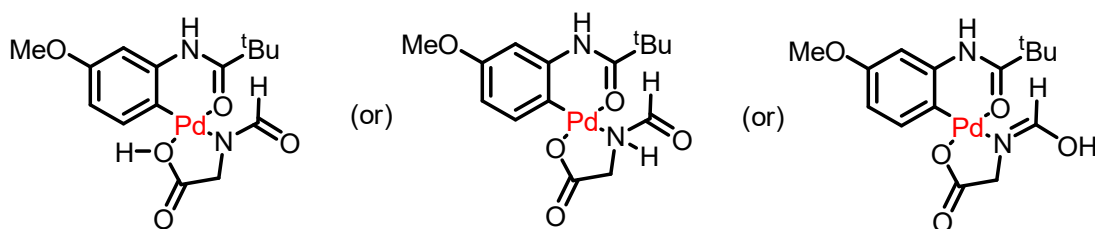


Figure 5A.9b. Possible intermediate complexes.

5A.7.5. Effect of Other Directing Group

The effect of substituent on the acyl group of anilides was further studied by changing the *N*-pivaloyl (i.e. *t*-Butyl) group to the *N*-acetyl (i.e. ethyl) group and gave the C-H arylated product in 31% yield only (mono/bis \approx 2:1). To further extend the scope of the reaction, we investigated different amides such as -NHCONMe₂ and -NHTs as the directing groups and found to be not suitable for the present arylation reaction. Due to the favourable conformation of the pivaloyl group good selectivity of the site-selective product was observed.

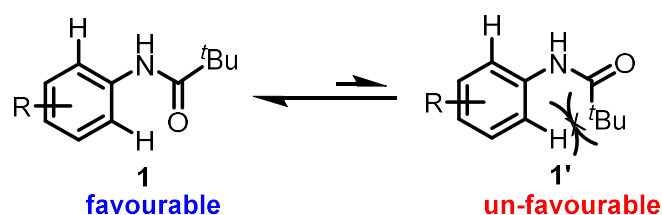
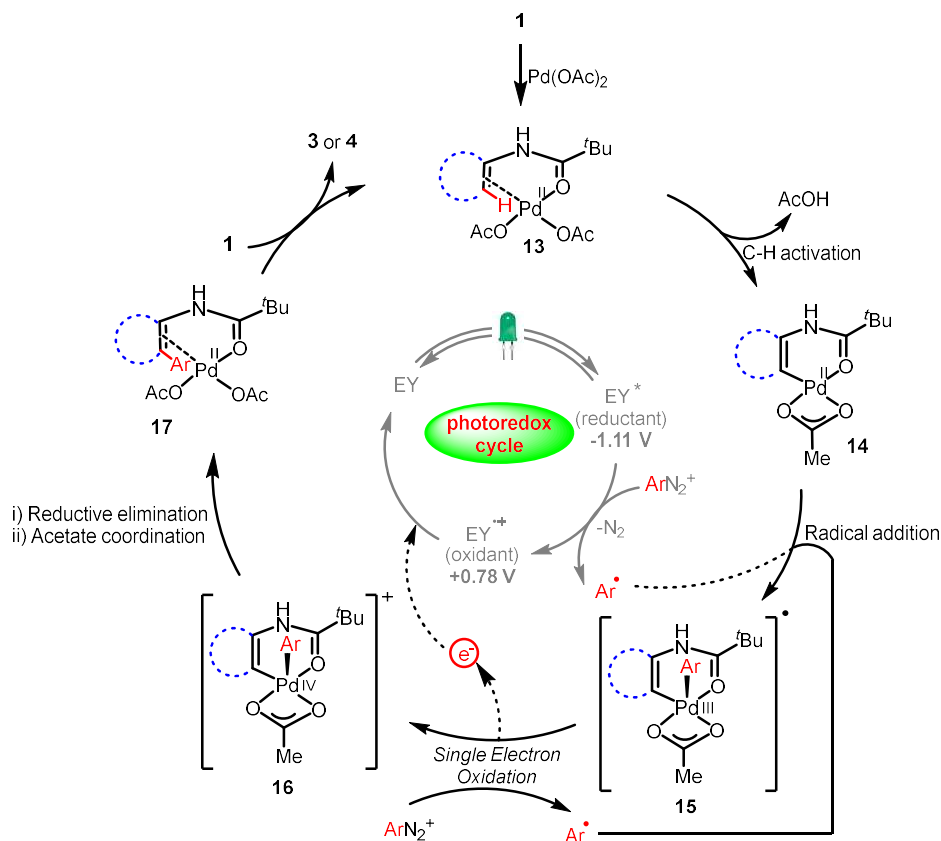


Figure 5A.10. A possible conformation of anilide **1**.

5A.7.6. Plausible Mechanism

Based on the above experimental findings and literature precedent^{12,13-15} a plausible mechanism for external-oxidant free C-H arylation of **1** is shown in Scheme 5A.5. Initially, eosin Y (EY) absorbs visible-light in the green light region ($\lambda_{\text{max}} = 539 \text{ nm}$) to give a photoexcited singlet state, ¹EY*, which undergoes rapid intersystem crossing to its lowest long-lived triplet state ³EY* with a lifetime of 24 μs .^{13d} This photoexcited ³EY* is a strong reductant ($E_{1/2}(\text{}^3\text{EY}^*/\text{EY}^+) = -1.15 \text{ V vs SCE}$)^{13d-e} and undergoes oxidative quenching followed by reducing the ArN₂BF₄. (the standard reduction potential of different ArN₂BF₄ are very close to SCE varying from a small positive to negative values; $E_{1/2}^{\text{red}} = -0.1 \text{ V vs SCE}$ for phenyldiazonium tetrafluoroborate)^{13f} to the corresponding electrophilic aryl radical with the concomitant generation of dinitrogen. Then the electrophilic aryl radical (Ar \cdot) reacts with palladacycle **14** (generated by the carboxylate assisted C-H bond activation of **1**) to afford the intermediate **15**.¹⁶ Single electron oxidation of **15** by EY⁺ (strongly oxidizing, $E_{1/2}(\text{EY}^+/\text{EY}) = +0.78 \text{ V vs SCE}$)¹³ to regenerate the photocatalyst (EY) and forms intermediate **16**. Indeed, the mechanistic studies show that a significant contribution of a radical chain process in the present catalytic system is operative.^{13a,13f}

Therefore, a second SET process between palladacycle **14** with another equivalent of the aryldiazonium salt contributes to the formation of **15** may also be feasible. Finally, the reductive elimination of **17** leads to an *ortho*-arylated anilide **3** or **4** via the C-C bond formation and followed by an acetate ion coordination regenerates the palladium catalyst.



Scheme 5A.5. A plausible catalytic cycle for a synergistic catalysis for C-H arylation of **1** under external oxidant-free condition.

5.8. Conclusion

In conclusion, a dual catalytic approach by successfully merging visible-light photoredox catalysis with palladium catalysis to room temperature external oxidant-free direct C-H arylation of anilides by using aryldiazonium tetrafluoroborates as a convenient aryl group donor, also working as an internal oxidant via C-N₂ bond cleavage has been reported. The unified approach operates under extremely mild conditions; silver-, additive-free, and redox-neutral conditions, and no generation of copious metal waste, and can thereby be scaled up in gram-scale synthesis. A consequence of this finding could be a safer and

cleaner process for the effective synthesis of a wide range of important *N*-heterocyclic commodities such as dibenzo[*b,d*]azepine, carbazole, and phenanthridine. In addition, a potential synthetic application of *ortho* C-H bond arylated anilides in agrochemical and material science has been successfully demonstrated. The broad substrate scope, functional group tolerance, and excellent selectivity of this process make it attractive for the facile construction of C-H arylated compounds of high utility in various research areas.

5.9. Experimental Section

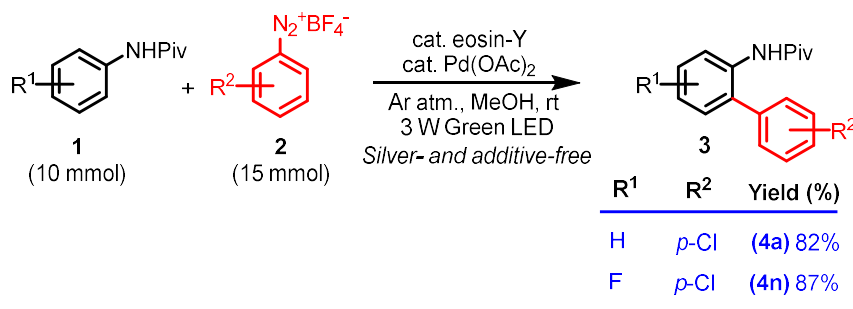
5A.9.1a. General Procedure for Room Temperature Oxidant- and Base-free Eosin-Y/Pd Catalyzed C-H Arylation of Anilides

In an oven-dried 15 mL, Schlenk tube with a magnetic stirring bar was charged with pivalamide **1** (0.2 mmol), aryldiazonium salt **2** (0.3 mmol), eosin-Y (1 mol %), Pd(OAc)₂ (10 mol %), and 1 mL of methanol under argon atmosphere. Then the reaction tube was freed in liquid N₂, degassed by the freeze-pump-thaw procedure (3×), refilled with argon gas. Then the Schlenk tube was placed on a magnetic stirrer with two 3 W green LED light bulbs kept about 5 cm away from it and irradiated at room temperature with constant stirring. After 18 h, the reaction mixture was quenched with saturated 15 mL NaHCO₃ solution, and was extracted with EtOAc (3 x 15 mL). Finally, the combined organic layer was washed with brine solution (15 mL), dried over Na₂SO₄ and concentrated in *vacuo*. The residue was purified by column chromatography on silica gel using mixture of EtOAc and petroleum ether to afford desired *ortho*-arylated product **3** or **4**.

5A.9.1b. General Procedure for Gram-scale Synthesis

In an oven-dried 100 mL Schlenk round-bottomed flask with a magnetic stirring bar was charged with pivalamide **1** (10 mmol), aryldiazonium salt **2** (15 mmol), Pd(OAc)₂ (10 mol %), eosin-Y (1.0 mol %), and 50 mL of anhydrous methanol under argon atmosphere. Then the reaction tube was freed in liquid N₂, degassed by the freeze-pump-thaw procedure (3×), refilled with argon gas. Then the round-bottomed flask was placed on a magnetic stirrer with two 3 W green LED light bulbs kept about 5 cm away from it and irradiated at room temperature with constant stirring. After 24 h, the reaction mixture was

quenched with saturated 100 mL NaHCO₃ solution, and the aqueous layer was extracted with EtOAc (2 x 100 mL). Finally, the combined organic layer was washed with brine solution (100 mL), dried over Na₂SO₄ and concentrated in *vacuo*. The residue was purified by column chromatography on silica gel with a mixture of EtOAc and petroleum ether to afford the desired *ortho*-arylated product in gram-scale.

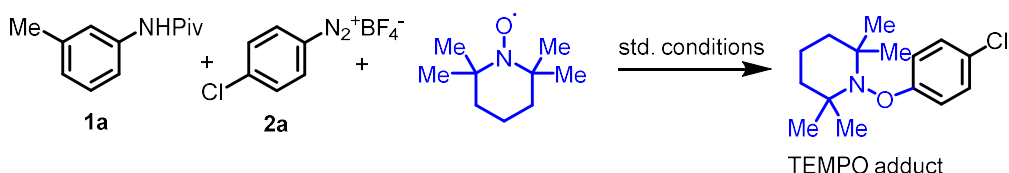


Scheme 5A.6. Gram-scale synthesis of C-H arylated anilides.

5A.9.2. Reusability of the Homogeneous System

The reusability of the present catalytic system was checked by following representative procedure (5A.9.1a.). After the first catalytic run between **1a** and **2a** in the presence of catalytic amounts of eosin-Y (1 mol%) and Pd(OAc)₂ (10 mol%) in methanol under standard conditions, the yield of the *ortho*-arylated product **3a** observed was 95% (GC yield). In the same reaction vessel were placed fresh **1a** and **2a**, and the reaction was continued further without the addition of catalysts. After 18 h, the yield determined for the second cycle was 91% (GC yield).

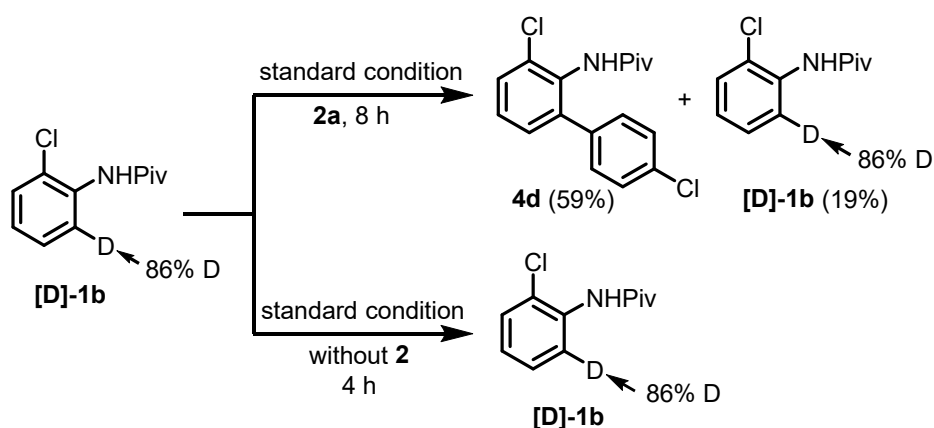
5A.9.3. Radical Trapping Experiment



In an oven-dried 15 mL Schlenk tube with a magnetic stirring bar was charged with pivalamide **1a** (0.2 mmol), aryldiazonium salt **2a** (0.3 mmol), eosin-Y (1 mol %), Pd(OAc)₂ (10 mol %), TEMPO (2.0 equivalent) and 1 mL of methanol under argon

atmosphere. Then the reaction tube was frozen in liquid N₂, degassed by the freeze-pump-thaw procedure (3×), refilled with argon gas. Then the Schlenk tube was placed on a magnetic stirrer with two 3 W green LED light bulbs kept about 5 cm away from it and irradiated at room temperature with constant stirring. After 18 h, the reaction mixture was analyzed on GC-MS and the formation of *O*-arylated-TEMPO product was observed.

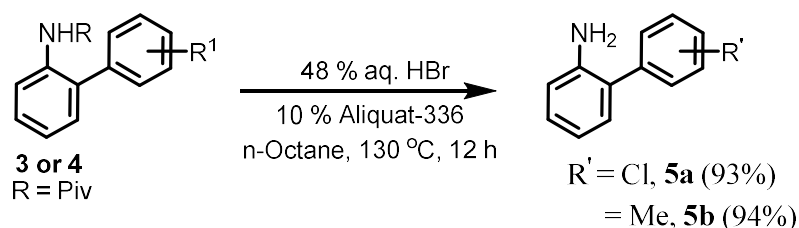
5A.9.4. H/D Exchange Experiments



Deuterium-labeled compound **[D]-1b** was prepared according to the reported literature procedure with 86% deuterium incorporation. Two independent experiments (i) with **2a** and (ii) without **2a** were performed under standard conditions using freshly distilled dry MeOH. In both the experiments the recovered starting material **1d** showed 86%. Thus, the C-H arylation of the isotopically labeled substrate **[D]-1d** was not accompanied by H/D exchange reactions, which is indicative of a kinetically relevant C-H palladation step.

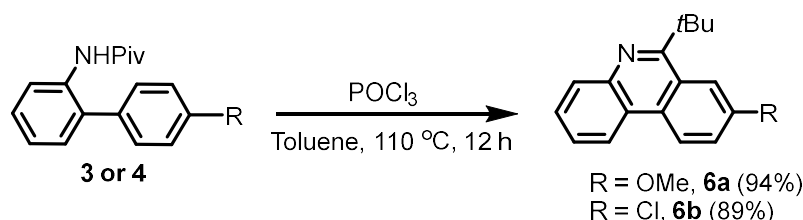
5A.9.5. Diversification of *ortho*-Arylaniline Derivatives

5A.9.5a. Removal of Directing Group



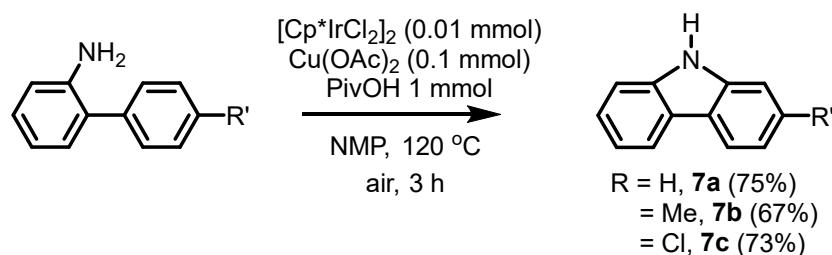
To a 10 mL screw-capped tube, *ortho*-aryl pivalamide (0.5 mmol), 10 weight percentage of Aliquat-336, 0.5 mL of 48 % aqueous HBr and 1.0 mL of *n*-octane were added under argon atmosphere. Then the tube was kept in a preheated oil bath at 130 °C for 12 h. After cooling to room temperature, the reaction mixture was neutralized with saturated Na₂CO₃. The compound was extracted with 25 mL of EtOAc three times. Then the organic layer was washed with 25 mL of brine solution, dried over Na₂SO₄ and concentrated in *vacuo*. The residue was purified by column chromatography on silica gel with a mixture of EtOAc and petroleum ether to afford desired *ortho*-arylated anilines (**5**).

5A.9.5b. Synthesis of Phenanthridine



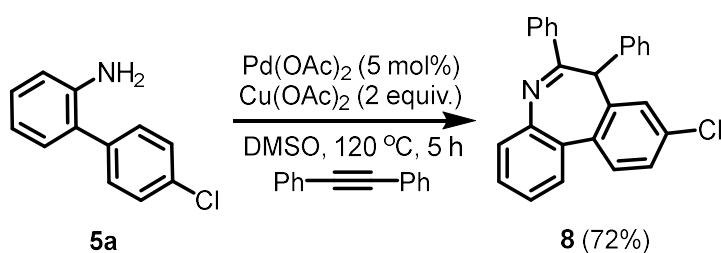
To an oven dried 10 mL sealed tube with the magnetic stirring bar was charged *ortho*-arylated pivalamide **3** or **4** (0.2 mmol), POCl₃ (0.6 mmol, 0.056 mL). To it 0.5 mL dry Toluene was added under an argon atmosphere. The Teflon screw cap was closed and the tube was kept in a preheated oil bath at 110 °C, the reaction was continued for 12 h. After completion, the reaction mixture was quenched by addition of aqueous NaHCO₃. The mixture was extracted with dichloromethane (3 × 10 mL). The combined extracts were washed with brine solution, dried over Na₂SO₄ and the solvent was removed in *vacuo*. The crude product was purified by column chromatography on silica gel using a mixture of hexanes and EtOAc as eluent to afford the corresponding phenanthridine derivatives.

5A.9.5c. Carbazole Synthesis



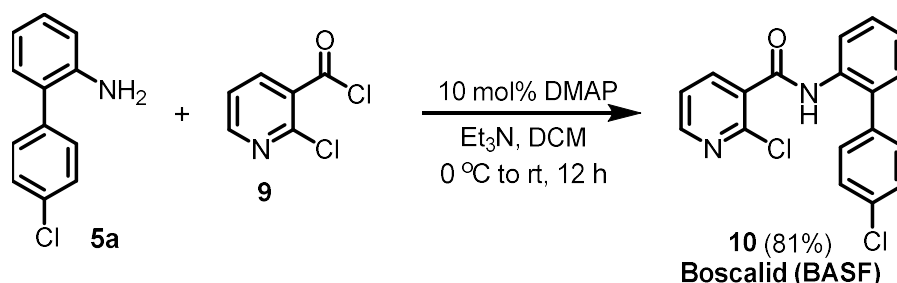
To a 20 mL two-necked flask with a reflux condenser and a rubber cup were added 2-aryl aniline (0.5 mmol), $[\text{Cp}^*\text{IrCl}_2]_2$ (0.01 mmol), $\text{Cu}(\text{OAc})_2$ (0.1 mmol), PivOH (1.0 mmol) in NMP (3 mL). The resulting mixture was stirred under air at 120 °C for 3h. After cooling, the reaction mixture was extracted with EtOAc (100 mL), washed with aqueous NaHCO_3 (100 mL, three times), and dried over Na_2SO_4 . Purification by column chromatography on silica gel using hexane-EtOAc (10:1, v/v) as eluent gave carbazole.

5A.9.5d. Cyclization with Diphenylacetylene



In a oven-dried, 5.0 mL vial equipped with a stirring bar was charged with $\text{Pd}(\text{OAc})_2$ (3.4 mg, 0.015 mmol), $\text{Cu}(\text{OAc})_2$ (114.4 mg, 0.63 mmol), **5a** (0.30 mmol) and diphenylacetylene (0.45 mmol), followed by sequential addition of DMSO (3.0 mL). The vial was sealed with a Teflon screw cap and then the reaction mixture was heated at 120 °C for 5 h. After the reaction vessel was cooled to room temperature, the mixture was extracted with EtOAc, dried over MgSO_4 , filtered, and concentrated in *vacuo*. The residue was then purified on silica gel to yield **8** in 72%.

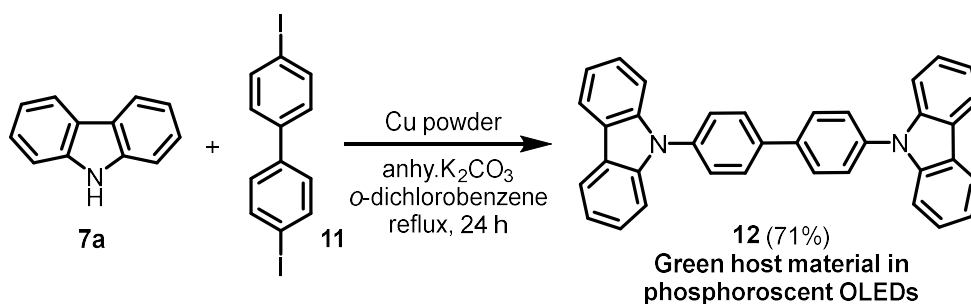
5A.9.5e. Synthesis of Boscalid



To a stirred solution of 2-chloronicotinoyl chloride **9** (88 mg, 0.5 mmol), DMAP (6 mg, 0.05 mmol) in 4 mL dichloromethane, 4'-chloro-[1,1'-biphenyl]-2-amine **5a** (102 mg, 0.5

mmol), Et₃N (0.14 mL, 1.0 mmol) in dichloromethane (1.0 mL) was added dropwise at 0 °C. The reaction was allowed to stir at 0 °C for 1 h, and another 12 h at room temperature followed by addition of dichloromethane (20 mL) and water (20 mL). The combined organic extracts were dried over Na₂SO₄ and the organic solvent was removed in *vacuo*. The crude residue was purified by column chromatography on silica gel (230-400 mesh) using a mixture of petroleum ether/EtOAc (*R_f* = 0.5, petroleum ether/EtOAc = 2:1), to afford 2-Chloro-*N*-(4'-chloro-[1,1'-biphenyl]-2-yl)nicotinamide (**10**, 104 mg, 81%) as a white solid.

5A.9.5f. Synthesis of a Green Host Material (**12**)



To a 50 mL round-bottomed flask carbazole **7a** (2.4 mmol, 334 mg), 4,4'-diiodobiphenyl **11** (1.0 mmol, 406 mg), K₂CO₃ (8.0 mmol, 1.11 g), copper powder (2.8 mmol, 178 mg) and 18-crown-6 (0.2 mmol, 53 mg) were taken under argon atmosphere. To it, 20 mL of *o*-dichlorobenzene was added and the mixture was allowed to reflux for 24 h. The reaction mixture was filtered through a small pad of celite and the residue was washed with chloroform. The combined solvent was removed in *vacuo* and the resulted residue was recrystallized from methanol at -20 °C to give the product **12** as a white solid (344 mg, 71%).

5.10. References

- (a) Corbet, J.-P.; Mignani, G. *Chem. Rev.* **2006**, *106*, 2651-2710. (b) Kay, E. R.; Leigh, D. A.; Zerbetto, F. *Angew. Chem., Int. Ed.* **2007**, *46*, 72-191. (c) Hughes, R. A.; Moody, C. J. *Angew. Chem., Int. Ed.* **2007**, *46*, 7930-7954. (d) Ackermann, L. *Modern Arylation Methods*, Wiley-VCH, Weinheim, **2009**. (e) Bringmann, G.; Gulder, T.; Gulder, T. A. M.; Breuning, M. *Chem. Rev.* **2011**, *111*, 563-639.
- (a) Beller, M.; Bolm, C. *Transition Metals for Organic Synthesis*, 2nd ed.; Wiley-VCH: Weinheim **2004**; (b) Meijere, A. de.; Diederich, F. *Metal-Catalyzed Cross-Coupling Reactions*; Wiley-VCH: Weinheim, **2004**.
- For representative reviews of direct C-H arylation, see: (a) Alberico, D.; Scott, M. E.; Lautens, M. *Chem. Rev.* **2007**, *107*, 174-238. (b) Ackermann, L. *Top. Organomet. Chem.* **2007**, *24*, 35-60. (c) Kakiuchi, F.; Kochi, T. *Synthesis* **2008**, 3013-3039. (d) Li, B.-J.; Yang, S.-D.; Shi, Z. *J. Synlett* **2008**, 949-957. (e) McGlacken, G. P.; Bateman, L. *Chem. Soc. Rev.* **2009**, *38*, 2447-2464. (f) Ackermann, L.; Vicente, R.; Kapdi, A. R. *Angew. Chem., Int. Ed.* **2009**, *48*, 9792-9826. (g) Daugulis, O.; Do, H. Q.; Shabashov, D. *Acc. Chem. Res.* **2009**, *42*, 1074-1086. (h) Chen, X.; Engle, K. M.; Wang, D.-H.; Yu, J.-Q. *Angew. Chem., Int. Ed.* **2009**, *48*, 5094-5115. (i) Lyons, T. W.; Sanford, M. S. *Chem. Rev.* **2010**, *110*, 1147-1169. (j) Daugulis, O. *Top. Curr. Chem.* **2010**, *292*, 57-84. (k) Chiusoli, G. P.; Catellani, M.; Costa, M.; Motti, E.; Ca, N. D.; Maestri, G. *Coord. Chem. Rev.* **2010**, *254*, 456-469. (l) Yamaguchi, J.; Yamaguchi, A. D.; Itami, K. *Angew. Chem., Int. Ed.* **2012**, *51*, 8960-9009.
- (a) Daugulis, O.; MacArthur, A. H. R.; Rix, F. C.; Templeton, J. L. *ACS Catal.* **2016**, *6*, 1518-1532. (b) Hubrich, J.; Himmler, T.; Rodefied, L.; Ackermann, L. *ACS Catal.* **2015**, *5*, 4089-4093. (c) Hubrich, J.; Himmler, T.; Rodefied, L.; Ackermann, L. *Adv. Synth. Catal.* **2015**, *357*, 474-480. (d) Suzuki, C.; Hirano, K.; Satoh, T.; Miura, M. *Org. Lett.* **2015**, *17*, 1597-1600. (e) Choi, S.; Chatterjee, T.; Choi, W. J.; You, Y.; Cho, E. J. *ACS Catal.* **2015**, *5*, 4796-4802. (f) Zuo, Z.; Liu, J.; Nan, J.; Fan, L.; Sun, W.; Wang, Y.; Luan, X. *Angew. Chem., Int. Ed.* **2015**, *54*, 15385-15389. (g) Feng, M.; Tang, B.; Xu, H.-X.; Jiang, X. *Org. Lett.* **2016**, *18*, 4352-4355.
- (a) Tremont, S. J.; Rahman, H. *J. Am. Chem. Soc.*, **1984**, *106*, 5759-5760. (b) Kalyani, D.; Deprez, N. R.; Desai, L. V.; Sanford, M. S. *J. Am. Chem. Soc.* **2005**, *127*, 7330-7331. (c) Daugulis, O.; Zaitsev, V. G. *Angew. Chem., Int. Ed.* **2005**, *44*, 4046-4048. (d) Shabashov, D.; Daugulis, O. *J. Org. Chem.* **2007**, *72*, 7720-7725. (e) Shi, Z.; Li, B.; Wan,

X.; Cheng, J.; Fang, Z.; Cao, B.; Qin, C.; Wang, Y. *Angew. Chem., Int. Ed.* **2007**, *46*, 5554-5558. (f) Yang, S.; Li, B.; Wan, X.; Shi, Z. *J. Am. Chem. Soc.* **2007**, *129*, 6066-6067. (g) Brasche, G.; Garcia-Fortanet, J.; Buchwald, S. L. *Org. Lett.* **2008**, *10*, 2207-2210. (h) Li, B.-J.; Tian, S.-L.; Fang, Z.; Shi, Z.-J. *Angew. Chem., Int. Ed.* **2008**, *47*, 1115-1118. (i) Deprez, N. R.; Sanford, M. S. *J. Am. Chem. Soc.* **2009**, *131*, 11234-11241. (j) Nishikata, T.; Abela, A. R.; Lipshutz, B. H. *Angew. Chem., Int. Ed.* **2010**, *49*, 781-784. (k) Nishikata, T.; Abela, A. R.; Huang, S.; Lipshutz, B. H. *J. Am. Chem. Soc.* **2010**, *132*, 4978-4979. (l) Mousseau, J. J.; Vallee, F.; Lorion, M. M.; Charette, A. B. *J. Am. Chem. Soc.* **2010**, *132*, 14412-14414. (m) Yeung, C. S.; Zhao, X.; Borduas, N.; Dong, V. M. *Chem. Sci.* **2010**, *1*, 331-336. (n) Zhao, X.; Yeung, C. S.; Dong, V. M. *J. Am. Chem. Soc.* **2010**, *132*, 5837-5844. (o) Truong, T.; Daugulis, O. *Org. Lett.* **2012**, *14*, 5964-5967. (p) Wencel-Delord, J.; Nimphius, C.; Wang, H.; Glorius, F. *Angew. Chem., Int. Ed.* **2012**, *51*, 13001-13005. (q) Jiao, L.-Y.; Oestreich, M. *Chem. -Eur. J.* **2013**, *19*, 10845-10849. (r) Yang, F.; Song, F.; Li, W.; Lan, J.; You, J. *RSC Adv.* **2013**, *3*, 9649-9652. (s) Liu, Y.-X.; Xue, D.; Wang, J.-D.; Zhao, C.-J.; Zou, Q.-Z.; Wang, C.; Xiao, J. *Synlett* **2013**, 507-513. (t) Uhlig, N.; Li, C.-J.; *Chem. -Eur. J.* **2014**, *20*, 12066-12067. (u) Li, D.; Xu, N.; Zhang, Y.; Wang, L. *Chem. Commun.* **2014**, *50*, 14862-14865. (v) Chinnagolla, R. A.; Jeganmohan, M. *Chem. Commun.* **2014**, *50*, 2442-2444. (w) Haridharan, R.; Muralirajan, K.; Cheng, C.-H. *Adv. Synth. Catal.* **2015**, *357*, 366-370. (x) Gao, P.; Guo, W.; Xue, J.; Zhao, Y.; Yuan, Y.; Xia, Y.; Shi, Z. *J. Am. Chem. Soc.* **2015**, *137*, 12231-12240. (y) Gao, P.; Liu, L.; Shi, Z.; Yuan, Y. *Org. Biomol. Chem.* **2016**, *14*, 7109-7113. (z) Nareddy, P.; Jordan, F.; Brenner-Moyer, S. E.; Szostak, M. *ACS Catal.* **2016**, *6*, 4755-4759.

6. Recent reviews on the utilization of aryldiazonium salts as an arylating agent, see: (a) Taylor, J. G.; Moro, A. V.; Correia, C. R. D. *Eur. J. Org. Chem.* **2011**, 1403-1428. (b) Mo, F.; Dong, G.; Zhang, Y.; Wang, J. *Org. Biomol. Chem.* **2013**, *11*, 1582-1593. (c) Hari, D. P.; König, B. *Angew. Chem., Int. Ed.* **2013**, *52*, 4734-4743. (d) Hari, D. P.; Hering, T.; König, B. *Chimica Oggi-Chemistry Today*, **2013**, *31*, 59.

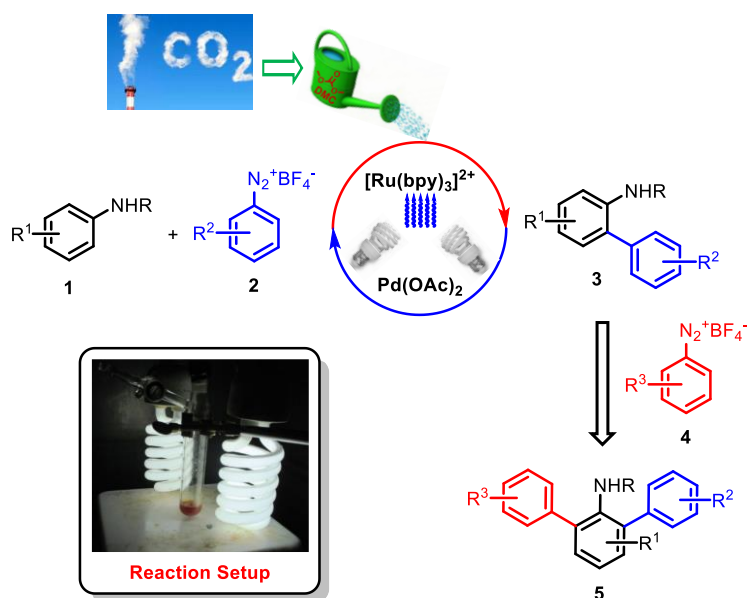
7. (a) Werner, E. W.; Sigman, M. S. *J. Am. Chem. Soc.* **2011**, *133*, 9692-9695. (b) Werner, E. W.; Mei, T.-S.; Burckle, A. J.; Sigman, M. S. *Science*, **2012**, *338*, 1455-1458. (c) Hari, D. P.; Schroll, P.; König, B. *J. Am. Chem. Soc.* **2012**, *134*, 2958-2961. (d) Hartmann, M.; Li, Y.; Studer, A. *J. Am. Chem. Soc.* **2012**, *134*, 16516-16519. (e) Schroll, P.; Hari, D. P.; König, B. *ChemistryOpen* **2012**, *1*, 130-133. (f) Sahoo, B.; Hopkinson, M. N.; Glorius, F. *J. Am. Chem. Soc.* **2013**, *135*, 5505-5508. (g) Shu, X.-Z.; Zhang, M.; He, Y.; Frei, H.;

- Toste, F. D. *J. Am. Chem. Soc.* **2014**, *136*, 5844-5847. (h) Oliveira, C. C.; Marques, M. V.; Godoi, M. N.; Regiani, T.; Santos, V. G.; dos-Santos, E. A. F.; Eberlin, M. N.; Sá, M. M.; Correia, C. R. D. *Org. Lett.* **2014**, *16*, 5180-5183. (i) Xue, D.; Jia, Z.-H.; Zhao, C.-J.; Zhang, Y.-Y.; Wang, C.; Xiao, J. *Chem. -Eur. J.* **2014**, *20*, 2960-2965. (j) Verbelen, B.; Boodts, S.; Hofkens, J.; Boens, N.; Dehaen, W. *Angew. Chem., Int. Ed.* **2015**, *54*, 4612-4616. (k) Nelson, H. M.; Williams, B. D.; Miró, J.; Toste, F. D. *J. Am. Chem. Soc.* **2015**, *137*, 3213-3216. (l) Huang, L.; Hackenberger, D.; Gooßen, L. J. *Angew. Chem., Int. Ed.* **2015**, *54*, 12607-12611. (m) Um, J.; Yun, H.; Shin, S. *Org. Lett.* **2016**, *18*, 484-487.
8. Kim, S.; Rojas-Martin, J.; Toste, F. D. *Chem. Sci.* **2016**, *7*, 85-88.
9. (a) Kalyani, D.; McMurtrey, K. B.; Neufeldt, S. R.; Sanford, M. S. *J. Am. Chem. Soc.* **2011**, *133*, 18566-18569. (b) Shin, K.; Park, S.-W.; Chang, S. *J. Am. Chem. Soc.* **2015**, *137*, 8584-8592.
10. Phipps, R. J.; Gaunt, M. J. *Science* **2009**, *323*, 1593-1597.
11. Neufeldt, S. R.; Sanford, M. S. *Adv. Synth. Catal.* **2012**, *354*, 3517-3522.
12. (a) Xuan, J.; Xiao, W.-J. *Angew. Chem., Int. Ed.* **2012**, *51*, 6828-6838. (b) Tucker, J. W.; Stephenson, C. R. J. *J. Org. Chem.* **2012**, *77*, 1617-1622. (c) Prier, C. K.; Rankic, D. A.; MacMillan, D. W. C. *Chem. Rev.* **2013**, *113*, 5322-5363. (d) Hopkinson, M. N.; Sahoo, B.; Li, J.-L.; Glorius, F. *Chem. Eur. J.* **2014**, *20*, 3874-3886. (e) Levin, M. D.; Kim, S.; Toste, F. D. *ACS Cent. Sci.* **2016**, *2*, 293-301. (f) Skubi, K. L.; Blum, T. R.; Yoon, T. P. *Chem. Rev.* **2016**, *116*, 10035-10074. (g) Romero, N. A.; Nicewicz, D. A. *Chem. Rev.* **2016**, *116*, 10075-10166. (h) Ghosh, I.; Marzo, L.; Das, A.; Shaikh, R.; König, B. *Acc. Chem. Res.* **2016**, *49*, 1566-1577.
13. For selected examples of photoredox catalysis by eosin-Y and radical chemistry, see: (a) Cismesia, M. A.; Yoon, T. P. *Chem. Sci.* **2015**, *6*, 5426-5434. (b) Studer, A.; Curran, D. P. *Angew. Chem., Int. Ed.* **2016**, *55*, 58-102. (c) Xu, P.; Wang, G.; Zhu, Y.; Li, W.; Cheng, Y.; Li, S.; Zhu, C. *Angew. Chem., Int. Ed.* **2016**, *55*, 2939-2943. (d) Hari, P.; König, B. *Chem. Commun.* **2014**, *50*, 6688-6699. (e) Neumann, M.; Földner, S.; König, B.; Zeitler, K. *Angew. Chem., Int. Ed.* **2011**, *50*, 951-954. (f) Majek, M.; Filace, F.; Wangelin, A. J. v. *Beilstein J. Org. Chem.* **2014**, *10*, 981-989.
14. Xiong, T.; Li, Y.; Lv, Y.; Zhang, Q. *Chem. Commun.* **2010**, *46*, 6831-6833.
15. Maestri, G.; Malacria, M.; Derat, E. *Chem. Commun.* **2013**, *49*, 10424-10426.
16. An alternative mechanism involving binuclear Pd species that may result in completely different catalytic cycle can't be rolled out. For seminal work on high oxidation state

bimetallic Pd species, see: (a) Powers, D. C.; Ritter, T. *Nat. Chem.* **2009**, *1*, 302-309. (b) Powers, D. C.; Geibel, M. A. L.; Klein, J. E. M. N.; Ritter, T. *J. Am. Chem. Soc.* **2009**, *131*, 17050-17051.

Chapter 5B

Direct Arylation of Anilides under External Oxidant-Free Conditions using CO₂-Derived Dimethyl Carbonate (DMC) as a 'Green' Solvent under [Ru]-Catalysis



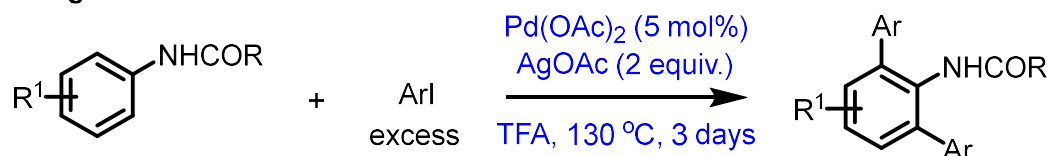
5B.1. Introduction

Development of new catalytic approaches based on direct utilization of ubiquitous inert C-H bonds for chemical production is an important field of research. In this context, *ortho*-arylaniline scaffold constitutes one of the important families of organic compound and find applications in pharmaceuticals, material sciences, and organometallic catalysis.¹ They have also been found to be key synthetic intermediates for various organic transformations and for synthesizing diverse *N*-heterocyclics.² Owing to their structural diversity, and remarkable synthetic utilities, development of an efficient and a practical methodology for the selective and straightforward synthesis of *ortho*-aryl anilides has long been of immense importance in the contemporary science. Despite the classical cross-coupling reactions, direct C-H arylation has emerged as more powerful and promising method to enable diverse *ortho*-arylated aniline derivatives.²⁻⁵ Research groups of Shi, Lipshutz, Daugulis, Ackermann, Cheng, Jeganmohan and others have extensively studied the catalytic C-H arylation of anilides with various aromatic electrophiles,^{2a-c,4} and aromatic organometallic reagents (Scheme 5B.1a and Scheme 5B.1b).^{1c,2d-e,5} However, the use of excess amounts of external oxidant, base/additives, the formation of mono- and di-arylated anilides (in case of symmetrical anilides), and performing the reactions at a higher temperature (80-120 °C)^{1c,2,4a-b,5a-c} are potential concerns.

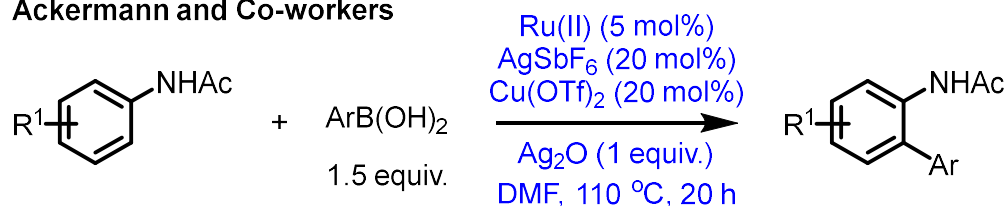
In recent times, aryldiazonium salts have been highlighted as convenient arylating reagents because, a) the aryl diazonium salt can be easily synthesized from inexpensive, abundantly available anilines and can be used for large-scale preparation, and b) their reactivity is higher than that of the corresponding halides.⁶ However, examples of utilization of aryldiazonium salts in the transition metal-catalyzed direct arylation of C-H bonds have rarely been achieved.⁷ Recently, direct C-H arylation of 2-phenylpyridine, which is a good substrate because of its chelating ability and electron-deficient cyclic *tert*-amides is reported under dual catalysis.^{7a} Sanford and co-workers reported a photoredox Ir/Pd-catalyzed (10 mol% of Pd(NO₃)₂ and 5 mol% of [Ir(ppy)₂(dtbbpy)]PF₆) arylation of *ortho*-substituted anilide (*only one example*) with aryldiazonium salt in methanol, albeit with a poor yield.^{5f} Gaunt and co-workers reported *meta*-selective C-H arylation of anilides using diaryliodonium salts as aryl coupling partner under copper catalysis.⁸ In this chapter, we report direct *ortho* C-H arylation of anilides by merging Ru-based photoredox catalysis with palladium catalysis using aryldiazonium salt as an expedient aryl group donor, under

CO₂-derived dimethyl carbonate (DMC) as a 'green' solvent, is described. Totally, unprecedented synthesis of unsymmetrical bis-C-H arylated anilines was also described. This bis-arylated anilines are good precursors for the synthesis of Brookhart-type polymerization catalyst.

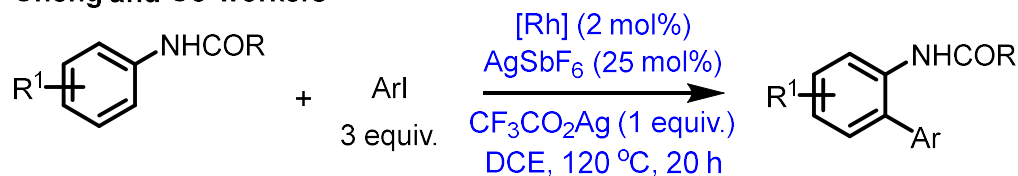
Daugulis and Co-workers



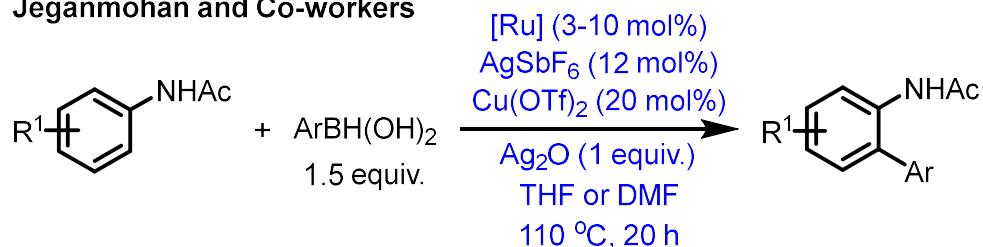
Ackermann and Co-workers



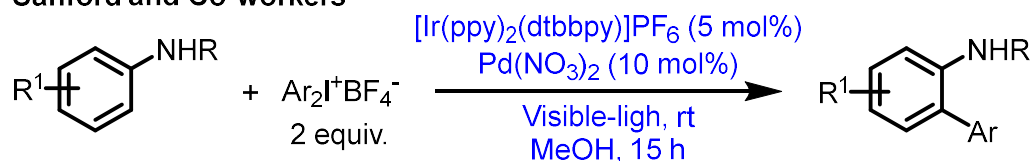
Cheng and Co-workers



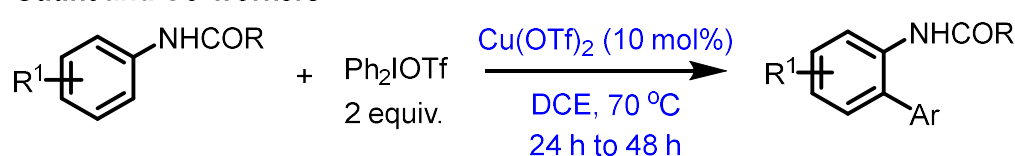
Jeganmohan and Co-workers



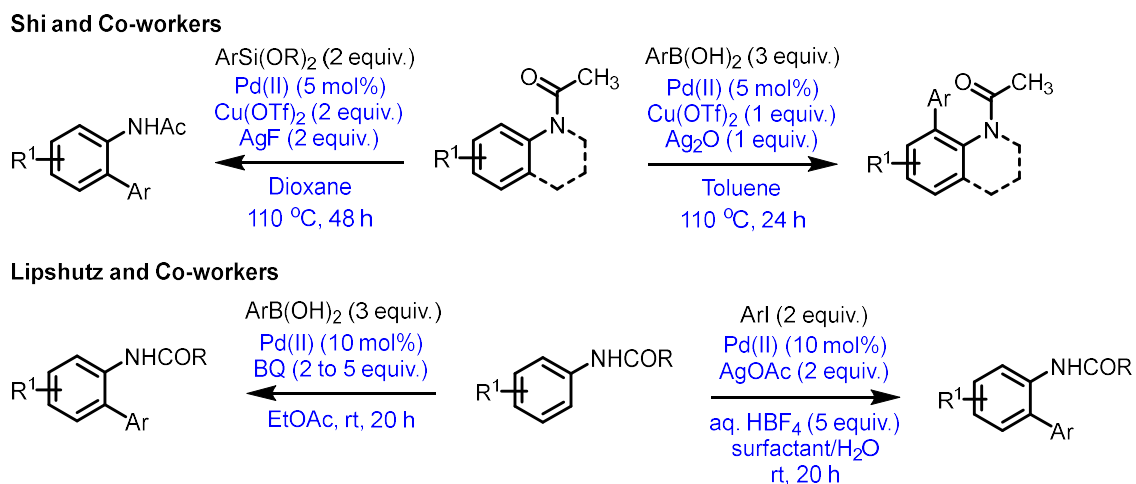
Sanford and Co-workers



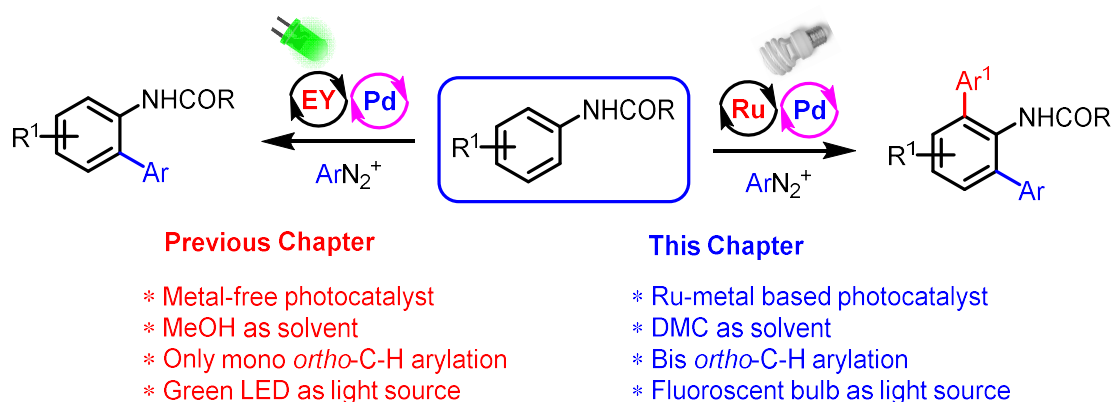
Gaunt and Co-workers



Scheme 5B.1a. Strategies for *ortho*-C-H arylation of anilides.



Scheme 5B.1b. Strategies for *ortho*-C-H arylation of anilides.



Scheme 5B.2. Comparisons between eosin-Y (Chapter 5A) and Ru-based (Chapter 5B) photoredox catalysis.

5B.2. Statement of the Problem

The 2,6-diaryl substituted anilines have been used in the synthesis of Brookhart type polymerization catalyst. These bis-arylated anilines were usually synthesized by coupling boronic acids with pre-functionalized 2,6-dihaloaniline derivatives. Again, synthesis of unsymmetrical 2,6-arylated aniline derivative is always problematic. In chapter 5A, we have disclosed the *ortho*-C-H arylation of anilines under dual palladium and eosin-Y photoredox catalytic condition. The above dual catalytic method is limited only to the synthesis of mono *ortho*-C-H arylated anilines. In the current chapter, we describe a similar

Initially, we have optimized for mono-C-H arylation of anilides. Thus, we began our external oxidant-free C-H arylation of anilides with an evaluation of a range of solvents, mol% of the photoredox catalyst, and palladium salts in presence of anilide **1a** and *p*-chlorobenzenediazonium salt **2a** as representative coupling partners (Table 5B.1). We found that the use of light with catalytic amounts of photoredox catalyst [Ru(bpy)₃]Cl₂, and Pd(OAc)₂ enabled the desired mono-selective *ortho* C-H arylated anilide **3aa** in 97% isolated yield (Table 5B.1, entry 1). The necessity of each of the key reaction components was demonstrated through a series of control experiments (Table 5B.1, entries 5-8). While a minor amount of **3aa** formed in the absence of photoredox catalyst, no reaction was observed upon exclusion of light source. Also, no desired product (**3aa**) was observed in the absence of Pd(OAc)₂ (Table 5B.1, entry 6). Performing the reaction at elevated temperature (80 °C) gave **3aa** only 32% yield (Table 5B.1, entry 8). Notably, biarylated product (self-coupled) of *p*-chlorobenzenediazonium salt **2a** was not observed, which may exclude the homolytic bond cleavage of **2a** to an aryl radical. Other palladium salts such as PdCl₂, Pd(acac)₂, and Pd(PPh₃)₄ are ineffective under optimal conditions (Table 5B.1, entries 9-11). Next, to exploit the better solubility of diazonium salts in the reaction medium, we have screened several polar solvents, and finally, the use of dimethyl carbonate as the reaction medium was found to provide excellent yields. DMC is inexpensive, low-toxic, biodegradable, and considered as an environmentally benign' solvent.⁹ Other solvents commonly employed in photoredox catalysis, such as MeOH, DMF, and THF afforded the product **3aa** in 46%, 0%, and 7% yields, respectively (Table 5B.1, entries 12-14).

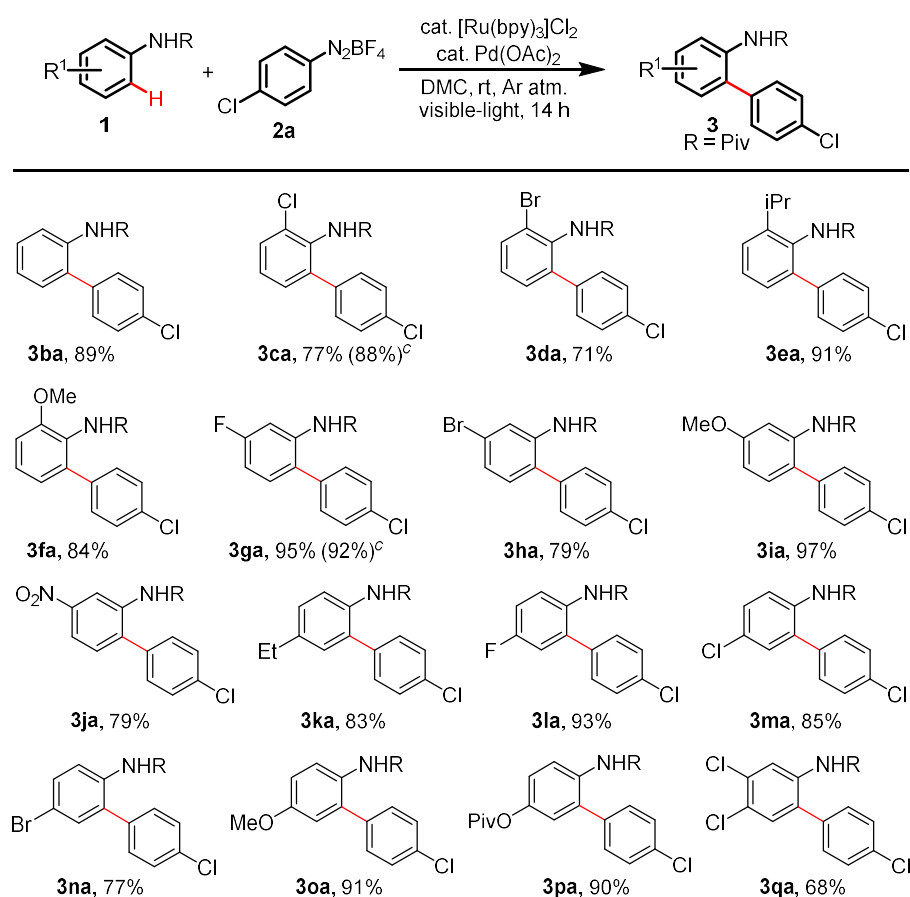
5B.4. Substrate Scope

5B.4.1. Scope for Mono *ortho*-C-H Arylation

Having identified 'green' conditions for direct C-H arylation using aryl diazonium salts, we sought to define the scope of the reaction. As shown in Table 5B.2, the present C-H arylation strategy displayed high functional-group tolerance and expedient method for the preparation of mono-selective *ortho* C-H arylated anilides in good to excellent yields (up to 97%) under very mild conditions. Thus, *N*-phenylpivalamide **1** with electron-donating substituents such as *o*-^{*i*}Pr, *o*-OMe, *m*-OMe, *p*-Et, and *p*-OMe afforded the corresponding

ortho-aryl anilides in excellent yields (Table 5B.2; products **3ea** in 91%, **3fa** in 84%, **3ia** in 97%, **3ka** in 83%, and **3oa** in 91% yields, respectively). Halide and electron-withdrawing substituents (*p*-F and *m*-NO₂) on the phenyl group of anilide are also tolerated and selectively gave the corresponding mono C-H arylated products in excellent yields (up to 95%). Notably, benzene ring substituted with *O*-pivaloyl group failed to give the corresponding *ortho* C-H arylated product. Thus, the reaction of **1p** with **2a** under optimized conditions selectively gave **3pa** in 90% isolated yield, highlighting the unique feature of the *N*-pivaloyl motif. The effect of substituent on the acyl group of anilides was further studied by changing *N*-pivaloyl (i.e. *t*-Butyl) to *N*-acetyl (i.e. methyl) and gave a mixture of mono- and bis-arylated products in 31% yields. To further extend the scope of the reaction, we also investigated different amide such as -NHTs as the directing group and found to be not suitable for the present C-H arylation strategy.

Table 5B.2. Substrate scope of anilides.^{a,b}

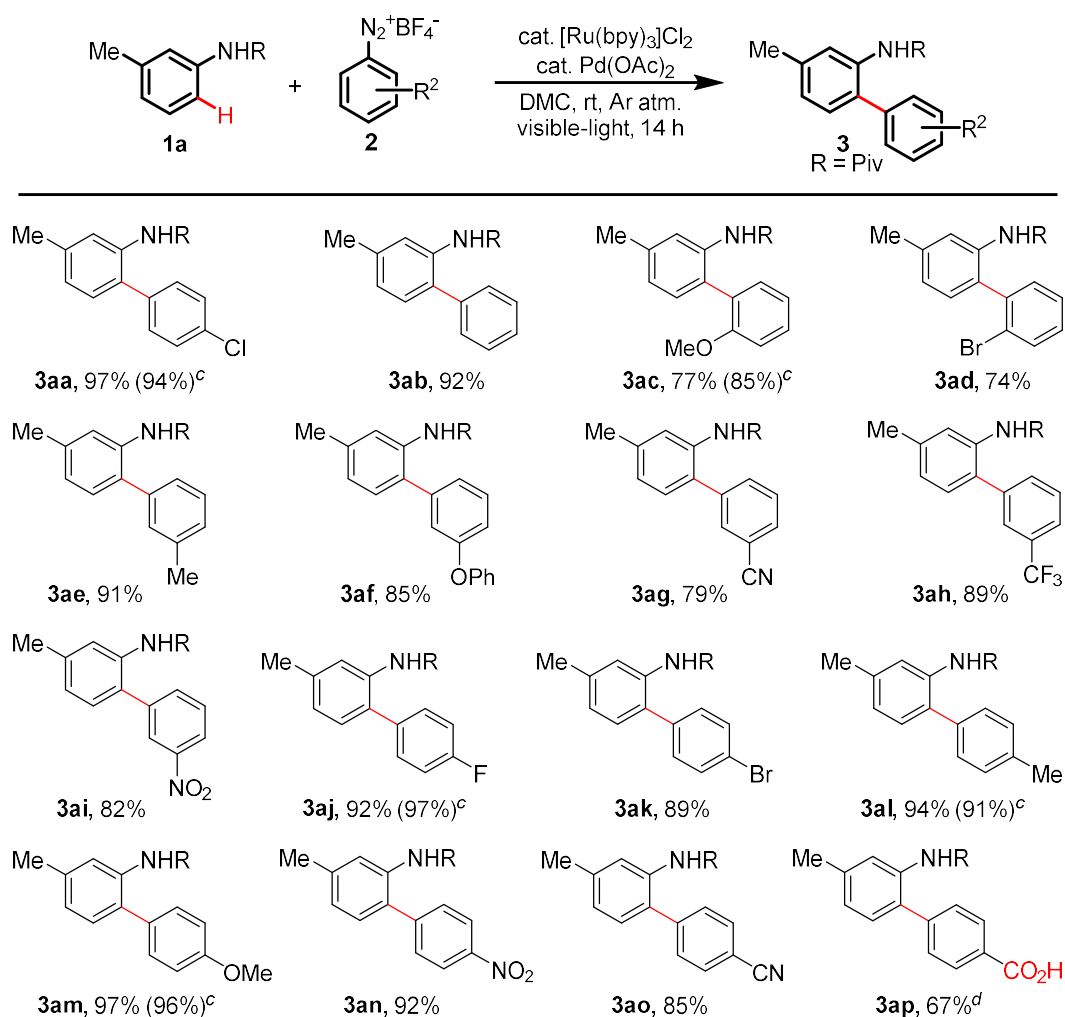


^aReaction conditions: **1** (0.1 mmol), **2a** (0.11 mmol), [Ru(bpy)₃]Cl₂ (2.5 mol%), Pd(OAc)₂ (5 mol%), DMC (0.5 mL) at rt for 14 h under visible-light irradiation. ^bIsolated yields.

^cUsing 10 mol% of Pd(OAc)₂ for 8 h.

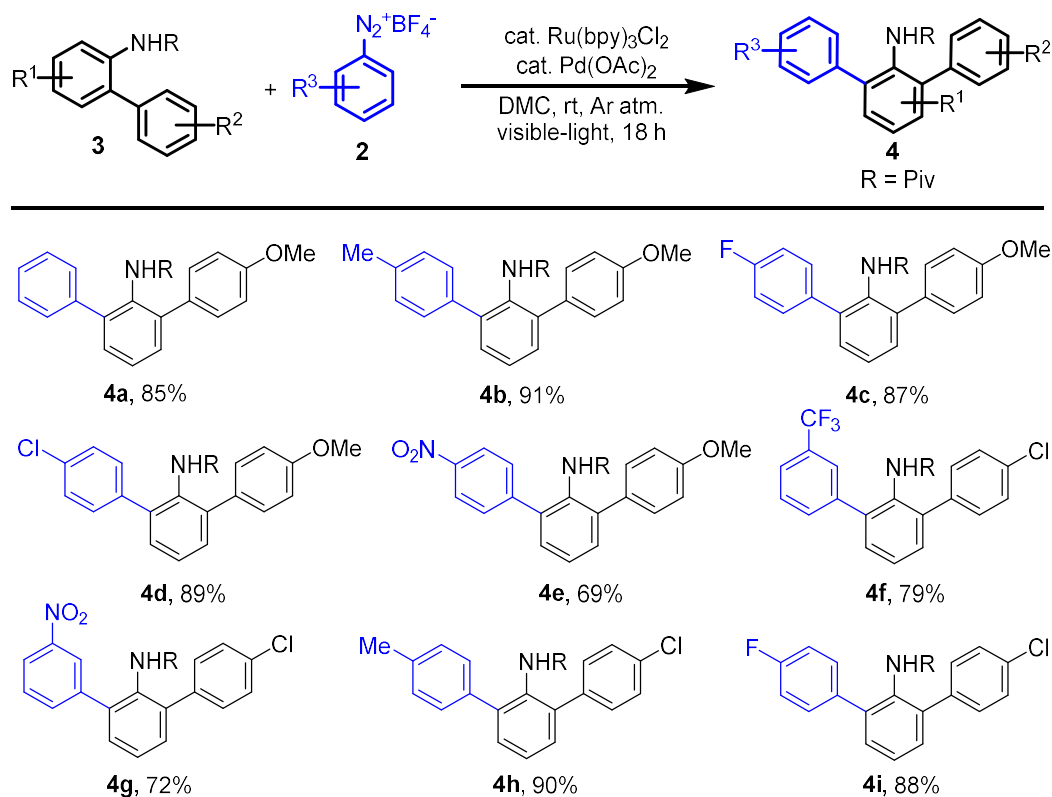
The scope of aryldiazonium salts **2** was explored using *N*-(*m*-tolyl)pivalamide **1a** as a benchmark substrate under optimal conditions (Table 5B.3). Various electronically diverse substituents, both electron-donating (-CH₃ and -OMe) and electron-withdrawing (-F, -CF₃, -NO₂ and -CN) groups, proceeded smoothly to afford the corresponding mono-selective *ortho* C-H arylated anilides in good to excellent yields (74% - 97%). It was observed that the electronic nature of the aryldiazonium salts has a minor influence on the room-temperature C-H arylation reaction. It should be noted that the use of an acid substituent on the aryl diazonium salt resulted in diminished reactivity under standard conditions and gave **3ap** in 67% isolated yield along with the decarboxylated product **3ab** in 8% yield.

Table 5B.3. Substrate scope of aryldiazonium salts.^{a,b}

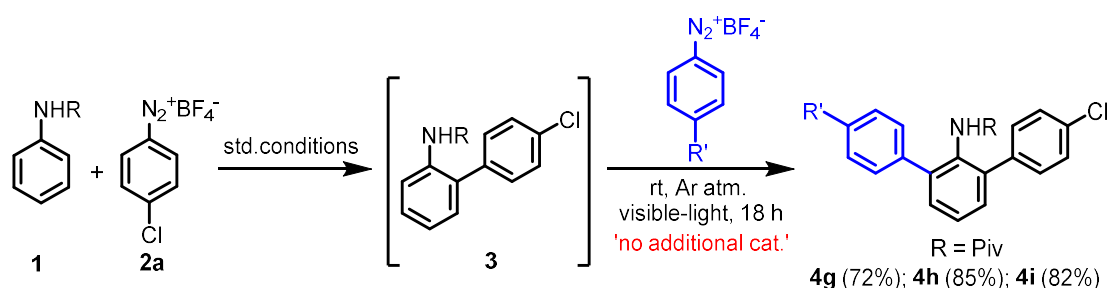


^aReaction conditions: **1a** (0.1 mmol), **2** (0.11 mmol), [Ru(bpy)₃]Cl₂ (2.5 mol%), Pd(OAc)₂ (5 mol%), DMC (0.5 mL) at room temperature for 14 h under visible-light irradiation.

^bIsolated yields. ^cUsing 10 mol% of Pd(OAc)₂ for 8 h. ^d0.2 mmol of **2** was used.

5B.4.2. Scope for 2,6-bis *ortho*-C-H ArylationTable 5B.4. Synthesis of unsymmetrical 2,6-diarylated anilines.^{a,b}

^aReaction conditions: **3** (0.1 mmol), **2** (0.11 mmol), $[\text{Ru}(\text{bpy})_3]\text{Cl}_2 \cdot 6\text{H}_2\text{O}$ (2.5 mol%), $\text{Pd}(\text{OAc})_2$ (8 mol%), DMC (0.5 mL) at room temperature for 18 h under visible-light irradiation. ^bIsolated yields.

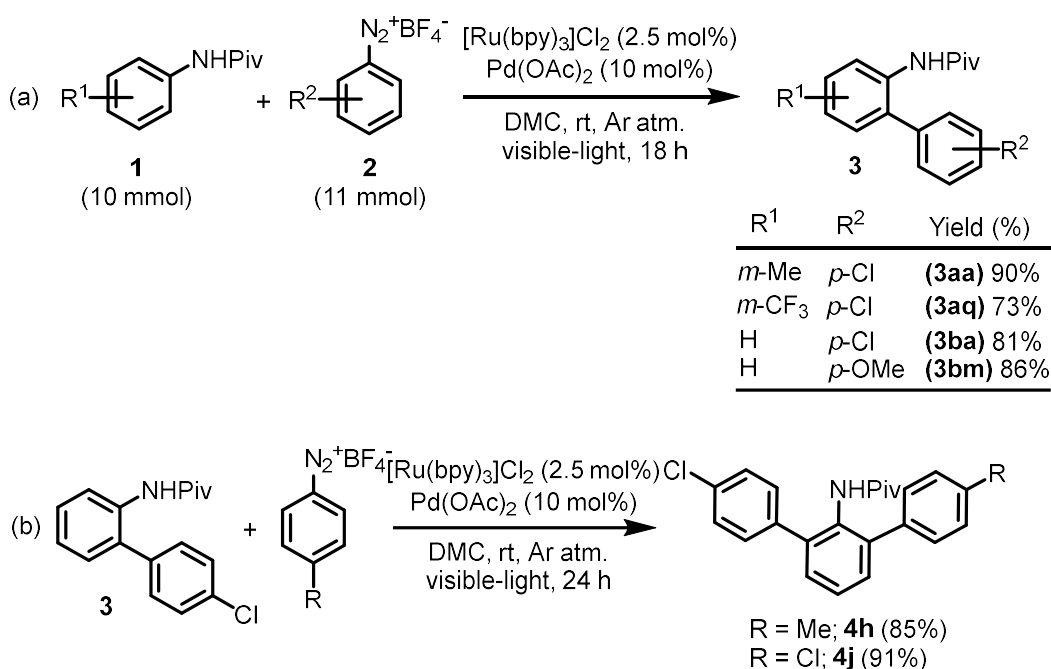


Scheme 5B.3. A one-pot sequential unsymmetrical bis-arylation.

Next, we have examined an efficient process for the sustainable synthesis of unsymmetrical 2,6-diarylated aniline derivatives (Table 5B.4). To our delight, treatment of mono-arylated anilides (**3**) and **2** with catalytic amounts of $[\text{Ru}(\text{bpy})_3]\text{Cl}_2$ and $\text{Pd}(\text{OAc})_2$

in DMC at room temperature for 18 h gave the expected product **4** in good yields (up to 91%). The reaction is general and possesses various functional group tolerance. A one-pot, sequential unsymmetrical bis-arylation of anilides is also demonstrated without the addition of any extra catalyst in the second stage (Scheme 5B.3). Thus, the developed silver- and oxidant-free dual catalytic approach showed high activity and can be used as a reusable homogeneous system for sustainable synthesis of 2,6-diarylated aniline derivatives. We have successfully shown the practical viability of this catalytic protocol under standard conditions. In this regard, the present strategy was tested for the gram-scale synthesis of both mono- and unsymmetrical bis-arylation of anilides, and it worked remarkably with the expected arylated product in very good yield under operationally simple conditions (Scheme 5B.4).

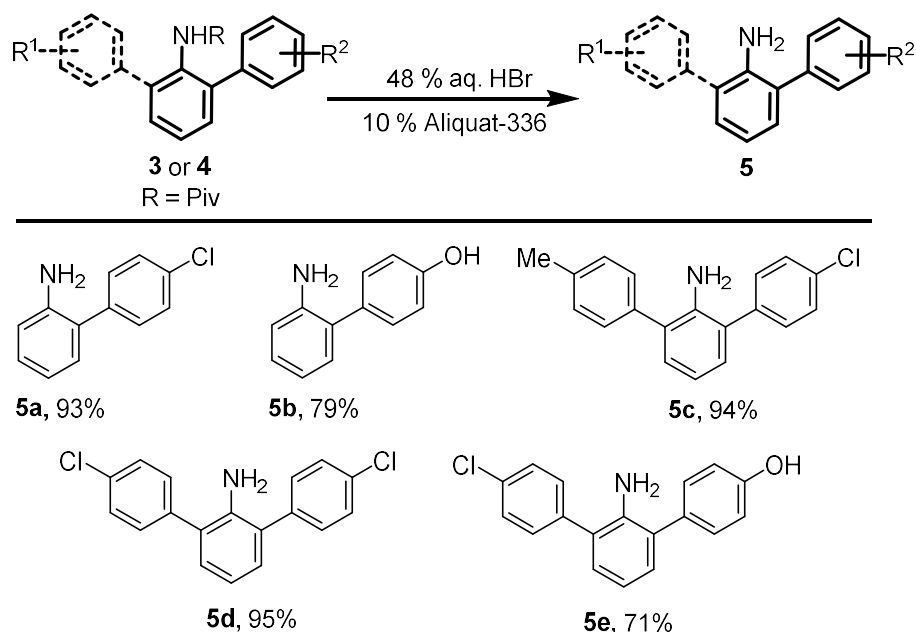
5B.4.3. Gram-scale *ortho*-C-H Arylation



Scheme 5B.4. Gram-scale synthesis of anilides.

5B.4.4. Directing Group Removal

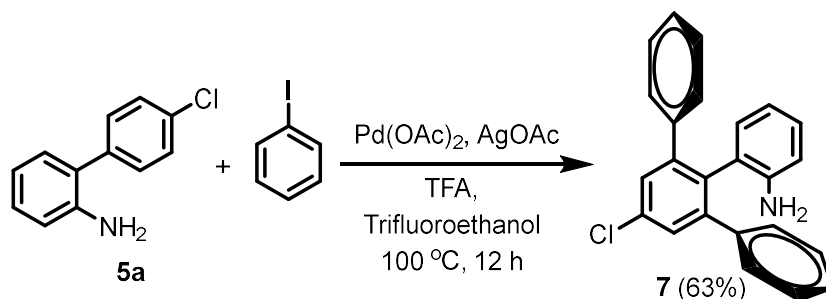
The removal of the directing group was accomplished under mild reaction conditions to access *ortho*-aryl anilines in excellent yields with chromatography-free method (Scheme 5B.5).



Scheme 5B.5. Removal of the directing group.

5B.4.5. Bis-arylation of Free Amine (5a)

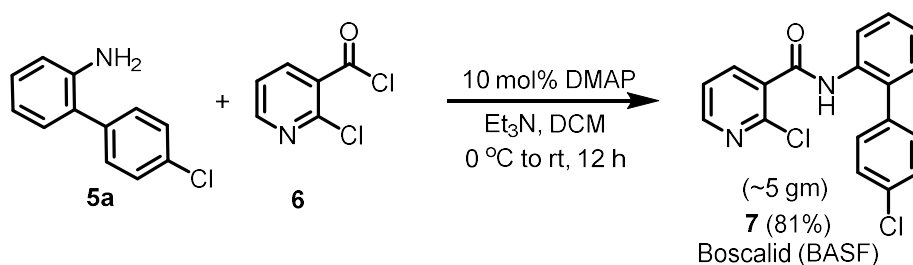
An efficient Pd(OAc)₂-catalyzed free-amine directed *ortho*-C-H arylation of **5a** with iodobenzene to the diarylated product (**7**) was done with exclusive regioselectivity.



Scheme 5B.6. Bis-arylation of 5a.

5B.4.6. Gram-scale Synthesis of Boscalid

Gratifyingly, a potential synthetic application of the present benign strategy in a concise and gram-scale synthesis of the BASF's agricultural fungicide, Boscalid (>1000 tons/year)^{1h} has been demonstrated (Scheme 5B.7). Thus, treatment of **5a** with 2-chloronicotinoyl chloride (**6**) in the presence of a catalytic amount of DMAP led to Boscalid (**7**) in 81% isolated yield.



Scheme 5B.7. Application in the gram-scale synthesis of Boscalid.

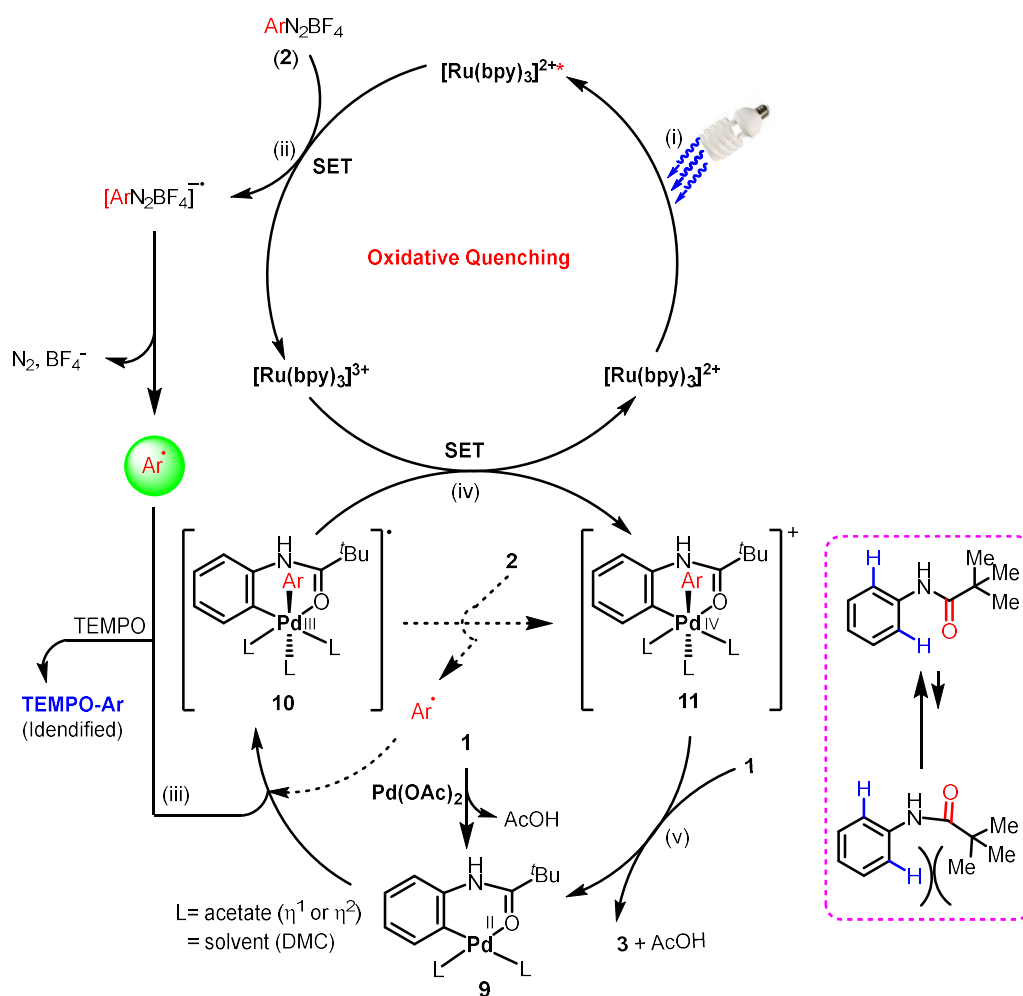
5B.5. Mechanistic Investigation

5B.5.1. Control Experiments

When we performed the reaction in the presence of the radical scavenger 2,2,6,6-tetramethylpiperidine-1-oxyl (TEMPO; 1.5 equiv.), the reaction was completely inhibited. Indeed, an *O*-arylated-TEMPO product was detected on GC-MS, indicating that the radical reaction pathway could be involved in the catalytic cycle. Reactions under dark conditions and at increased temperature (80 °C) gave the desired product in very poor yield (32%), which excludes the homolytic bond cleavage of aryldiazonium salt to an aryl radical under these conditions. In order to find the possibility of other reaction pathways such as chain reaction, a “light/dark” experiment¹⁰ was carried out. Thus, for the initial 60 minutes, the reaction was carried out under visible-light irradiation and then continued under dark condition. Interestingly, the formation of the product **3a** still occurs. This experimental result indicates that a radical chain process in the present dual catalytic system may be operative. This was further confirmed by performing the reaction using alternating intervals of light and dark; we have observed that the product formation occurs during the periods of irradiation as well as in the dark conditions.

5B.5.2. Plausible Mechanism

Based on preliminary results and known literature precedent,¹¹⁻¹³ a plausible catalytic cycle may involve the following key steps, (i) photoexcitation of $[\text{Ru}(\text{bpy})_3]^{2+}$ catalyst to generate a triplet state $[\text{Ru}(\text{bpy})_3]^{2+*}$ ($E_R^\circ = -0.81\text{V/SCE}$), (ii) the standard reduction potential of different ArN_2BF_2 are very close to SCE varying from a small positive to negative values,^{10c} and can be easily reduced by the triplet $[\text{Ru}(\text{bpy})_3]^{2+*}$ to aryl radical (Ar^\cdot) with the concomitant oxidation of Ru-centre to $[\text{Ru}(\text{bpy})_3]^{3+}$, (iii) reaction of aryl radical (Ar^\cdot) with palladacycle, (iv) one-electron oxidation of palladacycle by $[\text{Ru}(\text{bpy})_3]^{3+}$ ($E_R^\circ = +1.29\text{V/SCE}$) to regenerate the photocatalyst, and finally, (v) C-C bond formation *via* reductive elimination to release **3** and regeneration of Pd catalyst. Notably, an alternative mechanism involving binuclear palladium species that may result in completely different catalytic cycle can't be rolled out.¹⁴

Scheme 5B.8. Plausible catalytic cycle of *ortho*-C-H arylation reaction.

5B.6. Conclusion

In conclusion, we have developed an efficient strategy for *ortho*-C-H arylation of anilides under external oxidant-free conditions. In the present catalytic approach, aryldiazonium salt was used as an expedient aryl group donor, also working as an internal oxidant *via* C-N₂ bond cleavage. This reaction proceeds readily at room temperature and uses CO₂-derived dimethyl carbonate as a 'green' solvent under visible-light photoredox conditions. The potential application of the present strategy for the gram-scale synthesis of Boscalid (BASF's agricultural fungicide) is also demonstrated. The broad substrate scope and excellent selectivity of this process make it attractive for facile construction of diverse *N*-heterocycles (e.g. dibenzo[*b,d*]azepine, phenanthridine and carbazole). Also, unsymmetrical bis-arylation of anilides has been described under redox neutral conditions.

5B.7. Experimental Procedures

5B.7.1. General Procedure for *ortho* C-H Bond Arylation of Anilides

In an oven-dried 15 mL Schlenk tube with a magnetic stirring bar was charged with pivalamide **1** (0.1 mmol), aryldiazonium salt **2** (0.11 mmol), Pd(OAc)₂ (5 mol %), [Ru(bpy)₃]Cl₂·6H₂O (2.5 mol %), and 0.5 mL of anhydrous DMC under argon atm. Then the reaction tube was frozen in liquid N₂, degassed by the freeze-pump-thaw procedure (3×), refilled with argon gas. Then the Schlenk tube was placed on a magnetic stirrer with two 32 W compact fluorescent light bulbs kept about 5 cm away from it and irradiated at room temperature with constant stirring. After 14 h, the reaction mixture was quenched with saturated 15 mL NaHCO₃ solution, and the aqueous layer was extracted with EtOAc (3 × 15 mL). Finally, the combined organic layer was washed with brine solution (15 mL), dried over Na₂SO₄ and concentrated in *vacuo*. The residue was purified by column chromatography on silica gel with a mixture of EtOAc and petroleum ether to afford the desired *ortho*-arylated product.

5B.7.2. General Procedure for Gram-scale Synthesis

In an oven-dried 100 mL Schlenk tube with a magnetic stirring bar was charged with pivalamide **1** (10 mmol), aryldiazonium salt **2** (11 mmol), Pd(OAc)₂ (10 mol %), [Ru(bpy)₃]Cl₂·6H₂O (2.5 mol %), and 50 mL of anhydrous DMC under argon atm. Then the reaction tube was frozen in liquid N₂, degassed by the freeze-pump-thaw procedure (3×), refilled with argon gas. Then the Schlenk tube was placed on a magnetic stirrer with two 32 W compact fluorescent light bulbs kept about 5 cm away from it and irradiated at room temperature with constant stirring. After 18 h, the reaction mixture was quenched with saturated 100 mL NaHCO₃ solution, and the aqueous layer was extracted with EtOAc (3× 100 mL). Finally, the combined organic layer was washed with brine solution (100 mL), dried over Na₂SO₄ and concentrated in *vacuo*. The residue was purified by column chromatography on silica gel with a mixture of EtOAc and petroleum ether to afford the desired *ortho*-arylated product in gram-scale.

5B.7.3. General Procedure for 2,6-bis C-H Bond Arylation

5B.7.3a. Symmetrical 2,6-bis C-H Bond Arylation

In an oven-dried 15 mL Schlenk tube with a magnetic stirring bar was charged with pivalamide **1** (0.1 mmol), aryldiazonium salt **2** (0.25 mmol), Pd(OAc)₂ (8 mol %), [Ru(bpy)₃]Cl₂·6H₂O (2.5 mol %), and 0.5 mL of anhydrous DMC under argon atm. Then the reaction tube was frozen in liquid N₂, degassed by the freeze-pump-thaw procedure (3×), refilled with argon gas. Then the Schlenk tube was placed on a magnetic stirrer with two 32 W compact fluorescent light bulbs kept about 5 cm away from it and irradiated at room temperature with constant stirring. After 18 h, the reaction mixture was quenched with saturated 15 mL NaHCO₃ solution, and the aqueous layer was extracted with EtOAc (3 × 15 mL). Finally, the combined organic layer was washed with brine solution (15 mL), dried over Na₂SO₄ and concentrated in *vacuo*. The residue was purified by column chromatography on silica gel with a mixture of EtOAc and petroleum ether to afford pure symmetrical bis *ortho*-arylated product.

5B.7.3b. Unsymmetrical 2,6-bis C-H Bond Arylation

In an oven-dried 15 mL Schlenk tube with a magnetic stirring bar was charged with *ortho*-aryl pivalamide **3** (0.1 mmol), aryldiazonium salt **2** (0.11 mmol), Pd(OAc)₂ (8 mol %), [Ru(bpy)₃]Cl₂·6H₂O (2.5 mol %), and 0.5 mL of anhydrous DMC under argon atm. Then the reaction tube was frozen in liquid N₂, degassed by the freeze-pump-thaw procedure (3×), refilled with argon gas. Then the Schlenk tube was placed on a magnetic stirrer with two 32 W compact fluorescent light bulbs kept about 5 cm away from it and irradiated at room temperature with constant stirring. After 18 h, the reaction mixture was quenched with saturated 15 mL NaHCO₃ solution, and the aqueous layer was extracted with EtOAc (3 × 15 mL). Finally, the combined organic layer was washed with brine solution (15 mL), dried over Na₂SO₄ and concentrated in *vacuo*. The residue was purified by column chromatography on silica gel with a mixture of EtOAc and petroleum ether to afford desired unsymmetrical bis *ortho* C-H arylated product.

5B.7.3c. One-pot Sequential Approach to Unsymmetrical 2,6-bis C-H Bond Arylation

In an oven-dried 15 mL Schlenk tube with a magnetic stirring bar was charged with pivalamide **1** (0.1 mmol), aryldiazonium salt **2** (0.11 mmol), Pd(OAc)₂ (8 mol %), [Ru(bpy)₃]Cl₂·6H₂O (2.5 mol %), and 0.8 mL of anhydrous DMC under argon atm. Then the reaction tube was frozen in liquid N₂, degassed by the freeze-pump-thaw procedure (3×), refilled with argon gas. Then the Schlenk tube was placed on a magnetic stirrer with two 32 W compact fluorescent light bulbs kept about 5 cm away from it and irradiated at room temperature with constant stirring. After 14 h, 0.11 mmol of the second aryldiazonium salt was added under inert gas and was allowed the irradiation at room temperature with constant stirring for an additional 14 h. Then, the reaction mixture was quenched with saturated 15 mL NaHCO₃ solution, and the aqueous layer was extracted with EtOAc (3 × 15 mL). Finally, the combined organic layer was washed with brine solution (15 mL), dried over Na₂SO₄ and concentrated in *vacuo*. The residue was purified by column chromatography on silica gel with a mixture of EtOAc and petroleum ether to afford desired unsymmetrical bis *ortho* C-H arylated product.

5B.7.3d. Gram-scale Synthesis of Unsymmetrical 2,6-bis C-H Bond Arylated Products

In an oven-dried 50 mL Schlenk tube with a magnetic stirring bar was charged with *ortho*-aryl pivalamide **3** (3 mmol), aryldiazonium salt **2** (3.3 mmol), Pd(OAc)₂ (10 mol %), [Ru(bpy)₃]Cl₂·6H₂O (2.5 mol %), and 15 mL of anhydrous DMC under argon atm. Then the reaction tube was frozen in liquid N₂, degassed by the freeze-pump-thaw procedure (3×), refilled with argon gas. Then the Schlenk tube was placed on a magnetic stirrer with two 32 W compact fluorescent light bulbs kept about 5 cm away from it and irradiated at room temperature with constant stirring. After 24 h, the reaction mixture was quenched with saturated 50 mL NaHCO₃ solution, and the aqueous layer was extracted with EtOAc (3 × 50 mL). Finally, the combined organic layer was washed with brine solution (40 mL), dried over Na₂SO₄ and concentrated in *vacuo*. The residue was purified by column chromatography on silica gel with a mixture of EtOAc and petroleum ether to afford pure unsymmetrical bis *ortho*-arylated product in gram-scale.

5B.7.4a. Radical Trapping Experiment

In an oven-dried 15 mL Schlenk tube with a magnetic stirring bar was charged with **1a** (0.1 mmol), **2a** (0.11 mmol), TEMPO (0.15 mmol), Pd(OAc)₂ (5 mol %), [Ru(bpy)₃]Cl₂·6H₂O (2.5 mol %), and 0.5 mL of anhydrous DMC under argon atm. Then the reaction tube was frozen in liquid N₂, degassed by the freeze-pump-thaw procedure (3 ×), refilled with argon gas. Then the Schlenk tube was placed on a magnetic stirrer with two 32 W compact fluorescent light bulbs kept about 5 cm away from it and irradiated at room temperature. After 14 h, the reaction mixture was analyzed on GC-MS and the formation of *O*-arylated-TEMPO product was observed.

5B.7.4b. Light-Dark Experiment

Two parallel experiments [A (Light) and B (Dark)] were carried out employing *N*-(3-methylphenyl)pivalamide **1a** (77 mg, 0.4 mmol), 4-chlorobenzenediazonium tetrafluoroborate **2a** (136 mg, 0.6 mmol), Pd(OAc)₂ (5 mol%), [Ru(bpy)₃]Cl₂·6H₂O (2.5 mol%) and mesitylene (0.056 mL, 0.4 mmol) as internal standard in 2.0 mL of dimethyl

carbonate. Reaction (A) was irradiated with continuous irradiation. However, the reaction (B) was irradiated with a light source under the standard condition for the first 60 minutes and then carried out in the dark condition. Continuous sampling was undertaken with the different time intervals, and yield of *ortho*-arylated product (**3aa**) was determined by gas chromatography.

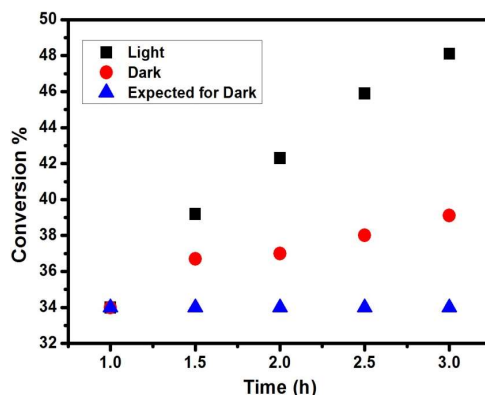


Figure 5B.1. Light-dark experiment.

5B.7.4c. Light-Dark Experiment (ON/OFF experiment)

The reaction was carried out employing *N*-(3-methylphenyl)pivalamide **1a** (77 mg, 0.4 mmol), 4-chlorobenzenediazonium tetrafluoroborate **2a** (136 mg, 0.6 mmol), Pd(OAc)₂ (5 mol%), [Ru(bpy)₃]Cl₂·6H₂O (2.5 mol%) and mesitylene (0.056 mL, 0.4 mmol) as internal standard in 2.0 mL of dimethyl carbonate. The reaction is conducted using alternating intervals of light and dark. In each interval, continuous sampling was undertaken with the different time intervals, and yield of *ortho*-arylated product (**3aa**) was determined by gas chromatography.

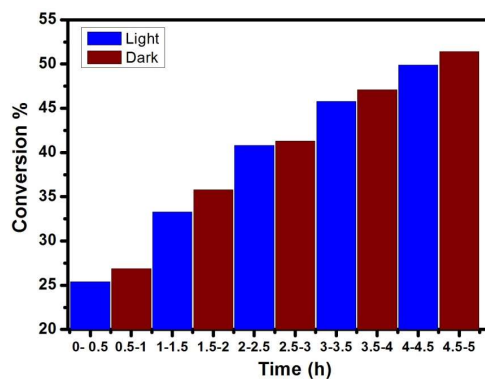


Figure 5B.2. Alternative Light on-off experiment.

5B.7.5a. Removal of Directing Group

To a 10 mL screw-capped tube, *ortho*-aryl pivalamide (0.5 mmol), 10 weight percentage of Aliquat-336, 0.5 mL of 48 % aqueous HBr and 1.0 mL of n-octane were added under argon atm. Then the tube was kept in a preheated oil bath at 130 °C for 12 h. After cooling to room temperature, the reaction mixture was neutralized with saturated Na₂CO₃ solution. The compound was extracted with 25 mL of EtOAc three times. Then the organic layer was washed with 25 mL of brine solution, dried over Na₂SO₄ and concentrated in *vacuo*. The residue was purified by column chromatography on silica gel with a mixture of EtOAc in petroleum ether to afford desired *ortho*-arylated anilines.

5B.7.5b. Removal of Directing Group in Gram-scale

To a 30 mL screw-capped tube, *ortho*-aryl pivalamide (4 mmol), Aliquat-336 (10 weight%), 4.0 mL of 48 % aqueous HBr and 8.0 mL of n-octane were added under argon atm. Then the sealed tube was kept in a preheated oil bath at 130 °C for 12 h. After cooling to room temperature, the reaction mixture was neutralized with saturated Na₂CO₃ solution. The compound was extracted with 100 mL of EtOAc three times. Then the organic layer was washed with 100 mL of brine solution, dried over Na₂SO₄ and concentrated in *vacuo*. The residue was purified by column chromatography on silica gel with a mixture of EtOAc and petroleum ether to afford desired *ortho*-arylated aniline in gram-scale.

5B.7.5c. Arylation of 6a with Phenyl Iodide by Palladium Catalysis

A 10 mL round-bottom flask with a magnetic stir bar and reflux condenser was charged with Pd(OAc)₂ (0.025 mmol, 6 mg, 5 mol%), AgOAc (1.5 mmol, 251 mg, 3.0 equiv.), **6a** (0.5 mmol, 1.0 equiv.), phenyl iodide (5.0 mmol, 1.02 g, 10 equiv.), TFA (1.0 mL) and trifluoroethanol (1.0 mL). The mixture was stirred for 10 minutes at room temperature, then heated to 100 °C and stirred for 12 h. After cooling to room temperature, the mixture was filtered through a plug of celite, the residue was washed with EtOAc (2 × 10 mL). Then saturated Na₂CO₃ solution (20 mL) was added, and the organic layer was collected. The aqueous phase was extracted with EtOAc (2 × 10 mL). The combined organic phases were washed with brine (20 mL), dried over Na₂SO₄, filtered and concentrated in *vacuo*.

The residue was purified by flash column chromatography with EtOAc and petroleum ether as eluent to afford **8** in 63% isolated yield.

5B.7.5d. Synthesis of Boscalid

To a stirred solution of 2-chloronicotinoyl chloride **10** (4.4 g, 25 mmol), DMAP (300 mg, 2.5 mmol) in 100 mL dichloromethane, 4'-chloro-[1,1'-biphenyl]-2-amine **5a** (5.1 g, 25 mmol), Et₃N (7 mL, 50 mmol) in dichloromethane (50 mL) was added dropwise at 0 °C. The reaction was allowed to stir at 0 °C for 2 h, and another 12 h at room temperature followed by addition of dichloromethane (20 mL) and water (50 mL). The combined organic extracts were dried over Na₂SO₄ and the organic solvent was removed in *vacuo*. The crude residue was purified by column chromatography on silica gel (230-400 mesh) using a mixture of petroleum ether/EtOAc ($R_f = 0.5$, petroleum ether/EtOAc = 2:1), to afford 2-Chloro-*N*-(4'-chloro-[1,1'-biphenyl]-2-yl)nicotinamide (**11**, 5.2 g, 81%) as a white solid.

5B.8. Reference

1. (a) Daugulis, O.; MacArthur, A. H. R.; Rix, F. C.; Templeton, J. L. *ACS Catal.* **2016**, *6*, 1518-1532. (b) Hubrich, J.; Himmler, T.; Rodefeld, L.; Ackermann, L. *ACS Catal.* **2015**, *5*, 4089-4093. (c) Hubrich, J.; Himmler, T.; Rodefeld, L.; Ackermann, L. *Adv. Synth. Catal.* **2015**, *357*, 474-480. (d) Suzuki, C.; Hirano, K.; Satoh, T.; Miura, M. *Org. Lett.* **2015**, *17*, 1597-1600. (e) Choi, S.; Chatterjee, T.; Choi, W. J.; You, Y.; Cho, E. J. *ACS Catal.* **2015**, *5*, 4796-4802. (f) Zuo, Z.; Liu, J.; Nan, J.; Fan, L.; Sun, W.; Wang, Y.; Luan, X. *Angew. Chem., Int. Ed.* **2015**, *54*, 15385-15389. (g) Feng, M.; Tang, B.; Xu, H.-X.; Jiang, X. *Org. Lett.* **2016**, *18*, 4352-4355. (h) Choi, J.; Fu, G. C. *Science* **2017**, *356*, DOI: 10.1126/science.aaf7230.
2. (a) Shabashov, D.; Daugulis, O. *J. Org. Chem.* **2007**, *72*, 7720-7725. (b) Li, B.-J.; Tian, S.-L.; Fang, Z.; Shi, Z.-J. *Angew. Chem., Int. Ed.* **2008**, *47*, 1115-1118. (c) Wencel-Delord, J.; Nimphius, C.; Wang, H.; Glorius, F. *Angew. Chem., Int. Ed.* **2012**, *51*, 13001-13005. (d) Chinnagolla, R. A.; Jeganmohan, M. *Chem. Commun.* **2014**, *50*, 2442-2444. (e) Haridharan, R.; Muralirajan, K.; Cheng, C.-H. *Adv. Synth. Catal.* **2015**, *357*, 366-370.
3. For representative reviews of C-H arylation of arenes, see: (a) Alberico, D.; Scott, M. E.; Lautens, M. *Chem. Rev.* **2007**, *107*, 174-238. (b) Ackermann, L. *Top. Organomet. Chem.* **2007**, *24*, 35-60. (c) Kakiuchi, F.; Kochi, T. *Synthesis* **2008**, 3013-3039. (d) Li, B.-J.; Yang, S.-D.; Shi, Z. J. *Synlett* **2008**, 949-957. (e) McGlacken, G. P.; Bateman, L. *Chem. Soc. Rev.* **2009**, *38*, 2447-2464. (f) Ackermann, L.; Vicente, R.; Kapdi, A. R. *Angew. Chem., Int. Ed.* **2009**, *48*, 9792-9826. (g) Daugulis, O.; Do, H. Q.; Shabashov, D. *Acc. Chem. Res.* **2009**, *42*, 1074-1086. (h) Chen, X.; Engle, K. M.; Wang, D.-H.; Yu, J.-Q. *Angew. Chem., Int. Ed.* **2009**, *48*, 5094-5115. (i) Ackermann, L. *Modern Arylation Method*, Wiley-VCH: Weinheim, **2009**. (j) Lyons, T. W.; Sanford, M. S. *Chem. Rev.* **2010**, *110*, 1147-1169. (k) Daugulis, O. *Top. Curr. Chem.* **2010**, *292*, 57-84.
4. (a) Daugulis, O.; Zaitsev, V. G. *Angew. Chem., Int. Ed.* **2005**, *44*, 4046-4048. (b) Brasche, G.; Garcia-Fortanet, J.; Buchwald, S. L. *Org. Lett.* **2008**, *10*, 2207-2210. (c) Nishikata, T.; Abela, A. R.; Lipshutz, B. H. *Angew. Chem., Int. Ed.* **2010**, *49*, 781-784.
5. (a) Shi, Z.; Li, B.; Wan, X.; Cheng, J.; Fang, Z.; Cao, B.; Qin, C.; Wang, Y. *Angew. Chem., Int. Ed.* **2007**, *46*, 5554-5558. (b) Yang, S.; Li, B.; Wan, X.; Shi, Z. *J. Am. Chem. Soc.* **2007**, *129*, 6066-6067. (c) Yeung, C. S.; Zhao, X.; Borduas, N.; Dong, V. M. *Chem. Sci.* **2010**, *1*, 331-336. (d) Nishikata, T.; Abela, A. R.; Huang, S.; Lipshutz, B. H. *J. Am. Chem. Soc.* **2010**, *132*, 4978-4979. (e) Truong, T.; Daugulis, O. *Org. Lett.* **2012**, *14*, 5964-

5967. (f) Neufeldt, S. R.; Sanford, M. S. *Adv. Synth. Catal.* **2012**, *354*, 3517-3522. (g) Li, D.; Xu, N.; Zhang, Y.; Wang, L. *Chem. Commun.* **2014**, *50*, 14862-14865. (h) Gao, P.; Guo, W.; Xue, J.; Zhao, Y.; Yuan, Y.; Xia, Y.; Shi, Z. *J. Am. Chem. Soc.* **2015**, *137*, 12231-12240. (i) Gao, P.; Liu, L.; Shi, Z.; Yuan, Y. *Org. Biomol. Chem.* **2016**, *14*, 7109-7113.
6. Recent reviews on the utilization of aryldiazonium salts as an arylating agent, see: (a) Roglans, A.; Pla-Quintana, A.; Moreno-Manas, M. *Chem. Rev.* **2006**, *106*, 4622-4643. (b) Felpin, F.-X.; Nassar-Hardy, L.; Callonnec, F. L.; Fouquet, E. *Tetrahedron* **2011**, *67*, 2815-2831. (c) Taylor, J. G.; Moro, A. V.; Correia, C. R. D. *Eur. J. Org. Chem.* **2011**, 1403-1428. (d) Mo, F.; Dong, G.; Zhang, Y.; Wang, J. *Org. Biomol. Chem.* **2013**, *11*, 1582-1593. (e) Hari, D. P.; König, B. *Angew. Chem., Int. Ed.* **2013**, *52*, 4734-4743. (f) Hari, D. P.; Hering, T.; König, B. *Chimica Oggi-Chemistry Today*, **2013**, *31*, 59.
7. (a) Kalyani, D.; McMurtrey, K. B.; Neufeldt, S. R.; Sanford, M. S. *J. Am. Chem. Soc.* **2011**, *133*, 18566-18569. (b) Shin, K.; Park, S.-W.; Chang, S. *J. Am. Chem. Soc.* **2015**, *137*, 8584-8592. (c) Sahoo, M. K.; Midya, S. P.; Landge, V. G.; Balaraman, E. *Green Chem.* **2017**, *19*, 2111-2117. (d) Jiang, J.; Zhang, W.-M.; Dai, J.-J.; Xu, J.; Xu, H.-J. *J. Org. Chem.* **2017**, *82*, 3622-3630.
8. Phipps, R. J.; Gaunt, M. J. *Science* **2009**, *323*, 1593-1597.
9. Tundo, P.; Selva, M. *Dimethyl Carbonate as a Green Reagent, in Methods and Reagents for Green Chemistry: An Introduction* (eds P. Tundo, A. Perosa, F. Zecchini), John Wiley & Sons, Inc.: Hoboken, NJ, **2007**.
10. (a) Cismesia, M. A.; Yoon, T. P. *Chem. Sci.* **2015**, *6*, 5426-5434. (b) Studer, A.; Curran, D. P. *Angew. Chem., Int. Ed.* **2016**, *55*, 58-102. (c) Xu, P.; Wang, G.; Zhu, Y.; Li, W.; Cheng, Y.; Li, S.; Zhu, C. *Angew. Chem., Int. Ed.* **2016**, *55*, 2939-2943.
11. (a) Campagna, S.; Puntoriero, F.; Nastasi, F.; Bergamini, G.; Balzani, V. *Top. Curr. Chem.* **2007**, *280*, 117-214. (b) Sehnal, P.; Taylor, R. J. K.; Fairlamb, I. J. S. *Chem. Rev.* **2010**, *110*, 824-889. (c) Narayanam, J. M. R.; Stephenson, C. R. J. *Chem. Soc. Rev.* **2011**, *40*, 102-113. (d) Koike, T.; Akita, M. *Inorg. Chem. Front.* **2014**, *1*, 562-576. (e) Levin, M. D.; Kim, S. Toste, F. D. *ACS Cent. Sci.* **2016**, *2*, 293-301. (f) Ghosh, I.; Marzo, L.; Das, A.; Shaikh, R.; König, B. *Acc. Chem. Res.* **2016**, *49*, 1566-1577.
12. (a) Prier, C. K.; Rankic, D. A.; MacMillan, D. W. C. *Chem. Rev.* **2013**, *113*, 5322-5363. (b) Hopkinson, M. N.; Sahoo, B.; Li, J.-L.; Glorius, F. *Chem. Eur. J.* **2014**, *20*, 3874-3886. (c) Skubi, K. L.; Blum, T. R.; Yoon, T. P. *Chem. Rev.* **2016**, *116*, 10035-10074.
13. Maestri, G.; Malacria, M.; Derat, E. *Chem. Commun.* **2013**, *49*, 10424-10426.

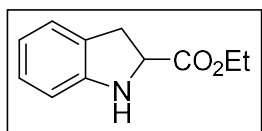
14. (a) Powers, D. C.; Ritter, T. *Nat. Chem.* **2009**, *1*, 302-309. (b) Powers, D. C.; Geibel, M. A. L.; Klein, J. E. M. N.; Ritter, T. *J. Am. Chem. Soc.* **2009**, *131*, 17050-17051. (c) Xiong, T.; Li, Y.; Lv, Y.; Zhang, Q. *Chem. Commun.* **2010**, *46*, 6831-6833.

Appendix

Appendix A

NMR and HRMS Data of Compounds

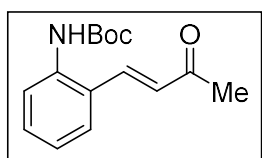
Chapter 2 and Chapter 3

**Ethyl indoline-2-carboxylate**

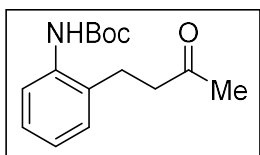
White solid; ¹H NMR (500 MHz, CDCl₃): δ = 7.10 (d, *J* = 7.2 Hz, 1H), 7.07 (t, *J* = 7.6 Hz, 1H), 6.77 (d, *J* = 7.2 Hz, 1H), 6.74 (d, *J* = 7.9 Hz, 1H), 4.47 (brs, 1H), 4.39 (dd, *J* = 10.7, 5.4 Hz, 1H), 4.22 (q, *J* = 7.4 Hz, 1H), 3.42 (dd, *J* = 16.0, 10.3 Hz, 1H), 3.33 (dd, *J* = 16.0, 5.4 Hz, 1H), 1.30 (t, *J* = 7.2 Hz, 3H); ¹³C NMR (126 MHz, CDCl₃): δ = 174.17, 150.06, 127.61, 126.66, 124.41, 119.44, 110.08, 61.41, 59.80, 33.68, 14.15; HRMS (ESI) *m/z* calculated for C₁₁H₁₄NO₂[M+H]⁺ 192.1019; found 192.1019.

**2,2,2-Trifluoroethyl indoline-2-carboxylate**

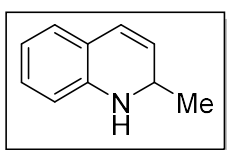
Colourless oil; ¹H NMR (500 MHz, CDCl₃): δ = 7.09 (d, *J* = 7.6 Hz, 1H), 7.06 (t, *J* = 7.6 Hz, 1H), 6.76 (t, *J* = 7.3 Hz, 1H), 6.71 (d, *J* = 8.0 Hz, 1H), 4.55-4.43 (m, 4H), 3.44 (dd, *J* = 16.0, 10.7 Hz, 1H), 3.29 (dd, *J* = 16.0, 4.9 Hz, 1H); ¹³C NMR (126 MHz, CDCl₃): δ = 172.78, 149.58, 127.76, 125.98, 124.42, 122.65 (q, *J*_{C-F} = 276.7 Hz), 119.35, 109.97, 60.72 (q, *J*_{C-F} = 35.3 Hz), 59.40, 33.53; HRMS (ESI) *m/z* calculated for C₁₁H₁₁F₃NO₂ [M+H]⁺ 246.0736; found 246.0736.

**tert-butyl (E)-(2-(3-oxobut-1-en-1-yl)phenyl)carbamate**

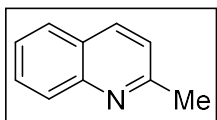
White solid; ¹H NMR (500 MHz, CDCl₃): δ = 7.73-7.70 (m, 2H), 7.57 (d, *J* = 7.6 Hz, 1H), 7.40 (t, *J* = 8.1 Hz, 1H), 7.17 (t, *J* = 7.8 Hz, 1H), 6.72 (d, *J* = 16.1 Hz, 1H), 6.55 (s, 1H), 2.41 (s, 3H), 1.55 (s, 9H); ¹³C NMR (126 MHz, CDCl₃): δ = 198.03, 153.09, 137.97, 136.80, 130.98, 128.48, 127.16, 124.81, 123.50, 81.11, 28.25; HRMS (ESI) *m/z* calculated for C₁₅H₁₉NO₃[M+Na]⁺ 284.1257; found 284.1253.

**tert-butyl (2-(3-oxobutyl)phenyl)carbamate**

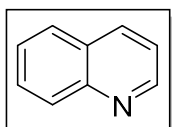
Colourless oil; ^1H NMR (500 MHz, CDCl_3): δ = 7.70 (d, J = 8.2 Hz, 1H), 7.55 (s, 1H); 7.19 (t, J = 7.8 Hz, 1H), 7.10 (d, J = 7.7 Hz, 1H), 7.03 (t, J = 7.2 Hz, 1H), 2.87-2.80 (m, 2H), 2.14 (s, 3H), 1.54 (s, 9H); ^{13}C NMR (126 MHz, CDCl_3): δ = 209.09, 153.80, 135.99, 129.37, 126.91, 124.16, 123.24, 80.01, 44.54, 29.91, 28.37, 24.04; HRMS (ESI) m/z calculated for $\text{C}_{15}\text{H}_{21}\text{NO}_3[\text{M}+\text{Na}]^+$ 286.1414; found 286.1408.

**2-methyl-1,2-dihydroquinoline**

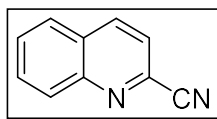
^1H NMR (500 MHz, CDCl_3): δ = 6.97 (t, J = 8.1 Hz, 1H), 6.87 (d, J = 7.3 Hz, 1H), 6.60 (t, J = 7.8 Hz, 1H), 6.40 (d, J = 7.6 Hz, 1H), 6.31 (d, J = 9.8 Hz, 1H), 5.55 (dd, J = 10.0, 3.8 Hz, 1H), 4.42 (m, 1H), 3.70 (brs, 1H), 1.31 (d, J = 6.6 Hz, 3H).

**2-Methylquinoline**

Colourless liquid; ^1H NMR (500 MHz, CDCl_3): δ = 8.04 (t, J = 8.3 Hz, 2H), 7.77 (d, J = 8.3 Hz, 1H), 7.68 (t, J = 7.6 Hz, 1H), 7.48 (t, J = 7.6 Hz, 1H), 7.29 (d, J = 8.6 Hz, 1H), 2.75 (s, 3H); ^{13}C NMR (126 MHz, CDCl_3): δ = 158.95, 147.74, 136.20, 129.42, 128.50, 127.44, 126.44, 125.66, 121.98, 25.28; HRMS (ESI) m/z calculated for $\text{C}_{10}\text{H}_{10}\text{N}[\text{M}+\text{H}]^+$ 144.0808; found 144.0809.

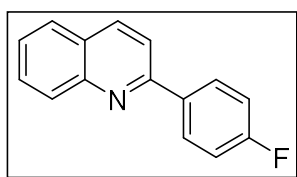
**Quinoline**

Colourless liquid; ^1H NMR (500 MHz, CDCl_3): δ = 8.92 (dd, J = 4.2, 1.5 Hz, 1H), 8.13 (t, J = 9.5 Hz, 2H), 7.81 (d, J = 8.4 Hz, 1H), 7.71 (t, J = 8.4 Hz, 1H), 7.54 (t, J = 7.3 Hz, 1H), 7.39 (dd, J = 8.4, 4.2 Hz, 1H); ^{13}C NMR (126 MHz, CDCl_3): δ = 150.25, 148.14, 135.87, 129.30, 129.29, 128.13, 127.63, 126.37, 120.91.



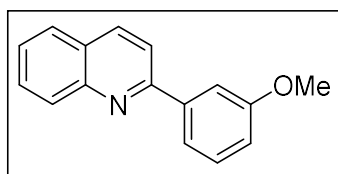
Quinoline-2-carbonitrile

White solid; ^1H NMR (500 MHz, CDCl_3): δ = 8.34 (d, J = 8.4 Hz, 1H), 8.19 (d, J = 8.8 Hz, 1H), 7.93 (d, J = 8.0 Hz, 1H), 7.87 (t, J = 8.4 Hz, 1H), 7.75-7.72 (m, 2H); ^{13}C NMR (126 MHz, CDCl_3): δ = 148.13, 137.44, 133.54, 131.19, 129.89, 129.40, 128.61, 127.74, 123.24, 117.50; HRMS (ESI) m/z calculated for $\text{C}_{10}\text{H}_7\text{N}_2[\text{M}+\text{H}]^+$ 155.0604; found 155.0604.



2-(4-Fluorophenyl)quinoline

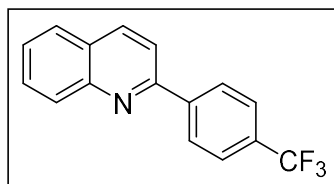
White solid; ^1H NMR (400 MHz, CDCl_3): δ = 8.22-8.16 (m, 4H), 7.83 (d, J = 8.6 Hz, 2H), 7.75 (t, J = 7.4 Hz, 1H), 7.55 (t, J = 7.4 Hz, 1H), 7.23 (t, J = 9.2 Hz, 2H); ^{13}C NMR (126 MHz, CDCl_3): δ = 163.76 (d, $J_{\text{C-F}}$ = 249.9 Hz), 156.17, 148.19, 136.85, 135.78, 129.74, 129.61, 129.36 (d, $J_{\text{C-F}}$ = 8.7 Hz), 127.43, 127.04, 126.30, 118.56, 115.72 (d, $J_{\text{C-F}}$ = 21.9 Hz); HRMS (ESI) m/z calculated for $\text{C}_{15}\text{H}_{11}\text{FN}$ $[\text{M}+\text{H}]^+$ 224.0870; found 224.0869.



2-(3-Methoxyphenyl)quinoline

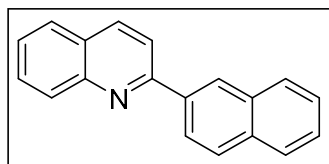
Colourless oil; ^1H NMR (400 MHz, CDCl_3): δ = 8.21 (dd, J = 8.5, 3.7 Hz, 2H), 7.86 (d, J = 8.6 Hz, 1H), 7.84-7.80 (m, 2H), 7.76-7.72 (m, 2H), 7.54 (t, J = 8.0 Hz, 1H), 7.45 (t, J =

8.0 Hz, 1H), 7.05 (dd, $J = 8.5, 1.9$ Hz, 1H), 3.94 (s, 3H); ^{13}C NMR (126 MHz, CDCl_3): $\delta = 160.08, 157.04, 148.15, 141.09, 136.68, 129.74, 129.68, 129.58, 127.39, 127.20, 126.25, 119.95, 119.02, 115.30, 112.66, 55.34$; HRMS (ESI) m/z calculated for $\text{C}_{16}\text{H}_{14}\text{NO}$ $[\text{M}+\text{H}]^+$ 236.1070; found 236.1068.



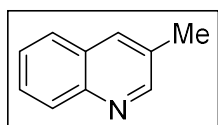
2-(4-(Trifluoromethyl)phenyl)quinoline

White solid; ^1H NMR (500 MHz, CDCl_3): $\delta = 8.29$ (d, $J = 8.5$ Hz, 2H), 8.26 (d, $J = 8.4$ Hz, 1H), 8.20 (d, $J = 8.4$ Hz, 1H), 7.88 (d, $J = 8.8$ Hz, 1H), 7.86 (d, $J = 8.0$ Hz, 1H), 7.80-7.75 (m, 3H), 7.58 (dt, $J = 8.1, 1.2$ Hz, 1H); ^{13}C NMR (126 MHz, CDCl_3): $\delta = 155.66, 148.29, 142.95, 137.12, 131.09$ (q, $J_{\text{C-F}} = 32.3$ Hz), 129.99, 129.87, 127.84, 127.54, 127.45, 126.86, 125.75 (q, $J_{\text{C-F}} = 3.8$ Hz), 124.24 (q, $J_{\text{C-F}} = 271.6$ Hz), 123.15, 118.77, 77.04; HRMS (ESI) m/z calculated for $\text{C}_{16}\text{H}_{11}\text{F}_3\text{N}$ $[\text{M}+\text{H}]^+$ 274.0838; found 274.0838.



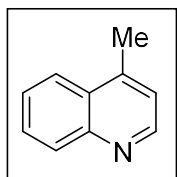
2-(Naphthalen-2-yl)quinoline

White solid; ^1H NMR (500 MHz, CDCl_3): $\delta = 8.64$ (s, 1H), 8.40 (d, $J = 8.7$ Hz, 1H), 8.26 (d, $J = 8.6$ Hz, 2H), 8.05-8.00 (m, 3H), 7.93-7.91 (m, 1H), 7.86 (d, $J = 8.2$ Hz, 1H), 7.77 (t, $J = 8.2$ Hz, 1H), 7.57-7.54 (m, 3H); ^{13}C NMR (126 MHz, CDCl_3): $\delta = 157.12, 148.35, 136.94, 136.76, 133.84, 133.48, 129.72, 129.68, 128.79, 128.54, 127.70, 127.46, 127.19, 127.11, 126.67, 126.30, 125.03, 119.11$; HRMS (ESI) m/z calculated for $\text{C}_{19}\text{H}_{14}\text{N}$ $[\text{M}+\text{H}]^+$ 256.1121; found 256.1120.



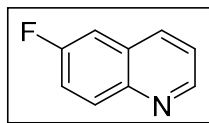
3-Methylquinoline

Colourless liquid; ^1H NMR (200 MHz, CDCl_3): δ = 8.69 (s, 1H), 8.03 (d, J = 8.4 Hz, 1H), 7.75 (s, 1H), 7.64-7.52 (m, 2H), 7.41 (t, J = 7.7 Hz, 1H), 2.37 (s, 3H); ^{13}C NMR (50 MHz, CDCl_3): δ = 152.03, 146.22, 134.30, 130.10, 128.82, 128.10, 127.79, 126.83, 126.20, 18.36; HRMS (ESI) m/z calculated for $\text{C}_{10}\text{H}_{10}\text{N}$ $[\text{M}+\text{H}]^+$ 144.0808; found 144.0808.



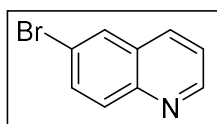
4-Methylquinoline

Colourless liquid; ^1H NMR (500 MHz, CDCl_3): δ = 8.76 (s, 1H), 8.10 (d, J = 8.3 Hz, 1H), 7.95 (d, J = 8.3 Hz, 1H), 7.68 (t, J = 7.7 Hz, 1H), 7.52 (t, J = 7.6 Hz, 1H), 7.18 (d, J = 3.5 Hz, 1H), 2.65 (s, 3H); ^{13}C NMR (126 MHz, CDCl_3): δ = 150.01, 147.88, 144.10, 129.90, 128.95, 128.17, 126.13, 123.68, 121.74, 18.48; HRMS (ESI) m/z calculated for $\text{C}_{10}\text{H}_{10}\text{N}$ $[\text{M}+\text{H}]^+$ 144.0808; found 144.0808.



6-Fluoroquinoline

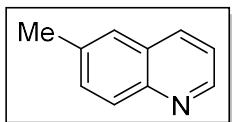
Colourless liquid; ^1H NMR (500 MHz, CDCl_3): δ = 8.87 (dd, J = 4.1, 1.1 Hz, 1H), 8.11-8.07 (m, 2H), 7.47 (dt, J = 9.1, 2.7 Hz, 1H), 7.42-7.38 (m, 2H); ^{13}C NMR (126 MHz, CDCl_3): δ = 160.32 (d, $J_{\text{C-F}}$ = 248.2 Hz), 149.62 (d, $J_{\text{C-F}}$ = 2.8 Hz), 145.33, 135.33 (d, $J_{\text{C-F}}$ = 5.6 Hz), 131.92 (d, $J_{\text{C-F}}$ = 9.5 Hz), 128.81 (d, $J_{\text{C-F}}$ = 9.5 Hz), 121.70, 119.68 (d, $J_{\text{C-F}}$ = 25.8 Hz), 110.62 (d, $J_{\text{C-F}}$ = 21.9 Hz); HRMS (ESI) m/z calculated for $\text{C}_9\text{H}_7\text{FN}$ $[\text{M}+\text{H}]^+$ 148.0557; found 148.0559.



6-Bromoquinoline

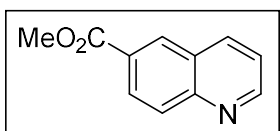
White solid; ^1H NMR (500 MHz, CDCl_3): δ = 8.92 (dd, J = 4.2, 1.5 Hz, 1H), 8.06 (d, J = 8.1 Hz, 1H), 7.99-7.97 (m, 2H), 7.78 (dd, J = 9.0, 2.3 Hz, 1H), 7.42 (dd, J = 8.3, 4.1 Hz,

1H); ^{13}C NMR (126 MHz, CDCl_3): $\delta = 150.69, 146.79, 135.01, 132.91, 131.18, 129.76, 129.31, 121.85, 120.42$; HRMS (ESI) m/z calculated for $\text{C}_9\text{H}_7\text{BrN}[\text{M}+\text{H}]^+$ 207.9756; found 207.9759.



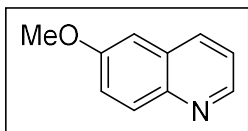
6-Methylquinoline

Colourless liquid; ^1H NMR (500 MHz, CDCl_3): $\delta = 8.84$ (s, 1H), 8.05 (d, $J = 8.6$ Hz, 1H), 8.00 (d, $J = 9.1$ Hz, 1H), 7.56-7.53 (m, 2H), 7.36-7.33 (m, 1H), 2.53 (s, 3H); ^{13}C NMR (126 MHz, CDCl_3): $\delta = 149.47, 146.83, 136.34, 135.33, 131.70, 129.03, 128.26, 126.53, 121.01, 21.52$; HRMS (ESI) m/z calculated for $\text{C}_{10}\text{H}_{10}\text{N} [\text{M}+\text{H}]^+$ 144.0808; found 144.0808.



Methyl quinoline-6-carboxylate

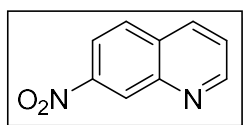
Yellow solid; ^1H NMR (500 MHz, CDCl_3): $\delta = 9.01$ (d, $J = 3.9$ Hz, 1H), 8.59 (s, 1H), 8.30 (d, $J = 8.7$ Hz, 1H), 8.26 (d, $J = 8.3$ Hz, 1H), 8.14 (d, $J = 8.8$ Hz, 1H), 7.47 (dd, $J = 8.3, 4.2$ Hz, 1H), 3.99 (s, 3H); ^{13}C NMR (126 MHz, CDCl_3): $\delta = 166.55, 152.47, 150.04, 137.28, 130.96, 129.78, 128.91, 128.09, 127.38, 121.80, 52.39$; HRMS (ESI) m/z calculated for $\text{C}_{11}\text{H}_{10}\text{NO}_2[\text{M}+\text{H}]^+$ 188.0706; found 188.0704.



6-Methoxyquinoline

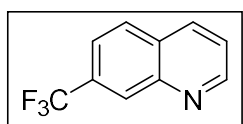
Colourless liquid; ^1H NMR (500 MHz, CDCl_3): $\delta = 8.76$ (dd, $J = 4.2, 1.8$ Hz, 1H), 8.03 (d, $J = 8.5$ Hz, 1H), 8.00 (d, $J = 9.2$ Hz, 1H), 7.37 (dd, $J = 9.2, 2.7$ Hz, 1H), 7.33 (dd, $J = 8.2, 4.2$ Hz, 1H), 7.06 (d, $J = 2.7$ Hz, 1H), 3.92 (s, 3H); ^{13}C NMR (126 MHz, CDCl_3): $\delta =$

157.70, 147.87, 144.41, 134.69, 130.81, 129.26, 122.19, 121.29, 105.10, 55.46; HRMS (ESI) m/z calculated for $C_{10}H_{10}NO[M+H]^+$ 160.0757; found 160.0754.



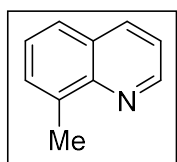
7-Nitroquinoline

Yellow solid; ¹H NMR (500 MHz, CDCl₃): δ = 9.10 (d, J = 2.8 Hz, 1H), 9.01 (d, J = 2.4 Hz, 1H), 8.33 (dd, J = 8.9, 2.1 Hz, 1H), 8.29 (d, J = 8.5 Hz, 1H), 8.00 (d, J = 9.2 Hz, 1H), 7.62 (dd, J = 8.2, 4.0 Hz, 1H); ¹³C NMR (126 MHz, CDCl₃): δ = 152.66, 148.03, 147.10, 135.89, 131.34, 129.45, 125.80, 123.91, 120.05; HRMS (ESI) m/z calculated for $C_9H_7N_2O_2[M+H]^+$ 175.0502; found 175.0503.



7-(Trifluoromethyl)quinoline

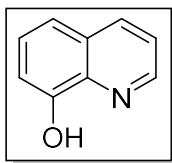
Colourless liquid; ¹H NMR (500 MHz, CDCl₃): δ = 9.01 (dd, J = 4.3, 1.5 Hz, 1H), 8.41 (s, 1H), 8.21 (d, J = 8.3 Hz, 1H), 7.93 (d, J = 8.5 Hz, 1H), 7.71 (dd, J = 8.5, 1.5 Hz, 1H), 7.52 (dd, J = 8.2, 4.3 Hz, 1H); ¹³C NMR (126 MHz, CDCl₃): δ = 151.73, 147.16, 135.89, 131.18 (q, J_{C-F} = 32.3 Hz), 129.64, 129.01, 127.30 (q, J_{C-F} = 4.7 Hz), 123.88 (q, J_{C-F} = 272.6 Hz), 122.87, 122.19 (q, J_{C-F} = 2.9 Hz); HRMS (ESI) m/z calculated for $C_{10}H_7F_3N[M+H]^+$ 198.0525; found 198.0526.



8-Methylquinoline

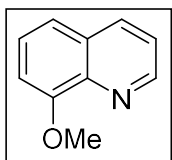
Colourless liquid; ¹H NMR (500 MHz, CDCl₃): δ = 8.96 (dd, J = 4.2, 1.6 Hz, 1H), 8.14 (dd, J = 8.0, 1.2 Hz, 1H), 7.67 (d, J = 8.0 Hz, 1H), 7.58 (d, J = 6.9 Hz, 1H), 7.44 (t, J = 7.7 Hz, 1H), 7.40 (dd, J = 8.0, 4.2 Hz, 1H), 2.84 (s, 3H); ¹³C NMR (126 MHz, CDCl₃): δ =

149.19, 147.31, 137.02, 136.23, 129.55, 128.20, 126.22, 125.81, 120.76, 18.09; HRMS (ESI) m/z calculated for $C_{10}H_{10}N$ $[M+H]^+$ 144.0808; found 144.0808.



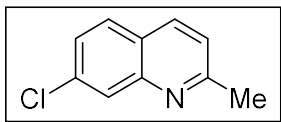
8-Quinolinol

White solid; 1H NMR (500 MHz, $CDCl_3$): δ = 8.80 (dd, J = 4.2, 1.5 Hz, 1H), 8.45 (br, 1H), 8.16 (d, J = 8.4 Hz, 1H), 7.47 (t, J = 8.0 Hz, 1H), 7.44 (dd, J = 8.0, 4.2 Hz, 1H), 7.34 (d, J = 8.4 Hz, 1H), 7.22 (d, J = 7.7 Hz, 1H); ^{13}C NMR (126 MHz, $CDCl_3$): δ = 152.26, 147.87, 138.29, 136.10, 128.51, 127.70, 121.75, 117.85, 110.11; HRMS (ESI) m/z calculated for C_9H_8NO $[M+H]^+$ 146.0600; found 146.0599.



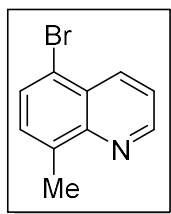
8-Methoxyquinoline

Red solid; 1H NMR (500 MHz, $CDCl_3$): δ = 8.89 (dd, J = 4.2, 1.9 Hz, 1H), 8.07 (dd, J = 8.0, 1.9 Hz, 1H), 7.41 (t, J = 8.4 Hz, 1H), 7.37 (dd, J = 8.4, 4.2 Hz, 1H), 7.34 (d, J = 8.4 Hz, 1H), 7.01 (d, J = 7.7 Hz, 1H), 4.05 (s, 3H); ^{13}C NMR (126 MHz, $CDCl_3$): δ = 155.25, 149.08, 140.06, 135.71, 129.20, 126.55, 121.52, 119.39, 107.38, 55.80; HRMS (ESI) m/z calculated for $C_{10}H_{10}NO$ $[M+H]^+$ 160.0757; found 160.0756.



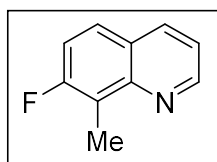
7-Chloro-2-methylquinoline

White solid; 1H NMR (500 MHz, $CDCl_3$): δ = 8.00-7.99 (m, 2H), 7.68 (d, J = 8.8 Hz, 1H), 7.42 (d, J = 8.8 Hz, 1H), 7.26 (d, J = 8.8 Hz, 1H), 2.72 (s, 3H); ^{13}C NMR (126 MHz, $CDCl_3$): δ = 160.15, 148.17, 135.85, 135.13, 128.62, 127.69, 126.63, 124.78, 122.14, 25.30; HRMS (ESI) m/z calculated for $C_{10}H_9ClN$ $[M+H]^+$ 178.0418; found 178.0419.



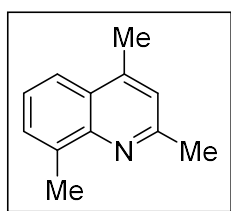
5-Bromo-8-methylquinoline

White solid; ^1H NMR (500 MHz, CDCl_3): $\delta = 8.92$ (dd, $J = 4.1, 1.6$ Hz, 1H), 8.47 (dd, $J = 8.3, 1.9$ Hz, 1H), 7.66 (d, $J = 7.6$ Hz, 1H), 7.45 (dd, $J = 8.4, 4.2$ Hz, 1H), 7.37 (d, $J = 7.6$ Hz, 1H), 2.75 (s, 3H); ^{13}C NMR (126 MHz, CDCl_3): $\delta = 149.64, 147.86, 137.22, 135.54, 129.86, 129.67, 127.33, 121.81, 119.14, 17.99$; HRMS (ESI) m/z calculated for $\text{C}_{10}\text{H}_9\text{BrN}[\text{M}+\text{H}]^+$ 221.9913; found 221.9915.



7-Fluoro-8-methylquinoline

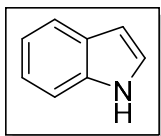
Colourless liquid; ^1H NMR (500 MHz, CDCl_3): $\delta = 8.95$ (d, $J = 4.4$ Hz, 1H), 8.10 (d, $J = 8.4$ Hz, 1H), 7.62 (t, $J = 8.6$ Hz, 1H), 7.35 (dd, $J = 7.8, 4.2$ Hz, 1H), 7.30 (t, $J = 8.6$ Hz, 1H), 2.71 (d, $J = 2.1$ Hz, 3H); ^{13}C NMR (126 MHz, CDCl_3): $\delta = 160.64$ (d, $J_{\text{C-F}} = 246.3$ Hz), $150.04, 148.16$ (d, $J_{\text{C-F}} = 9.1$ Hz), $136.18, 126.58$ (d, $J_{\text{C-F}} = 10.0$ Hz), $125.18, 120.98$ (d, $J_{\text{C-F}} = 14.7$ Hz), 119.90 (d, $J_{\text{C-F}} = 1.9$ Hz), 116.72 (d, $J_{\text{C-F}} = 27.5$ Hz), 8.99 (d, $J_{\text{C-F}} = 4.6$ Hz); HRMS (ESI) m/z calculated for $\text{C}_{10}\text{H}_9\text{FN}[\text{M}+\text{H}]^+$ 162.0714; found 162.0713.



2,4,8-Trimethylquinoline

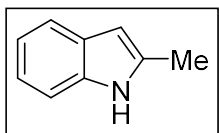
White solid; ^1H NMR (400 MHz, CDCl_3): $\delta = 7.81$ (d, $J = 8.1$ Hz, 1H), 7.54 (d, $J = 6.7$ Hz, 1H), 7.39 (t, $J = 7.8$ Hz, 1H), 7.12 (s, 1H), 2.86 (s, 3H), 2.74 (s, 3H), 2.65 (s, 3H); ^{13}C NMR (101 MHz, CDCl_3): $\delta = 157.30, 146.76, 143.91, 136.86, 129.17, 126.32, 124.80$,

122.34, 121.41, 25.44, 18.76, 18.34; HRMS (ESI) m/z calculated for $C_{12}H_{14}N[M+H]^+$ 172.1121; found 172.1120.



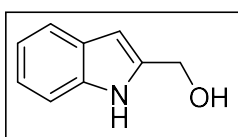
1H-indole

White solid; 1H NMR (500 MHz, $CDCl_3$): δ = 8.03 (brs, 1H), 7.75 (d, J = 8.4 Hz, 1H), 7.42 (d, J = 8.2 Hz, 1H), 7.29 (t, J = 7.7 Hz, 1H), 7.24-7.19 (m, 2H), 6.64 (s, 1H); ^{13}C NMR (126 MHz, $CDCl_3$): δ = 135.69, 127.76, 124.13, 121.89, 120.66, 119.74, 111.00, 102.45.



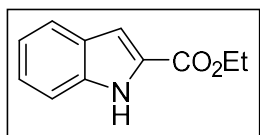
2-Methyl-1H-indole

White solid; 1H NMR (500 MHz, $CDCl_3$): δ = 7.64-7.62 (m, 2H), 7.29 (d, J = 8.2 Hz, 1H), 7.24-7.17 (m, 2H), 6.31 (t, J = 1.0 Hz, 1H), 2.44 (s, 3H); ^{13}C NMR (126 MHz, $CDCl_3$): δ = 135.94, 135.07, 128.94, 120.80, 119.53, 110.23, 100.19, 13.50; HRMS (ESI) m/z calculated for $C_9H_{10}N[M+H]^+$ 132.0808; found 132.0809.



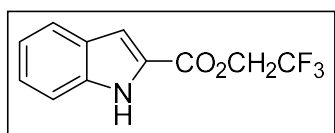
(1H-indole)methanol

White solid; 1H NMR (500 MHz, $CDCl_3$): δ = 8.40 (brs, 1H), 7.60 (d, J = 7.9 Hz, 1H), 7.32 (d, J = 8.0 Hz, 1H), 7.20 (dt, J = 8.0, 1.1 Hz, 1H), 7.13 (dt, J = 8.1, 1.1 Hz, 1H), 6.41 (s, 1H), 4.77 (s, 2H), 2.26 (brs, 1H); ^{13}C NMR (126 MHz, $CDCl_3$): δ = 137.49, 136.33, 128.00, 122.15, 120.58, 119.90, 110.97, 100.52, 58.60; HRMS (ESI) m/z calculated for $C_9H_{10}NO[M+H]^+$ 148.0757; found 148.0756.



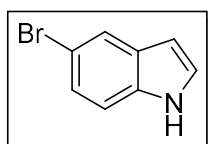
Ethyl 1*H*-indole-2-carboxylate

White solid; ¹H NMR (400 MHz, CDCl₃): δ = 9.32 (brs, 1H), 7.72 (d, *J* = 7.7 Hz, 1H), 7.46 (d, *J* = 8.0 Hz, 1H), 7.35 (t, *J* = 7.7 Hz, 1H), 7.27 (s, 1H), 7.18 (t, *J* = 8.0 Hz, 1H), 4.46 (q, *J* = 6.8 Hz, 2H), 1.45 (t, *J* = 7.3 Hz, 3H); ¹³C NMR (101 MHz, CDCl₃): δ = 162.22, 136.91, 127.43, 125.26, 122.54, 120.70, 111.90, 108.60, 61.04, 14.35; HRMS (ESI) *m/z* calculated for C₁₁H₁₁NNaO₂[M+Na]⁺ 212.0682; found 212.0682.



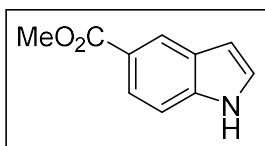
2,2,2-Trifluoroethyl 1*H*-indole-2-carboxylate

White solid; ¹H NMR (400 MHz, CDCl₃): δ = 9.03 (brs, 1H), 7.73 (d, *J* = 7.7 Hz, 1H), 7.45 (d, *J* = 8.1 Hz, 1H), 7.39 (t, *J* = 8.5 Hz, 2H), 7.20 (t, *J* = 7.7 Hz, 1H), 4.75 (q, *J* = 8.3 Hz, 2H); ¹³C NMR (101 MHz, CDCl₃): δ = 160.16, 137.36, 127.27, 126.22, 125.08, 122.96 (q, *J*_{C-F} = 277.4 Hz), 122.88, 121.20, 111.97, 110.78, 60.52 (q, *J*_{C-F} = 40.0 Hz); HRMS (ESI) *m/z* calculated for C₁₁H₉F₃NO₂[M+H]⁺ 244.0580; found 244.0583.



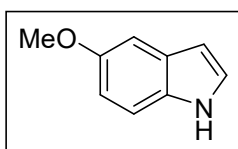
5-Bromo 1*H*-indole

White solid; ¹H NMR (500 MHz, CDCl₃): δ = 8.11 (brs, 1H), 7.76 (d, *J* = 2.1 Hz, 1H), 7.26 (dd, *J* = 8.5, 1.8 Hz, 1H), 7.22 (d, *J* = 8.6 Hz, 1H), 7.17 (t, *J* = 2.8 Hz, 1H), 6.48 (t, *J* = 3.0 Hz, 1H); ¹³C NMR (126 MHz, CDCl₃): δ = 134.35, 129.58, 125.34, 124.79, 123.16, 112.98, 112.41, 102.25; HRMS (ESI) *m/z* calculated for C₈H₇BrN[M+H]⁺ 195.9756; found 195.9757.



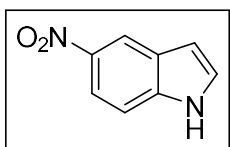
Methyl 1*H*-indole-5-carboxylate

White solid; ¹H NMR (500 MHz, CDCl₃): δ = 8.45 (s, 1H), 8.42 (brs, 1H), 7.94 (dd, *J* = 8.4, 1.5 Hz, 1H), 7.44 (d, *J* = 8.4 Hz, 1H), 7.30 (t, *J* = 3.1 Hz, 1H), 6.68 (s, 1H), 3.96 (s, 3H); ¹³C NMR (126 MHz, CDCl₃): δ = 168.24, 138.37, 127.45, 125.47, 123.77, 123.38, 121.94, 110.70, 104.03, 51.85; HRMS (ESI) *m/z* calculated for C₁₀H₁₀NO₂[M+H]⁺ 176.0706; found 176.0706.



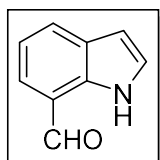
5-Methoxy 1*H*-indole

White solid; ¹H NMR (500 MHz, CDCl₃): δ = 8.07 (brs, 1H), 7.29 (d, *J* = 8.7 Hz, 1H), 7.18 (t, *J* = 2.6 Hz, 1H), 7.16 (s, 1H), 6.92 (d, *J* = 8.7 Hz, 1H), 6.52 (s, 1H), 3.90 (s, 3H); ¹³C NMR (126 MHz, CDCl₃): δ = 154.12, 130.92, 128.23, 124.87, 112.29, 111.69, 102.29, 55.81; HRMS (ESI) *m/z* calculated for C₉H₁₀NO[M+H]⁺ 148.0757; found 148.0758.



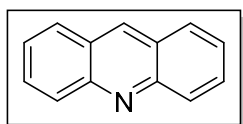
5-Nitro 1*H*-indole

Orange solid; ¹H NMR (500 MHz, CDCl₃): δ = 9.68 (brs, 1H), 8.59 (d, *J* = 1.5 Hz, 1H), 8.08 (dd, *J* = 8.8, 1.9 Hz, 1H), 7.44 (d, *J* = 9.2 Hz, 1H), 7.36 (t, *J* = 2.6 Hz, 1H), 6.69 (s, 1H); ¹³C NMR (126 MHz, CDCl₃): δ = 141.66, 138.98, 127.59, 127.16, 117.84, 117.31, 111.10, 104.58; HRMS (ESI) *m/z* calculated for C₈H₇N₂O₂[M+H]⁺ 163.0502; found 163.0500.



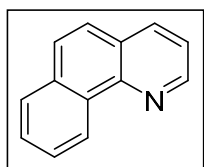
1H-indole-7-carbaldehyde

Pale yellow solid; ^1H NMR (400 MHz, CDCl_3): $\delta = 10.15$ (brs, 1H), 10.11 (s, 1H), 7.93 (d, $J = 7.8$ Hz, 1H), 7.64 (d, $J = 7.3$ Hz, 1H), 7.33 (t, $J = 3.0$ Hz, 1H), 7.26 (t, $J = 7.8$ Hz, 1H), 6.63-6.62 (m, 2H); ^{13}C NMR (101 MHz, CDCl_3): $\delta = 193.50, 133.51, 129.05, 128.76, 128.10, 125.90, 120.40, 119.36, 102.56$; HRMS (ESI) m/z calculated for $\text{C}_9\text{H}_8\text{NO}[\text{M}+\text{H}]^+$ 146.0600; found 146.0601.



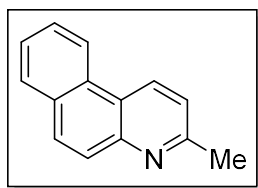
Acridine

White solid; ^1H NMR (500 MHz, CDCl_3): $\delta = 8.70$ (d, $J = 9.8$ Hz, 1H), 8.25 (d, $J = 8.9$ Hz, 2H), 7.95 (t, $J = 8.3$ Hz, 2H), 7.78-7.74 (m, 2H), 7.52-7.48 (m, 2H); ^{13}C NMR (126 MHz, CDCl_3): $\delta = 149.01, 135.92, 130.18, 129.35, 128.11, 126.50, 125.57$; HRMS (ESI) m/z calculated for $\text{C}_{13}\text{H}_{10}\text{N}[\text{M}+\text{H}]^+$ 180.0808; found 180.0807.



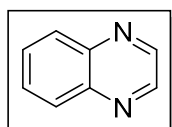
Benzo[h]quinoline

White solid; ^1H NMR (500 MHz, CDCl_3): $\delta = 9.35$ (d, $J = 8.1$ Hz, 1H), 9.02 (dd, $J = 4.2, 2.0$ Hz, 1H), 8.15 (dd, $J = 7.9, 1.9$ Hz, 1H), 7.92 (d, $J = 8.3$ Hz, 1H), 7.80 (d, $J = 8.8$ Hz, 1H), 7.77 (dt, $J = 7.0, 1.3$ Hz, 1H), 7.71 (dt, $J = 7.1, 1.5$ Hz, 1H), 7.66 (d, $J = 8.8$ Hz, 1H), 7.50 (dd, $J = 8.0, 4.2$ Hz, 1H); ^{13}C NMR (126 MHz, CDCl_3): $\delta = 148.73, 146.52, 135.69, 133.55, 131.46, 128.11, 127.73, 127.66, 126.99, 126.32, 125.25, 124.33, 121.68$; HRMS (ESI) m/z calculated for $\text{C}_{13}\text{H}_{10}\text{N}[\text{M}+\text{H}]^+$ 180.0808; found 180.0806.



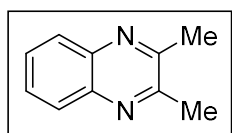
3-Methylbenzo[f]quinoline

White solid; ^1H NMR (500 MHz, CDCl_3): δ = 8.80 (d, J = 8.4 Hz, 1H), 8.56 (d, J = 8.1 Hz, 1H), 7.95-7.90 (m, 3H), 7.68-7.60 (m, 2H), 7.41 (d, J = 8.4 Hz, 1H), 2.79 (s, 3H); ^{13}C NMR (126 MHz, CDCl_3): δ = 158.35, 147.65, 131.30, 130.89, 130.69, 129.61, 128.57, 127.74, 126.91, 126.75, 123.15, 122.30, 121.78, 24.91; HRMS (ESI) m/z calculated for $\text{C}_{14}\text{H}_{12}\text{N}$ $[\text{M}+\text{H}]^+$ 194.0964; found 194.0964.



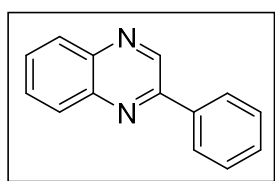
Quinoxaline

White solid; ^1H NMR (500 MHz, CDCl_3): δ = 8.54-8.51 (m, 2H), 7.81-7.77 (m, 2H), 7.42-7.41 (m, 2H); ^{13}C NMR (126 MHz, CDCl_3): δ = 144.34, 142.27, 129.31, 128.83; HRMS (ESI) m/z calculated for $\text{C}_8\text{H}_7\text{N}_2$ $[\text{M}+\text{H}]^+$ 131.0604; found 131.0605.



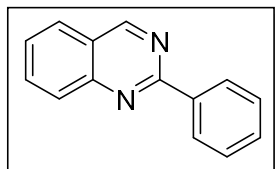
2,3-Dimethylquinoxaline

White solid; ^1H NMR (500 MHz, CDCl_3): δ = 7.95-7.93 (m, 2H), 7.63-7.61 (m, 2H), 2.68 (s, 6H); ^{13}C NMR (126 MHz, CDCl_3): δ = 153.34, 140.97, 128.71, 128.20, 23.07; HRMS (ESI) m/z calculated for $\text{C}_{10}\text{H}_{11}\text{N}_2$ $[\text{M}+\text{H}]^+$ 159.0917; found 159.0916.



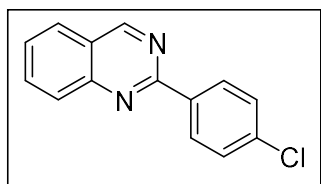
2-Phenylquinoxaline

White solid; ^1H NMR (500 MHz, CDCl_3): $\delta = 9.33$ (s, 1H), 8.20 (d, $J = 8.3$ Hz, 2H), 8.16 (d, $J = 8.0$ Hz, 1H), 8.13 (d, $J = 8.0$ Hz, 1H), 7.80-7.73 (m, 2H), 7.59-7.51 (m, 3H); ^{13}C NMR (126 MHz, CDCl_3): $\delta = 151.78, 143.31, 142.25, 141.53, 136.73, 130.22, 130.13, 129.58, 129.48, 129.10, 129.08, 127.50$; HRMS (ESI) m/z calculated for $\text{C}_{14}\text{H}_{11}\text{N}_2[\text{M}+\text{H}]^+$ 207.0917; found 207.0917.



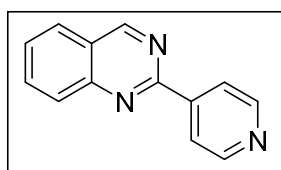
2-Phenylquinazoline

White solid; ^1H NMR (500 MHz, CDCl_3): $\delta = 9.49$ (s, 1H), 8.63 (d, $J = 8.4$ Hz, 2H), 8.11 (d, $J = 8.4$ Hz, 1H), 7.95-7.91 (m, 2H), 7.63 (t, $J = 7.6$ Hz, 1H), 7.57-7.51 (m, 3H); ^{13}C NMR (126 MHz, CDCl_3): $\delta = 161.08, 160.50, 150.79, 138.04, 134.11, 130.60, 128.64, 128.57, 127.26, 127.12, 123.61$; HRMS (ESI) m/z calculated for $\text{C}_{14}\text{H}_{11}\text{N}_2[\text{M}+\text{H}]^+$ 207.0917; found 207.0917.



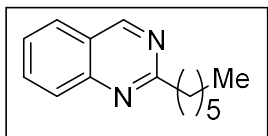
2-(4-Chlorophenyl)quinazoline

White solid; ^1H NMR (500 MHz, CDCl_3): $\delta = 9.41$ (s, 1H), 8.57 (d, $J = 8.4$ Hz, 2H), 8.06 (d, $J = 8.8$ Hz, 1H), 7.91-7.88 (m, 2H), 7.60 (t, $J = 7.7$ Hz, 1H), 7.50 (d, $J = 8.4$ Hz, 2H); ^{13}C NMR (126 MHz, CDCl_3): $\delta = 160.39, 159.87, 150.55, 136.72, 136.42, 134.13, 129.82, 128.70, 128.49, 127.34, 127.04, 123.49$; HRMS (ESI) m/z calculated for $\text{C}_{14}\text{H}_{10}\text{ClN}_2[\text{M}+\text{H}]^+$ 241.0527; found 241.0528.



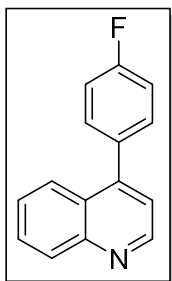
2-(Pyridin-4-yl)quinazoline

White solid; ^1H NMR (500 MHz, CDCl_3): $\delta = 9.41$ (s, 1H), 8.77(d, $J = 5.0$ Hz, 2H), 8.40 (d, $J = 5.5$ Hz, 2H), 8.05 (d, $J = 9.1$ Hz, 1H), 7.90-7.88 (m, 2H), 7.62(t, $J = 7.6$ Hz, 1H); ^{13}C NMR (126 MHz, CDCl_3): $\delta = 160.57, 158.73, 150.38, 150.32, 145.14, 134.36, 128.72, 128.16, 127.04, 123.99, 122.20$; HRMS (ESI) m/z calculated for $\text{C}_{13}\text{H}_{10}\text{N}_3[\text{M}+\text{H}]^+$ 208.0869; found 208.0869.



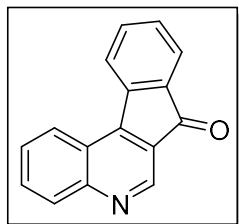
2-Hexylquinazoline

Colourless oil; ^1H NMR (500 MHz, CDCl_3): $\delta = 9.28$ (s, 1H), 7.92 (d, $J = 7.7$ Hz, 1H), 7.80 (t, $J = 7.2$ Hz, 2H), 7.51 (t, $J = 7.8$ Hz, 1H), 3.07 (t, $J = 8.1$ Hz, 2H), 1.87 (quin, $J = 7.3$ Hz, 2H), 1.40-1.24 (m, 6H) 0.82 (t, $J = 7.8$ Hz, 3H); ^{13}C NMR (126 MHz, CDCl_3): $\delta = 167.76, 160.21, 150.20, 133.82, 127.73, 126.91, 126.73, 122.89, 39.87, 31.57, 29.10, 28.85, 22.42, 13.93$; HRMS (ESI) m/z calculated for $\text{C}_{14}\text{H}_{19}\text{N}_2[\text{M}+\text{H}]^+$ 215.1543; found 215.1541.



4-(4-Fluorophenyl)quinoline

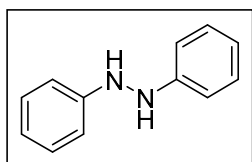
White solid; ^1H NMR (500 MHz, CDCl_3): $\delta = 8.95$ (d, $J = 4.4$ Hz, 1H), 8.19 (d, $J = 8.9$ Hz, 1H), 7.88 (d, $J = 8.5$ Hz, 1H), 7.74 (t, $J = 8.2$ Hz, 1H), 7.54-7.47 (m, 3H), 7.32 (d, $J = 4.2$ Hz, 1H), 7.23 (t, $J = 8.5$ Hz, 2H); ^{13}C NMR (126 MHz, CDCl_3): $\delta = 162.89$ (d, $J_{\text{C-F}} = 247.7$ Hz), 149.91, 148.63, 147.39, 133.90 (d, $J_{\text{C-F}} = 3.8$ Hz), 131.21 (d, $J_{\text{C-F}} = 8.5$ Hz), 129.89, 129.41, 126.76, 126.69, 125.56, 121.36, 115.64 (d, $J_{\text{C-F}} = 21.1$ Hz); ^{19}F NMR (376 MHz, D_2O): $\delta = -113.26$; HRMS (ESI) m/z calculated for $\text{C}_{15}\text{H}_{11}\text{FN}[\text{M}+\text{H}]^+$ 224.0870; found 224.0871.



7H-indeno[2,1-c]quinolin-7-one

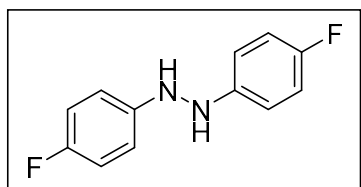
Yellow solid; ^1H NMR (500 MHz, CDCl_3): $\delta = 9.09$ (s, 1H), 8.40 (d, $J = 8.4$ Hz, 1H), 8.13 (d, $J = 8.8$ Hz, 1H), 8.04 (d, $J = 7.6$ Hz, 1H), 7.81 (t, $J = 8.0$ Hz, 1H), 7.72 (d, $J = 7.2$ Hz, 1H), 7.65 (t, $J = 8.0$ Hz, 1H), 7.58 (t, $J = 7.7$ Hz, 1H), 7.45 (t, $J = 7.6$ Hz, 1H); ^{13}C NMR (126 MHz, CDCl_3): $\delta = 192.90, 152.50, 151.02, 144.74, 142.40, 134.64, 133.90, 132.09, 131.06, 131.03, 128.18, 124.92, 124.81, 124.75, 124.44, 123.53$; HRMS (ESI) m/z calculated for $\text{C}_{16}\text{H}_{10}\text{NO}[\text{M}+\text{H}]^+$ 232.0757; found 232.0755.

Chapter 4



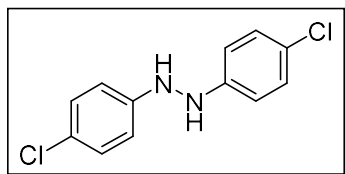
1,2-diphenylhydrazene

White solid; ^1H NMR (500 MHz, CDCl_3): $\delta = 7.19$ (t, $J = 7.6$ Hz, 4H), 6.83-6.80 (m, 6H), 5.51 (s, 2H); ^{13}C NMR (126 MHz, CDCl_3): $\delta = 148.80, 129.29, 119.81, 112.26$.



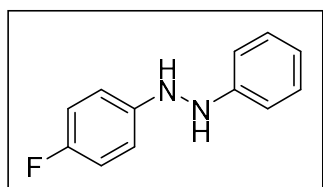
1,2-bis(4-fluorophenyl)hydrazine

White solid; ^1H NMR (200 MHz, CDCl_3): $\delta = 7.14\text{-}7.23$ (m, 3H), 6.78-6.86 (m, 5H), 5.61 (s, 1H); ^{13}C NMR (50 MHz, CDCl_3): $\delta = 148.40, 147.43, 129.39, 129.21, 124.39, 120.16, 113.48, 112.31$.



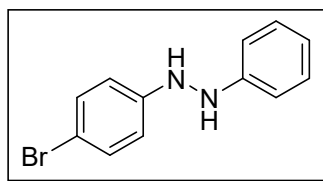
1,2-bis(4-chlorophenyl)hydrazine

White solid; ^1H NMR (500 MHz, CDCl_3): $\delta = 7.18$ (d, $J = 8.8$ Hz, 4H), 6.77 (d, $J = 8.8$ Hz, 4H), 5.63 (s, 2H); ^{13}C NMR (126 MHz, CDCl_3): $\delta = 146.97, 129.25, 124.64, 113.45$.



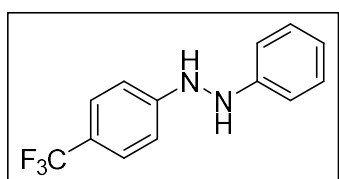
1-(4-fluorophenyl)-2-phenylhydrazine

Pale yellow solid; ^1H NMR (200 MHz, CDCl_3): $\delta = 7.23$ (t, 2H, $J=7.63$ Hz), 6.79-6.95 (m, 7H) 5.61 (s, 1H), 5.53 (s, 1H); ^{13}C NMR (50 MHz, CDCl_3): $\delta = 158.27, 155.92, 148.67, 144.97, 129.35, 119.98, 115.90, 115.67, 113.36, 113.29, 112.29$.



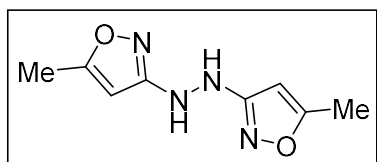
1-(4-bromophenyl)-2-phenylhydrazine

^1H NMR (200 MHz, CDCl_3): $\delta = 7.30 - 7.36$ (m, 4H), 6.78 - 6.89 (m, 5H), 5.68 (s, 2H); ^{13}C NMR (50 MHz, CDCl_3): $\delta = 112.32, 113.95, 120.20, 122.93, 124.34, 129.40, 132.10, 147.93, 148.35$.

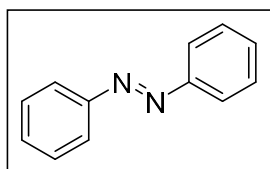


1-phenyl-2-(4-(trifluoromethyl)phenyl)hydrazine

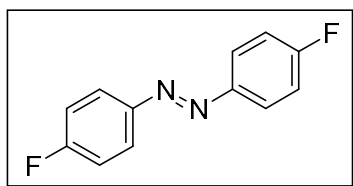
^1H NMR (200 MHz, CDCl_3): $\delta = 7.50$ (d, 2H, $J = 8.0$ Hz), 7.24 – 7.32 (m, 2H), 6.84 – 6.97 (m, 5H), 5.91 (s, 1H), 5.74 (s, 1H); ^{13}C NMR (50 MHz, CDCl_3): $\delta = 112.32, 113.95, 120.20, 122.93, 124.34, 129.40, 132.10, 147.93, 148.35$.

**1,2-bis(5-methylisoxazol-3-yl)hydrazine**

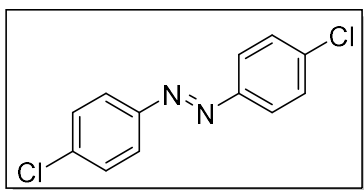
White solid; ^1H NMR (200 MHz, CDCl_3): $\delta = 6.30$ (s, 2H), 5.74 (s, 2H), 2.32 (s, 6H); ^{13}C NMR (50 MHz, CDCl_3): $\delta = 169.87, 166.69, 92.83, 12.58$.

**1,2-diphenyldiazene**

Orange solid; ^1H NMR (500 MHz, CDCl_3): $\delta = 7.96$ (d, $J = 7.1$ Hz, 4H), 7.55 (t, $J = 7.8$ Hz, 4H), 7.50 (t, $J = 7.1$ Hz, 2H); ^{13}C NMR (126 MHz, CDCl_3): $\delta = 152.63, 130.96, 129.07, 122.83$; HRMS (ESI) m/z calculated for $\text{C}_{12}\text{H}_{11}\text{N}_2$ $[\text{M}+\text{H}]^+$ 183.0917; found 183.0913.

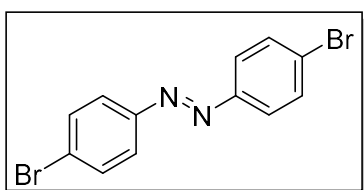
**1,2-bis(4-fluorophenyl)diazene**

Orange solid; ^1H NMR (500 MHz, CDCl_3): $\delta = 7.94$ (dd, $J = 8.9, 4.9$ Hz, 4H), 7.21 (t, $J = 8.6$ Hz, 4H); ^{13}C NMR (126 MHz, CDCl_3): $\delta = 164.34$ (d, $J = 252.8$ Hz), 148.96 (d, $J = 2.0$ Hz), 124.80 (d, $J = 8.5$ Hz), 116.03 (d, $J = 22.8$ Hz); HRMS (ESI) m/z calculated for $\text{C}_{12}\text{H}_9\text{F}_2\text{N}_2$ $[\text{M}+\text{H}]^+$ 219.0728; found 219.0727.



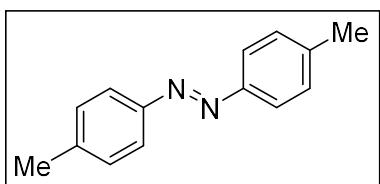
1,2-bis(4-chlorophenyl)diazene

Yellow solid; ^1H NMR (500 MHz, CDCl_3): $\delta = 7.88$ (d, $J = 7.2$ Hz, 4H), 7.50 (d, $J = 7.5$ Hz, 4H); ^{13}C NMR (126 MHz, CDCl_3): $\delta = 150.77$, 137.22, 129.39, 124.18; HRMS (ESI) m/z calculated for $\text{C}_{12}\text{H}_9\text{Cl}_2\text{N}_2$ $[\text{M}+\text{H}]^+$ 251.0137; found 251.0133.



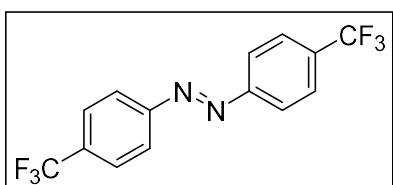
1,2-bis(4-bromophenyl)diazene

Orange solid; ^1H NMR (400 MHz, CDCl_3): $\delta = 7.80$ (d, $J = 8.6$ Hz, 4H), 7.66 (d, $J = 8.6$ Hz, 4H); ^{13}C NMR (101 MHz, CDCl_3): $\delta = 151.14$, 132.40, 125.76, 124.41; HRMS (ESI) m/z calculated for $\text{C}_{12}\text{H}_9\text{Br}_2\text{N}_2$ $[\text{M}+\text{H}]^+$ 340.9107; found 340.9104.



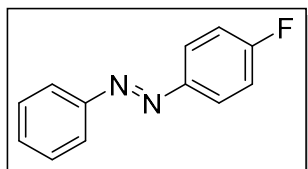
1,2-di-p-tolyldiazene

Orange solid; ^1H NMR (500 MHz, CDCl_3): $\delta = 7.84$ (d, $J = 7.3$ Hz, 4H), 7.33 (d, $J = 7.3$ Hz, 4H), 2.54 (s, 6H); ^{13}C NMR (126 MHz, CDCl_3): $\delta = 150.82$, 141.17, 129.68, 122.71, 21.45; HRMS (ESI) m/z calculated for $\text{C}_{14}\text{H}_{15}\text{N}_2$ $[\text{M}+\text{H}]^+$ 211.1230; found 211.1229.



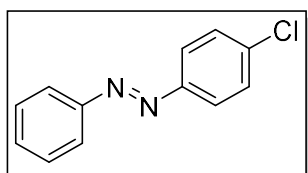
1,2-bis(4-(trifluoromethyl)phenyl)diazene

Red solid; ^1H NMR (500 MHz, CDCl_3): $\delta = 8.05$ (d, $J = 8.6$ Hz, 4H), 7.82 (d, $J = 8.3$ Hz, 4H); ^{13}C NMR (126 MHz, CDCl_3): $\delta = 154.09$, 132.99 (q, $J = 32.4$ Hz), 126.43 (q, $J = 3.7$ Hz), 123.79 (q, $J = 271.8$ Hz), 123.33; HRMS (ESI) m/z calculated for $\text{C}_{14}\text{H}_9\text{F}_6\text{N}_2$ $[\text{M}+\text{H}]^+$ 319.0664; found 319.0657.



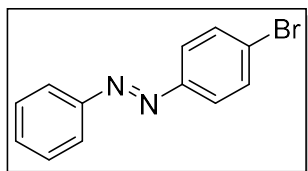
1-(4-fluorophenyl)-2-phenyldiazene

Yellow solid; ^1H NMR (500 MHz, CDCl_3): $\delta = 8.00$ -7.95 (m, 4H), 7.55 (t, $J = 7.3$ Hz, 2H), 7.51 (t, $J = 7.2$ Hz, 1H), 7.23 (t, $J = 8.4$ Hz, 2H); ^{13}C NMR (126 MHz, CDCl_3): $\delta = 164.32$ (d, $J = 251.7$ Hz), 152.43, 149.12 (d, $J = 2.9$ Hz), 130.97, 129.05, 124.83 (d, $J = 8.6$ Hz), 122.79, 115.96 (d, $J = 22.9$ Hz); HRMS (ESI) m/z calculated for $\text{C}_{12}\text{H}_{10}\text{FN}_2$ $[\text{M}+\text{H}]^+$ 201.0823; found 201.0819.



1-(4-chlorophenyl)-2-phenyldiazene

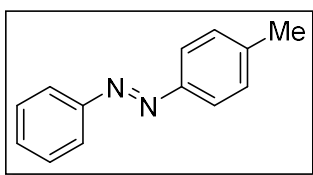
Orange solid; ^1H NMR (500 MHz, CDCl_3): $\delta = 7.96$ (d, $J = 7.7$ Hz, 2H), 7.91 (d, $J = 8.8$ Hz, 2H), 7.57-7.50 (m, 5H); ^{13}C NMR (126 MHz, CDCl_3): $\delta = 152.37$, 150.89, 136.83, 131.21, 129.26, 129.08, 124.08, 122.89; HRMS (ESI) m/z calculated for $\text{C}_{12}\text{H}_{10}\text{ClN}_2$ $[\text{M}+\text{H}]^+$ 217.0527; found 217.0526.



1-(4-bromophenyl)-2-phenyldiazene

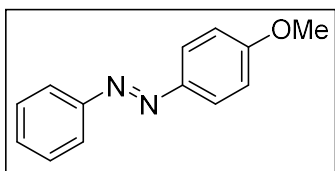
Orange solid; ^1H NMR (500 MHz, CDCl_3): $\delta = 7.95$ (d, $J = 7.4$ Hz, 2H), 7.83 (d, $J = 8.4$ Hz, 2H), 7.67 (d, $J = 8.4$ Hz, 2H), 7.56-7.49 (m, 3H); ^{13}C NMR (126 MHz, CDCl_3): $\delta =$

152.41, 151.28, 132.28, 131.28, 129.11, 125.34, 124.32, 122.92; HRMS (ESI) m/z calculated for $C_{12}H_{10}BrN_2$ $[M+H]^+$ 261.0022; found 261.0020.



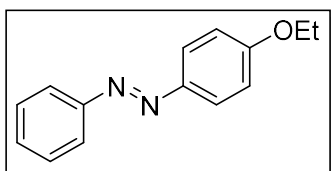
1-phenyl-2-(p-tolyl)diazene

Orange solid; 1H NMR (500 MHz, $CDCl_3$): δ = 7.97 (d, J = 7.6 Hz, 2H), 7.90 (d, J = 8.1 Hz, 2H), 7.56 (t, J = 7.6 Hz, 2H); 7.50 (t, J = 7.3 Hz, 1H) 7.36 (d, J = 7.9 Hz, 2H), 2.47 (s, 3H); ^{13}C NMR (126 MHz, $CDCl_3$): δ = 152.69, 150.73, 141.48, 130.64, 129.69, 129.00, 122.83, 122.69, 21.44; HRMS (ESI) m/z calculated for $C_{13}H_{13}N_2$ $[M+H]^+$ 197.1073; found 197.1073.



1-(4-methoxyphenyl)-2-phenyldiazene

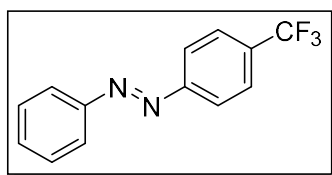
Red solid; 1H NMR (500 MHz, $CDCl_3$): δ = 8.03-7.99 (m, 4H), 7.57 (t, J = 7.3 Hz, 2H), 7.53-7.48 (m, 1H), 7.06 (d, J = 8.8 Hz, 2H), 3.87 (s, 3H); ^{13}C NMR (126 MHz, $CDCl_3$): δ = 161.93, 152.63, 146.87, 130.23, 128.90, 124.65, 122.48, 114.08, 55.34; HRMS (ESI) m/z calculated for $C_{13}H_{13}N_2O$ $[M+H]^+$ 213.1022; found 213.1020.



1-(4-ethoxyphenyl)-2-phenyldiazene

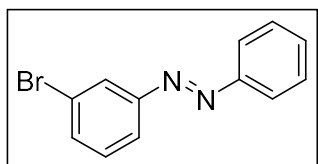
Yellow solid; 1H NMR (500 MHz, $CDCl_3$): δ = 7.95 (d, J = 8.9 Hz, 2H), 7.92 (d, J = 7.9 Hz, 2H), 7.53 (t, J = 8.1 Hz, 2H), 7.46 (t, J = 7.3 Hz, 1H), 7.02 (d, J = 8.9 Hz, 2H), 4.13 (q, J = 7.3, 6.8 Hz, 2H), 1.47 (t, J = 7.3 Hz, 3H); ^{13}C NMR (126 MHz, $CDCl_3$): δ = 161.45,

152.74, 146.83, 130.26, 128.97, 124.71, 122.50, 114.61, 63.75, 14.71; HRMS (ESI) m/z calculated for $C_{14}H_{15}N_2O$ $[M+H]^+$ 227.1179; found 227.1175.



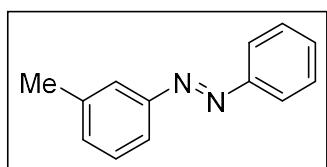
1-phenyl-2-(4-(trifluoromethyl)phenyl)diazene

Orange solid; 1H NMR (500 MHz, $CDCl_3$): δ = 8.04 (d, J = 8.1 Hz, 2H), 7.99 (d, J = 8.4 Hz, 2H), 7.82 (d, J = 8.4 Hz, 2H), 7.60-7.54 (m, 3H); ^{13}C NMR (126 MHz, $CDCl_3$): δ = 154.42, 152.42, 132.20 (q, J = 32.6 Hz), 131.80, 129.19, 126.28 (q, J = 3.8 Hz), 123.92 (q, J = 272.5 Hz), 123.16, 123.00; HRMS (ESI) m/z calculated for $C_{13}H_{10}F_3N_2$ $[M+H]^+$ 251.0791; found 251.0784.



1-(3-bromophenyl)-2-phenyldiazene

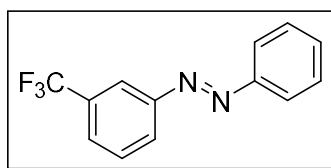
Orange solid; 1H NMR (500 MHz, $CDCl_3$): δ = 8.09 (s, 1H), 7.96 (d, J = 7.1 Hz, 2H), 7.91 (d, J = 8.2 Hz, 1H), 7.62 (d, J = 7.7 Hz, 1H), 7.56-7.52 (m, 3H), 7.41 (t, J = 8.0 Hz, 1H); ^{13}C NMR (126 MHz, $CDCl_3$): δ = 153.45, 152.27, 133.53, 131.48, 130.37, 129.11, 124.58, 123.08, 123.02, 122.93; HRMS (ESI) m/z calculated for $C_{12}H_{10}BrN_2$ $[M+H]^+$ 261.0022; found 261.0023.



1-phenyl-2-(m-tolyl)diazene

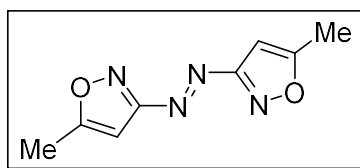
Red oil; 1H NMR (500 MHz, $CDCl_3$): δ = 7.95 (d, J = 8.0 Hz, 2H), 7.76 (s, 2H), 7.54 (t, J = 7.6 Hz, 2H), 7.49 (t, J = 7.6 Hz, 1H), 7.43 (t, J = 7.8 Hz, 1H), 7.32 (d, J = 7.2 Hz, 1H), 2.49 (s, 3H); ^{13}C NMR (126 MHz, $CDCl_3$): δ = 152.76, 152.71, 138.95, 131.75, 130.85,

129.05, 128.87, 122.92, 122.77, 120.47, 21.33; HRMS (ESI) m/z calculated for $C_{13}H_{13}N_2$ $[M+H]^+$ 197.1073; found 197.1073.



1-phenyl-2-(3-(trifluoromethyl)phenyl)diazene

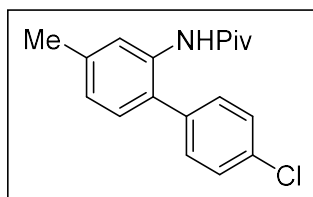
Red solid; 1H NMR (400 MHz, $CDCl_3$): δ = 8.22 (s, 1H), 8.13 (d, J = 8.0 Hz, 1H), 7.99-7.97 (m, 2H), 7.75 (d, J = 8.0 Hz, 1H), 7.66 (t, J = 8.0 Hz, 1H), 7.58-7.53 (m, 3H); ^{13}C NMR (101 MHz, $CDCl_3$): δ = 152.55, 152.32, 131.69 (q, J = 32.4 Hz), 131.68, 129.66, 129.18, 127.17 (q, J = 3.9 Hz), 126.23, 123.86 (q, J = 272.9 Hz), 123.10, 119.55 (q, J = 3.9 Hz); HRMS (ESI) m/z calculated for m/z calculated for $C_{13}H_{10}F_3N_2$ $[M+H]^+$ 251.0791; found 251.0788.



1,2-bis(5-methylisoxazol-3-yl)diazene

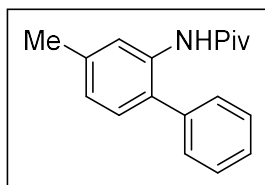
Yellow solid; 1H NMR (500 MHz, $CDCl_3$): δ = 6.43 (s, 2H), 2.53 (s, 6H); ^{13}C NMR (126 MHz, $CDCl_3$): δ = 173.83, 172.01, 91.94, 12.79; HRMS (ESI) m/z calculated for $C_8H_9N_4O_2$ $[M+H]^+$ 193.0720; found 193.0723.

Chapter 5



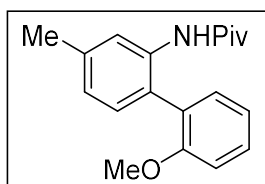
N-(4'-chloro-4-methyl-[1,1'-biphenyl]-2-yl)pivalamide

White solid; ^1H NMR (200 MHz, CDCl_3): δ = 8.08 (s, 1H), 7.38 (d, J = 8.6 Hz, 2H), 7.25-7.19 (m, 3H), 7.02 (d, J = 7.8 Hz, 1H), 6.91 (d, J = 7.8 Hz, 1H), 2.32 (s, 3H), 1.05 (s, 9H); ^{13}C NMR (50 MHz, CDCl_3): δ = 176.38, 138.91, 136.62, 134.64, 133.90, 130.76, 129.57, 129.14, 128.40, 125.01, 122.05, 39.77, 27.40, 21.45; HRMS (ESI) m/z calculated for $\text{C}_{18}\text{H}_{20}\text{ClNO}$ $[\text{M}+\text{H}]^+$ 302.1312; found 302.1306.



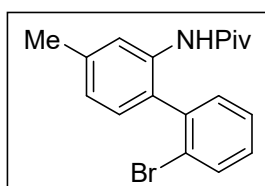
***N*-(4-methyl-[1,1'-biphenyl]-2-yl)pivalamide**

White solid; ^1H NMR (500 MHz, CDCl_3): δ = 8.25 (s, 1H), 7.49 (t, J = 7.6 Hz, 2H), 7.46 (brs, 1H), 7.41 (t, J = 7.6 Hz, 1H), 7.36 (d, J = 7.3 Hz, 2H), 7.15 (d, J = 7.6 Hz, 1H), 6.99 (d, J = 8.3 Hz, 1H), 2.41 (s, 3H), 1.11 (s, 9H); ^{13}C NMR (126 MHz, CDCl_3): δ = 176.30, 138.46, 138.08, 134.83, 129.48, 129.39, 128.95, 127.82, 124.63, 121.37, 39.74, 27.31, 21.45; HRMS (ESI) m/z calculated for $\text{C}_{18}\text{H}_{21}\text{NO}$ $[\text{M}+\text{H}]^+$ 268.1701, found .268.1696.



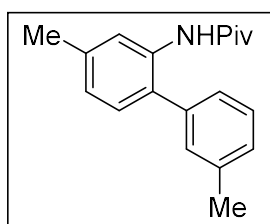
***N*-(2'-methoxy-4-methyl-[1,1'-biphenyl]-2-yl)pivalamide**

White solid; ^1H NMR (500 MHz, CDCl_3): δ = 8.00 (s, 1H), 7.75 (brs, 1H), 7.41 (t, J = 8.4 Hz, 1H), 7.23 (d, J = 8.4 Hz, 1H), 7.13 (d, J = 8.0 Hz, 1H), 7.08 (t, J = 7.6 Hz, 1H), 7.04-7.00 (m, 2H), 3.84 (s, 3), 2.41 (s, 3H), 1.09 (s, 9H); ^{13}C NMR (126 MHz, CDCl_3): δ = 176.35, 155.84, 138.22, 135.45, 132.21, 130.27, 129.46, 127.32, 127.27, 125.07, 122.67, 121.54, 110.88, 55.74, 39.42, 27.27, 21.38; HRMS (ESI) m/z calculated for $\text{C}_{19}\text{H}_{23}\text{NO}_2$ $[\text{M}+\text{H}]^+$ 298.1807, found 298.1802.

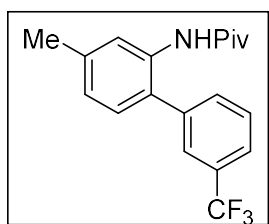


***N*-(2'-bromo-4-methyl-[1,1'-biphenyl]-2-yl)pivalamide**

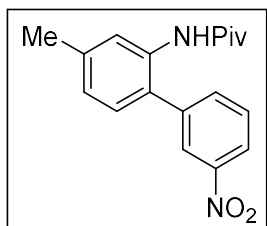
Colourless oil; ^1H NMR (500 MHz, CDCl_3): δ = 8.14 (s, 1H), 7.72 (d, J = 8.0 Hz, 1H), 7.42 (t, J = 7.6 Hz, 1H), 7.31-7.27 (m, 2H), 7.10 (brs, 1H), 7.06 (d, J = 7.6 Hz, 1H), 7.01 (d, J = 7.6 Hz, 1H), 2.42 (s, 3H), 1.05 (s, 9H); ^{13}C NMR (126 MHz, CDCl_3): δ = 176.22, 139.09, 138.82, 134.92, 132.87, 131.94, 129.74, 129.06, 128.95, 127.94, 124.71, 124.12, 121.76, 39.54, 27.15, 21.53; HRMS (ESI) m/z calculated for $\text{C}_{18}\text{H}_{20}\text{BrNO}$ $[\text{M}+\text{H}]^+$ 346.0807, found 346.0801.

***N*-(3',4-dimethyl-[1,1'-biphenyl]-2-yl)pivalamide**

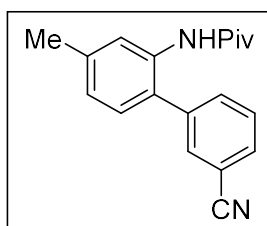
White solid; ^1H NMR (200 MHz, CDCl_3): δ = 8.25 (s, 1H), 7.52 (brs, 1H), 7.38 (t, J = 7.6 Hz, 1H), 7.24-7.12 (m, 4H), 6.98 (d, J = 7.7 Hz, 1H), 2.41 (m, 6H), 1.12 (s, 9H); ^{13}C NMR (50 MHz, CDCl_3): δ = 176.28, 138.65, 138.35, 137.95, 134.82, 130.12, 129.44, 129.35, 128.89, 128.51, 126.39, 124.58, 121.25, 39.77, 27.33, 21.47, 21.38; HRMS (ESI) m/z calculated for $\text{C}_{19}\text{H}_{23}\text{NO}$ $[\text{M}+\text{H}]^+$ 282.1858, found 282.1852.

***N*-(4-methyl-3'-(trifluoromethyl)-[1,1'-biphenyl]-2-yl)pivalamide**

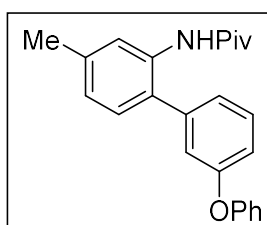
Colourless oil; ^1H NMR (500 MHz, CDCl_3): δ = 8.11 (s, 1H), 7.67 (d, J = 7.6 Hz, 1H), 7.64 (s, 1H), 7.61 (t, J = 7.6 Hz, 1H), 7.56 (d, J = 7.7 Hz, 1H), 7.26 (brs, 1H), 7.14 (d, J = 7.9 Hz, 1H), 7.02 (d, J = 7.9 Hz, 1H), 2.40 (s, 3H), 1.11 (s, 9H); ^{13}C NMR (126 MHz, CDCl_3): δ = 176.48, 139.28, 139.14, 134.52, 132.88, 131.26 (q, $J_{\text{C-F}}$ = 32.2 Hz), 129.63, 129.54, 128.50, 126.12 (q, $J_{\text{C-F}}$ = 3.8 Hz), 125.36, 124.51 (q, $J_{\text{C-F}}$ = 4.0 Hz), 123.86 (q, $J_{\text{C-F}}$ = 272.8 Hz), 122.68, 39.68, 27.27, 21.41; HRMS (ESI) m/z calculated for $\text{C}_{19}\text{H}_{20}\text{F}_3\text{NO}$ $[\text{M}+\text{H}]^+$ 336.1575; found 336.1570.

***N*-(4-methyl-3'-nitro-[1,1'-biphenyl]-2-yl)pivalamide**

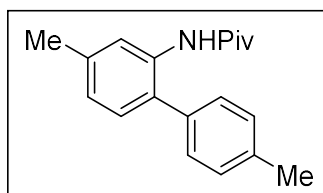
White solid; ^1H NMR (400 MHz, CDCl_3): δ = 8.25-8.22 (m, 2H), 7.96 (s, 1H), 7.72 (d, J = 7.8 Hz, 1H), 7.65 (t, J = 7.8 Hz, 1H), 7.25 (brs, 1H), 7.17 (d, J = 7.8 Hz, 1H), 7.06 (d, J = 7.8 Hz, 1H), 2.41 (s, 3H), 1.13 (s, 9H); ^{13}C NMR (50 MHz, CDCl_3): δ = 176.47, 148.35, 140.23, 139.67, 135.48, 134.30, 129.82, 129.70, 128.42, 125.95, 124.09, 123.82, 122.47, 39.60, 27.31, 21.34; HRMS (ESI) m/z calculated for $\text{C}_{18}\text{H}_{20}\text{N}_2\text{O}_3$ $[\text{M}+\text{H}]^+$ 313.1552; found 313.1546.

***N*-(3'-cyano-4-methyl-[1,1'-biphenyl]-2-yl)pivalamide**

Colourless oil; ^1H NMR (500 MHz, CDCl_3): δ = 7.98 (s, 1H), 7.69 (d, J = 7.1 Hz, 1H), 7.66 (s, 1H), 7.62 (d, J = 7.6 Hz, 1H), 7.58 (t, J = 7.1 Hz, 1H), 7.17 (brs, 1H), 7.13 (d, J = 7.6 Hz, 1H), 7.05 (d, J = 7.8 Hz, 1H), 2.40 (s, 3H), 1.14 (s, 9H); ^{13}C NMR (126 MHz, CDCl_3): δ = 176.43, 139.84, 139.59, 134.34, 133.80, 132.81, 131.20, 129.65, 129.55, 128.41, 125.81, 123.55, 118.24, 113.08, 39.63, 27.34, 21.37; HRMS (ESI) m/z calculated for $\text{C}_{19}\text{H}_{20}\text{N}_2\text{O}$ $[\text{M}+\text{H}]^+$ 293.1654; found 293.1648.

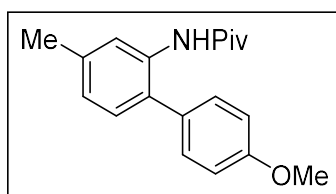
***N*-(4-methyl-3'-phenoxy-[1,1'-biphenyl]-2-yl)pivalamide**

Colourless oil; ^1H NMR (500 MHz, CDCl_3): δ = 8.22 (s, 1H), 7.50 (s, 1H), 7.44 (t, J = 8.1 Hz, 1H), 7.37 (t, J = 8.1 Hz, 2H), 7.16-7.12 (m, 2H), 7.08 (d, J = 7.6 Hz, 1H), 7.06-7.04 (m, 3H), 6.99 (s, 1H), 6.97 (d, J = 7.6 Hz, 1H), 2.39 (s, 3H), 1.14 (s, 9H); ^{13}C NMR (126 MHz, CDCl_3): δ = 176.30, 158.12, 156.46, 139.92, 138.74, 134.73, 130.27, 129.89, 129.43, 128.69, 124.68, 123.90, 123.84, 121.45, 119.36, 119.24, 117.78, 39.80, 27.39, 21.46; HRMS (ESI) m/z calculated for $\text{C}_{24}\text{H}_{25}\text{NO}_2$ $[\text{M}+\text{H}]^+$ 360.1964; found 360.1958.



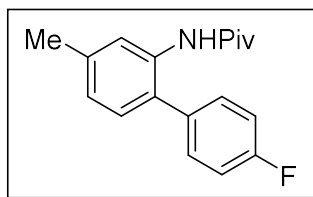
***N*-(4,4'-dimethyl-[1,1'-biphenyl]-2-yl)pivalamide**

White solid; ^1H NMR (200 MHz, CDCl_3): δ = 8.24 (s, 1H), 7.50 (brs, 1H), 7.31-7.20 (m, 4H), 7.11 (d, J = 7.7 Hz, 1H), 6.96 (d, J = 7.8 Hz, 1H), 2.41 (s, 3H), 2.39 (s, 3H), 1.11 (s, 9H); ^{13}C NMR (50 MHz, CDCl_3): δ = 176.28, 138.20, 137.57, 134.98, 134.88, 129.62, 129.58, 129.22, 124.56, 121.20, 39.74, 27.35, 21.43, 21.17; HRMS (ESI) m/z calculated for $\text{C}_{19}\text{H}_{23}\text{NO}$ $[\text{M}+\text{H}]^+$ 282.1858, found 282.1852.

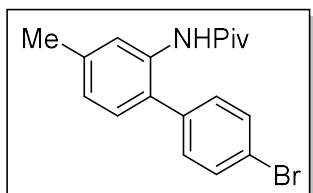


***N*-(4'-methoxy-4-methyl-[1,1'-biphenyl]-2-yl)pivalamide**

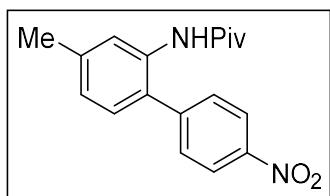
White solid; ^1H NMR (500 MHz, CDCl_3): δ = 8.23 (s, 1H), 7.48 (brs, 1H), 7.27 (d, J = 8.7 Hz, 2H), 7.10 (d, J = 7.9 Hz, 1H), 7.01 (d, J = 8.9 Hz, 2H), 6.95 (d, J = 7.7 Hz, 1H), 3.86 (s, 3), 2.39 (s, 3H), 1.12 (s, 9H); ^{13}C NMR (126 MHz, CDCl_3): δ = 176.34, 159.26, 138.22, 135.08, 130.62, 130.23, 129.74, 128.99, 124.62, 121.29, 114.40, 77.05, 55.37, 39.81, 27.44, 21.49; HRMS (ESI) m/z calculated for $\text{C}_{19}\text{H}_{23}\text{NO}_2$ $[\text{M}+\text{H}]^+$ 298.1807, found 298.1802.

***N*-(4'-fluoro-4-methyl-[1,1'-biphenyl]-2-yl)pivalamide**

White solid; ^1H NMR (400 MHz, CDCl_3): δ = 8.18 (s, 1H), 7.35-7.30 (m, 3H), 7.17 (t, J = 8.7 Hz, 2H), 7.11 (d, J = 7.8 Hz, 1H), 6.98 (d, J = 8.8 Hz, 1H), 2.40 (s, 3H), 1.12 (s, 9H); ^{13}C NMR (50 MHz, CDCl_3): δ = 176.31, 162.32 (d, $J_{\text{C-F}}$ = 248.0 Hz), 138.67, 134.79, 134.03 (d, $J_{\text{C-F}}$ = 3.7 Hz), 131.11 (d, $J_{\text{C-F}}$ = 8.0 Hz), 129.61, 128.50, 124.83, 121.77, 115.91 (d, $J_{\text{C-F}}$ = 21.3 Hz), 39.71, 27.34, 21.42; HRMS (ESI) m/z calculated for $\text{C}_{18}\text{H}_{20}\text{FNO}$ $[\text{M}+\text{H}]^+$ 286.1654; found 286.1648.

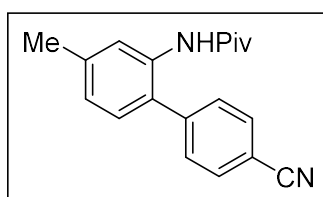
***N*-(4'-bromo-4-methyl-[1,1'-biphenyl]-2-yl)pivalamide**

White solid; ^1H NMR (200 MHz, CDCl_3): δ = 8.15 (s, 1H), 7.60 (d, J = 8.6 Hz, 2H), 7.33 (brs, 1H), 7.23 (d, J = 8.4 Hz, 2H), 7.09 (d, J = 7.8 Hz, 1H), 6.98 (d, J = 7.8 Hz, 1H), 2.39 (s, 3H), 1.13 (s, 9H); ^{13}C NMR (50 MHz, CDCl_3): δ = 176.31, 138.87, 137.09, 134.55, 132.04, 131.03, 129.48, 128.42, 125.02, 122.13, 121.98, 39.72, 27.37, 21.41; HRMS (ESI) m/z calculated for $\text{C}_{18}\text{H}_{20}\text{BrNO}$ $[\text{M}+\text{H}]^+$ 346.0807, found 346.0801.

***N*-(4-methyl-4'-nitro-[1,1'-biphenyl]-2-yl)pivalamide**

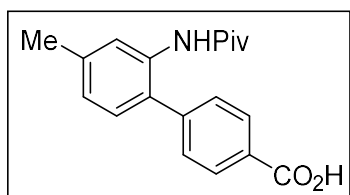
White solid; ^1H NMR (200 MHz, CDCl_3): δ = 8.32 (d, J = 9.0 Hz, 2H), 7.99 (s, 1H), 7.55 (d, J = 8.8 Hz, 2H), 7.23 (brs, 1H), 7.16 (d, J = 7.8 Hz, 1H), 7.06 (d, J = 7.8 Hz, 1H), 2.41 (s, 3H), 1.14 (s, 9H); ^{13}C NMR (50 MHz, CDCl_3): δ = 176.45, 147.14, 145.45, 139.91,

134.26, 130.22, 129.54, 128.53, 125.83, 123.96, 123.66, 39.64, 27.35, 21.37; HRMS (ESI) m/z calculated for $C_{18}H_{20}N_2O_3$ $[M+H]^+$ 313.1552; found 313.1546.



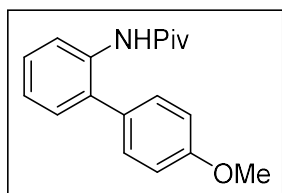
***N*-(4'-cyano-4-methyl-[1,1'-biphenyl]-2-yl)pivalamide**

Colourless oil; 1H NMR (500 MHz, $CDCl_3$): δ = 8.02 (s, 1H), 7.76 (d, J = 7.9 Hz, 2H), 7.49 (d, J = 8.4 Hz, 2H), 7.20 (brs, 1H), 7.12 (d, J = 7.6 Hz, 1H), 7.04 (d, J = 7.7 Hz, 1H), 2.40 (s, 3H), 1.13 (s, 9H); ^{13}C NMR (126 MHz, $CDCl_3$): δ = 176.40, 143.40, 139.71, 134.27, 132.54, 130.13, 129.45, 128.70, 125.69, 123.33, 118.49, 111.53, 39.66, 27.34, 21.39; HRMS (ESI) m/z calculated for $C_{19}H_{20}N_2O$ $[M+H]^+$ 293.1654; found 293.1648.



4'-methyl-2'-pivalamido-[1,1'-biphenyl]-4-carboxylic acid

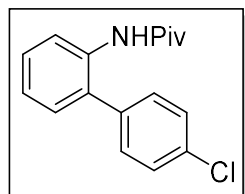
White solid; 1H NMR (500 MHz, $CDCl_3$): δ = 1.01 (s, 9H), 2.29 (s, 3H), 6.91 (d, J = 7.2 Hz, 1H), 7.05 (d, J = 7.7 Hz, 1H), 7.35-7.32 (m, 3H), 7.99 (s, 1H), 8.05 (d, J = 8.0 Hz, 2H); ^{13}C NMR (126 MHz, $CDCl_3$): δ = 21.16, 27.09, 39.42, 122.28, 124.93, 129.01, 129.25, 130.06, 134.31, 138.65, 142.44, 167.86, 176.22; HRMS (ESI) m/z calculated for $C_{19}H_{21}NO_3$ $[M+H]^+$ 312.1594; found 312.1593.



***N*-(4'-methoxy-[1,1'-biphenyl]-2-yl)pivalamide**

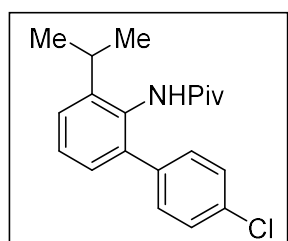
White solid; 1H NMR (200 MHz, $CDCl_3$): δ = 1.12 (s, 9H), 3.87 (s, 3H), 7.01 (d, J = 8.8 Hz, 2H), 7.23-7.09 (m, 2H), 7.29 (d, J = 8.7 Hz, 2H), 7.51 (brs, 1H), 8.35 (d, J = 8.2 Hz,

1H); ^{13}C NMR (50 MHz, CDCl_3): $\delta = 27.40, 39.76, 55.33, 114.40, 120.75, 123.81, 128.15, 129.91, 130.15, 130.49, 131.76, 135.28, 159.34, 176.25$; HRMS (ESI) m/z calculated for $\text{C}_{18}\text{H}_{21}\text{NO}_2$ $[\text{M}+\text{H}]^+$ 284.1645; found 284.1643.



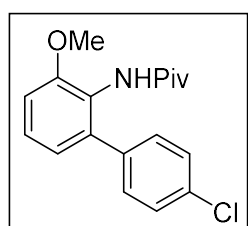
***N*-(4'-chloro-[1,1'-biphenyl]-2-yl)pivalamide**

Yellow solid; ^1H NMR (400 MHz, CDCl_3): $\delta = 8.29$ (d, $J = 8.2$ Hz, 1H), 7.49-7.46 (m, 2H), 7.40-7.34 (m, 2H), 7.33-7.30 (m, 2H), 7.21 (dd, $J = 7.8, 1.8$ Hz, 1H), 7.19-7.15 (m, 1H), 1.13 (s, 1H); ^{13}C NMR (101 MHz, CDCl_3): $\delta = 176.30, 136.56, 134.90, 134.10, 131.21, 130.66, 129.75, 129.16, 128.76, 124.22, 121.57, 39.73, 27.38$; HRMS (ESI) m/z calculated for $\text{C}_{17}\text{H}_{18}\text{ClNO}$ $[\text{M}+\text{H}]^+$ 288.1155; found 288.1150.



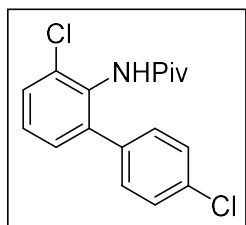
***N*-(4'-chloro-3-isopropyl-[1,1'-biphenyl]-2-yl)pivalamide**

White solid; ^1H NMR (500 MHz, CDCl_3): $\delta = 7.38$ -7.33 (m, 4H), 7.24 (d, $J = 8.4$ Hz, 2H), 7.13 (d, $J = 7.3$ Hz, 1H), 6.75 (s, 1H), 3.05 (sep, $J = 6.9$ Hz, 1H), 1.25 (d, $J = 6.9$ Hz, 6H), 1.11 (s, 9H); ^{13}C NMR (126 MHz, CDCl_3): $\delta = 177.27, 146.93, 139.53, 138.61, 133.17, 131.42, 130.32, 128.13, 127.81, 127.60, 125.62, 38.96, 28.54, 27.42, 23.42$; HRMS (ESI) m/z calculated for $\text{C}_{20}\text{H}_{24}\text{ClNO}$ $[\text{M}+\text{H}]^+$ 330.1625; found 330.1619.



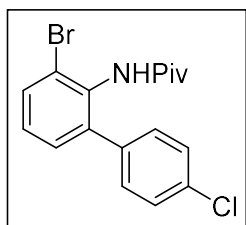
***N*-(4'-chloro-3-methoxy-[1,1'-biphenyl]-2-yl)pivalamide**

White solid; ^1H NMR (500 MHz, CDCl_3): $\delta = 7.30$ (s, 4H), 7.26 (t, $J = 8.0$ Hz, 1H), 6.94 (brs, 1H), 6.91 (d, $J = 8.1$ Hz, 2H), 3.84 (s, 3H), 1.14 (s, 9H); ^{13}C NMR (126 MHz, CDCl_3): $\delta = 176.71, 154.42, 139.50, 138.32, 132.90, 129.79, 128.10, 127.43, 123.21, 122.11, 110.35, 55.94, 39.08, 27.37$; HRMS (ESI) m/z calculated for $\text{C}_{18}\text{H}_{20}\text{ClNO}_2$ $[\text{M}+\text{H}]^+$ 318.1261; found 318.1255.



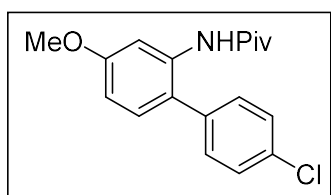
***N*-(3,4'-dichloro-[1,1'-biphenyl]-2-yl)pivalamide**

White solid; ^1H NMR (500 MHz, CDCl_3): $\delta = 7.43$ (d, $J = 7.9$ Hz, 1H), 7.34 (d, $J = 8.5$ Hz, 2H), 7.28-7.25 (m, 3H), 7.21 (d, $J = 7.6$ Hz, 1H), 7.05 (s, 1H), 1.14 (s, 9H); ^{13}C NMR (126 MHz, CDCl_3): $\delta = 176.53, 141.04, 137.51, 133.56, 132.75, 131.77, 129.89, 129.04, 128.75, 128.27, 128.03, 39.14, 27.31$; HRMS (ESI) m/z calculated for $\text{C}_{17}\text{H}_{17}\text{Cl}_2\text{NO}$ $[\text{M}+\text{H}]^+$ 322.0765; found 322.0760.



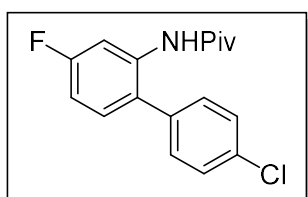
***N*-(3-bromo-4'-chloro-[1,1'-biphenyl]-2-yl)pivalamide**

White solid; ^1H NMR (500 MHz, CDCl_3): $\delta = 7.61$ (d, $J = 8.0$ Hz, 1H), 7.43 (d, $J = 8.4$ Hz, 2H), 7.27-7.24 (m, 3H), 7.20 (t, $J = 8.2$ Hz, 1H), 7.05 (brs, 1H), 1.13 (s, 9H); ^{13}C NMR (126 MHz, CDCl_3): $\delta = 176.27, 141.27, 137.77, 133.56, 133.15, 132.24, 129.89, 129.55, 128.45, 128.26, 123.44, 39.17, 27.31$; HRMS (ESI) m/z calculated for $\text{C}_{17}\text{H}_{17}\text{BrClNO}$ $[\text{M}+\text{H}]^+$ 366.0260; found 366.0255.

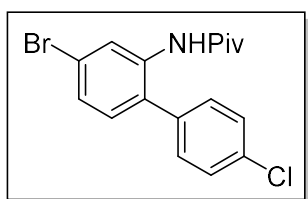


***N*-(4'-chloro-4-methoxy-[1,1'-biphenyl]-2-yl)pivalamide**

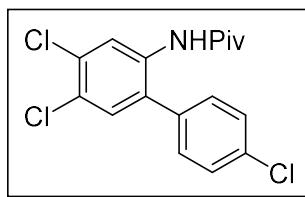
White solid; ^1H NMR (500 MHz, CDCl_3): δ = 8.08 (d, J = 2.6 Hz, 1H), 7.46 (d, J = 8.4 Hz, 2H), 7.43 (brs, 1H), 7.29 (d, J = 8.4 Hz, 2H), 7.11 (d, J = 8.4 Hz, 1H), 6.73 (dd, J = 8.4, 2.7 Hz, 1H), 3.86 (s, 3H), 1.14 (s, 9H); ^{13}C NMR (126 MHz, CDCl_3): δ = 176.46, 159.93, 136.42, 136.01, 133.83, 130.91, 130.43, 129.22, 123.09, 110.91, 105.63, 55.46, 39.92, 27.40; HRMS (ESI) m/z calculated for $\text{C}_{18}\text{H}_{20}\text{ClNO}_2$ $[\text{M}+\text{H}]^+$ 318.1261; found 318.1255.

***N*-(4'-chloro-4-fluoro-[1,1'-biphenyl]-2-yl)pivalamide**

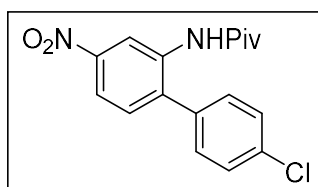
White solid; ^1H NMR (500 MHz, CDCl_3): δ = 8.21 (d, J = 11.1 Hz, 1H), 7.48 (d, J = 8.4 Hz, 2H), 7.44 (s, 1H), 7.28 (d, J = 7.9 Hz, 2H), 7.15 (t, J = 7.8 Hz, 1H), 6.84 (t, J = 7.8 Hz, 1H), 1.12 (s, 9H); ^{13}C NMR (126 MHz, CDCl_3): δ = 176.31, 162.52 (d, $J_{\text{C-F}}$ = 245.2 Hz), 136.34 (d, $J_{\text{C-F}}$ = 11.6 Hz), 135.61, 134.33, 130.74, 130.66 (d, $J_{\text{C-F}}$ = 10.3 Hz), 129.34, 126.36 (d, $J_{\text{C-F}}$ = 3.1 Hz), 110.62 (d, $J_{\text{C-F}}$ = 21.8 Hz), 108.23 (d, $J_{\text{C-F}}$ = 27.6 Hz), 39.83, 27.25; HRMS (ESI) m/z calculated for $\text{C}_{17}\text{H}_{17}\text{ClFNO}$ $[\text{M}+\text{H}]^+$ 306.1061; found 306.1055.

***N*-(4-bromo-4'-chloro-[1,1'-biphenyl]-2-yl)pivalamide**

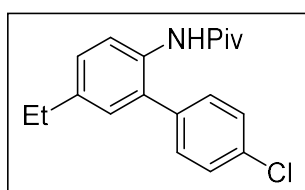
White solid; ^1H NMR (200 MHz, CDCl_3): δ = 8.61 (d, J = 2.0 Hz, 1H), 7.48 (d, J = 8.6 Hz, 2H), 7.36 (brs, 1H), 7.32-7.26 (m, 3H), 7.06 (d, J = 8.2 Hz, 1H), 1.12 (s, 9H); ^{13}C NMR (50 MHz, CDCl_3): δ = 176.35, 136.05, 135.45, 134.54, 130.84, 130.50, 129.56, 129.41, 127.05, 123.97, 122.53, 39.84, 27.30; HRMS (ESI) m/z calculated for $\text{C}_{17}\text{H}_{17}\text{BrClNO}$ $[\text{M}+\text{H}]^+$ 366.0260; found 366.0255.

***N*-(4,4',5-trichloro-[1,1'-biphenyl]-2-yl)pivalamide**

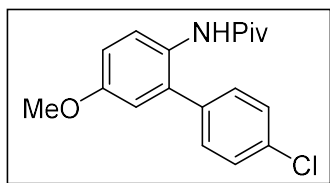
White solid; ^1H NMR (500 MHz, CDCl_3): δ = 8.57 (s, 1H), 7.50 (d, J = 8.6 Hz, 2H), 7.34 (s, 1H), 7.29-7.27 (m, 3H), 1.12 (s, 9H); ^{13}C NMR (126 MHz, CDCl_3): δ = 176.34, 135.03, 134.35, 134.22, 132.52, 130.76, 130.56, 130.42, 129.56, 127.18, 122.71, 39.85, 27.25; HRMS (ESI) m/z calculated for $\text{C}_{17}\text{H}_{16}\text{Cl}_3\text{NO}$ $[\text{M}+\text{H}]^+$ 356.0376; found 356.0370.

***N*-(4'-chloro-4-nitro-[1,1'-biphenyl]-2-yl)pivalamide**

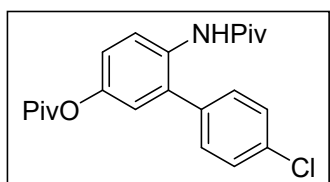
White solid; ^1H NMR (500 MHz, CDCl_3): δ = 9.24 (s, 1H), 7.99 (d, J = 6.9 Hz, 1H), 7.55-7.53 (m, 3H), 7.37-7.32 (m, 3H), 1.15 (s, 9H); ^{13}C NMR (126 MHz, CDCl_3): δ = 176.61, 147.98, 136.76, 136.14, 135.53, 134.48, 130.45, 130.25, 129.77, 118.71, 116.26, 77.07, 39.98, 27.29; HRMS (ESI) m/z calculated for $\text{C}_{17}\text{H}_{17}\text{ClN}_2\text{O}_3$ $[\text{M}+\text{H}]^+$ 333.1006; found 333.1000.

***N*-(4'-chloro-5-ethyl-[1,1'-biphenyl]-2-yl)pivalamide**

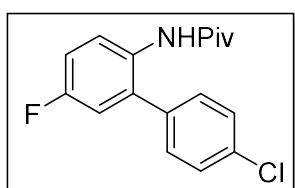
White solid; ^1H NMR (200 MHz, CDCl_3): δ = 8.15 (d, J = 8.4 Hz, 1H), 7.47 (d, J = 8.6 Hz, 2H), 7.35-7.26 (m, 3H), 7.22 (dd, J = 8.4, 2.2 Hz, 1H), 7.05 (d, J = 2.2 Hz, 1H), 2.65 (q, J = 7.6 Hz, 2H), 1.24 (t, J = 7.6 Hz, 3H), 1.13 (s, 9H); ^{13}C NMR (50 MHz, CDCl_3): δ = 176.23, 140.38, 136.89, 133.94, 132.48, 131.43, 130.67, 129.14, 129.07, 128.13, 121.91, 39.65, 28.26, 27.42, 15.62; HRMS (ESI) m/z calculated for $\text{C}_{19}\text{H}_{22}\text{ClNO}$ $[\text{M}+\text{H}]^+$ 316.1468; found 316.1462.

***N*-(4'-chloro-5-methoxy-[1,1'-biphenyl]-2-yl)pivalamide**

White solid; ^1H NMR (500 MHz, CDCl_3): δ = 8.02 (d, J = 8.9 Hz, 1H), 7.45 (d, J = 8.3 Hz, 2H), 7.30 (d, J = 8.5 Hz, 2H), 7.15 (brs, 1H), 6.92 (dd, J = 9.1, 3.1 Hz, 1H), 6.77 (d, J = 3.2 Hz, 1H), 3.81 (s, 3H), 1.13 (s, 9H); ^{13}C NMR (126 MHz, CDCl_3): δ = 176.30, 156.34, 136.65, 134.05, 133.63, 130.49, 128.99, 127.90, 124.19, 115.27, 113.56, 55.49, 39.45, 27.40; HRMS (ESI) m/z calculated for $\text{C}_{18}\text{H}_{20}\text{ClNO}_2$ $[\text{M}+\text{H}]^+$ 318.1261; found 318.1255.

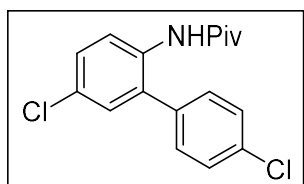
**4'-chloro-6-pivalamido-[1,1'-biphenyl]-3-yl pivalate**

White solid; ^1H NMR (500 MHz, CDCl_3): δ = 8.31 (d, J = 8.9 Hz, 1H), 7.47 (d, J = 8.5 Hz, 2H), 7.33 (d, J = 8.6 Hz, 2H), 7.30 (brs, 1H), 7.08 (dd, J = 8.9, 2.7 Hz, 1H), 6.95 (d, J = 2.7 Hz, 1H), 1.35 (s, 9H), 1.13 (s, 9H); ^{13}C NMR (126 MHz, CDCl_3): δ = 177.12, 176.27, 147.09, 135.75, 134.47, 132.46, 132.23, 130.64, 129.26, 122.71, 122.58, 121.60, 39.74, 39.06, 27.40, 27.12; HRMS (ESI) m/z calculated for $\text{C}_{22}\text{H}_{26}\text{ClNO}_3$ $[\text{M}+\text{H}]^+$ 388.1679; found 388.1674.

***N*-(4'-chloro-5-fluoro-[1,1'-biphenyl]-2-yl)pivalamide**

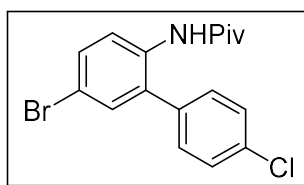
White solid; ^1H NMR (500 MHz, CDCl_3): δ = 8.14 (dd, J = 9.1, 3.7 Hz, 1H), 7.46 (d, J = 8.4 Hz, 2H), 7.29 (d, J = 8.4 Hz, 2H), 7.25 (brs, 1H), 7.05 (dt, J = 8.4, 3.5 Hz, 1H), 6.93 (dd, J = 8.8, 3.0 Hz, 1H), 1.12 (s, 9H); ^{13}C NMR (126 MHz, CDCl_3): δ = 176.33, 159.10 (d, $J_{\text{C-F}}$ = 245.2 Hz), 135.55, 134.52, 133.60 (d, $J_{\text{C-F}}$ = 7.6 Hz), 130.90, 130.39, 129.21,

124.04 (d, $J_{C-F} = 8.6$ Hz), 116.43 (d, $J_{C-F} = 23.0$ Hz), 115.13 (d, $J_{C-F} = 20.9$ Hz), 39.55, 27.31; HRMS (ESI) m/z calculated for $C_{17}H_{17}ClFNO$ $[M+H]^+$ 306.1061; found 306.1055.



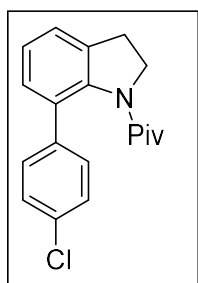
***N*-(4',5-dichloro-[1,1'-biphenyl]-2-yl)pivalamide**

White solid; 1H NMR (500 MHz, $CDCl_3$): $\delta = 8.27$ (d, $J = 8.9$ Hz, 1H), 7.49 (d, $J = 8.4$ Hz, 2H), 7.34 (dd, $J = 8.7, 2.7$ Hz, 1H), 7.32-7.28 (m, 3H), 7.20 (d, $J = 2.7$ Hz, 1H), 1.12 (s, 9H); ^{13}C NMR (126 MHz, $CDCl_3$): $\delta = 176.30, 135.23, 134.69, 133.60, 132.62, 130.48, 129.46, 129.38, 129.14, 128.61, 122.77, 39.77, 27.33$; HRMS (ESI) m/z calculated for $C_{17}H_{17}Cl_2NO$ $[M+H]^+$ 322.0765; found 322.0760.



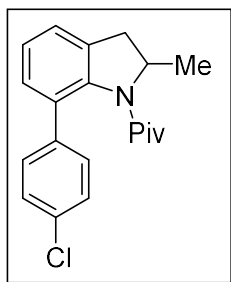
***N*-(5-bromo-4'-chloro-[1,1'-biphenyl]-2-yl)pivalamide**

White solid; 1H NMR (200 MHz, $CDCl_3$): $\delta = 8.23$ (d, $J = 8.8$ Hz, 1H), 7.52-7.45 (m, 3H), 7.35 (d, $J = 2.4$ Hz, 1H), 7.32-7.26 (m, 3H), 1.11 (s, 9H); ^{13}C NMR (50 MHz, $CDCl_3$): $\delta = 176.31, 135.09, 134.73, 134.13, 132.85, 132.33, 131.59, 130.50, 129.41, 122.93, 116.75, 39.81, 27.34$; HRMS (ESI) m/z calculated for $C_{17}H_{17}BrClNO$ $[M+H]^+$ 366.0260; found 366.0255.



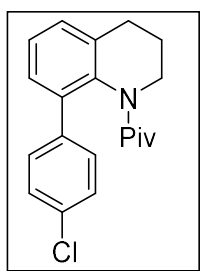
1-(7-(4-chlorophenyl)indolin-1-yl)-2,2-dimethylpropan-1-one

White solid; ^1H NMR (500 MHz, CDCl_3): $\delta = 7.33$ (s, 4H), 7.23 (d, $J = 7.2$ Hz, 1H), 7.18-7.14 (m, 2H), 4.20 (t, $J = 7.6$ Hz, 2H), 3.12 (t, $J = 7.6$ Hz, 2H), 1.19 (s, 9H); ^{13}C NMR (126 MHz, CDCl_3): $\delta = 177.28, 141.79, 140.03, 134.76, 132.35, 131.87, 128.48, 128.43, 127.88, 125.11, 123.52, 50.63, 39.73, 31.09, 28.01$; HRMS (ESI) m/z calculated for $\text{C}_{19}\text{H}_{21}\text{ClNO}$ $[\text{M}+\text{H}]^+$ 314.1312; found 314.1306.



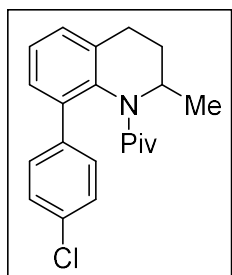
1-(7-(4-chlorophenyl)-2-methylindolin-1-yl)-2,2-dimethylpropan-1-one

Brown solid; ^1H NMR (500 MHz, CDCl_3): $\delta = 7.38$ (d, $J = 8.3$ Hz, 2H), 7.33 (d, $J = 8.3$ Hz, 2H), 7.25 (d, $J = 6.6$ Hz, 1H), 7.21-7.17 (m, 2H), 4.78 (quin, $J = 6.6$ Hz, 1H), 3.33 (dd, $J = 14.9, 6.7$ Hz, 1H), 2.62 (d, $J = 14.9$ Hz, 1H), 1.43 (d, $J = 6.2$ Hz, 3H), 1.20 (s, 9H); ^{13}C NMR (126 MHz, CDCl_3): $\delta = 177.15, 140.74, 139.76, 134.47, 133.56, 132.36, 128.42, 127.90, 127.85, 125.58, 124.18, 57.03, 40.04, 38.28, 28.52, 20.59$; HRMS (ESI) m/z calculated for $\text{C}_{20}\text{H}_{23}\text{ClNO}$ $[\text{M}+\text{H}]^+$ 328.1468; found 328.1463.



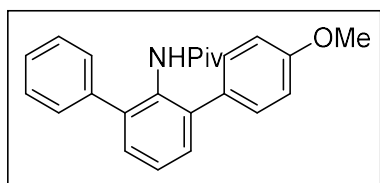
1-(8-(4-chlorophenyl)-3,4-dihydroquinolin-1(2H)-yl)-2,2-dimethylpropan-1-one

Colourless oily liquid; ^1H NMR (500 MHz, CDCl_3): $\delta = 7.35$ -7.31 (m, 7H), 4.40 (s, 1H), 3.40 (s, 1H), 2.85-2.76 (m, 2H), 2.16 (s, 1H), 2.04 (s, 1H), 1.10 (s, 9H); ^{13}C NMR (126 MHz, CDCl_3): $\delta = 176.60, 139.17, 138.80, 137.83, 133.77, 132.31, 129.77, 127.89, 127.82, 127.60, 125.75, 45.15, 39.02, 28.10, 25.73, 24.74$; HRMS (ESI) m/z calculated for $\text{C}_{20}\text{H}_{23}\text{ClNO}$ $[\text{M}+\text{H}]^+$ 328.1468; found 328.1462.



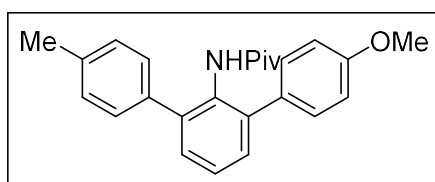
1-(8-(4-chlorophenyl)-2-methyl-3,4-dihydroquinolin-1(2H)-yl)-2,2-dimethylpropan-1-one

White solid; ^1H NMR (500 MHz, CDCl_3): δ = 7.32 (d, J = 8.3 Hz, 2H), 7.24 (d, J = 8.3 Hz, 2H), 7.19-7.13 (m, 2H), 7.05 (d, J = 6.9 Hz, 1H), 4.64-4.61 (m, 1H), 2.90-2.79 (m, 2H), 2.18-2.11 (m, 1H), 1.80-1.77 (m, 1H), 1.30 (d, J = 6.5 Hz, 3H), 1.05 (s, 9H); ^{13}C NMR (126 MHz, CDCl_3): δ = 178.10, 139.66, 139.13, 135.67, 132.34, 131.86, 130.30, 128.09, 127.95, 127.76, 125.46, 77.07, 48.64, 39.73, 29.82, 28.26, 23.56, 18.14; HRMS (ESI) m/z calculated for $\text{C}_{21}\text{H}_{25}\text{ClNO}$ $[\text{M}+\text{H}]^+$ 342.1625; found 342.1619.



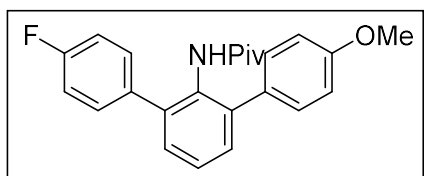
N-(4-methoxy-[1,1',3',1''-terphenyl]-2'-yl)pivalamide

White solid; ^1H NMR (500 MHz, CDCl_3): δ = 0.86 (s, 9H), 3.83 (s, 3H), 6.81 (brs, 1H), 6.91 (d, J = 8.8 Hz, 2H), 7.33-7.28 (m, 5H), 7.39-7.35 (m, 5H); ^{13}C NMR (126 MHz, CDCl_3): δ = 27.06, 38.67, 55.22, 113.39, 127.05, 127.15, 127.91, 128.82, 129.27, 129.68, 129.95, 131.74, 132.06, 139.81, 140.39, 140.88, 158.79, 176.43; HRMS (ESI) m/z calculated for $\text{C}_{24}\text{H}_{25}\text{NO}_2$ $[\text{M}+\text{H}]^+$ 360.1958; found 360.1958.



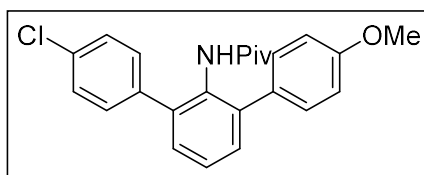
N-(4-methoxy-4''-methyl-[1,1',3',1''-terphenyl]-2'-yl)pivalamide

White solid; ^1H NMR (500 MHz, CDCl_3): δ = 0.86 (s, 9H), 2.37 (s, 3H), 3.82 (s, 3H), 6.75 (brs, 1H), 6.91 (d, J = 8.2 Hz, 2H), 7.18 (d, J = 8.0 Hz, 2H), 7.25 (d, J = 8.0 Hz, 2H), 7.34-7.28 (m, 4H), 7.36 (t, J = 7.8 Hz, 1H); ^{13}C NMR (126 MHz, CDCl_3): δ = 21.15, 27.15, 38.76, 55.27, 113.44, 127.16, 128.69, 128.73, 129.43, 129.59, 129.99, 131.77, 132.28, 136.80, 136.87, 140.39, 140.67, 158.80, 176.40; HRMS (ESI) m/z calculated for $\text{C}_{25}\text{H}_{27}\text{NO}_2$ $[\text{M}+\text{H}]^+$ 374.2115; found 374.2114.



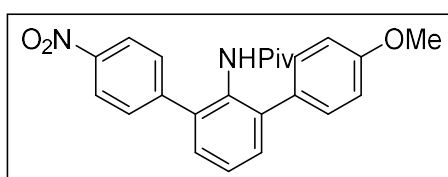
***N*-(4-fluoro-4''-methoxy-[1,1',3',1''-terphenyl]-2'-yl)pivalamide**

White solid; ^1H NMR (200 MHz, CDCl_3): δ = 0.88 (s, 9H), 3.83 (s, 3H), 6.72 (brs, 1H), 6.92 (d, J = 8.8 Hz, 2H), 7.06 (t, J = 8.8 Hz, 2H), 7.38-7.26 (m, 7H); ^{13}C NMR (126 MHz, CDCl_3): δ = 27.15, 38.77, 55.30, 113.53, 114.80 (d, $J_{\text{C-F}}$ = 21.9 Hz), 127.27, 129.45, 129.86, 130.02, 130.46 (d, $J_{\text{C-F}}$ = 8.6 Hz), 131.81, 131.83, 135.94 (d, $J_{\text{C-F}}$ = 3.8 Hz), 140.06, 140.38, 158.95, 162.10 (d, $J_{\text{C-F}}$ = 245.9 Hz), 176.56; HRMS (ESI) m/z calculated for $\text{C}_{24}\text{H}_{24}\text{FNO}_2$ $[\text{M}+\text{H}]^+$ 378.1864; found 378.1863.



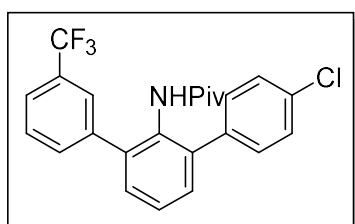
***N*-(4-chloro-4''-methoxy-[1,1',3',1''-terphenyl]-2'-yl)pivalamide**

White solid; ^1H NMR (500 MHz, CDCl_3): δ = 0.88 (s, 9H), 3.83 (s, 3H), 6.76 (brs, 1H), 6.92 (d, J = 8.7 Hz, 2H), 7.34-7.25 (m, 8H), 7.37 (t, J = 7.5 Hz, 1H); ^{13}C NMR (126 MHz, CDCl_3): δ = 27.14, 38.78, 55.29, 113.55, 127.33, 128.09, 129.34, 130.02, 130.18, 131.68, 133.09, 138.46, 139.81, 140.37, 158.98, 176.60; HRMS (ESI) m/z calculated for $\text{C}_{24}\text{H}_{24}\text{ClNO}_2$ $[\text{M}+\text{H}]^+$ 394.1568; found 394.1568.

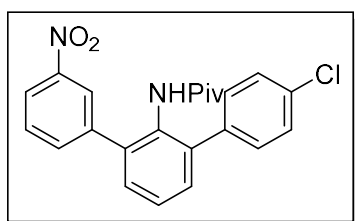


***N*-(4-methoxy-4''-nitro-[1,1',3',1''-terphenyl]-2'-yl)pivalamide**

White solid; ^1H NMR (200 MHz, CDCl_3): δ = 0.87 (s, 9H), 3.85 (s, 3H), 6.83 (brs, 1H), 6.95 (d, J = 8.8 Hz, 2H), 7.30-7.24 (m, 7H), 7.43-7.36 (m, 2H), 7.56 (d, J = 8.8 Hz, 2H), 8.24 (d, J = 8.8 Hz, 2H); ^{13}C NMR (126 MHz, CDCl_3): δ = 27.09, 38.86, 55.36, 113.83, 123.21, 127.36, 129.23, 129.63, 130.10, 130.78, 130.98, 131.54, 138.62, 139.87, 146.81, 147.31, 159.28, 176.43; HRMS (ESI) m/z calculated for $\text{C}_{24}\text{H}_{24}\text{N}_2\text{O}_4$ $[\text{M}+\text{H}]^+$ 405.1809; found 405.1806.

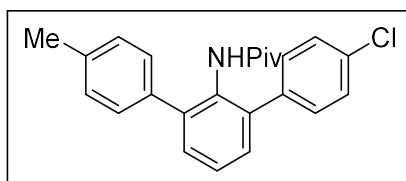
***N*-(4''-chloro-3-(trifluoromethyl)-[1,1',3',1''-terphenyl]-2'-yl)pivalamide**

White solid; ^1H NMR (500 MHz, CDCl_3): δ = 0.84 (s, 9H), 6.75 (brs, 1H), 7.29-7.26 (m, 2H), 7.37-7.34 (m, 4H), 7.43 (t, J = 7.8 Hz, 1H), 7.52 (t, J = 7.6 Hz, 1H), 7.60-7.57 (m, 3H); ^{13}C NMR (126 MHz, CDCl_3): δ = 26.96, 38.73, 124.02 (q, $J_{\text{C-F}}$ = 3.9 Hz), 124.07 (q, $J_{\text{C-F}}$ = 272.8 Hz), 125.45 (q, $J_{\text{C-F}}$ = 4.7 Hz), 127.64, 128.32, 128.76, 129.95, 130.15, 130.24, 130.20 (q, $J_{\text{C-F}}$ = 32.4 Hz), 131.55, 132.47, 133.55, 137.71, 139.79, 139.81, 140.39, 176.72; HRMS (ESI) m/z calculated for $\text{C}_{24}\text{H}_{21}\text{ClF}_3\text{NO}$ $[\text{M}+\text{H}]^+$ 432.1337; found 432.1335.

***N*-(4''-chloro-3-nitro-[1,1',3',1''-terphenyl]-2'-yl)pivalamide**

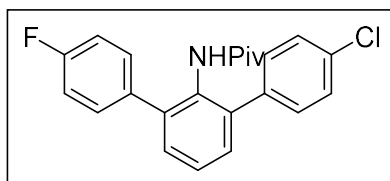
White solid; ^1H NMR (500 MHz, CDCl_3): δ = 0.86 (s, 9H), 6.84 (s, 1H), 7.29 (d, J = 8.3 Hz, 2H), 7.39 (t, J = 8.2 Hz, 4H), 7.48-7.45 (m, 1H), 7.58 (t, J = 7.8 Hz, 1H), 7.77 (d, J = 8.0 Hz, 1H), 8.20 (d, J = 8.0 Hz, 1H), 8.24 (s, 1H); ^{13}C NMR (126 MHz, CDCl_3): δ = 27.00, 38.80, 122.08, 123.53, 127.74, 128.48, 129.21, 129.92, 130.27, 130.48, 131.51, 133.81,

135.25, 137.32, 138.73, 139.53, 141.46, 147.75, 176.60; HRMS (ESI) m/z calculated for $C_{23}H_{21}ClN_2O_3$ $[M+H]^+$ 409.1313; found 409.1312.



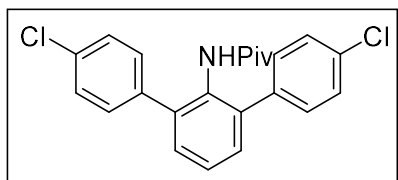
***N*-(4-chloro-4''-methyl-[1,1',3',1''-terphenyl]-2'-yl)pivalamide**

White solid; 1H NMR (400 MHz, $CDCl_3$): δ = 0.86 (s, 9H), 2.37 (s, 3H), 6.75 (s, 1H), 7.23-7.18 (m, 4H), 7.34-7.27 (m, 6H), 7.39-7.36 (m, 1H); ^{13}C NMR (101 MHz, $CDCl_3$): δ = 21.17, 27.10, 38.78, 127.31, 128.10, 128.75, 128.83, 129.45, 129.95, 130.18, 131.59, 133.08, 136.35, 137.12, 138.48, 139.75, 140.60, 176.53; HRMS (ESI) m/z calculated for $C_{24}H_{24}ClNO$ $[M+H]^+$ 378.1619; found 378.1617.



***N*-(4-chloro-4''-fluoro-[1,1',3',1''-terphenyl]-2'-yl)pivalamide**

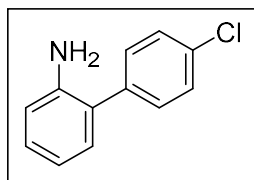
White solid; 1H NMR (400 MHz, $CDCl_3$): δ = 0.87 (s, 9H), 6.71 (brs, 1H), 7.07 (t, J = 8.7 Hz, 2H), 7.36-7.26 (m, 8H), 7.40 (t, J = 7.8 Hz, 1H); ^{13}C NMR (101 MHz, $CDCl_3$): δ = 27.11, 38.78, 114.96 (d, J_{C-F} = 21.1 Hz), 127.50, 128.20, 129.74, 129.99, 130.22, 130.53 (d, J_{C-F} = 7.7 Hz), 131.66, 133.35, 135.45 (d, J_{C-F} = 3.8 Hz), 138.07, 139.91, 140.14, 162.22 (d, J_{C-F} = 246.3 Hz), 176.74; HRMS (ESI) m/z calculated for $C_{23}H_{21}ClFNO$ $[M+H]^+$ 382.1368; found 382.1373.



***N*-(4,4''-dichloro-[1,1',3',1''-terphenyl]-2'-yl)pivalamide**

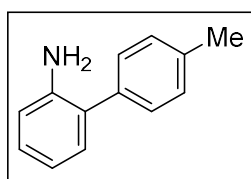
White solid; 1H NMR (500 MHz, $CDCl_3$): δ = 0.89 (s, 9H), 6.73 (brs, 1H), 7.29 (d, J = 8.6 Hz, 4H), 7.33 (d, J = 7.6 Hz, 2H), 7.36 (d, J = 8.6 Hz, 4H), 7.41 (t, J = 7.5 Hz, 1H); ^{13}C

NMR (126 MHz, CDCl_3): $\delta = 27.12, 38.79, 127.57, 128.23, 129.89, 130.22, 131.49, 133.39, 137.95, 139.87, 176.72$; HRMS (ESI) m/z calculated for $\text{C}_{23}\text{H}_{21}\text{Cl}_2\text{NO}$ $[\text{M}+\text{H}]^+$ 398.1073; found 398.1072.



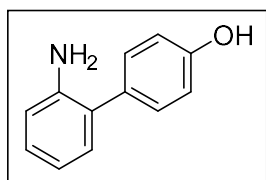
4'-chloro-[1,1'-biphenyl]-2-amine

Pale brown oil; ^1H NMR (500 MHz, CDCl_3): $\delta = 3.74$ (brs, 2H), 6.78 (dd, $J = 7.9, 1.0$ Hz, 1H), 6.85 (dt, $J = 7.6, 1.2$ Hz, 1H), 7.12 (dd, $J = 7.7, 1.5$ Hz, 1H), 7.19 (dt, $J = 7.7, 1.5$ Hz, 1H), 7.45-7.41(m, 4H); ^{13}C NMR (126 MHz, CDCl_3): $\delta = 115.68, 118.72, 126.24, 128.78, 128.94, 130.29, 130.41, 133.03, 137.85, 143.36$; HRMS (ESI) m/z calculated for $\text{C}_{12}\text{H}_{10}\text{ClN}$ $[\text{M}+\text{H}]^+$ 204.0575; found 204.0576.



4'-methyl-[1,1'-biphenyl]-2-amine

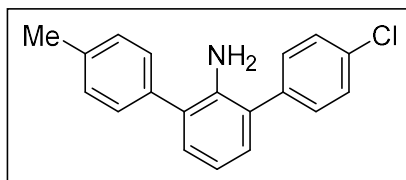
Pale brown oil; ^1H NMR (500 MHz, CDCl_3): $\delta = 7.43$ (d, $J = 8.1$ Hz, 2H), 7.33 (d, $J = 8.1$ Hz, 2H), 7.24-7.19 (m, 2H), 6.90 (dt, $J = 7.2, 0.8$ Hz, 1H), 6.82 (d, $J = 8.1$ Hz, 1H), 3.74 (s, 2H), 2.48 (s, 3H); ^{13}C NMR (126 MHz, CDCl_3): $\delta = 143.50, 136.73, 136.45, 130.37, 129.42, 128.86, 128.22, 127.52, 118.53, 115.46, 21.11$; HRMS (ESI) m/z calculated for $\text{C}_{13}\text{H}_{13}\text{N}$ $[\text{M}+\text{H}]^+$ 184.1126; found 184.1121



2'-amino-[1,1'-biphenyl]-4-ol

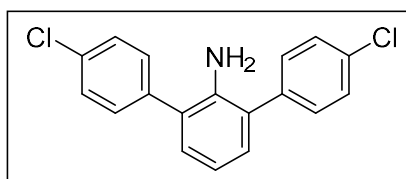
Brown solid; ^1H NMR (500 MHz, CDCl_3): $\delta = 6.78$ (d, $J = 7.9$ Hz, 1H), 6.82 (t, $J = 7.6$ Hz, 1H), 6.91 (dd, $J = 8.6, 2.2$ Hz, 2H), 7.11 (dd, $J = 7.3, 1.2$ Hz, 1H), 7.15 (dt, $J = 7.6,$

1.5 Hz, 1H), 7.33 (dd, $J = 8.6, 2.2$ Hz, 2H); ^{13}C NMR (126 MHz, CDCl_3): $\delta = 115.56, 115.63, 118.71, 127.37, 128.20, 130.38, 130.46, 131.81, 143.51, 154.78$; HRMS (ESI) m/z calculated for $\text{C}_{12}\text{H}_{11}\text{NO}$ $[\text{M}+\text{H}]^+$ 186.0913; found 186.0912.



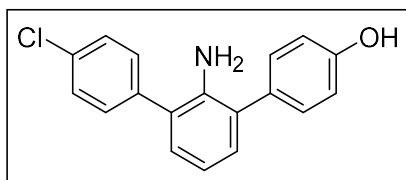
4-chloro-4''-methyl-[1,1',3',1''-terphenyl]-2'-amine

Brown solid; ^1H NMR (500 MHz, CDCl_3): $\delta = 2.43$ (s, 3H), 3.82 (s, 2H), 6.89 (t, $J = 7.6$ Hz, 1H), 7.10 (d, $J = 7.7$ Hz, 1H), 7.15 (d, $J = 7.7$ Hz, 1H), 7.30 (d, $J = 8.1$ Hz, 2H), 7.42 (d, $J = 8.1$ Hz, 2H), 7.45 (d, $J = 8.7$ Hz, 2H), 7.48 (d, $J = 8.4$ Hz, 2H); ^{13}C NMR (126 MHz, CDCl_3): $\delta = 21.18, 118.19, 126.52, 128.08, 128.98, 129.11, 129.42, 129.55, 130.04, 130.68, 133.13, 136.48, 137.03, 138.21, 140.78$; HRMS (ESI) m/z calculated for $\text{C}_{19}\text{H}_{16}\text{ClN}$ $[\text{M}+\text{H}]^+$ 294.1044; found 294.1048.



4,4''-dichloro-[1,1',3',1''-terphenyl]-2'-amine

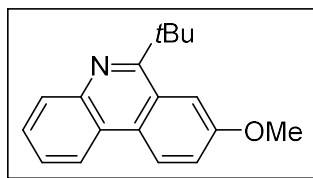
Brown solid; ^1H NMR (500 MHz, CDCl_3): $\delta = 3.78$ (brs, 2H), 6.89 (t, $J = 7.6$ Hz, 1H), 7.11 (d, $J = 7.6$ Hz, 2H), 7.45 (s, 8H); ^{13}C NMR (126 MHz, CDCl_3): $\delta = 118.35, 126.77, 129.06, 129.92, 130.65, 133.30, 137.87, 140.62$; HRMS (ESI) m/z calculated for $\text{C}_{18}\text{H}_{13}\text{Cl}_2\text{N}$ $[\text{M}+\text{H}]^+$ 314.0498; found 314.0499.



2'-amino-4''-chloro-[1,1',3',1''-terphenyl]-4-ol amine

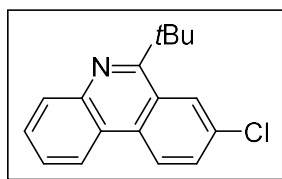
Brown solid; ^1H NMR (400 MHz, CDCl_3): $\delta = 3.82$ (br, 2H), 5.31 (br, 1H), 6.92-6.87 (m, 3H), 7.08 (d, $J = 7.5$ Hz, 1H), 7.12 (d, $J = 7.9$ Hz, 1H), 7.37 (d, $J = 8.1$ Hz, 2H), 7.44 (t,

$J = 8.8$ Hz, 4H); ^{13}C NMR (101 MHz, CDCl_3): $\delta = 115.74, 118.42, 126.74, 127.95, 129.00, 129.36, 130.07, 130.57, 130.66, 131.71, 133.18, 138.09, 140.67, 154.93$; HRMS (ESI) m/z calculated for $\text{C}_{18}\text{H}_{14}\text{ClNO}$ $[\text{M}+\text{H}]^+$ 296.0837; found 296.0837.



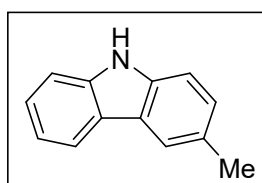
6-(*tert*-butyl)-8-methoxyphenanthridine

White solid; ^1H NMR (200 MHz, CDCl_3): $\delta = 8.61$ (d, $J = 9.2$ Hz, 1H), 8.45 (dd, $J = 7.6, 2.2$ Hz, 1H), 8.11 (dd, $J = 7.4, 2.3$ Hz, 1H), 8.01 (d, $J = 2.6$ Hz, 1H), 7.69-7.55 (m, 2H), 7.45 (dd, $J = 9.1, 2.7$ Hz, 1H), 4.01 (s, 3H), 1.75 (s, 9H); ^{13}C NMR (50 MHz, CDCl_3): $\delta = 165.68, 157.23, 142.14, 130.20, 128.20, 127.37, 126.49, 125.46, 124.42, 123.46, 121.09, 119.09, 109.66, 55.45, 40.04, 30.95$; HRMS (ESI) m/z calculated for $\text{C}_{18}\text{H}_{19}\text{NO}$ $[\text{M}+\text{H}]^+$ 226.1545; found 226.1539.



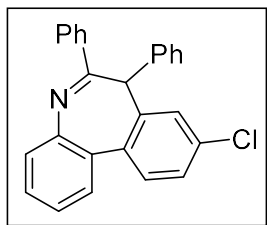
6-(*tert*-butyl)-8-chlorophenanthridine

Colourless liquid; ^1H NMR (500 MHz, CDCl_3): $\delta = 8.61$ (d, $J = 8.8$ Hz, 1H), 8.59 (d, $J = 2.2$ Hz, 1H), 8.47 (d, $J = 7.9$ Hz, 1H), 8.13 (d, $J = 8.2$ Hz, 1H), 7.75-7.70 (m, 2H), 7.63 (dt, $J = 8.2, 1.2$ Hz, 1H), 1.73 (s, 9H); ^{13}C NMR (126 MHz, CDCl_3): $\delta = 165.57, 142.81, 132.37, 131.81, 130.36, 129.76, 128.68, 127.54, 126.85, 125.12, 124.62, 122.75, 121.45, 40.16, 31.11$; HRMS (ESI) m/z calculated for $\text{C}_{17}\text{H}_{16}\text{ClN}$ $[\text{M}+\text{H}]^+$ 270.1050; found 270.1044.



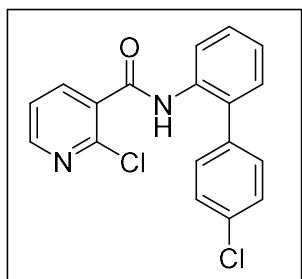
3-methyl-9H-carbazole

White solid; ^1H NMR (500 MHz, CDCl_3): $\delta = 8.05$ (d, $J = 7.6$ Hz, 1H), 7.97 (d, $J = 8.0$ Hz, 1H), 7.93 (s, 1H), 7.41-7.38 (m, 2H), 7.25-7.22 (m, 2H), 7.08 (d, $J = 8.0$ Hz, 1H), 2.54 (s, 3H); ^{13}C NMR (126 MHz, CDCl_3): $\delta = 139.95$, 139.45, 135.99, 125.25, 123.43, 121.03, 120.96, 119.98, 119.31, 110.71, 110.45, 22.03.



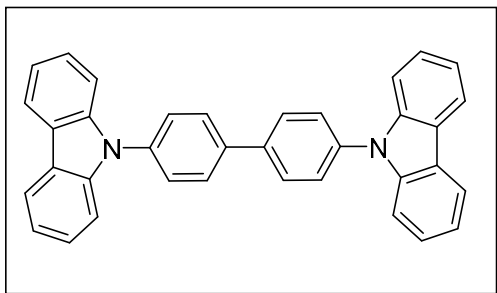
9-chloro-6,7-diphenyl-7H-dibenzo[b,d]azepine

White solid; ^1H NMR (500 MHz, CDCl_3): $\delta = 8.09$ (dd, $J = 7.6$, 2.2 Hz, 2H), 7.69 (d, $J = 8.2$ Hz, 1H), 7.54-7.51 (m, 3H), 7.48-7.45 (m, 2H), 7.41 (d, $J = 8.6$ Hz, 1H), 7.25 (d, $J = 8.3$ Hz, 1H), 7.17 (t, $J = 8.6$ Hz, 1H), 6.99 (t, $J = 8.6$ Hz, 1H), 6.95-6.92 (m, 3H), 6.78-6.76 (m, 2H), 6.00 (s, 1H); ^{13}C NMR (126 MHz, CDCl_3): $\delta = 165.70$, 146.08, 140.10, 139.96, 136.54, 135.32, 134.26, 130.97, 130.61, 129.65, 129.32, 128.76, 128.36, 128.00, 127.87, 127.78, 127.63, 126.55, 126.41, 126.28, 124.29, 53.32.

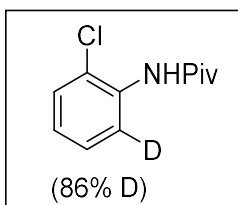


2-Chloro-N-(4'-chloro-[1,1'-biphenyl]-2-yl)nicotinamide

White solid; ^1H NMR (500 MHz, CDCl_3): $\delta = 8.42$ (d, $J = 4.6$ Hz, 1H), 8.39 (d, $J = 8.4$ Hz, 1H), 8.17 (s, 1H), 8.11 (d, $J = 7.6$ Hz, 1H), 7.47-7.44 (m, 1H), 7.43 (d, $J = 8.4$ Hz, 2H), 7.35-7.32 (m, 3H), 7.27 (d, $J = 3.8$ Hz, 2H); ^{13}C NMR (126 MHz, CDCl_3): $\delta = 162.48$, 151.23, 146.65, 140.03, 136.23, 134.37, 134.26, 132.28, 131.05, 130.74, 130.19, 129.23, 128.83, 125.31, 122.84, 122.16; HRMS (ESI) m/z calculated for $\text{C}_{21}\text{H}_{25}\text{ClNO}$ $[\text{M}+\text{H}]^+$ 343.0405; found 343.0399.

**4,4'-di(9H-carbazol-9-yl)-1,1'-biphenyl**

White solid; ^1H NMR (500 MHz, CDCl_3): δ = 8.24 (d, J = 7.6 Hz, 4H), 7.95 (d, J = 8.4 Hz, 4H), 7.75 (d, J = 8.4 Hz, 4H), 7.58 (d, J = 8.0 Hz, 4H), 7.51 (t, J = 7.6 Hz, 4H), 7.38 (t, J = 7.3 Hz, 4H); ^{13}C NMR (126 MHz, CDCl_3): δ = 140.81, 139.24, 137.24, 128.48, 127.46, 126.01, 123.49, 120.37, 120.07, 109.81.

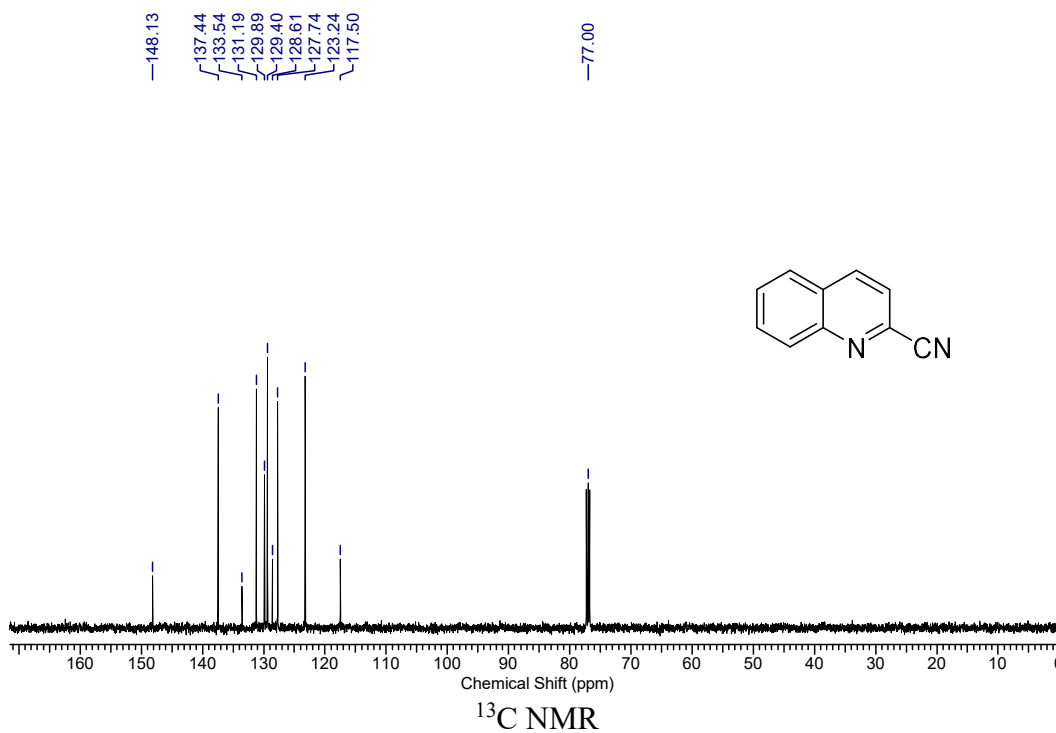
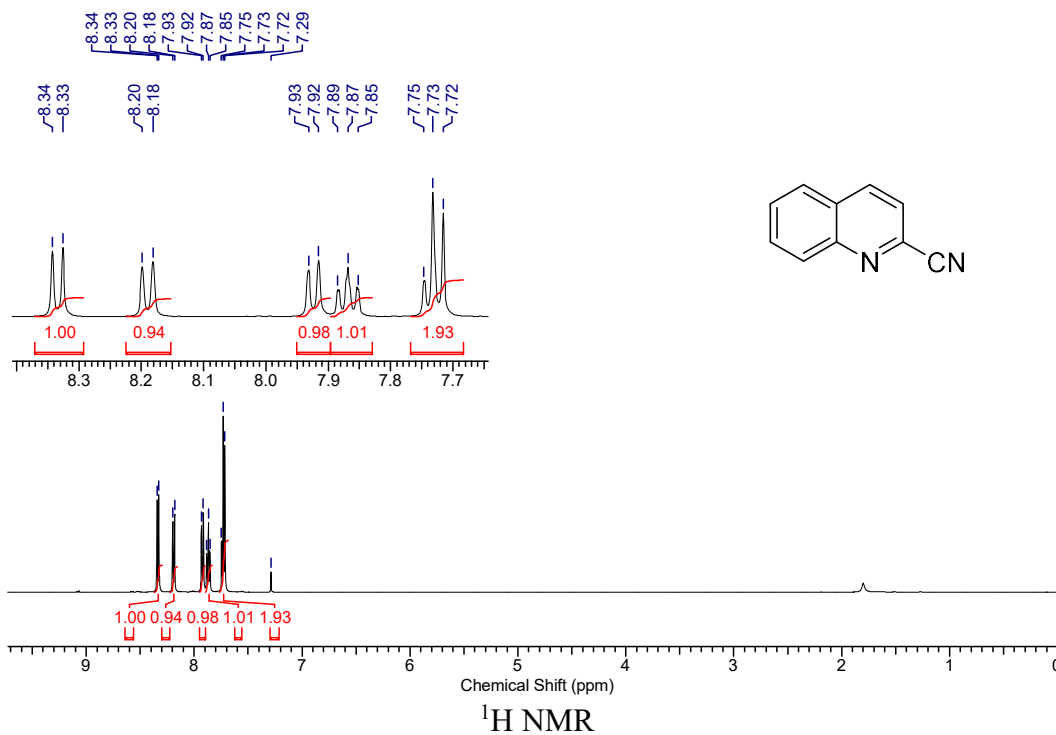
***N*-(2-chlorophenyl-6-*d*)pivalamide**

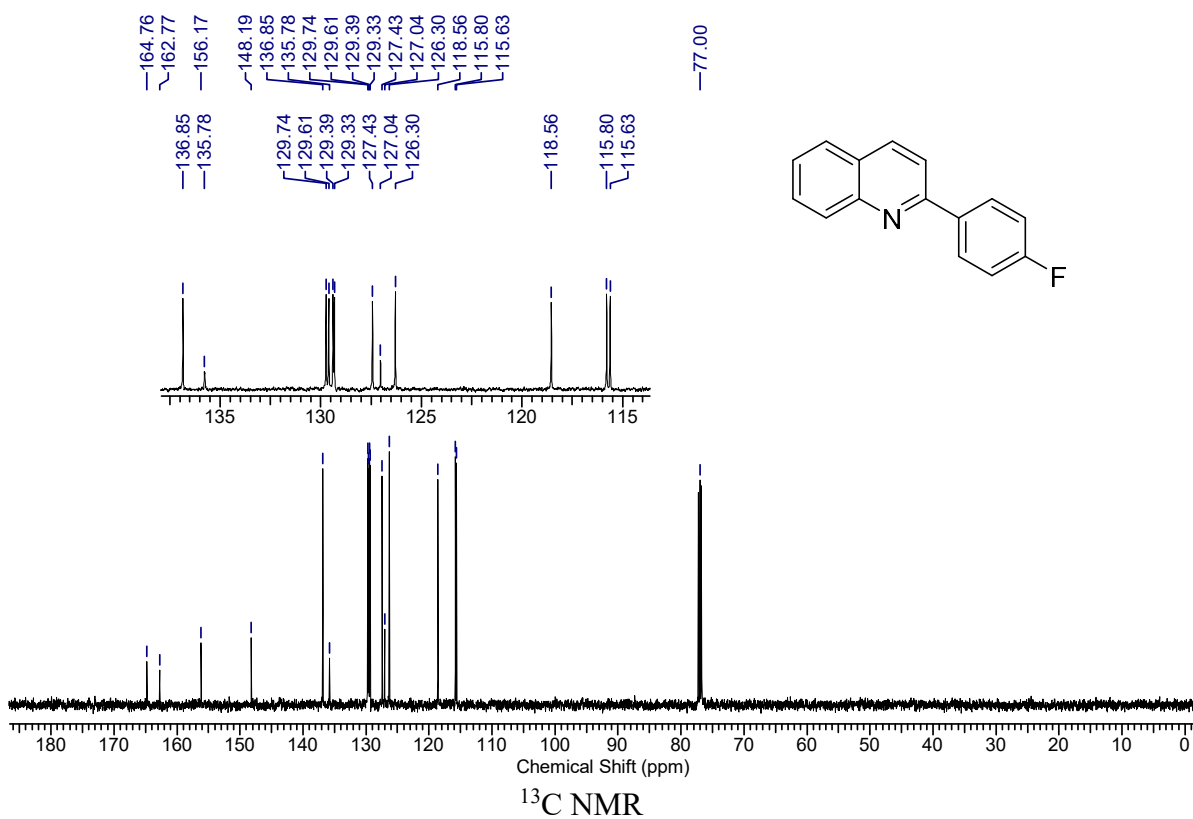
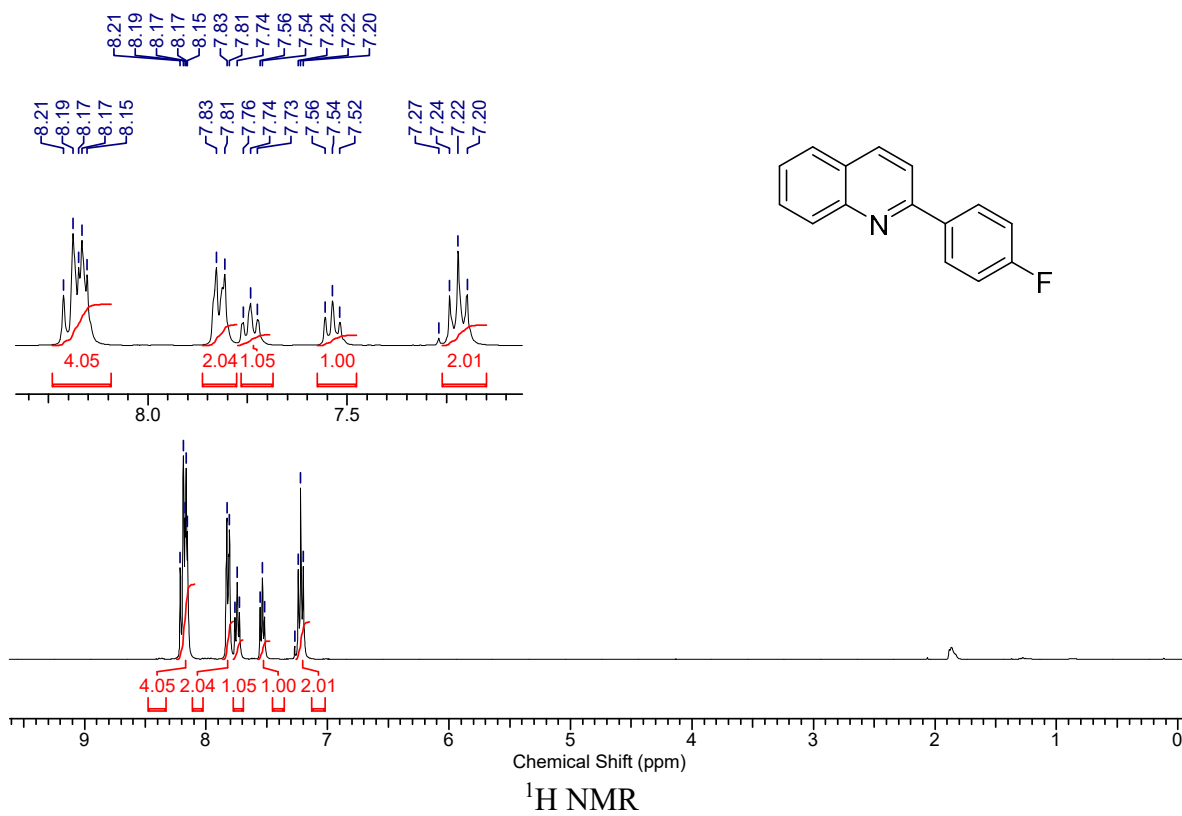
White solid; ^1H NMR (500 MHz, CDCl_3): δ = 8.44 (d, J = 7.7 Hz, 0.14H), 8.04 (s, 1H), 7.38 (d, J = 8.0 Hz, 1H), 7.31-7.28 (m, 1H), 7.05 (t, J = 8.0 Hz, 1H), 1.37 (s, 9H).

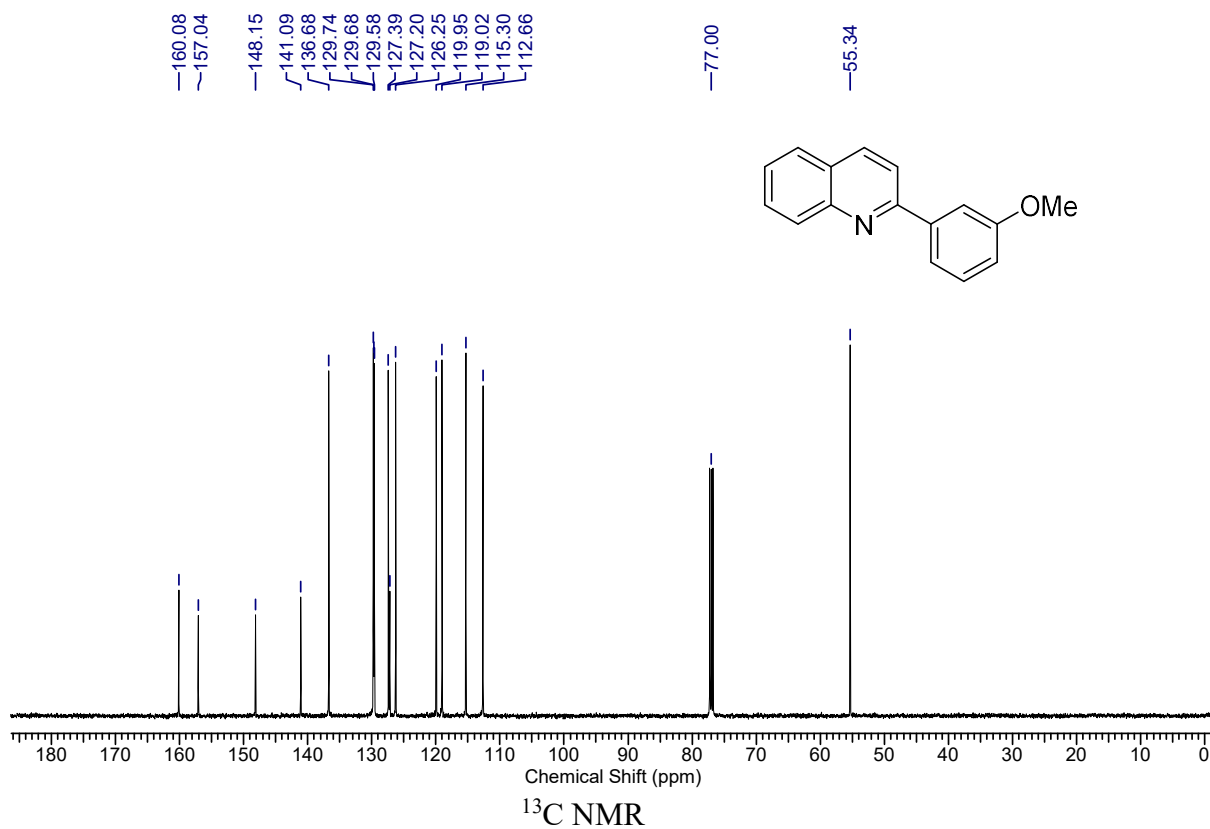
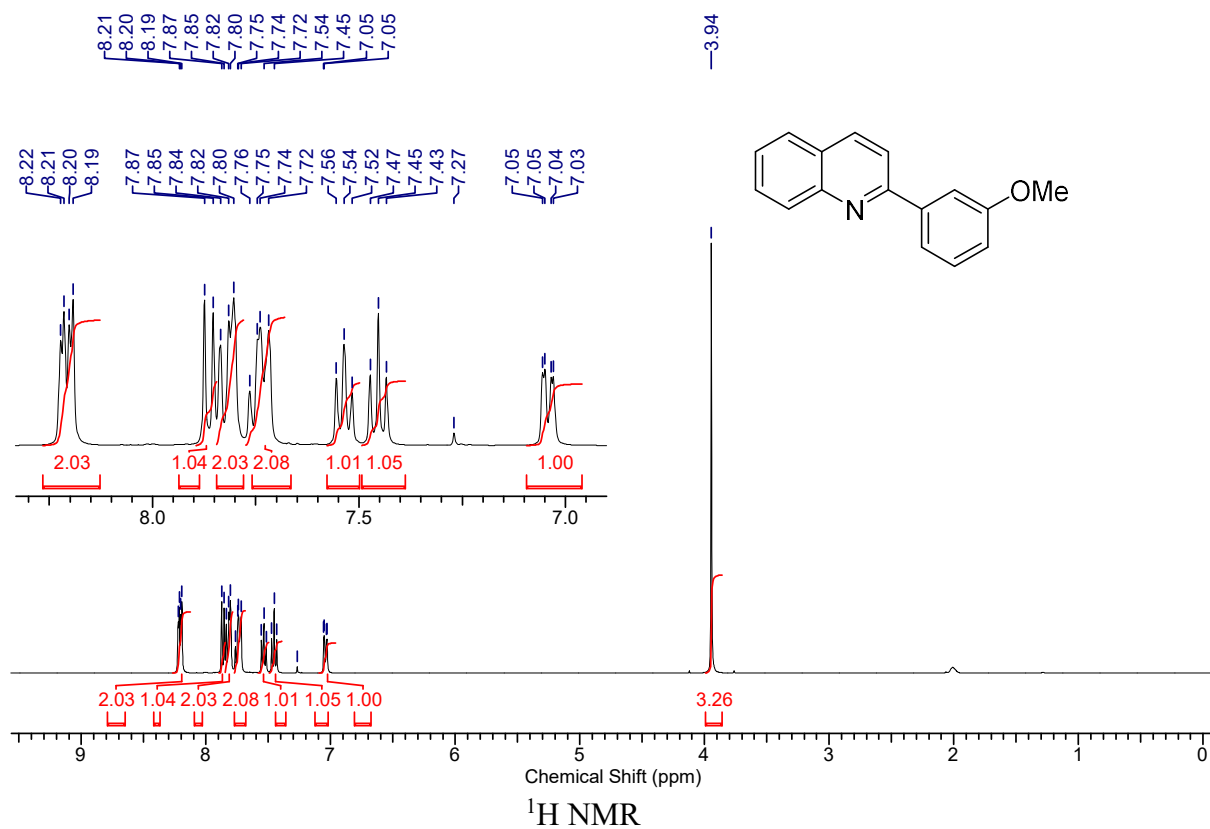
Appendix B

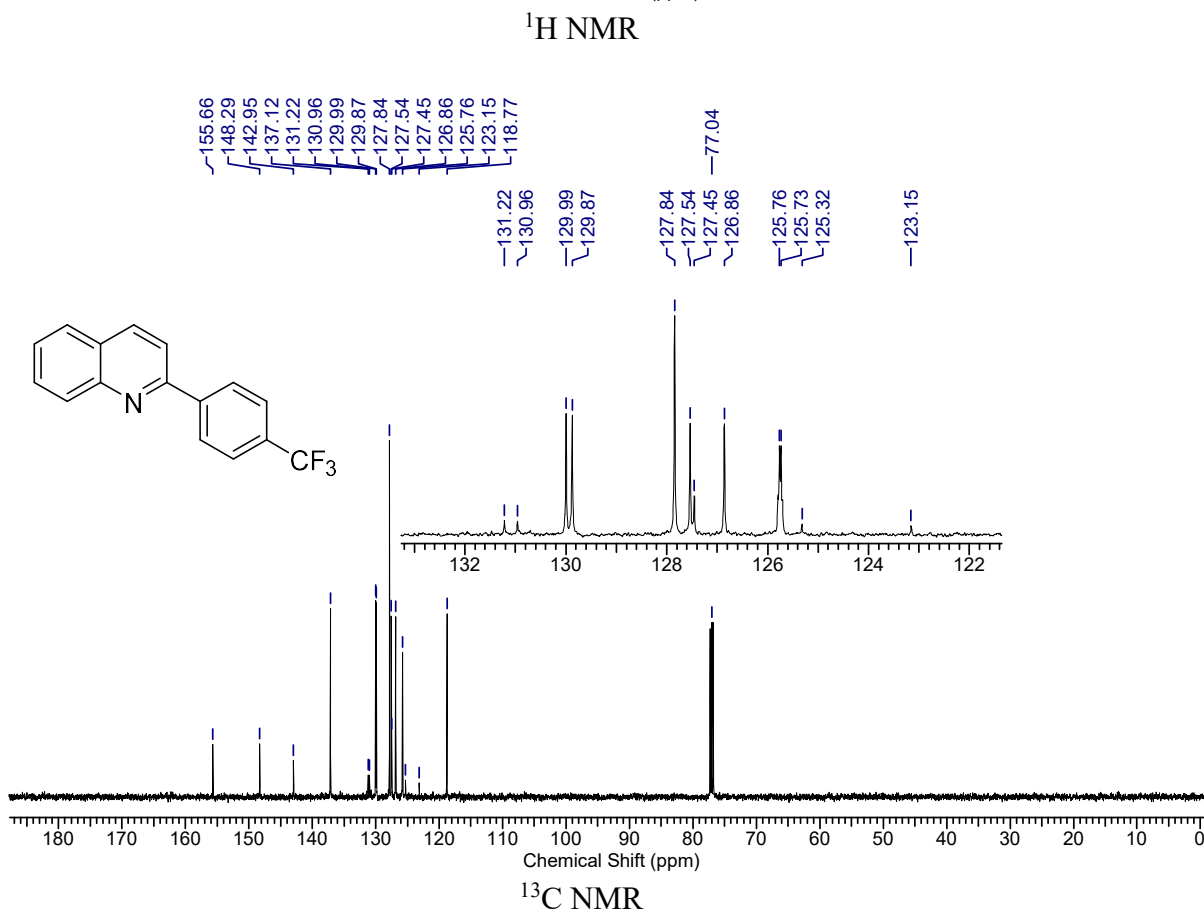
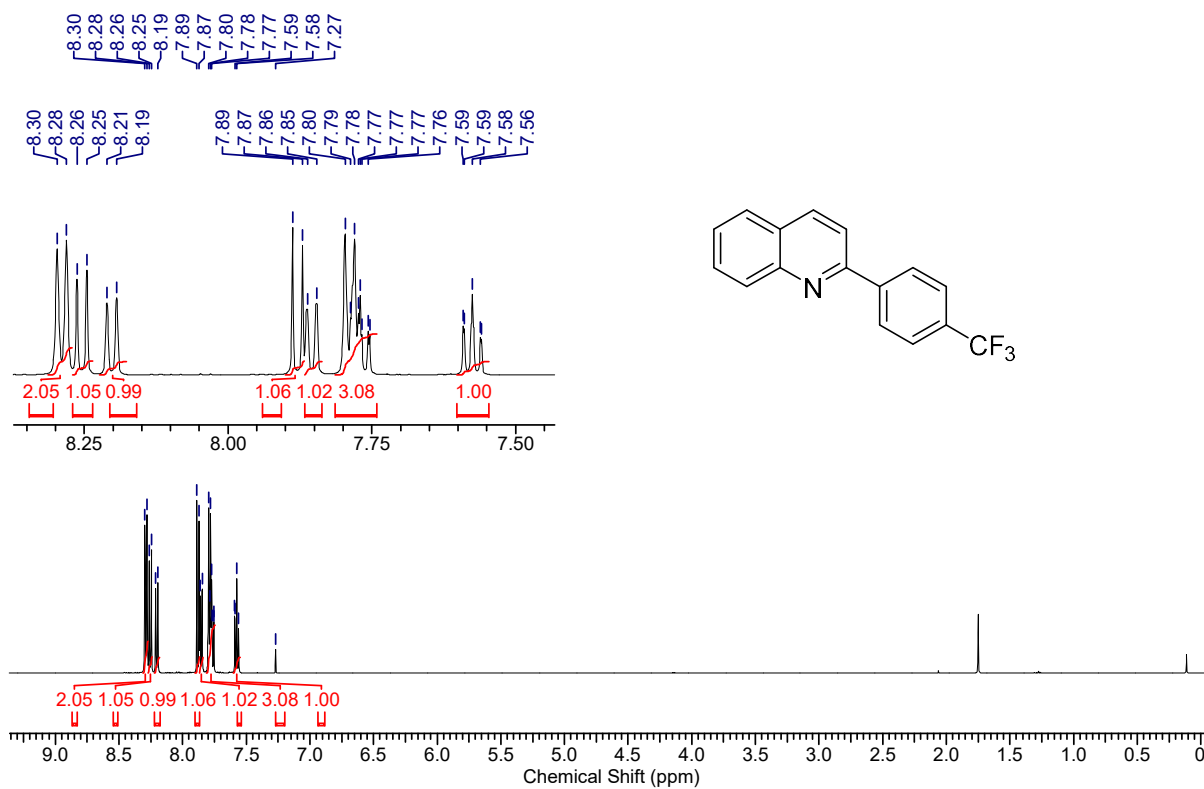
Copy of ^1H and ^{13}C Spectra

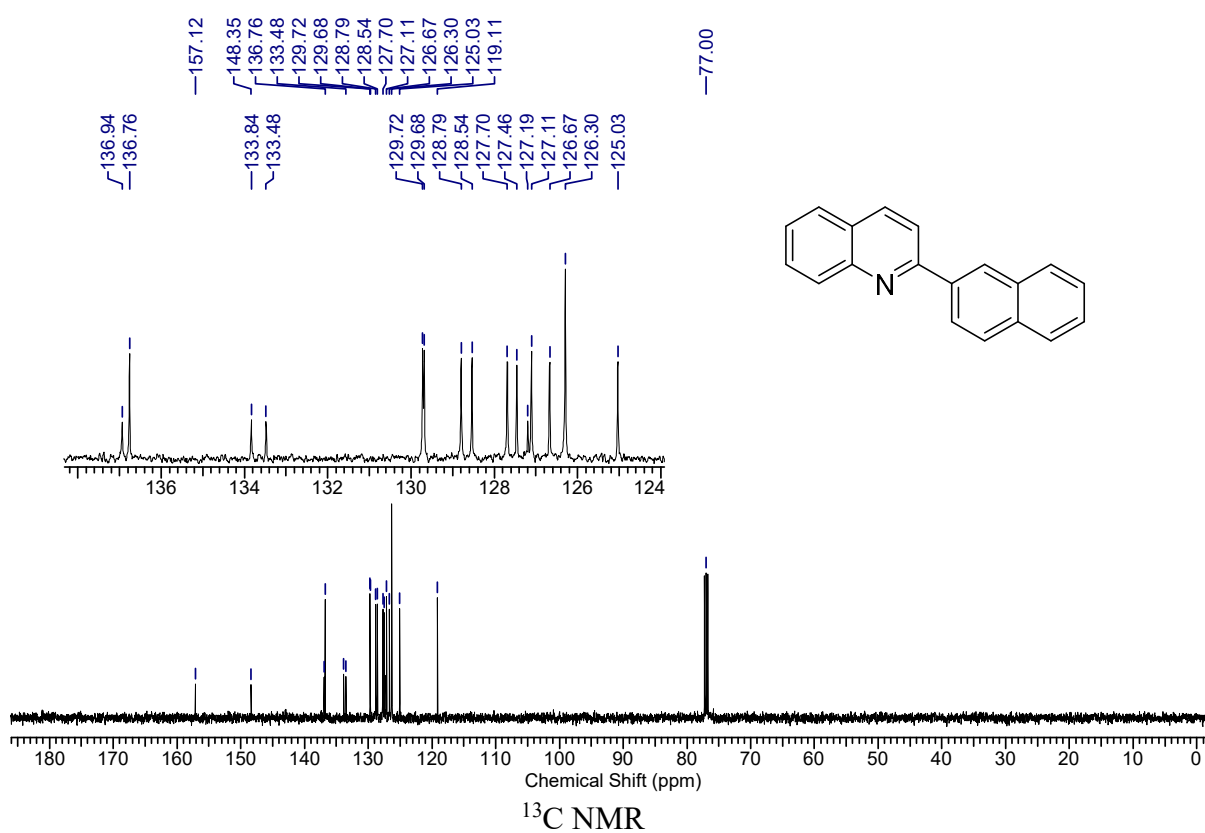
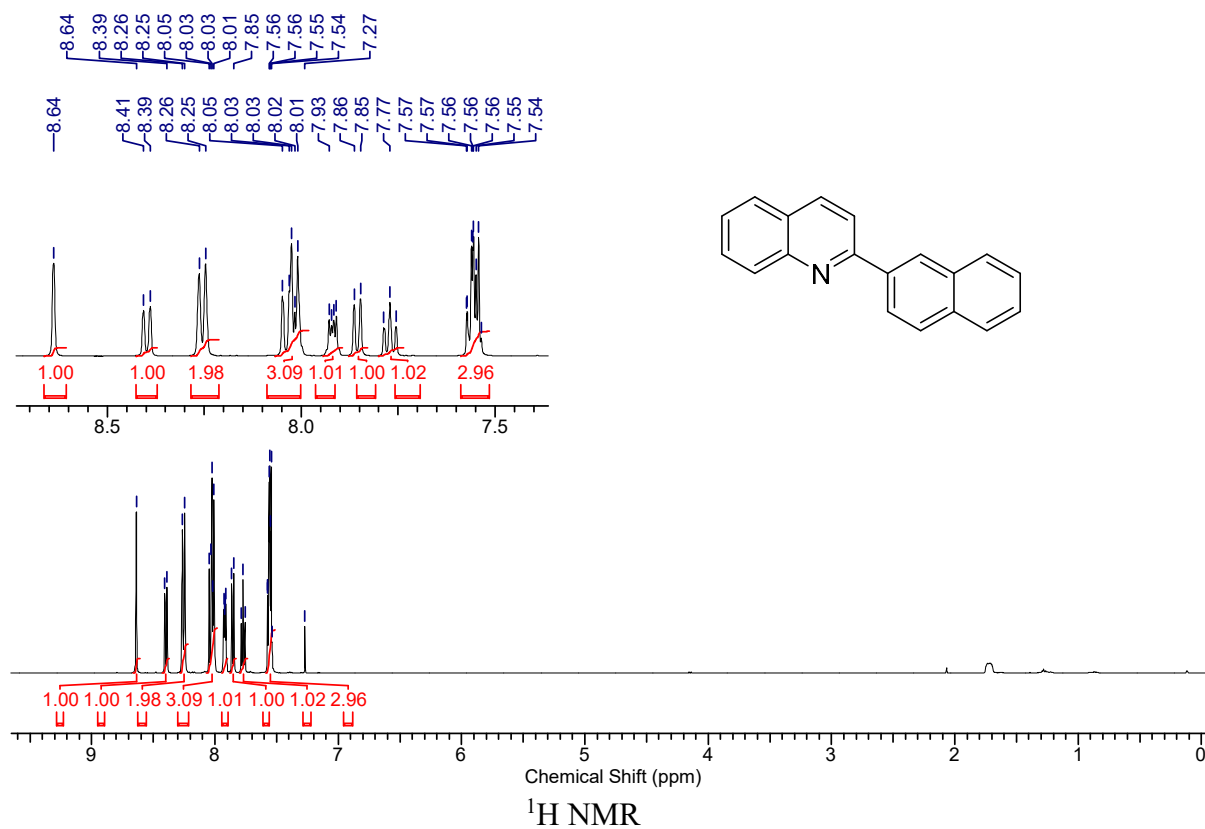
Chapter-2 and Chapter 3

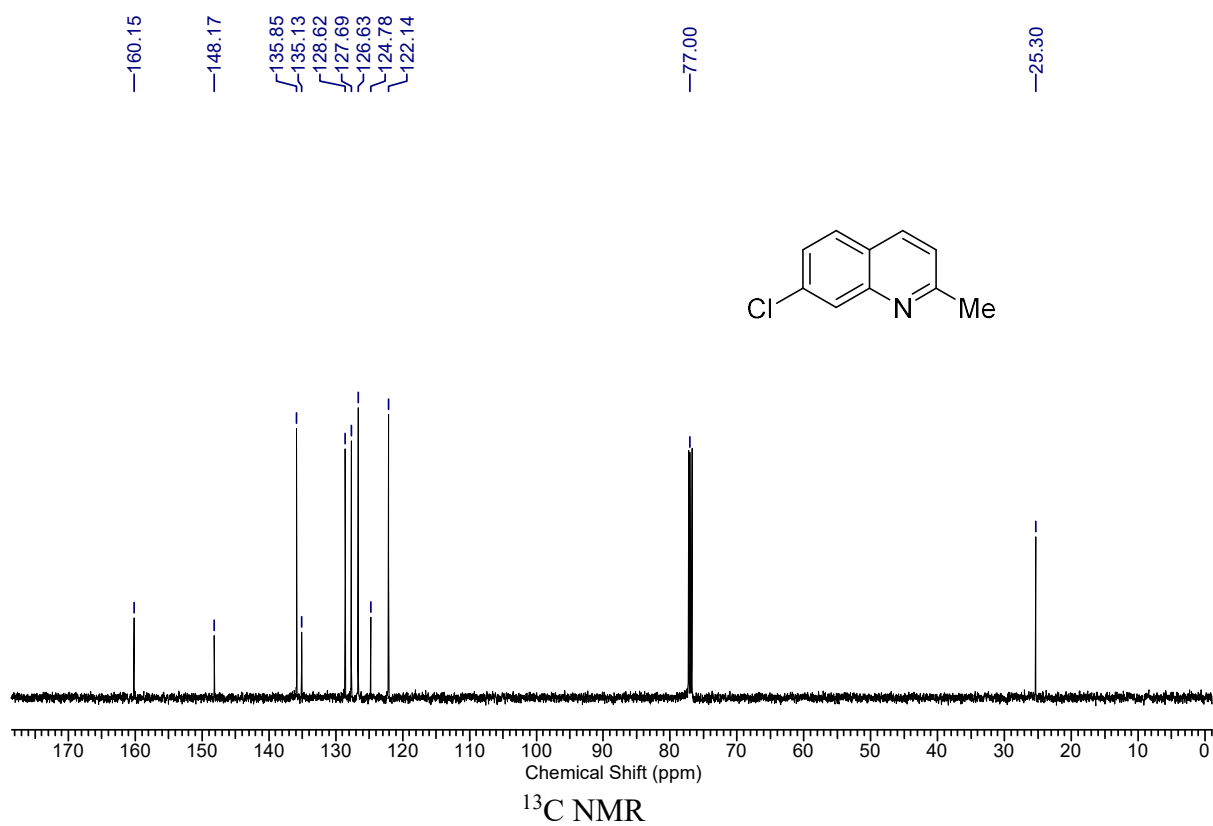
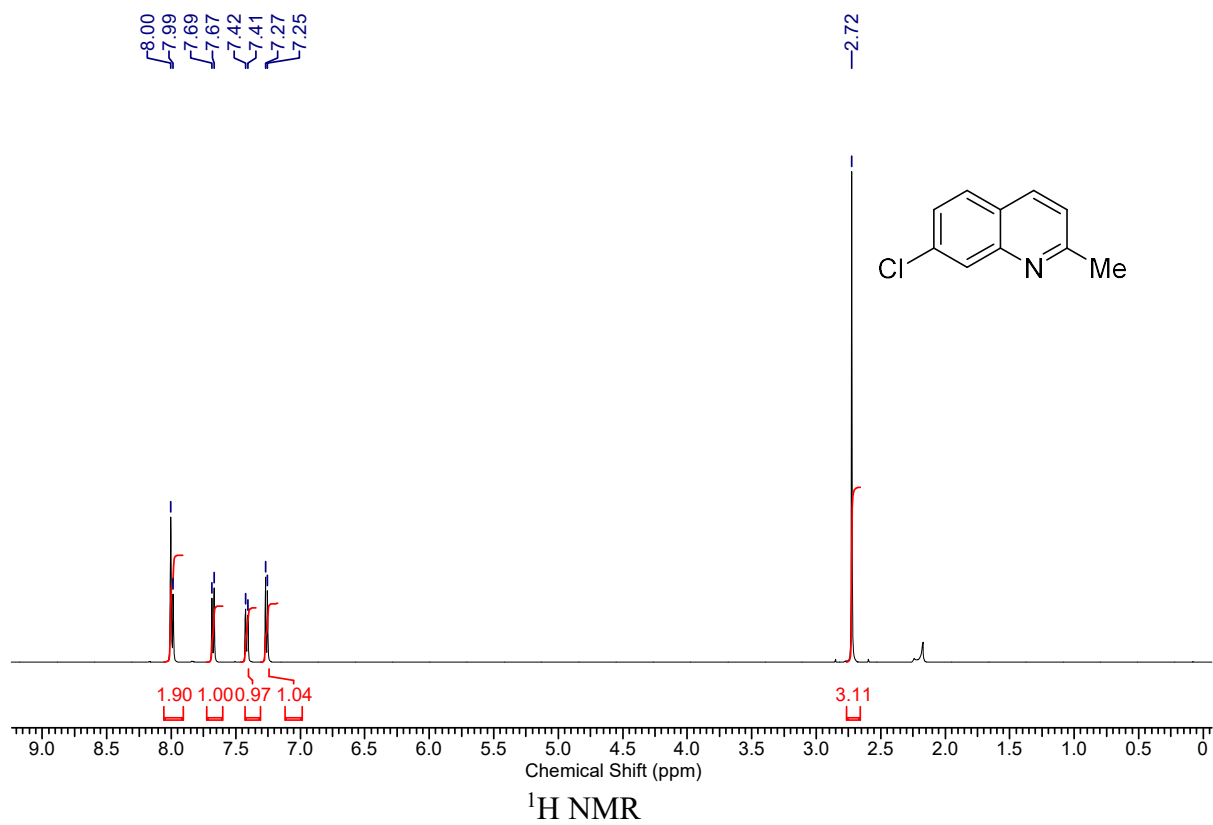


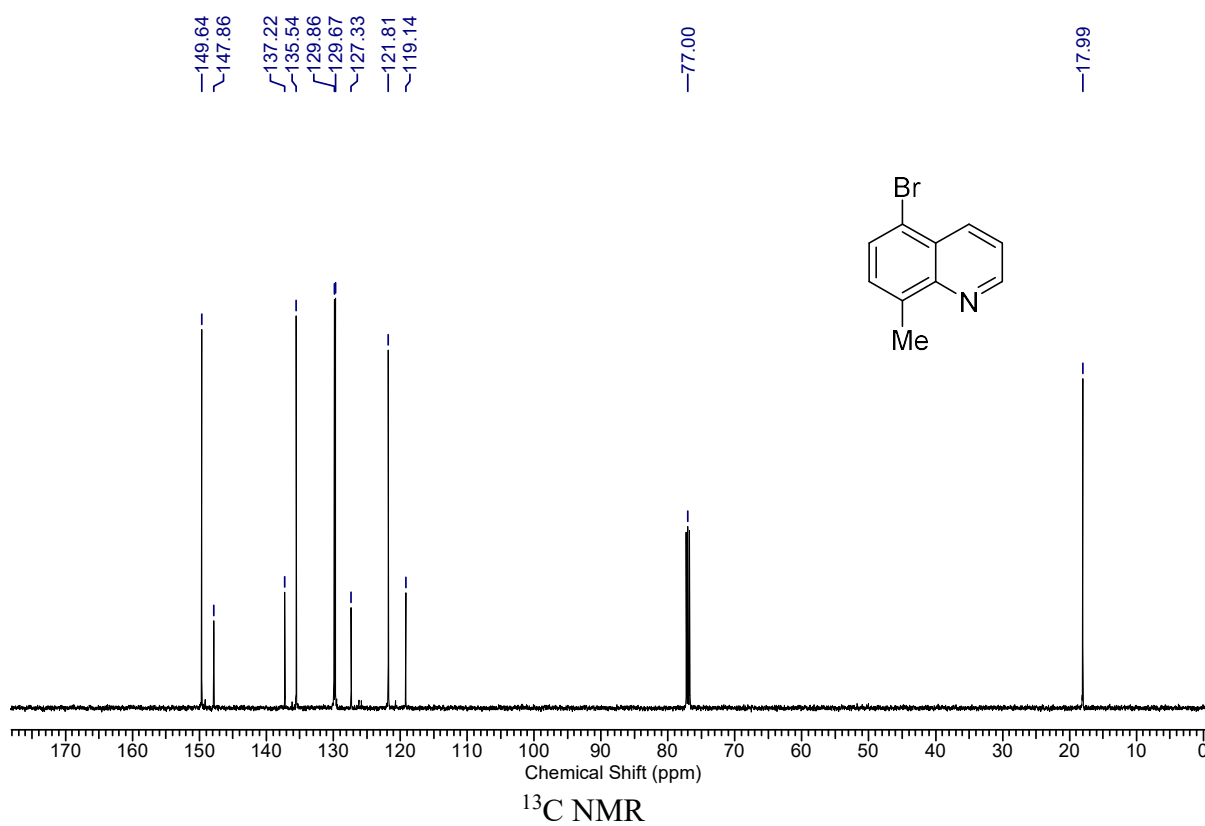
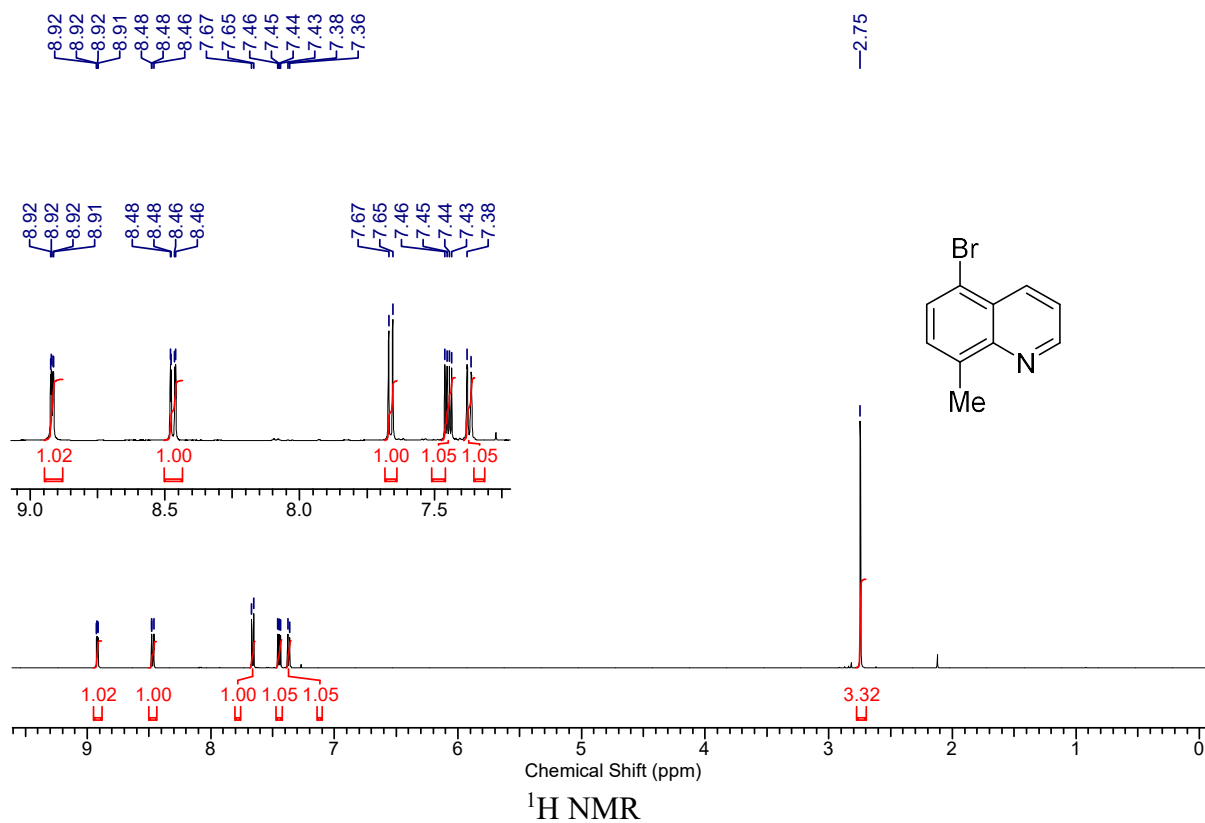


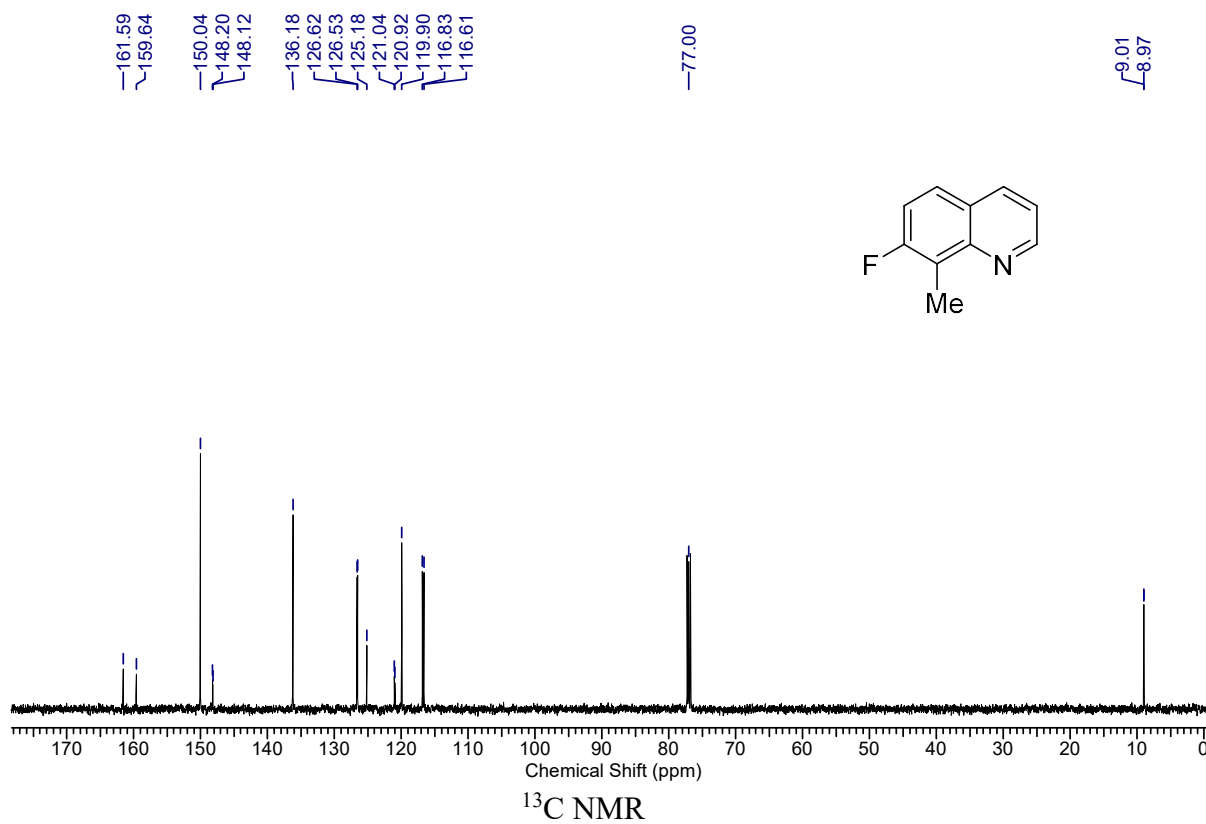
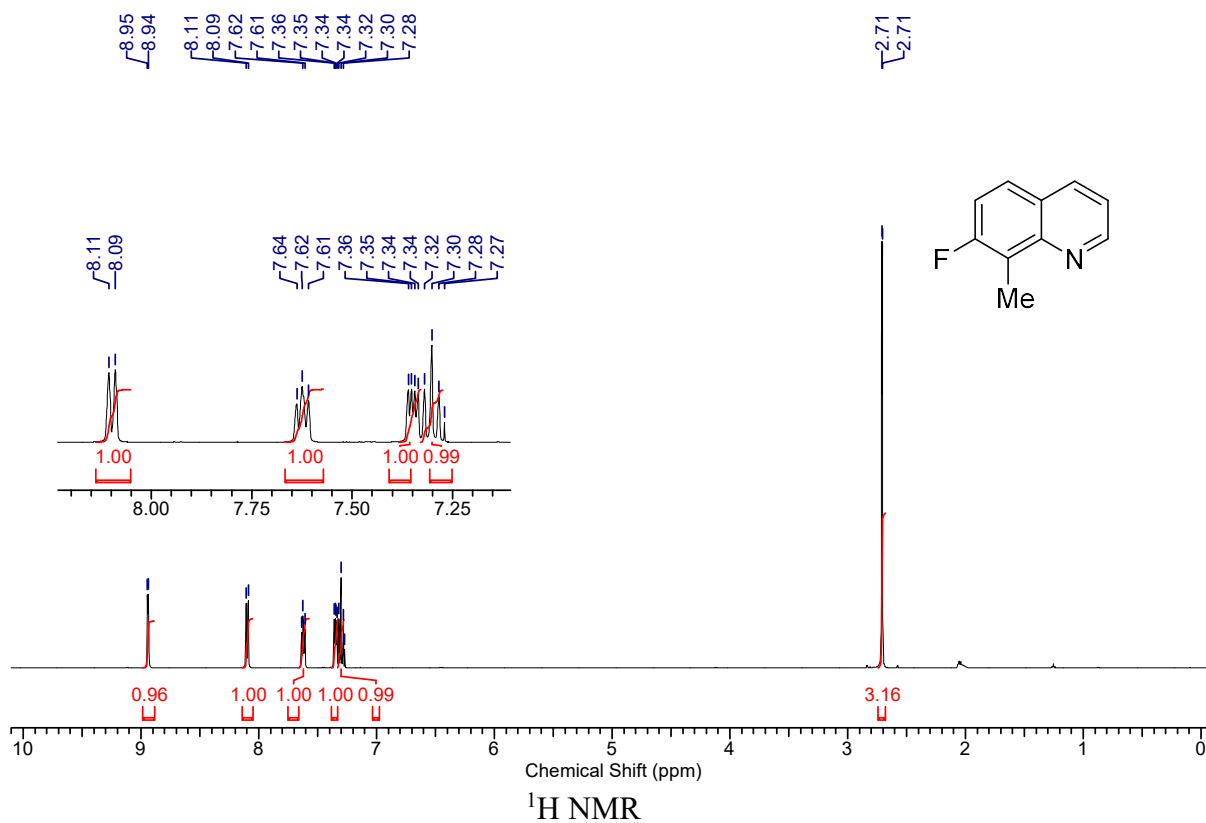


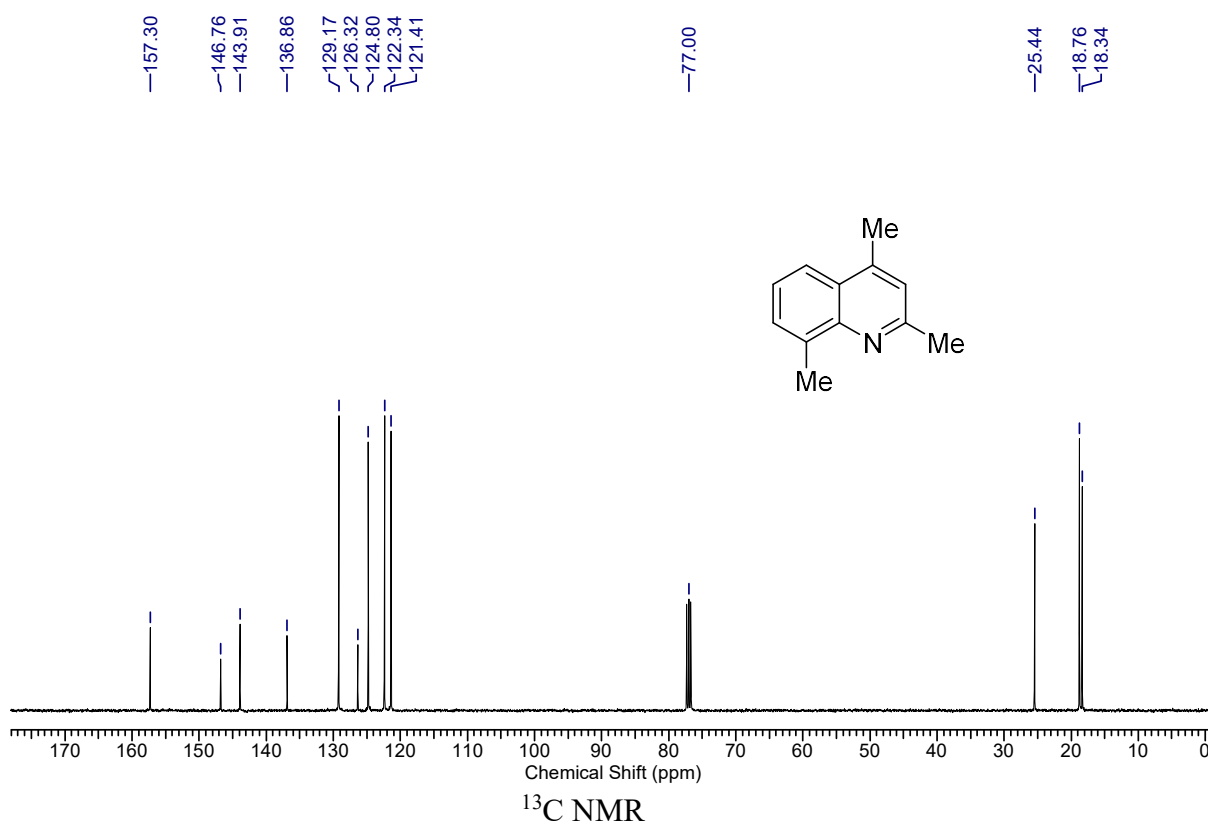
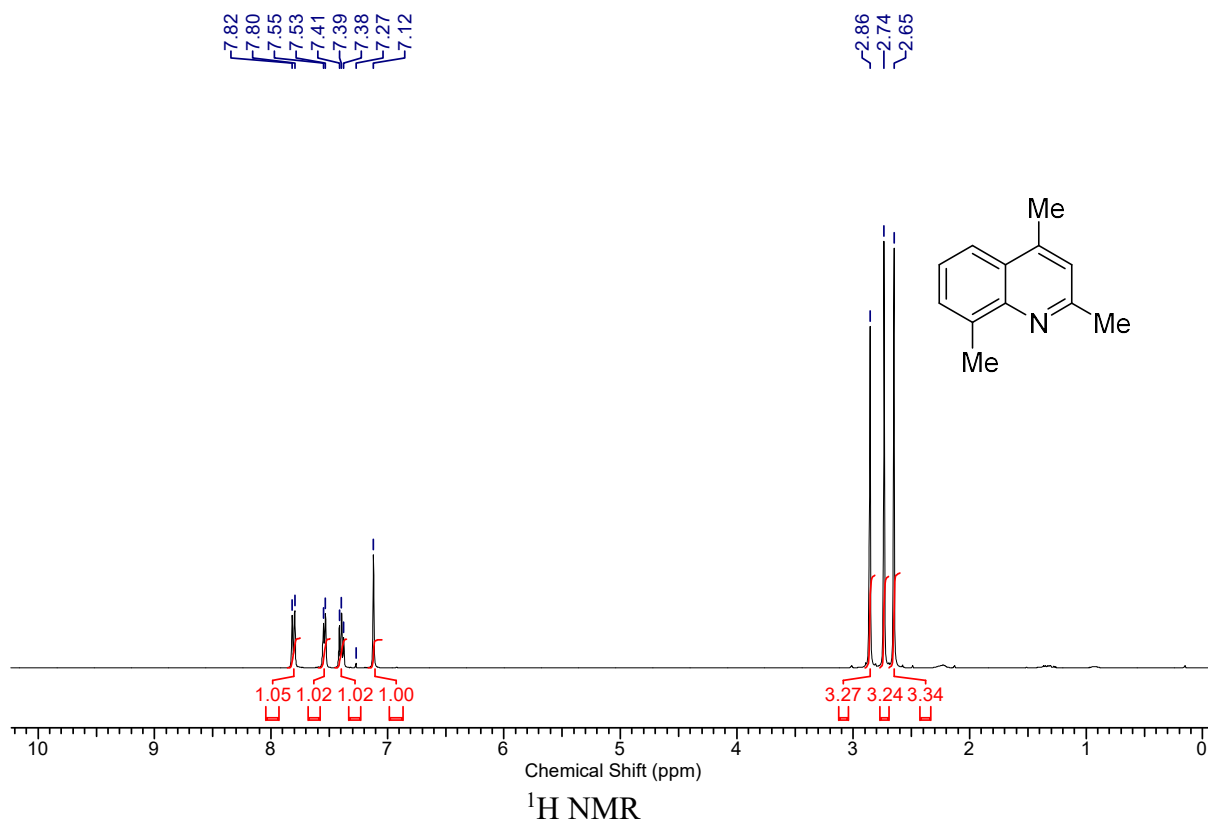


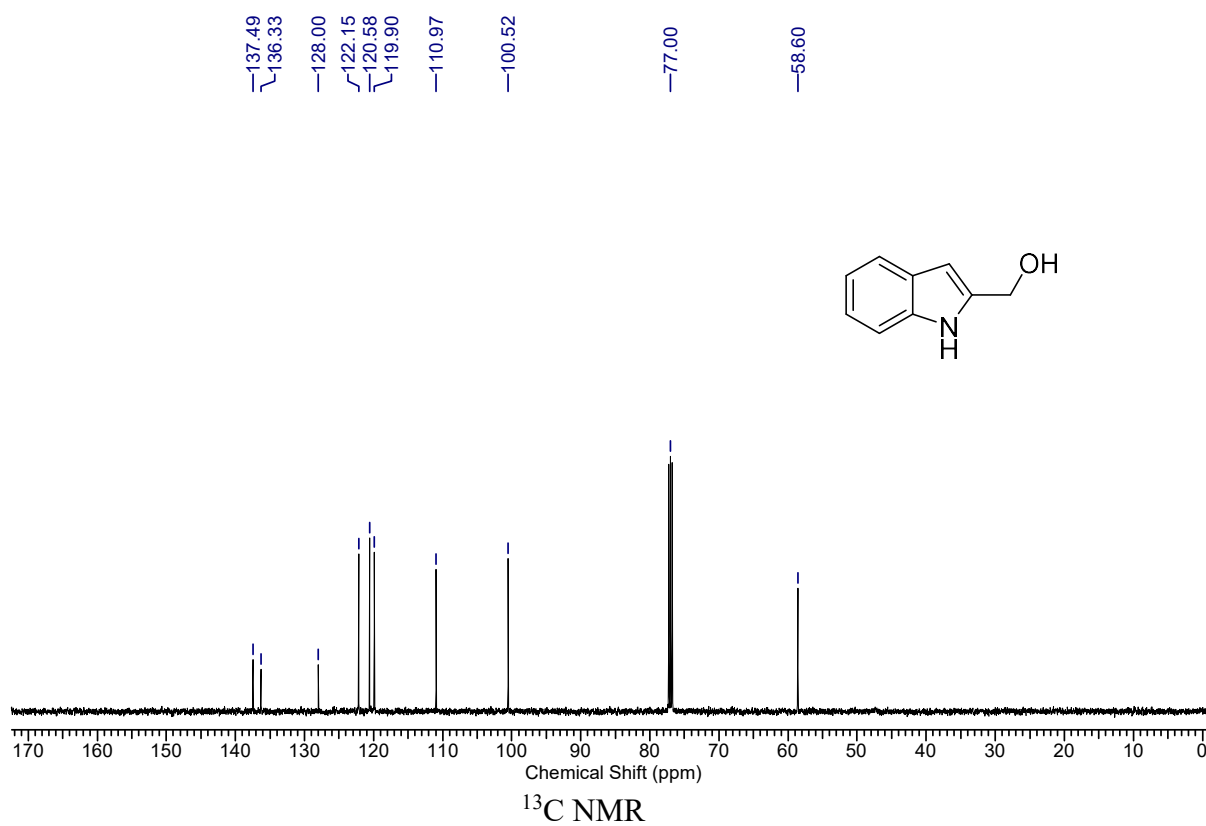
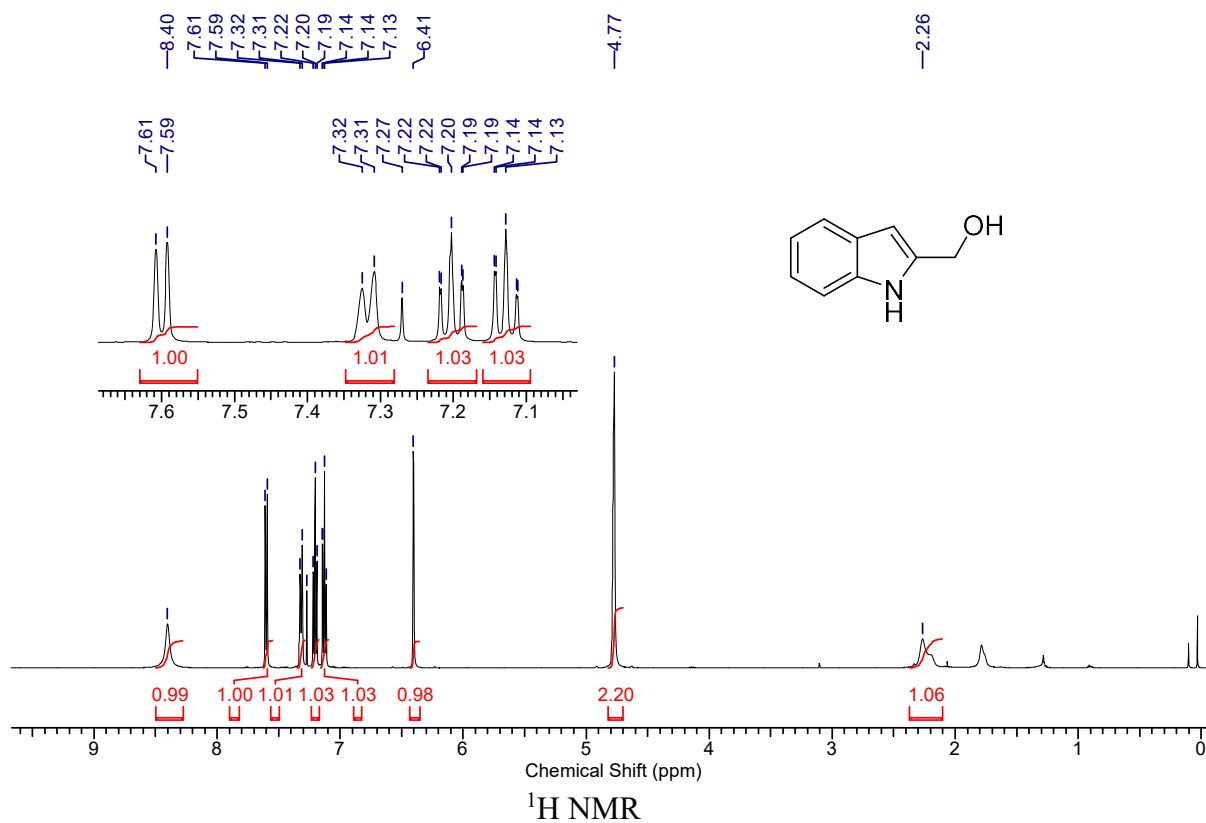


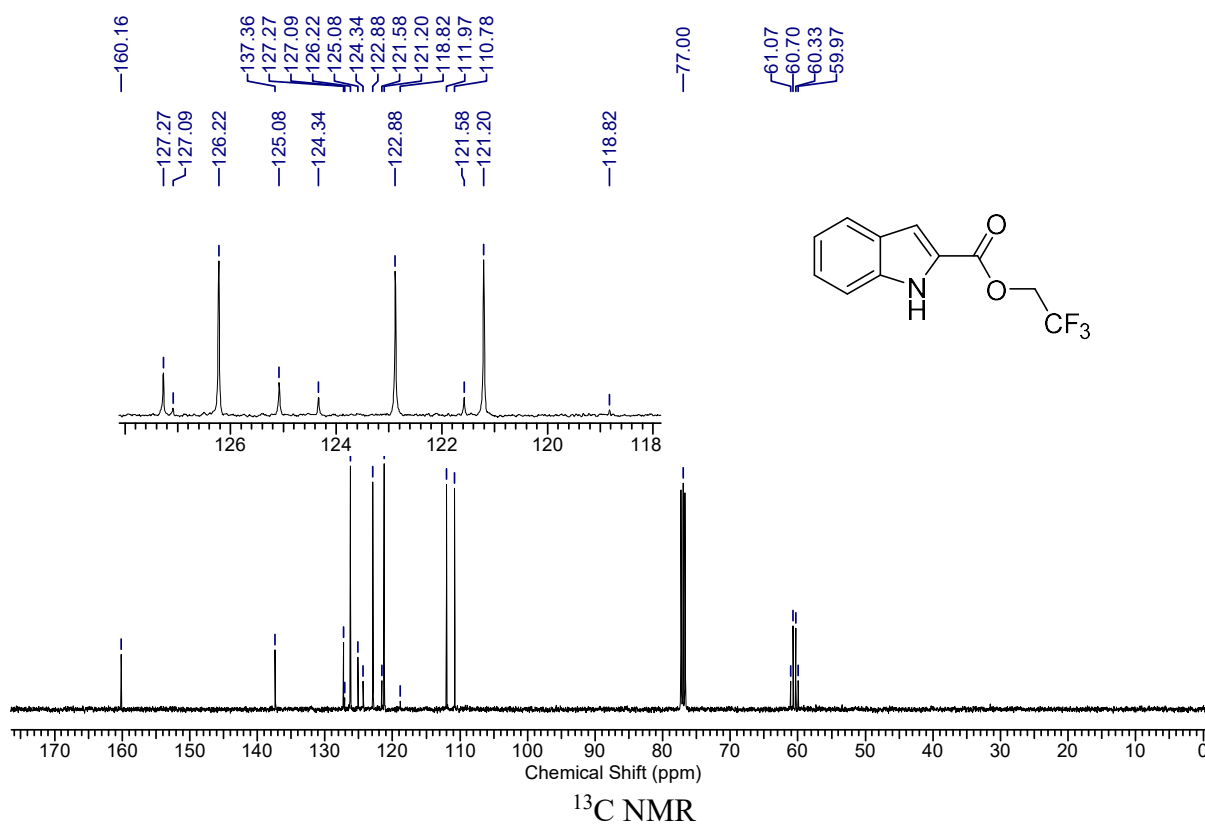
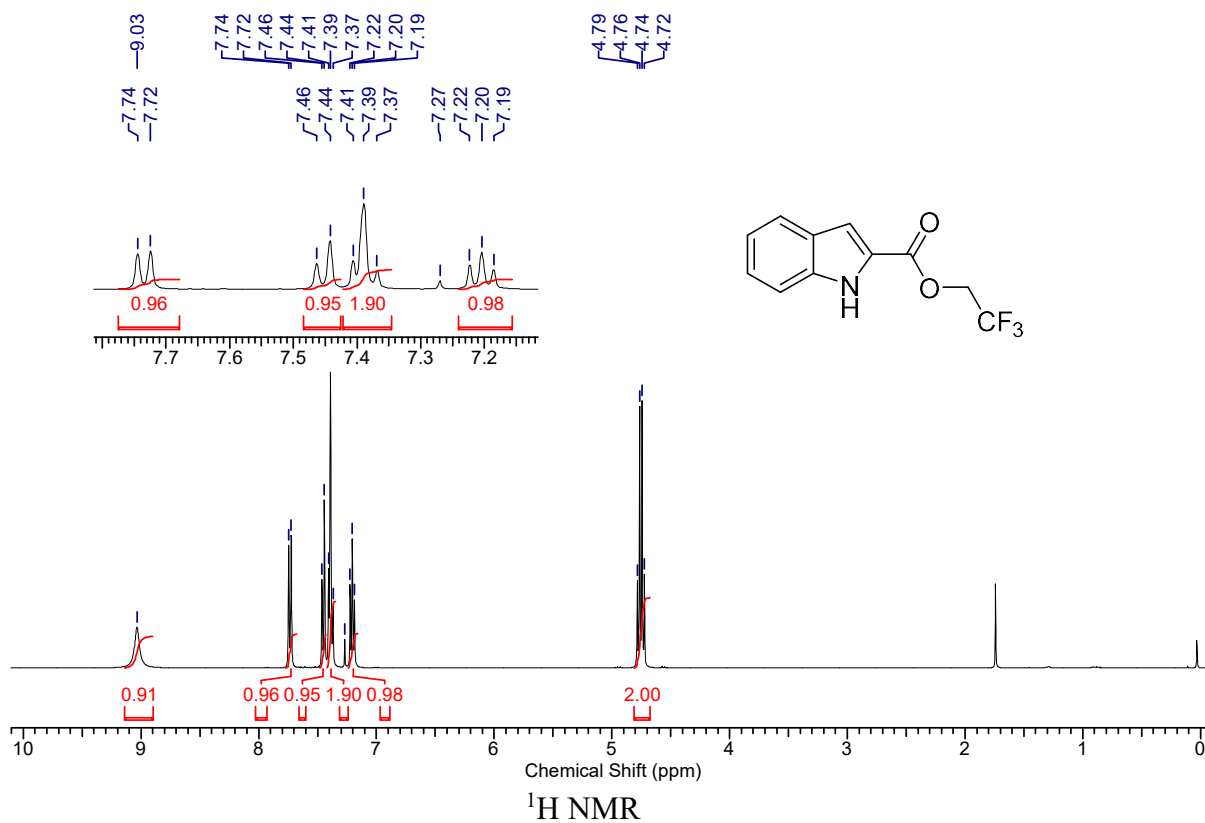


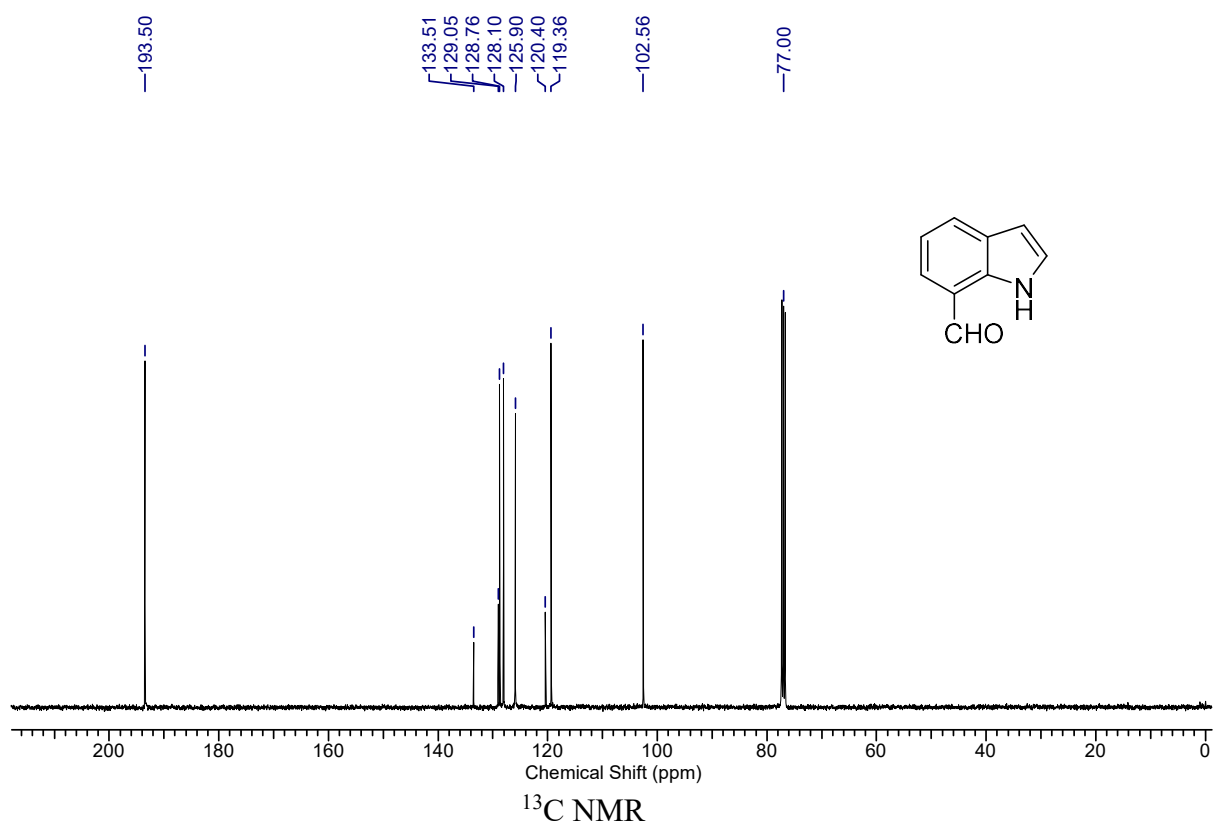
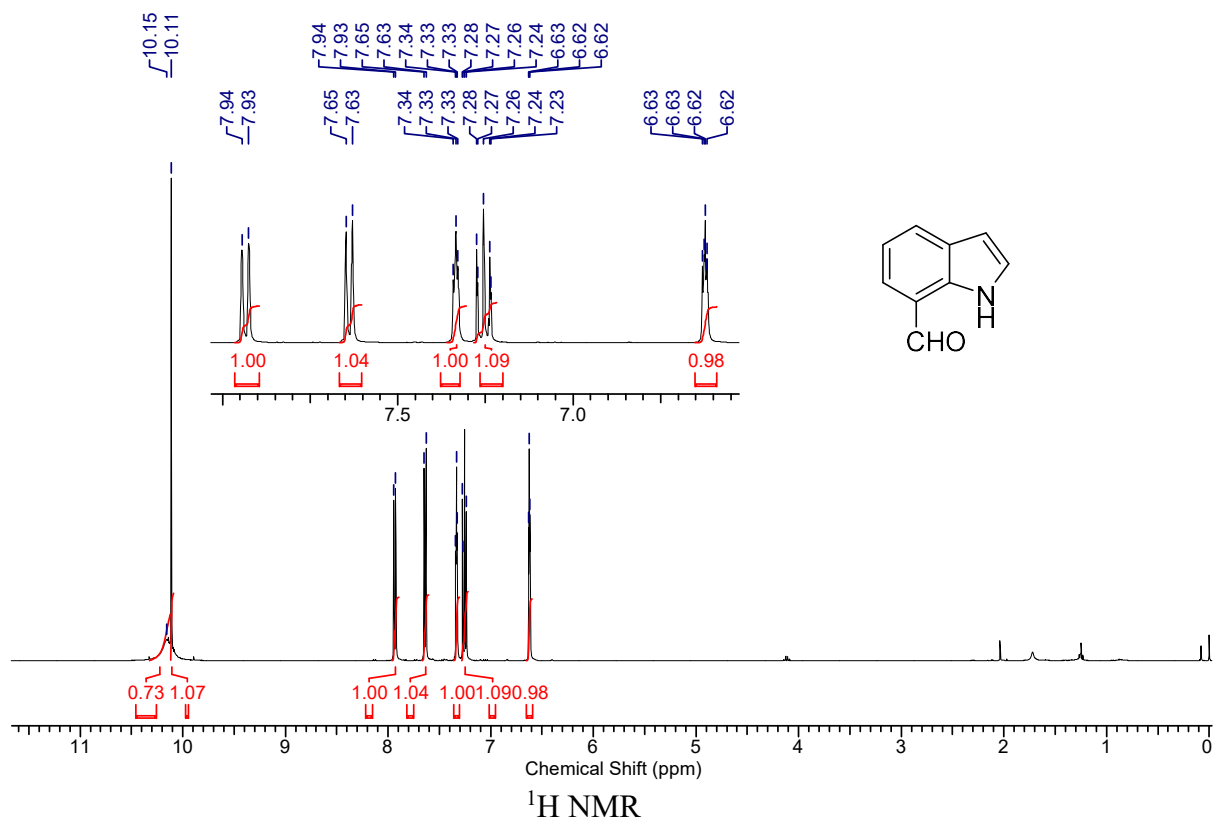


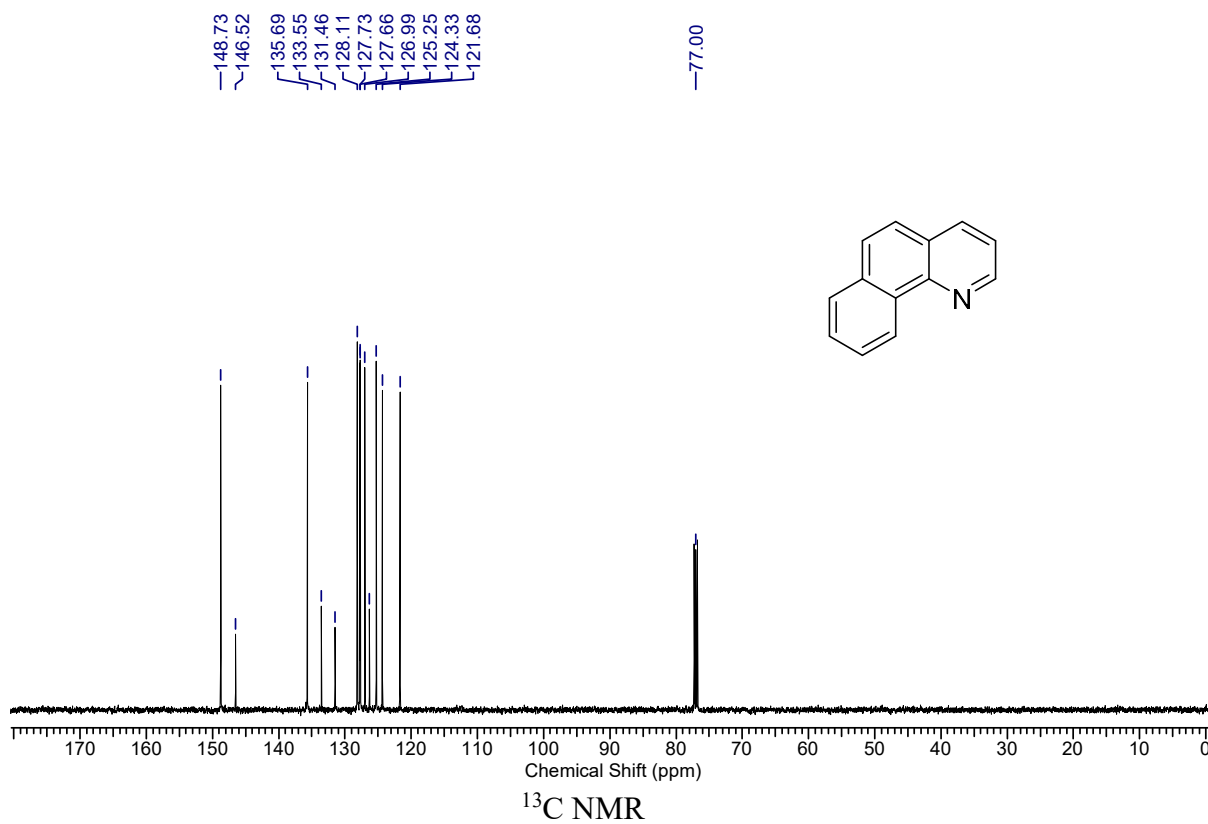
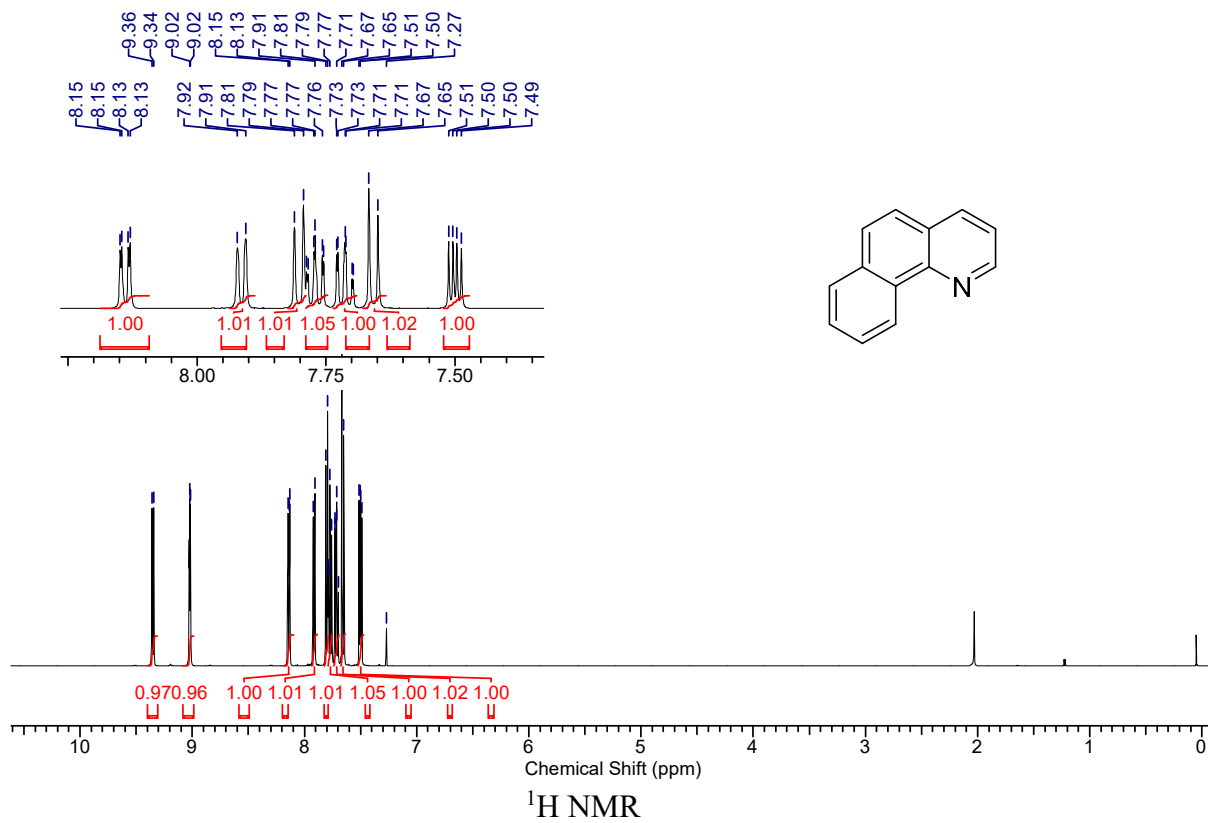


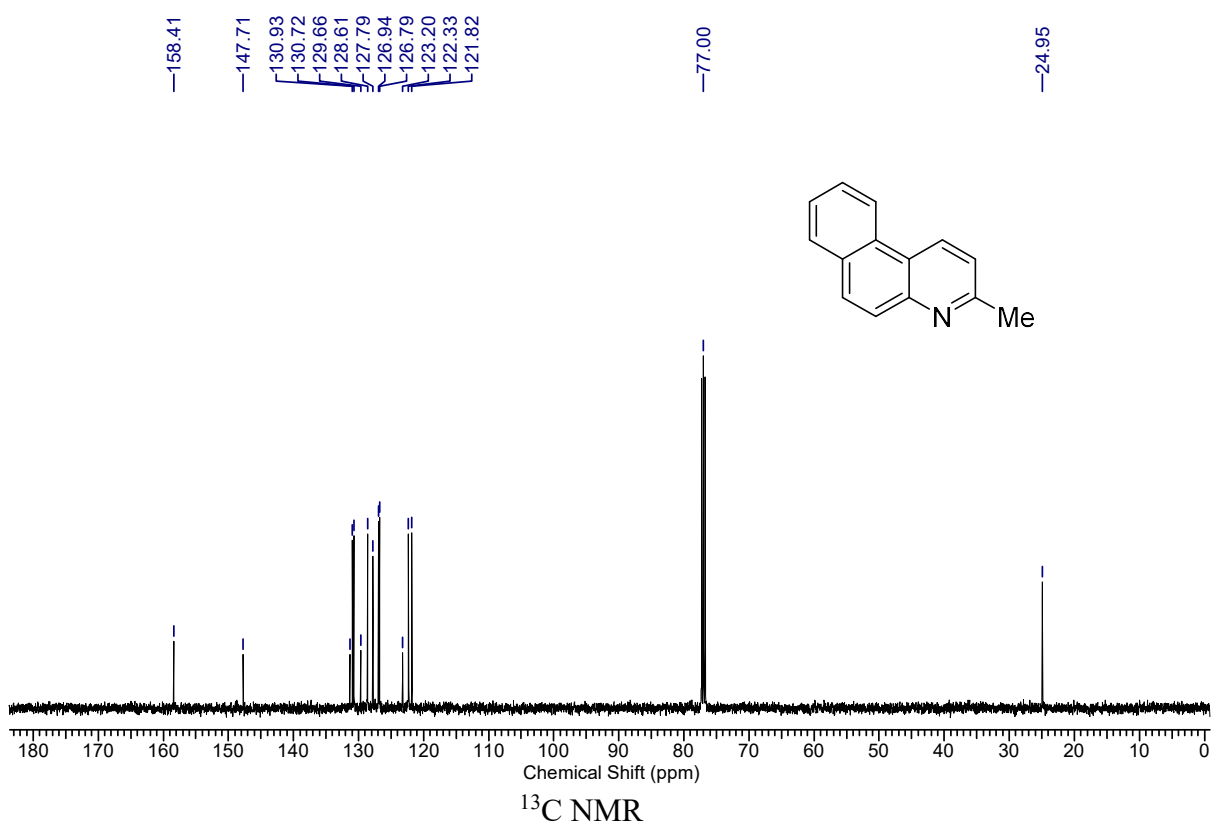
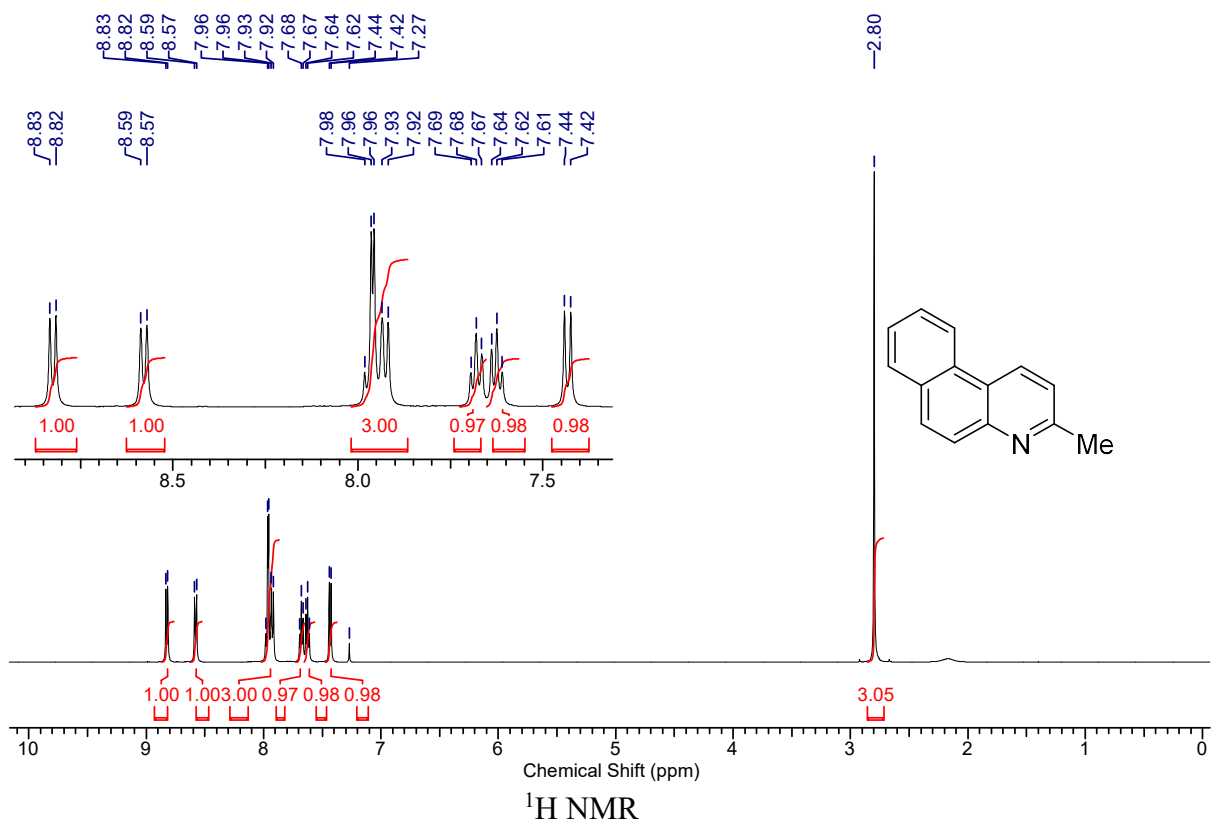


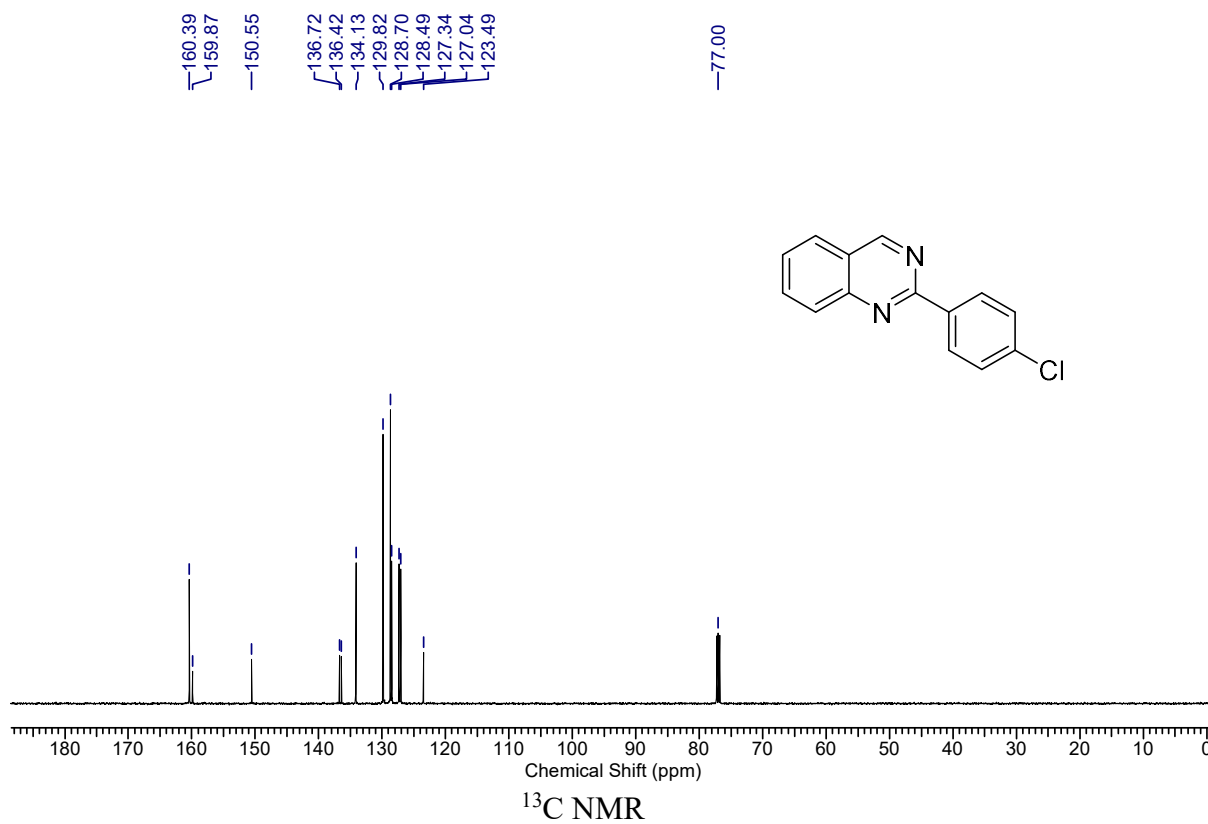
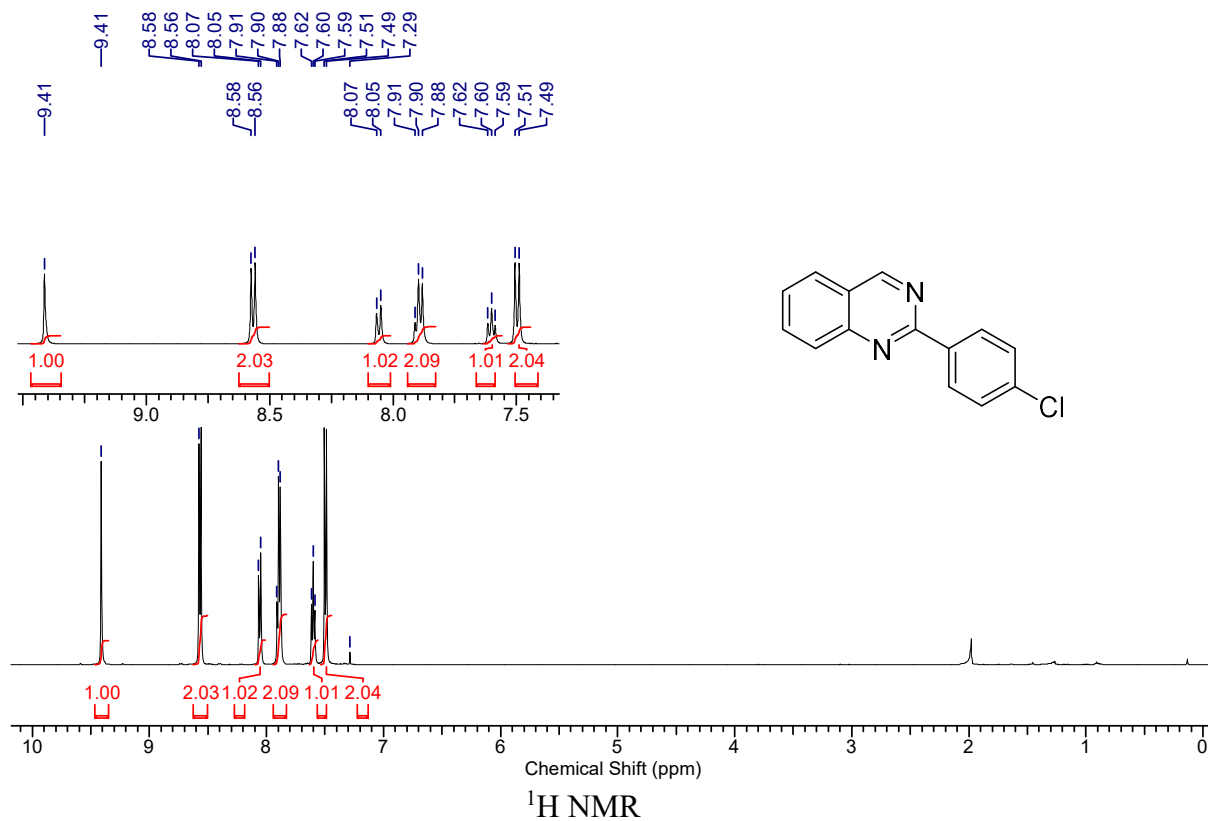


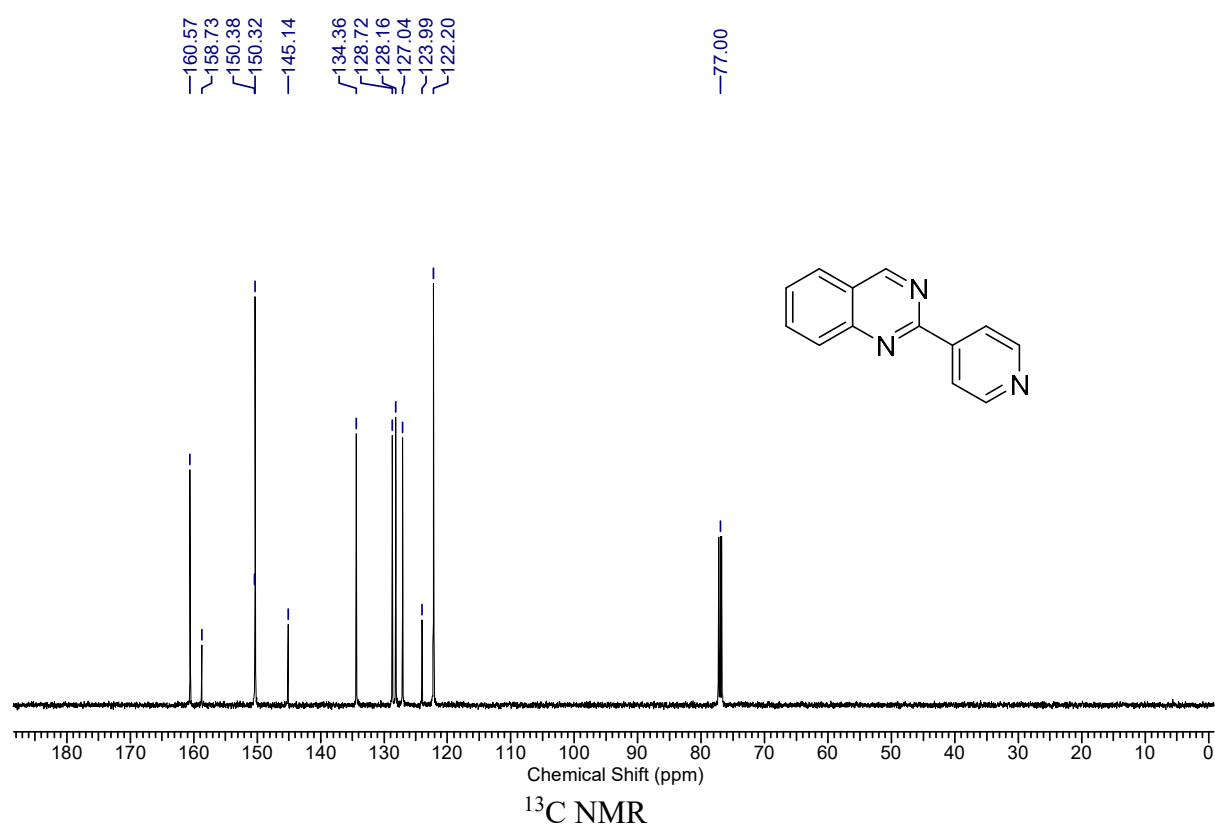
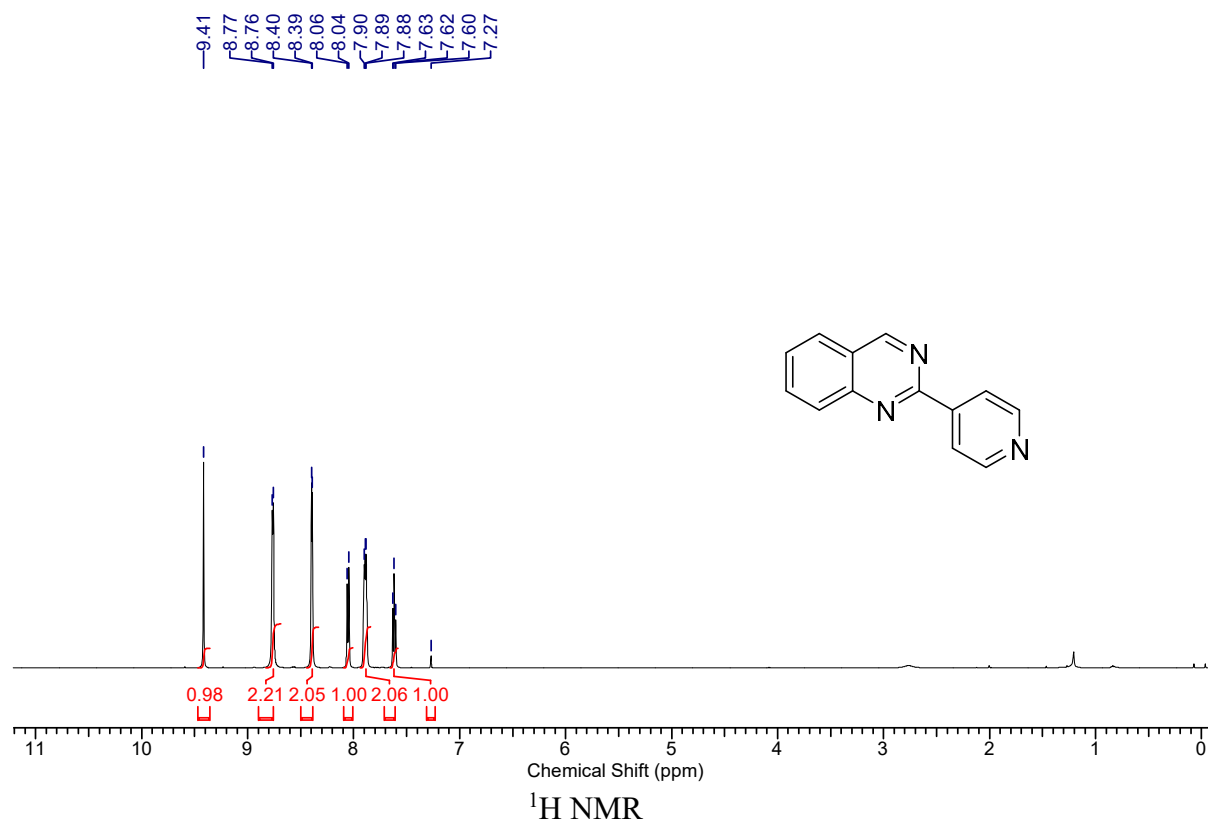


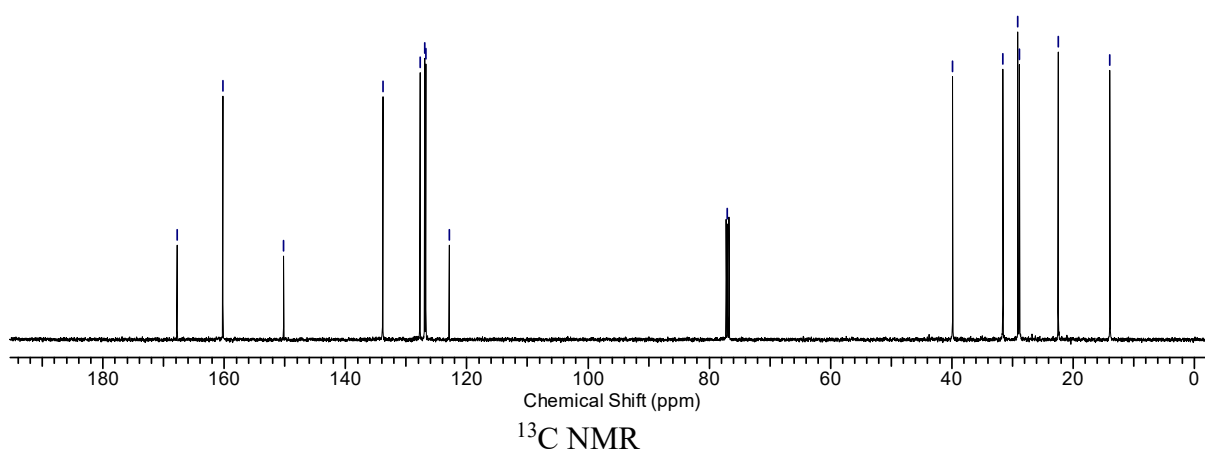
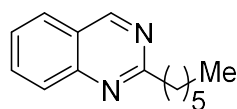
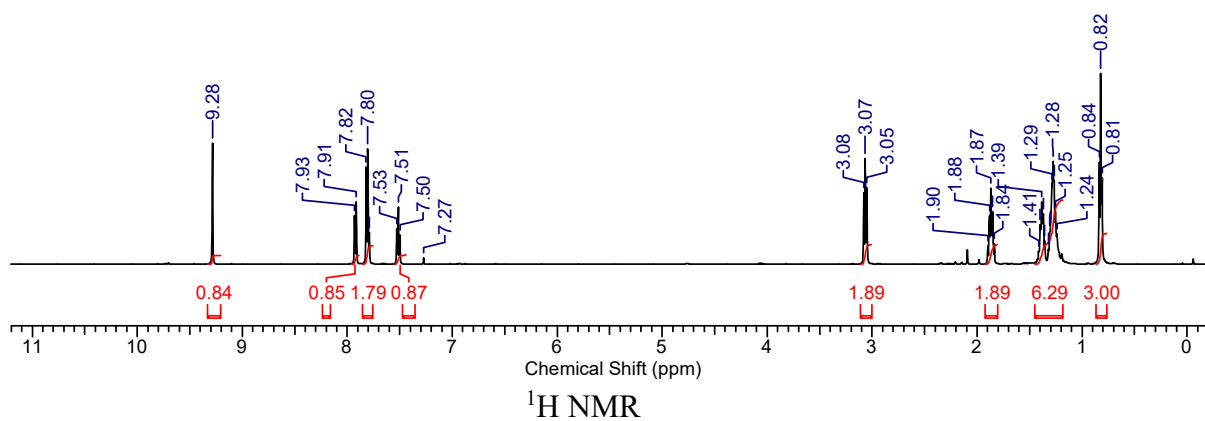
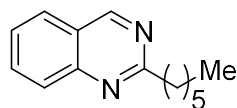




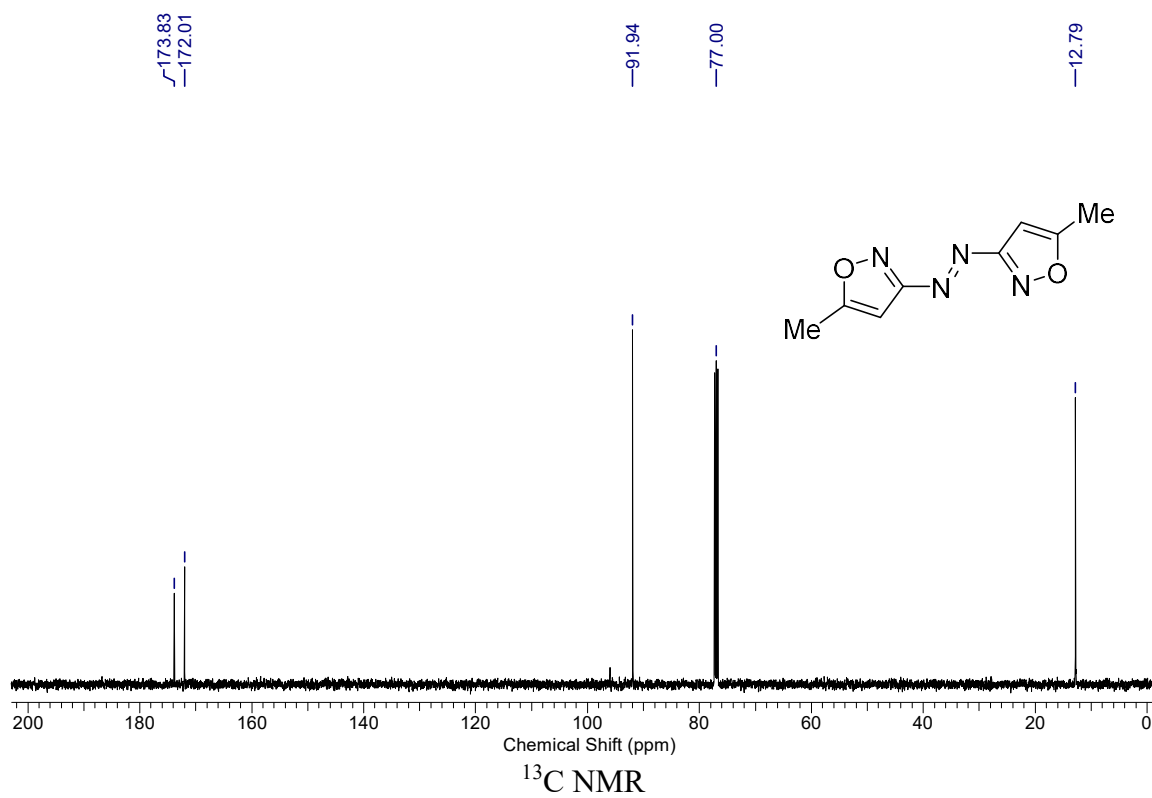
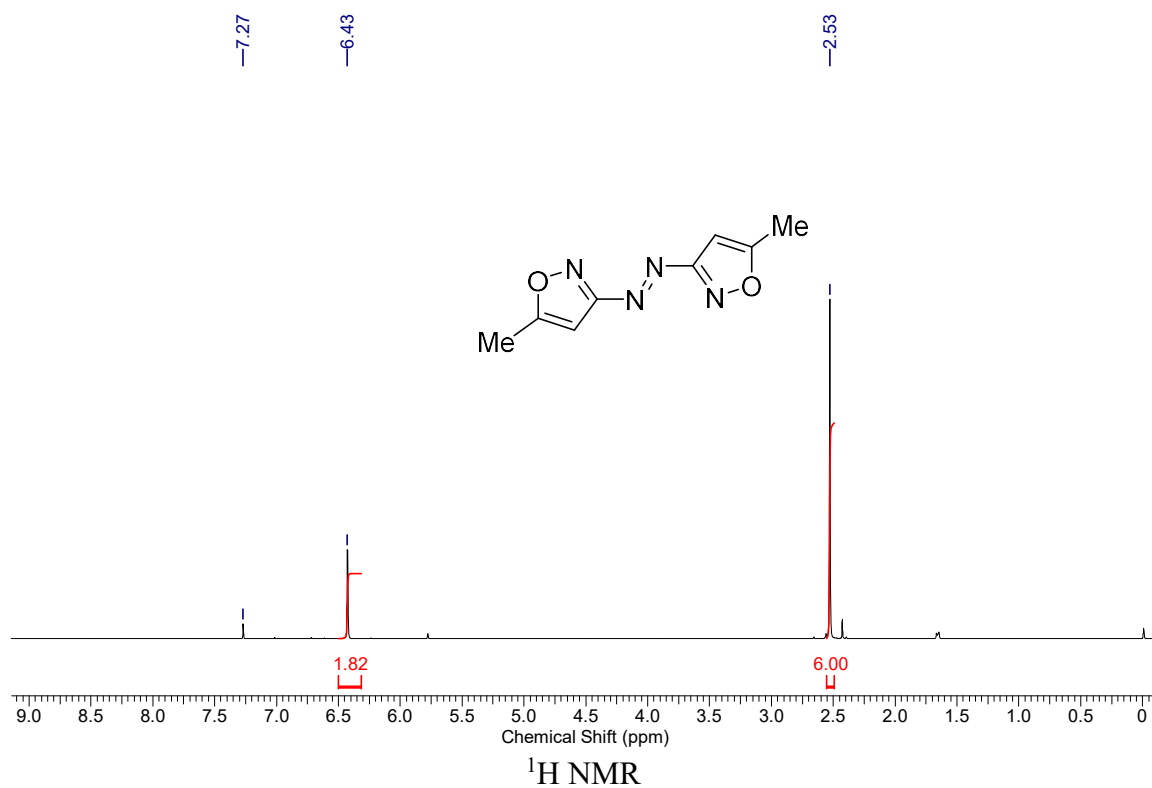




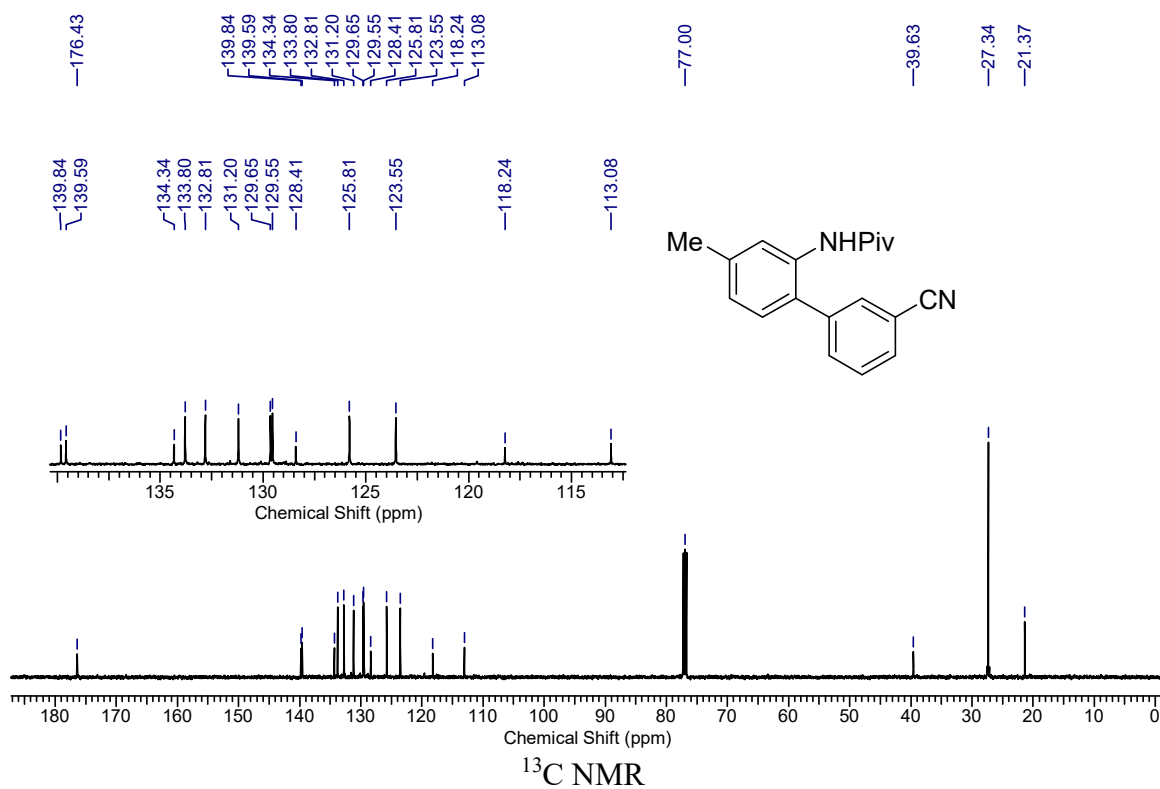
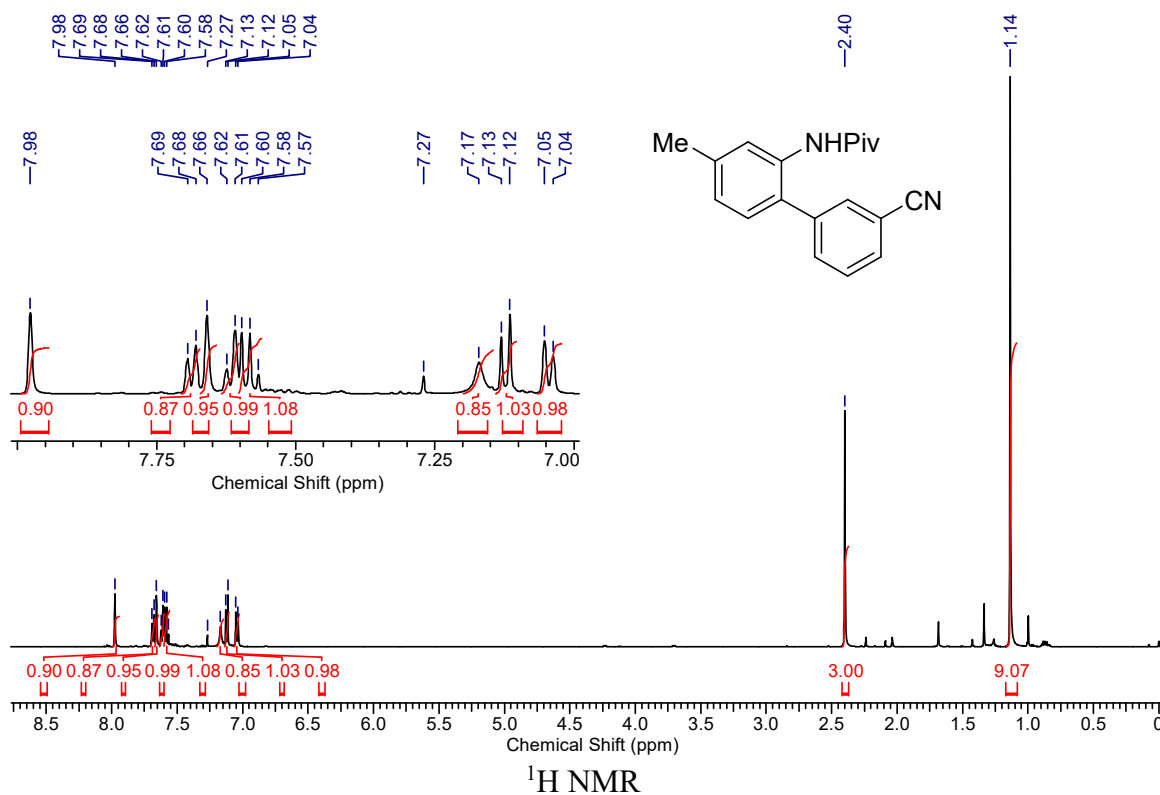


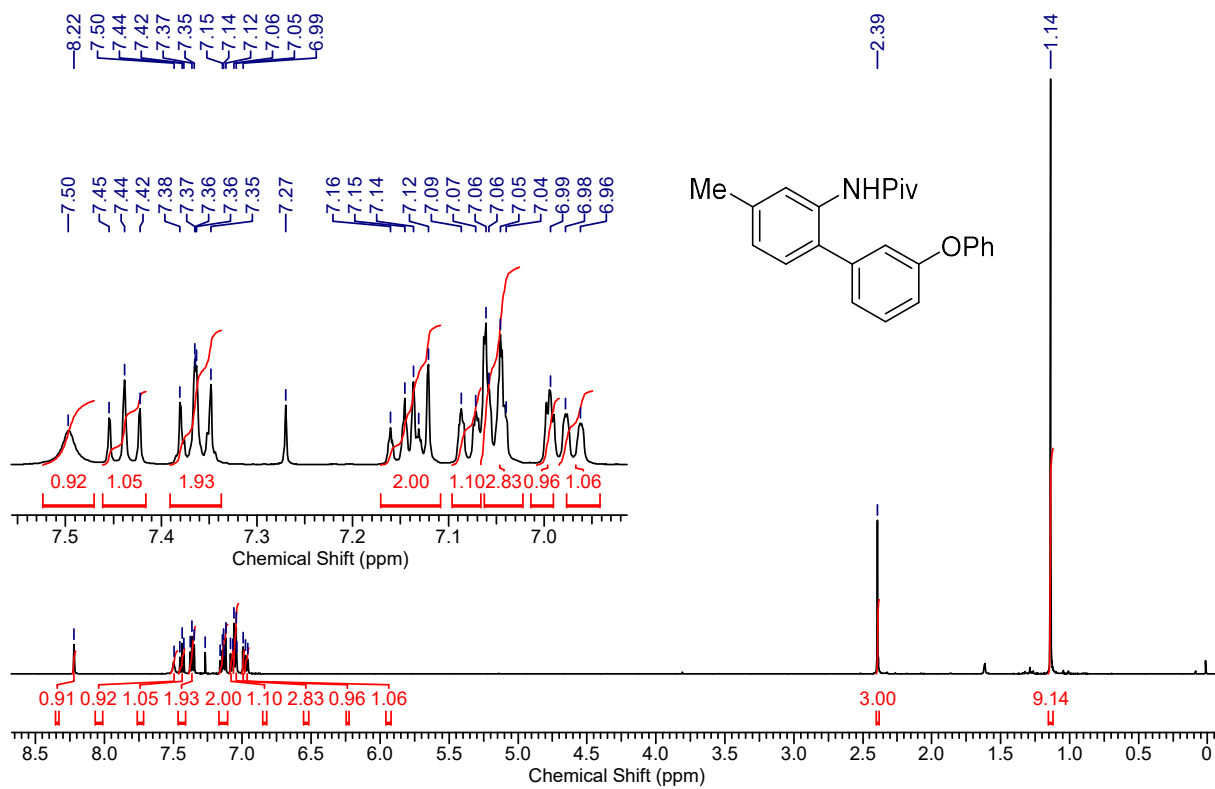
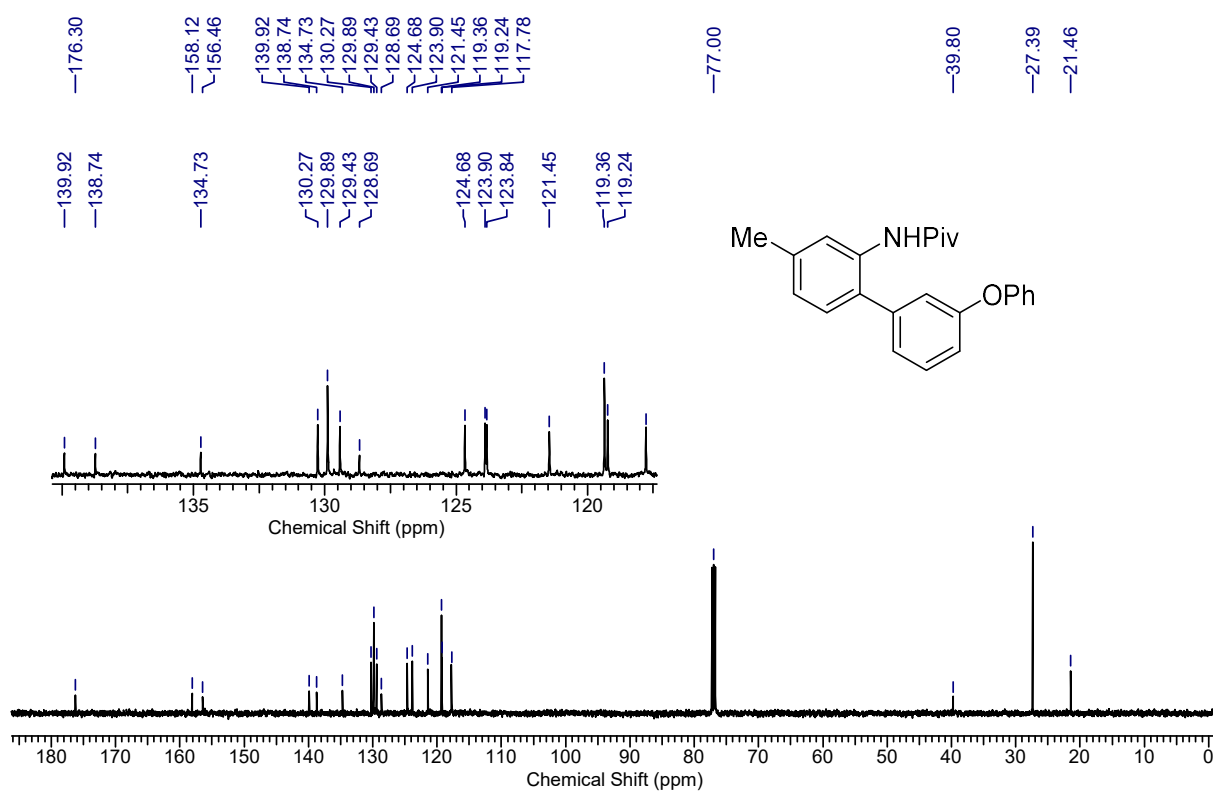


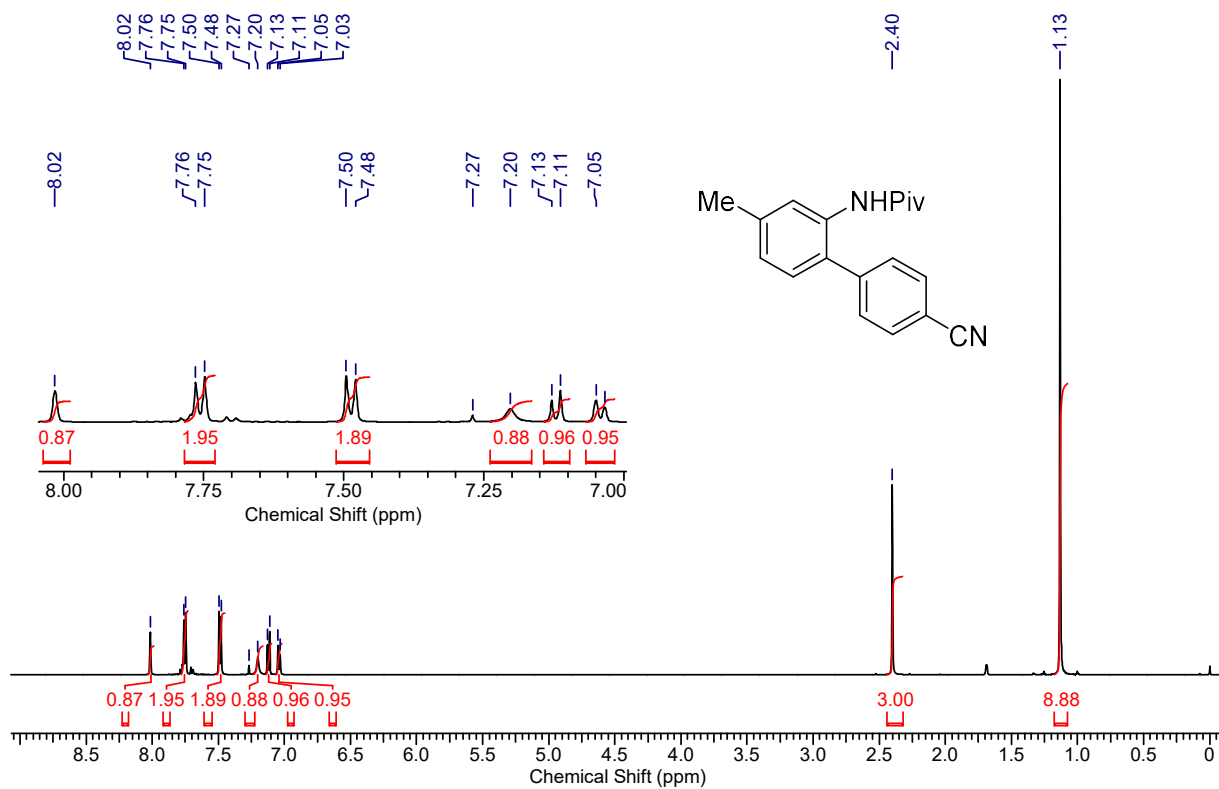
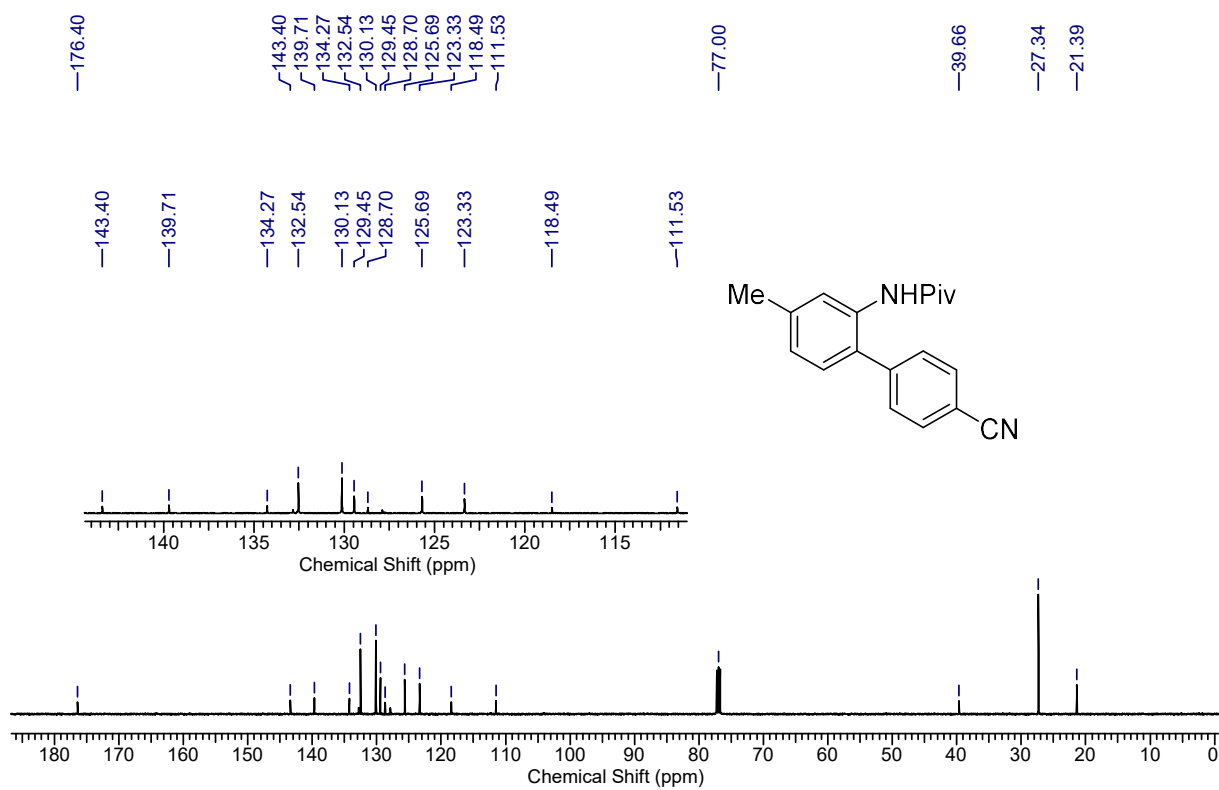
Chapter 4

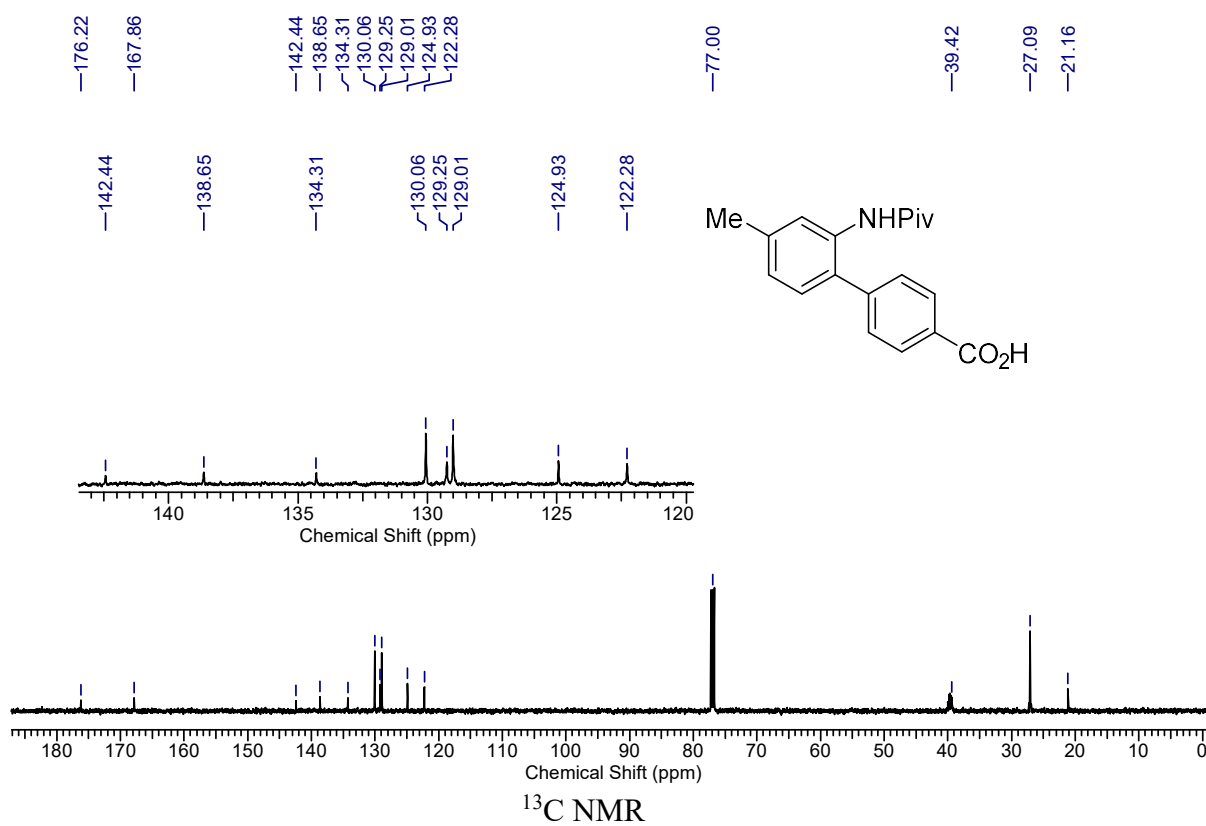
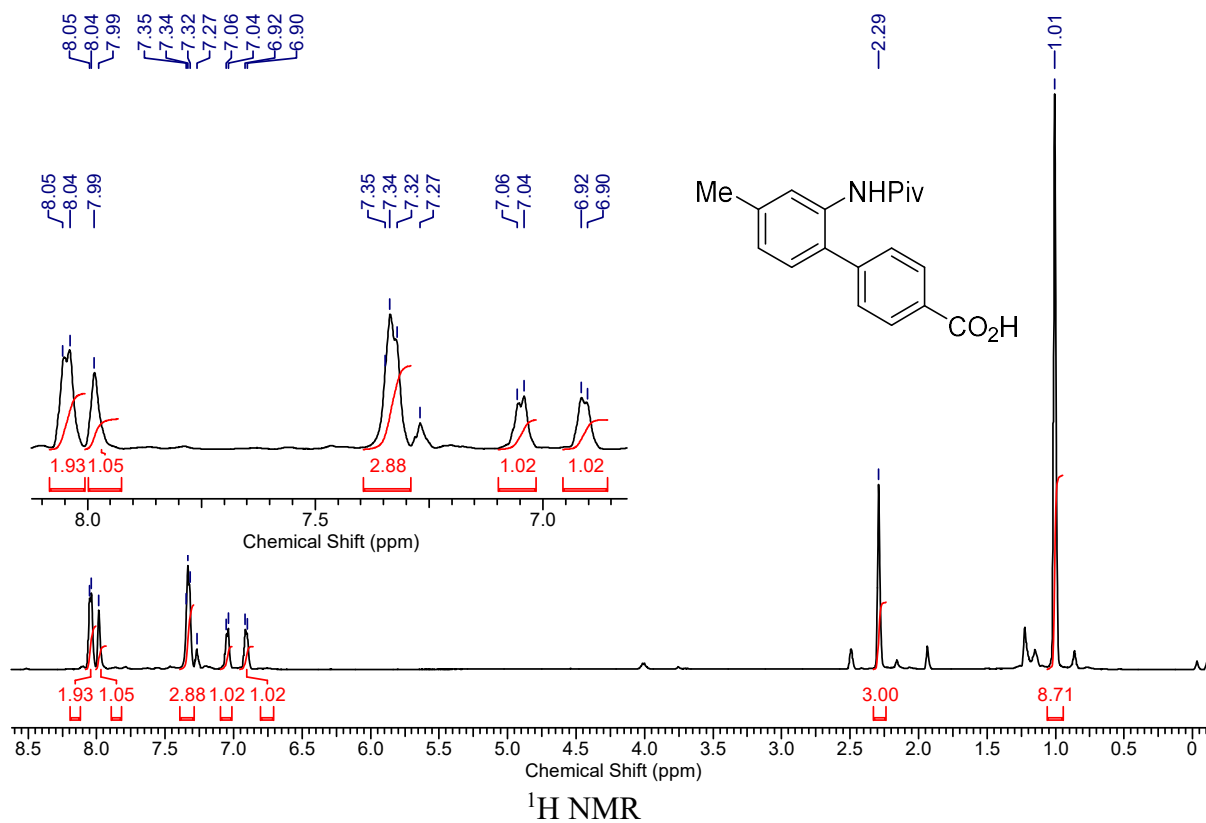


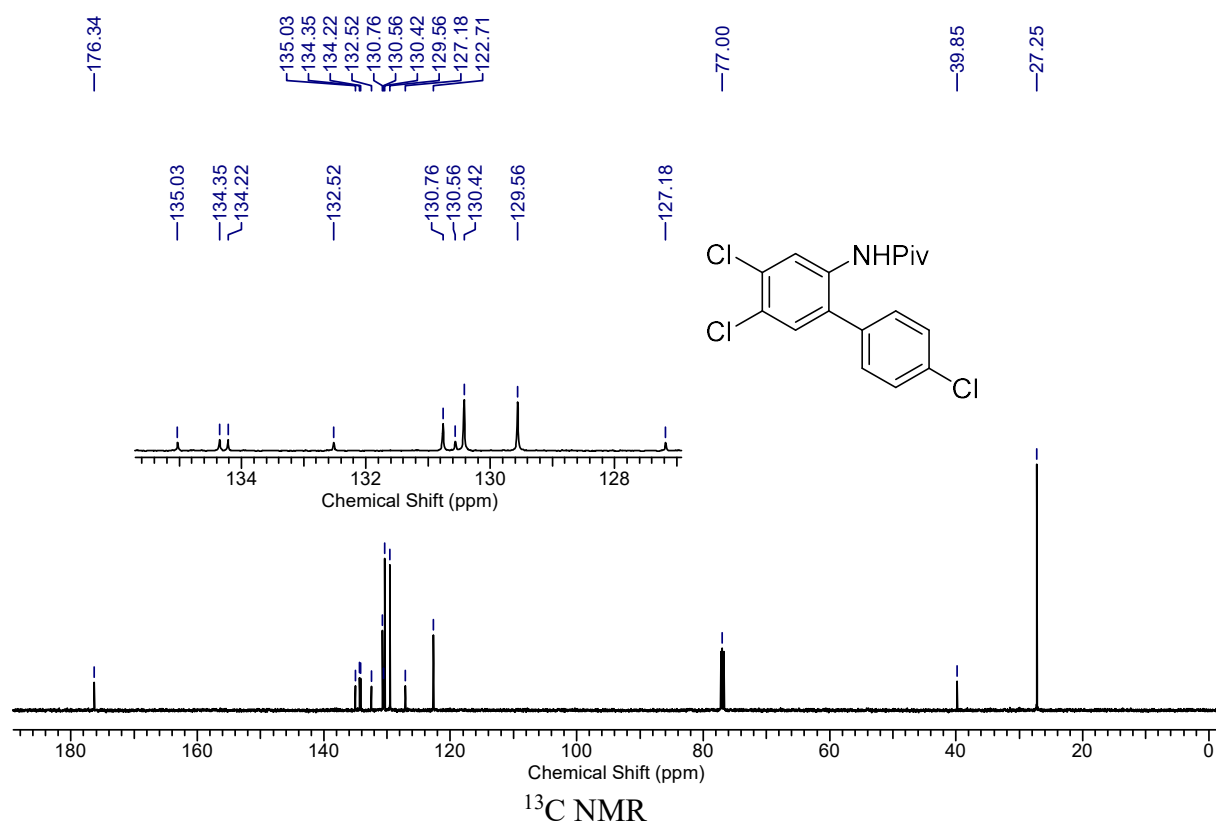
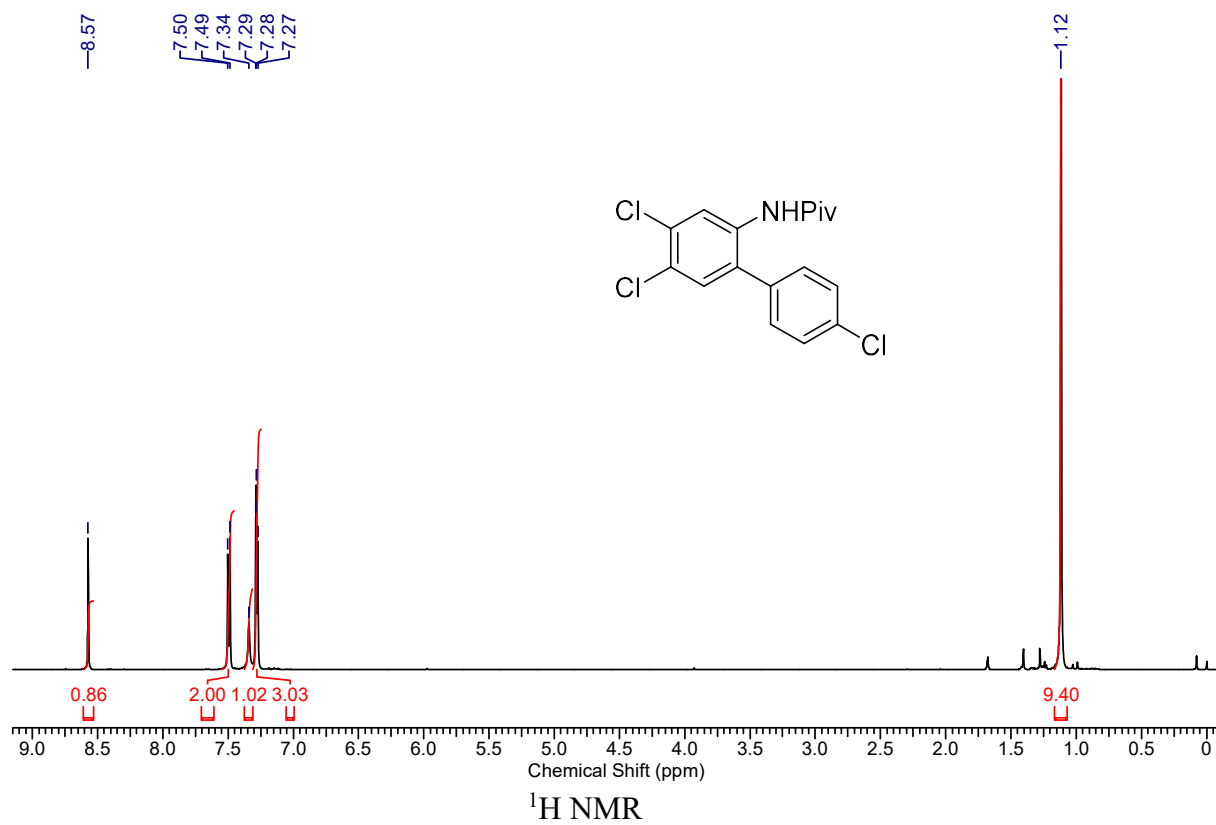
Chapter 5

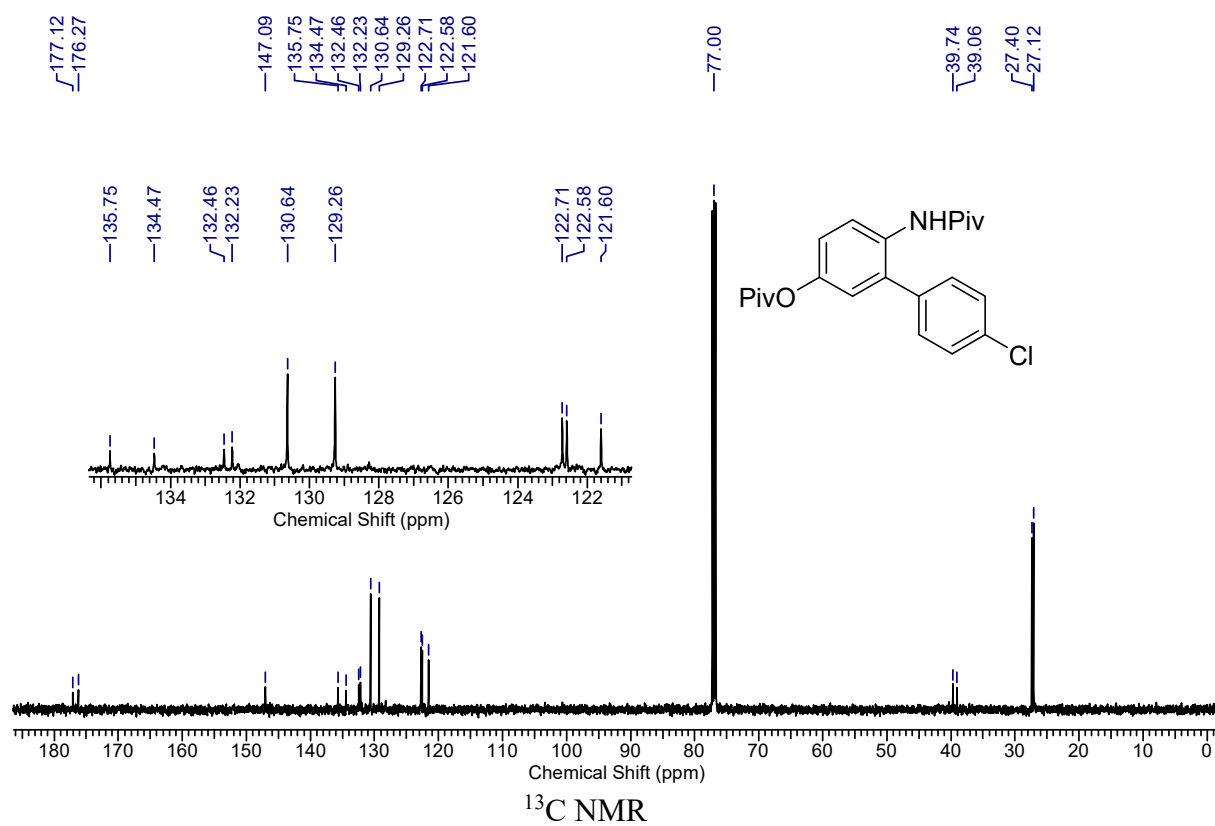
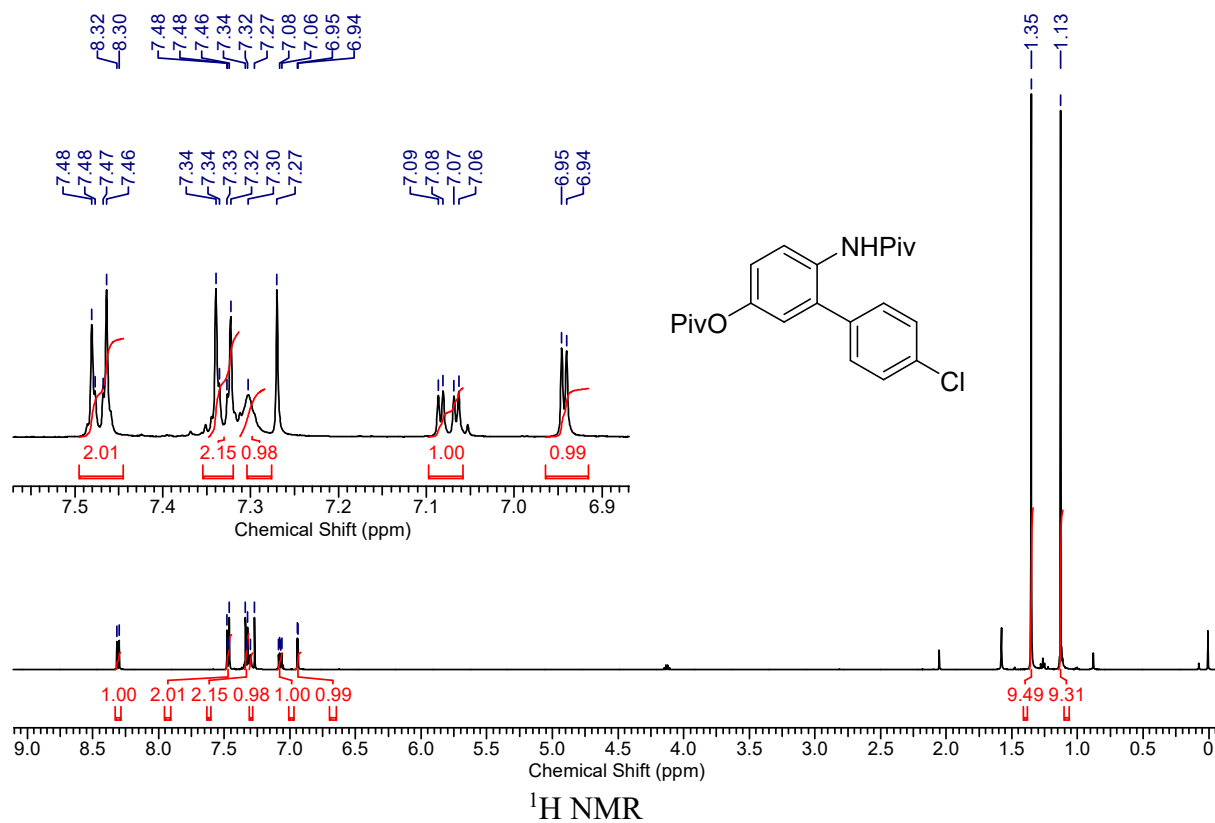


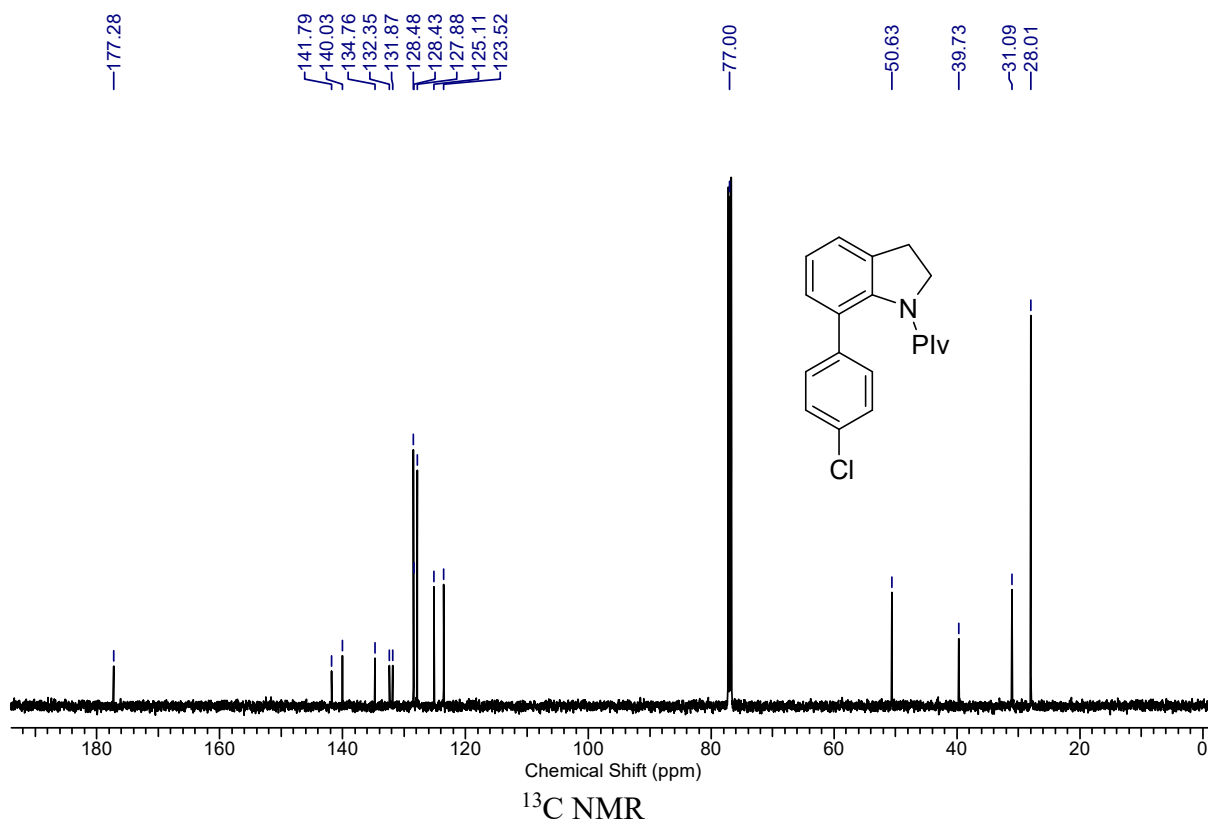
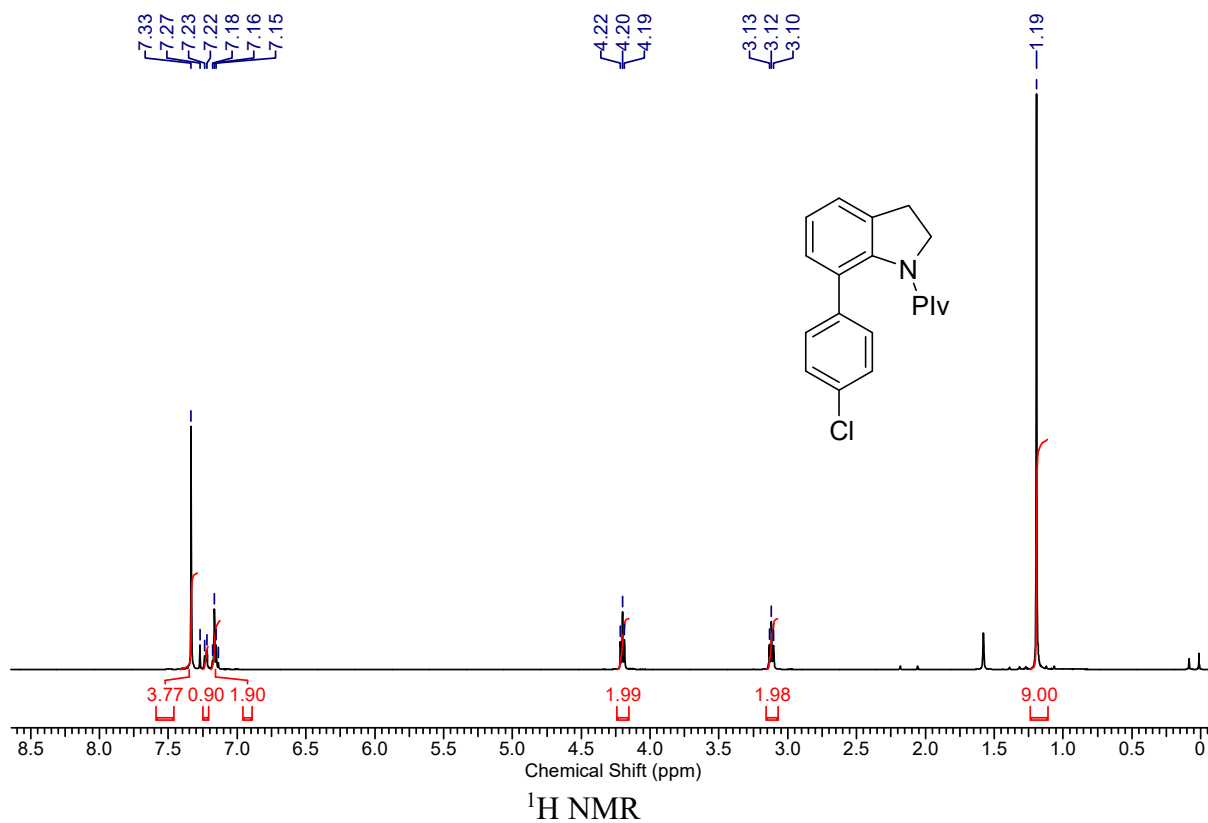
¹H NMR¹³C NMR

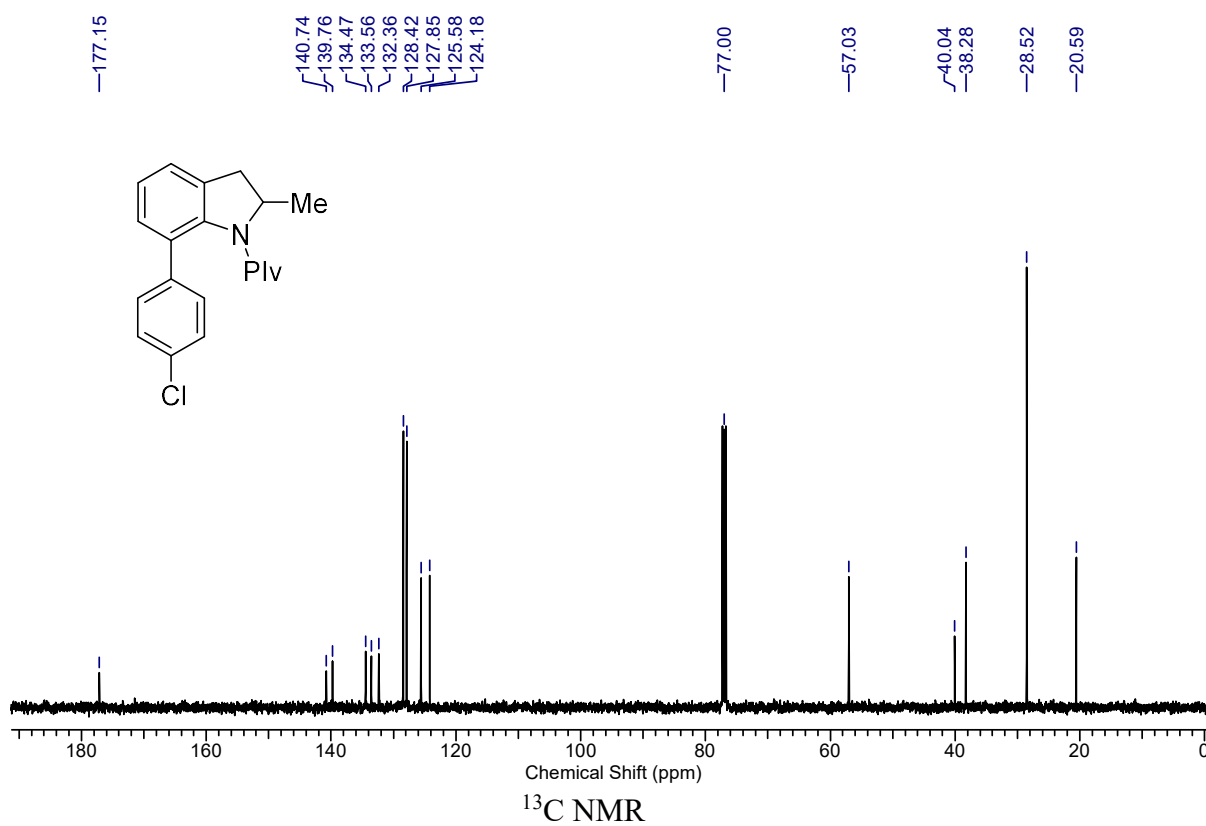
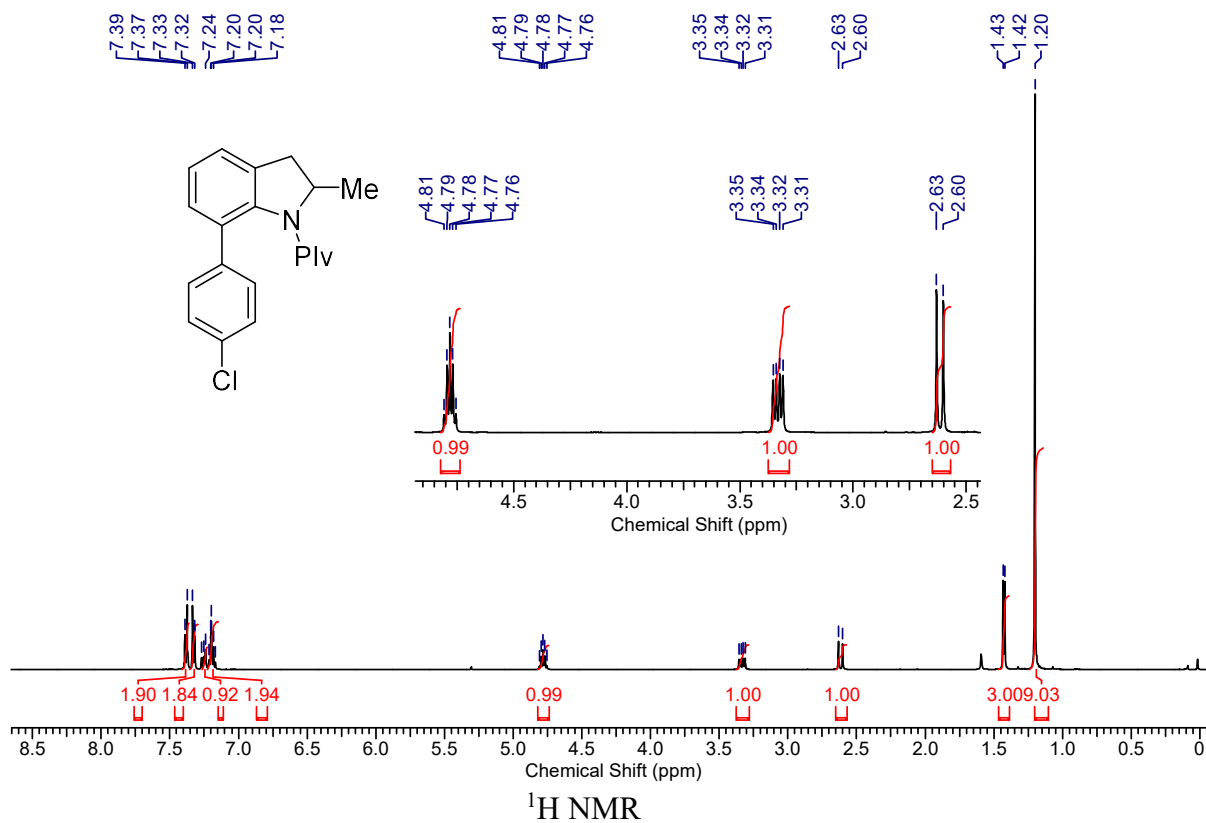
¹H NMR¹³C NMR

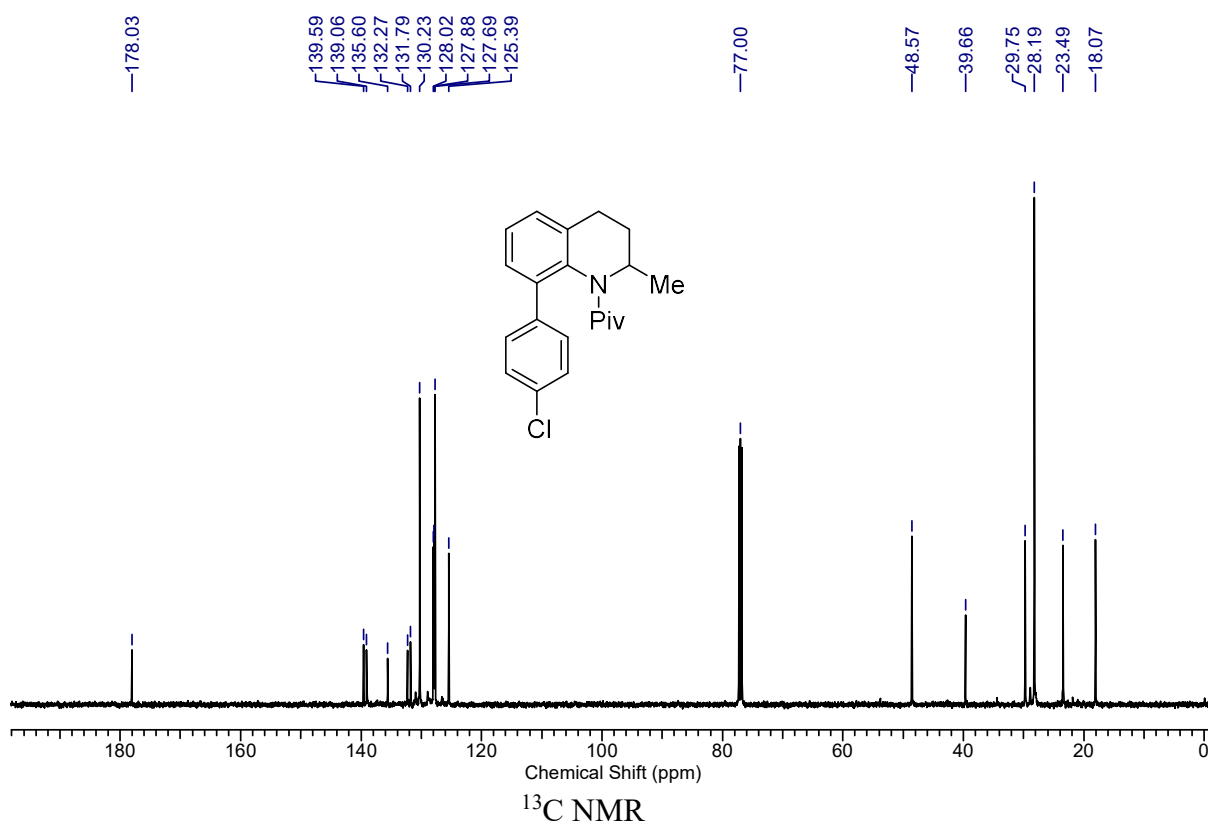
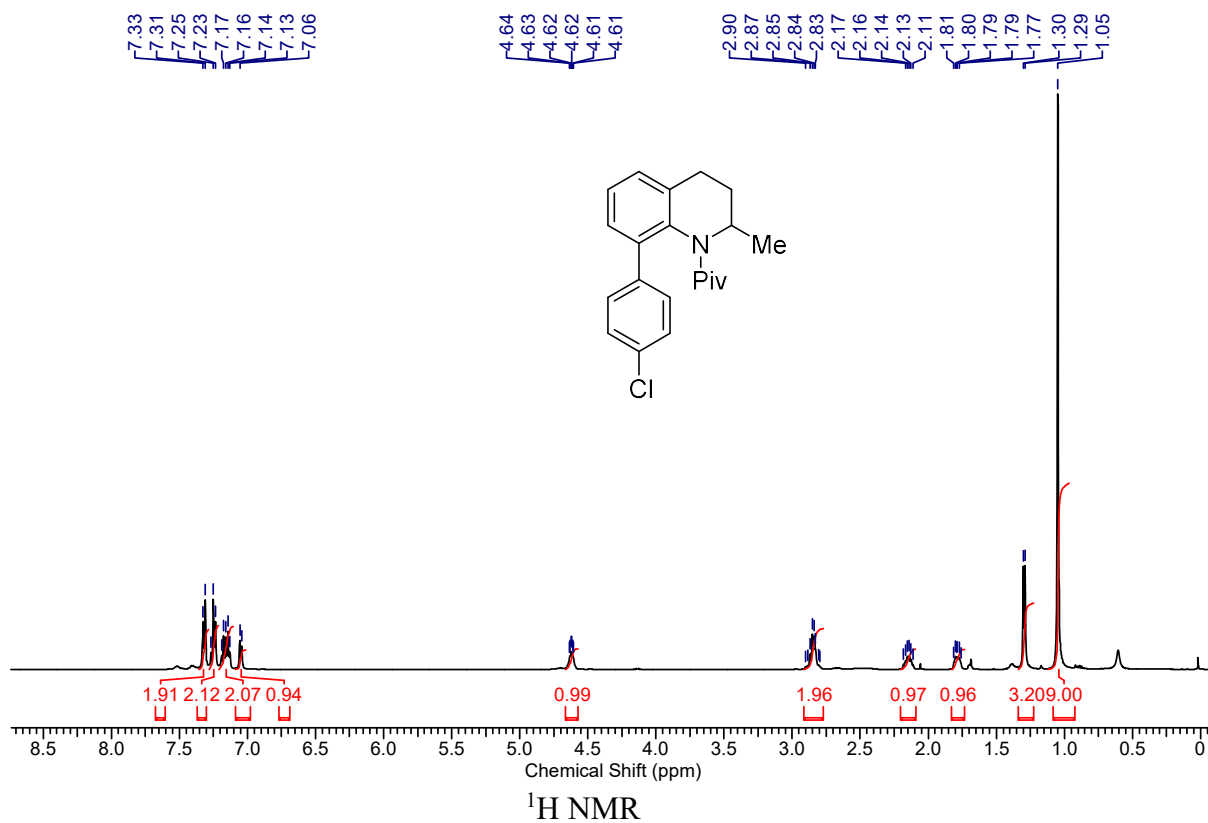


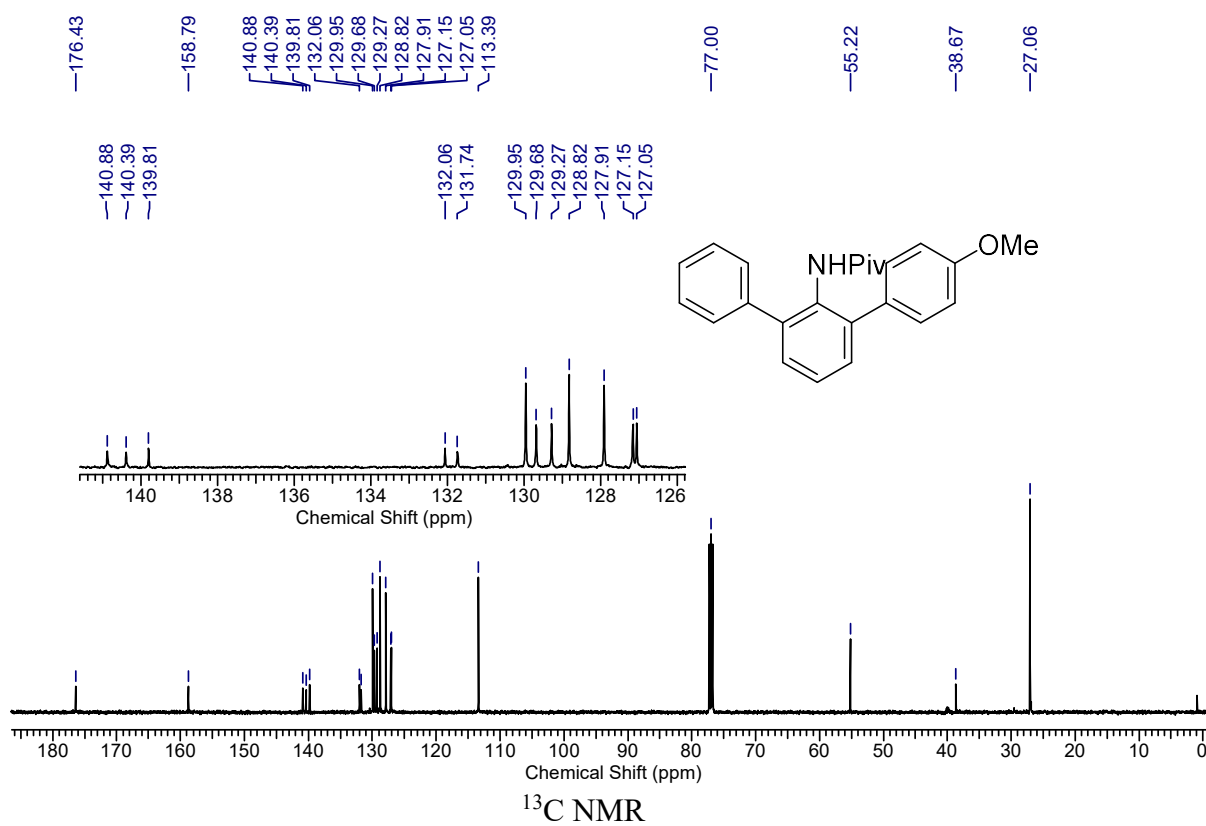
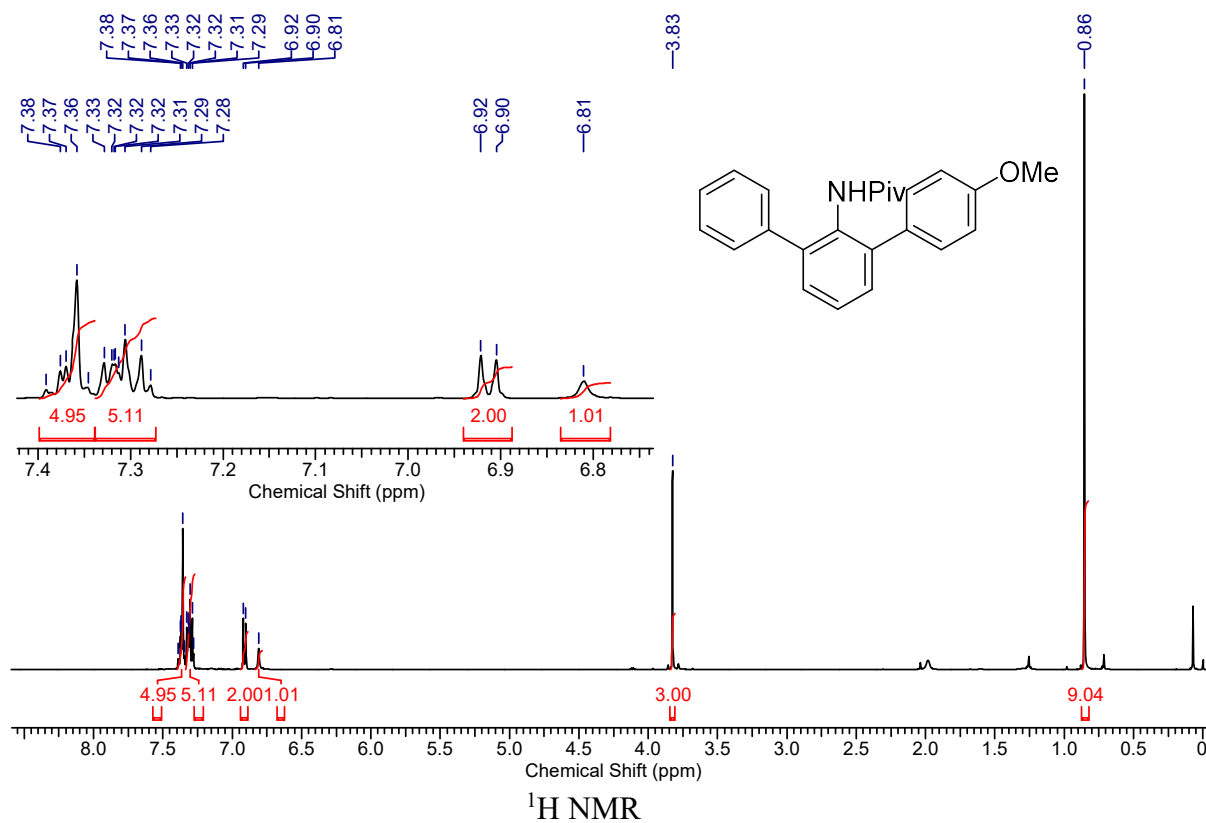


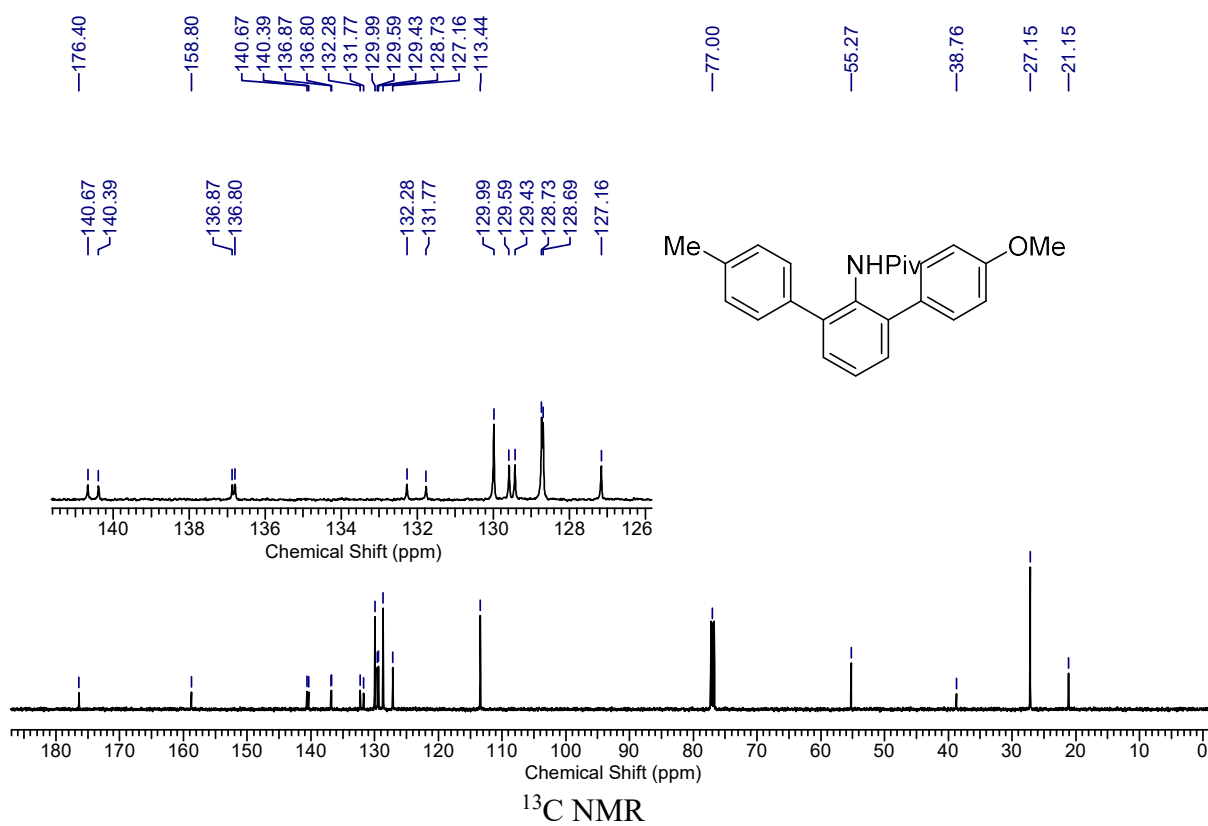
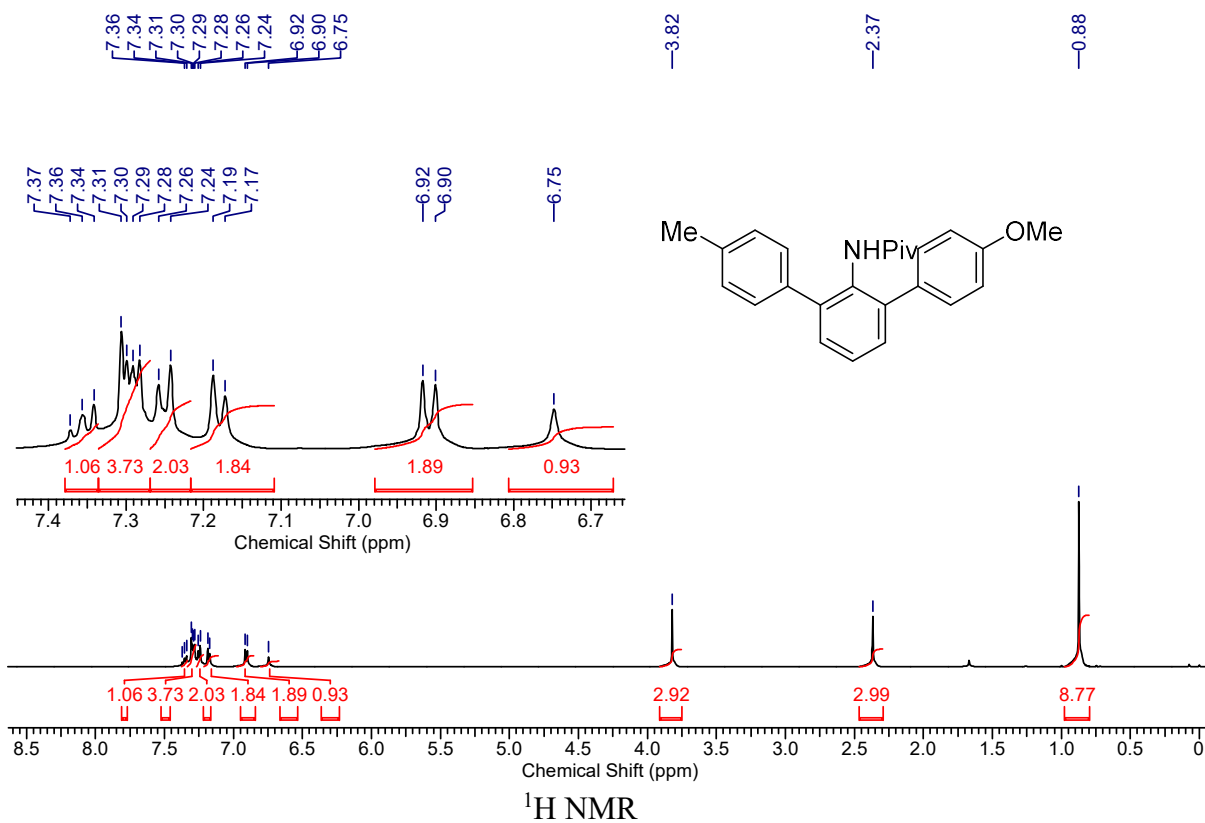


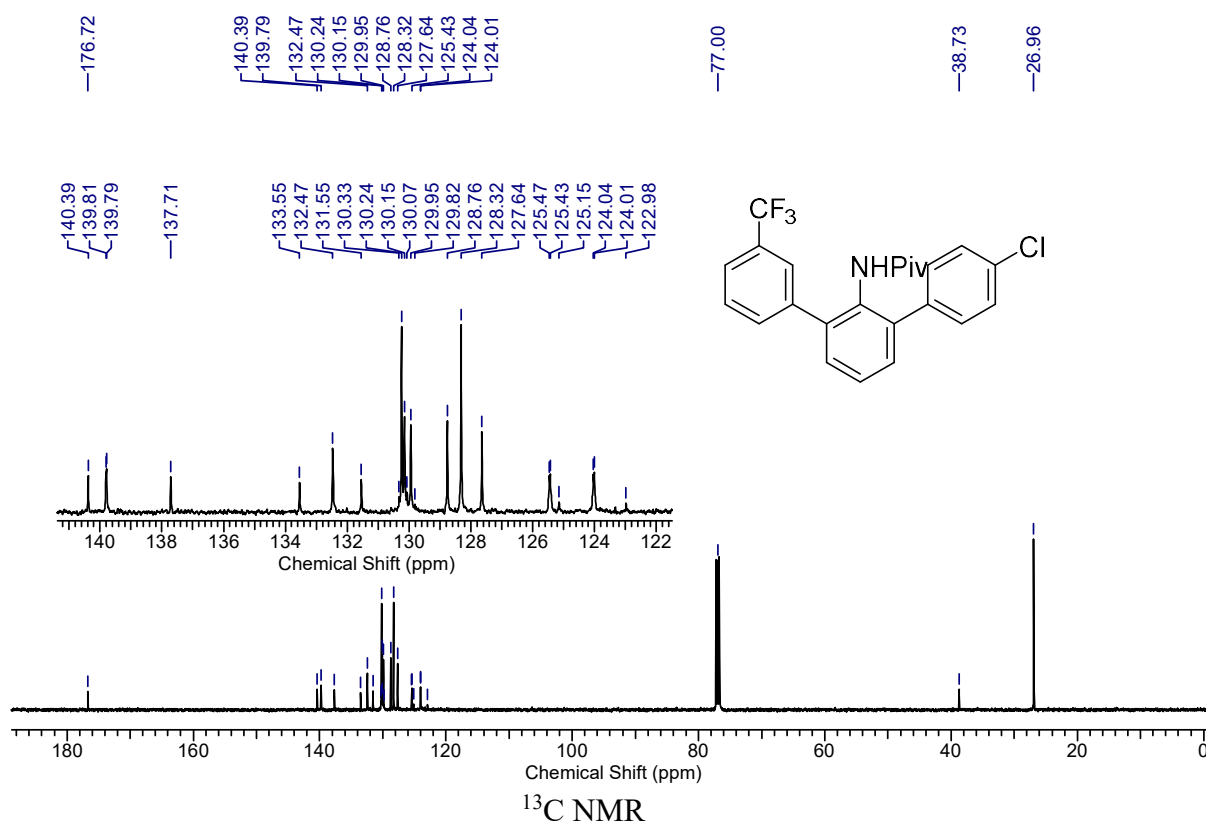
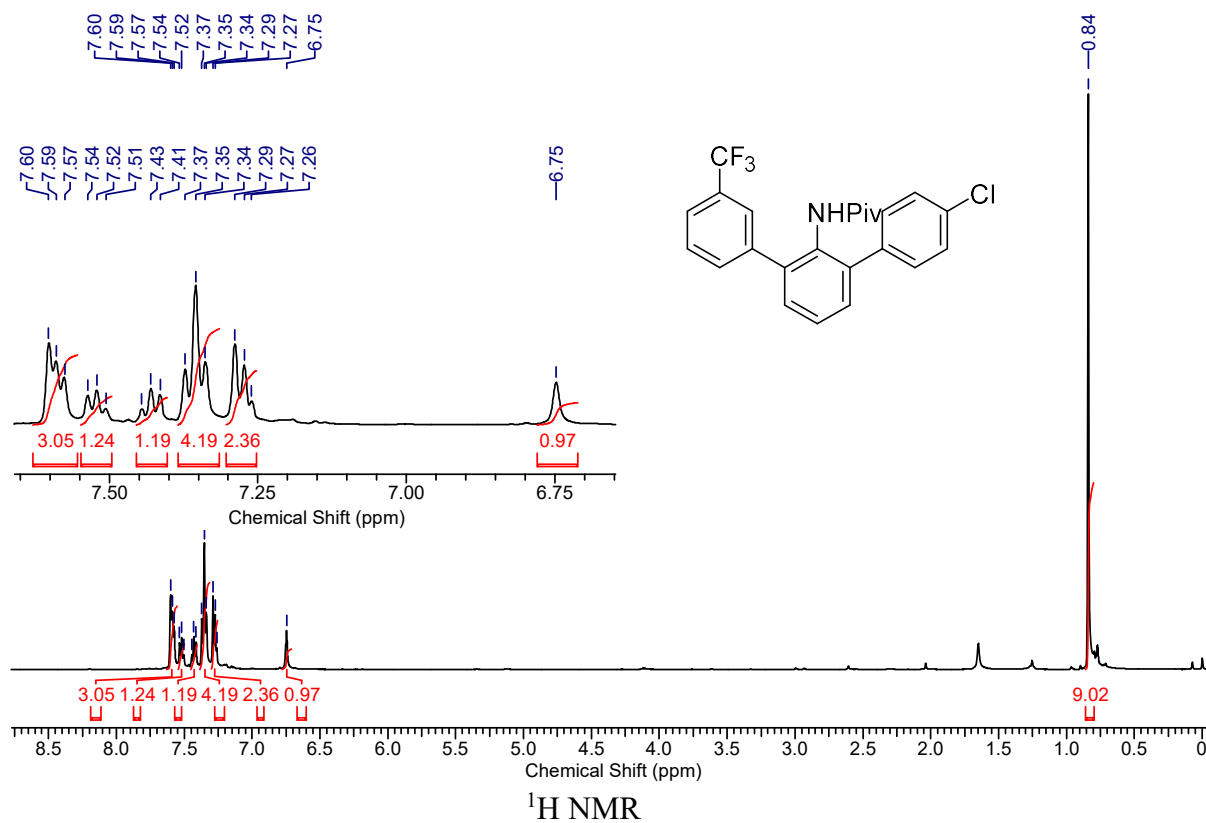


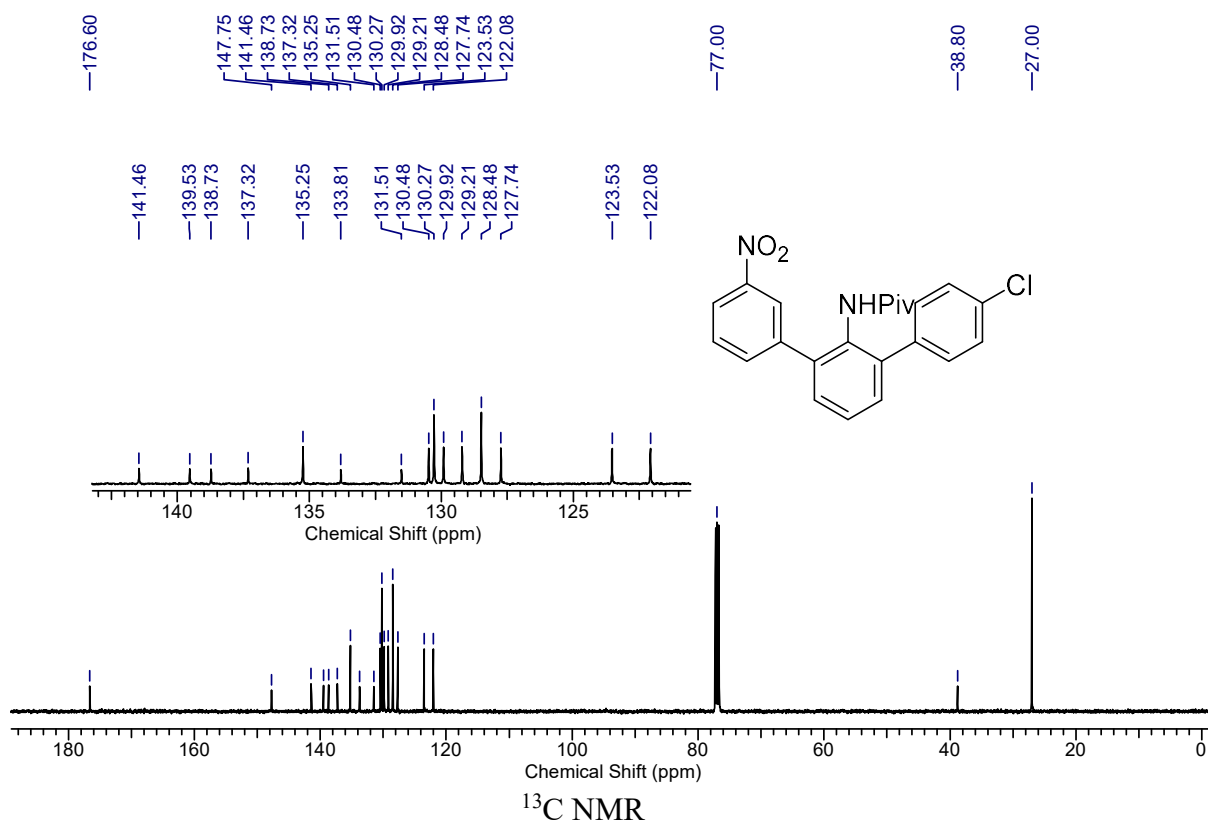
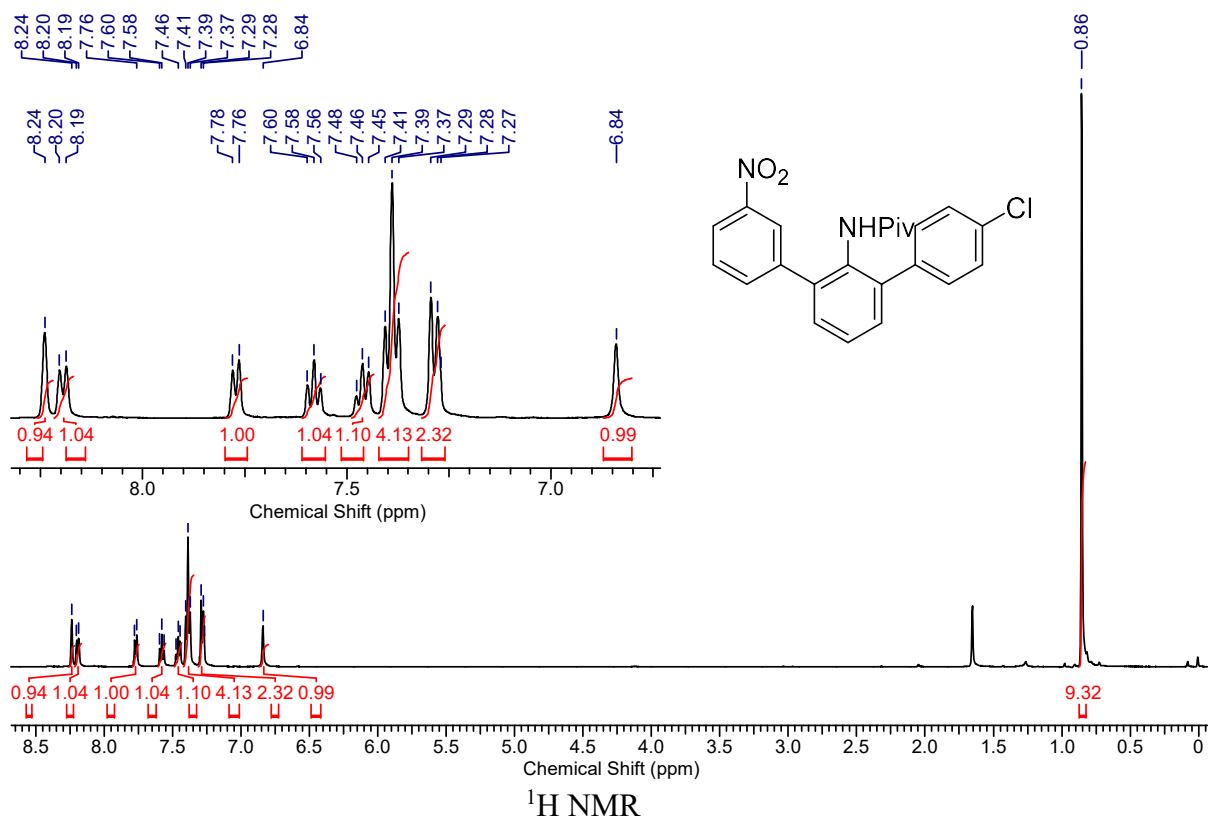


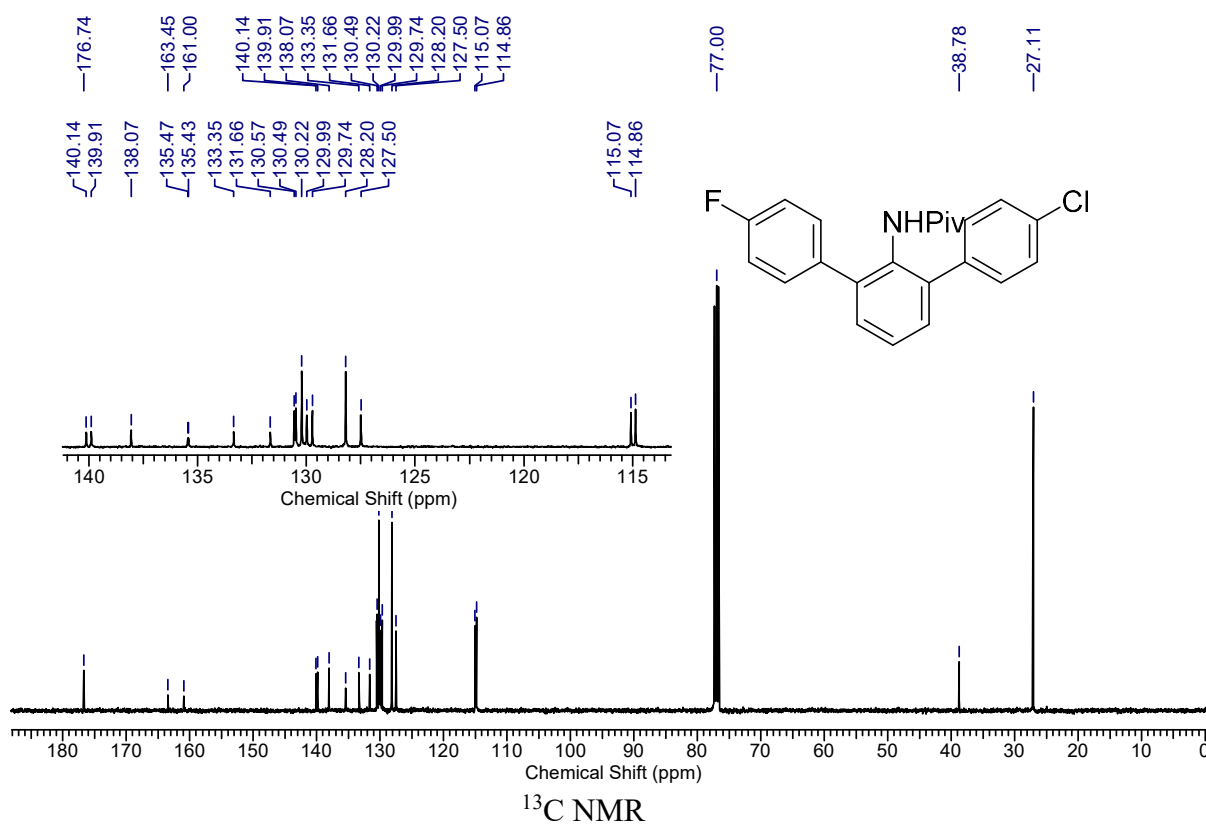
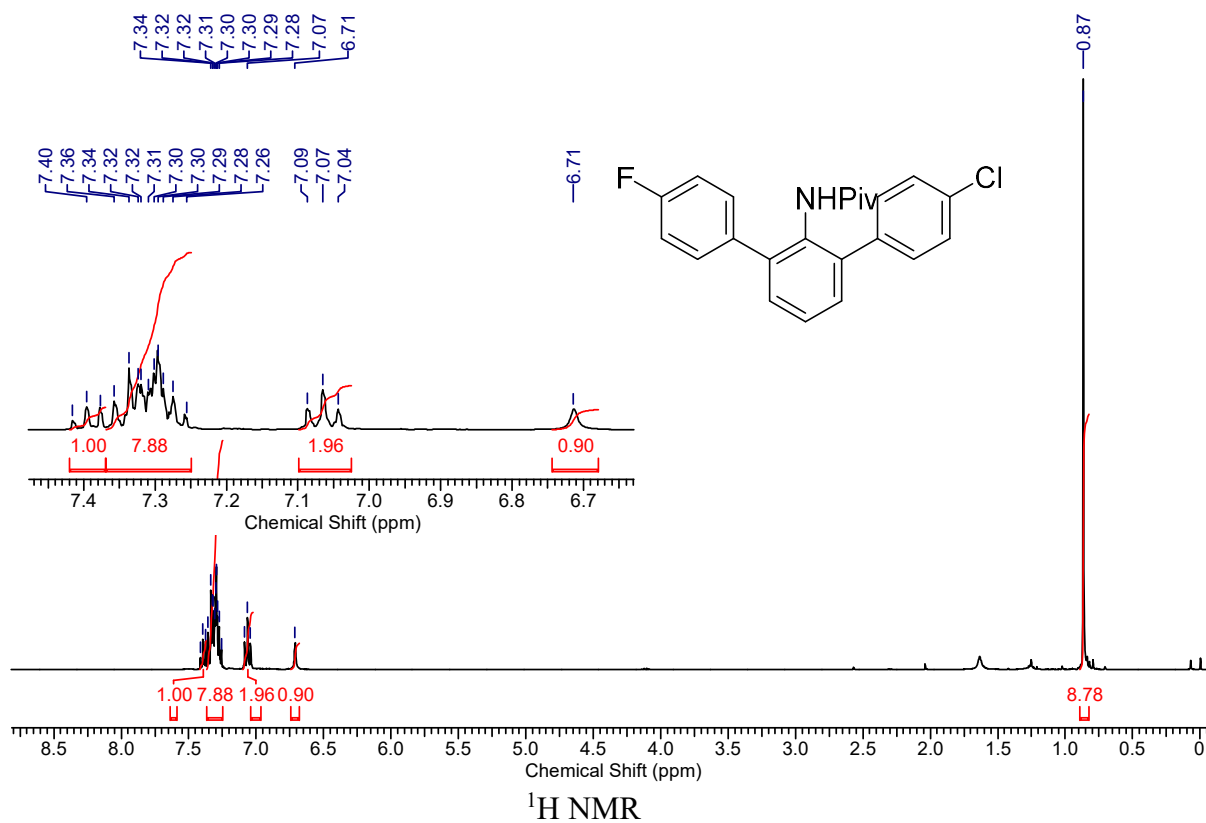


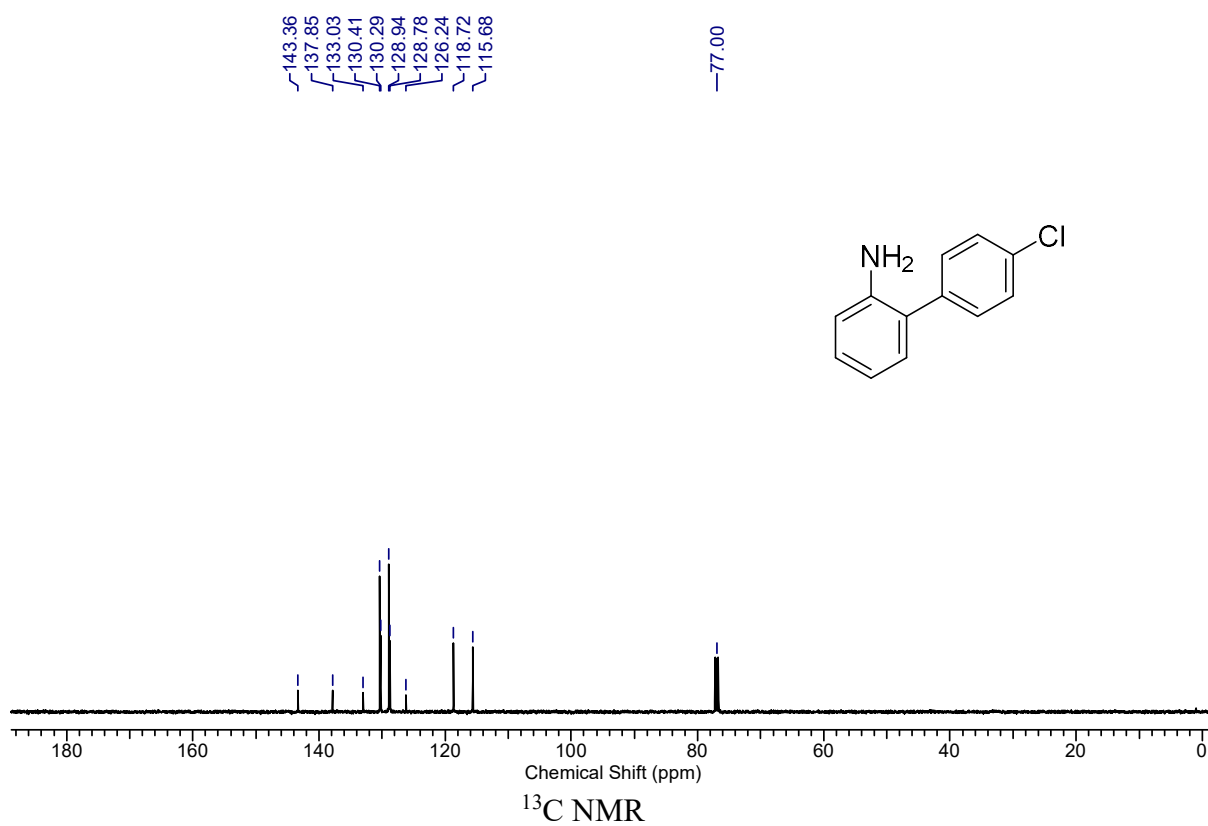
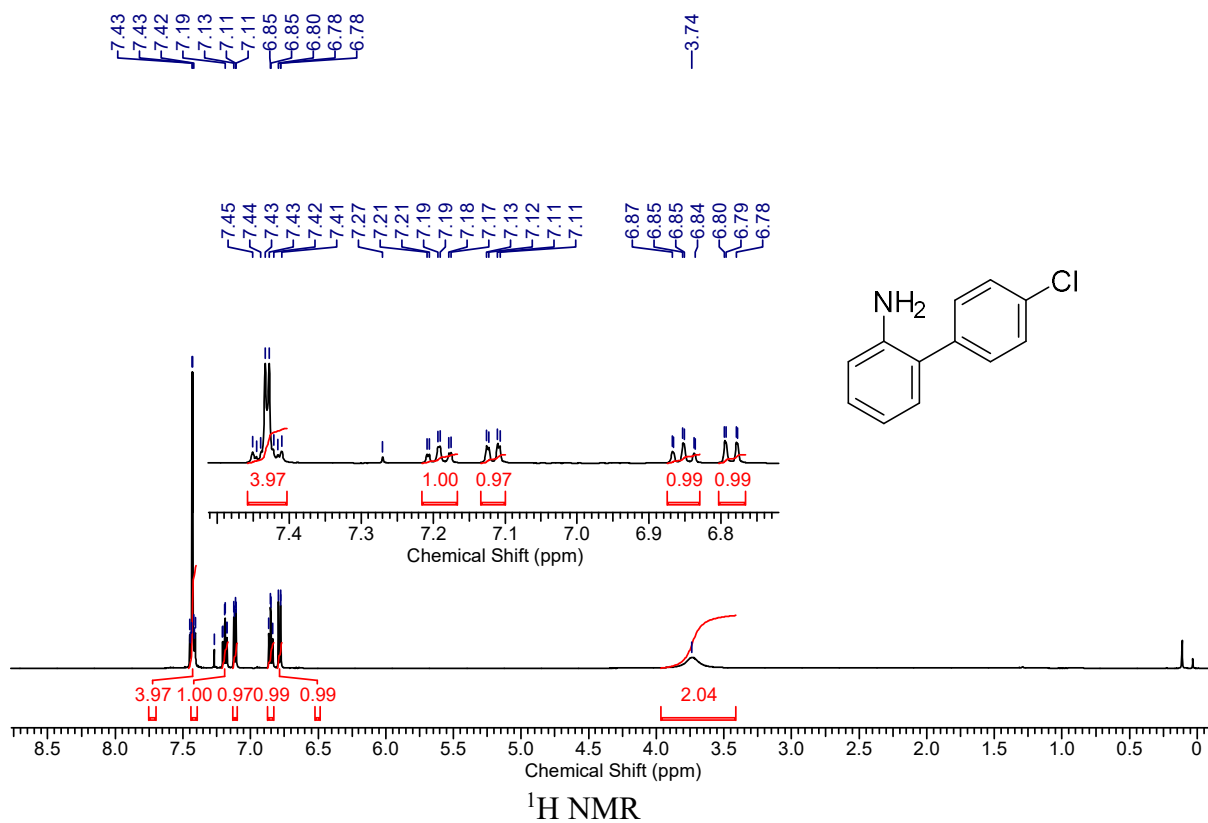


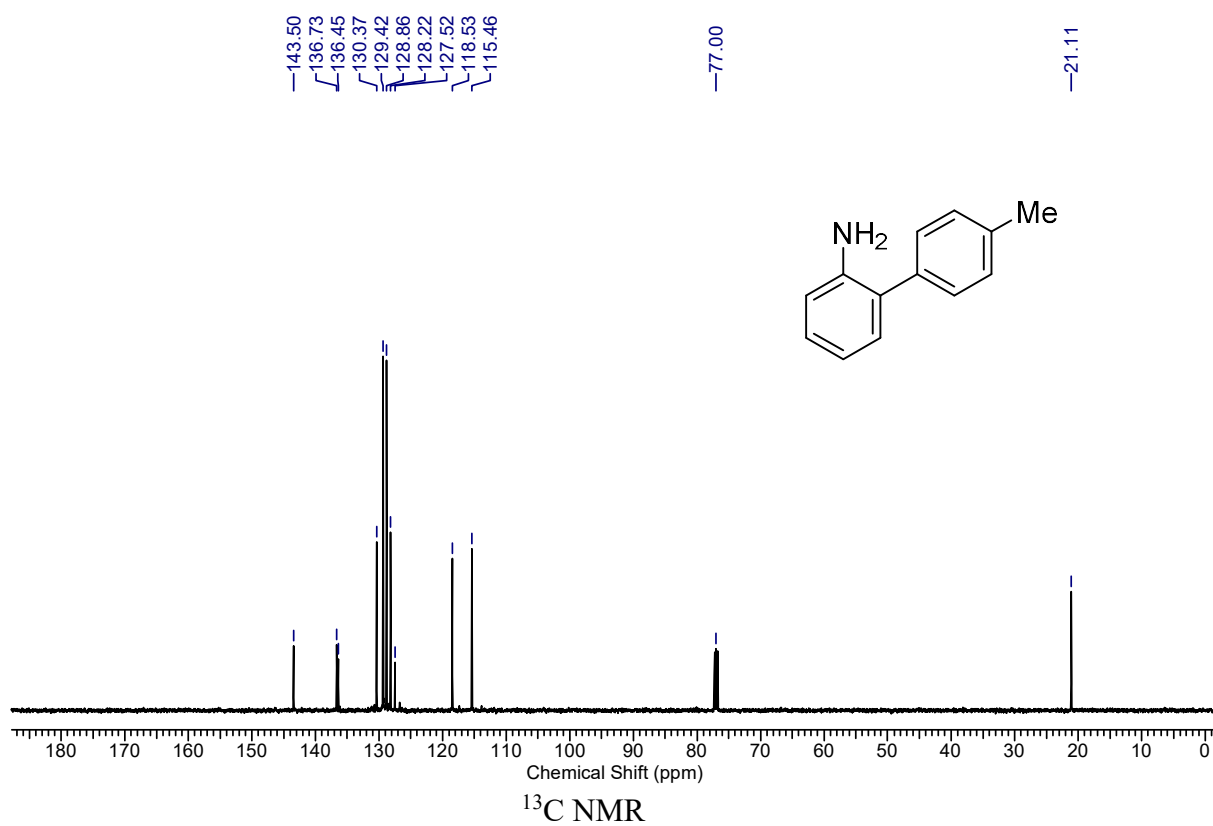
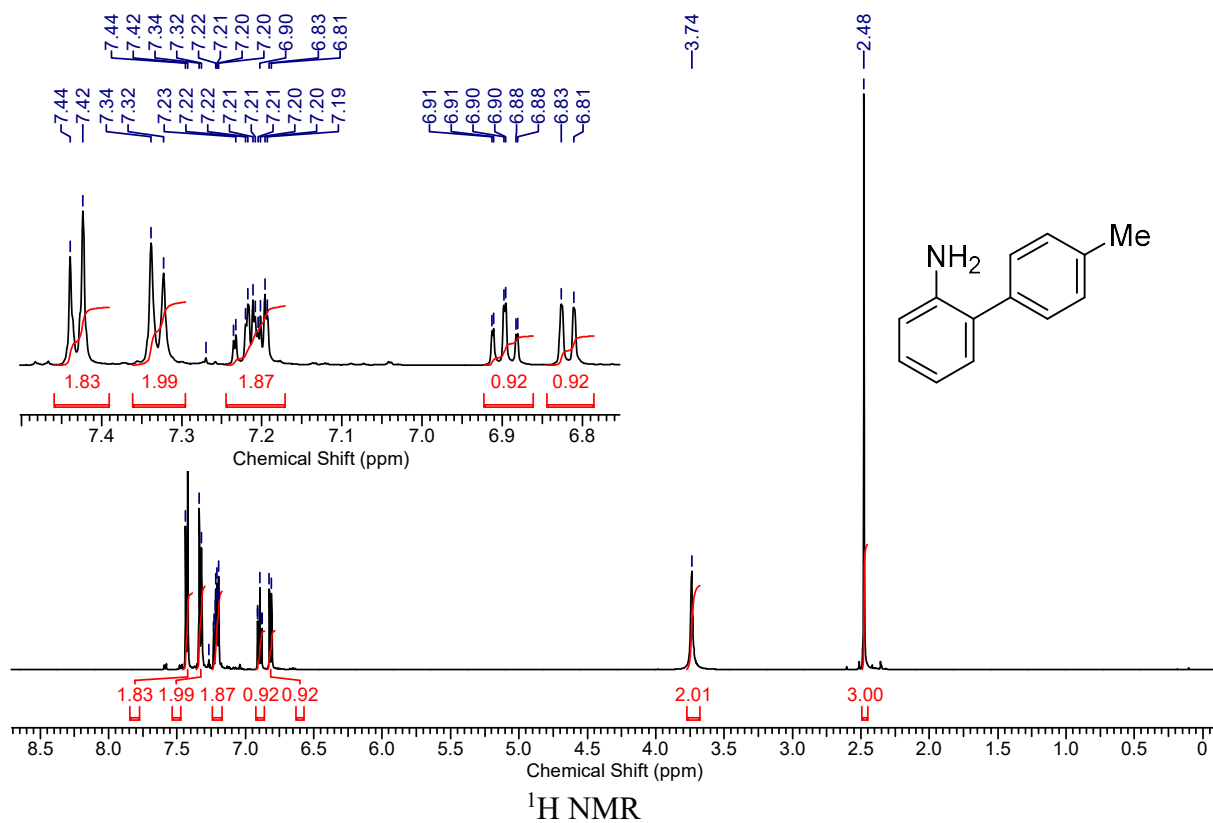


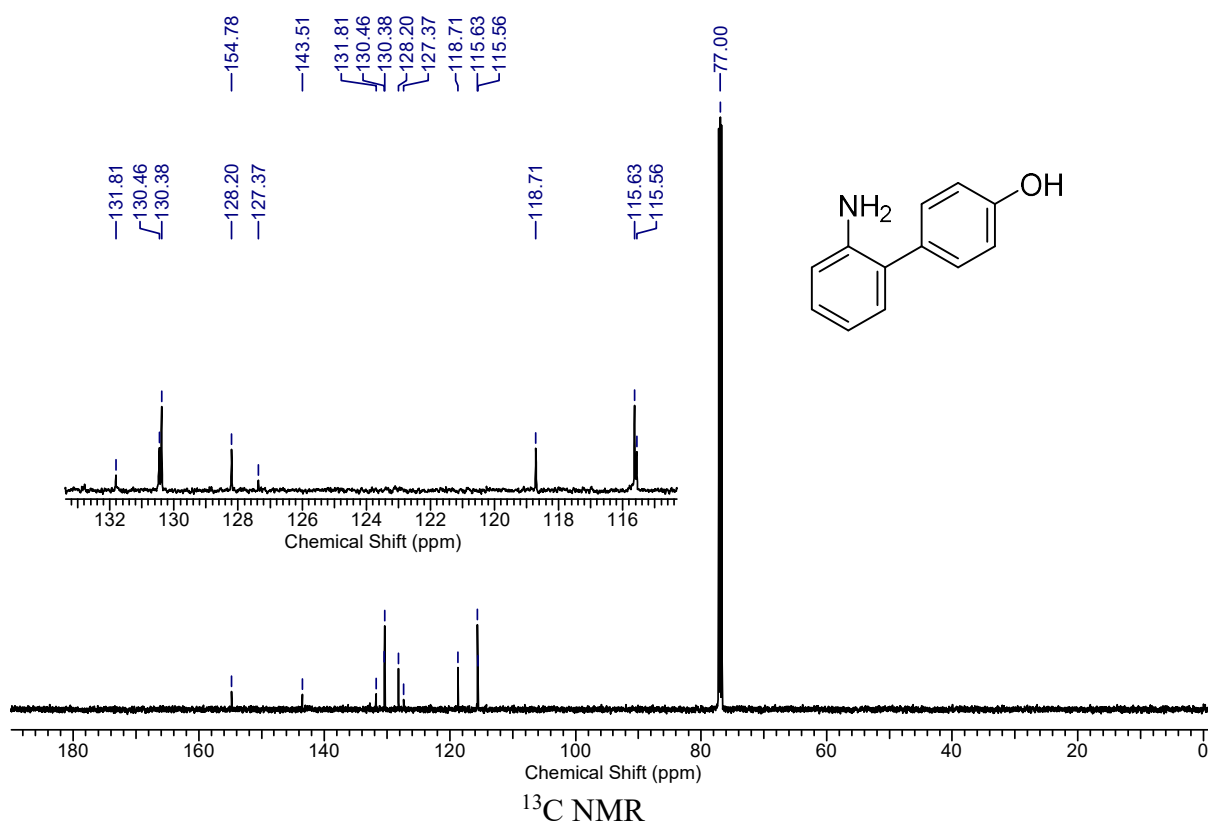
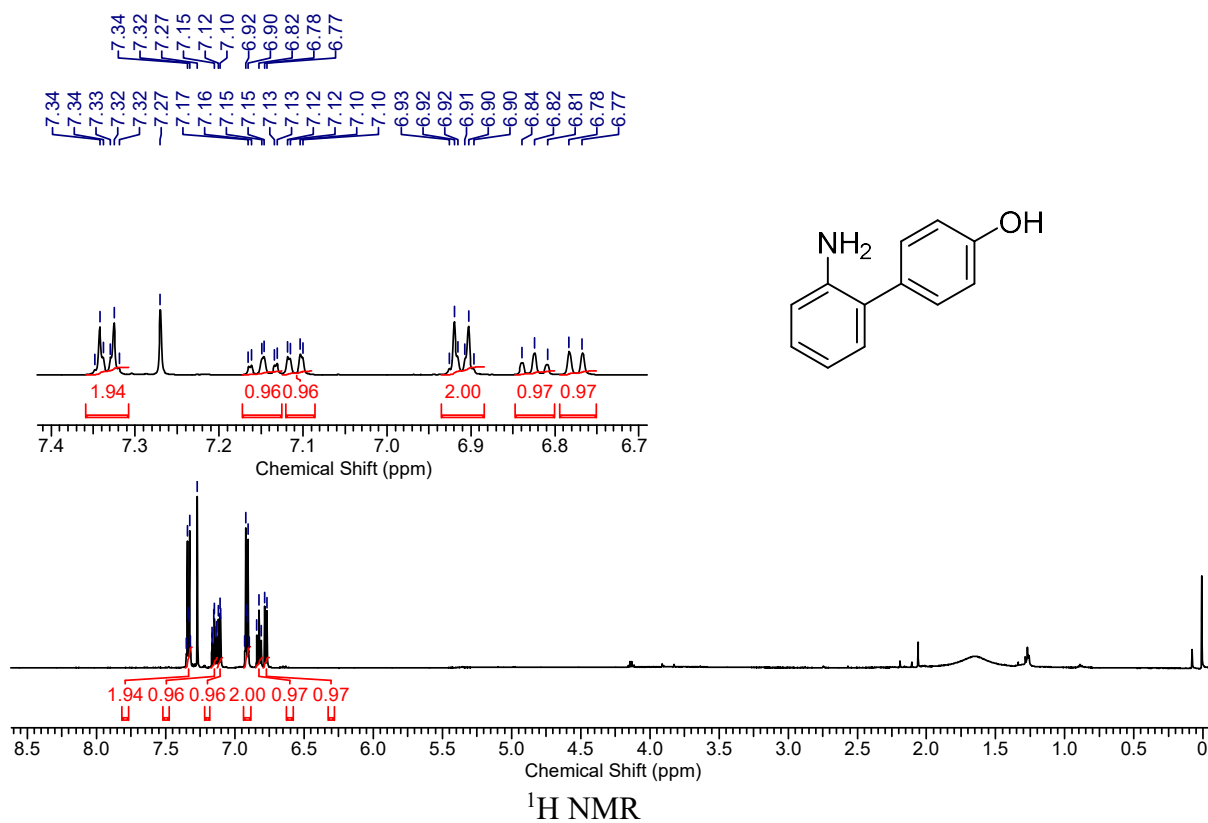


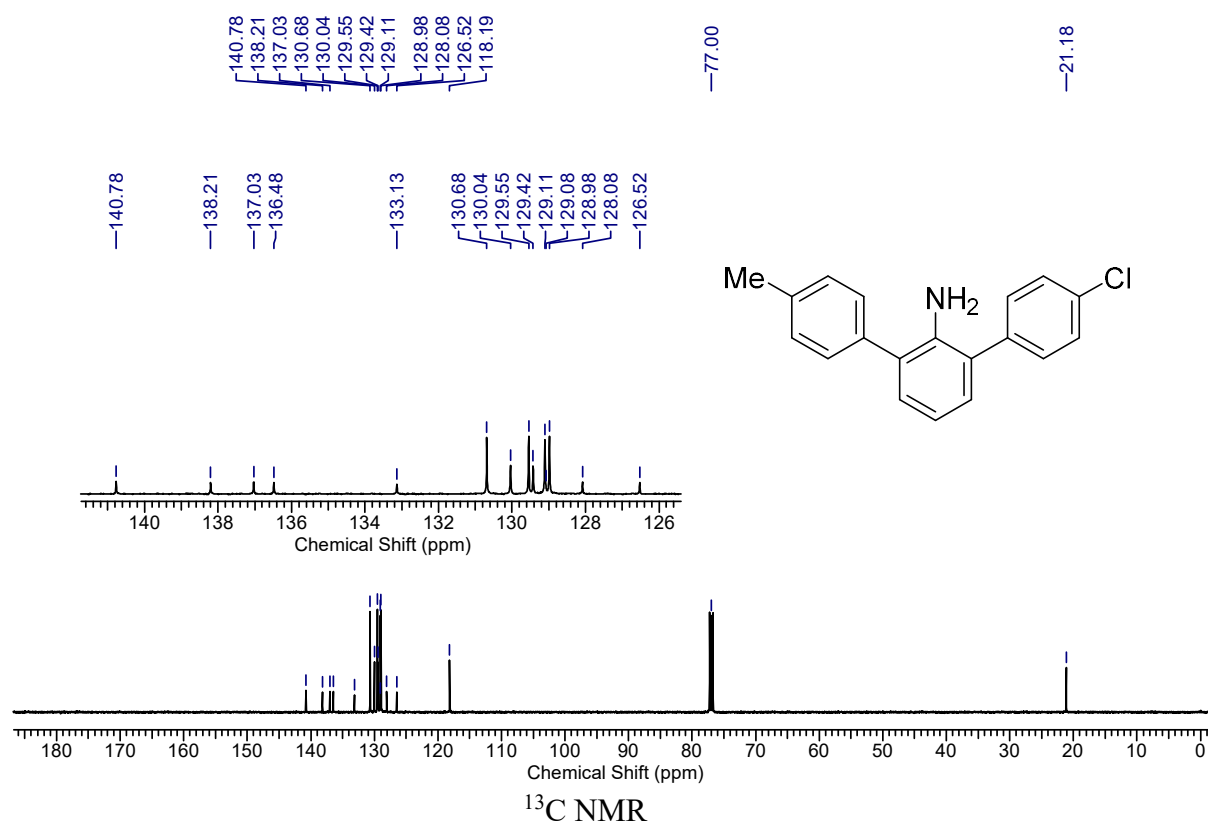
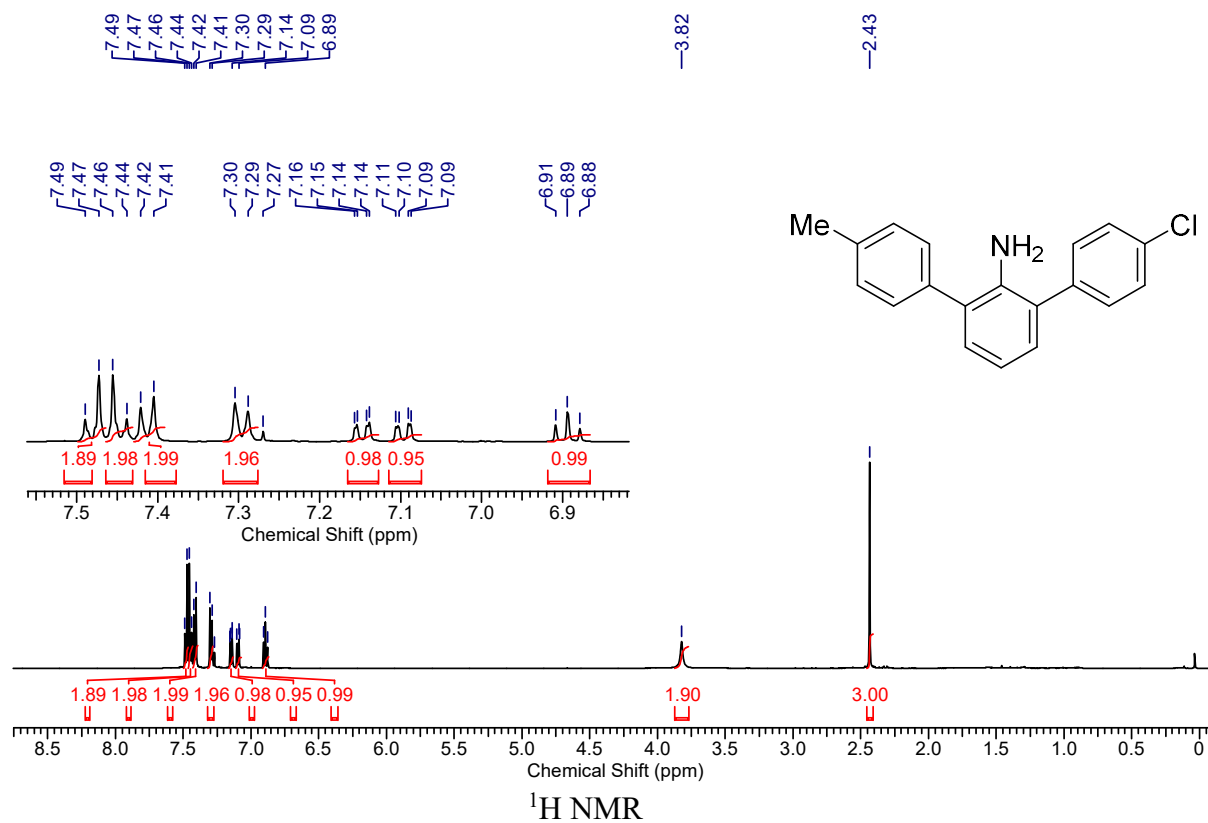


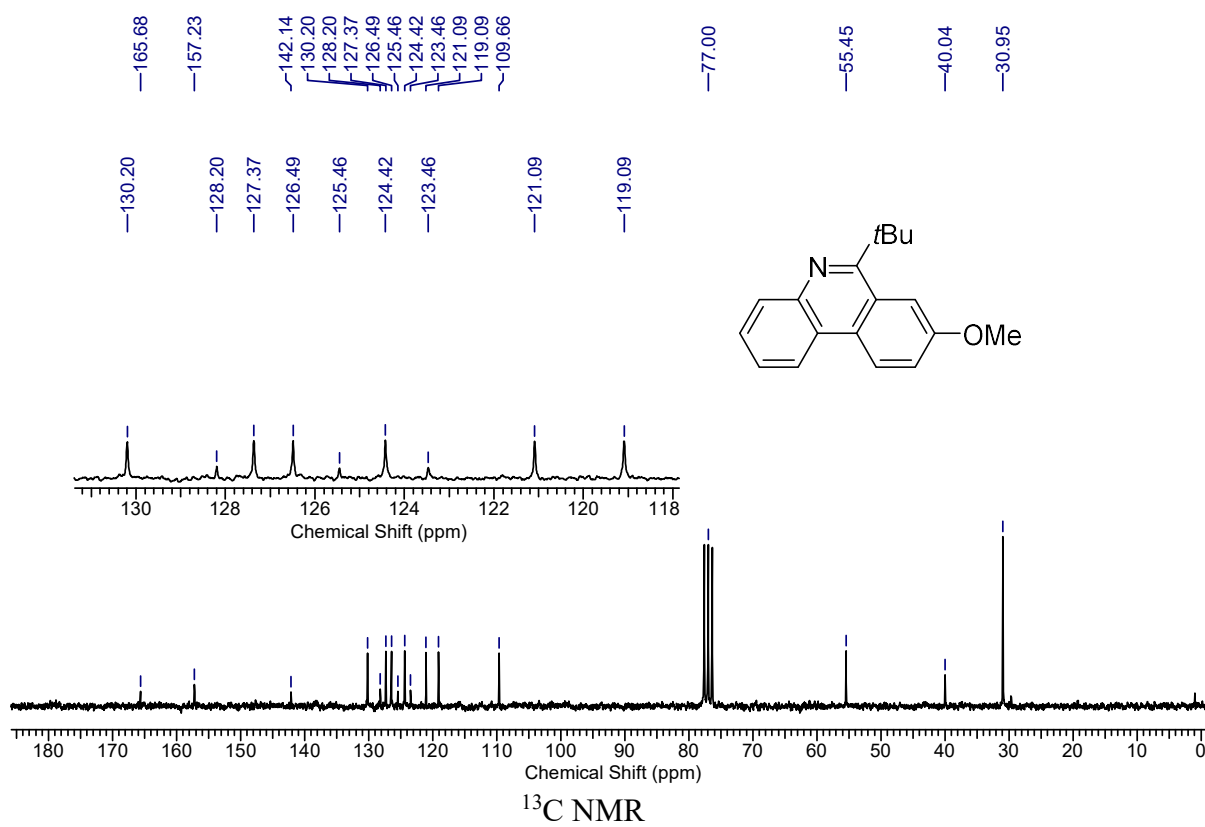
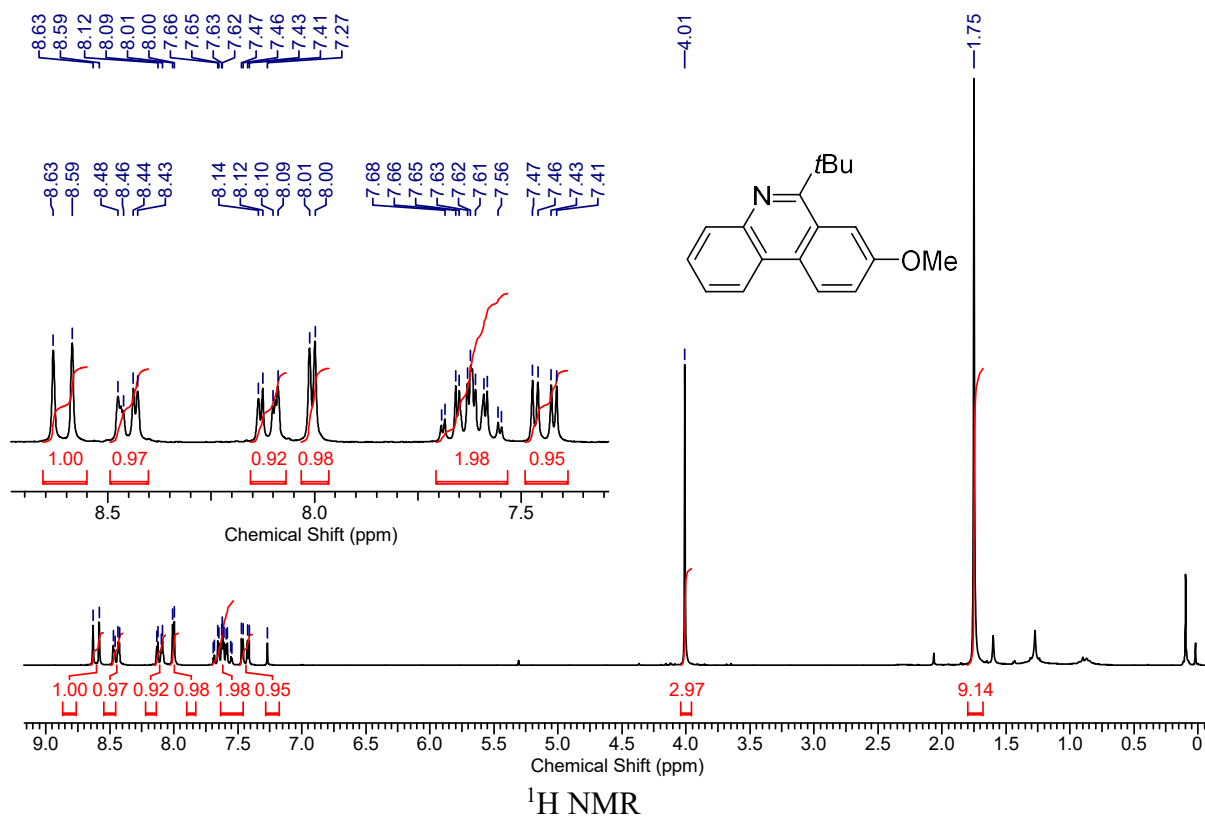


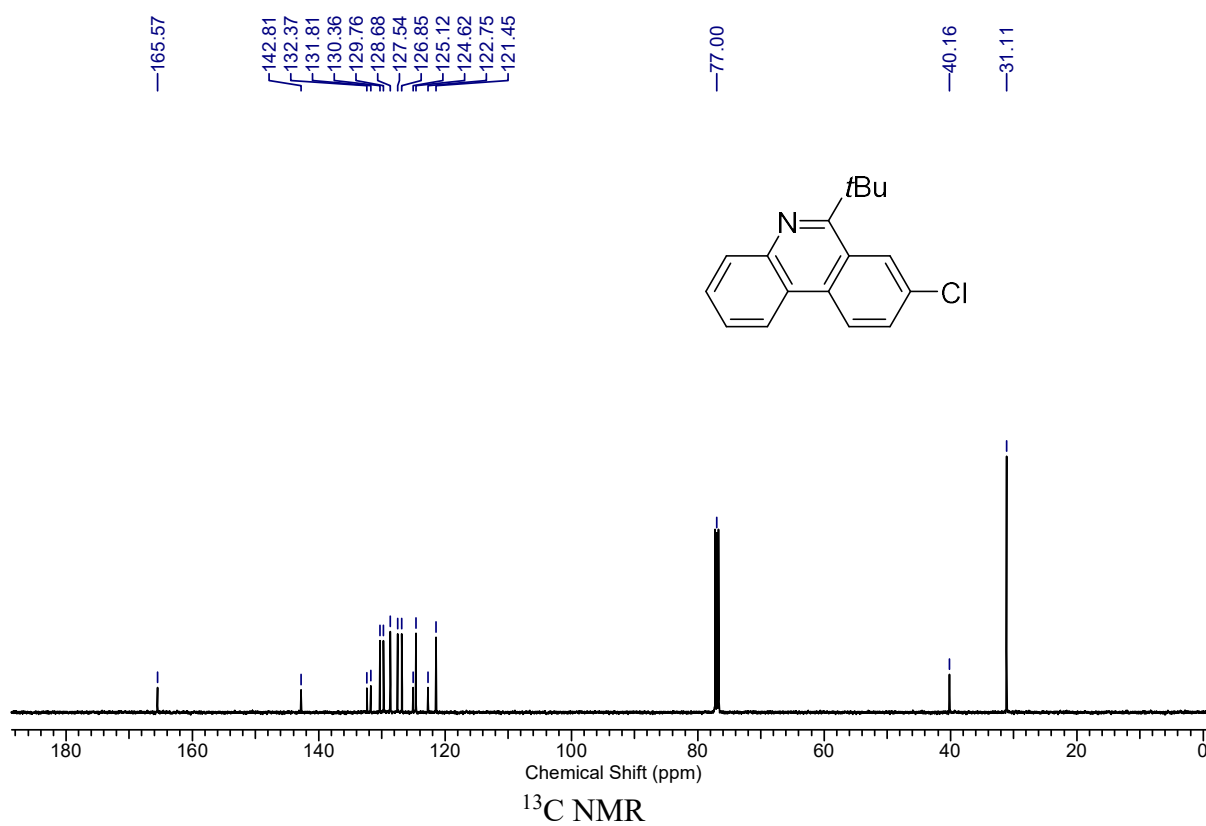
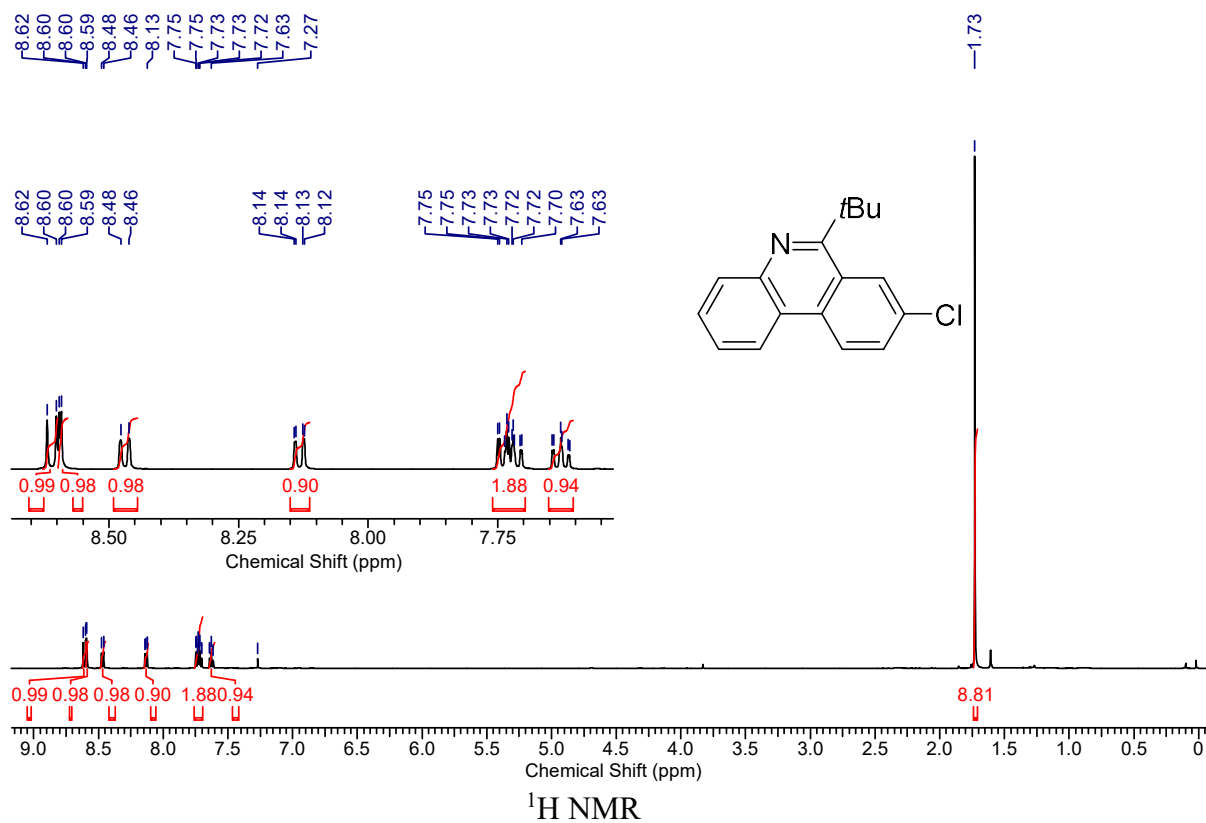


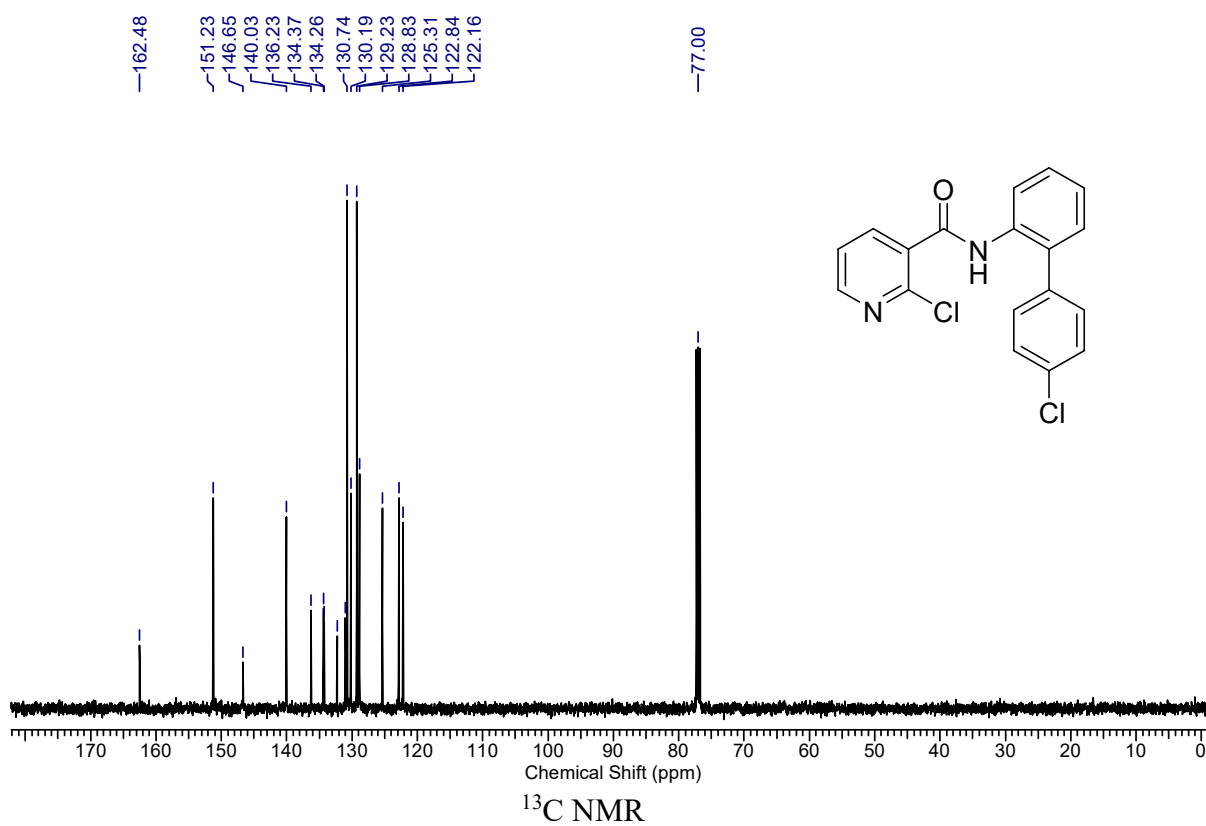
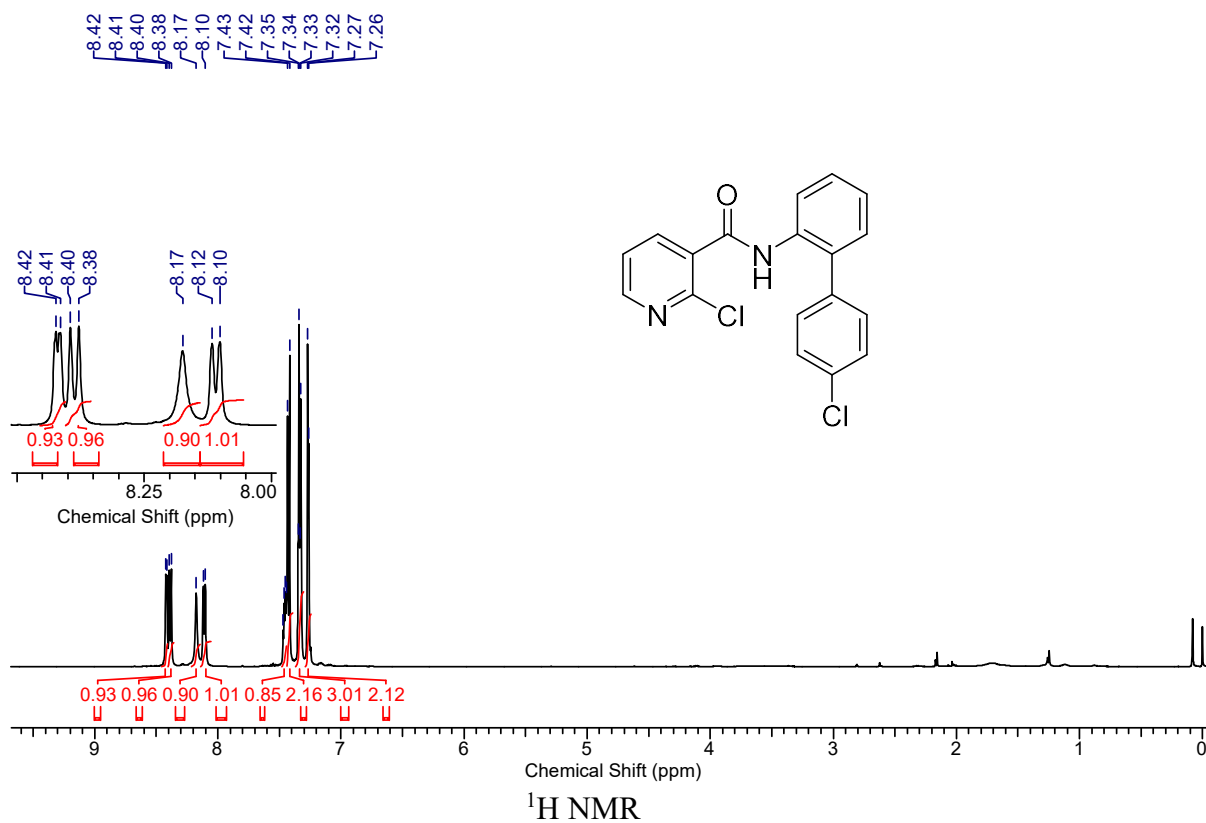


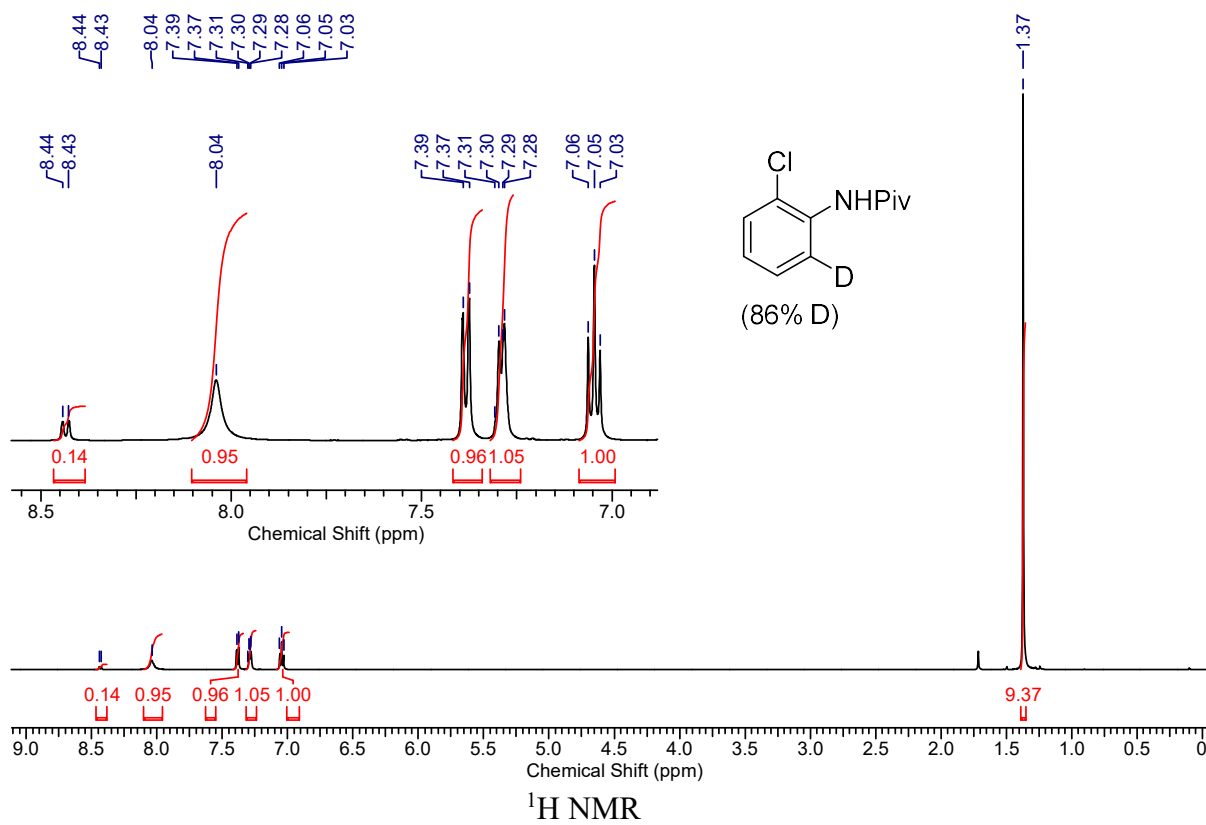






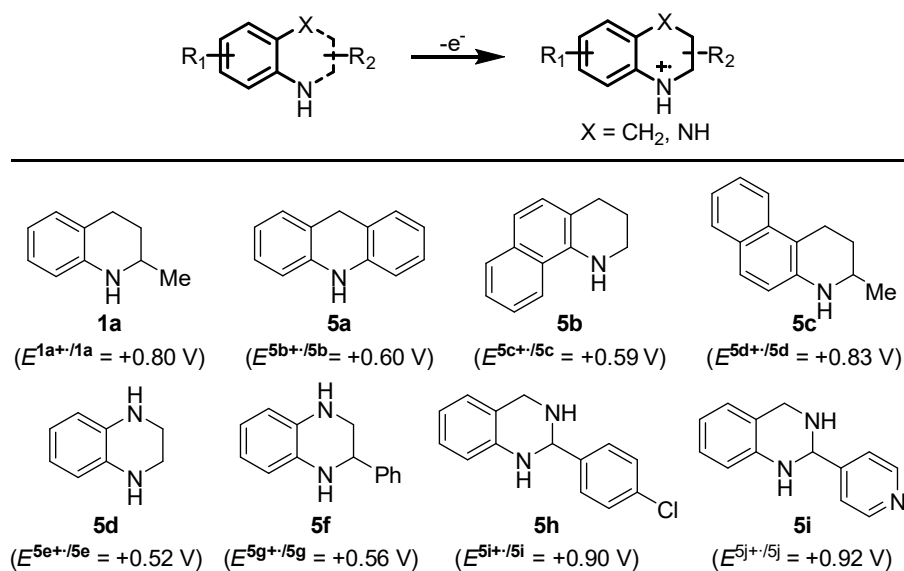






Appendix C

Cyclic Voltammetry Data



Scheme C.1. Oxidation potential of key starting materials (+0.52 V - +1.07 V vs Ag/Ag^+).

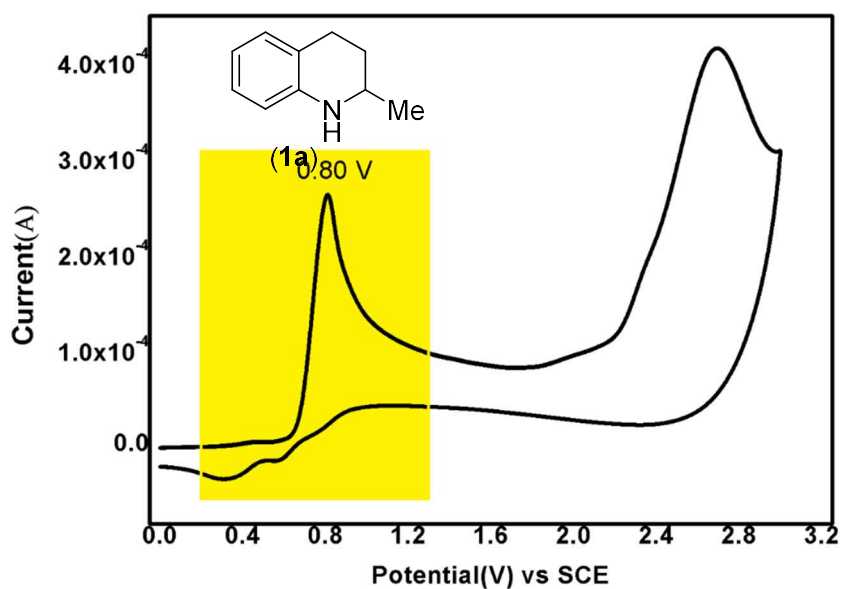


Figure C.1. CV spectra **1a** (0.01 M) in 0.1 M NBu_4ClO_4 in degassed CH_3CN with scan rate 10 mV/s.

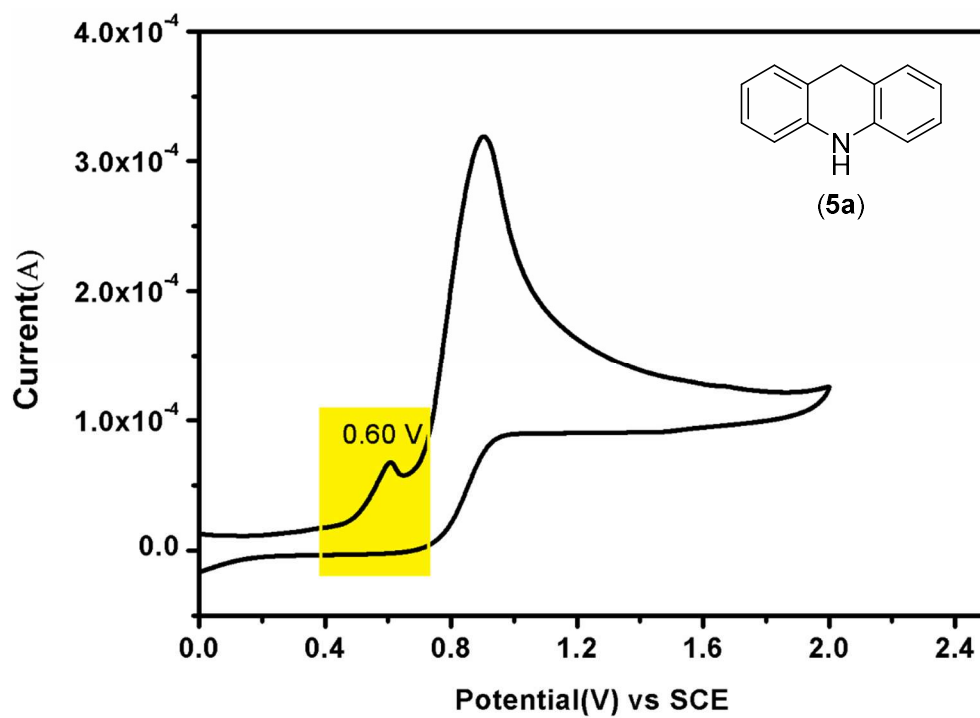


Figure C.2. CV spectra **5a** (0.01 M) in 0.1 M NBu_4ClO_4 in degassed CH_3CN with scan rate 10 mV/s.

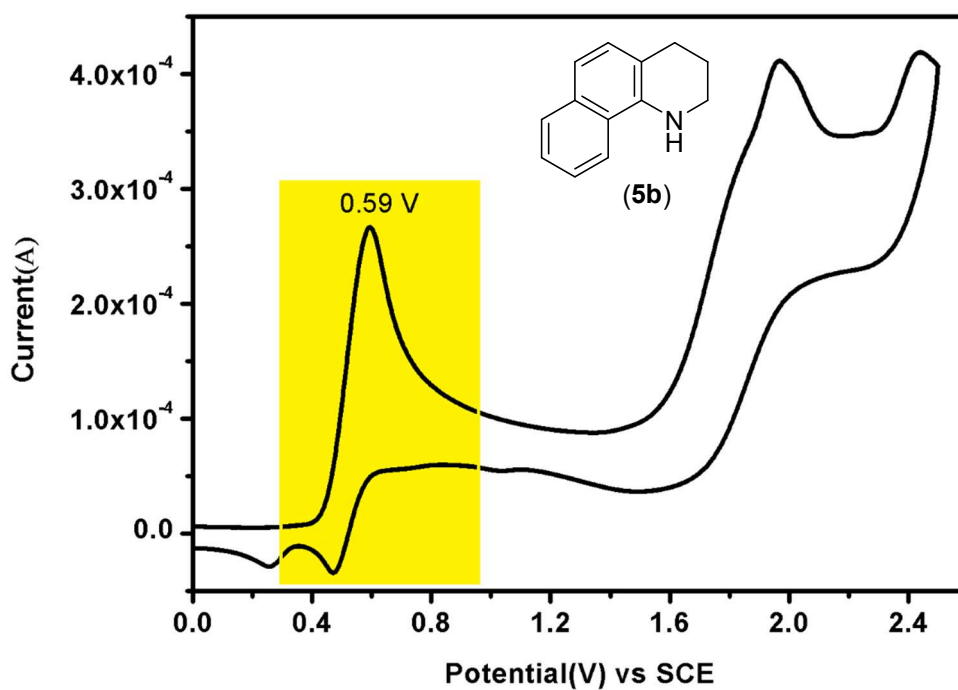


Figure C.3. CV spectra **5b** (0.01 M) in 0.1 M NBu_4ClO_4 in degassed CH_3CN with scan rate 10 mV/s.

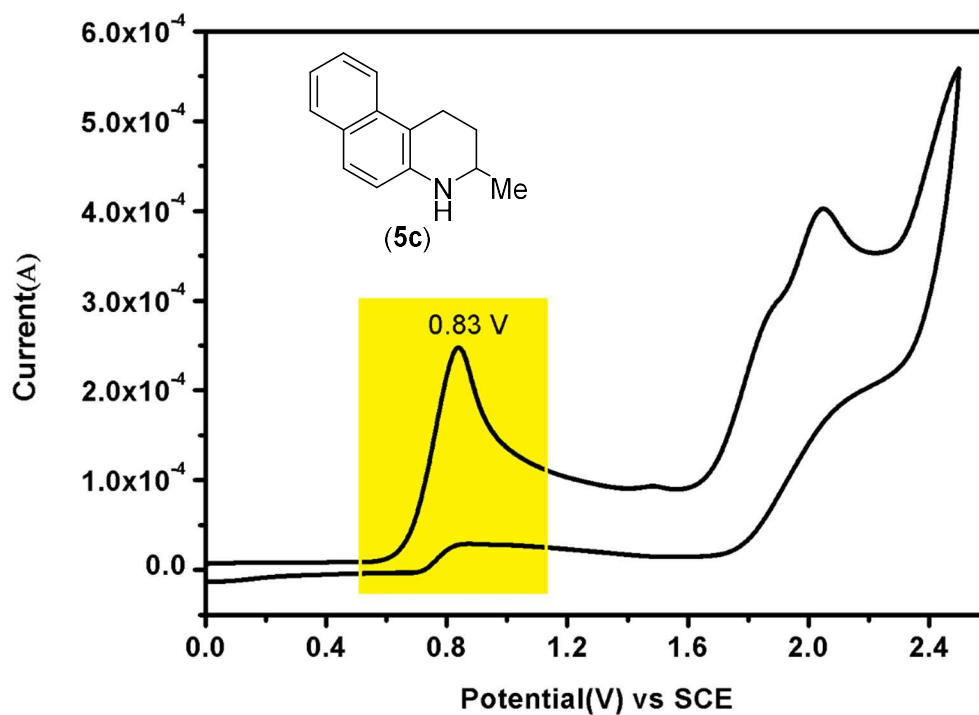


Figure 2D. CV spectra **5c** (0.01 M) in 0.1 M NBu_4ClO_4 in degassed CH_3CN with scan rate 10 mV/s.

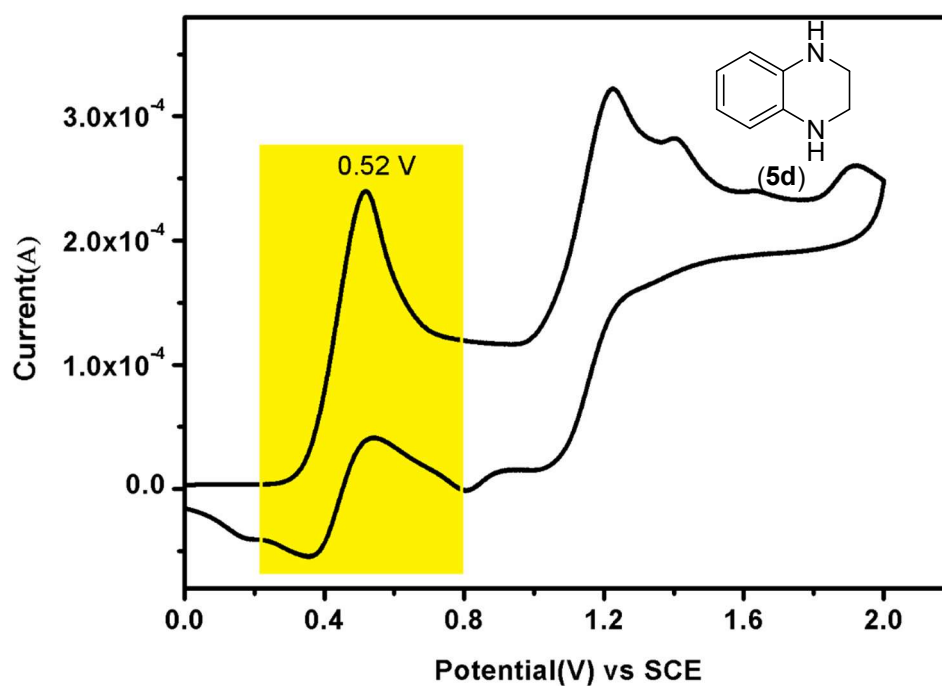


Figure 2E. CV spectra **5d** (0.01 M) in 0.1 M NBu_4ClO_4 in degassed CH_3CN with scan rate 10 mV/s

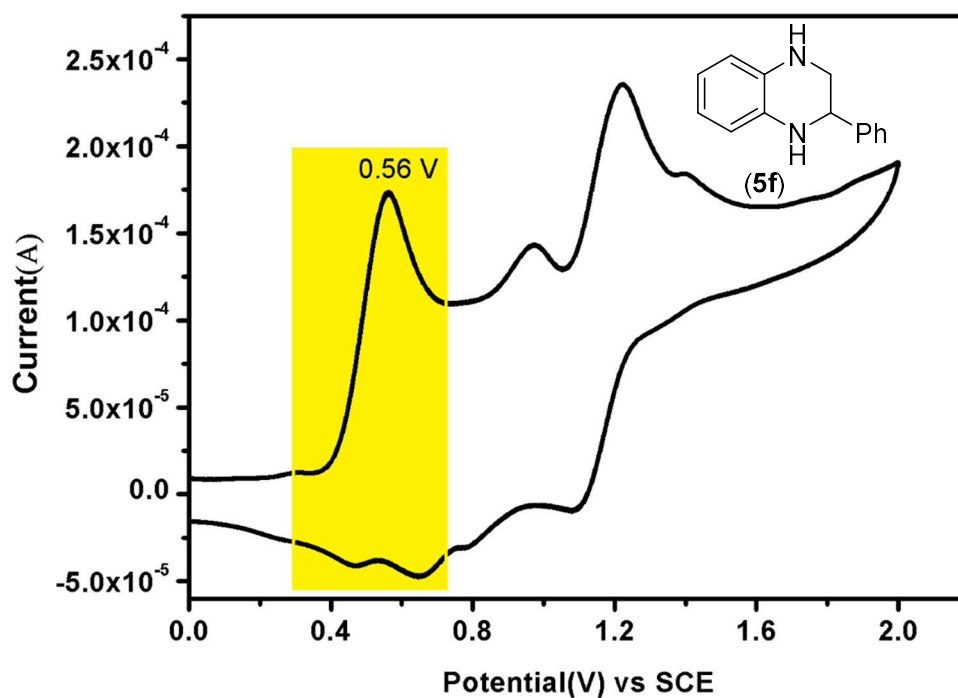


Figure 2F. CV spectra **5f** (0.01 M) in 0.1 M NBu₄ClO₄ in degassed CH₃CN with scan rate 10 mV/s.

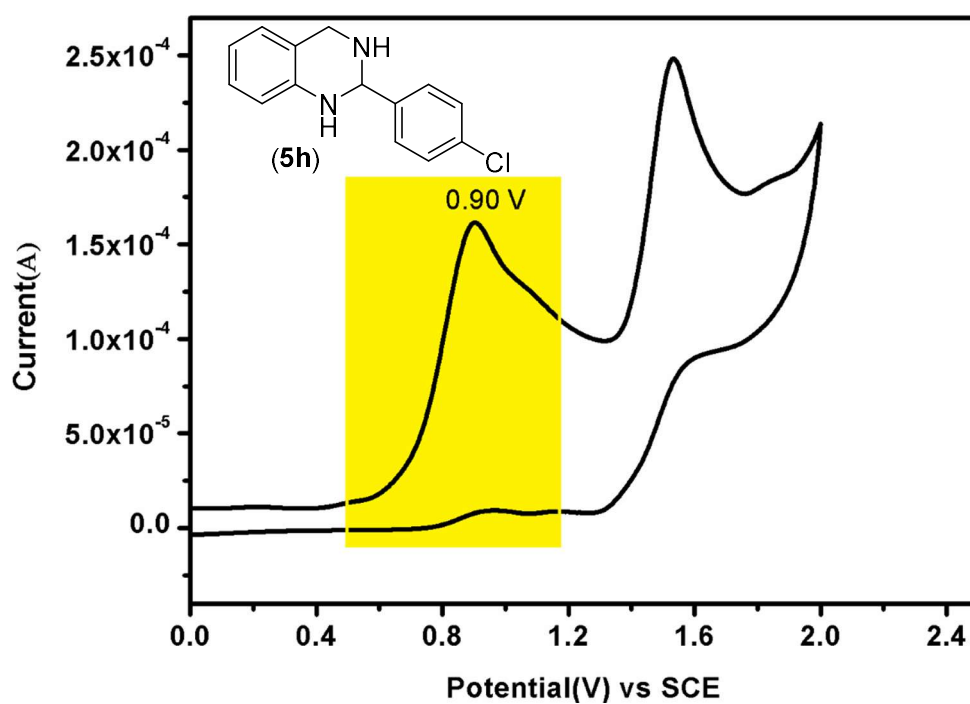


Figure 2G. CV spectra **5h** (0.01 M) in 0.1 M NBu₄ClO₄ in degassed CH₃CN with scan rate 10 mV/s.

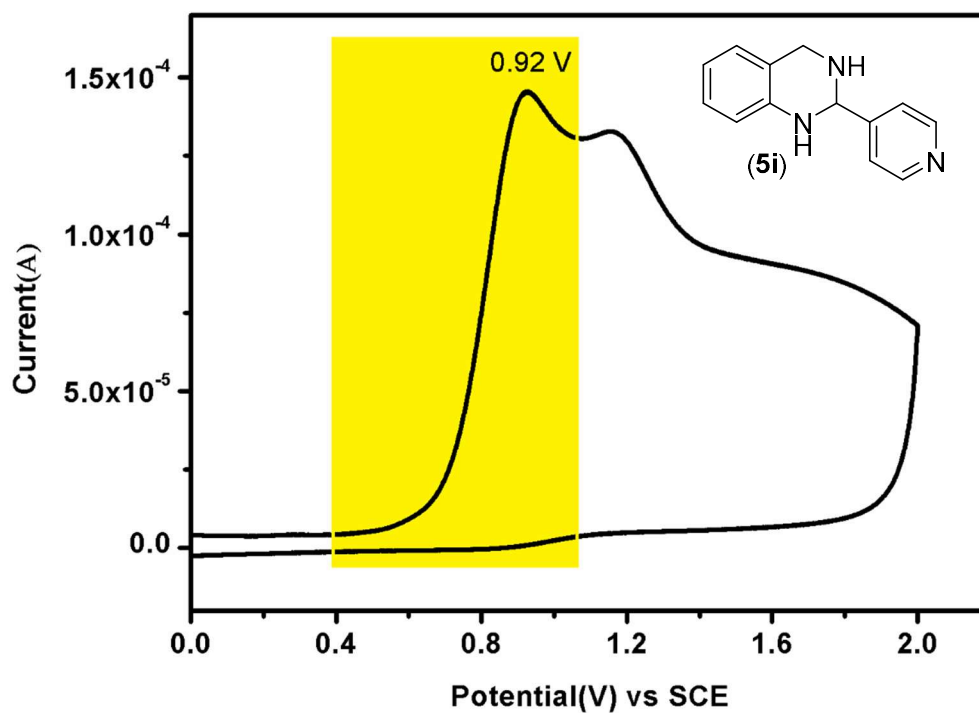


Figure 2H. CV spectra **5i** (0.01 M) in 0.1 M NBu_4ClO_4 in degassed CH_3CN with scan rate 10 mV/s.

CURRICULUM VITAE

Manoj Kumar Sahoo

CSIR-National Chemical Laboratory (CSIR-NCL)

Dr. Homi Bhabha Road

Pune - 411008, India.

Email: mk.sahoo@ncl.res.in



Academic qualification

Present status

From July 2013 to till date working as Ph.D. Scholar with Dr. E. Balaraman at CSIR-National Chemical Laboratory. I will be completing my doctoral work by July 2018.

Educational Qualification:

PhD in Visible-Light Mediated Photoredox Catalytic Organic Transformations.

(Expected to be complete by July-2018)

CSIR-Senior Research Fellow, Registered with AcSIR-New Delhi at CSIR-National Chemical Laboratory, Pune, India.

M. Sc., General Chemistry with First Class (71%), Utkal University - Bhubaneswar, Odisha, India, 2009-2011.

B. Sc., Chemistry, Physics, Mathematics, First Class with Distinction (70%), Narasingha Choudhury (Autonomous) College, Jajpur, Odisha, 2005- 2008.

Research Experience

1) CSIR-Junior Research Fellow for PhD from 29th July 2013 on the topic “*Ortho*-C-H arylation of anilides under dual catalysis by merging photoredox catalysis with transition-metal catalysis” with **Dr. E. Balaraman** at CSIR-National Chemical Laboratory, Pune.

3) CSIR-Senior Research Fellow for PhD from 30th July 2015 on the topic “Dehydrogenation of partially saturated *N*-heterocycles and application towards liquid organic storage materials” with **Dr. E. Balaraman** at CSIR-National Chemical Laboratory, Pune.

Pre-Synopsis done on 13th March 2018, PhD is expected to be complete in July 2018.

Duration: 29th July 2013 to till date.

Symposia Attended

National conferences:	2 (Participation) 3 (Poster presentation)
International conferences:	2 (Participation) 1 (Poster presentation)

Details of Publications:

1. **Sahoo, M. K.;** Saravanakumar, K.; Jaiswal, G.; Balaraman, E. Photocatalysis Enabling Acceptorless Dehydrogenation of Diaryl hydrazines at Room Temperature, *ACS Catal.* **2018**, *8*, 7727-7733.
2. **Sahoo, M. K.;** Midya, S. P.; Landge, V. G.; Balaraman, E. A unified strategy for silver-, base-, and oxidant free direct arylation of C-H bonds, *Green Chem.*, **2017**, *19*, 2111-2117.
3. **Sahoo, M. K.;** Jaiswal, G.; Rana, J.; Balaraman, E. Organo-photoredox catalyzed oxidative dehydrogenation of N-heterocycles, *Chem. Eur. J.*, **2017**, *23*, 14167-14172.
4. **Sahoo, M. K.;** Rana, J.; Subramanian, M.; Balaraman, E. Room-temperature direct arylation of anilides under external oxidant-free conditions using CO₂ derived dimethyl carbonate (DMC) as 'green' solvent, *ChemistrySelect.*, **2017**, *2*, 7565-7569.
5. **Sahoo, M. K.;** Jaiswal, G.; Balaraman, E. Room Temperature Visible-light Mediated Acceptorless Dehydrogenation of N-Heterocycles with Liberation of H₂ in Water, *Manuscript under Revision*.
6. Midya, S. P.; Landge, V. G.; **Sahoo, M. K.;** Rana, J.; Balaraman, E. Cobalt-Catalyzed Acceptorless Dehydrogenative Coupling of Aminoalcohols with alcohols: Direct Access to Pyrrole, Pyridine and Pyrazine Derivatives, *Chem. Commun.*, **2018**, *54*, 90-93.
7. Balaraman, E.; Nandakumar, A.; Jaiswal, G.; **Sahoo, M. K.;** Iron-catalyzed dehydrogenation reactions and its applications in sustainable energy and catalysis (Review Article), *Catal. Sci. Technol.*, 2017, *7*, 3177-3195.
8. Landge, V. G.; Shewale, C. H.; Jaiswal, G.; **Sahoo, M. K.;** Midya, S. P.; Balaraman, E. Nickel-catalyzed direct alkynylation of C(sp²)-H bonds of amides: An

“inverse Sonogashira strategy” to *ortho*-alkynylbenzoic acids. *Catal. Sci. Technol.*, **2016**, *6*, 1946-1951.

9. Midya, S. P.; **Sahoo, M. K.**; Landge, V. G.; Rajamohanam, P. R.; Balaraman, E. Reversed reactivity of anilines with alkynes in the rhodium-catalyzed C-H activation/carbonylation tandem, *Nature Commun.*, **2015**, *6*, 8591.

10. Landge, V. G.; **Sahoo, M. K.**; Midya, S. P.; Jaiswal, G.; Balaraman, E. Well-defined palladium(II) complexes for ligand enabled C(sp³)-alkynylation. *Dalton Trans.*, **2015**, *44*, 15382-15386.

11. Nandakumar, A.; **Sahoo, M. K.**; Balaraman, E. Reverse-hydroformylation: a missing reaction explored. (Highlight) *Org. Chem. Front.*, **2015**, *2*, 1422-1424.

Details of Patents:

1. Novel *ortho*-diarylaniline their derivatives and preparation thereof. Balaraman, E; **Sahoo, M. K.**; Jaiswal, G.; Borikar, S. P. Indian Pat. Appl. (**2017**), IN 2015DE02331 A 20170203.

2. Catalytic hydrogenation process for the synthesis of terminal diols from terminal dialkyl aliphatic esters.

Balaraman, E; **Sahoo, M. K.**

International Application No.: PCT/IN2016/050013

- 131/DEL/2015 (IN)
- WO2016113758 (A1)
- US2017349514 (A1)

3. Phenanthroline based pincer complexes useful as catalysts for the preparation of methanol from carbondioxide.

Balaraman, E.; Landge, V. G.; Midya, S. P.; **Sahoo M. K.**; Jaiswal, G.

International Application No.: PCT/IN2016/050050

- 358/DEL/2015 (IN) and 417/DEL/2015 (IN)
- WO2016128997 (A1)
- US2018021766 (A1)
- EP3256250 (A1)

4. Novel CF₃ pertaining fatty acid donors for olefin polymerization.

Virendrakumar Gupta, E. Balaraman, K. Vanka, Manoj K. Sahoo, J. Kumawat

- DN20170159

5. A process for the synthesis of azobenzene derivatives.

Balaraman, E.; **Sahoo, M. K.**; Mondal, A.

Indian Patent Appl. No. 201811000292. Provisional application filed.

6. One step one pot transition metal-free process for synthesis of heterocycles.

Balaraman, E.; **Sahoo, M. K.**; Rana, J.

Indian Patent Appl. No. 201711031976. Provisional application filed.